

NASA TECHNICAL NOTE



NASA TN D-3870

NASA TN D-3870

FACILITY FORM 602

N 67 19279

(ACCESSION NUMBER)	467	(THRU)	
(PAGES)		(CODE)	31
(NASA CR OR TMX OR AD NUMBER)		(CATEGORY)	

GEMINI LAND LANDING SYSTEM DEVELOPMENT PROGRAM

VOLUME II - SUPPORTING INVESTIGATIONS

by Leland C. Norman, Jerry E. McCullough, and Jerry C. Coffey

*Manned Spacecraft Center
Houston, Texas*

GEMINI LAND LANDING SYSTEM
DEVELOPMENT PROGRAM

VOLUME II - SUPPORTING INVESTIGATIONS

By Leland C. Norman, Jerry E. McCullough,
and Jerry C. Coffey

Manned Spacecraft Center
Houston, Texas

NATIONAL AERONAUTICS AND SPACE ADMINISTRATION

For sale by the Clearinghouse for Federal Scientific and Technical Information
Springfield, Virginia 22151 - CFSTI price \$3.00

ABSTRACT

Volume II of the Gemini Land Landing System Development Program contains detailed presentations of the scaled-model tests, component development and verification efforts, and test systems, which led to and supported the full-scale investigation presented in Volume I.

CONTENTS

Section	Page
SUMMARY	1
INTRODUCTION	1
SECTION I - ONE-THIRD-SCALE FLIGHT DYNAMICS TESTS	3
ONE-THIRD-SCALE FLIGHT DYNAMICS TESTS	5
SUMMARY	5
INTRODUCTION	5
TEST PROGRAM	6
SYSTEM DESCRIPTION	7
Parachute	7
Rigging	7
Vehicle	8
Impact Attenuation	8
Control System	9
Data Acquisition	9
RESULTS	10
Parachute Performance	10
Load Distribution and Center of Pressure	12
SECTION II - LANDING DYNAMICS TEST OF A ONE-THIRD-SCALE PARA-SAIL/LANDING-ROCKET MODEL	27
LANDING DYNAMICS TEST OF A ONE-THIRD-SCALE PARA-SAIL/LANDING-ROCKET MODEL	29
SUMMARY	29

Section	Page
INTRODUCTION	30
GEMINI SPACECRAFT LANDING-ROCKET SYSTEM DESIGN	30
MODEL DESCRIPTION	31
TEST PROCEDURE	33
MODEL TEST	33
Phase I - Impact Test on Sod and Soil	34
Phase II - Impact Tests on Canvas with Active Propulsion System	34
RESULTS AND DISCUSSION	35
Stability on Sod and Soil Surfaces without Propulsion	36
Stability on Canvas Surface with Active Propulsion System	36
Accelerations	37
Coefficients of Friction	38
Surface Erosion	39
CONCLUSIONS	39
SECTION III - PARACHUTE DEVELOPMENT	57
PARACHUTE DEVELOPMENT	59
APPENDIX A - PARA-SAIL EVALUATION DROP-TEST PROGRAM	61
SUMMARY	61
INTRODUCTION	61
EQUIPMENT	62
TEST PROCEDURE	63

Section	Page
TEST RESULTS	63
Deployment	63
Rate of Turn	63
Free Descent	64
CONCLUSIONS AND RECOMMENDATIONS	64
HELICOPTER DROP TESTS	64
APPENDIX B - DEVELOPMENT TESTS OF THE 80-FOOT-DIAMETER PARA-SAIL	73
DEVELOPMENT TESTS OF THE 80-FOOT-DIAMETER PARA-SAIL	75
SUMMARY	75
INTRODUCTION	75
DISCUSSION	76
RESULTS	80
Opening Loads	81
Opening Times	81
Riser-Load Distribution	81
The Effect of Wing Loading on Steady-State Performance	82
Oscillation	82
Evaluation of the Internal Parachute as an Inflation Aid	83
Internal-Parachute Behavior	83
Fixed-Turn Potential	84
Effect of Stabilization Panels on Steady-State Performance	84

Section	Page
CONCLUSIONS	85
TEST DESCRIPTION AND RESULTS	87
APPENDIX C - RESULTS AND ANALYSES OF DROP TESTS WITH A 70-FOOT-DIAMETER PARA-SAIL	105
RESULTS AND ANALYSES OF DROP TESTS WITH A 70-FOOT- DIAMETER PARA-SAIL	107
SUMMARY	107
INTRODUCTION	107
SYMBOLS	109
DROP-TEST PROGRAM	111
TEST RESULTS	112
Total and Individual Riser Forces	112
Canopy Depth and Aspect Ratio	113
Rate of Descent	113
Aerodynamic Centerline	113
Effective Drag Coefficient	114
Lift and Drag Coefficients	114
Lift-to-Drag Ratio	115
Turn Rate	115
Control-Line Forces	116
OPENING CHARACTERISTICS	116
Force and Trajectory Curves	116
Internal Parachute Performance	117
Projected Planform Area-Time History	117

Section	Page
THE DEPLOYMENT SYSTEM	118
Para-Sail Deployment Aids	118
Primary Reefing	119
PACKING METHODS AND AIDS	120
STRUCTURAL INTEGRITY	120
SYSTEM WEIGHT AND VOLUME	121
CANOPY CONFIGURATION	121
CONCLUDING REMARKS	122
SECTION IV - ROCKET-MOTOR DEVELOPMENT	215
USE OF PARAMETRIC EQUATIONS TO OPTIMIZE A LANDING ROCKET AND SUBSEQUENT MODEL TESTING	217
SUMMARY	217
INTRODUCTION	217
SYMBOLS	218
DERIVATION OF MOTION RELATIONSHIPS	220
APPLICATION	226
Case A	228
Case B	228
SUSTAIN PHASE	229
CONCLUDING REMARKS	231
APPENDIX A - DEVELOPMENT OF THE MODEL-100 LANDING ROCKET	232

Section	Page
BASIC MOTOR ASSEMBLIES	235
The Loaded Case Assembly	235
The Nozzle Assembly	235
The Igniter Assembly	236
APPENDIX B - PROPULSION-MODEL DESCRIPTION AND TESTING	238
SECTION V - ALTITUDE-SENSOR DEVELOPMENT	271
ALTITUDE-SENSOR DEVELOPMENT	273
REQUIREMENT	273
SCOPE	273
Manned Spacecraft Center Development	273
Mechanical Probe	274
SYSTEM DESCRIPTIONS	274
Pendulum-Type Device	274
DeHavilland-Type Altitude-Sensing Device	277
CONCLUSIONS	280
SECTION VI - TURN-CONTROL MOTOR DEVELOPMENT	289
TURN-CONTROL MOTOR DEVELOPMENT	291
REQUIREMENT	291
SCOPE	291
Aircraft Armaments Contract	291
Manned Spacecraft Center Development	291

Section	Page
Future Development	291
SYSTEM DESCRIPTION	292
Functional and Physical Description	292
Test Results	294
Problem Areas and Improvements	295
Final Configuration and Conclusions	296
SECTION VII - INVESTIGATION OF THE VISUAL-REFERENCE REQUIREMENTS FOR PILOT CONTROL OF GLIDING PARACHUTES FOR LAND LANDING OF SPACECRAFT	303
INVESTIGATION OF THE VISUAL-REFERENCE REQUIREMENTS FOR PILOT CONTROL OF GLIDING PARACHUTES FOR LAND LANDING OF SPACECRAFT	305
SUMMARY	305
INTRODUCTION	305
General	305
Mode of Operation	306
Test-Program Objectives	307
TEST-PROGRAM DESCRIPTION	307
Phase I	307
Phase II	307
Phase III	308
DESCRIPTION OF TEST VEHICLES AND SYSTEMS	308
Phase I	308
Phase II	308

Section	Page
Phase III	309
TEST PROCEDURES	310
Phase I	310
Phase II	311
Phase III	311
RESULTS AND DISCUSSION	312
Phase I	312
Phase II	312
Phase III	314
CONCLUSIONS AND RECOMMENDATIONS	316
SECTION VIII - GEMINI FLIGHT-TEST VEHICLE FOR PARA-SAIL/LANDING-ROCKET DEVELOPMENT PROGRAM	333
GEMINI FLIGHT-TEST VEHICLE FOR PARA-SAIL/LANDING- ROCKET DEVELOPMENT PROGRAM	335
INTRODUCTION	335
TEST VEHICLE	335
EXTERIOR MODIFICATIONS OF THE GEMINI SPACECRAFT BOILERPLATE	336
RENDEZVOUS AND RECOVERY CANISTER	337
Purpose	337
Description	337
RENDEZVOUS AND RECOVERY RELEASE MECHANISM	338
Purpose	338

Section	Page
Description	338
RESERVE PARACHUTE INSTALLATION	338
Purpose	338
Description	339
MAIN LANDING-GEAR INSTALLATION	339
Purpose	339
Description	339
NOSE LANDING GEAR	340
Purpose	340
Description	340
INSTRUMENTATION INSTALLATION	340
Purpose	340
Description	340
DEHAVILLAND ALTITUDE-SENSOR INSTALLATION	341
Purpose	341
Description	341
ZERO ALTITUDE SENSOR	341
Purpose	341
Operation	342
INTERIM ALTITUDE SENSOR	342
Purpose	342
Operation	342

Section	Page
SEPARATION SWITCH	343
Purpose	343
Description	343
RETRACTABLE ATTACH POINT	344
Purpose	344
Description	344
RETROROCKET ALINEMENT HARDWARE	344
Purpose	344
Description	344
BLAST DEFLECTOR	345
Purpose	345
Operation	345
LOAD CELLS	346
Purpose	346
Descriptions	346
PARACHUTE DISCONNECT AND ATTITUDE-CHANGE MECHANISM	346
Purpose	346
Description	347
TENSION-MEASUREMENT DEVICE	347
Purpose	347
Description	347

Section	Page
NEW TURN-CONTROL MOTORS	348
Purpose	348
Description	348
CABLE CUTTER	349
Purpose	349
Description	349
CAMERA INSTALLATION	349
Purpose	349
Operation	349
RADIO ANTENNA INSTALLATION	350
Purpose	350
Description	350
AIRBORNE LAUNCH CRADLE	351
Purpose	351
Description	351
GEAR-STROKE SENSOR	351
NOSE LANDING-GEAR SKID PROTECTOR	352
Purpose	352
Description	352
SECTION IX - VERIFICATION OF THE LANDING GEAR AND THE TEST HARDWARE	381
VERIFICATION OF THE LANDING GEAR AND THE TEST HARDWARE	383

Section	Page
SUMMARY	383
INTRODUCTION	383
LANDING-GEAR VERIFICATION	384
Deployment Tests	384
Impact Attenuation Tests	386
TEST VEHICLE AND SUPPORTING HARDWARE	389
Rendezvous and Recovery Canister Release Mechanism	389
Attitude-Change Tests	390
Zero Altitude Sensors	391
Disconnect Hardware	392
Cable Cutters	394
Load Cells	395
Rocket Motor Mounting and Alinement Hardware	395
Flotation Tests	397
TEST IMPLEMENTATION DEVICES	397
Launch-Cradle Tests	397
Blast Deflector	398
CONCLUDING REMARKS	401
SECTION X - OPERATIONAL PERFORMANCE STUDY	421
OPERATIONAL PERFORMANCE STUDY	423
SECTION XI - INSTRUMENTATION AND ELECTRONIC SYSTEMS IMPLEMENTATION FOR THE GEMINI SPACECRAFT PARA-SAIL RETROCKET SYSTEM	425

Section	Page
INSTRUMENTATION AND ELECTRONIC SYSTEMS IMPLEMENTATION FOR THE GEMINI SPACECRAFT PARA-SAIL RETROROCKET SYSTEM	427
INTRODUCTION	427
MEASUREMENT CHANGES, PROBLEMS AND TECHNIQUES	428
Signal Conditioning	428
Control-Line Load Measurements	428
Chamber Pressure Measurement P-42 and P-44	429
Attitude Gyroscope	429
Angle of Attack	429
Batteries	430
Ground Receiving Station	430
Antenna Systems	431
CALIBRATIONS	432
DATA HANDLING	432
SECTION XII - SEQUENCING AND IGNITION SYSTEMS FOR THE GEMINI SPACECRAFT LAND LANDING PROGRAM	457
SEQUENCING AND IGNITION SYSTEMS FOR THE GEMINI SPACECRAFT LAND LANDING PROGRAM	459
INTRODUCTION	459
DISCUSSION	459
System Checkout Philosophy	461
Sequencing System	462

TABLES

Table	Page
I-I DROP CONDITIONS	15
II-I LANDING IMPACT AND STABILITY TEST OF ONE-THIRD- SCALE GEMINI SPACECRAFT MODEL	
(a) Test conducted on St. Augustine sod; propulsion system not used	41
(b) Test conducted on compacted earth; propulsion system not used	42
(c) Test conducted on canvas; propulsion system used . . .	43
III-I HOUSTON TEST PROGRAM	123
III-II EL CENTRO TEST PROGRAM	124
III-III DROP-TEST PROGRAM	126
III-IV SUMMARY OF DROP-TEST INFORMATION DURING INFLATION	128
III-V SUMMARY OF PARA-SAIL TEST INFORMATION DURING STEADY STATE	129
III-VI PARA-SAIL TEST DATA SUMMARY	130
III-VII STEADY-STATE RISER FORCES	132
III-VIII GEOMETRIC PARAMETERS FOR VARIOUS PARA-SAIL CONFIGURATIONS DURING STEADY STATE	133
III-IX OPENING FORCES ON INDIVIDUAL RISERS	134
III-X DIMENSIONLESS DIAMETER, TIME-HISTORY COORDINATES	135
III-XI PARA-SAIL WEIGHT AND VOLUME	137
III-XII PERFORMANCE EVALUATION OF PARA-SAIL CONFIG- URATIONS 70A-4 AND 70A-5	138

Table	Page
IV-I TIME AND PRESSURE RELATIONSHIPS OBTAINED DURING SYSTEM CHARACTERIZATION	242
VI-I PARA-SAIL FLIGHT TEST RESULTS	297
IX-I GEAR IMPACT TEST RESULTS	402
XI-I MEASUREMENT REQUIREMENTS, AIR DROP 1	433
XI-II MEASUREMENT REQUIREMENTS, AIR DROPS 2 THROUGH 5	434
XI-III MEASUREMENT REQUIREMENTS, AIR DROPS 6 THROUGH 12	436
XII-I PYROTECHNIC NOMENCLATURE LIST	466

FIGURES

Figure		Page
I-1	Vehicle drop method	16
I-2	Slotted front configuration	17
I-3	Solid front configuration	18
I-4	Bridle system for phases I and II	19
I-5	Final bridle configuration	20
I-6	Major dimensions of test vehicle	21
I-7	Landing gear with honeycomb struts	22
I-8	Yielding metal landing gear	23
I-9	Positions and fields of view for onboard cameras	24
I-10	General arrangement (shell removed), top view	25
I-11	General arrangement (shell removed), side view	26
II-1	Landing system	
	(a) Complete full-scale system	45
	(b) One-third-scale test model	46
II-2	Model dimensions, center-of-gravity location, weight, and inertias	47
II-3	Main landing-gear detail	48
II-4	Main landing-gear shock attenuator	49
II-5	Nose landing gear	50
II-6	Schematic of propulsion system (one-third-scale Gemini spacecraft)	51
II-7	Test facility	52

Figure		Page
II-8	Drop carriage	53
II-9	Coefficients of friction	54
II-10	Soil erosion caused by model at 0 horizontal velocity	55
II-11	Soil erosion caused by model at 3.5 ft/sec horizontal velocity	56
III-1	Para-Sail parachute	139
III-2	Drop aircraft and test vehicle	140
III-3	Test vehicles housing the parachute bag, camera, and batteries (side view)	141
III-4	Test vehicle housing the parachute bag, camera, and batteries (top view)	142
III-5	Special variable length risers	
	(a) Shortened condition	143
	(b) Extended position	144
III-6	Peak-load data for tests 5, 6, 7, and 8	145
III-7	Peak-load data for tests 14 and 15	146
III-8	Turn with front riser shortened	147
III-9	Turn with rear riser shortened	148
III-10	Turn with right exhaust ports closed	149
III-11	Turn with right exhaust ports closed	150
III-12	Turn with left exhaust ports closed	151
III-13	Turn with left exhaust ports closed	152
III-14	Original 23.2-ft-diameter Para-Sail	153

Figure	Page	
III-15	Original 80-ft Para-Sail, 3 solid gores. Configuration for Houston tests 1 and 2	154
III-16	Eighty-foot Para-Sail, 7 solid gores	
	(a) Configuration for Houston test 3	155
	(b) Configuration for Houston tests 4 and 5	156
III-17	Thirty-six-line pilot parachute and bridle arrangement . . .	157
III-18	Twenty-four-foot d_o Para-Sail, solid front elliptical cutout (front view)	158
III-19	Eighty-foot Para-Sail, solid front, elliptical cutout	
	(a) Configuration for Houston tests 6 and 7	159
	(b) Configuration for Houston test 8	160
	(c) Configuration for Houston tests 9, 10, and 11; and El Centro tests 1, 2, 3, and 4	161
III-20	Internal parachute arrangement	162
III-21	Reefed inflation, airstream lines	163
III-22	Eighty-foot Para-Sail, no centerline	
	(a) Configuration for El Centro test 5	164
	(b) Configuration for El Centro tests 6 to 15 inclusive . . .	165
	(c) Final 80-ft configuration	166
III-23	Eighty-foot Para-Sail, no centerline	167
III-24	Expected opening loads	168
III-25	Expected opening times	169
III-26	Individual riser loads, test 14	170
III-27	Individual riser loads, test 16	171
III-28	Individual riser loads, test 19	172
III-29	Riser schematic	173

Figure		Page
III-30	Glide ratio versus wing loading	174
III-31	Rate of descent versus wing loading	175
III-32	Lift-to-drag ratio versus rate of descent	176
III-33	Opening dynamics with and without the internal parachute	177
III-34	Force-time history, internal parachute and Para-Sail, test 14	178
III-35	Force-time history, internal parachute and Para-Sail, test 16	179
III-36	Force-time history, internal parachute and Para-Sail, test 19	180
III-37	Lift-to-drag ratio with and without stabilization panels . . .	181
III-38	Rate of descent with and without stabilization panels	182
III-39	Schematic of parachute test items	183
III-40	Schematic cording diagram for Para-Sails 70A-4 and 70A-5	184
III-41	Location of aerodynamic centerline for a 69.8-ft Para-Sail (based upon wind-tunnel studies)	185
III-42	Average effective drag coefficient versus canopy loading for various Para-Sail configurations (based upon nominal area)	186
III-43	Average effective drag coefficient versus rate of descent at sea level for various Para-Sail configurations (based upon nominal area)	187
III-44	Average effective drag coefficient versus turn rate for a 70-ft d_o Para-Sail ($W/S_o = 1.24 \text{ lb/ft}^2$; $C_{D_{eff}}$ based upon nominal area)	188

Figure	Page
III-45	Average lift coefficient versus canopy loading for various Para-Sail configurations (based upon nominal area) 189
III-46	Average drag coefficient versus canopy loading for various Para-Sail configurations (based upon nominal area) 190
III-47	Lift coefficient versus drag coefficient for various Para-Sail configurations (based upon nominal area) 191
III-48	Average lift-to-drag ratio versus canopy loading for various Para-Sail configurations (based upon nominal area) 192
III-49	Turn rate versus elapsed time for a 69.8-ft d_o Para-Sail 193
III-50	Ground track for drop 4 (turn test) 194
III-51	Ground track for drop 12 (turn test) 195
III-52	Ground track for drop 13 (turn test) 196
III-53	Control-line force versus control-line stroke for a 69.8-ft d_o Para-Sail 197
III-54	Force versus time traces for drops 2 through 5 (configuration 70A-4), and drops 6 through 11 (configuration 70A-5) 198
III-55	Maximum force ratio versus maximum dynamic-pressure ratio for a 70-ft Para-Sail 199
III-56	Altitude versus time curves for drops 5, 6, and 11 200
III-57	Trajectory angle versus time for drops 5, 6, and 11 201
III-58	Total velocity versus time for drops 5, 6, and 11 202
III-59	Projected diameter ratio versus time ratio, stage I 203
III-60	Projected diameter ratio versus time ratio, stage II 204

Figure		Page
III-61	Total opening time versus maximum dynamic-pressure ratio for a 70-ft d_o Para-Sail ($q_{\text{design}} = 80 \text{ lb/ft}^2$)	205
III-62	Total force-to-dynamic pressure ratio versus time	206
III-63	Pictorial view of Para-Sail deployment aids	207
III-64	Aluminum bridle-attaching vent ring	208
III-65	Para-Sail pressure packing equipment	208
III-66	Composite damage chart, drop tests 2 through 15, configura- tions 70A-4 and 70A-5	209
III-67	Calculated weight and volume for Para-Sail recovery para- chutes	210
III-68	General geometry of a 69.8-ft d_o Para-Sail (deflated condition). Configurations 70A-4 and 70A-5 (72 gores)	211
III-69	Typical gore pattern of a 69.8-ft d_o Para-Sail. Configura- tions 70A-4 and 70A-5 (72 gores)	212
III-70	Para-Sail, 69.8-ft d_o engineer plan view, based upon gore without fullness. Configurations 70A-4 and 70A-5 (72 gores)	213
IV-1	Dimensionless performance, boost phase	243
IV-2	Dimensionless performance, sustain phase, $\nu_1 = 0.00$. . .	244
IV-3	Dimensionless performance, sustain phase, $\nu_1 = 0.05$. . .	245
IV-4	Dimensionless performance, sustain phase, $\nu_1 = 0.10$. . .	246
IV-5	Dimensionless performance, sustain phase, $\nu_1 = 0.15$. . .	247
IV-6	Dimensionless performance, sustain phase, $\nu_1 = 0.20$. . .	248

Figure		Page
IV-7	Dimensionless performance, sustain phase, $\nu_1 = 0.25$. . .	249
IV-8	Dimensionless performance, sustain phase, $\nu_1 = 0.30$. . .	250
IV-9	Dimensionless performance, sustain phase, $\nu_1 = 0.35$. . .	251
IV-10	Dimensionless performance, sustain phase, $\nu_1 = 0.40$. . .	252
IV-11	Dimensionless performance, sustain phase, $\nu_1 = 0.45$. . .	253
IV-12	Dimensionless performance, sustain phase, $\nu_1 = 0.50$. . .	254
IV-13	Use of boost-phase parametric charts	255
IV-14	Use of sustain-phase parametric charts	255
IV-15	Illustration of iteration scheme	256
IV-16	Envelope requirements	257
IV-17	Envelope of M-100 landing rocket (flight weight)	258
IV-18	Typical thrust-time trace	259
IV-19	Schematic of propulsion system (one-third-scale Gemini spacecraft)	260
IV-20	Thrust stand used to calibrate cold-gas propulsion system	261
IV-21	Cold-gas system thrust-chamber pressure, calibration curve	262
IV-22	Overall view of model propulsion system	263
IV-23	Actuation time relationships for cold-gas propulsion system	264
IV-24	Dome pressure-manifold pressure, calibration curve	265

Figure		Page
IV-25	Dome-pressure ratio as a function of valve open time	266
IV-26	Overall model test set up	267
IV-27	Typical cold-gas thrust-time variation (drop 25)	268
IV-28	Typical vertical acceleration, velocity, distance, and time relationships	269
V-1	Full-scale landing-dynamics test using pendulum altitude sensor	281
V-2	Cable stowage spool for pendulum altitude sensor	282
V-3	Pendulum sensor head	823
V-4	Disassembled pendulum sensor head	284
V-5	Deployment test of the deHavilland altitude sensor	285
V-6	Container for the deHavilland altitude sensor	286
V-7	DeHavilland altitude-sensor head	287
V-8	DeHavilland sensor deployed from spacecraft in flight	288
VI-1	Turn-control motors, assembled	298
VI-2	Turn-line, load-stroke characteristics	299
VI-3	Installation, left and right turn motors	300
VI-4	Turn-motor assembly	301
VII-1	UH-1 helicopter showing camera attachments	318
VII-2	H-13 helicopter with fiber-optics bundle and glide-angle indicator	319
VII-3	Examples of reticles investigated	320

Figure	Page
VII-4 One-third-scale Gemini spacecraft Para-Sail vehicle with television camera	321
VII-5 One-third-scale Gemini spacecraft vehicle attached to a UH-1 helicopter	322
VII-6 Internal view of Para-Sail control van showing television monitor, control box, and video-tape recorder	323
VII-7 Typical ground track (Ellington Air Force Base, Texas)	324
VII-8 Typical ground track (Ellington Air Force Base, Texas)	325
VII-9 Typical ground track (Ellington Air Force Base, Texas)	326
VII-10 Typical ground track (Ellington Air Force Base, Texas)	327
VII-11 Map of Fort Hood Military Reservation, Texas, showing landing points	328
VII-12 Typical ground track (Fort Hood Military Reservation, Texas)	329
VII-13 Typical ground track (Fort Hood Military Reservation, Texas)	330
VII-14 Typical ground track (Fort Hood Military Reservation, Texas)	331
VII-15 Typical ground track (Fort Hood Military Reservation, Texas)	332
VIII-1 Gemini spacecraft boilerplate station and nomenclature diagram (200 series)	353
VIII-2 Top view of Gemini spacecraft boilerplate (200 series)	354
VIII-3 Bottom view of Gemini spacecraft boilerplate (200 series)	355

Figure		Page
VIII-4	Rendezvous and recovery canister. (See fig. VIII-5 for detail.)	356
VIII-5	Overcenter link	357
VIII-6	Rendezvous and recovery release mechanism. (See fig. VIII-5 for detail.)	358
VIII-7	Reserve parachute installation	359
VIII-8	Main landing-gear installation	360
VIII-9	Nose landing-gear installation. (See fig. VIII-18 for detail.)	361
VIII-10	Instrumentation mounting surfaces	362
VIII-11	DeHavilland altitude-sensor installation	363
VIII-12	Altitude sensors	
	(a) Zero altitude sensor	364
	(b) Interim altitude sensor	364
VIII-13	Gemini spacecraft boilerplate equipment	
	(a) Separation switch	365
	(b) Retractable attach point	365
VIII-14	Retrorocket alinement hardware	366
VIII-15	Retrorocket alinement fixture	367
VIII-16	Blast deflector and installation	
	(a) Blast-deflector installation	368
	(b) Blast-deflector construction	368
VIII-17	Load cell	369
VIII-18	Parachute disconnect hardware	370
VIII-19	Parachute attach and disconnect hardware	371

Figure	Page	
VIII-20	Tension-measurement device installation	
	(a) Tension-measurement device	372
	(b) Tension-measurement installation	372
VIII-21	Modified turn-control motor	373
VIII-22	Cable cutter	374
VIII-23	Camera locations	375
VIII-24	Whip antenna installation and location	376
VIII-25	Airborne launch cradle	377
VIII-26	Gear-stroke sensor	378
VIII-27	Skid-protector installation	379
IX-1	Nose-gear pressurization system	403
IX-2	Main-gear deployment actuators	404
IX-3	Gear deployment test	405
IX-4	Landing-gear extension and stroke dimensions	406
IX-5	Landing-gear static-load test	407
IX-6	Landing-gear crane drop	408
IX-7	Riser and turn-line stowage	409
IX-8	Attitude change, test setup	410
IX-9	Rear V-bridle disconnect and cable cutters	411
IX-10	Door-seal integrity test	412
IX-11	Flotation attitude, forward section flooded	413
IX-12	Flotation attitude, two-thirds of forward section sealed	414

Figure		Page
IX-13	Test vehicle after a water landing	415
IX-14	Test vehicle and launch cradle	416
IX-15	Test vehicle and launch cradle, in aircraft	417
IX-16	Blast deflector I	418
IX-17	Blast deflector II	419
IX-18	Blast deflector II, test in progress	420
XI-1	Instrumentation pallet, BP-205	439
XI-2	Complete instrumentation system, BP-205	440
XI-3	Instrument systems, BP-206	441
XI-4	Instrumentation for first deployment test	442
XI-5	Instrumentation and electronic systems for airdrop 1. (F, force; P, pressures; and A, acceleration.)	443
XI-6	Measurement locations, top view. (F, force.)	444
XI-7	Instrumentation breadboard, airdrops 2 to 5	445
XI-8	Instrumentation and electronic systems for airdrops 2 to 5. (A, acceleration; D, positions or strokes; E, events; F, force; 0, attitude; P, pressures; R, rates; T, temperature; and V, voltage.)	446
XI-9	Telemetry system	447
XI-10	Instrumentation and electronic systems	448
XI-11	Battery pallet	449
XI-12	Instruments at the center of gravity	450
XI-13	Instrumentation breadboard, airdrops 6 to 12	451

Figure	Page
XI-14 Instrumentation and electronic systems for airdrops 6 to 12. (A, acceleration; D, positions or strokes; E, events; F, force; O, attitude; P, pressures; R, rates; T, temperature; and V, voltage.)	452
XI-15 Measurement locations, inside view. (A, acceleration; D, positions or strokes; E, events; O, attitude; P, pressures; R, rates; T, temperature; and V, voltage.)	453
XI-16 Control-line transducer	454
XI-17 Measurement locations, bottom view. (P, pressures.) . . .	455
XI-18 Data flow chart	456
XII-1 Block diagram of event-sequencing system for drop 1 of the Gemini spacecraft land landing system	468
XII-2 Block diagram of event-sequencing system for drops 2, 3, 8, and 9 of the Gemini spacecraft land landing system	469
XII-3 Block diagram of event-sequencing system for drops 4 and 5 of the Gemini spacecraft land landing system	470
XII-4 Block diagram of event-sequencing system for drops 6 and 7 of the Gemini spacecraft land landing system	471
XII-5 Block diagram of event-sequencing system for drops 10, 11, and 12 of the Gemini spacecraft land landing system . . .	472
XII-6 Block diagram of event-sequencing system of crane-drop tests of impact-attenuation system	473
XII-7 Sequence board for drops 10, 11, and 12	474

GEMINI LAND LANDING SYSTEM

DEVELOPMENT PROGRAM

VOLUME II - SUPPORTING INVESTIGATIONS

By Leland C. Norman, Jerry E. McCullough,
and Jerry C. Coffey
Manned Spacecraft Center

SUMMARY

Volume I of the Gemini Land Landing System Development Program contains a description of the landing system and full-scale testing, with a detailed presentation and discussion of the test results. Volume II contains the analyses, scaled-model tests, and component development efforts which defined and developed the system to the point where the full-scale testing reported in Volume I began.

INTRODUCTION

Volume I of the Gemini Land Landing System Development Program contains a detailed description of the full-scale system, the full-scale test program, and a presentation and discussion of the test results. Prior to testing full scale, many supporting investigations, scaled-model tests, and component development programs were conducted to define and develop the system. This volume contains detailed presentations of the more important of these efforts. Several authors were involved in preparing the individual sections of this volume and are credited on the appropriate section title pages.

Two scaled-model system test programs were conducted to obtain preliminary flight and landing characteristics of the integrated system. These two investigations were conducted before final development of the components began and provided an accurate prediction of the full-scale system characteristics which were obtained 1 to 2 years later.

Once the design requirement studies and integration analyses were completed, development specifications were prepared for each component. Separate, concurrent development programs were then conducted. These efforts are presented in detail in separate sections.

Forty-one hardware items were designed, manufactured, and developed especially for this program. In many cases, the requirements were unique. The physical and functional characteristics of the more important of these are discussed in a separate section, and the verification tests of all major hardware are discussed. Presentations of the data acquisition system and the sequencing system complete this volume.

SECTION I - ONE-THIRD-SCALE FLIGHT DYNAMICS TESTS

By Robert B. West and David L. Brown

ONE-THIRD-SCALE FLIGHT DYNAMICS TESTS

By Robert B. West and David L. Brown
Manned Spacecraft Center

SUMMARY

Prior to full-scale system tests, a drop-test program was conducted with a one-third-scaled model of the Gemini spacecraft vehicle and a 24-foot d_0 Para-Sail parachute to obtain preliminary flight and control dynamics information. Twenty-five drops were made from altitudes of 900 to 4000 feet.

The results of these tests indicated that the vehicle/canopy combination was dynamically stable, with oscillations of less than 5° about all three axes in straight and level flight, and that a change of vehicle attitude from heat-shield down reentry to horizontal flying posed no stability problems. Turn rates of up to 70 deg/sec were obtained with 24 inches of control-line travel with a corresponding force of 25 pounds. It was possible to maneuver the system to a preselected area and land with the correct wind alinement.

INTRODUCTION

The analytical studies conducted to determine the combined gliding parachute and Gemini spacecraft system performance were based upon the assumption that the flight dynamics encountered would not impose unacceptable behavior characteristics. To insure the validity of this assumption and to provide preliminary flight information, the scaled-model test program was conducted.

The specific objectives of this program were: to obtain data relating to the dynamic behavior of the vehicle when suspended from a controllable gliding parachute; to determine the load distribution on the Para-Sail, the control-line forces, and response of the system with the controls actuated from within the suspended vehicle; and to evaluate the visual requirements of the pilot which would be necessary to utilize fully the capabilities of the system in executing a controlled glide to the desired touchdown point.

To insure that the results could be related to the planned full-scale tests, the model vehicle duplicated the proposed flight configuration as closely as possible. In addition, the performance of the 24-foot parachute was representative of that expected of the larger version.

TEST PROGRAM

The test program, consisting of 25 drop tests, was conducted as a three-phase effort. The first 10 tests, which constituted phase I, were conducted primarily to establish test procedures, to verify rigging techniques, and to determine the general dynamic characteristics of the system. This was accomplished prior to the installation of a major portion of the instrumentation. Phase II consisted of tests 11 to 17, which were fully instrumented drops to record riser loads, control response, vehicle dynamics, and various accelerations. Tests 18 to 25, which constituted phase III, were fully instrumented tests using a canopy modified to produce considerably higher turn rates. In addition, a much improved control system and a different type of landing gear were incorporated.

The test procedure for all 25 drops was virtually the same. The drop aircraft was an Army UH-19 helicopter. The test vehicle was suspended on a carriage (fig. I-1) which extended out of the cargo door of the helicopter. An Air Force MA-4A electrically actuated bomb release was used to support the model. The drop altitudes ranged from 900 to 4000 feet, with a majority of the drops made from an altitude of 3500 feet. The vehicle was released at indicated airspeeds between 15 and 30 knots. Table I-I presents a complete list of drop conditions. The drop area for all tests was Ellington Air Force Base, Texas.

The parachute was packed in a bag which was attached to the side of the vehicle by four lengths of 30-pound breakcord. At release, a 6-foot static line separated the parachute bag from the vehicle and deployed the parachute. A 42-inch hemispherical guide-surface pilot parachute was permanently attached to the crown of the Para-Sail as an inflation aid. After parachute opening, a series of preplanned turns were executed, then the vehicle was maneuvered to the target area and faced into the wind prior to landing.

SYSTEM DESCRIPTION

Parachute

Two versions of the 24-foot d_0 Para-Sail were employed during the test program. The configuration used in phases I and II featured slotted front panels and single turn vents located on each side of the canopy (fig. I-2). In phase III, a modified version of the canopy was used which featured solid front panels with a semielliptical cutout in the leading edge and four turn vents arranged circumferentially on each side of the canopy (fig. I-3).

Directional control of the system was achieved by opening and closing the vents by means of a miniature cable and winch system located within the test vehicle. When a turn line was shortened, the airflow through these vents was changed from aft when they were fully open, to forward when they were inverted. The reaction to this redirected airflow, and the undisturbed flow on the opposite turn vents, produced the turning moment. Simultaneously inverting the turn vents on both sides of the canopy produced an effective means of modulating the lift-to-drag ratio (L/D).

Rigging

Throughout the program an effort was made to determine the rigging configuration which could be used on a Gemini-type vehicle. As a result, several changes were made during the program to duplicate more closely the actual Gemini spacecraft attach points. During phase I the rear risers were attached at separate points on each side of the vehicle directly adjacent to the heat-shield area. The front risers were attached on each side of the vehicle at the confluence of the tapered portion and the cylindrical nose section. The centerline was attached 11 inches from the rear edge on the top surface of the vehicle (fig. I-4). During phase II the two front-riser attach points were moved to the forward edge of the cylindrical section, and the centerline was moved aft to a point 8.5 inches from the rear edge of the vehicle.

The final configuration tested in phase III of the program used the actual Gemini spacecraft hard-point locations consisting of one front and two rear attach points. The centerline connected to a bridle attached to the front and rear of the vehicle on the upper surface (figs. I-3 and I-5). In four of the phase III tests, the Gemini spacecraft deployment sequence involving attitude change was simulated by initially passing all the risers and the apex line through a single nose attach point. Therefore, the vehicle was placed in an approximate 80° nose-high pitch attitude during inflation of the canopy. After 12 seconds, a reefing cutter severed a line which held the risers at this point

allowing them to assume their normal position, which in turn resulted in a horizontal vehicle attitude.

On each of the configurations tested, the suspension-line distribution consisted of seven lines to the two rear risers and five lines to the two front risers. It was determined during the program that shifting the location of the centerline attach point along the longitudinal axis of the vehicle provided an effective means of adjusting the vehicle attitude while maintaining the proper load distribution between the main risers.

Vehicle

The test vehicle was a 1/3-dimensionally scaled model of the Gemini spacecraft. The major dimensions are shown in figure I-6. The model was constructed of 1-inch welded steel tubing covered with a 1/8-inch fiber-glass shell. Lead ballast was used to vary the model weight and to obtain the proper center-of-gravity location. The drop weight of the vehicle during the initial tests was as much as 402 pounds in an effort to attain a rate of descent of 25 ft/sec. It was determined, however, that the effective drag coefficient of the parachute was much higher than was anticipated; and, that in order to obtain this descent velocity, the vehicle weight would have to be approximately 580 pounds. Since the canopy was designed for personnel use and was not constructed to support this amount of weight, the weight of the vehicle was reduced and the remainder of the tests was conducted at a reduced rate of descent. During the phase II test series the vehicle weighed 365 pounds, and for phase III the weight of the vehicle was reduced to 345 pounds.

Impact Attenuation

Two means of impact-energy attenuation were employed during the drop-test program. Neither method was designed to represent the planned full-scale attenuation system which featured landing rockets. Both methods were employed solely to protect the vehicle, the instrumentation, and the cameras. During phases I and II, impact attenuation was achieved through three stroking struts which used aluminum honeycomb for energy absorption. One strut was located on the nose, and the other two were placed, one on either side, at the rear of the vehicle (fig. I-7). This method proved quite adequate for absorbing vertical accelerations; but it was ineffective for landings with horizontal velocity on unprepared surfaces, since the vehicle resisted slideout and provided for no stroke in the horizontal direction.

A yielding-metal-type landing gear (fig. I-8) was designed for phase III. This tricycle gear absorbed most of the kinetic energy in the vertical

direction and part of the kinetic energy in the horizontal direction by permanently deforming a fully annealed, 1/4-inch yellow brass rod. The remaining energy in the horizontal direction was dissipated by vehicle slideout. This gear improved the landing stability of the vehicle over a greater range of landing conditions.

Control System

Two separate control systems were used during the model test program, both of which were actuated by radio-command control from a ground station. During phase I and II testing, the control system consisted of two takeup pulleys on a common shaft, driven by a single reversible motor. The pulleys, which provided 12 inches of travel to each turn line, were free on the shaft and designed to be driven in opposite directions. When the motor was in the neutral position, both turn lines were fully extended. When the motor was engaged in a particular direction, one of the pulleys was engaged and wound in the turn line until it was stopped by a limit switch. When the turn command was released, the motor reversed and unwound the pulley until it was stopped by the neutral-position limit switch. This procedure was reversed to obtain turn in the opposite direction. Approximately 3 seconds were required for maximum travel. Although this system provided satisfactory turn control, the rates were limited by the amount of available travel, and the system was incapable of simultaneous operation of both turn lines to provide L/D modulation.

During phase II testing, a control system was used which employed independent motors and reels capable of producing 24 inches of travel for each turn line. These units either could operate individually to produce turn or simultaneously to provide a means of modulating glide. There were no means for providing proportional control. This system either provided full turn upon command or no turn when the command was released. Trim was accomplished by individually adjusting the turn lines prior to flight. Approximately 7 seconds were required to reach the maximum turn-line travel.

Data Acquisition

Three onboard 16-mm TKB-3A Fotodata motion-picture cameras were used throughout the test program. One camera was oriented vertically upward to study the parachute inflation characteristics as affected by variations in rigging techniques, and to investigate the canopy action resulting from control inputs. A second camera, oriented vertically downward, was used to obtain turn-rate and dynamic-response data and to study the vehicle yaw stability characteristics. The third camera initially was mounted in a horizontal

plane looking directly out of the nose of the vehicle, but was later rotated to an angle 30° below the longitudinal axis of the vehicle. This camera was used to study the vehicle pitch and roll characteristics with reference to the horizon and to provide the data concerning the pilot visual-reference requirements. Figure I-9 shows the placements and the fields of view of the cameras. During the two latter phases of the program, a 12-channel Consolidated Electronic Corporation (CEC) light-beam oscillograph was incorporated in the vehicle to record turn commands, individual riser loads, turn-line loads, rate of descent, and various accelerations; and to provide an accurate means for correlation of the motion-picture films.

Strain-gage-type load links were inserted in the individual risers and turn lines to obtain the riser and turn-line loads. For several tests, two $\pm 0.5g$ linear accelerometers were coupled to record accelerations about the yaw axis. Due to their limited sensitivity, these units did not provide sufficient quantitative information to warrant their continued usage.

During phase III testing, a pressure transducer was installed in the vehicle to record the rate of descent. The unit was sealed on one side at a constant pressure and, on the opposite side, was vented to the atmosphere. The variation in differential pressure provided a good indication of the overall rate of descent; however, due to a lack of sensitivity of the system, the effect of turns on the rate of descent could not be measured accurately.

The signal from an Adtrol Timing Light Generator, Model TLG-111, set at 100 cps, was recorded by the oscillograph and on the motion-picture films for correlation of events. Two additional channels of the oscillograph were used to record the direction and duration of the turn commands which were received from the ground station. The general arrangement of the test model and the onboard instrumentation is shown in figures I-10 and I-11.

RESULTS

Parachute Performance

Deployment and opening. - The average time from release to line stretch was 1.4 seconds. Due to the static-line deployment method, the snatch forces were quite low, never exceeding 200 pounds. Filling time averaged 2.9 seconds during phases I and II and 1.6 seconds during phase III. The opening load averaged 3.0g for the test series, with a maximum of 4.5g and a minimum of 2.4g.

In general, the opening loads produced by the solid front canopy were slightly higher than those obtained with the slotted front configuration. This was attributed to the more positive and faster opening characteristics of the solid front canopy.

Although there were no failures, the slotted front version of the parachute exhibited a strong tendency for the front of the canopy to tuck in during inflation. This tendency was reduced considerably by the inclusion of the solid front canopy. During several of the tests, it was noted that as the parachute bag separated from the vehicle, the bag would rotate several turns before the parachute was extracted. This caused the parachute to inflate with a corresponding number of turns in the risers and suspension lines. However, the turns appeared to have no noticeable adverse effect on the opening characteristics of the parachute; and within a few seconds following full inflation the vehicle would rotate, correcting the situation.

Turn rates. - The original version of the parachute (fig. I-2), which featured the single turn vents and slotted front panels, produced turn rates up to 12 deg/sec with angular accelerations of 4 deg/sec/sec. The modified version (fig. I-3), which employed a series of turn vents and solid front panels, achieved turn rates up to 70 deg/sec with angular accelerations of 12 deg/sec/sec. It should be noted that these acceleration values are somewhat dependent upon the rates at which the turn lines are reeled in. As discussed previously, the turn condition was terminated by releasing the turn-line takeup pulley and allowing the line to payout. With the higher performance turn system the payout occurred in 0.2 second, resulting a termination of the turn within a 5° change in heading. The load in the control lines in the no-turn position was approximately 5 pounds, ranged upward to 15 pounds at the maximum turn rate available with the initial parachute configuration, and up to 25 pounds with the final parachute configuration.

Stability. - Oscillations during steady-state descent were most prevalent about the pitch axis and were determined to be approximately $\pm 5^\circ$ in magnitude. Oscillations about the roll and yaw axes were essentially nonexistent. During turns, the canopy banked in the direction of turn and pitched down, both phenomena being a function of turn rate. After the bank and pitch attitude was achieved in a constant-rate turn, the parachute was extremely stable. When the turn was released, the canopy quickly returned to its flying attitude.

During vehicle attitude change from heat-shield down to horizontal, the front of the canopy initially pitched upward due to a sudden loss of load in the front riser, then returned to the normal flying attitude. Very little canopy distortion was evident as the vehicle repositioned in the horizontal attitude.

The vehicle fell in the original attitude until the load was assumed by the rear risers, then the vehicle rotated forward, passing through horizontal attitude to a pitch attitude of approximately -15° , then returned to the horizontal position, oscillating slightly due to the elastic suspension system. An average of four oscillations was required to reach a completely damped-out condition.

Load Distribution and Center of Pressure

The riser-load distribution for the two parachute configurations was determined as follows:

	Slotted front	Solid front
Front riser, percent of total load	21	29
Centerline, percent of total load	28	23
Rear risers, percent of total load	51	48

In order to determine the location of the center of pressure on a projected area of the inflated parachute in a horizontal plane, it was assumed that the load carried by each riser was uniformly distributed over the elliptical quarter-section corresponding to each riser attachment. Then the loads of each riser were considered to act through the centroid of the corresponding elliptical quarter-section, and the centerline load was assumed to act through the apex. By summing the moments about the apex and using the riser loads determined from the drop tests, the center of pressure was determined to be approximately 11 inches aft of the apex for the solid front configuration. This calculated value is in close accordance with results obtained in the wind tunnel at the University of Minnesota, which indicated the center of pressure was 10.4 inches aft of the apex.

Lift-to-drag ratio. - During the test program, the system was observed visually to maintain some forward velocity when oriented directly into winds measured at 10 to 11 knots. From observations of this type, it can be stated that the 1.1 L/D value measured in the wind tunnel is valid for the solid front configuration. Although no quantitative data exist on the amount of L/D modulation achieved by simultaneous activation of the turn lines, the same kind of wind-attenuation evidence exists which indicates a definite modulation of glide.

Rate of descent. - An average rate of descent was determined by dividing the release altitude by the total downtime. For phase II, the average rate of descent was 17.8 ft/sec. The difference can be attributed to the lower vehicle

weight during phase III and the slightly increased drag produced by the solid front canopy. During turns, the system was observed to descend at a higher rate.

Vehicle dynamics. - In steady-state descent, the vehicle was extremely stable about all three axes, with no oscillations exceeding $\pm 5^\circ$.

During the 70-deg/sec turn rate experienced during phase III, the vehicle rolled up to 30° as the system banked into the turn. This banking action was caused by the forward inertia of the vehicle which tended to keep it traveling in a straight line while the canopy turned away from it. This change in roll attitude was accompanied by a change in pitch attitude from 0 to approximately -15° caused by the strong canopy pitch-down characteristic previously described. Upon release of the turn command, the vehicle attitude returned to nominal in less than 1 second with no apparent oscillation.

During the earlier phases, when the turn rates were approximately 12 deg/sec, this same phenomenon was evident, but to a lesser degree. In these tests, the vehicle exhibited a maximum roll attitude of 15° and a pitch down of 5° .

The separated riser-suspension system employed during the tests formed a strong couple between the parachute and the vehicle such that rotation of the canopy induced the same rotation in the vehicle. When the turn command was released, the vehicle also ceased to turn with no discernible tendency to continue turning or to oscillate.

It was also determined that adjusting the length of the individual bridle legs caused a corresponding change in the suspension attitude of the vehicle as the tendency of the parachute to remain at its maximum glide angle overrode the ability of the vehicle weight to disturb it.

Control capability. - During the test program, the system was controlled by radio command from a point on the ground located near the desired landing point. Wind drift was determined by visual observation of the system in flight.

Since the majority of the tests conducted during this program were initiated from an altitude of 3500 feet, there were approximately 3 minutes per drop during which turn control of the system could be exercised. During the initial tests conducted in phases I and II of the program, the limited control response required that the last 30 seconds of the drop be devoted primarily to achieving proper orientation of the system for landing into the wind. In every case, the test vehicle was aligned within 5° of the indicated surface wind

at touchdown. The average distance from the actual point of impact to the target was approximately 150 feet.

During the final phase of the program when the higher performance turn-control system was incorporated, it was possible to initiate the final turn at a much lower altitude. Consequently, additional time for accurate maneuvering was available. Again, no difficulty was encountered in alining within 5° of the indicated surface wind at touchdown. With the additional maneuvering time available, the average miss distance to the target was decreased to 50 feet. Throughout the program, there was no difficulty in placing the system on the desired heading. A factor which contributed strongly to this capability was the rapid rate at which the turn condition was terminated.

In striving to land the system on a desired target, the technique which proved to be most satisfactory was to release the vehicle from the helicopter at a point considerably upwind. This was followed immediately by whatever turns were required to satisfy the requirements of the particular test, noting continuously the effect of wind drift. The desired touchdown point could then be reached with a relatively high degree of accuracy by setting up a glide with the wind to a point nearly over the target area. The location of this point varied, depending upon the wind conditions. By executing a turn into the wind, the forward glide of the parachute compensated for horizontal wind drift and resulted in a nearly vertical descent at touchdown.

Preliminary visual requirements. - Analysis of the onboard film coverage of the tests indicated that a flight crew would require a view centered slightly forward of vertical to allow continuous observation of all of the possible landing points.

TABLE I-I. - DROP CONDITIONS

Drop	Drop altitude, ft	Drop velocity, knots	Surface winds, knots	Opening shock, g	Descent rate, avg, ft/sec
1	900	25	20		21.4
2	900	25	10		29.2
3	1740	25	12		23.5
4	1700	35	15		25
5	2100	30	25		21.5
6	3500	30	20		23.4
7	3700	30	20		22.9
8	3800	30	20		--
9	3800	30	15		--
10	3800	30	25	--	25
11	3750	25	8	2.44	21.9
12	3620	23	8	2.64	18.8
13	4000	12	10	3.07	15.0
14	2500	23	--	2.96	22.7
15	2500	25	5	3.47	20.0
16	3000	--	--	--	21.4
17	3000	22	5	--	19.6
18	2750	20	5	--	41.7
19	3360	--	--	4.55	18.25
20	3600	25	10	--	17.1
21	3500	25	8	--	17.9
22	3500	25	10	3.4	18.2
23	3500	30	--	--	17.7
24	3500		--	2.74	17.3
25	3500		10	2.56	18.4

NASA-S-66-9821 OCT 24

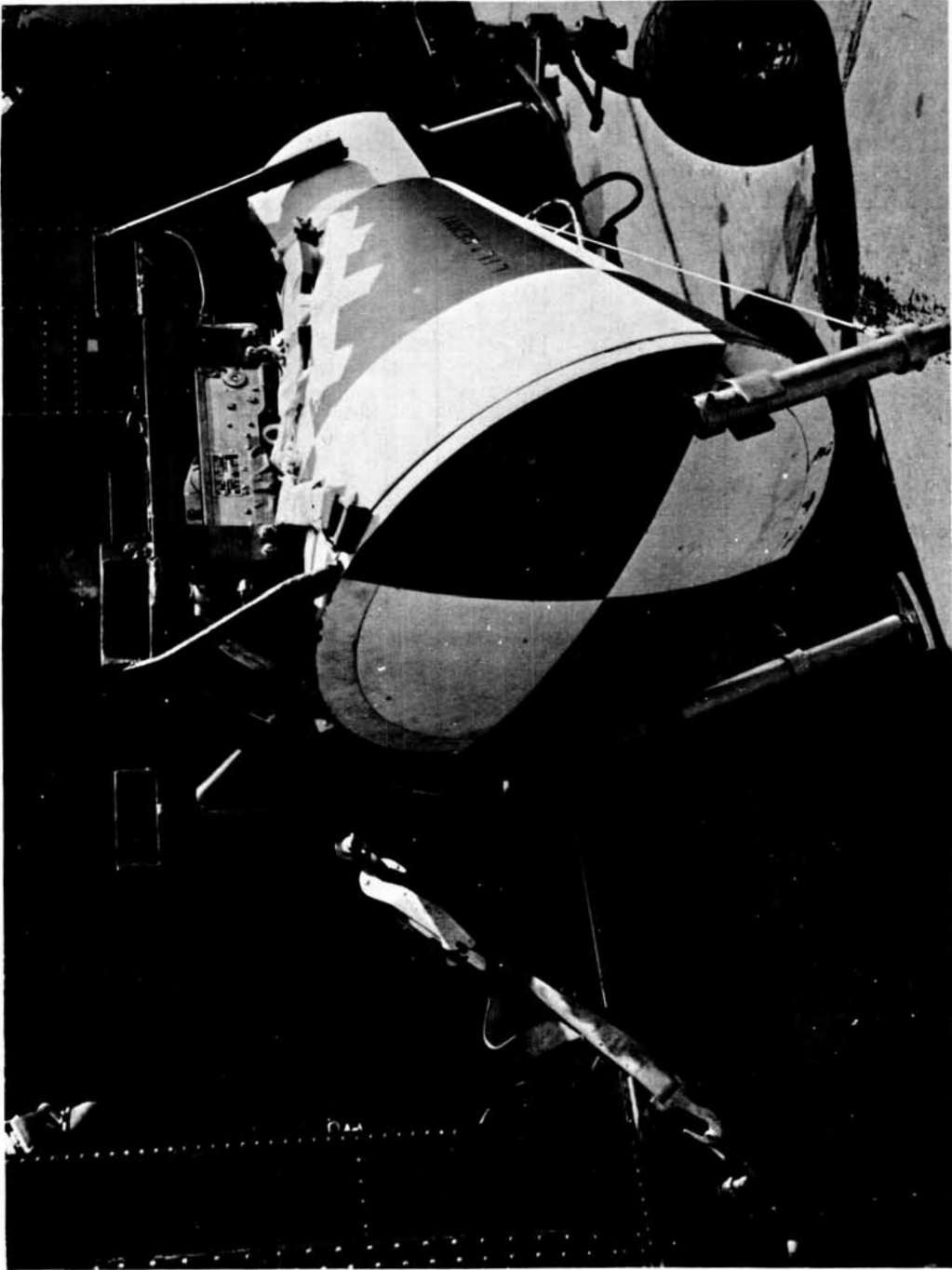


Figure I-1.- Vehicle drop method.

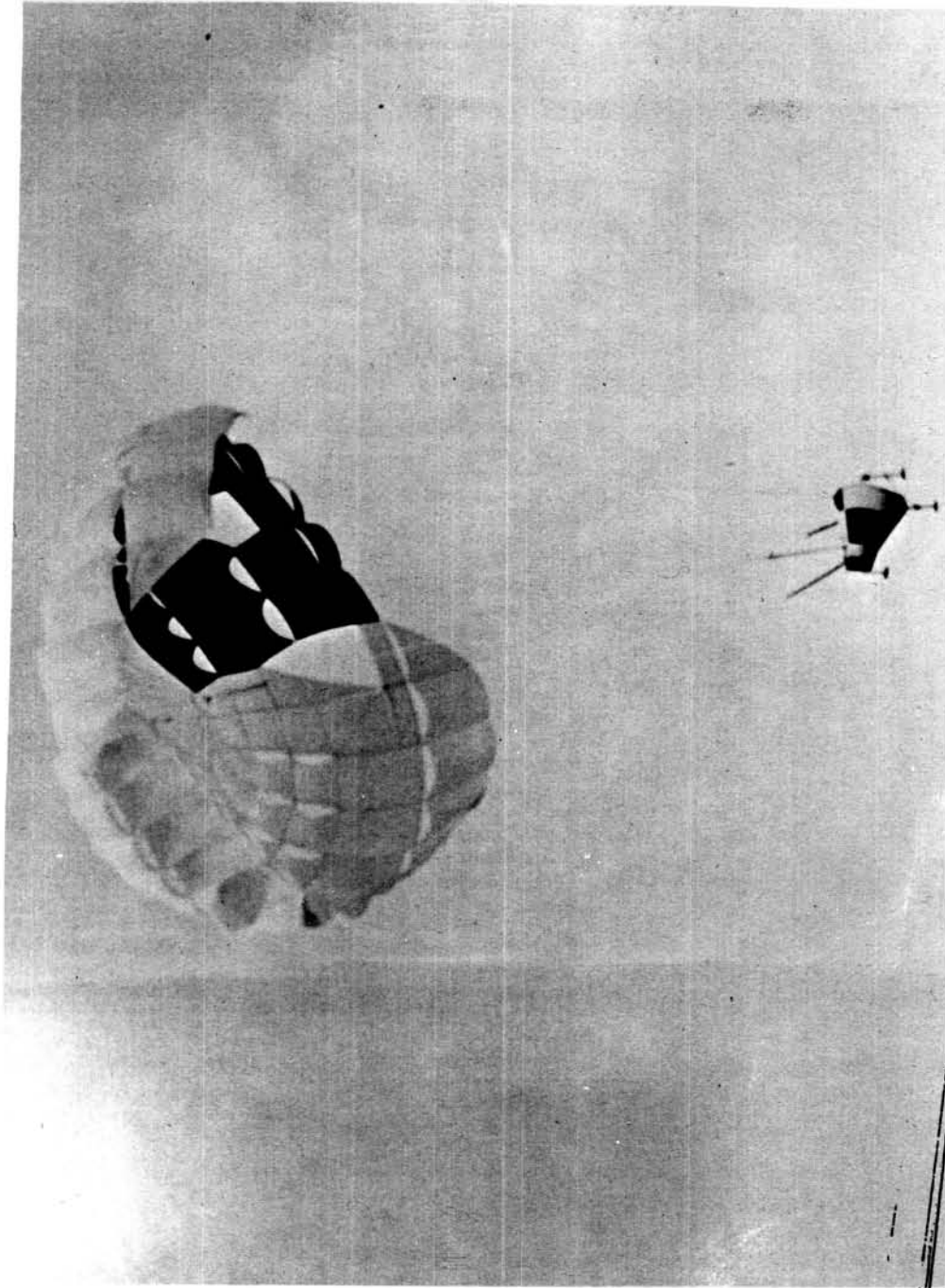


Figure I-2.- Slotted front configuration.

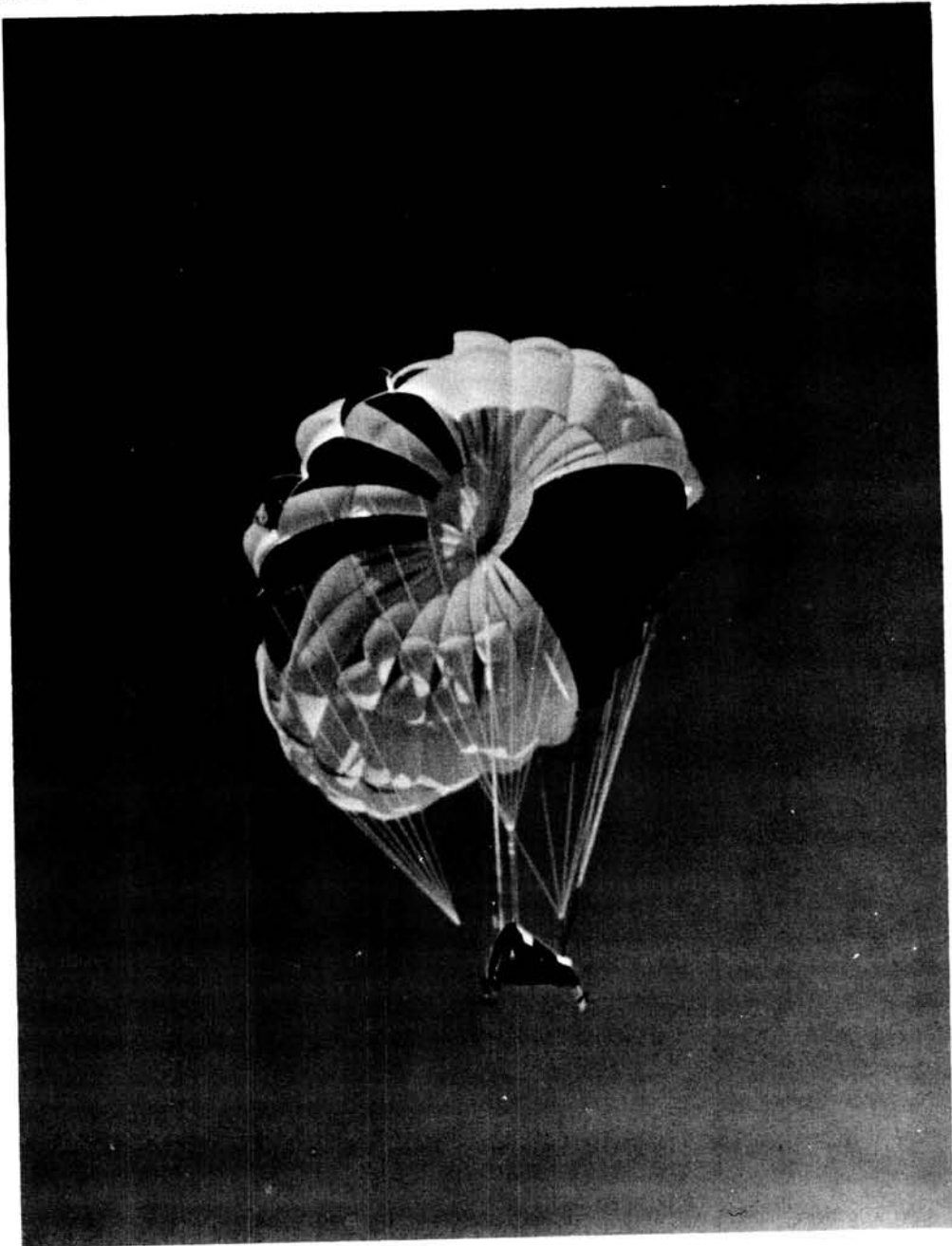


Figure I-3.- Solid front configuration.

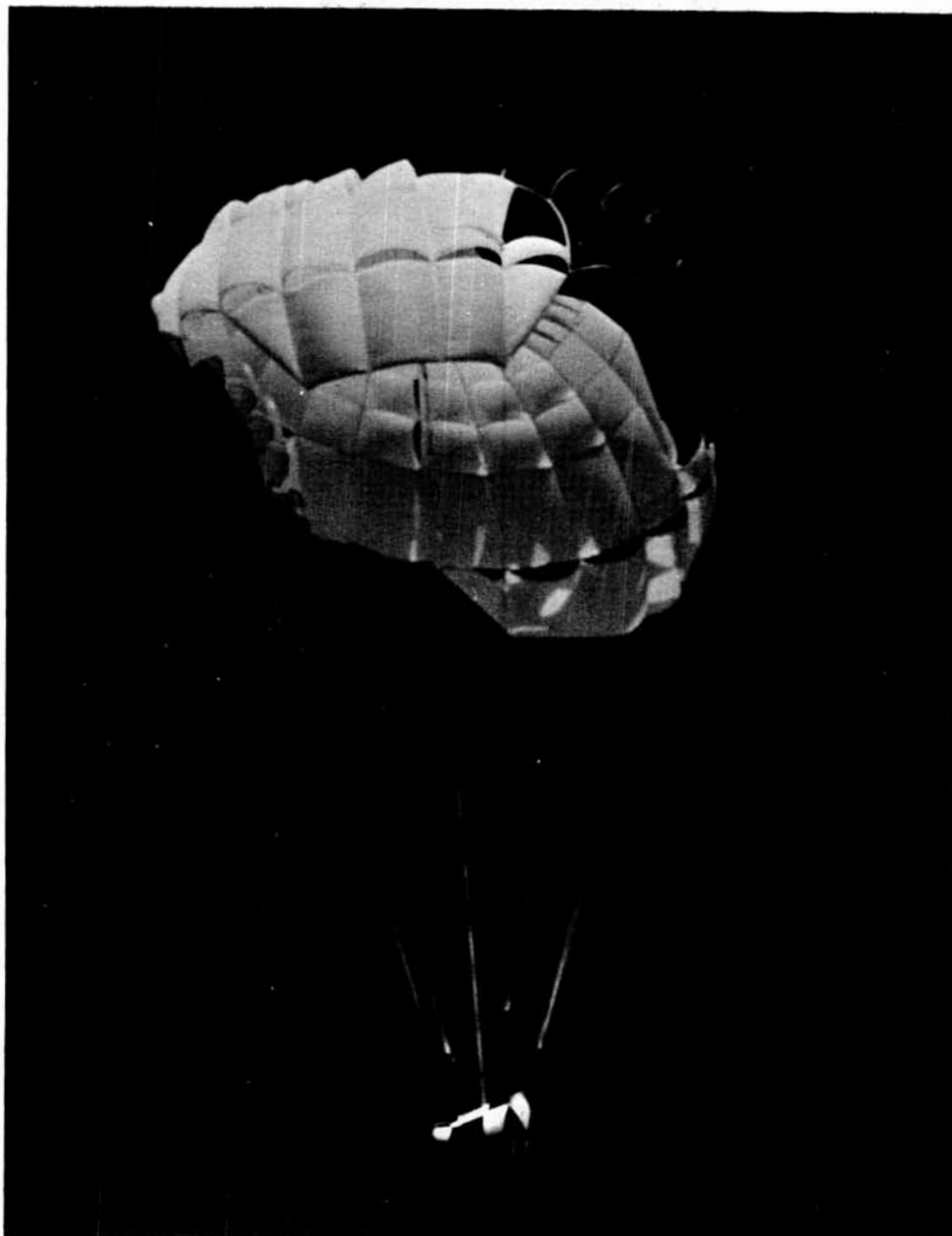


Figure I-4.- Bridle system for phases I and II.

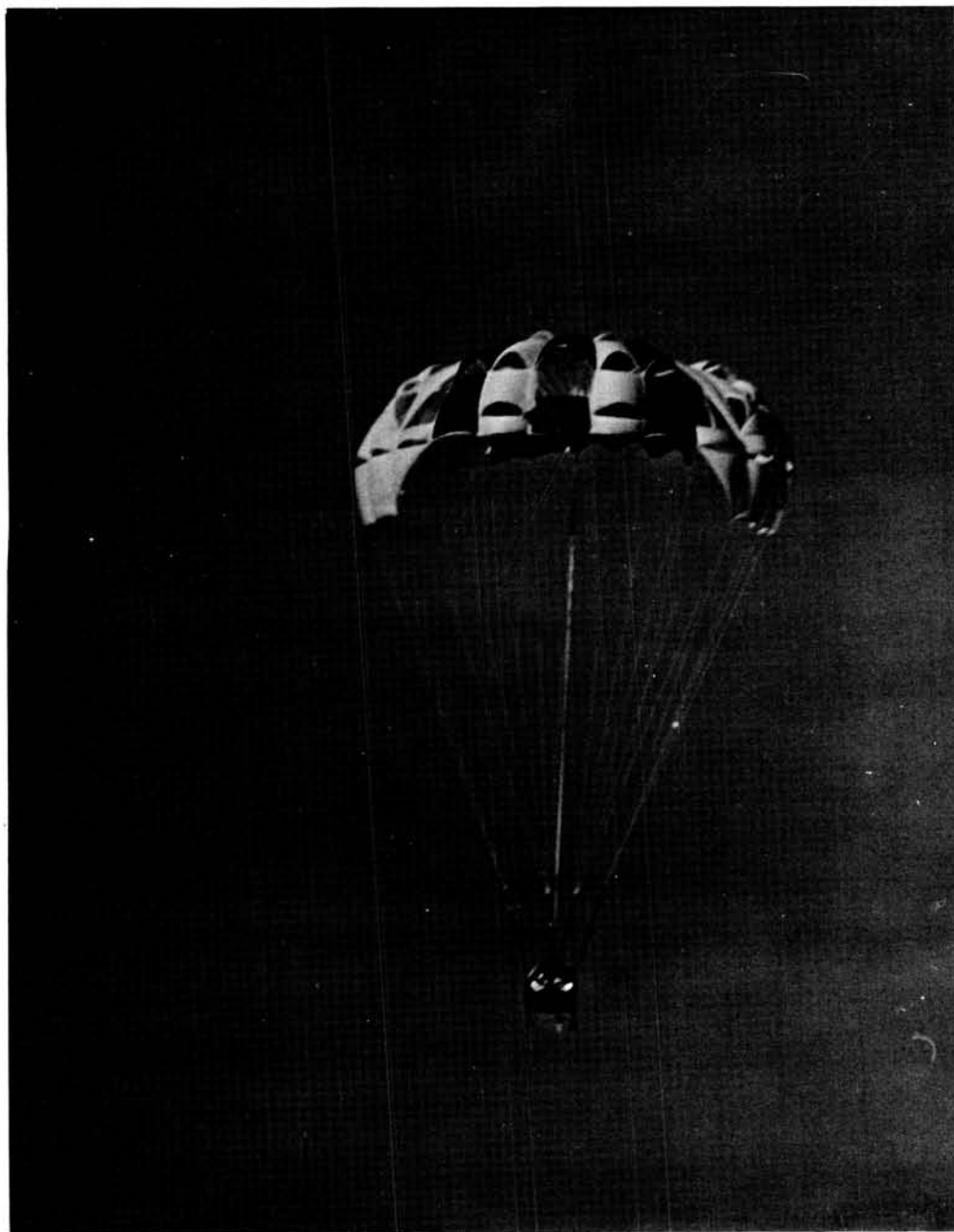


Figure I-5.- Final bridle configuration.

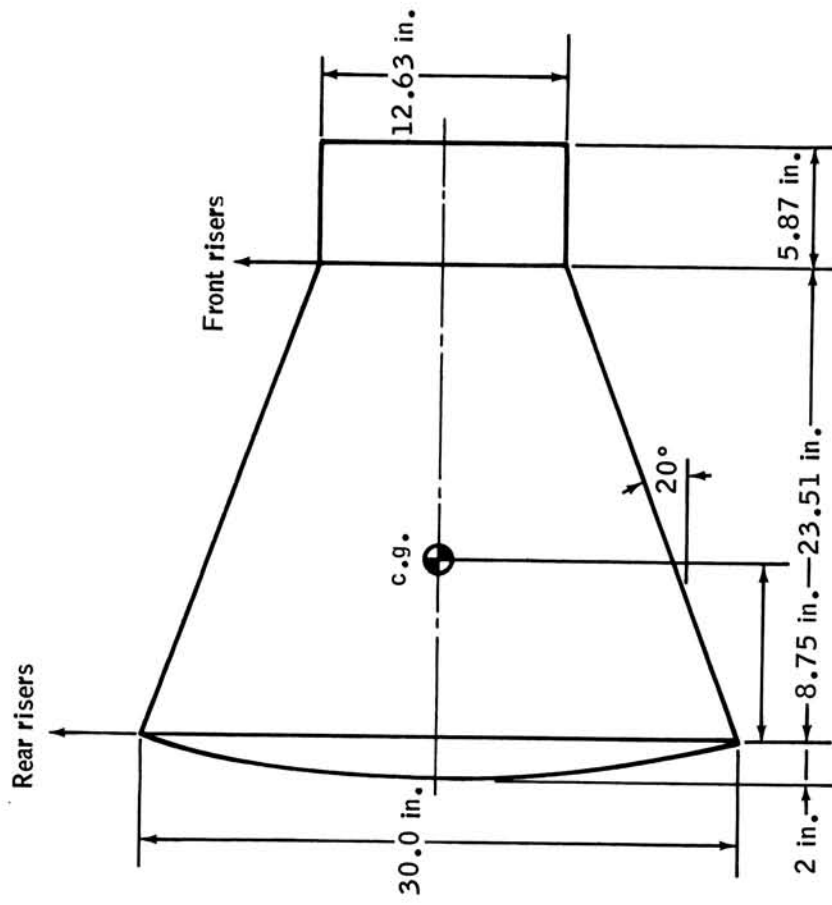


Figure I-6.- Major dimensions of test vehicle.

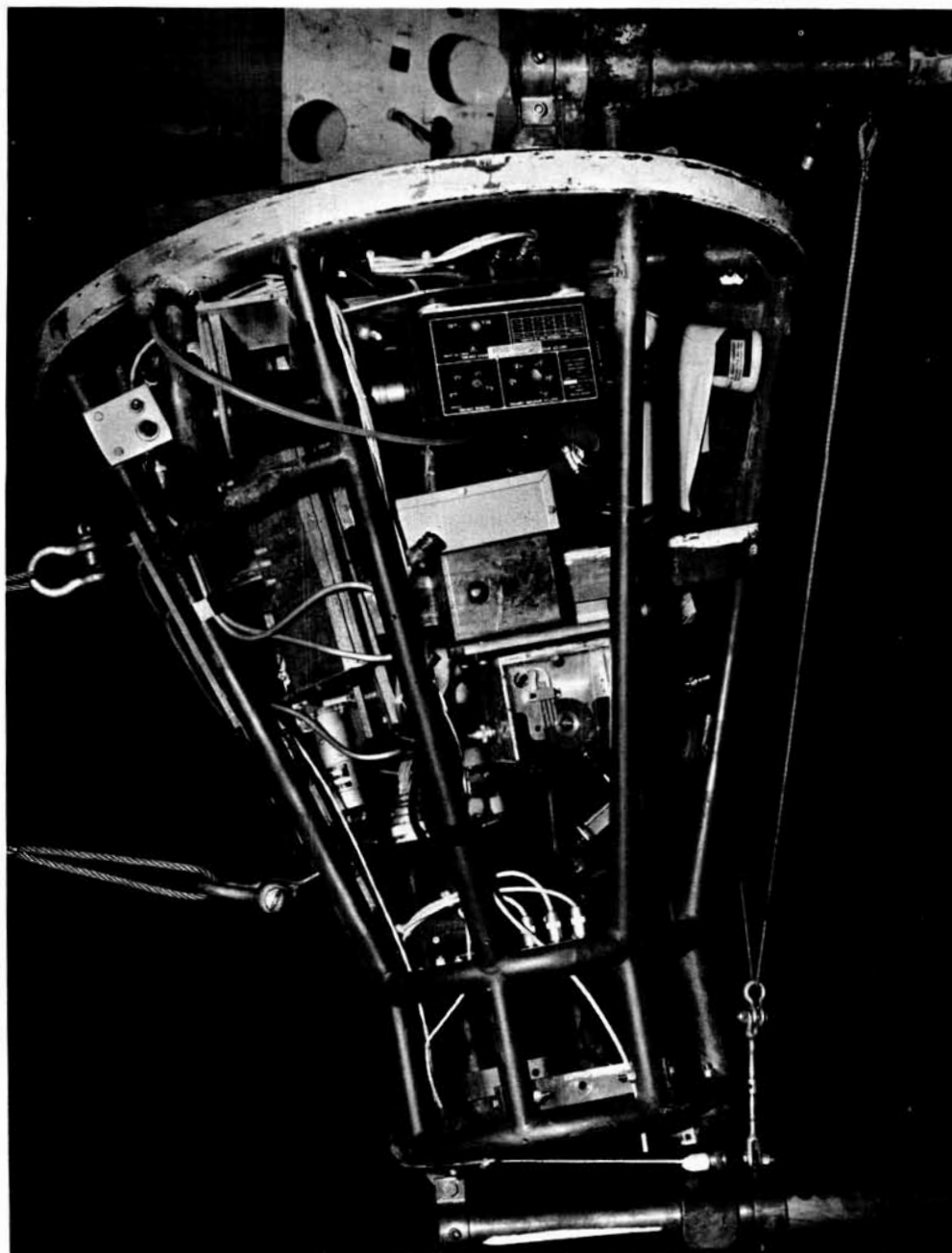


Figure I-7.- Landing gear with honeycomb struts.

NASA-S-66-9828 OCT 24

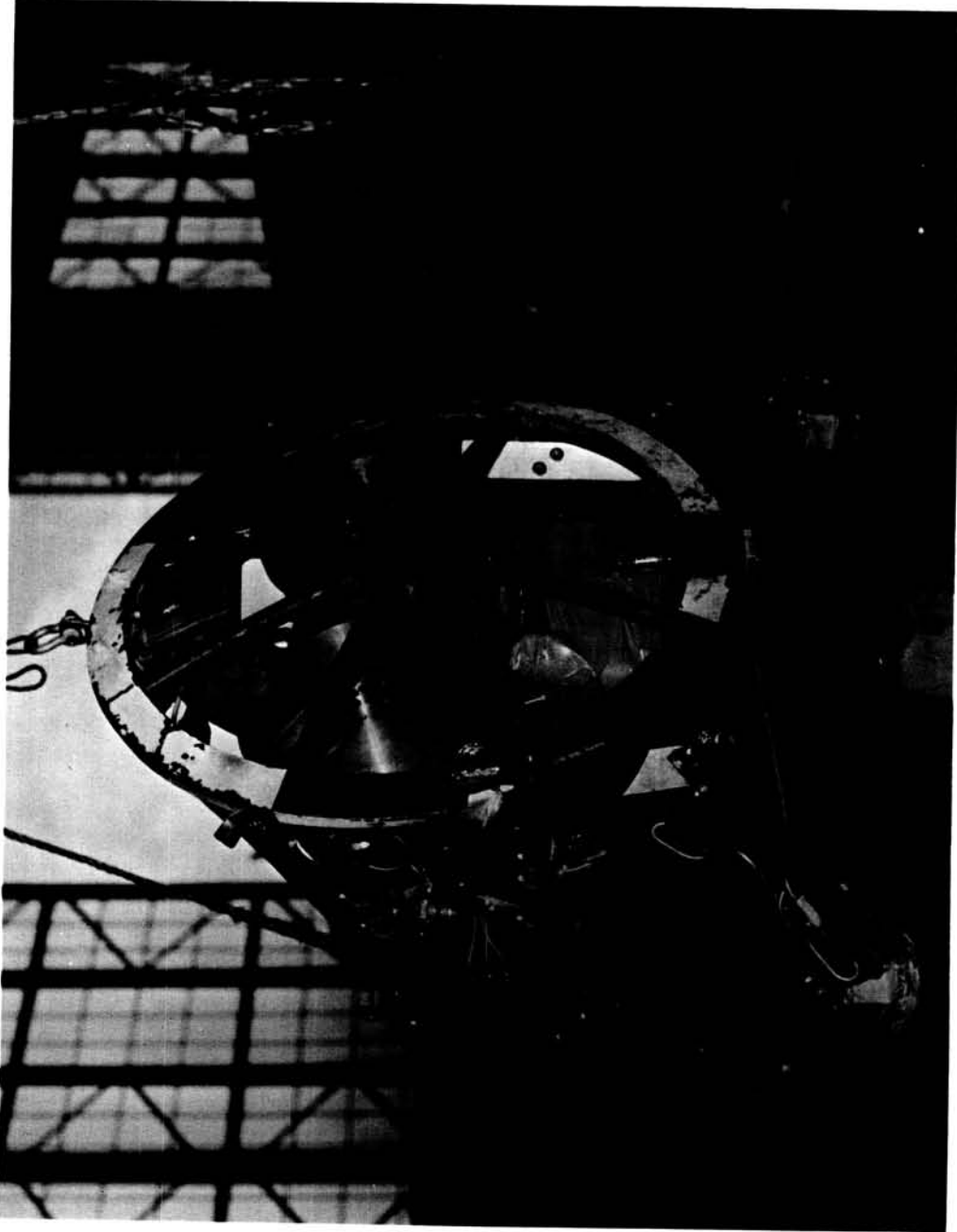


Figure I-8.- Yielding metal landing gear.

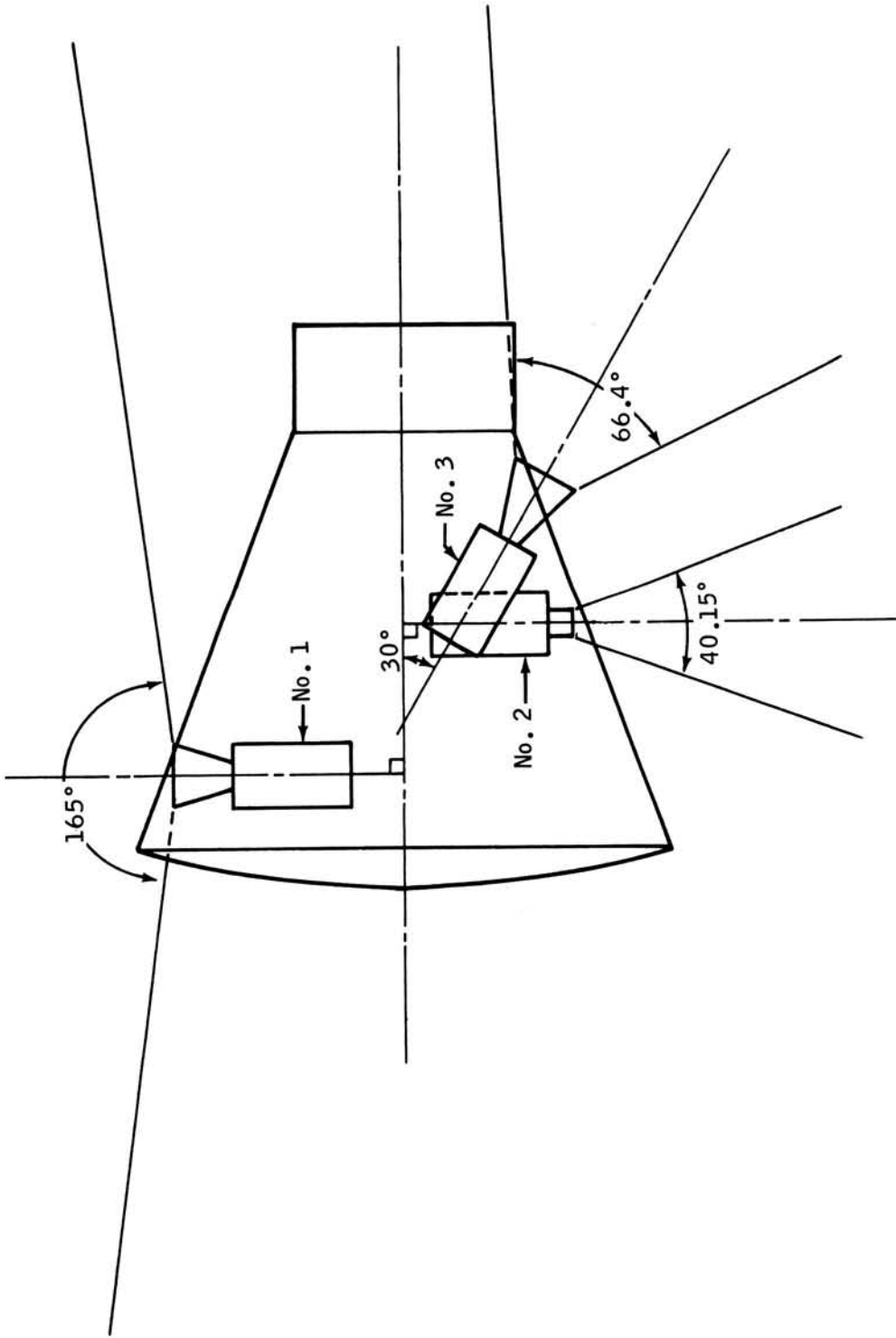


Figure I-9.- Positions and fields of view for onboard cameras

NASA-S-66-9830 OCT 24

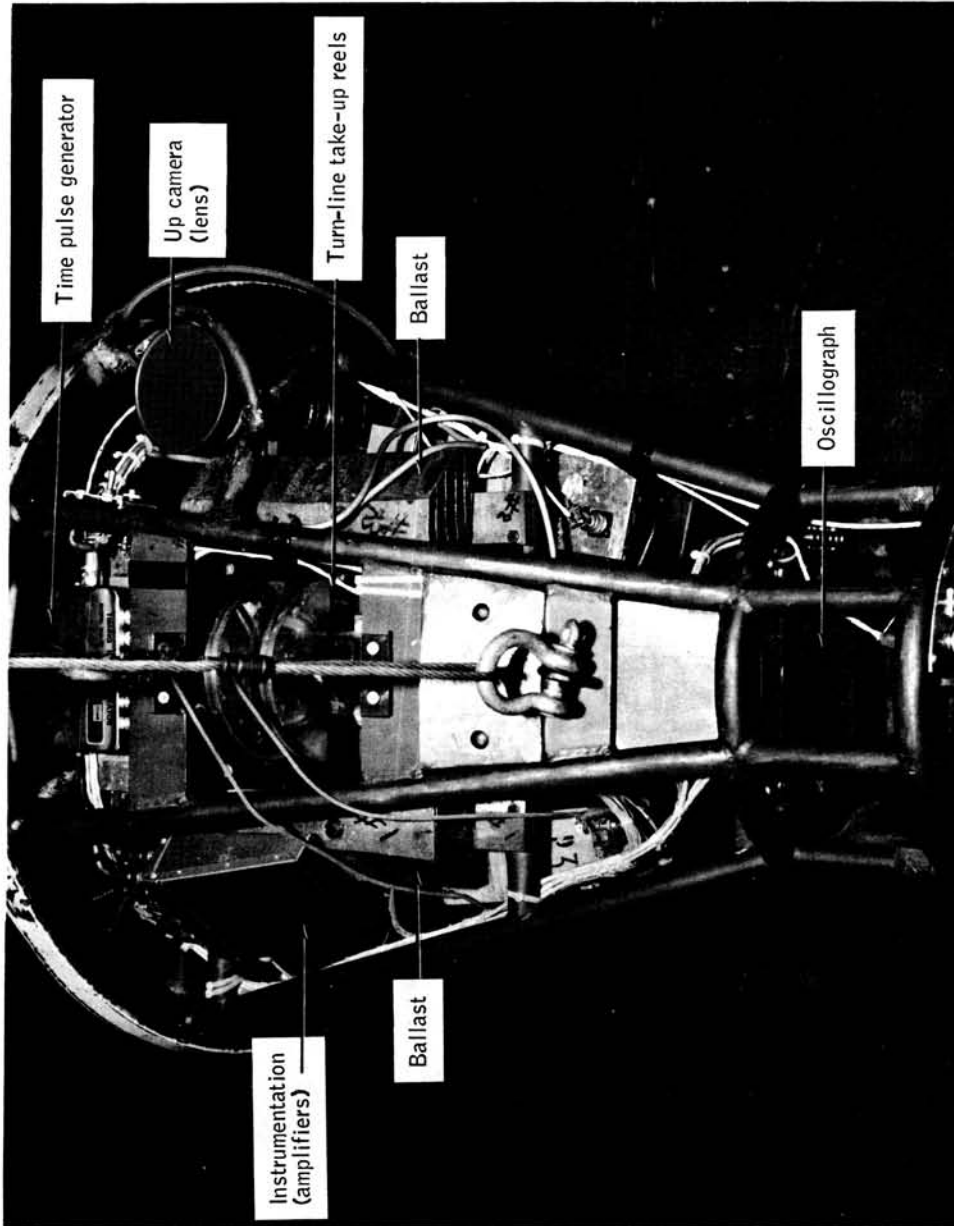


Figure I-10.- General arrangement (shell removed), top view.

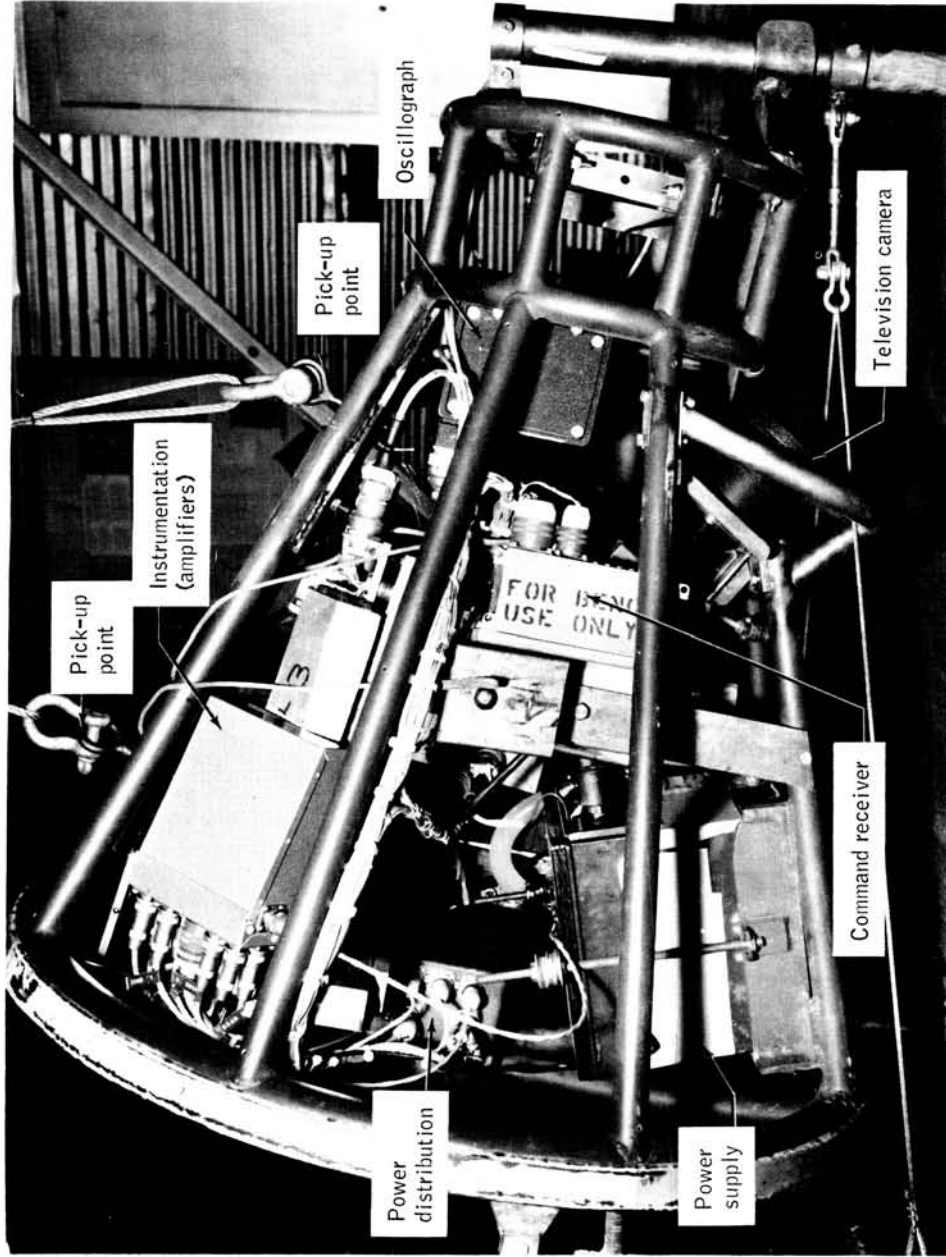


Figure I-11.- General arrangement (shell removed), side view.

SECTION II - LANDING DYNAMICS TEST OF A ONE-THIRD-SCALE

PARA-SAIL/LANDING-ROCKET MODEL

By Jerry E. McCullough and Harold E. Benson

LANDING DYNAMICS TEST OF A ONE-THIRD-SCALE
PARA-SAIL/LANDING-ROCKET MODEL

By Jerry E. McCullough and Harold E. Benson
Manned Spacecraft Center

SUMMARY

Investigations of a 1/3-scale Gemini spacecraft model were conducted to determine the feasibility of using the Para-Sail/landing-rocket combination as the landing system on the present Gemini spacecraft. The model used in these tests was a dynamically scaled Gemini spacecraft configuration which incorporated a cold-gas retrorocket-deceleration system and a tricycle-skid landing gear.

A high-pressure nitrogen system was used in the model to simulate the thrust-time curve of a solid-propellant retrorocket, and the full-size landing gear was simulated in the model with respect to the force-stroke curve of the energy absorber.

Instrumentation of the model included accelerometers on the three axes of the vehicle to record impact accelerations, and the necessary pressure transducers to determine the performance of the cold-gas landing-rocket systems. In addition, high-speed motion pictures were made of each test.

This test series consisted of impacting the model at simulated horizontal velocities of 0, 15, 30, and 50 ft/sec with a simulated vertical impact velocity of 10 ft/sec. Also, one test was conducted with the vehicle landing backward at a horizontal velocity of 10 ft/sec. The pitch attitude of the model was varied $\pm 5^\circ$ from the nominal design of -13° , and the model was yawed in increments of 5° to a maximum of 15° . The recorded impact accelerations were low, with a maximum of 7.4g occurring parallel to the Y-axis of the model. The other two accelerometers recorded 3.65g or less.

The results of these landing tests indicate that the Gemini spacecraft is capable of making safe aircraft-type landings on flat, smooth, compact terrain through the complete range of test conditions, with the exception of backward horizontal velocities. In the presence of irregular or soft landing

surfaces where skid penetration or tripping occurs, the vehicle will tumble. Also, landing-gear failure is probable in the event of extreme yaw or negative (backward) velocity conditions.

INTRODUCTION

An initial requirement of the Gemini spacecraft was that it could be recovered with no damage and, therefore, could be reused. This design goal led to the adoption of the paraglider-tricycle-skid landing system. In the event that any of the stages in the development of the paraglider system could not be fulfilled in the designated time, a possible alternate recovery system (the Para-Sail/landing-rocket system) was conceived.

The design philosophy for incorporating the Para-Sail/landing-rocket system into the existing Gemini spacecraft was based upon a minimum modification. With this approach, the present tricycle-skid landing gear was retained. The location of the rocket motors in the vehicle also was based upon a minimum modification with due consideration to the attitude of the vehicle during descent.

GEMINI SPACECRAFT LANDING-ROCKET SYSTEM DESIGN

In order to retain the present Gemini spacecraft tricycle-skid landing gear in the Para-Sail/landing-rocket system, the attitude of the vehicle at touchdown must remain essentially the same as that for the paraglider system. With this constraint and with the design philosophy of minimum modification, the landing rockets were located in the lower equipment bay of the Gemini spacecraft vehicle. Photographs of the full-scale and 1/3-scale landing system are shown in figures II-1(a) and II-1(b).

The performance requirements for the solid-propellant rocket motor were chosen to decrease the terminal vertical velocity of the vehicle descending on the Para-Sail parachute from 30 ft/sec to 10 ft/sec or less. The length and depth of the center equipment bay dictate the use of a pair of rocket motors to achieve the desired performance. The motors are rolled 6.5° about their longitudinal axis to enable the thrust vector for each motor to pass through the nominal center of gravity of the vehicle. The location also dictates that the thrust vector must be perpendicular to the longitudinal centerline of the motor. The boost thrust level is 5950 pounds of thrust for 0.4 second; and the sustain thrust level is 1220 pounds of thrust for 1.1 seconds for

each motor. One or more probes were used to sense the correct altitude for igniting the rocket motors.

MODEL DESCRIPTION

The Para-Sail has lower horizontal and higher vertical velocities than the paraglider; therefore, it became necessary to study and test the present Gemini spacecraft configuration to determine how these changes in velocities affect the landing impact and the stability of the vehicle. Prior to the full-scale testing of the system, a 1/3-scaled-model test program was initiated. The specific objectives of this program were to determine the accelerations during impact and the stability characteristics of the Gemini spacecraft vehicle under simulated Para-Sail/landing-rocket landing conditions. This program was designed to establish critical test parameters, to furnish design data, to verify design, and to obtain test data prior to full-scale testing.

The model used for these tests was a 1/3-dynamically scaled model of the Gemini spacecraft. The overall dimensions of the model, center of gravity, location, weight, and moments of inertia (fig. II-2) are proportional to the Gemini spacecraft. The Gemini spacecraft landing gear and shock absorbers were simulated both in size and in action. Tapered aluminum honeycomb was used in the shock attenuators as the energy absorbing material. An effort was made to duplicate the load-stroke curve of the Gemini spacecraft shock attenuators, as furnished by McDonnell Aircraft Corporation. Photographs of the landing gear and shock attenuators are included in figures II-3 to II-5.

The model parameters were obtained by scaling the prototype parameters. The only prototype parameter that could not easily be simulated was the drag force of the parachute. Therefore, the effect of the parachute drag force was compensated for in the model program by adjusting the initial velocity of the model using the equations of motion. However, it should be emphasized that all other parameters were scaled, including the model velocity, at the instant of boost-phase thrust. The following scale factors are applicable (γ was chosen as 1/3 for the model used in the test).

Quantity	Full size	Scale factor	Model
Length	l	y	yl
Time	t	\sqrt{y}	$\sqrt{y} t$
Mass	m	y^3	$y^3 m$
Weight	w	y^3	$y^3 w$
Acceleration	a	1	a
Coefficient of friction	u	1	u
Force	F	y^3	$y^3 F$
Velocity	V	\sqrt{y}	$\sqrt{y} V$
Moment of inertia	I	y^5	$y^5 I$

The propulsion system used to simulate the solid-propellant rocket motors used compressed nitrogen gas, expanding from a common manifold through two nozzles. The propulsion system is shown schematically in figure II-6. The nitrogen gas was stored in the tanks at a pressure of 3000 lb/in.² and was regulated to the pressure required at the nozzle to produce the desired thrust. The two nozzles, mounted in the manifold, were run on a thrust stand to obtain the net resultant thrust as a function of nozzle pressure. The boost thrust level was governed by the regulator-dome pressure setting. In order to obtain the sustain thrust, it was necessary to reduce the regulator-dome pressure. This was achieved by opening the regulator-dome solenoid valve momentarily to allow the regulator-dome pressure to decrease to the desired value.

In order to control the system, an electronic sequencer was used to control the time intervals within a few milliseconds. The sequencer contained two reaction-control (R-C) network channels, one for opening and closing the regulator-dome solenoid valve and one for opening and closing the nozzle solenoid valve. A start signal was fed into the sequencer by the closing of a microswitch when the model physically separated from the drop tower. This start signal initiated both R-C networks; however, both the bandwidth and the total time for each R-C network were controlled individually by variable potentiometers.

Section IV presents a complete discussion of the full-scale solid-propellant motors and the cold-gas system used in these tests.

TEST PROCEDURE

The model was suspended from the compound pendulum carriage (figs. II-7 and II-8), and its vertical height above the impact surface was adjusted for a calculated vertical velocity. The pendulum was then pulled back by a cable winch to a specific height so that its horizontal component of velocity was also established. The supporting carriage fixture was adjustable so that the model could be given any desired initial pitch and yaw attitude. Because of the nature of the pendulum, the model retained the initial pitch throughout the swing. On release, the pendulum swung through its arc and actuated a microswitch which, in turn, caused the attachment mechanism to release the model at the neutral position on the swing arc of the pendulum. The model then impacted and slid to a stop on the prepared surfaces without any restraint except its trailing umbilical cable. To neutralize this effect as much as possible, the cable was given an initial horizontal velocity equal to that of the model.

Onboard instrumentation consisted of four strain-gage accelerometers and two pressure transducers. Three accelerometers were installed at the center of gravity of the model along the three principal axes to record impact accelerations. Another accelerometer was mounted at the nozzle manifold to record accelerations along the thrust axis. The pressure transducers were installed so that nozzle pressures were recorded. Output signals from these instruments were transmitted through an umbilical cable to the amplifying and recording equipment. Model impact attitudes, in addition to motions and displacements which occurred after contact, were recorded by three stationary 16-mm high-speed motion-picture cameras.

MODEL TEST

Tests were made in two general phases. In the first, without using the propulsion system, the model was tested on two types of possible landing terrains, and it was assumed that the rockets had performed under nominal conditions. In the second phase, the propulsion system was employed as an active system.

Phase I - Impact Test on Sod and Soil

In phase I, two types of landing surfaces were used to determine to what degree terrain conditions affect stability. The propulsion system was not used, and the model was dropped at velocities that would be present if the rocket motors had fired under normal conditions.

Tests 1 to 11 were conducted on a landing surface prepared by covering hard-packed soil with a mat of St. Augustine grass composed of 1-foot-square sections of sod placed close together. Loose sand was packed between the squares to fix the sod rigidly into a reasonably uniform surface and to prevent the squares from slipping. For tests 12 to 24, the sod and sand were removed, and the hard-packed soil was leveled to remove surface irregularities.

Before testing on each of the two surfaces, data were recorded to permit calculation of coefficients of friction, penetration, and relative roughness. To obtain the coefficient of friction, the force required to slide the model over the surface was recorded with a load cell. The coefficient of friction was calculated to be 0.49 for the sod surface and 0.50 for the hard-packed soil.

The relative hardness of the impact surfaces was obtained by dropping a sphere, which measured 5 inches in diameter and weighed 16 pounds, from a height of 7 feet and measuring the depth of impact impression. The sphere was dropped 10 times on each of the two surfaces, and the average depressions were calculated. The average depressions were calculated to be 1.44 and 1.38 inches for the sod and the compacted soil, respectively.

The average difference in ground elevation was 0.3 inch every 2 feet, with a maximum difference of 1.0 inch every 2 feet for the sod surface. No attempt was made to calculate the relative roughness of the soil because the surface was leveled by dragging prior to testing. Throughout these tests the pitch and vertical velocity were maintained at a constant -13° (nose-down attitude) and 10 ft/sec (full-scale), respectively. The yaw angle was varied in increments of 5° from 0° to 15° for each of the horizontal velocities of 0, 15, 30, and 50 ft/sec. In addition, one test was made landing the model backward (180° yaw) at 10-ft/sec (full-scale) horizontal velocity.

Phase II - Impact Tests on Canvas with Active Propulsion System

The conditions for phase II, tests 25 to 50, were basically the same as those for the first phase, except that an active propulsion system was used. The purpose of phase II was to verify the results of phase I in which impact conditions were based upon assumptions that the propulsion system had

performed properly. Also, phase II investigated the effect of the sustainer thrust of the rockets on the vehicular stability during slideout.

The landing surface for phase II was the smooth, compacted soil covered with canvas tarpaulin to reduce the amount of dust activated by the rocket blast. The coefficient of friction for the canvas was calculated to be 0.42 by using data taken prior to rocket thrust. A second coefficient of friction obtained during employment of the propulsion system was calculated to be 0.55. It is believed that this higher coefficient can be attributed to removal of dust from the surface of the canvas by the rocket exhaust.

The model was dropped from a predetermined height and allowed to free fall until the desired initial velocity was achieved. The sequencer was preset so that approximately 90 percent of boost thrust was achieved at the instant the desired initial velocity was reached. The sequencer was also preset to allow the proper time interval for the boost- and sustain-thrust phases.

The nominal initial vertical velocity for this test series was constant at 14.3 ft/sec. The only variations in initial vertical velocity were due to variations in the sequencer and the response of the propulsion system. The horizontal velocities tested were 0, 15, 22.5, and 30 ft/sec. The pitch angle was varied from a nominal of -13° (nose down) to $\pm 5^\circ$. The yaw angle was varied in increments of 5° from 0° to 15° . Tests were performed with combinations of these horizontal velocities and pitch and yaw angles.

One additional test was conducted with the canvas tarpaulin removed. In this test the model was pulled along with an average horizontal velocity of 3.5 ft/sec, with the retrorockets thrusting at the sustainer level. The purpose of this test was to obtain preliminary data on the amount of soil erosion resulting from the rocket thrust.

RESULTS AND DISCUSSION

The general landing behavior was similar for all conditions. It was characterized by an approach at the predetermined attitude, impact on the main gear, angular rotation to nose-gear impact, and by the slideout. On initial contact of the main skids, a portion of the sink-speed energy was absorbed by the rear shock attenuators, and the vehicle was given a rotational impulse in pitch. The resulting vertical and rotational energy in the system was then absorbed during primary nose-gear impact, by both the nose- and the main-gear energy absorbers. Energy due to the horizontal landing velocity was largely dissipated by skid-friction forces during slideout, and by the resistance force of the skids riding over or shearing the impact indentations

in the landing surface. During yawed landings without the propulsion system, the vehicle returned to an approximately unyawed slideout position during the time between the initial impact of the main and nose gears.

Stability on Sod and Soil Surfaces Without Propulsion

In all of the tests on the sod surface where the horizontal velocity and yaw angle did not exceed 30 ft/sec and 0° , respectively, the model appeared to be dynamically stable. However, a horizontal velocity of 30 ft/sec combined with a yaw angle of 5° caused the nose-skid drag force to become large enough so that the model turned over or rolled slowly over in the direction of travel. This tendency recurred at 30-ft/sec horizontal velocity and 10° yaw; therefore, tests were not made at greater yaw angles.

Tumbling also occurred at 50-ft/sec horizontal velocity and 0° yaw. This was a violent end-over-end motion in which the model nose skid dug into the turf, pitched 360° about the Y-axis with the nose skid as a pivot point, and landed upright on the landing gear. In test 11, the yaw angle was set at 180° and the model was given a backward horizontal velocity of 10 ft/sec. In this test, the left rear main landing gear failed at the strut-hinge point, and the drag-brace member buckled. Tests 12 to 24 were conducted on the hard-packed soil surface with horizontal velocities from 15 to 50 ft/sec and yaw angles from 0° to 15° . The vehicle proved quite stable on this surface and remained upright for all test conditions.

Stability on Canvas Surface with Active Propulsion System

In the tests employing the propulsion system, there were three specific problems:

1. The thrust vector was initially misaligned with the center of gravity of the model. The resulting torque was of sufficient magnitude to pitch the vehicle over on the heat shield when the model was not traveling at a horizontal velocity. After the proper thrust-vector alignment was achieved, the vehicle exhibited good pitch stability.

2. The drop-tower carriage imparted a tip-off torque to the model in the pitch plane upon release. The resultant angular pitch rate was in the direction for pitching the nose of the model up. Thus, the horizontal component of the thrust imparted a backward velocity to the model. By the time the rear gear impacted, the pitch attitude had changed sufficiently so that the backward horizontal velocity coupled with the horizontal component of the thrust vector was sufficient to pitch the model over on its heat shield, using

the rear gear as a pivot point. This problem was corrected by moving the attachment bracket on the model so that it was directly above the center of gravity of the model when the vehicle was trimmed for an attitude of -13° .

3. At horizontal velocities of 20 ft/sec the trailing umbilical cable exerted an inertia force which caused the model to change its pitch and yaw attitudes prior to impact. This problem was overcome by accelerating the cable to a horizontal velocity equal to that of the model.

All tests in which one of these three problems occurred were rerun after the conditions were corrected. Two of these problems are inherent only in the model program. However, the alignment of the thrust vector through the center of gravity is a problem in the prototype vehicle. The thrust vector must pass through the center of gravity within close limits ($\pm 1/2$ inch) or the vehicle will acquire undesirable motion, such as pitching over on the heat shield or rolling off the landing gear. However, the alignment of the thrust vector for the prototype vehicle should be less sensitive since it will be used in conjunction with a parachute; and the parachute will be attached so that the parachute line loads will produce a torque to oppose any torque produced by a thrust-vector misalignment.

The function of the propulsion system was to attenuate the vertical component of velocity. The thrust-time relationship was obtained from the nozzle pressure-time trace. The velocity and distance-traveled time relationships were derived by direct integration of Newton's second law. Since the total drop height of the vehicle was known, the method of determining the velocity and distance traveled as a function of time is accurate, providing that the time required to travel the total distance analytically is equal to the total time to impact derived from the accelerometer data. The time required to travel the drop distance, as determined analytically, was compared with the total time to impact, as derived from the accelerometer data. This comparison was made with favorable results on all tests in which the propulsion system was used. The vehicle motion during rocket firing, with combinations of present errors in the pitch angle of $\pm 5^\circ$ and yaw angles up to 15° and with horizontal velocities up to a simulated 30 ft/sec, was satisfactory. The vertical component of velocity at impact ranged from a simulated 5 to 10.5 ft/sec. This range of velocities was due to deviations in the sequencer and in the magnitude of the thrust.

Accelerations

Acceleration histories were recorded by means of accelerometers installed on the three major axes of the vehicle and in the direction of the thrust vector. Table II-I presents a summary of test results, including the vertical

and horizontal velocities at impact, the model slideout distance, the average coefficient of friction for the main landing gear, the peak-impact accelerations along the principal axes of the vehicle, and comments on the stability of the vehicle. The range of impact accelerations for test conditions with and without the propulsion system was very comparable. Although tumbling and end-over-end flipping occurred, the accelerations encountered were relatively low and were well below the level of human endurance.

The maximum accelerations were recorded along the Y-axis. The accelerations ranged from 1.38g to 7.4g, with the higher values recorded during testing on the hard-packed soil surface without the propulsion system. The higher accelerations may be attributed to the fact that the apparent weight of the vehicle during sustainer phase thrusting is only one-half the real weight without the propulsion system, and the sod attenuated more of the impact shock than the other landing surfaces.

No attempt was made to change the roll position from 0° during these tests; and the accelerations measured along the X-axis of the vehicle were negligible. The X-axis accelerations shown in table II-I were insignificant in magnitude and can be attributed to the irregularity of the landing surfaces, which caused the model to bounce and tip.

The accelerations recorded along the Z-axis were, likewise, small, ranging from a minimum of $-0.24g$ to a maximum of $3.65g$, which occurred during vehicle tumbling. These accelerations were proportional to the vehicle pitch attitude, the landing-gear drag, and the bouncing of the model about its pitch axis. It should be noted that in the test in which the gear failed, accelerations were approximately the same as those in the preceding test and the backward horizontal velocity caused the gear failure.

Coefficients of Friction

For purposes of comparison, the average coefficient of friction for each test was calculated by the same method as that used in the McDonnell Aircraft Corporation 1/4-scale model test report, TR 052-042.10. This method arrives at a coefficient of friction by assuming that all horizontal energy is dissipated only by friction forces. It is derived by dividing the square of the horizontal velocity by twice the acceleration of gravity multiplied by the slideout distance. This equation is not entirely valid because some of the horizontal energy is dissipated by the skids either riding over or shearing the impact indentations in the landing surface. Although there is some fallacy in this equation, it is the best method available without more complex instrumentation. The average coefficients of friction are plotted in figure II-9. The band between 0.4 and 0.6 represents values obtained with the load-cell

method. All tagged points are for tests which did not use the cold-gas system. All of these points are higher than the band values, which indicates that the coefficient of restitution and surface irregularities affected these tests to a much greater extent than the tests made with the propulsion system.

Table II-I shows the slideout distances used in calculating the coefficients of friction for each run. On tests 3 and 12, which were made on sod and soil without the propulsion system, slide distances of about 1 foot were recorded. These tests were made with horizontal velocities of 15 ft/sec and vertical velocities of 10 ft/sec. While under the same landing conditions, a slideout distance of 7-1/3 feet was recorded on test 26, with the active propulsion system. However, the coefficients of friction for the three surfaces are comparable. The difference in slideout distance with the propulsion system is attributed to the lower drag force on the skids as a result of the reduction in normal force because of sustainer thrust.

In test 33, where the pitch attitude of the vehicle was increased to -18° nose down, the slideout distance for the model increased to 11 feet. This increase was caused by the horizontal component of the propulsion-system thrust vector attributed to the change in attitude.

Surface Erosion

The results of the test, in which the propulsion system was exhausted directly upon the compacted soil surface, were of interest as qualitative data only. It would not be correct to say that this soil was entirely representative of either a prepared or an unprepared landing surface that could be used for a spacecraft recovery. The exhaust plume of the sustain phase of the cold-gas system blasted a hole in the surface approximately 30 inches in diameter and 8 inches deep when the model had no horizontal velocity (fig. II-10).

The model was then given a horizontal velocity of 3.62 ft/sec, and the propulsion system was again activated at sustainer level. Two ruts approximately 8 inches wide and 2 inches deep were made (fig. II-11). These preliminary data indicate that if a landing-rocket recovery system were used, then soil erosion caused by rocket plume would require additional study.

CONCLUSIONS

Tests were conducted to determine the feasibility of using the Para-Sail/landing-rocket combination as the landing system on the present Gemini spacecraft. A 1/3-scale Gemini spacecraft with a cold-gas deceleration

system and a tricycle-skid landing gear was used. From the results of the tests, the following conclusions may be drawn:

1. By using directional control furnished by the Para-Sail and with the low, vertical rate of descent made possible by the use of landing rockets, accelerations will be small, with magnitudes in the order of 10g or less. During these tests, the maximum accelerations recorded were 7.4g (Y-axis), 3.1g (X-axis), and 1.62g (Z-axis).

2. The present Gemini spacecraft landing gear will operate satisfactorily on a smooth, prepared surface; however, tumbling is imminent on sod or on other irregular surfaces where penetration can occur, causing the landing gear to trip.

3. The present Gemini spacecraft landing gear is not designed for extreme yaw conditions. At 180° yaw (backward) landing, the gear will probably fail; however, accelerations will be low. It is not feasible to redesign the landing gear to compensate for this handicap because of the tendency of the spacecraft to turn over on the heat shield when the landing rockets are thrusting.

4. Proper thruster alinement with the center of gravity of the vehicle is critical. Also, wide variations in the weight and the attitudes of the vehicle cannot be tolerated from the standpoint of impact accelerations and vehicle stability.

5. Tests are required where a parachute is used in conjunction with the landing rockets to determine the drag force and the vehicle stability as a function of time during rocket firing.

6. Under certain landing conditions, soil erosion caused by the propulsion system may create ruts large enough to cause the gears to trip. With the data presently available it appears that erosion could be a problem.

TABLE II-I. - LANDING IMPACT AND STABILITY TEST OF ONE-THIRD-SCALE GEMINI SPACECRAFT MODEL

(a) Test conducted on St. Augustine sod; propulsion system not used

Test	Horizontal velocity, ft/sec		Pitch angle, deg	Yaw angle, deg	Slideout distance, ft		Average coefficient of friction		Peak impact acceleration, g			Vertical impact velocity, ft/sec		Stability
	Actual	Full scale			Right, ft	Left, ft	Right	Left	Y	X	Z	Actual	Full scale	
1	0	0	-13	0	0	0	--	--	--	--	--	5.77	10	Good
2	0	0	-13	0	0	0	--	--	4.0	--	0.3	5.77	10	Good
3	8.65	15	-13	0	1.00	1.00	1.16	1.16	3.0	0.2	1.0	5.77	10	Good
4	8.65	15	-13	5	.90	.92	1.31	1.28	5.1	.4	1.0	5.77	10	Good
5	8.65	15	-13	10	.90	.92	1.31	1.28	5.8	2.3	1.1	5.77	10	Good
6	8.65	15	-13	15	.88	.90	1.34	1.30	6.3	.5	1.1	5.77	10	Good
7	17.30	30	-13	0	6.00	6.00	.78	.78	7.2	.3	1.4	5.77	10	Good
8	17.30	30	-13	5	--	--	--	--	6.2	.2	1.4	5.77	10	Tumbled
9	17.30	30	-13	10	--	--	--	--	7.4	.7	1.5	5.77	10	Tumbled
10	28.8	50	-13	0	--	--	--	--	6.0	.4	1.6	5.77	10	360° flip
11	5.78	10	-13	180	--	--	--	--	4.0	.2	.6	5.77	10	Damaged both main landing gears.

TABLE II-I. - LANDING IMPACT AND STABILITY TEST OF ONE-THIRD-SCALE GEMINI SPACECRAFT MODEL - Continued

(b) Test conducted on compacted earth; propulsion system not used

Test	Horizontal velocity, ft/sec		Pitch angle, deg	Yaw angle, deg	Slideout distance		Average coefficient of friction		Peak impact acceleration, g			Vertical impact velocity, ft/sec		Stability
	Actual	Full scale			Right, ft	Left, ft	Right	Left	Y	X	Z	Actual	Full scale	
12	8.65	15	-13	0	1.04	1.04	1.12	1.12	5.50	2.30	1.00	5.77	10	Good
13	0	0	-13	0	0	0	--	--	5.50	.70	1.00	5.77	10	Good
14	8.65	15	-13	5	.96	.96	1.27	1.21	5.70	.80	1.40	5.77	10	Good
15	8.65	15	-13	10	.96	.96	1.27	1.21	6.30	2.20	1.10	5.77	10	Good
16	8.65	15	-13	10	.71	.73	1.64	1.60	6.30	3.10	1.00	5.77	10	Good
17	17.30	30	-13	0	6.29	6.59	.74	.71	5.90	2.10	1.20	5.77	10	Good
18	17.30	30	-13	5	6.59	7.13	.71	.66	6.20	1.00	1.20	5.77	10	Good
19	17.30	30	-13	10	6.17	7.00	.75	.67	6.16	.18	1.12	5.77	10	Good
20	17.30	30	-13	15	7.00	7.67	.67	.61	5.90	.08	1.26	5.77	10	Good
21	28.80	50	-13	0	18.38	18.68	.76	.69	5.35	.14	.60	5.77	10	Good
22	28.80	50	-13	5	18.91	19.17	.68	.67	6.80	.28	1.50	5.77	10	Good
23	28.80	50	-13	10	21.00	21.82	.62	.59	5.75	-	1.33	5.77	10	Good
24	28.80	50	-13	15	20.70	21.60	.63	.60	5.10	.06	1.20	5.77	10	Good

TABLE II-I. - LANDING IMPACT AND STABILITY TEST OF ONE-THIRD-SCALE GEMINI SPACECRAFT MODEL - Continued

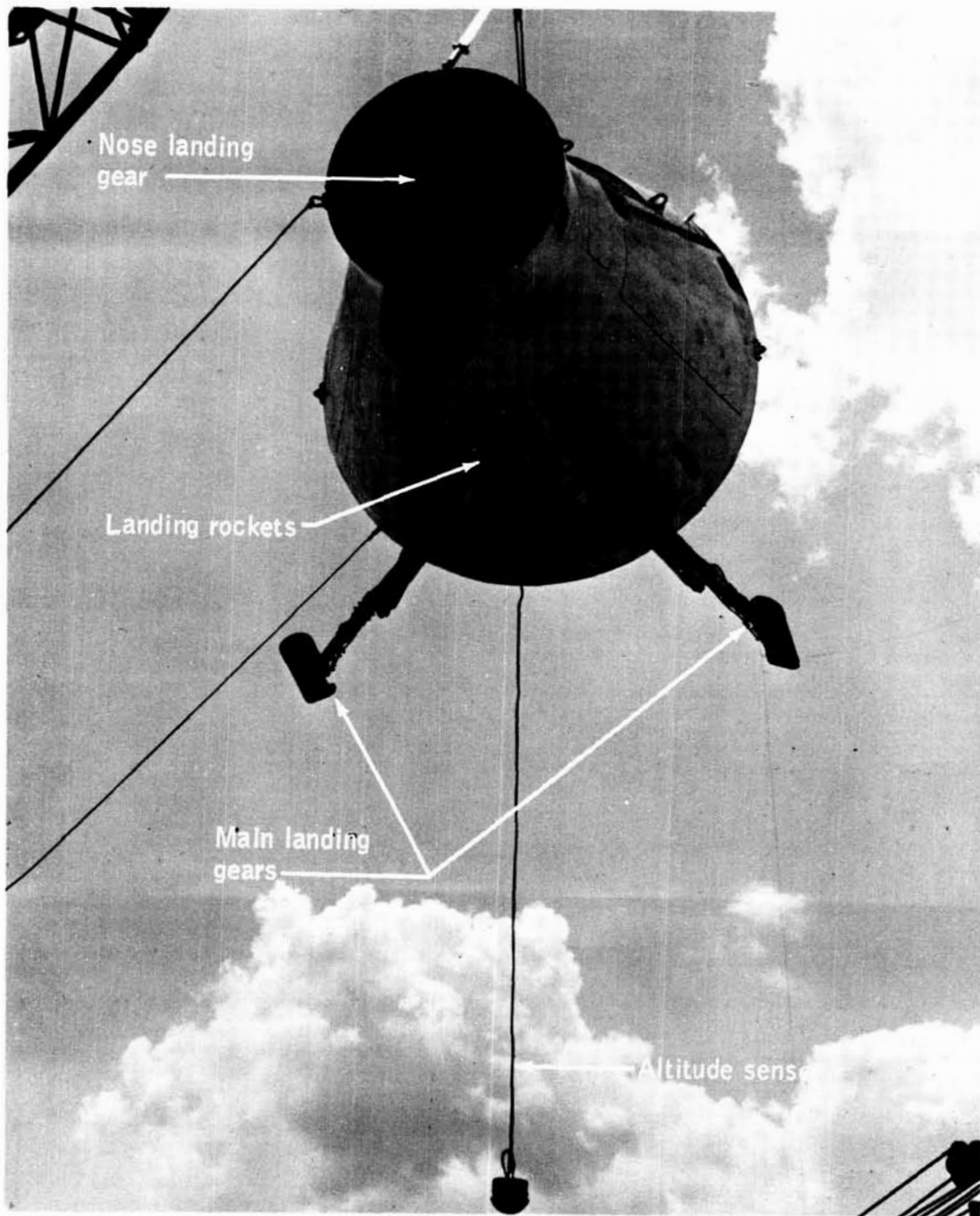
(c) Test conducted on canvas; propulsion system used

Test	Horizontal velocity, ft/sec		Pitch angle, deg	Yaw angle, deg	Slideout distance, ft		Average coefficient of friction		Peak impact acceleration, g			Vertical impact velocity, ft/sec		Stability
	Actual	Full scale			Right, ft	Left, ft	Right	Left	Y	X	Z	Actual	Full scale	
25	0	0	-13	0	--	--	--	--	3.76	0.80	1.11	5.95	10.30	Good
26	8.65	15	-13	0	7.33	7.33	0.318	0.318	3.49	.00	1.22	4.72	8.20	Good
27	8.65	15	-13	5	8.33	8.17	.280	.289	2.42	.00	.61	5.29	9.15	Good
28	8.65	15	-13	10	6.50	6.58	.359	.400	3.49	.00	1.45	4.58	7.94	Good
29	8.65	15	-13	15	--	--	--	--	3.49	1.12	1.12	4.85	8.40	Good
30	0	0	-18	0	.42	.42	--	--	7.00	1.13	1.33	3.74	6.50	Model translated 9 in. forward; stable
31	8.65	15	-18	0	10.92	11.17	.214	.300	2.84	2.36	1.62	4.83	8.35	Good (model appeared yawed)
32	8.65	15	-18	5	--	--	--	--	3.22	1.39	1.62	4.28	7.40	Good
33	8.65	15	-18	10	11.17	11.08	.300	.210	4.35	--	1.62	4.32	7.32	Good
34	8.65	15	-18	15	10.58	10.25	.220	.227	3.77	1.85	1.22	4.32	7.32	Good
35	8.65	15	-8	0	6.00	6.42	.388	.363	1.57	.00	1.22	5.05	8.75	Good
36	8.65	15	-8	15	6.25	6.67	.373	.350	3.67	1.93	.81	4.85	8.40	Good
37	8.65	15	-13	0	--	--	--	--	4.20	1.85	1.42	4.42	7.66	Good
38	17.30	30	-13	0	--	--	--	--	5.10	--	3.65	4.50	7.80	Cable fouled R/H MLG causing model to tumble 360°
39	17.30	30	-13	0	13.25	14.25	.704	.655	4.32	.93	1.62	5.62	9.75	Good

TABLE II-I. - LANDING IMPACT AND STABILITY TEST OF ONE-THIRD-SCALE GEMINI SPACECRAFT MODEL - Concluded

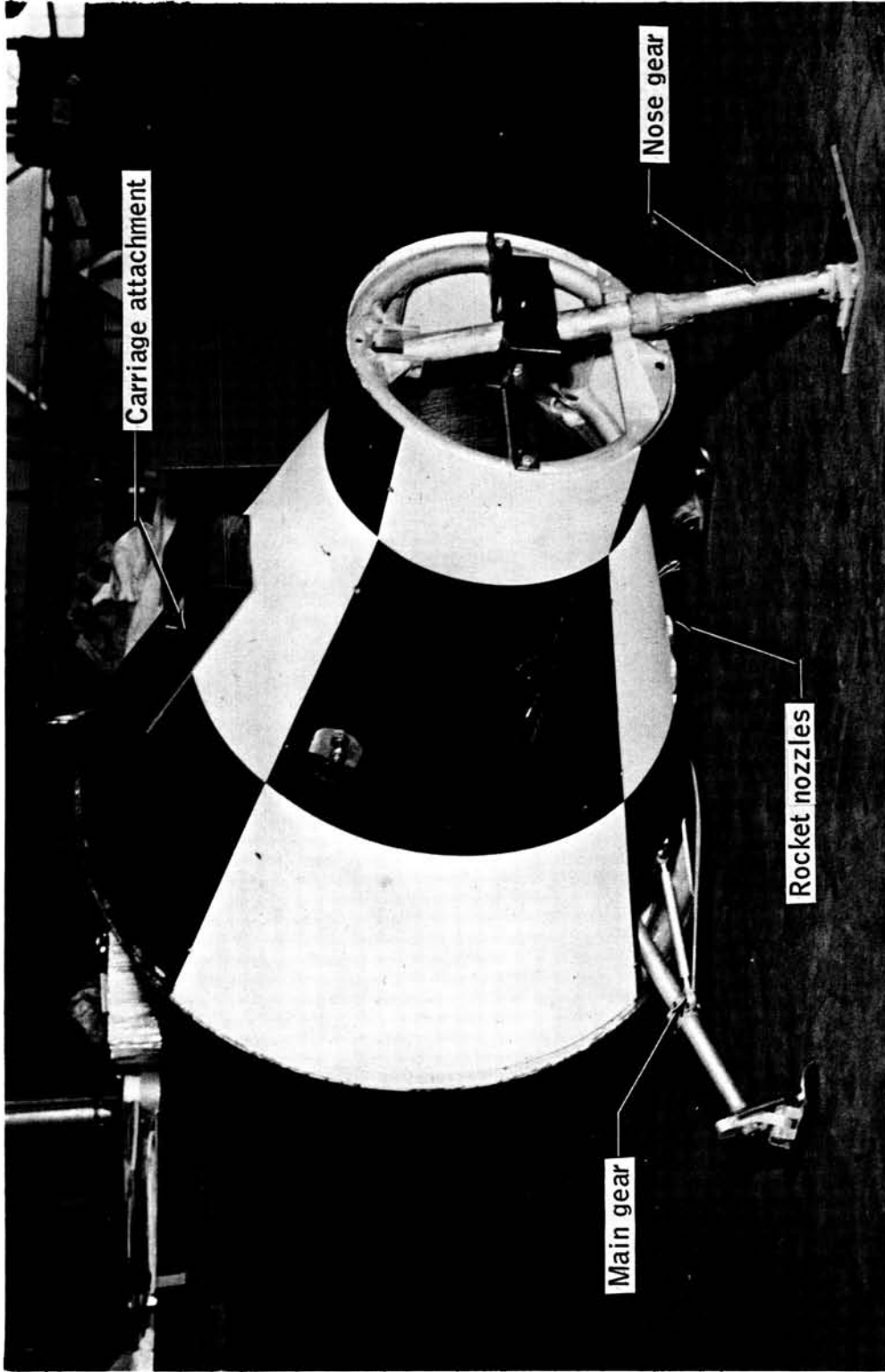
(c) Test conducted on canvas; propulsion system used

Test	Horizontal velocity, ft/sec		Pitch angle, deg	Yaw angle, deg	Slideout distance		Average coefficient of friction		Peak impact acceleration, g			Vertical impact velocity, ft/sec		Stability
	Actual	Full scale			Right, ft	Left, ft	Right	Left	Y	X	Z	Actual	Full scale	
40	11.52	20	-13	0	11.50	11.25	0.360	0.368	2.69	1.85	1.45	3.82	6.60	Good
41	14.20	25	-13	0	13.75	13.67	.456	.456	5.36	.00	.94	3.31	5.72	Good
42	12.95	22.5	-13	0	10.17	11.00	.514	.473	4.94	.00	1.21	4.20	7.30	Good
43	17.30	30	-18	0	16.25	18.42	.574	.506	3.22	.95	1.11			Good
44	17.30	30	-8	0	13.42	14.25	.695	.655	3.22	.00	1.55			Good
45	17.30	30	-13	15	14.00	15.00	.666	.623	5.66	.00	1.33			Good
46	17.30	30	-13	15	15.50	16.00	.601	.584	3.31	1.01	1.33			Good
47	17.3	30	-13	15	13.92	15.58	.67	.60	4.54	1.01	1.55			Good
48	17.3	30	-13	5	12.83	14.33	.72	.65	1.38	.00	1.30			Good
49	17.3	30	-8	15	14.83	15.17	.63	.62	3.41	1.01	1.33			Good
50	17.3	30	-18	15	18.58	19.25	.50	.48	3.24	2.02	1.55			Good

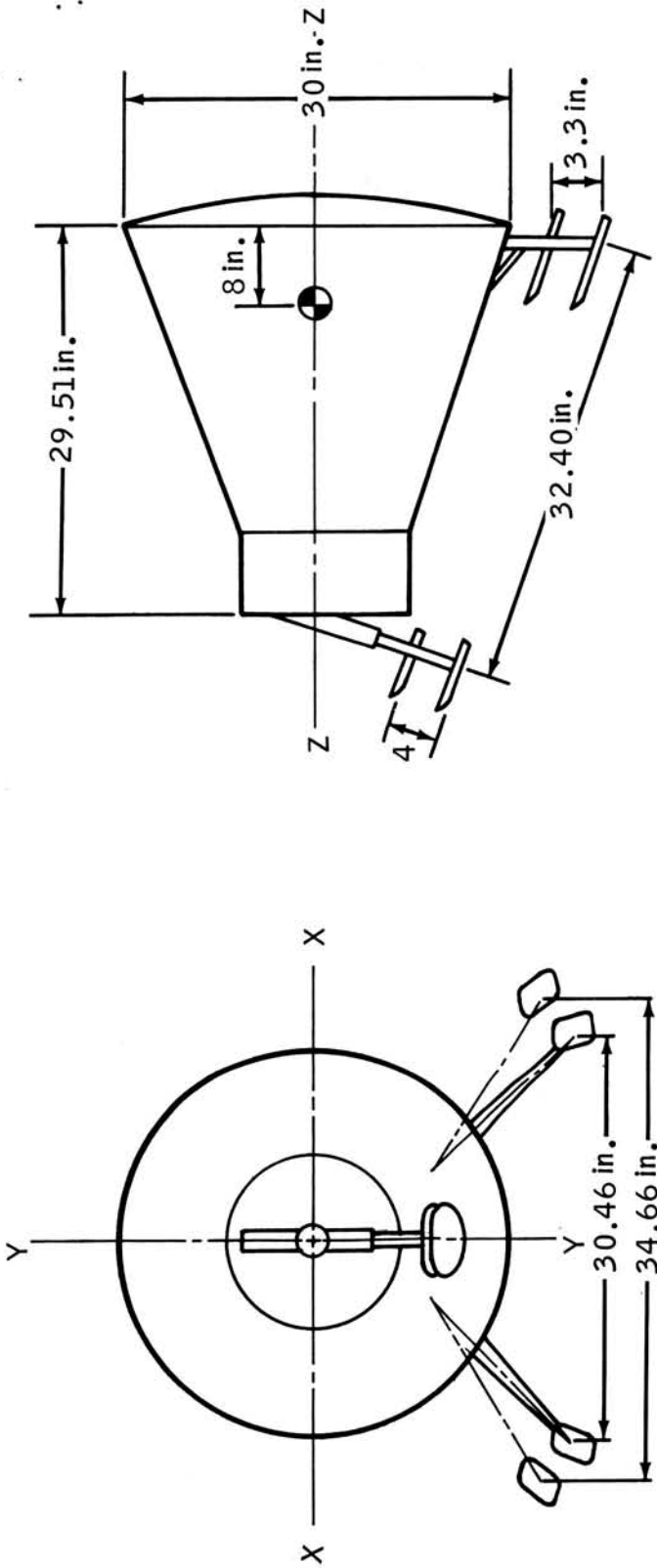


(a) Complete full-scale system.
Figure II-1.- Landing system.

NASA-S-66-9833 OCT 24



(b) One-third-scale test model.
Figure II-1.- Concluded.



	Model	Scale factor	Full scale
Weight	176.6 lb	3^3	4768.2 lb
Inertia, X-X (yaw)	4.18 slugs/ft ²	3^5	1016 slugs/ft ²
Inertia, Y-Y (pitch)	4.35 slugs/ft ²	3^5	1058 slugs/ft ²
Inertia, Z-Z (roll)	3.15 slugs/ft ²	3^5	766 slugs/ft ²

Figure II-2.- Model dimensions, center-of-gravity location, weight, and inertias.

NASA-S-66-9835 OCT 24

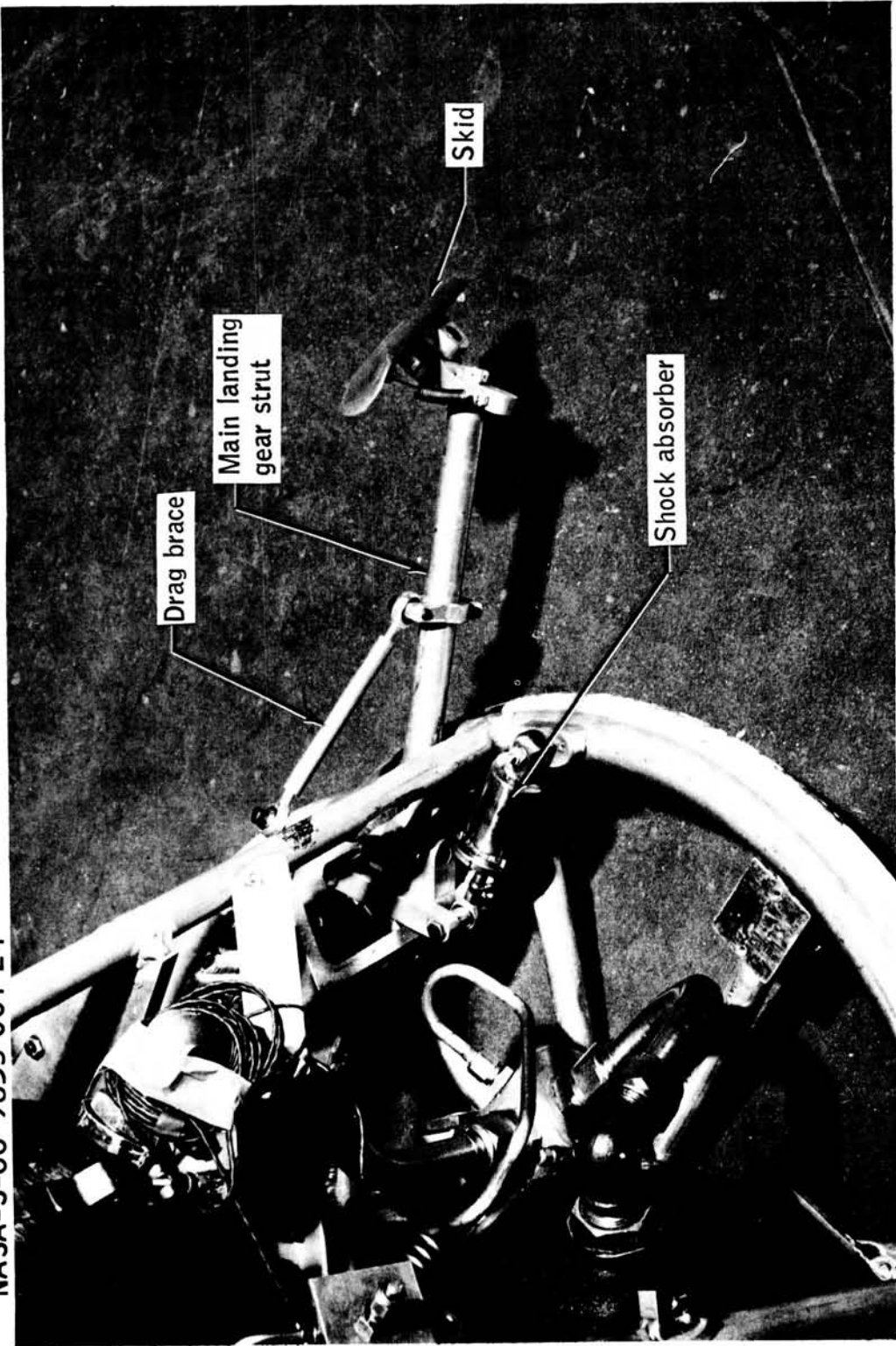


Figure II-3.- Main landing-gear detail.

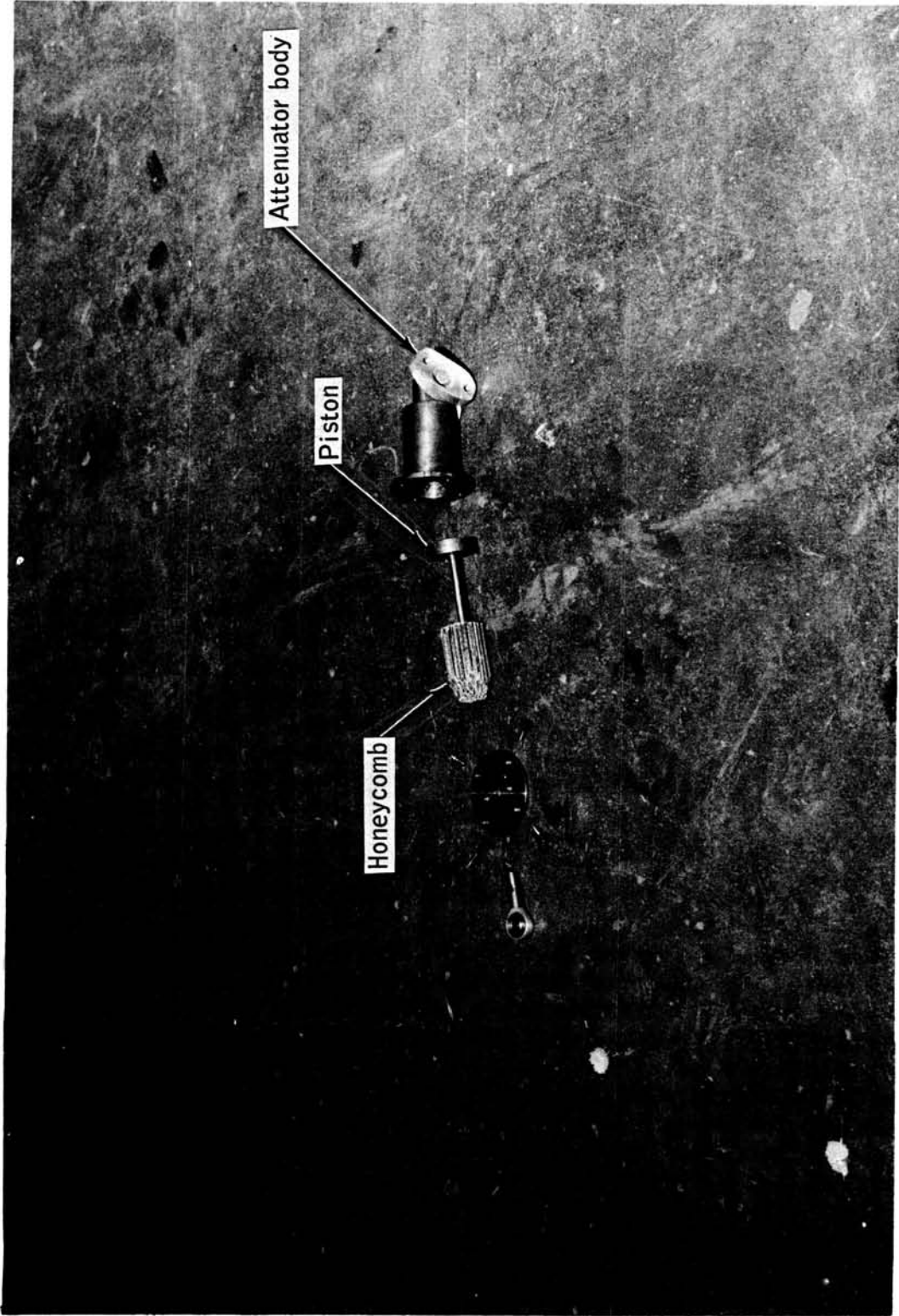


Figure II-4.- Main landing-gear shock attenuator.

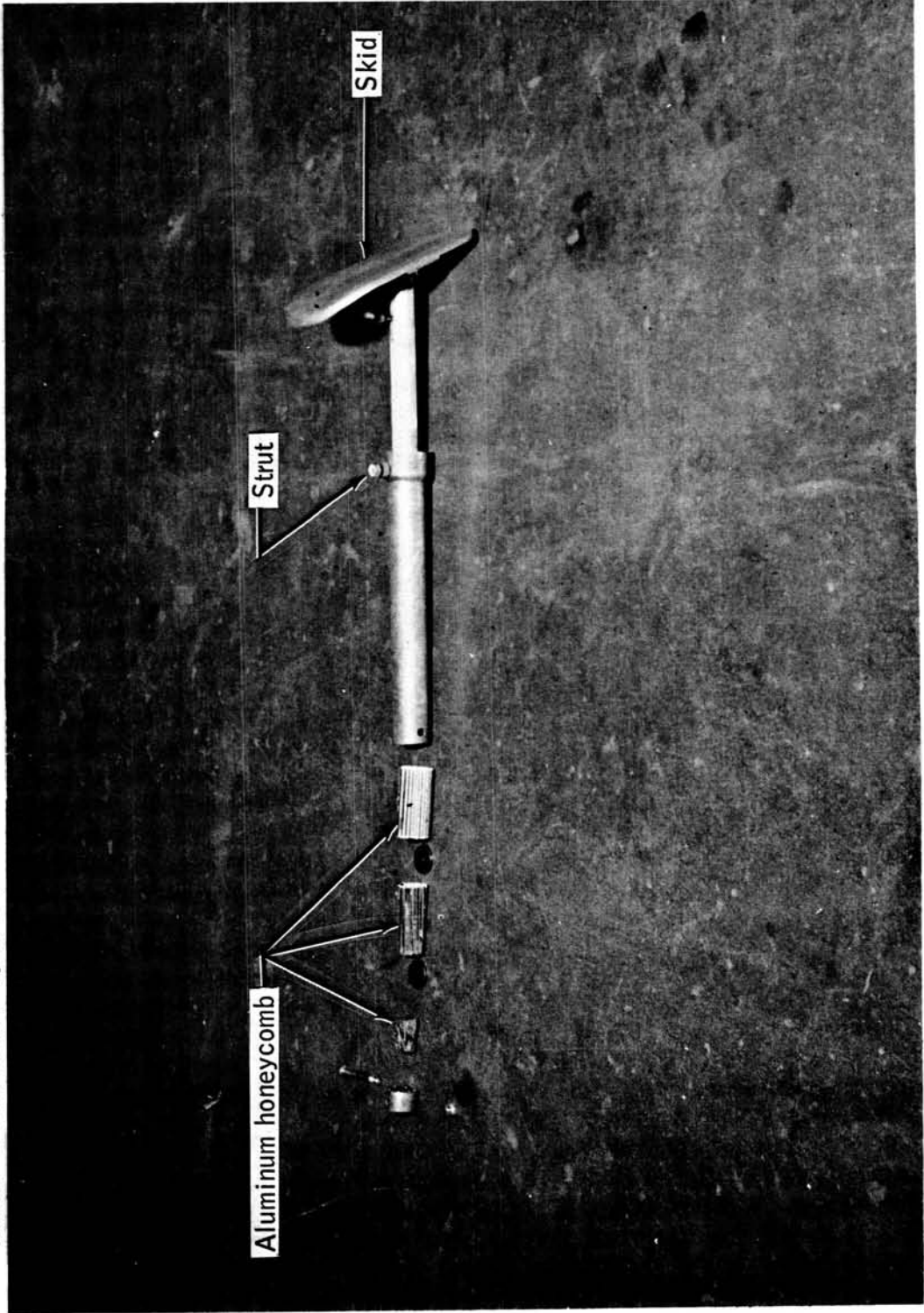


Figure II-5.- Nose landing gear.

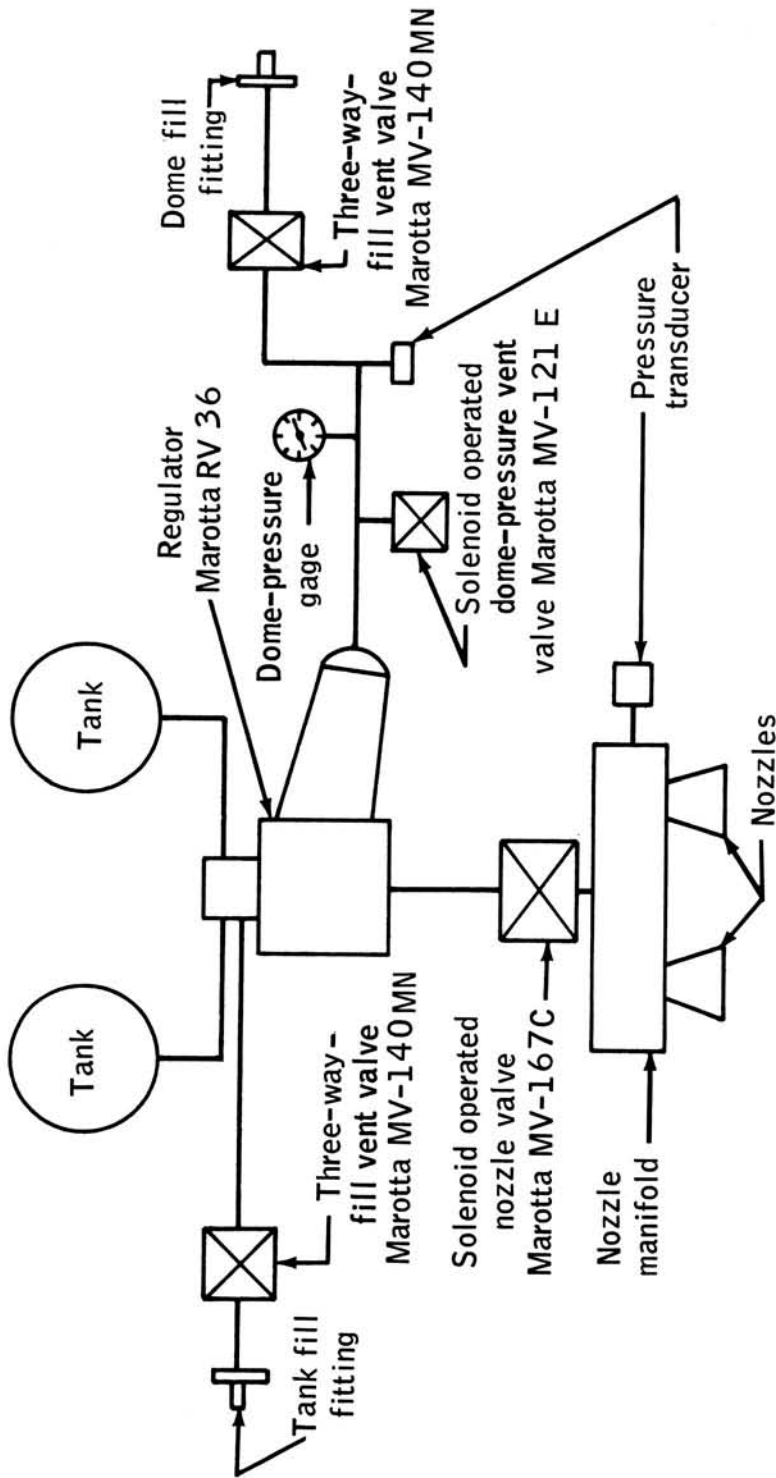


Figure II-6. - Schematic of propulsion system (one-third-scale Gemini spacecraft).

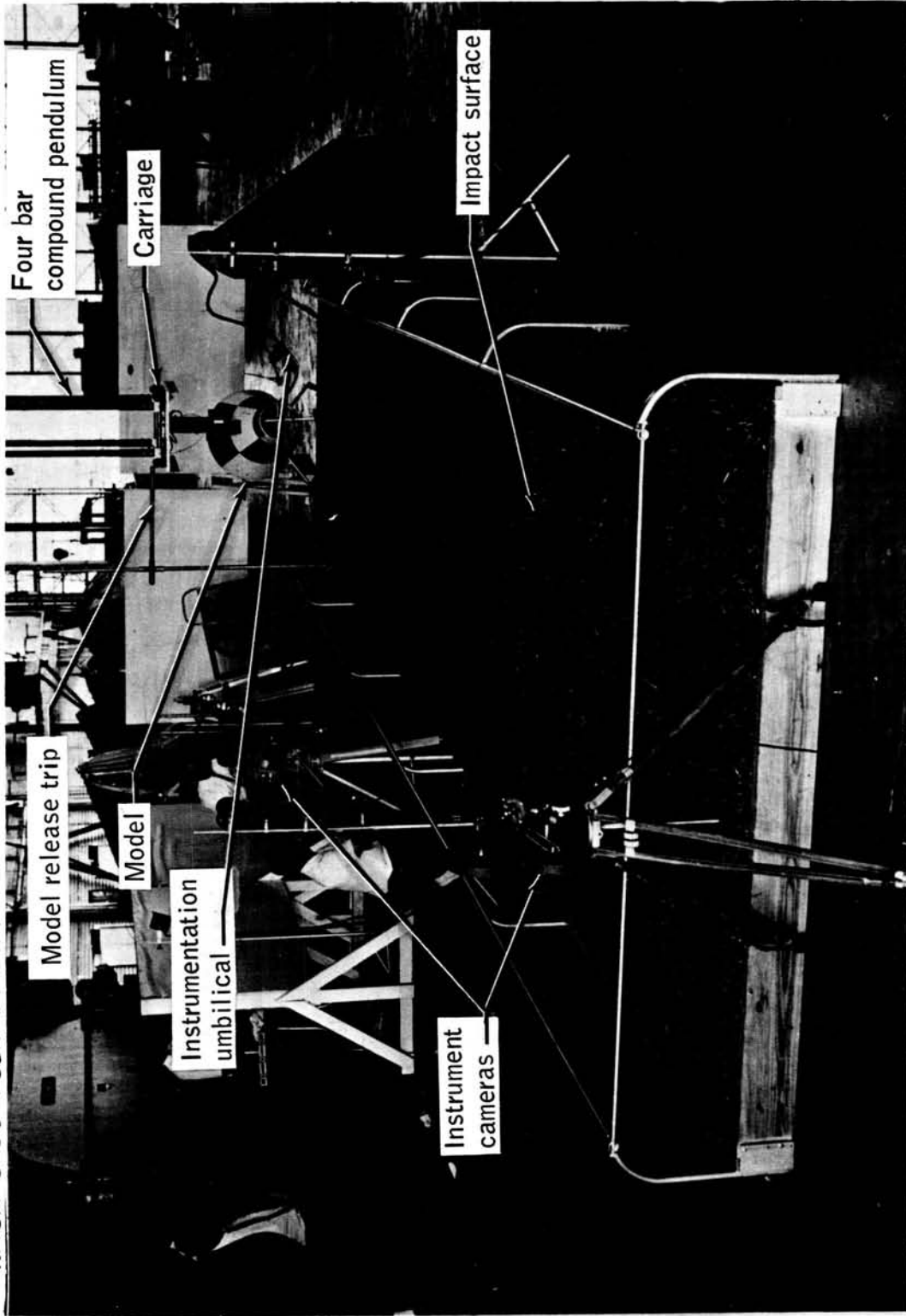


Figure II-7.- Test facility.

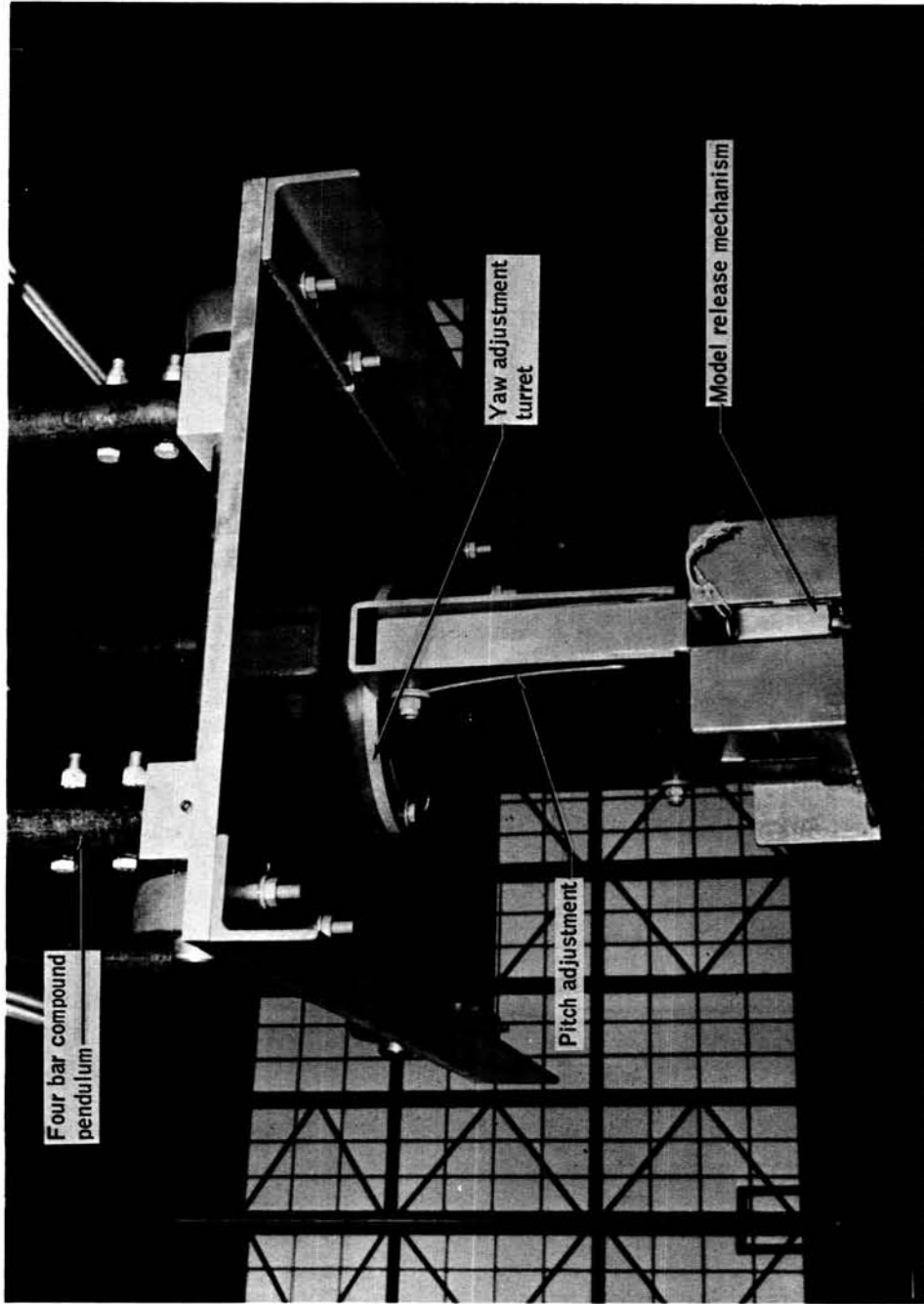


Figure II-8.- Drop carriage.

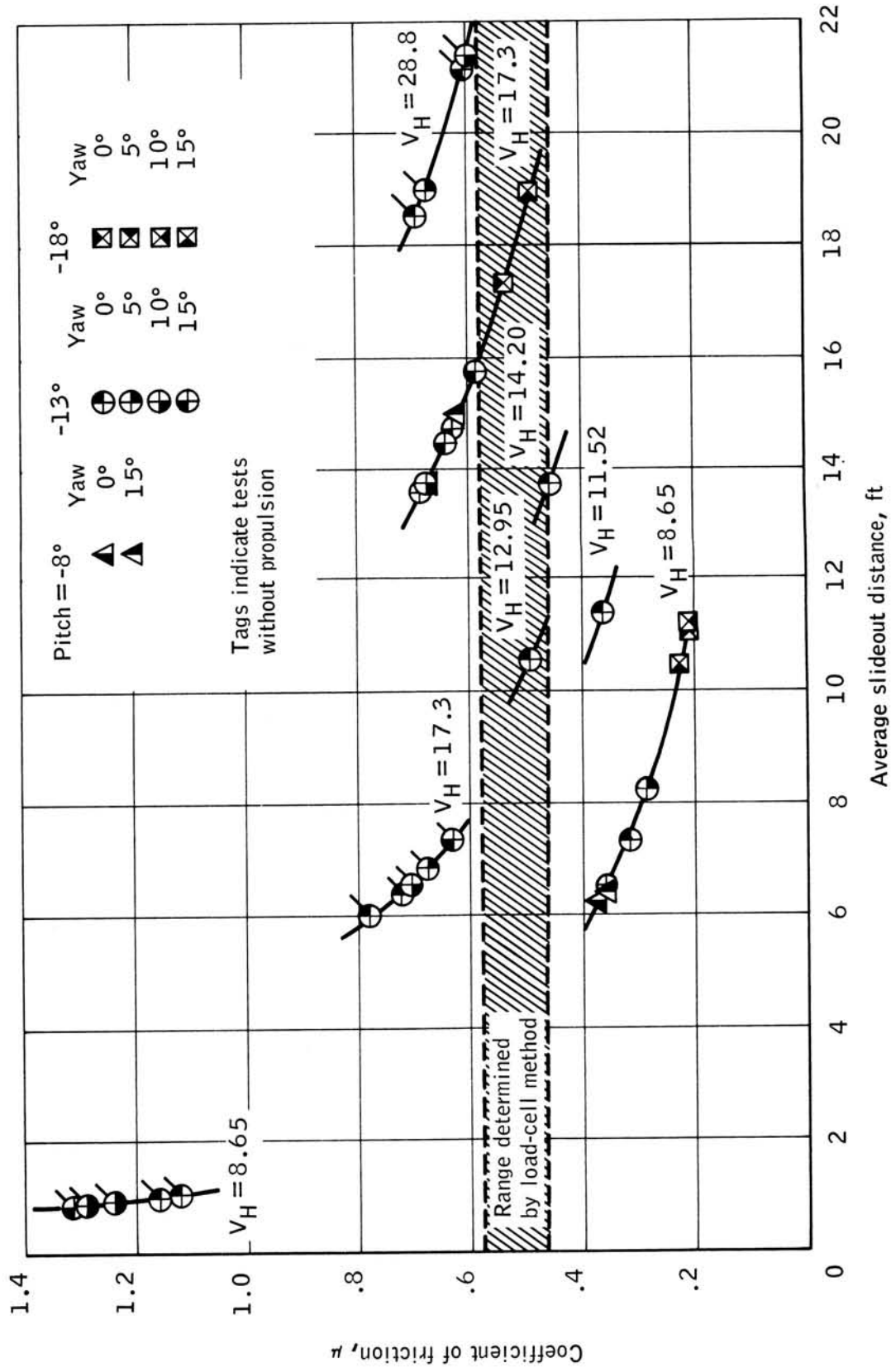


Figure II-9.- Coefficients of friction.

NASA-S-66-9842 OCT 24

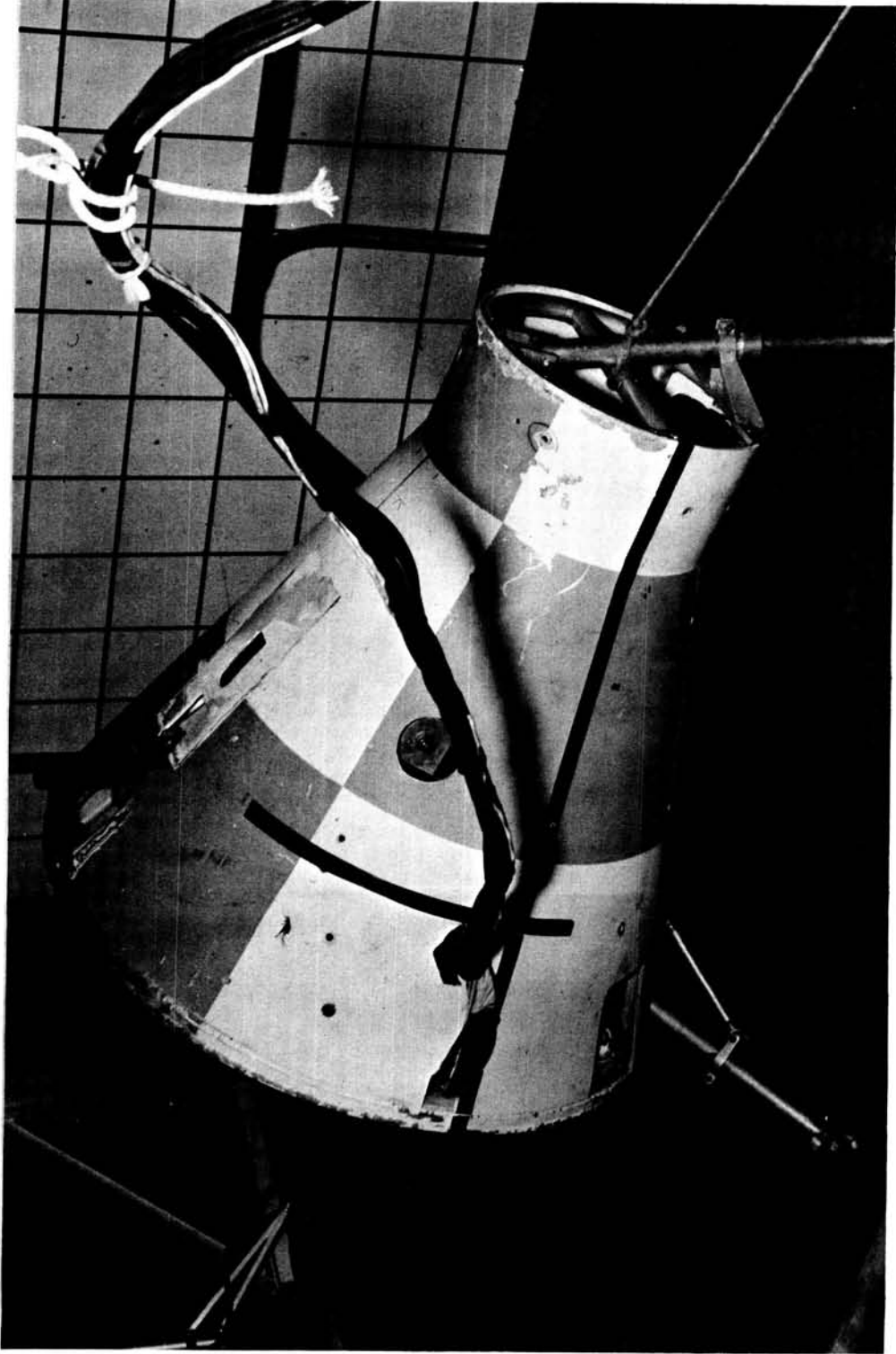


Figure II-10.- Soil erosion caused by model at 0 horizontal velocity.

NASA-S-66-9843 OCT 24

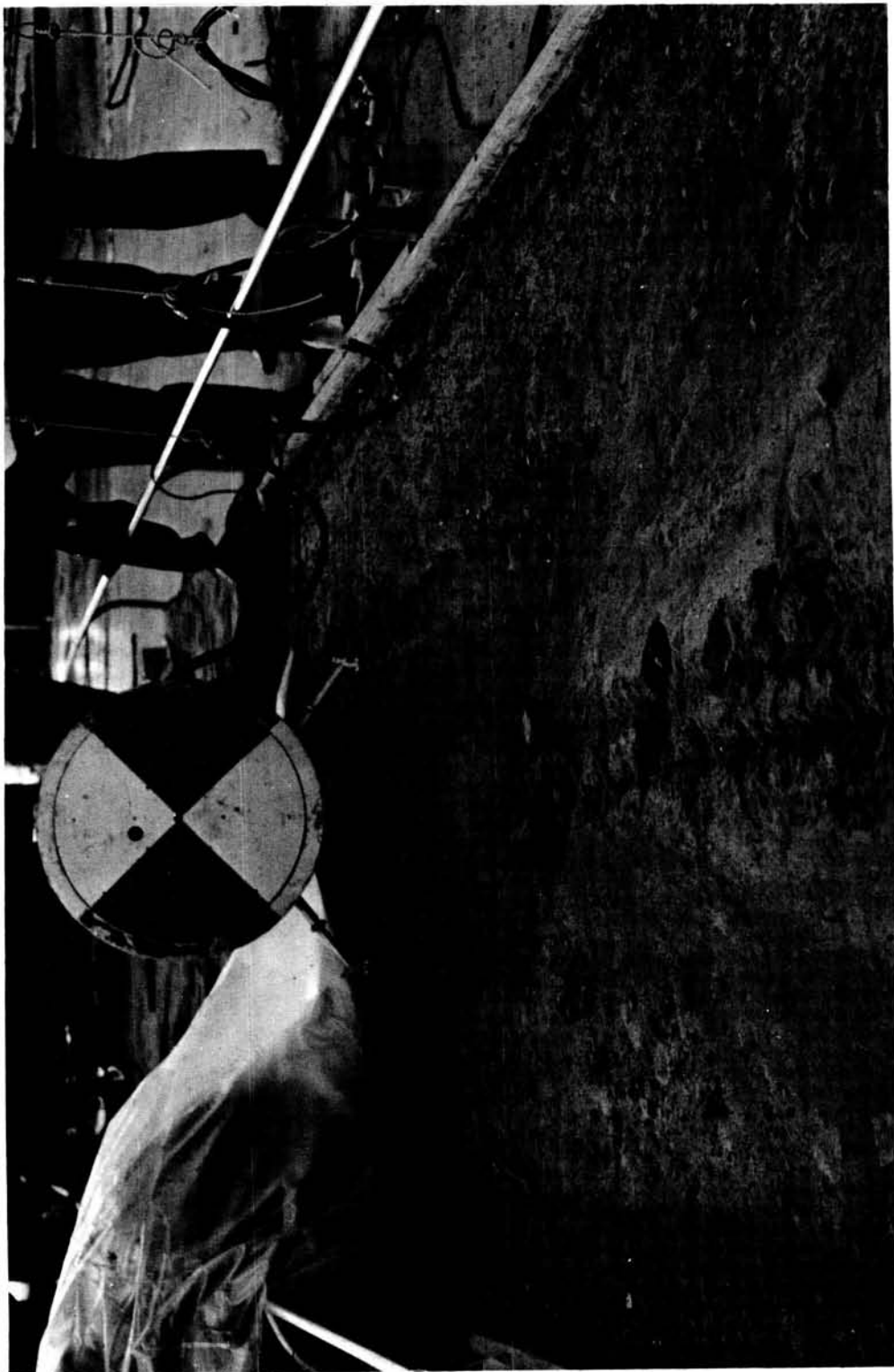


Figure II-11.- Soil erosion caused by model at 3.5 ft/sec horizontal velocity.

SECTION III - PARACHUTE DEVELOPMENT

APPENDIX A - PARA-SAIL EVALUATION DROP-TEST PROGRAM

By Leland C. Norman

PRECEDING PAGE BLANK NOT FILMED.

PARACHUTE DEVELOPMENT

Section III contains three parts. The first describes the initial 17 deployments of the original 23.2-foot d_0 parachute configuration. The second contains all of the development tests of the 80-foot d_0 version of the parachute. The third presents the verification tests of the final 70-foot d_0 parachute configuration.

PRECEDING PAGE BLANK NOT FILMED.

PARA-SAIL EVALUATION DROP-TEST PROGRAM

By Leland C. Norman
Manned Spacecraft Center

SUMMARY

The Para-Sail evaluation drop-test program was conducted to determine the deployment characteristics, reefing parameters, and turn sensitivity of a 23.2-foot-diameter Para-Sail parachute. Seventeen parachute drops were made at altitudes from 600 to 2000 feet and speeds from 0 to 118 knots. Loads were recorded with a self-recording tensiometer and turn data were obtained from photographic coverage. These data are presented in appropriate sections of the report.

The tests showed that the Para-Sail can be packed and deployed in the conventional manner at velocities up to 120 knots when methods are employed which allow the parachute to take a more normal hemispherical shape during opening. Rates of turn from 13.3 deg/sec to 29.3 deg/sec were obtained.

INTRODUCTION

The Para-Sail ascending parachute, designed in France by Mr. Pierre LeMoigne, is a gliding parachute based upon the jet exhaust principle (fig. III-1). Preliminary evaluations of glide capability conducted by the Manned Spacecraft Center indicated lift-to-drag ratios (L/D) of 0.8 to 1.0. Moreover, the canopy was found to be sensitive to turn control. The high L/D ratios and turn sensitivity offer two desirable characteristics for spacecraft earth-landing systems in that they provide capability for avoiding local obstacles and negating some surface winds.

The Para-Sail was designed to be towed in the full-open position. Deployment and free-descent characteristics were not known. Because the shape of the canopy is radically different from normal parachutes, some modification of the conventional deployment methods had to be devised. It was felt that the low-porosity cloth and the apex-down canopy shape would result in very high opening shock forces. This investigation of the Para-Sail

parachute was conducted to determine its deployment characteristics, reefing parameters, and turn sensitivity.

EQUIPMENT

The canopy tested was a 23.2-foot-diameter Para-Sail (fig. III-1). The pilot parachute was a 42-inch spring-loaded guide vane. For 15 drop tests, two types of helicopters, H-19 and H-21, were used as drop aircraft. The only modification required was the installation of a second cargo-hook attachment (fig. III-2). A C-119 aircraft was used in tests 16 and 17. The launch velocities for these tests were 100 knots and 118 knots, respectively. A 125-pound test vehicle was constructed to house the parachute bag, a 16-mm Gun Sight Aiming Point (GSAP) camera, and batteries. This vehicle is shown in figures III-3 and III-4.

An H-19 helicopter accompanied the drop aircraft in flight for the purpose of obtaining motion-picture records of the tests. The H-19 helicopter was equipped with a 16-mm Bell and Howell 3-inch Ekta lens camera. A 70-mm Hulcher Tracking Camera located near the impact point recorded all of the tests. A 16-mm Aeroflex camera with 28-inch Big Bertha lens recorded all of the tests from the ground. A self-recording tensiometer with a range of from 0 to 7500 pounds was used to record the parachute opening forces.

A special set of variable length or snubbing risers was fabricated by Pioneer Parachute Company for these tests. These risers are shown in figure III-5(a) in the snubbed or shortened condition, and in figure III-5(b) in the fully extended position. The apex was pulled down inside the canopy when the parachute was in the inflated position, as shown in figure III-1. In order to give the canopy a more normal parachute shape during inflation and to reduce opening shock, it was necessary to shorten the circumferential suspension lines with respect to the apex lines. This was accomplished by a snubber line tied between the rings on the risers. This snubber line allowed the canopy to take a normal hemispherical parachute shape during inflation and opening shock. After the opening shock was encountered, reefing cutters cut the snubber line and allowed the circumferential suspension lines to extend to normal length. This action has the effect of pulling the apex down to its glide position.

TEST PROCEDURE

These tests were performed with the drop helicopter in either a hover attitude or in straight and level flight. The test vehicle was carried under the helicopter and suspended by a carrying loop held in a standard cargo hook. The test vehicle was dropped by electrically releasing the cargo hook from inside the drop helicopter. On drops 16 and 17, the test vehicle was pushed from the C-119 left paratrooper door. A static line to the pilot-parachute ripcord activated the spring-loaded pilot parachute in tests 1, 2, and 3. In the remaining tests, the static line was attached directly to the deployment bag. The time-delay reefing cutters were activated by a lanyard at line stretch.

TEST RESULTS

The test results of the 17 tests are summarized.

Deployment

The 23.2-foot-diameter Para-Sail was packed and deployed in the conventional manner at velocities up to 75 knots with modifications to the risers. It was deployed at velocities up to 120 knots with the risers modified and the canopy skirt reefed. Peak-load data for tests 5, 6, 7, and 8 are presented in figure III-6. Figure III-7 contains peak-load data for tests 14 and 15. Opening shock loads are shown to be approximately 7.5g.

Rate of Turn

The rate of turn was found to be relatively independent of wind velocity and direction. A rate of turn of 21.2 deg/sec was obtained on the prototype by shortening one front riser 24 inches, as shown in figure III-8. A rate of turn of 16.4 deg/sec was obtained on the prototype by shortening one rear riser 24 inches. Figure III-9 presents these data. A rate of turn of 13.3 deg/sec was obtained by closing the side exhaust ports. These data are presented in figures III-10 to III-13. A rate of turn of 29.3 deg/sec was obtained by shortening the two risers on one side by 40 inches and the opposite front riser by 30 inches.

Free Descent

The maximum free-descent glide was obtained by shortening both front risers 10 inches. The maximum free descent L/D was approximately 1.0 on the prototype. The canopy was extremely stable.

CONCLUSIONS AND RECOMMENDATIONS

The Para-Sail could be deployed at velocities up to 120 knots. It was believed that deployment could be accomplished at considerably higher speeds if the slots were arranged to form a vented doughnut shape around the crown area. This shape would allow opening shock-pressure relief in the same manner as the vent in standard canopies.

Rates of turn from 13.3 deg/sec to 29.3 deg/sec were obtained. The rate of turn perhaps could be increased by the addition of vertical slots in the sides of the canopy.

This parachute was designed for towed ascension in flights for sport. Considerable improvement for spacecraft application probably could be attained if the various design parameters, shape, porosity, and exhaust-port size and location were optimized for deployed free-fall performance.

HELICOPTER DROP TESTS

Test 1 - Ellington Air Force Base, September 4, 1962

Launch conditions. - Altitude = 1000 feet; velocity = 0 (hover).

Rigging. - The 42-inch pilot parachute was permanently attached to the main canopy apex. The pilot parachute was spring loaded, and a 15-pound breakcord was tied from the static line to the apex of the pilot parachute. A breakcord was tied from the bag to loops on lines 12 and 24 of the main parachute.

Riser shortening. - None.

Results. - The parachute deployed satisfactorily. When the main canopy opened, the pilot parachute and deployment bag fell on the left rear of the main canopy and temporarily collapsed that portion. The parachute was completely stable and made a normal gliding descent.

Remarks. - The pilot parachute was very slow entering the airstream. This was a result of the bag being tightly wedged into the test vehicle and a possible low-pressure area immediately above the test vehicle while it was in free fall.

Test 2 - Ellington Air Force Base, September 4, 1962

Launch conditions. - Altitude = 1000 feet; velocity = 0.

Rigging. - The 42-inch pilot parachute was permanently affixed to the deployment bag. A breakcord was tied from the bag to loops on lines 12 and 24. A static line was attached to the ripcord. The pilot parachute was spring loaded.

Riser shortening. - Full (no distance between the reefing rings; all risers were shortened 40 inches).

Results. - Total malfunction. The pilot parachute did not enter the airstream; consequently, the main canopy did not deploy.

Remarks. - It is believed that the reason the pilot parachute failed to get into the airstream was due to the fact that the packed parachute wedged in the test vehicle.

Recommendations. - Modify the test vehicle to accommodate the packed parachute. More positive pilot-parachute deployment.

Test 3 - Ellington Air Force Base, September 11, 1962

Launch conditions. - Altitude = 1000 feet; velocity = 0.

Ringing. - The 42-inch pilot parachute was permanently affixed to the deployment bag. A breakcord was tied from the bag to loops on lines 12 and 24 of the main canopy. A static line was attached to the ripcord and a 40-pound breakcord was tied to the apex of the pilot parachute. The pilot parachute was spring loaded.

Riser shortening. - Full.

Results. - The main canopy deployed satisfactorily without the characteristic post-opening shock rebound (heavy breath). The reefing cutters fired as scheduled, and the canopy was completely stable and made a normal gliding descent. The average rate of descent was 12.5 ft/sec.

Remarks. - The pilot parachute was again slow in getting into the air-stream, and thereby delayed opening of the main canopy. The test vehicle was modified to fit the packed parachute.

Test 4 - Ellington Air Force Base, September 11, 1962

Launch conditions. - Altitude = 1000 feet; velocity = 0.

Rigging. - The static line was permanently attached to the deployment bag. A breakcord was tied from the bag to loops on lines 12 and 24 of the main canopy.

Riser shortening. - Full.

Results. - The main canopy deployed satisfactorily without the characteristic post-opening shock rebound. The reefing cutters fired as scheduled, and the canopy was completely stable and made a normal gliding descent.

Remarks. - Since the static line actuated, bag strip-off deployment occurred immediately following separation. The average rate of descent was 12.1 ft/sec.

Test 5 - Ellington Air Force Base, September 18, 1962

Launch conditions. - Altitude = 700 feet; velocity = 0.

Rigging. - The static line was permanently attached to the deployment bag. A breakcord was tied from the bag to the loops on lines 12 and 24 of the main canopy. A tensiometer was placed in the riser between the canopy and the test-vehicle attachment.

Riser shortening. - Full.

Results. - The main canopy deployed satisfactorily without the characteristic post-opening shock rebound. The reefing cutters fired on schedule. The tensiometer recorded load data.

Remarks. - The parachute deployed so that it was alined facing into the wind (12 to 15 knots) and made a near vertical descent, remaining completely stable. Load data from this test are presented in figure III-6.

Test 6 - Ellington Air Force Base, September 18, 1962

Launch conditions. - Altitude = 600 feet; velocity = 0.

Rigging. - Same as test 5.

Riser shortening. - Half (20 inches).

Results. - The main canopy deployed satisfactorily but exhibited a slight post-opening shock rebound. The reefing cutters fired on schedule and the tensiometers recorded load data. These load data are presented in figure III-6.

Remarks. - The canopy deployed facing with the wind, was completely stable, and made a long gliding descent.

Test 7 - Ellington Air Force Base, September 18, 1962

Launch conditions. - Altitude = 700 feet; velocity = 0.

Rigging. - Same as test 5.

Riser shortening. - 26 inches.

Results. - The main canopy deployed satisfactorily but exhibited a slight post-opening shock rebound that damped out quickly. The reefing cutters fired on schedule and the tensiometers recorded load data. These load data are presented in figure III-6.

Remarks. - The canopy deployed facing into the wind (7 to 8 knots), made a very shallow gliding descent, and remained completely stable.

Test 8 - Galveston Bay, September 26, 1962

Launch conditions. - Altitude = 1000 feet; velocity = 67 knots.

Rigging. - Same as test 5.

Riser shortening. - Full.

Results. - The main canopy deployed satisfactorily but exhibited a moderate post-opening shock breathing in the reefed condition. The reefing

cutters fired on schedule and the tensiometer recorded the load data. These load data are presented in figure III-6.

Remarks. - This was the first drop made with an initial velocity. No canopy damage occurred. The parachute made a spiral gliding descent.

Test 9 - Galveston Bay, September 26, 1962

Launch conditions. - Altitude = 1000 feet; velocity = 63 knots.

Rigging. - Same as test 5.

Riser shortening. - Full.

Results. - The parachute deployed satisfactorily with no post-opening shock breathing. The reefing cutters fired on schedule. No loads were recorded because the tensiometer lanyard apparently fouled and broke.

Remarks. - No canopy damage occurred. The parachute was completely stable and made a long gliding descent.

Test 10 - Galveston Bay, October 2, 1962

Launch conditions. - Altitude = 1500 feet; velocity = 0.

Rigging. - Same as test 5.

Riser shortening. - Full.

Results. - The canopy deployed satisfactorily and the reefing cutters fired on schedule. The canopy rotated 3-1/4 turns clockwise after disreef. The exhaust ports on lines 5, 6, 7, and 8 were sewed closed so that the canopy would rotate. The average rate of descent was 13.05 ft/sec. The average rate of turn was 13.3 deg/sec.

Remarks. - The chase helicopter inadvertently hovered close to the canopy and partially collapsed it at one point. This drop was made in a 20-knot wind, and the rate of turn did not appear to be affected by the direction of the wind relative to the canopy.

Test 11 - Galveston Bay, October 2, 1962

Launch conditions. - Altitude = 1500 feet; velocity = 0.

Rigging. - Same as test 5.

Riser shortening. - Full.

Results. - The canopy deployed satisfactorily and the reefing cutters fired on schedule. The canopy rotated 3-3/4 turns counterclockwise. The exhaust ports on lines 17, 18, 19, and 20 were sewed closed so that the canopy would rotate. Time from release to impact was 1 minute 47.2 seconds, and the canopy did not begin to rotate until 8.1 seconds after release. The average rate of descent was 12.6 ft/sec.

Remarks. - This drop was made in a 20-knot wind, and the rate of turn did not appear to be affected by the direction of the wind relative to the canopy. The average rate of turn was 13.4 deg/sec. These turn data are presented in figures III-12 and III-13.

Test 12 - Galveston Bay, October 9, 1962

Launch conditions. - Altitude = 1000 feet; velocity = 0.

Rigging. - Same as test 5 plus the right front riser was shortened 24 inches.

Riser shortening. - Full.

Results. - The parachute deployed satisfactorily and the reefing cutters fired on schedule. The parachute descended in a left spiralling turn. Time from release to impact was 60.0 seconds. The average rate of descent was 12.5 ft/sec.

Remarks. - It is postulated that the unexpected left turn resulted from the following:

1. The right-hand exhaust ports increased in size as a result of the foreshortened right front riser.

2. The right front scoop panels inverted and raised the right front of the canopy so that it assumed a left bank angle of 10°. The average rate of turn was 21.2 deg/sec to the left. These turn data are presented in figure III-8.

Test 13 - Galveston Bay, October 9, 1962

Launch conditions. - Altitude = 1000 feet; velocity = 0.

Rigging. - Same as test 5 plus the right rear riser was shortened 24 inches.

Riser shortening. - Full.

Results. - The parachute deployed satisfactorily and the reefing cutters fired on schedule. The parachute descended in a slow right turn, slipping rearward. Time from release to impact was 78.1 seconds. The average rate of descent was 12.2 ft/sec.

Remarks. - The average rate of turn was 16.4 deg/sec to the right. Turn data are presented in figure III-9.

Test 14 - Galveston Bay, October 11, 1962

Launch conditions. - Altitude = 1500 feet; velocity = 70 knots.

Rigging. - Same as test 5 plus permanent 10-inch lines (30-inch pull down) were added to the front risers. A tensiometer was placed in one riser.

Riser shortening. - Full.

Results. - The reefing cutter on the left riser malfunctioned; consequently, the parachute descended with the left risers pulled down 40 inches and the right front riser pulled down 30 inches. The right rear riser was fully extended. The parachute descended in a left banking turn and rotated. The average rate of turn was 29.3 deg/sec. The average rate of descent was 14.4 ft/sec. The tensiometer recorded the loads which are presented in figure III-7.

Test 15 - Galveston Bay, October 9, 1962

Launch conditions. - Altitude = 1800 feet; velocity = 73 knots.

Rigging. - Same as test 5 plus both front risers were permanently pulled down 30 inches. A tensiometer was placed in the riser.

Riser shortening. - Full.

Results. - The canopy deployed satisfactorily and the reefing cutters fired on schedule. The high negative angle of the canopy caused by shortening the front risers stalled the front of the canopy. It descended with the front half of the canopy alternately stalling and reinflating. The time from release to impact was 1 minute 50 seconds. The average rate of descent was 15 ft/sec. The tensiometer recorded the loads which are presented in figure III-7.

Test 16 - Galveston Bay, October 23, 1962

Launch conditions. - Altitude = 2000 feet; velocity = 100 knots.

Rigging. - Same as test 5 plus the front risers permanently shortened 10 inches.

Riser shortening and skirt reefing. - The circumferential suspension lines were shortened 40 inches (full) and held until released by 10-second cutters. The skirt was reefed to 14 percent (105 inches) until released by 5-second cutters.

Results. - The canopy deployed satisfactorily and was stable in the skirt reefed condition. After skirt disreef, the parachute remained stable in the apex-up position. After the snubber line was released, the parachute aligned itself with the wind (23 knots) and made a long gliding descent covering approximately 2 miles. The rate of descent was 12.3 ft/sec.

Test 17 - Galveston Bay, October 23, 1962

Launch conditions. - Altitude = 2000 feet; velocity = 118 knots.

Rigging. - Same as test 16.

Riser shortening and skirt reefing. - The circumferential suspension lines were shortened 40 inches (full) and held until released by 10-second cutters. The skirt was reefed to 10 percent (75 inches) until released by 5-second cutters.

Results. - The canopy deployed satisfactorily and was reasonably stable in the skirt reefed condition. The canopy inflated through the vents in the sides. After skirt disreef, the parachute was facing into a 23-knot wind, and during the descent very little ground was lost in view of the existing wind conditions. The average rate of descent was 12.3 ft/sec.

PRECEDING PAGE BLANK NOT FILMED.

APPENDIX B - DEVELOPMENT TESTS OF THE
80-FOOT-DIAMETER PARA-SAIL

By Leland C. Norman and Jerry C. Coffey

PRECEDING PAGE BLANK NOT FILMED.

DEVELOPMENT TESTS OF THE 80-FOOT-DIAMETER PARA-SAIL

By Leland C. Norman and Jerry C. Coffey
Manned Spacecraft Center

SUMMARY

This report documents the 80-foot-diameter Para-Sail parachute developmental test program conducted by the Landing Technology Branch of the NASA Manned Spacecraft Center. The Para-Sail evolution is traced from its inception as a towable, ascending parachute for sport to a demonstration of an 80-foot-diameter version meeting second generation spacecraft criteria. A detailed description of a preliminary test program conducted at Houston and the subsequent developmental test program conducted at the Joint Parachute Test Facility, El Centro, California, is included with a presentation of the raw test data and the analyses of the composite results.

INTRODUCTION

In the consideration of a land landing system for low lift-to-drag ratio spacecraft, the requirement exists for some means of offsetting horizontal drift induced by surface winds, since it is difficult to provide impact attenuation and post-impact stability if high horizontal velocities must be accommodated. As a possible solution, several types of gliding parachute systems have been evaluated. A gliding parachute can, by heading into the wind, negate a horizontal drift equal to its own forward speed. In mid-1962, preliminary evaluation of one of these gliding parachutes, called the Para-Sail, indicated L/D ratios of 0.8 to 1.0. Moreover, the canopy was found to be responsive to turn control.

The original configuration, shown in figure III-14, employed a central suspension line (centerline) which pulled the apex down to increase vertical drag area and decrease profile drag area. The canopy was designed as a towable, ascending parachute for sport use. The front was slotted to facilitate canopy filling at the initiation of tow, and two stabilization panels were added below the skirt for directional stability during tow.

Since the inclusion of a central suspension line which pulled the apex down inside the canopy presented a shape basically different from standard parachutes, the Para-Sail deployment and inflation characteristics were recognized as an important unknown. It was also recognized that the extremely low-porosity Para-Sail fabric might result in unusually high opening loads. In the development of a gliding parachute for a particular application, the normal practice was to select a standard canopy with good inflation characteristics and then to develop the required steady-state performance with a series of stepwise modifications, taking care not to introduce modifications which compromise inflation. Since this effort started with a canopy design essentially capable of meeting the steady-state performance requirements, it was necessary to plan a program designed to develop inflation techniques and to correct design deficiencies affecting inflation without compromising steady-state performance.

In September and October of 1962, 17 low-speed deployment tests of the 23.2-foot-diameter d_0 canopy, shown in figure III-14, were conducted at the Manned Spacecraft Center. These tests indicated that the Para-Sail could be packed and deployed in a conventional manner at velocities up to 120 knots when methods were employed which allowed the parachute to take a more normal hemispherical shape during opening. For this initial series, the Para-Sail was deployed with the centerline extended to permit normal apex-up inflation. These deployment tests were successful, although the front of the canopy exhibited a slight tendency to tuck in during inflation.

In conjunction with these deployment tests, the University of Minnesota began a wind-tunnel evaluation of 4-foot-diameter models in an effort to achieve a maximum L/D of at least 1.0. In December 1962, a Para-Sail model on which the front had been replaced with solid panels exhibited an L/D of 1.2. On the basis of information gained up to this point, a program was initiated through Pioneer Parachute Company, Incorporated, to investigate the inflation characteristics and performance of an 80-foot-diameter version of the Para-Sail.

DISCUSSION

Development of the large Para-Sail parachute has been a joint effort by MSC, Pioneer Parachute Company, and the University of Minnesota, with most of the exploratory work being conducted by the MSC at Houston. The initial configuration, shown in figure III-15, featured rear and side exhaust slots, two rows of turn slots on each side, the centerline pulling the apex down, three panel-width stabilization panels, and a scooped front similar to

the towable 23.2-foot d_0 parachute configuration. The three front gores were solid material (no slots). This configuration and the configuration having seven solid front gores (figs. III-16(a) and III-16(b)) exhibited a serious front tuck-in characteristic during inflation. While this same tendency had been evident in tests of the 23.2-foot-diameter canopies, it had been of short duration and the front panels would pop out to the fully inflated state. This was not always true of the larger canopy. As reefed inflation began, the rear of the canopy would open immediately and begin to glide while the front half would fold back against the centerline and rear of the canopy in an attempt to follow the stream lines created by air flowing into the skirt and out of the rear exhaust slots. The tucking in of the front gores during inflation presented an ideal situation for inversion, which was often the result as the canopy disreefed. The front, in tucking back, would essentially close the skirt. At disreef, the rear would open fully and increase forward velocity, driving still further over the tucked in front.

A permanent pilot parachute and bridle arrangement (fig. III-17) was added to the system to distribute the pilot parachute force evenly around the doughnut-shaped crown area. This bridle arrangement was an attempt to provide tension in the front gores which would prevent the front lip from dropping below the level of the rear canopy edge. The pilot parachute and bridle aided greatly in preventing inversion, but did not solve the basic aerodynamic tuck-in problem.

Analysis of the tests to this point indicated that the concept of a slotted front air-flow inlet area during inflation was aerodynamically unsound. The slots provided a means of internal-pressure escape and allowed the canopy to tuck back and follow the stream lines formed by air exiting through the rear exhaust slots. For the front to inflate and remain fully open during glide, sufficient internal pressure would have to exist to prevent tuck in.

A deployment investigation was initiated at MSC with 24-foot-diameter canopies on which the slotted front had been replaced with solid gores. The results of this study indicated that the solid front had a positive inflation tendency. With the slotted front 24-foot d_0 parachute models, the front would tuck in momentarily before popping out to the fully inflated state. With the solid front modification, this momentary tuck in did not occur, and the front was the first portion of the canopy to reach the fully inflated state.

In steady-state glide, the lower front panels would buckle slightly and flatten out in the profile plane. At the higher glide angles, positive pressure differential could not be maintained at the leading edge; leading edge buckling further increased canopy drag. To reduce the buckling tendency, the front skirt was modified with a semielliptical cutout, with a 12-inch maximum

height (fig. III-18). This configuration retained the positive inflation tendency during deployment, and the front buckling due to glide was significantly reduced. Wind-tunnel studies at the University of Minnesota indicated that the solid front and semielliptical cutout slightly increased L/D and did not adversely affect the rate of descent or stability. Based upon the results of the 24-foot-diameter parachute model drop-test program and the wind-tunnel studies, the 80-foot-Para-Sail configuration was modified to include the solid front and semielliptical cutout (figs. III-19(a) to III-19(c)). It should be noted that the stabilization panels were also reduced to single panel width. The 80-foot solid front parachute configuration showed a decrease in magnitude of the tuck in, but not an elimination of the basic tendency. The addition of pocket bands was ineffective.

One test was conducted in which the rear exhaust slot gores were zero reefed at the skirt in an attempt to prevent the rear portion of the canopy from inflating first and creating the strong airflow stream lines causing the front to tuck in. This also proved ineffective.

At this point, it was evident that the best solution was to alter the airflow stream lines during inflation. The University of Minnesota was directed to investigate the effect of an internal parachute as an inflation aid (fig. III-20). The internal parachute inflates first and acts as a stream-line deflector, providing a strong radial-flow component with respect to the axis of symmetry of the large parachute. This radial flow provides a force which tends to spread the cloth surface of the large canopy outward, resulting in an increased rate of change of the skirt inlet area. The strength of the radial flow is highest as main canopy inflation begins, and diminishes as the main canopy gains size. At the time of maximum force, the radial flow is quite weak. This provides an appreciable reduction in opening time without a correspondingly large increase in opening force.

After the wind-tunnel studies indicated the internal parachute was effective in producing symmetrical canopy inflation, a 10-foot-diameter guide-surface internal canopy was added to the system. Drop tests of the 80-foot Para-Sail with the internal parachute showed a marked improvement in inflation. Inflation in the reefed stage was essentially symmetrical, with good skirt inlet shape. The canopy opened rapidly to the fully inflated position after disreef, with no tuck-in tendency. The airflow during inflation, with and without the internal parachute, is diagramed in figure III-21.

At this point, the deployment and inflation characteristics were sufficiently improved to warrant extensive testing at the Joint Parachute Test Facility, El Centro, California. The test program conducted at Houston had been of a qualitative nature, with relatively low payload weights and deployment speeds. The first four tests at El Centro indicated that opening forces

were excessive, and the canopy could not withstand deployment at nominal airspeeds with a payload weight of approximately 4800 pounds. In earlier tests, it had proved necessary to close the slots in the doughnut-shaped crown area to allow development of an acceptable reefed shape. The reopening of these slots would reduce the reefed opening shock, but it would also result in the loss of reefed drag area and, consequently, a significant increase in full opening shock.

A wind-tunnel study was initiated to investigate the effect of removing the centerline and replacing the existing crown area with a flat, circular section. The results of these studies indicated a possible reduction of reefed opening loads with no adverse effect on L/D, stability, or rate of descent. Based upon these results, the 80-foot parachute configuration was modified by removing the centerline and replacing the crown area with a flat, circular section of 2-1/4-ounce ripstop. This configuration modification is shown in figures III-22(a) through III-22(c). The Para-Sail without centerline exhibited deployment characteristics similar to those of a conventional ringsail canopy; that is, a large, reefed airball and rapid opening after disreef. Trajectory data indicated a slight increase in L/D and an insignificant increase in rate of descent.

With the centerline removed, the question of the necessity of the internal parachute arose, since the canopy was allowed to take a more normal parachute shape during opening. One full-scale test was made with the internal parachute removed. During this test, the canopy streamed for approximately 3 seconds in the reefed state, then slowly began to fill, with a poorly formed and partially closed skirt opening. At disreef, the skirt flopped around randomly, with the front tucked in. Time from disreef to full inflation was 10.6 seconds, approximately three times that required with the internal parachute. Based upon the results of this test, the internal parachute was retained.

Testing up to this point had been conducted at altitudes up to 5000 feet, with weights up to 3700 pounds and dynamic pressures up to 50 lb/ft^2 . Figure III-23 shows the configuration at this stage, with the original scooped rear and turn slots; a solid front with the semielliptical cutout in the skirt; no centerline; a flat, circular crown; a 10-foot internal parachute; and a 6-foot vent parachute.

In additional tests, the altitude was increased to 10 600 feet, the weight to 4750 pounds, and the dynamic pressure to 64 lb/ft^2 . At this test condition, another deployment problem arose. In all prior tests, the stabilization panels had been tightly folded and tied off with multiple breakcords. During two tests, as the stabilization panels emerged from the bag at strip-off, the

breakcords failed; and the stabilization panels inflated through opposing suspension lines; causing partial canopy inversion and heavy damage during opening.

Full-scale testing was suspended, and a two-phase study was initiated: the first, a wind-tunnel evaluation of steady-state performance with the stabilization panels removed; and the second, a drop-test program with 24-foot-diameter canopies to develop a means of controlled retention of the stabilization panels during deployment. When the wind-tunnel investigation indicated the decrease in steady-state performance was negligible, a full-scale canopy was drop tested with the stabilization panels removed. Trajectory information from this test showed a 17 percent decrease in L/D and an 18 to 20 percent increase in rate of descent. In descent, the canopy appeared deeper and less elliptical, with excess fullness in the front.

The drop-test program with 24-foot-diameter canopies indicated that it is possible to control inflation of the stabilization panels without affecting the basic opening characteristics of the main canopy. This was done by zero reefing the stabilization panels independent of the skirt reefing and retaining the panels with breakcords. It was necessary to disreef the stabilization panels prior to skirt disreef to avoid excessive localized skirt loads. This controlled retention system was incorporated into full-scale testing and proved to be a satisfactory solution. The deployment investigation was concluded with two satisfactory tests from an altitude of 10 600 feet at a dynamic pressure of 80 lb/ft^2 and with a 4750-pound payload.

In addition to the deployment investigation, two fixed-turn tests were made to evaluate canopy rate-of-turn potential. The first, with one row of turn slots closed, resulted in an average rate of turn of approximately 12 deg/sec, and the second, with both rows of turn slots closed on one side, resulted in an average rate of turn of approximately 19 deg/sec.

RESULTS

Tables III-I and III-II contain a detailed description of each test, including configuration, rigging, and results. The preliminary test program conducted in Houston (table III-I) was of a qualitative nature and very little quantitative data were obtained. The results discussed in this section were obtained from the El Centro test program (table III-II).

Opening Loads

Figure III-24 presents the peak opening loads as a function of dynamic pressure. All data points are based upon comparable altitude, payload, and reefing parameters. The curve indicates that the 80-foot Para-Sail does not exceed the 16 000-pound opening force limit when deployed at a dynamic pressure of 80 lb/ft².

Opening Times

Figure III-25 presents the measured opening times as a function of dynamic pressure. Reefed filling time, shown as a solid line on the figure, decreases slightly as dynamic pressure increases, furnishing a value of approximately 1.25 seconds at 80 lb/ft². The dotted line, representing full-open filling time, was faired through the locus of points as a straight line, since the canopy reached a 1g condition prior to disreef in every case. These opening times are similar to those of conventional parachutes having close to optimum reefing parameters.

Riser-Load Distribution

Figures III-26 to III-28 present the individual riser loads and total load for three representative tests. Figure III-29 shows the portion of the canopy applying to each riser. The loads obtained from these figures indicate the following percentages of total load are distributed in the front, side, and rear riser groups during the peak opening forces and in steady state.

Riser group	Reefed opening	Full open	Steady state
Front, lines 25 to 36; 37 to 48	25.5	27.6	24.2
Sides, lines 13 to 24; 49 to 60	30.4	27.8	40.7
Rear, lines 1 to 12; 61 to 72	34.9	44.1	35.1
Internal parachute	9.2	.5	0

It should be noted that the opening peaks in the individual risers do not exactly align with the peaks in the total-force trace, due to the elasticity in the suspension system as well as slight variation in the rate of loading of different sections of the canopy.

Analysis of the films of various tests indicates that the rear portion of the canopy is the first to inflate in both the reefed and fully open states. This fact is borne out by the load distribution during opening. In steady-state descent, the canopy is elliptically shaped due to the radial force exerted by the stabilization panels. The long dimension of the ellipse is normal to the direction of flight. The canopy sides, being forced farther out, exert higher force than the front or rear. This fact is substantiated by the steady-state load distribution.

The Effect of Wing Loading on Steady-State Performance

In steady-state descent, the vertical velocity is a function of the projected area in the vertical direction, and the glide ratio is a function of both the horizontal and vertical velocities. When payload weight is increased, the projected drag area is decreased and, correspondingly, the profile, or frontal area, is increased. Therefore, it is assumed that heavier payloads will result in lower values for L/D and in higher rates of descent. The results of the test program indicate the validity of this assumption.

Figure III-30 presents glide ratio (L/D) as a function of wing loading. As shown in the figure, the L/D decreases uniformly with increased payload weight. An analysis of test films indicates that the canopy banks while in a turn, thereby rotating the lift vector, which, in turn, decreases the effective lift and increases the rate of descent. This effect varies with rate of turn. The dotted line in figure III-30 represents L/D while the canopy is rotating at approximately 20 deg/sec.

Figure III-31 presents the rate of descent as a function of wing loading and shows an evenly increasing rate of descent with increased canopy loading. Since the drop altitude varied from 5000 to 11 000 feet, rates of descent are based upon an altitude of 3000 feet to allow uniform comparison. The thermal interference at low altitudes prevents sea-level comparison. The rates of descent at sea level will be approximately 4 percent lower than the values at 3000 feet. The dotted line in figure III-31 represents the increased rate of descent while the canopy is rotating at approximately 20 deg/sec. A cross plot of L/D and rate of descent obtained from the two wing-loading curves is presented in figure III-32.

Oscillation

During the development program, the Para-Sail exhibited essentially zero oscillation in steady-state descent. Efforts were made to measure oscillation from the cine-theodolite and Contraves film coverage of the various

tests. All of the attempted oscillation measurements indicated maximum excursions on the order of $\pm 1^\circ$.

Evaluation of the Internal Parachute as an Inflation Aid

When the canopy was modified by removal of the centerline and replacement of the crown area with a solid flat section, the parachute was allowed to take a more normal parachute shape during opening. To reevaluate the necessity of the internal parachute as an inflation aid, comparative tests were conducted with and without the internal parachute. Figure III-33 presents the force-time histories for these two tests. Analysis of the figure shows the following opening times:

	With internal parachute	Without internal parachute
Reefed filling time, sec	1.9	No reefed peak
Disreef to full opening shock, sec . . .	1.3	9.1
Disreef to full inflation, sec	3.7	10.6

A comparison of the force buildup indicates that the canopy with the internal parachute exhibited a reasonably smooth buildup to reefed opening shock, decelerated in a steady reefed state, and opened immediately following disreef. Without the internal parachute, the force record indicates that the canopy failed to reach a fully inflated reefed condition, and the canopy was unable to inflate fully for several seconds following disreef. Analysis of the film from the test without the internal parachute showed the canopy front was severely tucked back, partially closing the skirt following disreef.

Internal-Parachute Behavior

Figures III-34 through III-36 present the force-time record of the internal canopy compared with the total-load record of the Para-Sail for three representative tests. As shown in the figures, the internal canopy opens immediately after line stretch and forms the symmetrical flow pattern for air entering the skirt. As the Para-Sail reaches maximum reefed force and continues to inflate in the reefed state, the load on the internal parachute decreases. At disreef, the internal parachute remains inflated until the canopy sides move outward; then it collapses.

A study of the test films shows that the radial flow about the internal parachute maintains a fully open Para-Sail skirt during reefed inflation, and the internal parachute normally remains open until after Para-Sail disreef. In some cases, the internal parachute collapses after the fully reefed state is attained, then reinflates at main disreef until the maximum full-open load is reached. The collapsed internal parachute does not affect steady-state operation of the Para-Sail.

Fixed-Turn Potential

Two tests were conducted to investigate the turning characteristics. In each case, the turn line was tied to suspension-line connector links while the canopy was in tension on the packing table. For the first test, one row of turn vents was closed. This resulted in an average time of 39.4 seconds for one 360° turn, or a turn potential of slightly over 9 deg/sec. For the second test, both rows of turn vents were closed. This resulted in an average time of 18.95 seconds for one 360° turn, or a turn potential of 19 deg/sec.

Effect of Stabilization Panels on Steady-State Performance

During the deployment investigation, preinflation of the stabilization panels resulted in two malfunctions. An investigation was conducted to determine the effect of stabilization panel removal on steady-state performance. When wind-tunnel studies indicated the degradation was negligible, a full-scale canopy was drop tested with the stabilization panels removed. Figure III-37 presents the L/D data obtained from this test as compared with those of the canopy with stabilization panels, under identical conditions. Average values derived from these curves indicate a decrease in L/D of approximately 17 percent when the stabilization panels are removed. Figure III-38 presents rate-of-descent information for the same two tests. At 5000 feet, the average rates of descent indicate an increase of 20 percent when the stabilization panels are removed.

Analysis of the films from this test indicates the canopy without stabilization panels is deeper and less elliptical, with excess fullness in the front. Minor oscillation in the fore-and-aft direction was also noted. The stabilization panels, in addition to providing directional (yaw axis) stability, obviously have a significant effect on general canopy shape. The outward spanwise force generated by these panels is required on present Para-Sail configurations to provide acceptable overall performance.

CONCLUSIONS

During the 80-foot d_0 Para-Sail parachute development program, significant modifications were made to the original design as follows:

1. The idea of a scooped front, providing an airflow inlet area, proved to be aerodynamically unsound for inflation since the scoops prevented the front gores from maintaining positive internal pressure. The slotted front gores were replaced with solid ones to allow retention of positive pressure, and to provide a lifting surface similar to a crude airfoil. A semielliptical cutout was added to the front lip to reduce leading-edge buckle due to glide.

2. The centerline pulling the apex down in the original configuration was designed to achieve better glide by increasing the vertical drag area and decreasing the profile drag area. During the development program, this design feature produced opening loads which were high and poorly distributed. The centerline was removed, and the crown area was replaced with a flat, circular section to allow more normal parachute opening and lower opening forces. Wind-tunnel studies indicated there was no decrease in L/D when the centerline was removed.

3. The stabilization panel area was reduced from approximately 16 percent to approximately 4 percent of the total area to alleviate deployment difficulties. This reduction in stabilization panel size had no detrimental effect on steady-state performance. Comparative tests to determine the necessity of the smaller stabilization panels indicated that these panels increased stability and L/D and decreased the rate of descent by forcing the canopy into a more elliptical planform.

The strong stream lines formed by air entering the skirt and exiting through the rear exhaust slots caused the front gores to tuck back toward the rear during the opening process. It was necessary to add a 10-foot-diameter internal parachute to the system to act as a stream-line deflector, and to direct a portion of the entering air to the front half of the canopy. The addition of the internal parachute provided a reliable opening process for the Para-Sail. Wind-tunnel studies were conducted to determine the approximate size and location of the internal parachute, but these parameters have never been completely optimized.

During the development program, the 80-foot-diameter Para-Sail met the following performance parameters:

Suspended weight, lb	4 750
Deployment altitude, ft	10 600
Deployment dynamic pressure, lb/ft ²	80
Rate of descent (at 5000-ft pressure altitude), ft/sec	24 to 25
Lift-to-drag ratio, max	1.0
Rate of turn, deg/sec	19
Stability, maximum oscillation, deg	±3
Maximum opening force (at 80 lb/ft ²), lb	16 000

TEST DESCRIPTION AND RESULTS

Test H1 - Houston, Texas, March 8, 1963

Objective. - Test H1 was the first attempted deployment of a Para-Sail parachute larger than 24 feet in diameter. The objective of this test was to determine the preliminary deployment characteristics.

Configuration. - I (fig. III-15 and table III-I).

Deployment system. - A 7.9 percent reefing line; bag stripped off; and two reefing cutters with a 6-second delay.

Payload weight. - 2500 pounds.

Launch conditions. - 110 knots, 2000 feet.

Results. - The front of the canopy tucked in at inflation and stayed in for 19 seconds, then came out for a fully inflated descent. Since this was a qualitative and not a quantitative test, no load data were obtained. Analysis of the film showed that in the reefed state the skirt was malformed and essentially closed, with the rear of the canopy inflating first and the front of the canopy folding against the centerline and back to the rear of the canopy. At disreef, the rear half of the canopy inflated fully, while the entire front half of the canopy folded back. The rate of descent was approximately 15 ft/sec.

Test H2 - Houston, Texas, March 12, 1963

Objective. - The objective of this test was to determine the effect of an increased reefing-line length on the deployment characteristics.

Configuration. - I (fig. III-15 and table III-I).

Deployment system. - A 14.2 percent reefing line; bag stripped off; and two reefing cutters with a 6-second delay.

Payload weight. - 2500 pounds.

Launch conditions. - 110 knots, 2600 feet.

Results. - The front of the canopy tucked in through the suspension lines at inflation and inflated inverted. In the reefed state, the skirt was malformed and essentially closed, with the rear of the canopy inflated fully,

and the front half of the canopy folded back against the centerline and the rear of the canopy. At disreef, the rear of the canopy inflated fully; and the front half tucked all the way back to the rear of the canopy, where a portion of the front skirt inflated inverted through two of the side suspension lines. The canopy was severely damaged.

Test H3 - Houston, Texas, March 28, 1963

Objective. - The objective of this test was to determine the deployment characteristics of the slotted front canopy with seven solid gores.

Configuration. - II (fig. III-16(a) and table III-I).

Deployment system. - A 14.2 percent reefing line; bag stripped off; and two reefing cutters with a 6-second delay.

Payload weight. - 2500 pounds.

Launch conditions. - 125 knots, 2600 feet.

Results. - The canopy inflated slowly in the reefed state, with the rear of the canopy fully inflated and the front half folded back against the centerline at the rear of the canopy. The skirt was malformed and essentially closed during reefed inflation. At disreef, the front right side and right stabilization panel tucked through adjacent suspension lines and inflated inverted, which caused serious canopy damage.

Test H4 - Houston, Texas, April 26, 1963

Objective. - The objective of this test was to determine the deployment characteristics and to evaluate the attempted means of preventing front tuck in.

Configuration. - III (fig. III-16(b) and table III-I). A 9-foot, 36-line bridle was attached to the permanent pilot parachute in an attempt to maintain an even force around the doughnut-shaped crown during inflation.

Deployment system. - The pilot parachute was permanently attached; and there was no skirt reefing for this test.

Payload weight. - 2500 pounds.

Launch conditions. - 125 knots, 2600 feet.

Results. - The addition of the pilot-parachute bridle arrangement appeared to decrease the severity of the front tuck in, but did not eliminate the tendency. The front tucked in at inflation, then came out slowly for a fully inflated descent. The crown area of the canopy was prevented from blossoming fully by the pilot parachute bridle, and it appeared to be pinched in.

Test H5 - Houston, Texas, May 2, 1963

Objective. - The objective of this test was to evaluate deployment characteristics, and to determine if the increased bridle length to the pilot parachute would decrease crown pinching.

Configuration. - III (fig. III-16(b) and table III-I). The bridle to the pilot parachute was increased in length to 18-1/2 feet in an attempt to prevent crown-area pinching.

Deployment system. - Same as test H4.

Payload weight. - 2500 pounds.

Launch conditions. - 125 knots, 2600 feet.

Results. - The front of the canopy tucked in at initial inflation, and the skirt panel of the front gore tucked through the two suspension lines in the rear center gore and partially inflated, holding the front at the rear of the canopy for the entire descent.

Test H6 - Houston, Texas, June 4, 1963

Objective. - The objective of this test was to evaluate the deployment characteristics of the solid front configuration.

Configuration. - IV (fig. III-19(a) and table III-I).

Deployment system. - A 36-line bridle to the permanently attached pilot parachute; and there was no reefing.

Payload weight. - 2500 pounds.

Launch conditions. - 110 knots, 2600 feet.

Results. - The front of the canopy tucked in during initial inflation, indicating the airflow was through the skirt and out through the rear exhaust

slots. The front of the canopy folded back in an attempt to follow the air stream. The solid front indicated an improved tendency to inflate to a normal shape after initial tuck in. The canopy inflated very slowly for a fully inflated descent.

Test H7 - Houston, Texas, June 11, 1963

Objective. - The objective of this test was to determine the effectiveness of zero reefing the rear gores during deployment as a means of preventing front tuck in.

Configuration. - IV (fig. III-19(a) and table III-I).

Deployment system. - The pilot parachute was permanently attached to the vent area with a 36-line bridle; the rear 21 gores were zero reefed at the skirt; and there was no full skirt reefing.

Payload weight. - 3600 pounds.

Launch conditions. - 110 knots, 2600 feet.

Results. - As seen in the previous tests, the front tucked back during the initial inflation. As the rear portion of the canopy began to inflate, the 2000 pound rear-gore reefing line failed, and one rear gore blew, excluding the skirt and vent band. The front of the canopy came out slowly to the fully inflated condition. In addition to the blown rear gore, seven rear exhaust panels failed.

Test H8 - Houston, Texas, July 3, 1963

Objective. - Analysis of prior tests indicated a differential height of 4 feet 3 inches between the front and rear of the canopy during inflation, caused by the rear of the canopy inflating first. The objective of this test was to evaluate deployment characteristics with the rear risers foreshortened.

Configuration. - V (fig. III-19(b) and table III-I). Pocket bands were added to the 21 solid front gores.

Deployment system. - The pilot parachute was permanently attached; the rear risers were pulled down 4 feet 3 inches; and there was no skirt reefing.

Payload weight. - 3600 pounds.

Launch conditions. - 110 knots, 2600 feet.

Results. - The front center gore and two rear gores blew during inflation, including the skirt band but not the vent band. The front tucked in, then came out slowly. The canopy was severely damaged.

Test H9 - Houston, Texas, July 9, 1963

Objective. - The objective of this test was to evaluate deployment characteristics with an internal parachute added to the system.

Configuration. - VI (fig. III-19(c) and table III-I).

Deployment system. - The pilot parachute was permanently attached; a 13.4 percent reefing line was used; and two reefing cutters with a 6-second delay.

Payload weight. - 2500 pounds.

Launch conditions. - 110 knots, 2600 feet.

Results. - The canopy inflated with the front crown tucked in, and, for the first time, the skirt had a reasonably good shape. The reefing line failed, and the canopy opened rapidly, then made a fully inflated descent. Analysis of the film indicated the reefing-line failure was due to the rear of the canopy inflating first, causing an uneven skirt, thereby transmitting suspension-line loads to the reefing line. This test marked a significant improvement in the deployment characteristics since, for the first time, the front of the canopy demonstrated a positive inflation tendency. The front crown tuck in was attributed to the pressure relief slots in the rear crown area.

Test H10 - Houston, Texas, July 16, 1963

Objective. - The objective of this test was to investigate deployment with an internal parachute. The rear crown-area slots were closed in an attempt to eliminate the tuck in on the front crown, and the rear risers were pulled down 4 feet 3 inches to effect an even skirt during inflation.

Configuration. - VI (fig. III-19(c) and table III-I).

Deployment system. - A permanent pilot parachute; a 14.5 percent reefing line; a 4 foot 3 inch pull down on rear risers; and two reefing cutters with a 6-second delay.

Payload weight. - 2500 pounds.

Launch conditions. - 110 knots, 2600 feet.

Results. - The canopy inflated in the reefed state, with a very large reefed airball, front crown tuck in, and a good skirt shape. At disreef, the canopy opened rapidly and evenly to the fully inflated state. This test demonstrated the marked improvement in deployment brought about by the inclusion of the internal parachute. The closing of the rear exhaust slots did not eliminate the front crown tuck in, but did decrease the magnitude of the tuck in. Damage was limited to two blown rear panels.

Test H11 - Houston, Texas, July 23, 1963

Objective. - This test was conducted to evaluate deployment quantitatively. The pilot parachute confluence was removed in an attempt to eliminate the front crown tuck in.

Configuration. - VI (fig. III-19(c) and table III-I).

Deployment system. - The pilot parachute confluence was removed by attaching the pilot parachute suspension lines directly to the canopy crown loops; a 14.5 percent reefing line; a 4 foot 3 inch pull down on rear risers; and two reefing cutters with a 6-second delay.

Payload weight. - 3500 pounds.

Launch conditions. - 110 knots, 2400 feet.

Results. - The reefed airball was very large, and reefed opening shock was 11 200 pounds. At disreef, the canopy opened rapidly and evenly to the fully inflated state, and the opening shock was 8900 pounds. The pilot parachute, with no confluence point, was considered ineffective. At this point, the deployment was considered sufficiently solved to warrant continued testing at El Centro and the termination of the Houston drop-series tests.

Test 1 - El Centro, California, June 11, 1963

Objective. - This was a functional test to determine the deployment characteristics of the parachute and to verify the C-130 drop system. This was a repeat of Test H11 in Houston.

Configuration. - VI (fig. III-19(c) and table III-II). Pocket bands were added to the front 21 gores; a 10-foot internal parachute; and a 36-line bridle to pilot parachute.

Deployment system. - Permanent pilot parachute with no confluence point; a 4 foot 3 inch pull down on rear risers; a 14.5 percent reefing; and two reefing cutters with a 6-second delay.

Payload weight. - 3782 pounds.

Launch conditions. - 119 knots, 4950 feet.

Results. - The canopy inflated with the front crown tucked in. The canopy had a good skirt shape and a very large reefed airball. Full inflation occurred in 10.8 seconds. The pilot parachute collapsed on reefed opening. The rate of descent was approximately 19 ft/sec. No load data were taken. Only minor burn damage was sustained on a few panels.

Test 2 - El Centro, California, August 12, 1963

Objective. - The objective of this test was to study further deployment and inflation characteristics of the 80-foot Para-Sail and to obtain the rate of descent, lift-to-drag ratio, and opening forces.

Configuration. - VI (fig. III-19(c) and table III-II). A permanent pilot parachute with a confluence point; the rear riser released to full extension with 20-second cutters; a 2000-pound, 14.5 percent reefing line; and two reefing cutters with a 6-second delay.

Deployment system. - Same as test 1.

Payload weight. - 3738 pounds.

Launch conditions. - 120 knots, 5020 feet.

Actual launch conditions. - $q = 40 \text{ lb/ft}^2$, 5350 feet.

Results. - The canopy inflated with the front crown tucked in, a very large reefed airball, and a good skirt shape. Full inflation occurred in 9.2 seconds. No force data were obtained because of a strain-link failure. The vertical accelerometer indicated a reefed opening shock of 11 950 pounds and a disreefed opening shock of 9700 pounds. Damage was limited to a split in one rear main-seam tape. The rate of descent was 19 ft/sec, with an L/D of 1.15.

Test 3 - El Centro, California, August 15, 1963

Objective. - The objective of this test was to study further the deployment and inflation characteristics; to obtain the rate of descent, lift-to-drag ratio, and opening forces; and to determine the effect on deployment characteristics caused by an increased payload weight.

Configuration. - VI (fig. III-19(c) and table III-II).

Deployment system. - Same as test 1.

Payload weight. - 4998 pounds.

Launch conditions. - 120 knots, 5000 feet.

Actual launch conditions. - $q = 41 \text{ lb/ft}^2$, 5325 feet.

Results. - The canopy inflated with the front crown tucked in and with a good skirt shape. The reefed airball grew very large; then the two rear risers failed where the riser release was stitched. The failure load was 16 700 pounds. The rate of descent was approximately 60 ft/sec. The rear of the canopy was severely damaged.

Test 4 - El Centro, California, August 27, 1963

Objective. - The objective of this test was the same as test 3.

Configuration. - VI (fig. III-19(c) and table III-II).

Deployment system. - Same as test 1, except for a 12.35 percent reefing line.

Payload weight. - 4998 pounds.

Launch conditions. - 120 knots, 5000 feet.

Actual launch conditions. - $q = 45 \text{ lb/ft}^2$, 5300 feet.

Results. - The deployment bag ripped free of the bridle and failed the pilot parachute bridle. The pilot parachute bridle rebounded into the main vent and released the centerline. The apex of the canopy came up after centerline failure and failed when the first airball hit it with a force of 12 000 pounds. The suspension lines separated from the canopy after disreef. The telemeter pack and the cameras were destroyed, and the canopy was severely damaged.

Test 5 - El Centro, California, September 25, 1963

Objective. - The objective of this test was to investigate the deployment characteristics of the canopy with the centerline removed and the crown area replaced with a flat circular section.

Configuration. - VII (fig. III-22(a) and table III-II). The centerline to the apex was removed, and the crown area was replaced with 2.25-ounce rip-stop with reinforcing tape, which made the parachute biconical. The vent size was increased to 5 feet in diameter.

Deployment system. - An 11.4 percent reefing line; a 10-ft-diameter guide-surface internal parachute; an 8-ft-diameter guide-surface pilot parachute attached to the vent; and two reefing cutters with a 6-second delay.

Payload weight. - 2785 pounds.

Launch conditions. - 120 knots, 5000 feet.

Actual launch conditions. - $q = 45 \text{ lb/ft}^2$, 5300 feet.

Results. - The canopy was very slow to inflate in the reefed state, with looseness in the crown area indicating that the vent area was near the inlet area. The maximum reefed opening shock was 4000 pounds, with a disreefed opening shock of 9300 pounds. The system exhibited a very stable steady-state descent at a descent rate of approximately 15.5 ft/sec and a lift-to-drag ratio of 1.2. The cover of one vent line was broken by the pilot parachute bridle.

Test 6 - El Centro, California, October 2, 1963

Objective. - The objective of this test was to investigate the effect of increased reefing-line length on the modified configuration.

Configuration. - VIII (fig. III-22(b) and table III-II).

Deployment system. - A 13 percent reefing line; a 10-ft-diameter guide-surface internal parachute; an 8-ft-diameter guide-surface pilot parachute attached to the vent; and two reefing cutters with a 6-second delay.

Payload weight. - 2785 pounds.

Launch conditions. - 120 knots, 5035 feet.

Actual launch conditions. - $q = 34.5$ ft/sec, 5300 feet.

Results. - The canopy inflated slowly in the reefed state to an almost filled condition at disreef. In the reefed state, the canopy sides in the lateral scoop area were folded. Reefed opening shock was 6600 pounds, with an excellent disreef, and an opening shock of 7600 pounds. The descent of the parachute was very stable. Three vent covers were broken by the pilot parachute bridle.

Test 7 - El Centro, California, October 8, 1963

Objective. - The objective of this test was to investigate the deployment characteristics of the modified configuration with the internal parachute removed.

Configuration. - VII (fig. III-22(b) and table III-II).

Deployment system. - A 13 percent reefing line; no internal parachute; and two reefing cutters with a 6-second delay.

Payload weight. - 2775 pounds.

Launch conditions. - 120 knots, 4930 feet.

Actual launch conditions. - $q = 43.5$ lb/ft², 5200 feet.

Results. - The canopy streamed for approximately 3 seconds in the reefed state, then slowly began to fill. The canopy was only partially filled

at disreef and had a poorly shaped skirt. The reefed opening shock was 4960 pounds. At disreef, the skirt flapped around randomly, with the front tucked in, then inflated, with the front coming out last. The disreef opening shock was 6790 pounds. The time from disreef to full inflation was approximately 7 seconds. Suspension line 70 broke at the skirt. Gores 41 and 42 sustained horizontal tears in the taffeta on panel 2 at the reinforcing tape. A comparison of test 6 with test 7 indicates the necessity for the internal parachute.

Test 8 - El Centro, California, October 22, 1963

Objective. - The objective of this test was to evaluate the deployment characteristics at design altitude.

Configuration. - VII (fig. III-22(b) and table III-II).

Deployment system. - A 13 percent reefing line; a 10-ft-diameter guide-surface internal parachute; an 8-ft-diameter guide-surface pilot parachute attached to the vent; and two reefing cutters with a 6-second delay.

Payload weight. - 2785 pounds.

Launch conditions. - 120 knots, 10 600 feet.

Actual launch conditions. - $q = 39 \text{ lb/ft}^2$, 11 100 feet.

Results. - The canopy inflated symmetrically in the reefed state and held a round airball. The reefed opening shock was 7800 pounds, with an even, symmetrical, and steady skirt. An excellent disreef was observed, with a disreefed opening shock of 5680 pounds. The canopy made a long, gliding descent, with no damage.

Test 9 - El Centro, California, October 29, 1963

Objective. - The objective of this test was to determine the effect on deployment characteristics of an increased payload weight at design altitude.

Configuration. - VIII (fig. III-22(b) and table III-II).

Deployment system. - A 12.35 percent reefing line; a 10-ft-diameter guide-surface internal parachute; an 8-ft-diameter guide-surface pilot parachute attached to vent; and two reefing cutters with a 6-second delay.

Payload weight. - 3880 pounds.

Launch conditions. - 119 knots, 10 590 feet.

Results. - As the stabilization panels emerged from the bag during strip off, the breakcord failed, thus allowing the left stabilization panel to unfold and inflate. The left stabilization panels pulled the bottom skirt panel out and inflated it. At this point, the upper canopy was still emerging from the bag, and there was no tension on the system. As the lower skirt panel inflated, it jerked the pleated canopy to one side, which then caused an entanglement. The remainder of the canopy filled. At disreef, several suspension lines failed, and the canopy streamed. Reefed opening shock was 7330 pounds. Preliminary examination indicated that the malfunction was caused by improper rigging of the stabilization ties. The vehicle impacted at approximately 100 ft/sec.

Test 10 - El Centro, California, November 6, 1963

Objective. - The objective of this test was to determine the effect on deployment characteristics of an increased payload weight at design altitude.

Configuration. - VIII (fig. III-22(b) and table III-II).

Deployment system. - A 12.4 percent reefing line; a 10-ft-diameter guide-surface internal parachute; an 8-ft-diameter guide-surface pilot parachute attached to the vent; and three reefing cutters with a 6-second delay.

Payload weight. - 3860 pounds.

Launch conditions. - 119 knots, 10 600 feet.

Actual launch conditions. - $q = 31.5 \text{ lb/ft}^2$, 11 000 feet.

Results. - The canopy inflated symmetrically in the reefed state and held a large, round airball. Reefed opening shock was 10 580 pounds, with an excellent disreef and a disreef opening shock of 8600 pounds. The canopy made a long spiraling descent, indicating a slight built-in turn.

Test 11 - El Centro, California, November 27, 1963

Objective. - The objective of this test was to determine the deployment characteristics at design payload weight and design altitude.

Configuration. - VIII (fig. III-22(b) and table III-II).

Deployment system. - Same as test 10.

Payload weight. - 4750 pounds.

Launch conditions. - 120 knots, 10 600 feet.

Actual launch conditions. - $q = 37 \text{ lb/ft}^2$, 10 750 feet.

Results. - The stabilization panel breakcord failed as the stabilization panels emerged from the bag during strip off. The left stabilization panel inflated inverted and pulled a large portion of the canopy through two suspension lines. The main canopy blew at disreef and descended with four gores blown. The reefed opening shock was 13 400 pounds. The descent rate was approximately 80 ft/sec.

Test 12 - El Centro, California, December 18, 1963

Objective. - The objective of this test was to determine the effectiveness of hesitator bags as a means of controlling the deployment of the stabilization panels.

Configuration. - VIII (fig. III-22(b) and table III-II).

Deployment system. - A 12.4 percent reefing line; hesitator bags on the stabilization panel; the same internal parachute and pilot parachute as in test 5; and three reefing cutters with a 6-second delay.

Payload weight. - 4755 pounds.

Launch conditions. - 120 knots, 10 600 feet.

Actual launch conditions. - $q = 46 \text{ lb/ft}^2$, 10 750 feet.

Results. - The canopy inflated rapidly to a large, symmetrical airball in the reefed shape. The reefed opening shock was 14 100 pounds. The canopy disreefed evenly, with an opening shock of 13 800 pounds. The canopy

made a long spiraling descent, indicating a slight built-in turn. Analysis of the film indicated that the hesitator bags blew off at line stretch and were therefore ineffective.

Test 13 - El Centro, California, December 19, 1963

Objective. - The objective of this test was to determine the deployment and steady-state characteristics of the canopy with the stabilization panels removed.

Configuration. - VIII (fig. III-22(b) and table III-II) with the stabilization panels removed.

Deployment system. - A 12.4 percent reefing line; a 10-ft-diameter guide-surface internal parachute; an 8-ft-diameter guide-surface pilot parachute attached to the vent; and two reefing cutters with a 6-second delay.

Payload weight. - 2820 pounds.

Launch conditions. - 120 knots, 10 600 feet.

Actual launch conditions. - $q = 49 \text{ lb/ft}^2$, 10 900 feet.

Results. - The canopy inflated rapidly to a very large reefed airball. The reefed opening shock was 8675 pounds. The disreef was rapid and even, with an opening shock of 6400 pounds. The loss of steady-state stability was evident. The preliminary rate of descent was approximately 12 percent higher than the previous tests with stabilization panels.

Test 14 - El Centro, California, January 13, 1964

Objective. - The objective of this test was to investigate the use of zero reefing the stabilization panels as a means of controlling their deployment.

Configuration. - VIII (fig. III-22(b), and table III-II).

Deployment system. - A 12.4 percent reefing line; stabilization panels were zero reefed with 4-second cutters; 1000-pound braided suspension line 37 was inadvertently left on from the previous test; the same internal and pilot parachutes as test 5; and three reefing cutters with a 6-second delay.

Payload weight. - 4750 pounds.

Launch conditions. - 140 knots, 10 600 feet.

Actual launch conditions. - $q = .73 \text{ lb/ft}^2$, 10 300 feet.

Results. - The canopy was damaged during reefed inflation. The front reefing rings pulled off, and two gores split in the front pressure area. The damage was attributed to the uneven skirt loading caused by the 1000-pound suspension line which was inadvertently left on from the previous test. Reefed opening shock was 15 900 pounds. The vehicle was recovered with no damage. The average rate of descent was 25 ft/sec.

Test 15 - El Centro, California, January 29, 1964

Objective. - This test was a repeat of test 14, with the 1000-pound braided-nylon suspension line 37 replaced by a 550-pound suspension line.

Configuration. - VIII (fig. III-22(b) and table III-II).

Deployment system. - A 12.4 percent reefing line; stabilization panels were zero reefed with 4-second cutters, and the 1000-pound suspension line inadvertently retained on test 13 was replaced by a 550-pound line; and three reefing cutters with a 6-second delay.

Payload weight. - 4750 pounds.

Launch conditions. - 140 knots, 10 600 feet.

Actual launch conditions. - $q = 65 \text{ lb/ft}^2$, 11 000 feet.

Results. - The reefing line failed before disreef. The reefed opening shock was 16 000 pounds. The full open shock was 16 600 pounds. Damage was limited to one split gore in the pressure area. The vehicle was recovered without damage. The rate of descent was 25 ft/sec.

Test 16 - El Centro, California, February 11, 1964

Objective. - This test was a repeat of test 15, with a 1500-pound tubular reefing line.

Configuration. - IX (fig. III-22(c) and table III-II). Reinforcing tapes were added in the crown area.

Deployment system. - A 12.4 percent, 1500-pound tubular reefing line; and two reefing cutters with a 6-second delay.

Payload weight. - 4750 pounds.

Launch conditions. - 140 knots, 10 600 feet.

Actual launch conditions. - $q = 71 \text{ lb/ft}^2$, 10 700 feet.

Results. - The canopy inflated to a very large, reefed, airball shape, with a reefed opening shock of 15 000 pounds. The canopy disreefed evenly, with an opening shock of 11 000 pounds. Two panels burned and blew in the pressure area during reefed inflation. Preliminary investigation indicates that the burn damage was caused by the upper canopy tie and the internal parachute riser not being sleeved.

Test 17 - El Centro, California, March 4, 1964

Objective. - The objective of this test was to increase the deployment dynamic pressure to 80 lb/ft^2 at design weight and altitude.

Configuration. - IX (fig. III-22(c) and table III-II).

Deployment system. - A 12.4 percent, 1500-pound braided nylon reefing line; and two reefing cutters with a 6-second delay.

Payload weight. - 4750 pounds.

Launch conditions. - 155 knots, 10 595 feet.

Results. - The canopy inflated to a reefed shape slightly smaller than in earlier tests. At disreef, the canopy inflated rapidly and evenly to the fully inflated state. Two panels were blown, and there were a few small burns. No force data were obtained due to a telemetry failure.

Test 18 - El Centro, California, March 9, 1964

Objective. - The objective of this test was to determine the rate of turn of the canopy with one row of turn slots closed.

Configuration. - IX (fig. III-22(c) and table III-II).

Deployment system. - A 12.4 percent, 1500-pound reefing line; the canopy was deployed by sled extraction; and three reefing cutters with a 6-second delay.

Payload weight. - 4750 pounds.

Launch conditions. - 105 knots, 10 600 feet.

Actual launch conditions. - $q = 31.5 \text{ lb/ft}^2$, 10 850 feet.

Results. - The reefed opening shock was 11 500 pounds, and the full opening shock was 13 700 pounds. The canopy descended in a spiraling turn at a rate of 12 deg/sec.

Test 19 - El Centro, California, March 13, 1964

Objective. - The objective of this test was to determine the performance of the canopy when deployed at design altitude, dynamic pressure, and weight.

Configuration. - IX (fig. III-22(c) and table III-II).

Deployment system. - A 12.4 percent, 1500-pound reefing line; and two reefing cutters with a 6-second delay.

Payload weight. - 4750 pounds.

Launch conditions. - 155 knots, 10 600 feet.

Results. - The canopy inflated rapidly to an excellent reefed shape. The reefed opening shock was 14 400 pounds. At disreef, the canopy opened rapidly and evenly to the full-open state, with a full-open shock of 12 600 pounds. Damage was limited to one blown number 10 panel and several small burns.

Test 20 - El Centro, California, March 18, 1964

Objective. - The objective of this test was to determine the rate of turn with both rows of turn slots closed.

Configuration. - IX (fig. III-22(c) and table III-II).

Deployment system. - A 12.4 percent, 1500-pound reefing line; the test vehicle and canopy were sled extracted; and two reefing cutters with a 6-second delay.

Payload weight. - 4750 pounds.

Launch conditions. - 105 knots, 10 600 feet.

Results. - The reefed opening shock was 12 000 pounds, with a full opening shock of 14 750 pounds. The canopy descended in a spiraling turn at a rate of 19 deg/sec. Damage was limited to light burns in the crown area.

APPENDIX C - RESULTS AND ANALYSES OF DROP TESTS

WITH A 70-FOOT-DIAMETER PARA-SAIL

By L. R. Jameson, Jr., W. J. Everett, and E. D. Vickery

RESULTS AND ANALYSES OF DROP TESTS

WITH A 70-FOOT-DIAMETER PARA-SAIL

By L. R. Jameson, Jr., W. J. Everett, and E. D. Vickery
Pioneer Parachute Company, Inc.

SUMMARY

The 70-foot version of the Para-Sail was based upon refinement of the final 80-foot configuration (80A-9). After the final 70-foot configuration was fixed by wind-tunnel and analytical studies, a drop-test program was conducted to verify deployment and steady-state performance characteristics. The completed drop-test program showed that the improved version of the Para-Sail was capable of recovering a suspended weight of 4750 pounds from an altitude of 10 600 feet at a speed of 188 KEAS (equivalent air speed in nautical miles per hour). The lift-to-drag ratio exceeded unity, the rate of turn amounted to approximately 48 deg/sec, and an average rate of descent at sea level of 27 ft/sec was recorded.

INTRODUCTION

To develop and to verify the performance of the final parachute configuration, the Pioneer Parachute Company was awarded Contract NAS 9-2860 on April 27, 1964. In scope, this program required the development of a Para-Sail configuration demonstrating the following performance characteristics:

Suspended weight, lb	4 750
Deployment pressure altitude, ft	10 600
Deployment q , design testing, lb/ft ²	80
Deployment q , strength testing (1.5 design q), lb/ft ²	120
Rate of descent (at 5000 ft, pressure altitude), ft/sec	30

Lift-to-drag ratio (maximum)	(at least) 1.0
Turn rate (maximum), deg/sec	(at least) 20
Maximum shock force at design q, lb	16 000
Steady-state stability, deg	±3
Parachute system weight and volume	minimized

The first phase of the contractual effort was to design a canopy capable of meeting the required performance. Descriptions of the deployment system and the parachute configuration will be discussed in this section. The two configuration identities (70A-4 and 70A-5) reflect a change in material from 2-ounce taffeta to 2-ounce low-porosity rip stop and the addition of reinforcing tapes. The basic planform was identical for both configurations.

The second phase was to perform a series of full-scale drop tests to verify the performance characteristics of the designed configuration. The series of drop tests adopted for this program was performed at the Joint Parachute Test Facility, El Centro, California, using standard data-recording and film-coverage techniques. Fourteen tests of the 70-foot version of the parachute were conducted, and all were adjudged successful. The measurements of the pertinent data will be presented, including the results from visual observations of the drop tests.

The Pioneer Parachute Company conducted the development and test program of the 70-foot-diameter Para-Sail parachute under NASA-MS Contract No. NAS 9-2860. The results of this program are presented in nine separate documents.

1. The Drag of Idealized Shapes of a Para-Sail Parachute during Inflation.
2. The Pressure Distribution on Idealized Shapes of an Inflating Para-Sail.
3. The Mass Flow through Idealized Shapes of an Inflating Para-Sail Parachute.
4. Stress Analysis of the 70-foot Para-Sail during Inflation and Steady Descent.
5. Determination of the Stability, Drag, and Aerodynamic Center of the Para-Sail.

6. The Effects of Some Design Parameters upon the Functioning of the Para-Sail.

7. Opening Characteristics of the Para-Sail with Several Internal Canopy Arrangements.

8. Materials and Fabrication Studies for a 70-foot-diameter Para-Sail.

9. Results and Analysis of Drop Tests with a 70-foot-diameter Para-Sail.

The first eight documents report the results of wind-tunnel and analytical studies conducted to define the final configuration as well as the material and fabrication tests conducted to define and to verify the structural integrity of the fabricated parachute. The ninth document presents the results and analysis of the full-scale drop-test program, and, as such, represents the culmination and confirmation of the efforts presented in the first eight documents.

This section will present edited excerpts from only the final document. The complete version of this report and the other eight reports are on file with the Landing and Docking Mechanics Branch, Structures and Mechanics Division, Manned Spacecraft Center, Houston, Texas.

SYMBOLS

$C_{D_{eff}}$	effective drag coefficient
C_{D_o}	drag coefficient based on nominal area
C_{L_o}	lift coefficient based on nominal area
D	drag force, lb
d_i	internal parachute projected diameter, ft
d_o	nominal diameter based on total canopy area, ft
d_p	projected diameter of inflated canopy, ft

d_v	vent diameter, ft
F	opening force, lb
F_{design}	design opening force = 16 000 lb
F_{max}	maximum opening shock, lb
h	altitude, ft
KEAS	equivalent air speed, knots
L	lift
L/D	lift-to-drag ratio
q	dynamic pressure $\equiv 1/2\rho V^2$, lb/ft ²
q_{design}	design dynamic pressure, lb/ft ²
q_{max}	maximum dynamic pressure, lb/ft ²
S	canopy area, ft ²
S_o	nominal canopy area $\equiv \frac{\pi d_o^2}{4}$, lb/ft ²
S_p	projected canopy area $\equiv \frac{\pi d_p^2}{4}$, ft ²
T	dimensionless time $\equiv t/t_f$
t	time, sec
t_d	deployment time, sec
t_f	filling time, sec

t_T	total opening time, sec
V	velocity, ft/sec
V_D	velocity at disreef, ft/sec
V_O	initial velocity, ft/sec
V_{max}	maximum velocity, ft/sec
V_v	rate of descent, ft/sec
W	suspended weight, lb
α	angle of attack = $\tan^{-1} L/D$
ρ	density, slugs/ft ³
ρ_O	density at sea level = 0.002378 slug/ft ³
σ	density ratio = ρ/ρ_O
ω	turn rate, deg/sec

Subscripts:

I	refers to stage I
II	refers to stage II

DROP-TEST PROGRAM

In May of 1964, test work was initiated at the Joint Parachute Test Facility through the 6511th Test Group under Air Force local project LIC 9221. The test program adopted consisted of a total of 14 tests, including general deployment and reefing studies, ultimate strength verification, turn,

lift-to-drag modulation, and deployment under simulated pad abort conditions. Table III-III summarizes this program.

The deployment system used for this drop-test program is similar to the system used for the 80-foot d_0 version of the Para-Sail. However, certain changes and modifications have been incorporated into the new system based upon this previous experience. These changes and modifications as well as the deployment system itself are discussed later. Figure III-39 indicates schematically the arrangement and location of the system components with respect to the vehicle/parachute combination.

This section presents all pertinent measurements, photographs, and related information from the drop-test program; a description of each test item including the number, observations, and purpose; and the data-reduction methods used. This section also includes a composite damage chart, environment data, aircraft and pilot parachute data plus, other miscellaneous data from the drop-test program.

The more important information has been extracted and listed in tables III-IV and III-V. These tables summarize the performance parameters during inflation and at steady state, respectively. It should be mentioned that only drop tests 2 through 11 were analyzed during the inflation sequence. Further analysis was not deemed necessary as these drops should provide representative information for those configurations examined. A complete summary of all drop-test information is included in table III-VI. This tabulation essentially summarizes all the data presented in section III in addition to weather and aircraft information.

TEST RESULTS

Total and Individual Riser Forces

The total and individual riser forces are listed in table III-VII for all the drops. The geometry of the suspension lines and individual risers with respect to the glide direction of the canopy is shown in figure III-40. From the values of the riser forces, it is apparent that the distribution of these forces is asymmetric, which is expected, due to the glide characteristic of the Para-Sail.

The riser and suspension lines attaching to the front carry approximately 23.6 percent of the suspended load. The side risers carry 37.4 percent (18.7 percent for each side) and the rear riser carries 39.7 percent of the load.

Canopy Depth and Aspect Ratio

The canopy depth and aspect ratio for the configurations used in the development program are tabulated in table III-VIII. These values were taken from films of the drops provided by the El Centro Test Facility. From these values it can be seen that the aspect ratio of configuration 70A-5 is 1.94, while that of the final 80-foot version (80A-9) is only 1.61. Thus, even though the canopy loading for configuration 70A-5 is 29 percent higher than 80A-9, the glide capability is much the same.

Rate of Descent

The rate of descent is affected by altitude. The average values of rate of descent at an altitude of 5000 feet are tabulated in table III-V. The values range from 27.8 ft/sec to 30.9 ft/sec excluding turn and minimum L/D drops, with an average value of 29.3 ft/sec.

Aerodynamic Centerline

The location of the aerodynamic centerline (ACL) has been determined from wind-tunnel measurements using small scale models. The results are presented in figure III-41. The direction of the resultant aerodynamic force was also calculated from steady-state loads measured during full-scale tests. From these calculations, the aerodynamic centerline acts approximately 4° rearward of the parachute centerline as compared with 1.5° rearward as determined in the wind tunnel.

There are several possible reasons for the apparent discrepancy in the two values shown here:

1. The exact location of the geometric centerline is difficult to determine for the full-size configuration.
2. The riser forces listed in table III-VII yield the following averages and standard deviation.

Riser	Average force, lb	Deviation, lb
Front	561	± 79
Rear	932	± 47
Side	894	± 63

From these variations, a corresponding variation in the aerodynamic centerline location was calculated, assuming the geometric centerline is correct. This resulted in a variation of the ACL from 3° to 4.5°.

3. The inflated shapes of the model and the full-scale parachute may differ slightly.

In view of these uncertainties, it is suggested that rearward slanting of 3° of the aerodynamic centerline be assumed to be a valid value.

Effective Drag Coefficient

Averages of the effective drag coefficient for each drop are presented in table III-V. These values were based upon the nominal area of the canopy. The averages for all drops with nominal rigging were calculated to be $C_{D_{eff}} = 1.43$.

Figures III-42 and III-43 present the values of $C_{D_{eff}}$ versus canopy loading and rate of descent at sea level, respectively. For comparative purposes, similar values measured for various other configurations are included. The large variation in the values for $C_{D_{eff}}$ at a constant canopy loading can be attributed to the variation in the wind currents for each drop test. It is interesting to note that for several of the drops the canopy was deployed with a turn incorporated into the rigging. By comparing $C_{D_{eff}}$ with the turn rates for these drops (table III-V), it is noted that $C_{D_{eff}}$ decreases significantly as turn rate increases. This variation is presented in figure III-44.

Lift and Drag Coefficients

Average values of the nominal lift and drag coefficients for each drop are presented in table III-V. These values were based upon the nominal area of the canopy. Averaging these values for those drop tests with normal rigging enables the determination of representative coefficients for lift and drag. These averaged values are $C_{L_0} = 0.51$ and $C_{D_0} = 0.49$.

It has been indicated that as canopy loading is increased, lift and drag coefficients decrease. Furthermore, the lift coefficient has been observed to

decrease at a faster rate than has the drag coefficient, thereby causing a net decrease in glide capability. This trend is shown in figures III-45 and III-46, which present C_{L_0} and C_{D_0} , respectively, versus canopy loading. As canopy loading increases, C_{L_0} decreases from approximately 0.65 to 0.5, while C_{D_0} remains almost constant.

The values from figures III-45 and III-46 are further correlated in figure III-47, which presents C_{L_0} versus C_{D_0} , with canopy loading as a parameter. As W/S_0 increases, the slope of C_{L_0} decreases, indicating a decrease in the glide characteristic. These same trends are also supported by the results from wind-tunnel experiments with scaled models of the various Para-Sail configurations.

Lift-to-Drag Ratio

Average lift-to-drag values for each drop are tabulated in table III-V. For those drops without rigging modifications, the average L/D was approximately 1.04, with a corresponding canopy load factor W/S_0 of 1.24 lb/ft².

Figure III-48 presents L/D versus canopy loading, indicating the results from this program as well as values measured for various other Para-Sail configurations. A decrease in L/D is observed as canopy loading is increased.

Turn Rate

The turn capability of the Para-Sail was tested on drops 4, 12, and 13. The procedure used was to shorten the left control line before the parachute was packed, thereby inverting the turn slots on the left side of the canopy and inducing a turn to the left. Figures III-49 to III-52 show the rates as a function of time during steady-state descent. Also shown are x-y plots of the parachute system ground track, from which an estimate of the radius of turn may be made.

Control-Line Forces

The canopy turn slots are actuated by retracting a control line (MIL-W-5625, 1000-lb tubular webbing) which passes from the riser suspension-line-connector link through rings attached to the four turn slots of one gore and attaches at the parachute vent. The control line is initially a single strand, branching into two and then into four strands, to control a total of 16 slots on each side of the canopy. The total force required to hold the slots in a nearly inverted position was measured on drops 12, 13, and 14. Based upon the results from these tests and photographic evidence of the approximate slot positions, a relationship between control-line load and stroke curve was established. This relationship is shown in figure III-53.

OPENING CHARACTERISTICS

Force and Trajectory Curves

Total-force traces for drops 2 to 11 are presented in figure III-54. The peak forces or opening shock values for each stage of inflation (stages I and II) for all drops are listed in table III-IX. From the force traces, it can be shown that the opening process is extremely uniform and consistent. The variation in the time to maximum force for stage II arises due to the various time delays incorporated into the opening process through the reefing-line cutters.

The reefed opening shock values for these drops are not constant, but rather increase with the deployment velocity. This variation is shown in figure III-55. In this case, the forces and dynamic pressures have been made dimensionless by respective design values. The variation in the maximum force ratio for stage I is almost linear with dynamic pressure. At design q ($q_{\max}/q_{\text{design}} = 1.0$), the force ratio is $F_{\max}/F_{\text{design}} = 0.97$, 3 percent below the design value of 1.0.

Trajectory data, including altitude, glide angle, and total velocity histories, are presented in figures III-56 to III-58. Only the maximum, minimum, and design conditions have been represented. The significant information from these data illustrate: the rapid decrease in trajectory angle approaching 90° before the completion of inflation; the similarity in variation of altitude with respect to time; and the consistency of the Para-Sail under varying deployment velocities to attain the same velocity prior to disreef, which is approximately 120 ft/sec.

Internal Parachute Performance

Previous experience with other Para-Sail configurations and conventional parachutes has proved the favorable effect of the internal parachute upon the opening characteristics of the main canopy. In addition, wind-tunnel studies using scaled models of Para-Sail configuration 70A-4 show a noticeable decrease in filling time and a more consistent and uniform canopy inflation sequence for all configurations utilizing a second canopy.

Projected Planform Area-Time History

The projected diameter variation during inflation is represented in figures III-59 and III-60 for stages I and II, respectively. In these figures, the diameter represents the area of a circle equivalent to the respective planform projected areas. The tabulation of the coordinates for figures III-59 and III-60 is listed in table III-X. Again a uniform filling process is indicated, as evidenced by the compact grouping of the data. The average diameter ratio based upon these data is $d_p/d_o = 0.17$ at the beginning of the inflation. The reefed diameter ratio, again averaged, is $d_p/d_o = 0.35$, while the full open ratio is $d_p/d_o = 0.67$.

Deployment and filling times. - The deployment times, stages I and II filling times, and the total inflation times for drops 2 through 11 are listed in table III-IV. The total opening time for these drops has been plotted versus the maximum dynamic-pressure ratio in figure III-61. The average opening time for these drops, which shows no noticeable variation with the dynamic-pressure ratio, is approximately 5.0 seconds. These values are not affected by the reefing-line cutter delay, for this time characteristic has been removed.

Individual riser forces. - Table III-IX summarizes the available data on individual riser forces for both reefed and disreefed cases (stages I and II) for all drop tests. Table III-IX includes the peak riser forces during these two stages plus the total opening shock.

A statistical analysis of the results in table III-IX reveals an appreciable variation in the maximum individual riser loads. Under all deployment conditions, the rear risers exhibited significantly higher loading than side and front risers. The rear riser-load deviation from the average value was in the order of 8.55 percent for the stage I opening and 18.21 percent for stage II. Since these values are important in design strength considerations, the standard deviations were determined for both cases. One standard deviation was calculated to be 7.35 percent for the stage I opening loads and 12.63 percent

for the stage II loads. Therefore, this would result in eccentric loading factors of 15.9 percent and 30.8 percent for the respective opening stages under one standard deviation.

Dynamic drag area. - The change in parachute drag area and the effects of apparent mass and other dynamic phenomena during the parachute opening process may be isolated by dividing total force by dynamic pressure. This has been done for three drops representative of deployment dynamic pressures (at line stretch) of 37, 91, and 119 lb/ft². The results (fig. III-62) show that the dynamic drag area increases at approximately the same rate regardless of deployment velocity and reaches a steady value after 2 seconds, or about 400 lb/ft². This variation of drag area with time may be used to calculate total-force-time histories for various initial conditions of velocity weight or flight-path angle.

THE DEPLOYMENT SYSTEM DESCRIPTION

Para-Sail Deployment Aids

Certain design features of the Para-Sail which enable it to achieve high steady-state performance characteristics also create deployment and inflation problems. In the course of development of large Para-Sail parachutes, specific techniques and procedures were adopted which produced reliable deployments. These problems have been eliminated by the use of special deployment aids and procedures which are described in later sections. Figure III-63 shows the arrangement of these deployment aids.

Internal parachute. - Arranged in the inlet or mouth of the Para-Sail, a comparatively small, ribless, guide-surface parachute has been found to be an effective aid to inflation. Size and position considerations of this aid were based upon experience with conventional types of parachutes. However, because of the uneven skirt characteristics of the Para-Sail, it became necessary to modify position slightly so that the internal parachute remained within the inlet of the primary canopy. Drop-test experience has shown that the selected parameters have been effective in achieving reliable and repeatable inflations.

Stabilizer reefing. - Previous experience has shown the necessity for a method of controlling the stabilizers during the inflation process. During the 80-foot Para-Sail test program, a method was developed which has provided satisfactory control and has prevented the semi-inversion type of malfunction which occurred prior to its adoption. This procedure utilizes a series of

reefing rings attached on the inside of each radial seam at the base of the stabilizers (lower edge). In packing, the stabilizers are pleated in a conventional manner and a reefing line is passed through the rings and adjacent reefing cutters, then the ends are joined. In effect, each group of stabilizers is reefed with a line of zero length. Additionally, the panels are held by an encasing sleeve which is secured by light break cords, protecting the panels from air blast but allowing them to unfurl when the skirt disreefs. Stabilizers are reefed for a period of, at most, 70 percent of that of the primary skirt reefing.

Primary Reefing

In conjunction with the reefing procedure adopted for the stabilizers, it became necessary to utilize a somewhat unorthodox method of skirt reefing. Since the skirt becomes bunched in the vicinity of the stabilizers, the reefing line is passed directly through the rings on these gores, allowing little or no spacing of the line. The remainder of the line is spaced equally fore and aft of these panels and tacked at each ring with light tie cord. In this manner, the spreading action of the skirt resulting from tension in the reefing line is minimized in the vicinity of the stabilizers.

Vent-stabilization parachute. - In order to center the vent of the Para-Sail during inflation, thereby reducing unequal loading and flutter damage to the canopy material, a small guide-surface parachute was permanently attached to the vent. Unfortunately, the attachment of the parachute bridle to the Para-Sail vent lines often resulted in damage to these lines. This was overcome by adoption of an aluminum connector ring, as shown in figure III-64. This ring had been used previously, by the testing agency, with 100-foot-diameter cargo parachutes.

Deployment bag. - Previous experience has indicated that the low-permeability materials used in Para-Sail construction may have a greater tendency toward friction burn damage as the result of self-contact or contact with deployment-bag materials. In an attempt to minimize such damage, a deployment bag was provided which offered an exceptionally clean opening through which to extract the canopy. This was accomplished by closure and protective flaps which were free to be blown away by the airstream after they had performed their function. In this manner, the bag opening would remain uncluttered by these flaps. Bag closure was accomplished by a simple break-cord drawstring in the hem of the closure hood. It was noted from onboard drop-test films that this hood would normally invert over the outside of the bag during deployment, allowing free passage of the canopy and lines. The bag was also provided with a slight taper to facilitate easier extraction. An exploded view is provided in figure III-63.

An expedient feature of this design was the manner in which pressure packing of the test item could be performed. With the packing aids mentioned in the following discussion, bag closure could be accomplished with the canopy under pressure.

PACKING METHODS AND AIDS

The packing procedure of the test item changed in only minor respects during the course of the test program. The techniques employed are similar to those for conventional large parachutes, with the exceptions noted for the stabilizers and reefing line.

In order to achieve the manipulation of slots necessary for turn and L/D modulation tests, it became necessary to modify packing techniques to obtain a fixed stroke of the individual control lines. This was accomplished by shortening the respective control line and attaching it at the riser during packing so that an effective stroke was produced by canopy inflation and elongation of suspension lines under opening and steady-state loads.

Fabrication of a special pressure packing aid made it possible to maintain pressure on the canopy while the difficult task of locking the canopy compartment was accomplished. This proved to be a substantial contribution to packing neatness and the time required for the packing cycle. A portion of this equipment is shown in figure III-65.

STRUCTURAL INTEGRITY

In the course of development of the final configuration, numerous destructive static tests were performed to substantiate or improve structural integrity of the test item. Some of these tests were made as the result of minor deficiencies disclosed by actual drop tests. The majority, however, were performed to provide evidence that structural integrity was adequate for the calculated component loading. Drop tests, as indicated by the composite damage chart (fig. III-66), substantiate the correctness of these findings and indicate the presence of more than adequate safety factors.

SYSTEM WEIGHT AND VOLUME

Table III-XI lists measured weights and volumes for the two test configurations 70A-4 and 70A-5. It will be noted that a slight weight increase occurred with the 70A-5 configuration. This is the result of slightly heavier, low-permeability materials in this unit, although nominally these materials are of the same weight (2.0 oz/yd^2). Figure III-67 presents a calculated weight and volume curve for a range of Para-Sail diameters. This figure is based upon the data available for the final configuration 70A-5.

It should be noted that volumes are determined at a 1 lb/in.^2 packing pressure. In order to meet system requirements, it was necessary to reduce the volume to 8012 cubic inches. This was accomplished under a packing pressure of less than 10 lb/in.^2 and resulted in a packed density of 32.5 lb/ft^3 .

CANOPY CONFIGURATION

The following figures present a graphical representation of the configuration tested during this program. Figure III-68 shows the general geometry in the inflated condition. Figure III-69 shows a typical gore pattern, with and without fullness, and figure III-70 shows the basic engineering plan view, including slot locations, porosity, and so forth.

Porosity distribution is indicated in figure III-70. These values were determined in the following manner.

The total area (A_T) of the canopy is defined as the area of a typical gore without fullness, including vent area, excluding slot area, and multiplied by the total number of gores. To this, the area of the stabilizers is added. This area neglects the effect of gores of varying length, as found in the leading surface of the canopy. The drag surface used in computing porosity is this same area minus the area of the stabilizers. The open area of the circumferential slots was calculated as the slot area in a plane perpendicular to the gore centerline. It was assumed in these calculations that the open area was bounded by an arc and a cord of a circle, the arc formed by the cloth bulge between suspension lines. The radial and turn slot areas were calculated in a similar manner, only with the exception that these areas were formed in a plane parallel rather than perpendicular to the gore centerline.

The term fullness, as used in this description, applies to the extra fabric introduced between main seams, which is in excess of that existing in the basic gore. The basic gore is defined as a representative gore from the basic canopy shape. Briefly, this basic shape is comprised of a flat, circular plate capping the small diameter of a truncated right circular cone.

CONCLUDING REMARKS

The primary objective of the drop-test program was to evaluate through measurement and observation the performance capability of the Para-Sail parachute and to correlate this information with results from wind-tunnel studies and analytical investigations. This objective has been met, and the 70-foot d_0 Para-Sail has adequately demonstrated the required performance.

Since proof of the structural integrity of each Para-Sail was one of the primary considerations of this program, it was important that accurate damage records be kept for each test. A composite damage chart for drops 2 to 15 is included (fig. III-66). This chart substantiates the structural integrity of the test item. Not noted on the damage chart is the fact that seam slippage was present to some degree in nearly all tests. The amount of slippage increased with the severity of deployment conditions; however, no failure resulted from this situation. Slippage was confined almost entirely to the upper sections fabricated of 2.25 oz/yd² MIL-C-7350, Type I. These records show that no significant damage occurred for the 69.8-foot d_0 Para-Sails during inflation or at steady state. Thus, the canopy satisfies the design requirements.

The evaluation of the aerodynamic performance characteristics of this configuration are summarized in table III-XII, which also lists the required values. It can be seen that these values are also equal or better than the required values.

In summary, the contractual performance requirements are considered to be fulfilled.

TABLE III-I - HOUSTON TEST PROGRAM

Drop	Launch conditions		Weight	Configuration	Purpose	Results
	Altitude, ft	Velocity, knots				
H1	2000	110	2500	I (fig. III-15)	Deployment study.	Canopy front tucked in for 19 seconds and then came out for fully inflated descent.
H2	2600	110	2500	I (fig. III-15)	Deployment study, increased reefing-line length.	Canopy front tucked back and inflated inverted. Canopy damaged.
H3	2600	125	2500	II (fig. III-16(a))	Deployment study, modified configuration.	Canopy front tucked back and inflated inverted.
H4	2600	125	2500	III (fig. III-16(b))	Deployment study with 36-line pilot parachute bridle.	Canopy front tucked back, then came out for fully inflated descent.
H5	2600	125	2500	III (fig. III-16(b))	Deployment study, pilot parachute bridle length increased.	Canopy front tucked back and inflated through rear suspension lines.
H6	2600	110	2500	IV (fig. III-19(a))	Deployment study, modified configuration.	Canopy front tucked back, then came out for fully inflated descent.
H7	2600	110	2600	IV (fig. III-19(a))	Deployment study, rear 21 gores zero reefed at skirt.	Rear skirt reefing line failed. Front tucked in, then came out slowly for fully inflated descent. Canopy damaged.
H8	2600	110	3600	V (fig. III-19(b))	Deployment study, rear risers shortened; pocket bands added to front.	Front tucked during inflation and two rear gores failed.
H9	2600	110	2500	VI (fig. III-19(c))	Deployment study with internal parachute.	First orderly deployment.
H10	2600	110	2500	VI (fig. III-19(c))	Deployment study.	Successful.
H11	2400	110	3500	VI (fig. III-19(c))	Deployment study.	Successful.

TABLE III-II. - EL CENTRO TEST PROGRAM

Drop	Launch conditions		Weight	Configuration	Purpose	Results
	Altitude, ft	Velocity, knots				
1	5 000	120	3600	VI (fig. III-19(c))	Deployment study.	Successful.
2	5 000	120	3500	VI (fig. III-19(c))	Deployment study.	Orderly deployment, high opening loads.
3	5 000	120	4823	VI (fig. III-19(c))	Deployment study, increased payload.	Two rear risers failed at reefed opening shock.
4	5 000	120	4823	VI (fig. III-19(c))	Deployment study, increased payload.	Canopy failed on opening.
5	5 000	120	2605	VII (fig. III-22(a))	Deployment study, modified configuration.	Successful.
6	5 000	120	2605	VIII (fig. III-22(b))	Deployment study, modified configuration.	Successful.
7	5 000	120	2650	VIII (fig. III-22(b))	Deployment study, internal parachute removed.	Slow inflation.
8	10 600	120	2605	VIII (fig. III-22(b))	Deployment study, increased altitude.	Successful.
9	10 600	120	3700	VIII (fig. III-22(b))	Deployment study, increased weight.	Failure. Stabilization panels caused partial inversion.
10	10 600	120	3700	VIII (fig. III-22(b))	Repeat of test 9.	Successful.
11	10 600	120	4750	VIII (fig. III-22(b))	Deployment study, increased weight.	Failure. Stabilization panels caused partial inversion.
12	10 600	120	4755	VIII (fig. III-22(b))	Deployment study, hesitator bags on stabilization panels.	Successful. Hesitator bags ineffective.
13	10 600	120	2785	VIII (fig. III-22(b))	Deployment study, stabilization panels removed.	Successful deployment. Loss of steady-state performance.
14	10 600	137	4755	VIII (fig. III-22(b))	Deployment study, increased q.	Canopy damaged during inflation due to 1000-lb suspension line inadvertently left on.
15	10 600	137	4755	VIII (fig. III-22(b))	Deployment study, increased q.	Successful, although reefing line failed.

TABLE III-II. - EL CENTRO TEST PROGRAM - Concluded

Drop	Launch conditions		Weight	Configuration	Purpose	Results
	Altitude, ft	Velocity, knots				
16	10 600	137	4755	IX (fig. III-22(c))	Deployment study, increased q .	Successful.
17	10 600	154	4750	IX (fig. III-22(c))	Deployment study, design q .	Successful.
18	10 600	120	4750	IX (fig. III-22(c))	Turn test.	Rate of turn was 12 deg/sec.
19	10 600	154	4750	IX (fig. III-22(c))	Deployment study, design q .	Successful.
20	10 600	120	4750	IX (fig. III-22(c))	Turn test.	Rate of turn was 19 deg/sec.

TABLE III-III. - DROP-TEST PROGRAM

[Cylindrical vehicle used on all tests weighed 4600 lb]

Test	Deployment, q/KEAS	Altitude, ft	Remarks
1	80/140	10 600	Exploratory test of Para-Sail. Configuration 80A-9. Without stabilizer panels.
2	66/140	10 600	Optimization of deployment technique and study of reefing parameters. Configuration 70A-4.
3	80/154	10 600	Optimization of deployment technique and study of reefing parameters. Configuration 70A-4.
4	37/105	10 600	Evaluation of fixed-turn capability. Configuration 70A-4.
5	37/105	10 600	Evaluation of fixed-lift/drag modulation. Configuration 70A-4.
6	80/154	10 600	Optimization of deployment technique and study of reefing parameters. Configuration 70A-5.
7	95/167	10 600	Optimization of deployment technique and study of reefing parameters. Configuration 70A-5.
8	110/180	10 600	Optimization of deployment technique and study of reefing parameters. Configuration 70A-5.
9	120/188	10 600	Determination of structural integrity at 1.5 design q. Configuration 70A-5.
10	120/188	10 600	Determination of structural integrity at 1.5 design q. Configuration 70A-5.
11	120/188	10 600	Determination of structural integrity at 1.5 design q. Configuration 70A-5.

TABLE III-III. - DROP-TEST PROGRAM - Concluded

[Cylindrical vehicle used on all tests weighed 4600 lb]

Test	Deployment, q/KEAS	Altitude, ft	Remarks
12	37/105	10 600	Evaluation of fixed-turn capability. Configuration 70A-5.
13	37/105	10 600	Evaluation of fixed-turn capability. Configuration 70A-5.
14	37/105	10 600	Evaluation of fixed-lift/drag modulation. Configuration 70A-5.
15	20/77	2 500	Low q, low altitude, simulated pad-abort conditions.

TABLE III-IV. - SUMMARY OF DROP-TEST INFORMATION DURING INFLATION^a

Config-uration	Drop	Deploy-ment altitude h (msl), ft	Deploy-ment velocity V _o ' ft/sec	Maximum velocity V _{max} ' ft/sec	Maximum dynamic pressure q _{max} ' lb/ft ²	Disreef velocity V _D ' ft/sec	Deploy-ment time t _d ' sec	Filling times t _f ' sec		Total opening time t _t ' sec	Opening shock F _{max} ' lb		Projected areas S _p ' ft ²	
								Stage I	Stage II		Stage I	Stage II	Stage I	Stage II
70A-4	2	11 190	294	306	74.6	118	1.40	2.72	1.40	5.52	14 000	14 700	495	1670
70A-4	3	11 249	337	338	94.0	112	1.40	2.80	1.53	5.53	16 250	16 000	481	1767
70A-4	4	11 244	202	215	37.6	113	2.26	1.49	1.16	4.91	11 000	14 360	480	1524
70A-4	5	11 250	194	212	37.0	121	2.04	2.16	1.44	5.64	9 750	15 500	522	1826
70A-5	6	11 336	320	333	91.2	117	1.42	2.22	1.59	5.23	15 000	15 900	481	1840
70A-5	7	11 220	347	350	100.6	116	1.31	1.85	1.52	4.68	18 000	16 000	491	1836
70A-5	8	10 720	368	370	119.2	114	1.35	1.87	1.16	4.38	22 000	17 200	480	1782
70A-5	9	11 128	387	388	124.1	120	1.22	2.10	1.45	4.77	22 200	16 600	481	1828
70A-5	10	11 066	383	385	122.2	113	1.17	2.73	1.35	5.25	21 000	16 800	465	1713
70A-5	11	10 731	387	388	127.7	119	1.17	2.86	1.29	5.32	21 600	14 600	470	1823

^aRemarks: Reefing percentage ≈ 12.5 (ratio of reefing-line diameter to nominal diameter d_o); $W/S_o = 1.24 \text{ lb/ft}^2$; and $\sigma = 0.70$; $\rho_o = 0.002378 \text{ slugs/ft}^3$.

TABLE III-V. - SUMMARY OF PARA-SAIL TEST INFORMATION
DURING STEADY STATE

Drop	Config- uration	L/D, avg	$C_{D_{eff}}$, avg	C_{D_o} , avg	C_{L_o} , avg	V_v , 5000 ft, ft/sec	Turn rate, deg/sec	Weight, lb
2	70A-4	0.981	1.271	0.479	0.470	30.9	--	4750
3	70A-4	1.082	1.297	.419	.453	30.6	--	4738
4	70A-4	.262	0.696	.648	.170	41.9	48	4740
5	70A-4	.985	1.396	.518	.510	29.6	--	4747
6	70A-5	1.148	1.456	.427	.490	28.9	--	4747
7	70A-5	1.087	1.548	.498	.541	28.0	--	4747
8	70A-5	1.105	1.574	.491	.543	27.8	--	4747
9	70A-5	.990	1.574	.585	.579	27.8	--	4747
10	70A-5	1.035	1.412	.492	.509	29.3	--	4747
11	70A-5	.929	1.271	.518	.481	30.9	--	4747
12	70A-5	.916	1.210	.502	.460	31.7	24	4747
13	70A-5	.848	1.054	.483	.410	34.0	27	4747
14	70A-5	.979	1.373	.517	.506	29.8	--	4747
15	70A-5	(a)	(a)	(a)	(a)	(a)	--	4747

^aLow altitude test, data not available.

TABLE III-VI. - PAR

Test	General data						Aircraft data			Pilot parachute		Parachute data						Weight data, lb				
	Air Force drop	Date	Temp, °F	Baro press, in. Hg	Rel humidity, percent	Ground wind, knots	Type	KIAS/KEAS, knots	Press alt, ft	Diameter - kind deployment (a)	Diameter - kind perm attach (a)	Diameter, ft	Parachute, serial no.	Configuration	Reefing line length, ft	Reefing delay, sec		Vehicle	Parachute	Accessory	Total	Reefed open time, sec
																Slab panels	Skirt					
1	0860 F64	1 June 1964	97	29.76	13	2	B-66	154	10 625	8-ft RGS	54-in. RGS	79.4	PS 63114	80A-10	31	-	10	4600	150	12	4750	2.8
2	1602 F64	15 Sept. 1964	91	29.80	21	4	B-66	140	10 600	6-ft RGS	51-in. RGS	69.8	PS 64500	70A-4	27-1/3	4	6	4600	140	12	4740	4.2
3	1657 F64	23 Sept. 1964	94	29.88	17	4	B-66	154	10 600	18-ft RGS ^b	51-in. RGS	69.8	PS 64527	70A-4	27-1/3	4	6	4600	140	12	4740	4.05
4	1704 F64	30 Sept. 1964	86	29.80	17	2	C-130	105	10 600	8-ft RGS	51-in. RGS	69.8	PS 64527	70A-4	27-1/3	4	6	4600	140	12	4740	4.50
5	1768 F64	7 Oct. 1964	94	29.86	39	4	C-130	105	10 600	8-ft RGS	51-in. RGS	69.8	PS 64527	70A-4	27-1/3	4	6	4600	140	12	4740	4.67
6	1876 F64	19 Oct. 1964	91	30.09	12	10	B-66	154	10 600	18-ft RGS ^b	51-in. RGS	69.8	PS 64570	70A-5a	27-1/3	4	6	4600	147	13	4747	3.86
7	1913 F64	6 Nov. 1964	71	30.05	22	4	B-66	167	10 600	18-ft RGS ^b	51-in. RGS	69.8	PS 64597	70A-5a	27-1/3	4	6	4600	147	13	4747	3.0
8	1949 F64	17 Nov. 1964	61	30.12	36	2	B-66	180	10 600	18-ft RGS ^b	51-in. RGS	69.8	PS 64685	70A-5b	27-1/3	4	8	4600	147	13	4747	3.5
9	2198 F64	20 Nov. 1964	51	30.18	42	8	B-66	188	10 600	18-ft RGS ^b	51-in. RGS	69.8	PS 64737	70A-5c	27-1/3	4	8	4600	147	13	4747	3.0

^aRGS = ring sail.^bReefed 12-1/2 percent.

FOLDOUT FRAME

130-1

III-VI. - PARA-SAIL TEST DATA SUMMARY

Total	Test data											Damage				Remarks
	Reefed open time, sec	Full-open time, sec	Downtime, sec	R/D, measured, ft/sec	C _D ^{eff} , average	L/D, average	Oscillation, deg	Snatch force, lb	Reefed open force, lb	Full-open force, lb	Light	Medium	Heavy	Test successful		
4750	2.8	-	111.7	90.6	-	-	-	6 600	18 600	-			X		Heavy tear. Broke 16 main seams.	Stabilization panels removed. Failure attributed to unexpected high reefed opening forces coupled with canopy fatigue from 6 previous drops.
4740	4.2	9.6	334.2	28.7	1.27	0.98	0	5 200	14 100	14 900				X	Slight evidence of strain in the upper two cross seams of each gore.	Continuous turn of 9 deg/sec and tuck in right front of canopy. Even with turn, canopy glide was apparent. Development and inflation appeared very orderly.
4740	4.05	12.7	340.72	28.4	1.30	1.08	0	6 250	16 250	16 000	X			X	Slight stress in seams of 2.25-oz nylon ripstop. Three damaged vent lines. Several small burn holes.	
4740	4.50	10.9	247.0	38.8	0.70	0.26		4 800	10 900	14 300	X			X	Two damaged vent lines and several small burn holes.	Rate of turn test, approximately 50 deg/sec. Control-line stroke = 6.9 ft.
4740	4.67	10.64	349.8	27.4	1.40	0.98	0	3 000	9 750	15 500	X			X	Three damaged vent lines and several small burn holes.	L/D-modulation test. Left and right control-line stroke = 6.9 ft.
4747	3.86	10.09	363.17	26.8	1.46	1.15	0	5 000	15 600	15 800	X			X	Negligible.	Canopy manufactured of 2.0-oz ripstop material.
4747	3.0	10.4	375.4	26.0	1.55	1.09	0	5 500	17 500	15 500	X			X	Negligible.	During steady-state descent the canopy was stable and exhibited no turn.
4747	3.5	11.4	364.5	25.8	1.57	1.10	0	5 800	22 000	17 250	X			X	Panel 8D blown, and several small burns.	During steady-state descent the canopy was stable and exhibited no turn.
4747	3.0	12.7	368.9	25.8	1.57	0.99	0	10 800	22 000	16 600	X			X	Few small holes.	1-1/2-design q test. During descent, canopy exhibited slow left turn.

FOLDOUT FRAME 2

TABLE III-VI. - PARA-SAIL TEST DATA

Test	General data						Aircraft data			Pilot parachute		Parachute data						Weight data, lb				Reefed open time, sec	Full-open time, sec
	Air Force drop	Date	Temp, °F	Baro press, in. Hg	Rel humidity, percent	Ground wind, knots	Type	KLAS/KEAS, knots	Press alt, ft	Diameter - kind deployment (a)	Diameter - kind perm attach (a)	Diameter, ft	Parachute, serial no.	Configuration	Reefing line length, ft	Stab panels	Reefing delay, sec	Skirt	Vehicle	Parachute	Accessory		
10	2226 F64	25 Nov. 1964	64	29.94	61	0	B-66	188	10 600	18-ft RGS ^b	51-in. RGS	69.8	PS 64835	70A-5d	27-1/3	4	8	4600	147	13	4747	3.4	11.6
11	2301 F64	3 Dec. 1964	65	29.81	24	8	B-66	188	10 600	18-ft RGS ^b	51-in. RGS	69.8	PS 64850	70A-5d	27-1/3	4	8	4600	147	13	4747	3.4	11.8
12	2385 F64	11 Dec. 1964	57	30.00	12	4	C-130	105	10 600	8-ft RGS	51-in. RGS	69.8	PS 64570	70A-5a	27-1/3	4	6	4600	147	13	4747	5.1	10.8
13	2407 F64	15 Dec. 1964	54	30.00	12	0	C-130	105	10 600	8-ft RGS	51-in. RGS	69.8	PS 64673	70A-5b	27-1/3	4	6	4600	147	13	4747	4.6	11.0
14	2422 F64	4 Jan. 1965	60	30.06	13	2	C-130	105	10 600	8-ft RGS	51-in. RGS	69.8	PS 64673	70A-5b	27-1/3	4	6	4600	147	13	4747	4.7	11.4
15	0032 F65	11 Jan. 1965	62	29.97	11	0	C-130	105	2 500	18-ft RGS ^b	51-in. RGS	69.8	PS 64570	70A-5a	27-1/3	4	6	4600	147	13	4747	7.2	15.0

^a RGS = ring sail.^b Reefed 12-1/2 percent.

131-1

FOLDOUT FRAME /

TEST DATA SUMMARY - Concluded

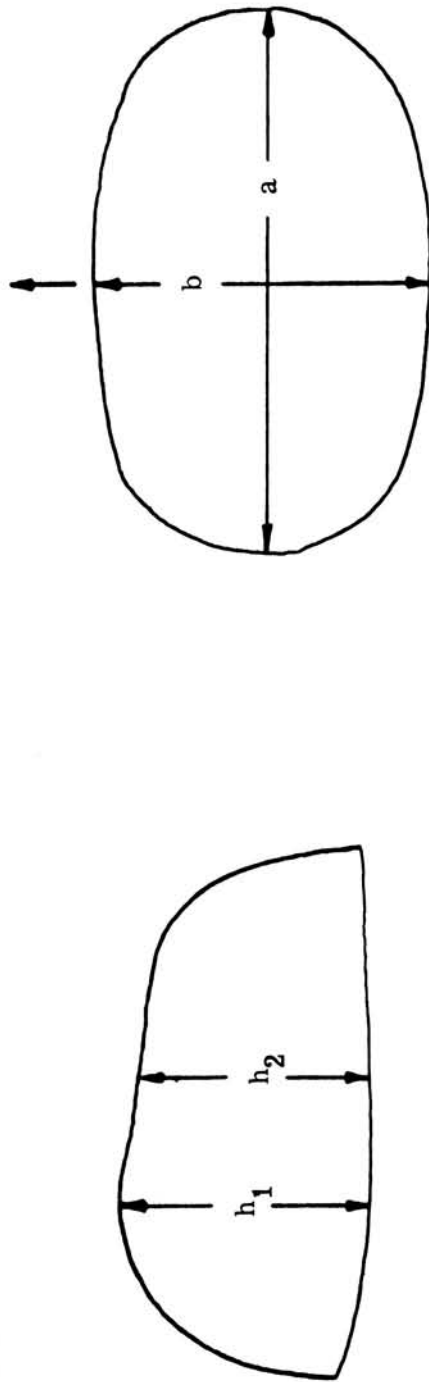
Test data									Damage				Remarks	
Full-open time, sec	Downtime, sec	R/D, measured, ft/sec	C _{Defl} average	L/D, average	Oscillation, deg	Snatch force, lb	Reefed open force, lb	Full-open force, lb	Light	Medium	Heavy	Test successful		
11.6	349.6	27.2	1.41	1.04	0	9000	20 800	16 800	X			X	Negligible.	1-1/2-design q test. During descent, canopy exhibited 7 deg/sec left turn.
11.8	325.0	28.7	1.27	0.93	0	6200	21 400	15 400	X			X	Three blown panels in rear of canopy.	1-1/2-design q test. Descent was stable and exhibited no turn.
10.8	315.0	29.4	1.21	0.92		3600	10 600	15 500				X	Air damage was negligible.	Rate-of-turn test approx 23.7 deg/sec. Control-line stroke = 6.4 ft. Peak control-line force = 400 lb. Steady-state control-line force, 80 to 100 lb.
11.0	300.3	31.4	1.05	0.85		4300	10 800	14 400				X	No damage.	Rate-of-turn test, approx 25.4 deg/sec. Control-line stroke = 7.4 ft. Peak control-line force, 660 lb. Steady-state control-line force, 150 lb.
11.4	338.0	27.6	1.37	0.98	0	4400	10 800	15 300				X	Air damage was negligible.	L/D-modulation test. Left and right control-line stroke = 7.4 ft. Steady-state control-line force, 120 and 150 lb. Peak control-line forces, 730 and 775 lb.
15.0	53.7	26.2	-	-	0	1800	9 000	12 800				X	Damage was negligible.	Low, slow test. Canopy full open at 1100 ft. Camera coverage revealed a malfunction of the internal canopy during which it slipped partially through the suspension lines in the front of the main canopy during reefed stage.

FOLDOUT FRAME 2

TABLE III-VII. - STEADY-STATE RISER FORCES

Drop	Rear riser		Side riser		Front riser		Total force
	1 to 12	61 to 72	49 to 60	13 to 24	25 to 36	37 to 48	
2	1000	975	1100	900	N/A	500	4600
3	975	1000	800	900	500	600	4600
4	1000	1000	1000	700	N/A	750	4600
5	900	950	800	850	800	600	4600
6	900	850	800	900	N/A	N/A	4600
7	900	900	1050	850	450	550	4600
8	900	850	1000	1000	600	650	4600
9	850	1050	925	800	500	550	4600
10	1075	750	750	1000	400	500	4600
11	850	900	900	950	500	350	4600
12	1000	975	925	800	N/A	575	4600
13	950	1000	950	725	N/A	600	4600
14	850	800	750	750	N/A	N/A	4600
15	1000	950	950	1200	600	725	4600

TABLE III-VIII. - GEOMETRIC PARAMETERS FOR VARIOUS PARA-SAIL CONFIGURATIONS DURING STEADY STATE



Side view

Planform

Config-uration	a, ft	b, ft	h_1 , ft	h_2 , ft	d_o' , ft	Aspect ratio, $\frac{a^2}{S_p}$	$\frac{h_1}{h_2}$	$\frac{h_1}{d_o}$	$\frac{h_2}{d_o}$
80A-9	64.4	52.0	22.6	21.5	79.4	1.61	1.05	0.285	0.271
70A-4	55.9	43.3	20.1	19.1	69.8	1.84	1.05	.288	.274
70A-5	58.9	45.6	19.8	19.4	69.8	1.94	1.02	.284	.278

TABLE III-IX. - OPENING FORCES ON INDIVIDUAL RISERS

Drop test	Stage	Rear riser		Side riser		Front riser		Total recorded force
		1 to 12	61 to 72	13 to 24	49 to 60	25 to 36	37 to 48	
2	I	2800	2450	2400	2500	N/A	1800	14 000
	II	3700	4100	2500	2500	N/A	1550	14 700
3	I	3300	3150	2850	2750	2300	2100	16 250
	II	4000	3600	2800	2850	3000	2300	16 000
4	I	1800	2100	1700	1900	1600	1500	11 000
	II	3000	3850	2250	2250	1450	2200	14 300
5	I	1750	2000	1650	1800	2000	1400	9 750
	II	3700	4200	2900	3200	3600	2150	15 500
6	I	2550	2700	2450	2900	2600	N/A	15 800
	II	3600	3400	3600	3500	N/A	N/A	15 900
7	I	3150	3100	2900	3500	2750	2650	18 000
	II	3450	3700	3000	3350	2100	2500	16 000
8	I	3800	3450	3400	3350	3300	3000	22 000
	II	3400	3300	3250	3100	2500	3300	17 200
9	I	3700	3800	3650	3600	3200	3200	22 200
	II	3500	3850	3000	2950	2900	2300	16 600
10	I	4300	3250	3800	3300	3000	2450	21 000
	II	3900	3600	2800	3400	3500	2250	16 800
11	I	4200	3500	3800	3100	3100	2600	21 600
	II	3600	3700	2700	2300	2400	1750	14 600
12	I	1800	1850	2000	1750	N/A	1350	10 800
	II	3450	3400	2750	2750	N/A	2750	15 500
13	I	1950	1950	1725	1850	N/A	1425	10 800
	II	3000	3250	2600	3100	N/A	2300	14 400
14	I	1800	1900	1825	1800	N/A	N/A	10 800
	II	3100	2900	2775	2800	N/A	N/A	15 400
15	I	1800	1825	1900	1600	1500	1400	9 000
	II	3050	3400	3050	2300	2250	2625	12 800

TABLE III-X. - DIMENSIONLESS DIAMETER, TIME-HISTORY COORDINATES

Stage I		Stage II		Stage I		Stage II		Stage I		Stage II	
t/t_{fI}	d_p/d_o	t/t_{fII}	d_p/d_o	t/t_{fI}	d_p/d_o	t/t_{fII}	d_p/d_o	t/t_{fI}	d_p/d_o	t/t_{fII}	d_p/d_o
Drop 2											
0	0.147	0	0.370	0	0.180	0	0.351	0	0.190	0	0.355
.2	.159	.2	.395	.2	.227	.2	.375	.2	.198	.2	.365
.4	.252	.4	.474	.4	.280	.4	.448	.4	.273	.4	.435
.6	.325	.6	.589	.6	.332	.6	.554	.6	.325	.6	.543
.8	.353	.8	.643	.8	.348	.8	.649	.8	.350	.8	.653
1.0	.360	1.0	.651	1.0	.354	1.0	.654	1.0	.356	1.0	.687
Drop 3											
0	0.162	0	0.360	0	0.174	0	0.370	0	0.185	0	0.350
.2	.185	.2	.377	.2	.220	.2	.412	.2	.220	.2	.392
.4	.276	.4	.465	.4	.251	.4	.465	.4	.276	.4	.459
.6	.332	.6	.570	.6	.309	.6	.560	.6	.310	.6	.533
.8	.352	.8	.650	.8	.347	.8	.690	.8	.327	.8	.637
1.0	.355	1.0	.684	1.0	.357	1.0	.747	1.0	.330	1.0	.656
Drop 6											
Drop 7											
Drop 9											
Drop 10											

TABLE III-X. - DIMENSIONLESS DIAMETER, TIME-HISTORY COORDINATES - Concluded

Stage I		Stage II		Stage I		Stage II		Stage I		Stage II	
t/t_{fI}	d_p/d_o	t/t_{fII}	d_p/d_o	t/t_{fI}	d_p/d_o	t/t_{fII}	d_p/d_o	t/t_{fI}	d_p/d_o	t/t_{fII}	d_p/d_o
Drop 5											
0	0.211	0	0.360	0	0.177	0	0.344	0	0.197	0	0.338
.2	.234	.2	.403	.2	.210	.2	.366	.2	.226	.2	.380
.4	.299	.4	.500	.4	.255	.4	.468	.4	.310	.4	.441
.6	.339	.6	.620	.6	.314	.6	.564	.6	.328	.6	.538
.8	.360	.8	.791	.8	.329	.8	.672	.8	.336	.8	.635
1.0	.370	1.0	.809	1.0	.341	1.0	.717	1.0	.340	1.0	.670
Drop 8											
Drop 11											

TABLE III-XI. - PARA-SAIL WEIGHT AND VOLUME

	Weight, lb		Volume, in. ³ (a)	
	70A-4	70A-5	70A-4	70A-5
Canopy, lines, internal para- chute, and riser	136	141	10 348	10 728
Vent stabilization para- chute, 51-in.-diameter ribless guide surface canopy	2	2	148.5	148.5
Bridle	1	1	67.5	67.5
Main canopy deployment bag	7	7	529	529
Total	146	151	11 093	11 473

^aUnder 1 lb/in.² packing pressure, hand pack.

TABLE III-XII. - PERFORMANCE EVALUATION OF PARA-SAIL
CONFIGURATIONS 70A-4 AND 70A-5

Performance description	Required	Demonstrated
Strength capability	Successful deployment, $q = 120 \text{ lb/ft}^2$	Successful deployment, $q = 127.7 \text{ lb/ft}^2$
Rate of descent	30 ft/sec, 5000 ft	29.3 ft/sec, 5000 ft
Lift-to-drag ratio	1.0 minimum	1.04 average
Turn rate	20 deg/sec, minimum	48 deg/sec average, drop 4
Steady-state stability	$\pm 3^\circ$	Negligible
Maximum shock force, 80 lb/ft^2	16 000 lb, maximum	15 700 lb



Figure III-1.- Para-Sail parachute.

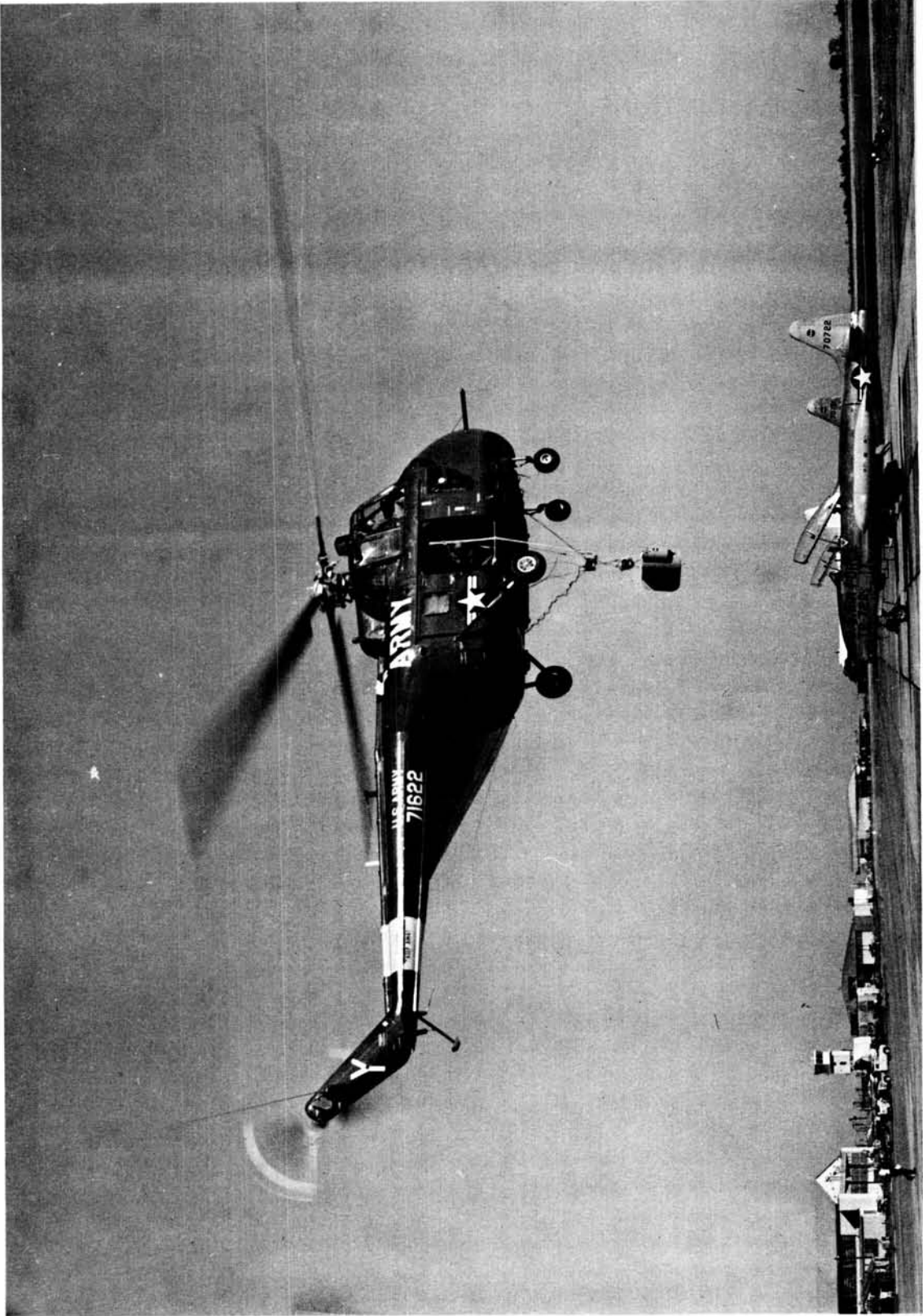


Figure III-2.- Drop aircraft and test vehicle.

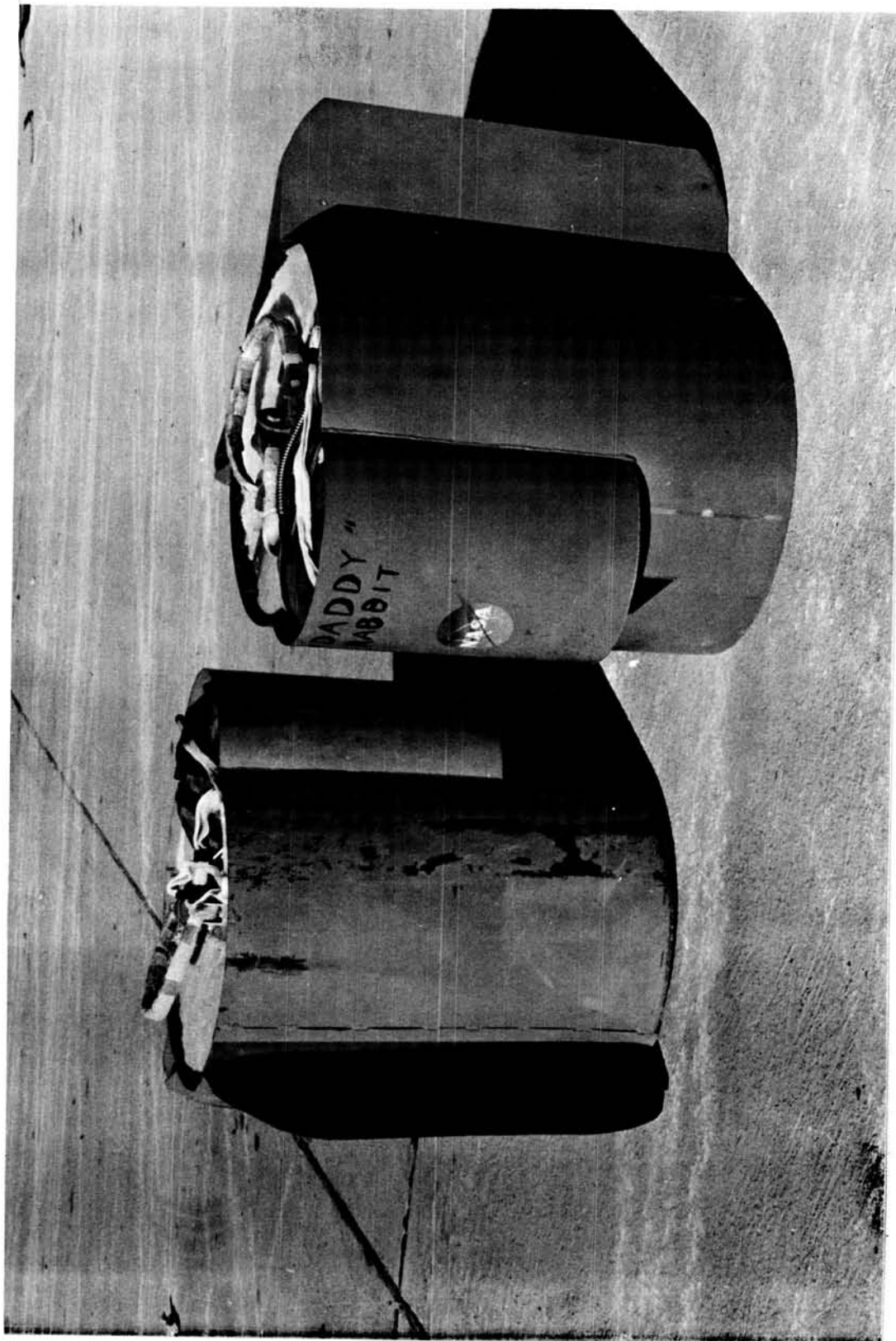


Figure III-3.- Test vehicles housing the parachute bag, camera, and batteries (side view).

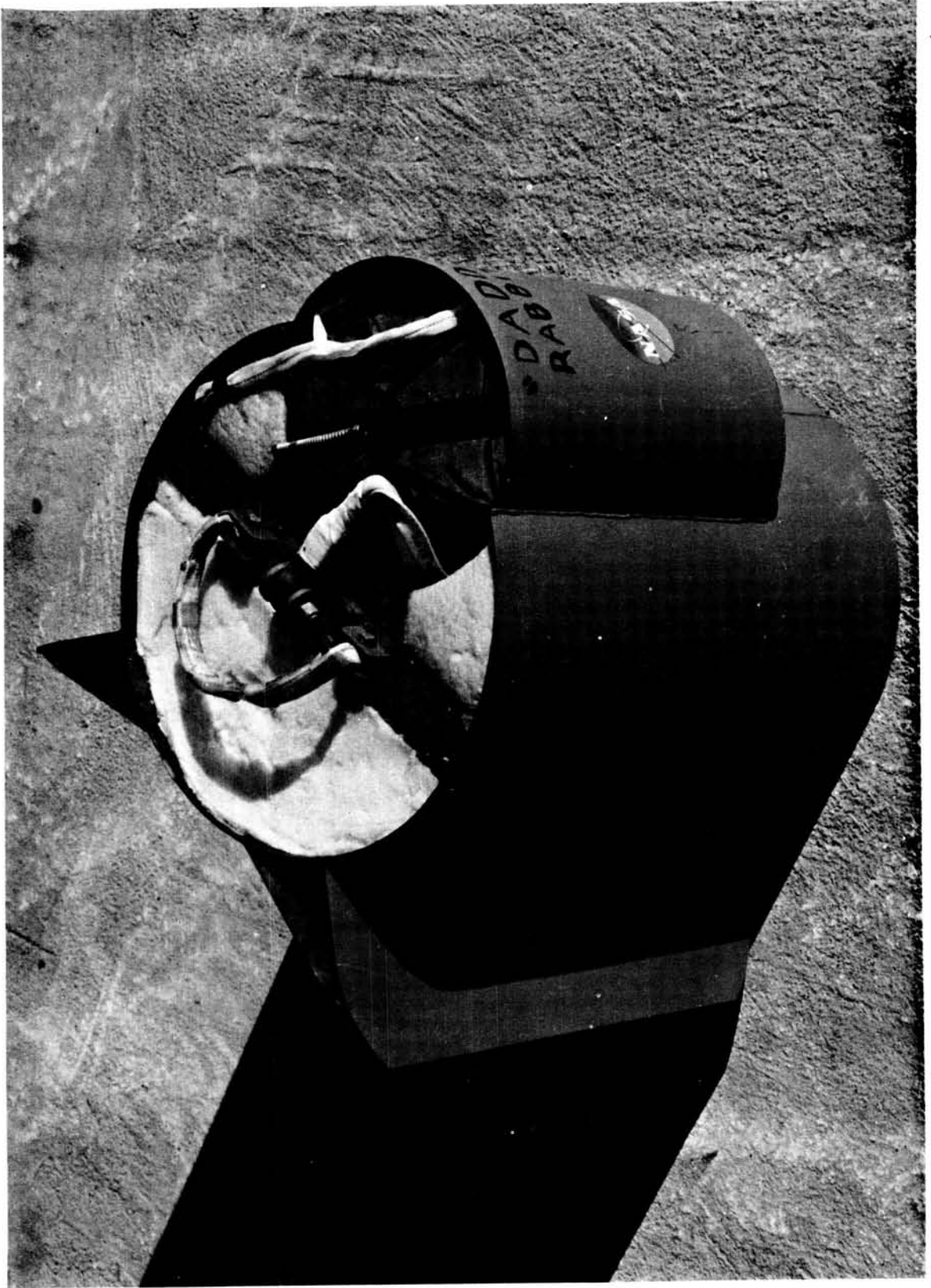


Figure III-4.- Test vehicle housing the parachute bag, camera, and batteries (top view).



(a) Shortened condition.

Figure III-5.- Special variable length risers.



(b) Extended per mission.
Figure III-5. - Concluded.

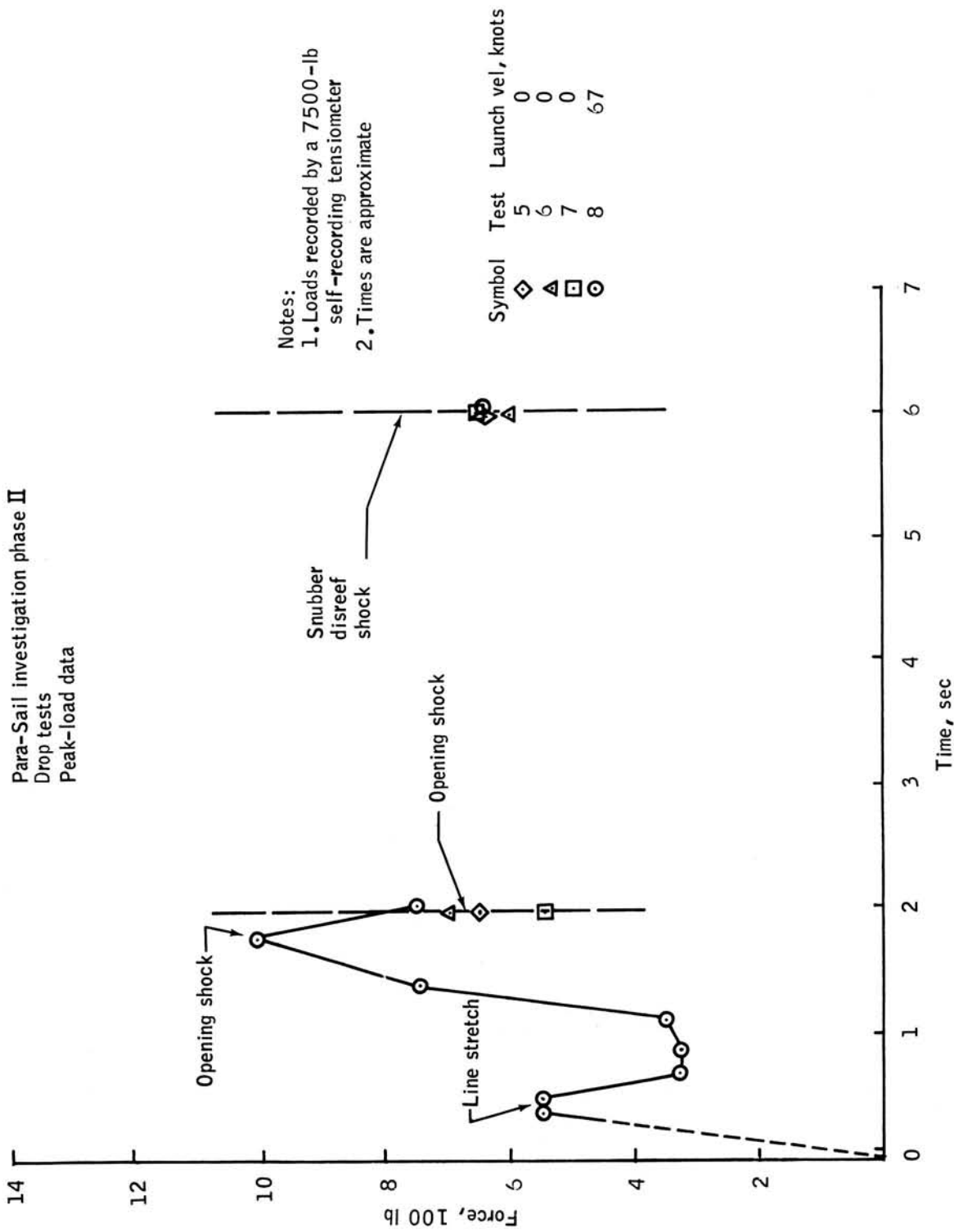


Figure III-6.- Peak-load data for tests 5, 6, 7, and 8.

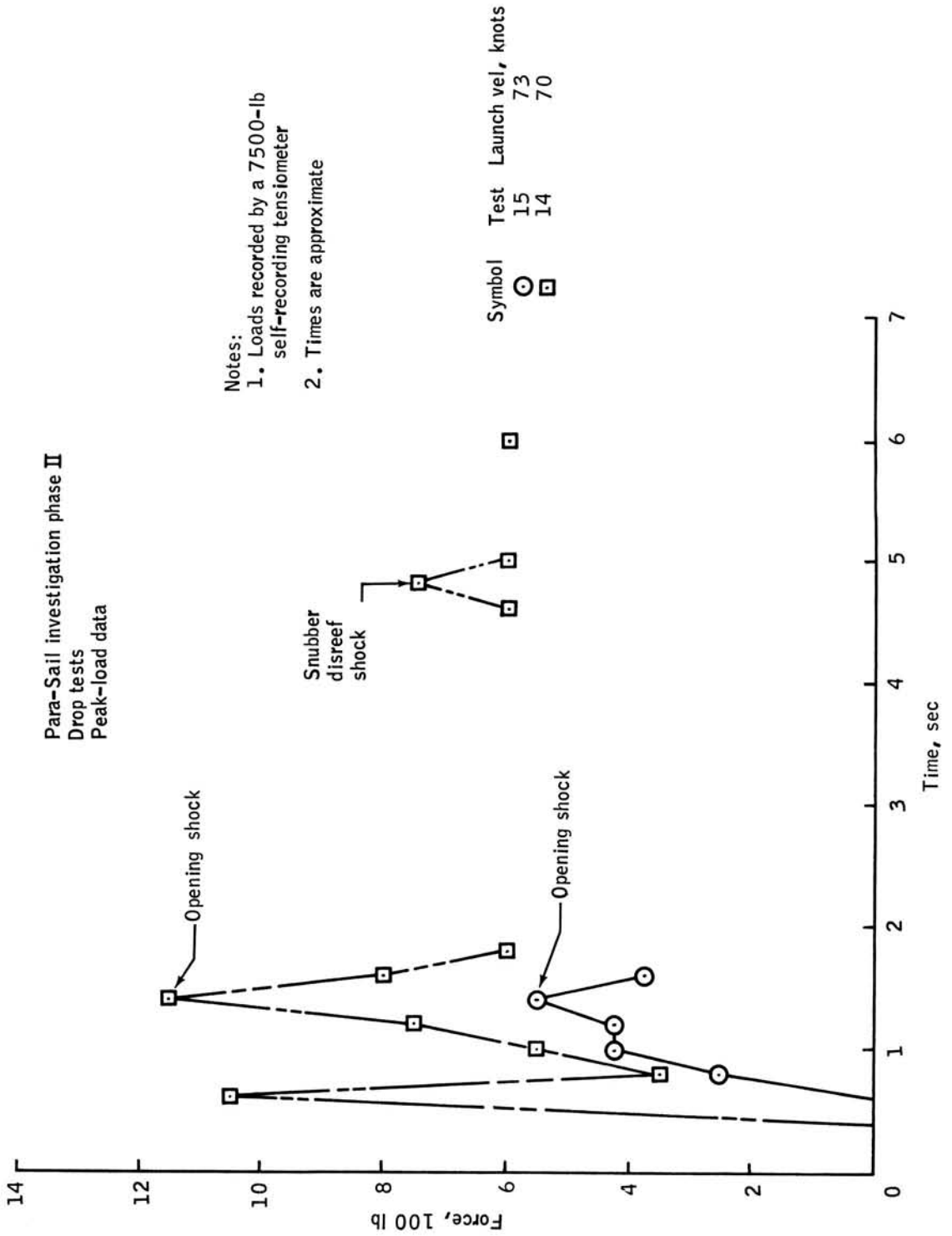


Figure III-7.- Peak-load data for tests 14 and 15.

Canopy rotation versus time
Test 12
Para-Sail
Right front riser
Shortened 24 in.

1. Time zero is disreef open
2. 16-mm tracking camera data
3. Launch conditions
A. Altitude 1000 ft
B. Velocity 0
4. Canopy rotated to left
5. Average turn rate 21.21 deg/sec

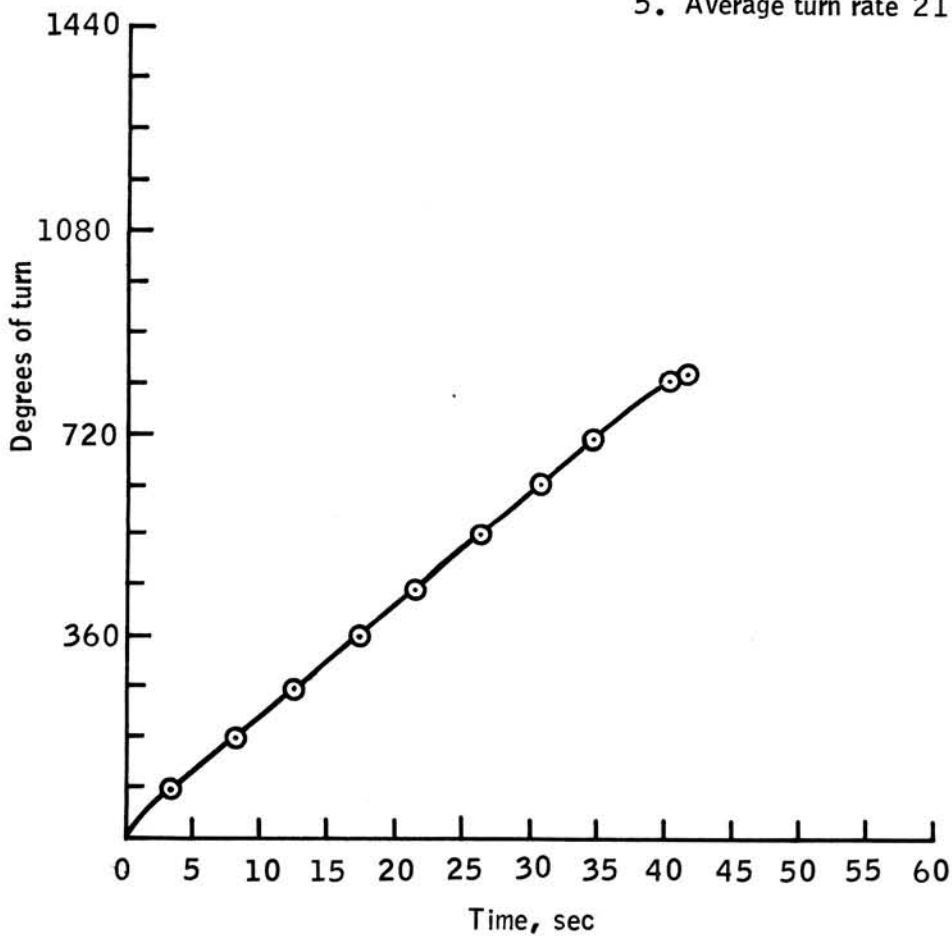


Figure III-8.- Turn with front riser shortened.

NASA-S-66-9853 OCT 24

Canopy rotation versus time
Test 13
Para-Sail
Right rear riser
Shortened 24 in.

1. Time zero is disreef open
2. 16-mm tracking camera data
3. Launch conditions
 - A. Altitude 1000 ft
 - B. Velocity 0
4. Canopy rotated to right
5. Average turn rate 16.4 deg/sec

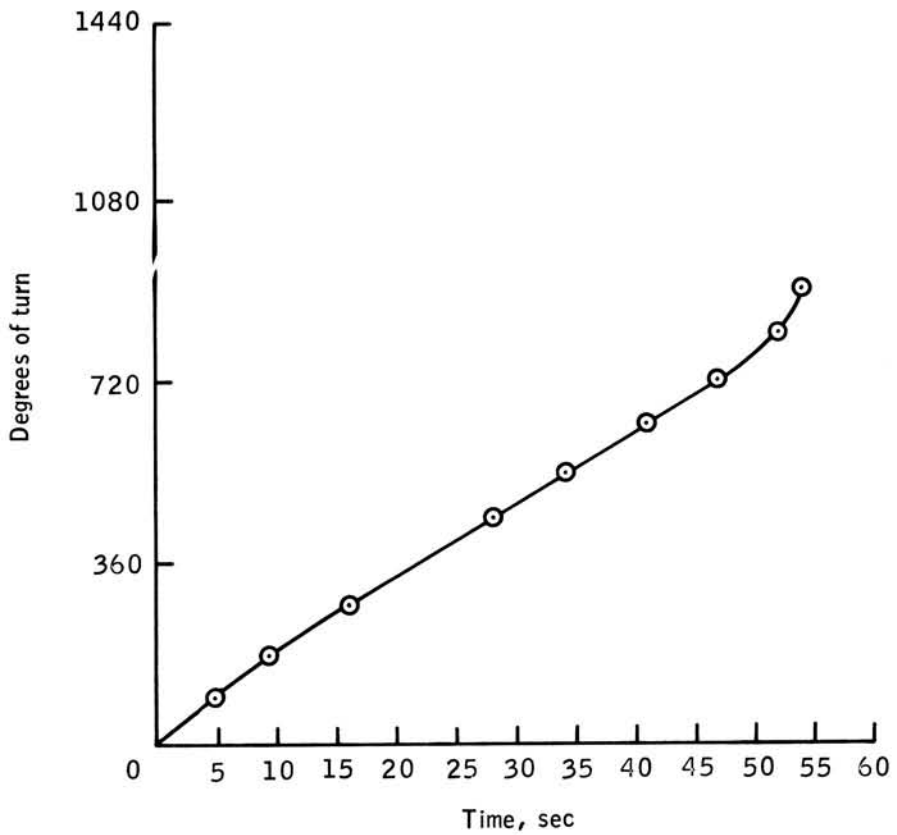


Figure III-9.- Turn with rear riser shortened.

Test 10
Para-Sail
Exhaust ports on lines
5,6,7, and 8 closed

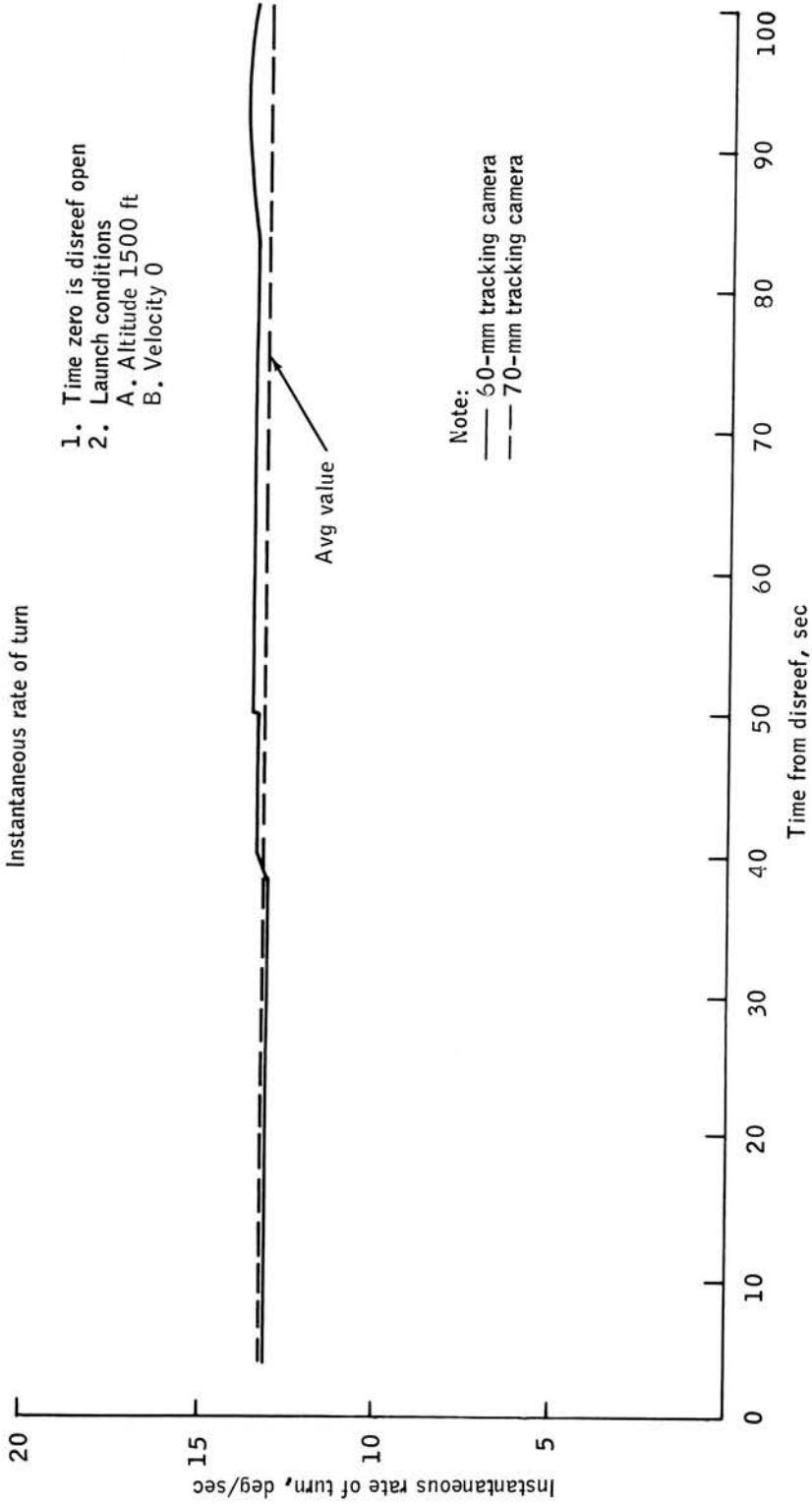


Figure III-10.- Turn with right exhaust ports closed.

Canopy rotation versus time
Test 10
Para-Sail
Exhaust ports of lines
5,6,7, and 8 closed

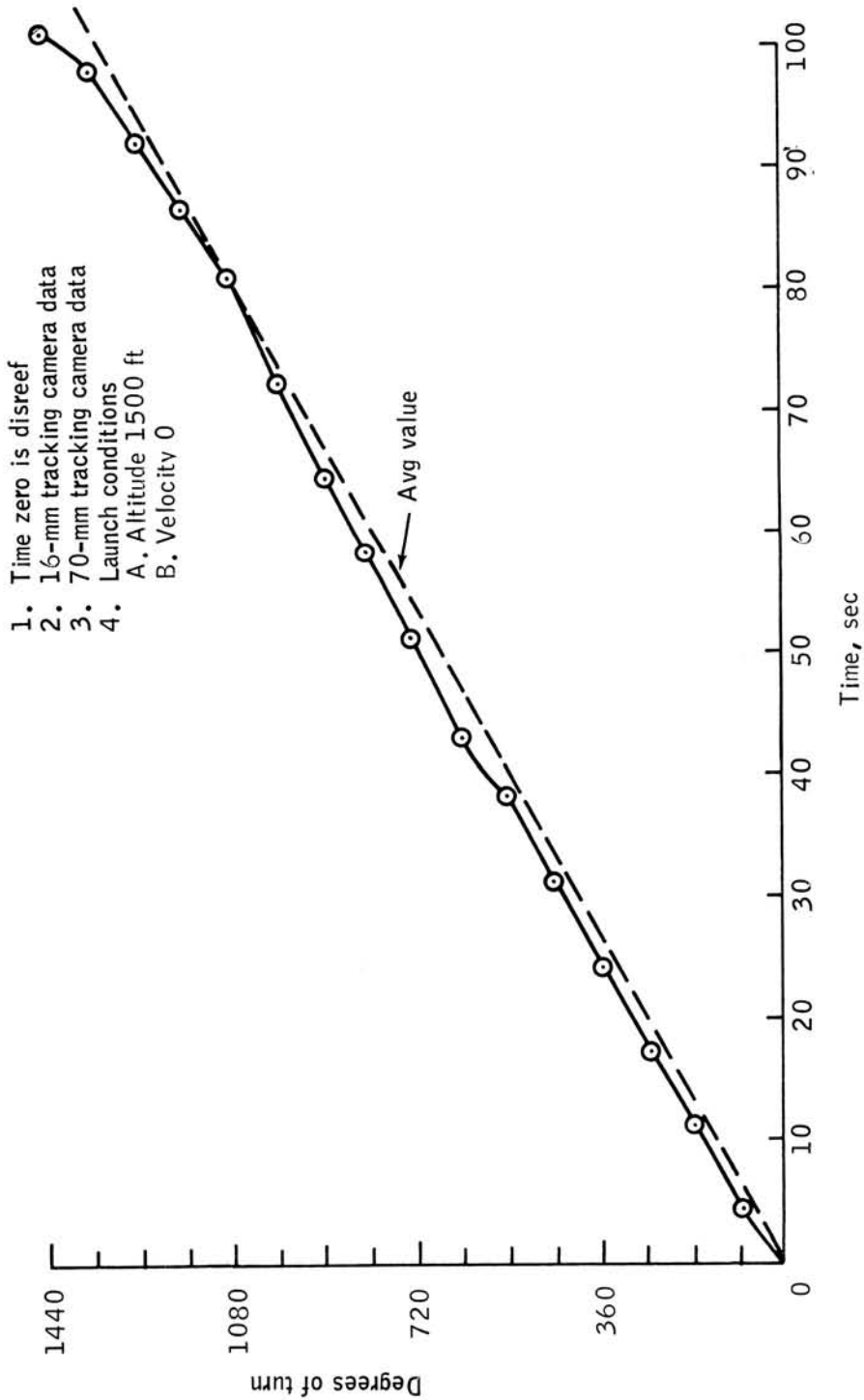


Figure III-11.- Turn with right exhaust ports closed.

Test II
Para-Sail
Exhaust ports on lines
17, 18, 19, and 20 closed

1. Time zero is disreef open
2. Launch conditions
A. Altitude 1500 ft
B. Velocity 0

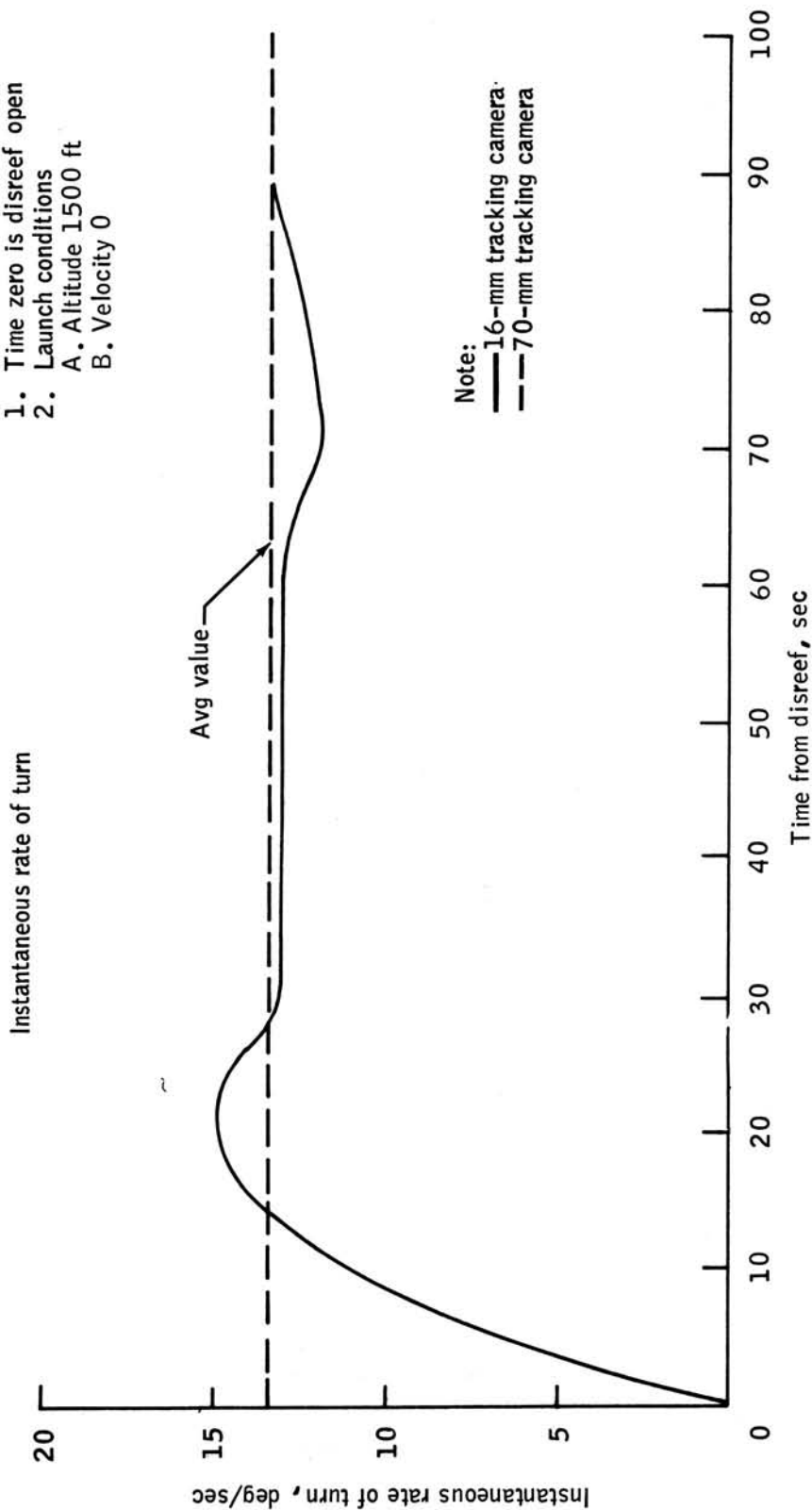


Figure III-12.- Turn with left exhaust ports closed.

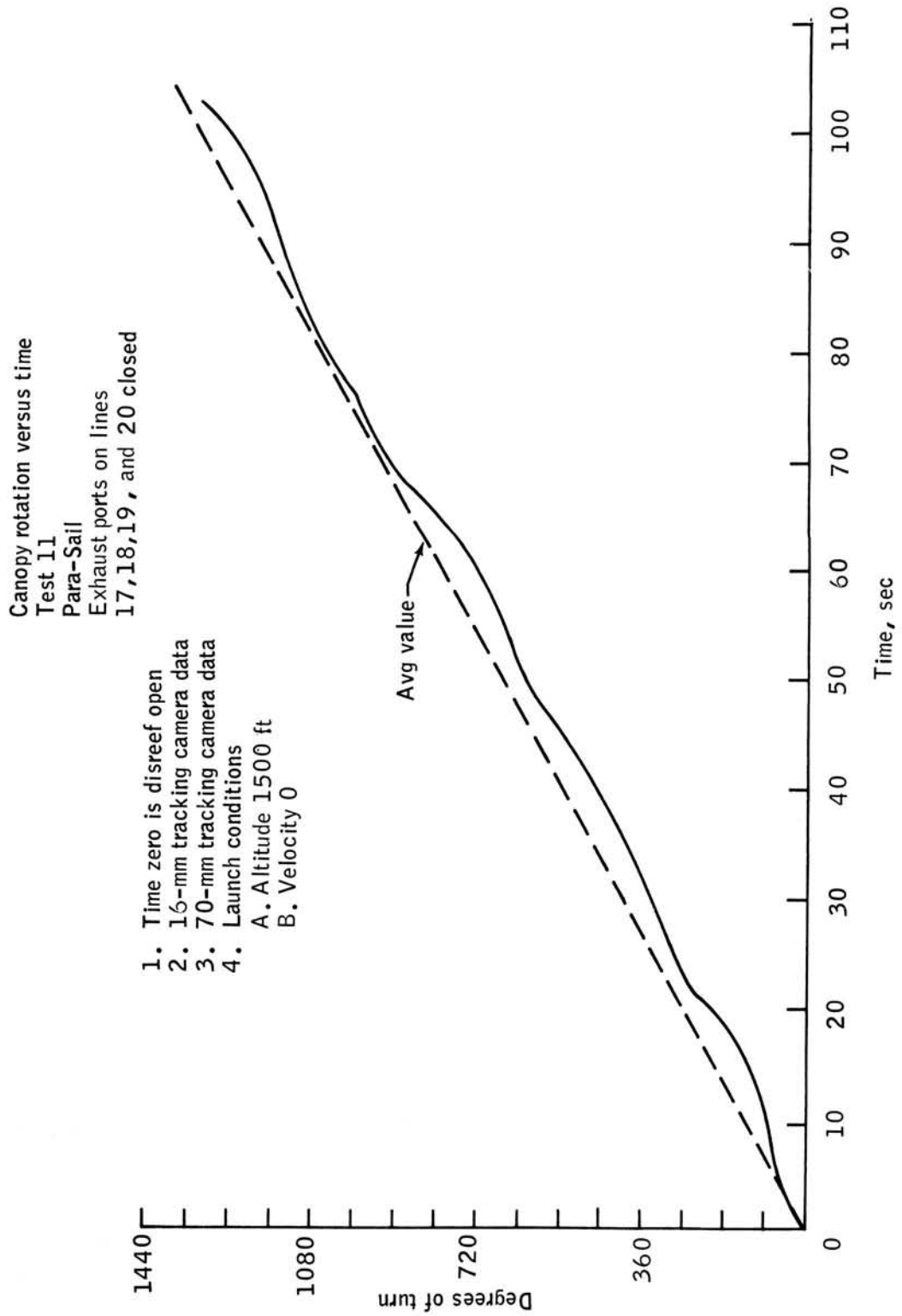


Figure III-13.- Turn with left exhaust ports closed.

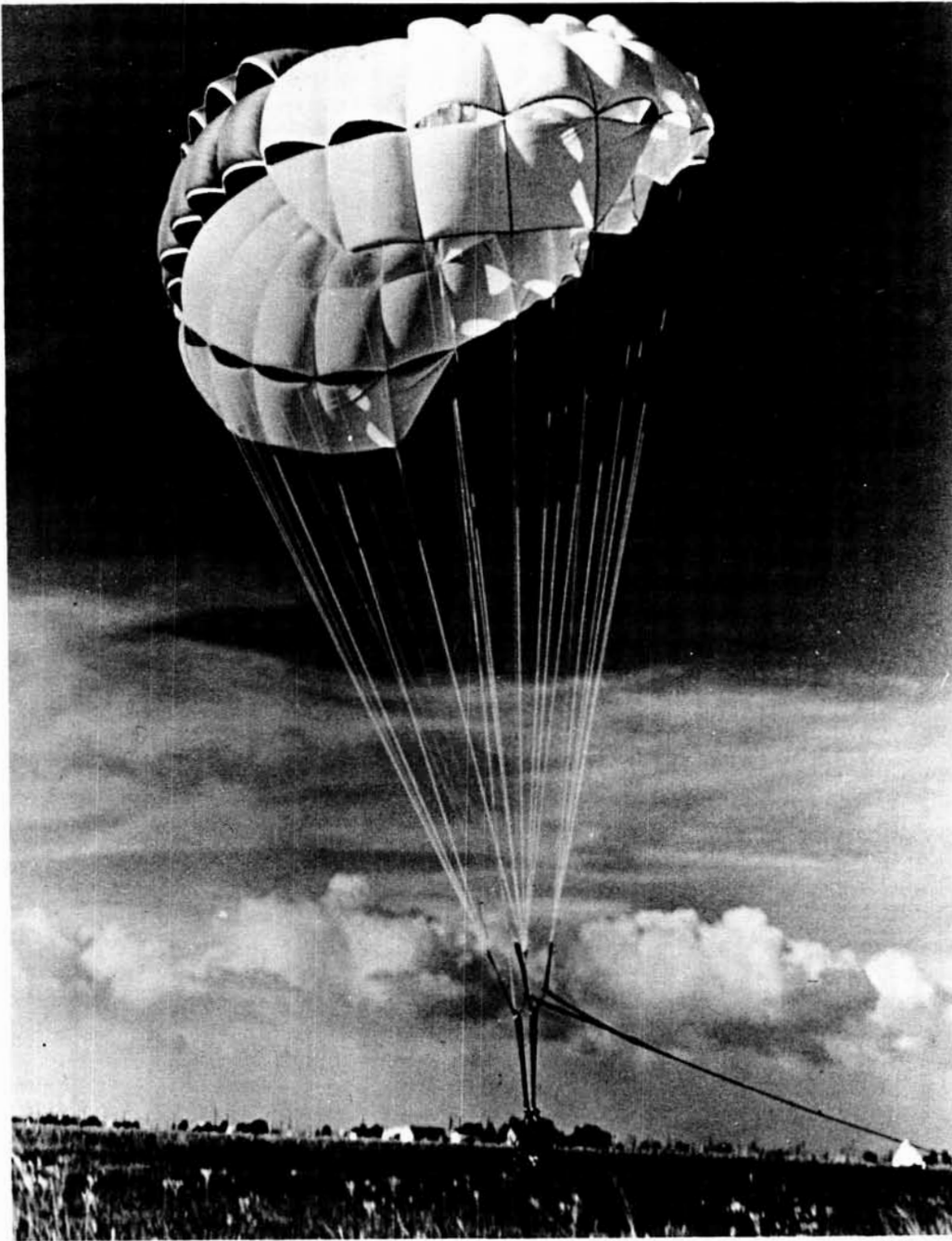


Figure III-14.- Original 23.2-ft-diameter Para-Sail.

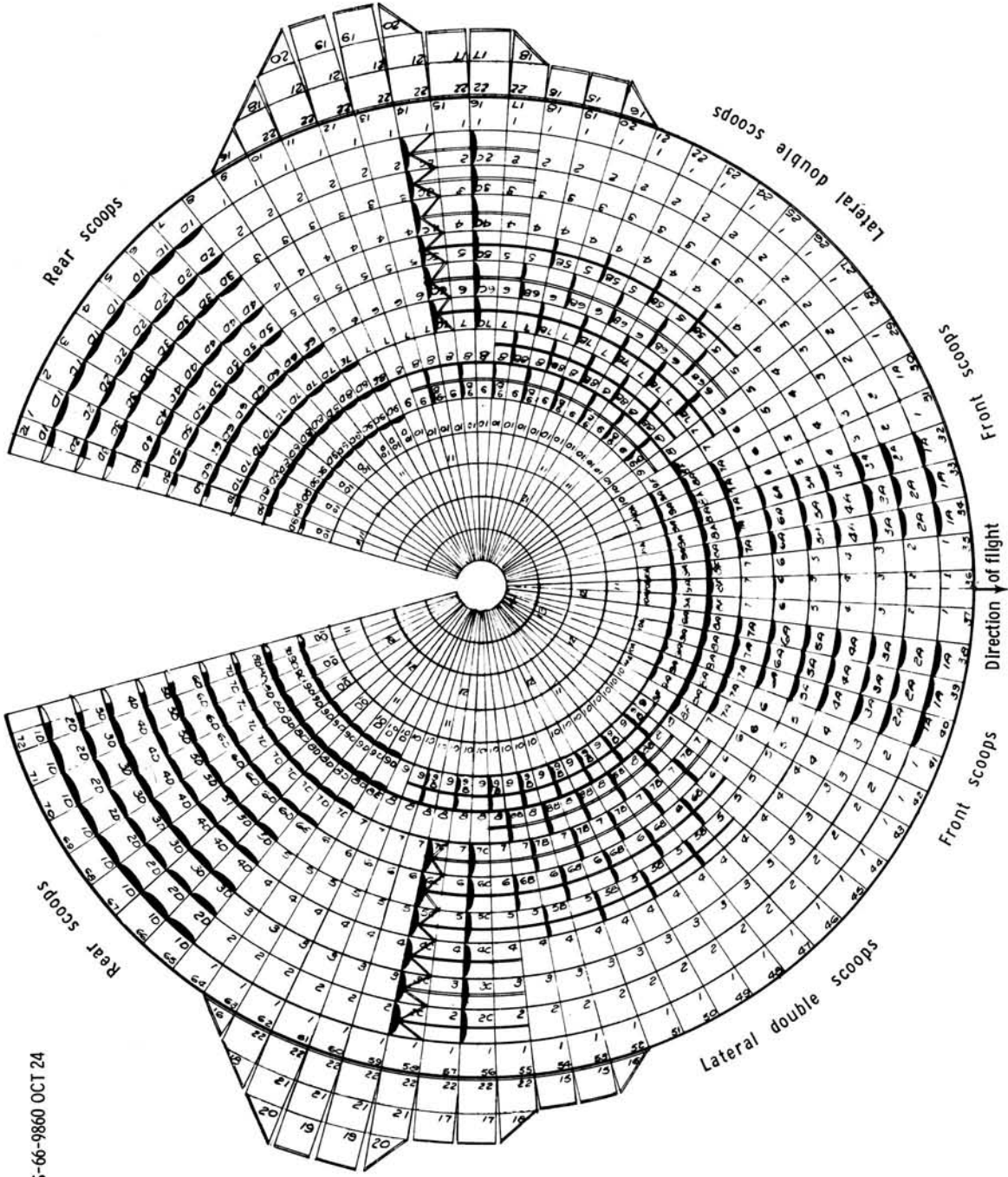
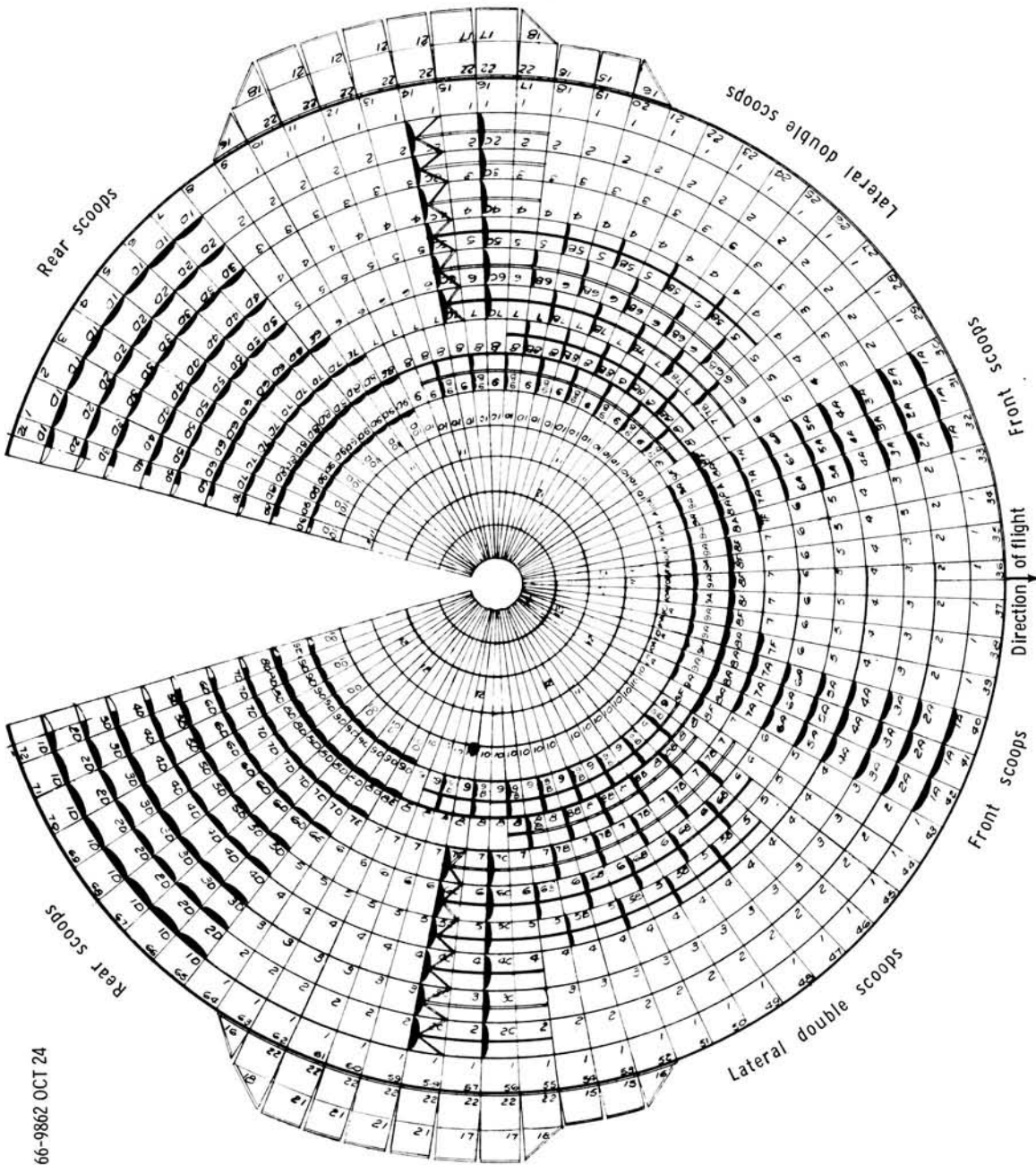


Figure III-15.- Original 80-ft Para-Sail, 3 solid gores. Configuration for Houston tests 1 and 2.



(b) Configuration for Houston tests 4 and 5.

Figure III-16.- Concluded.

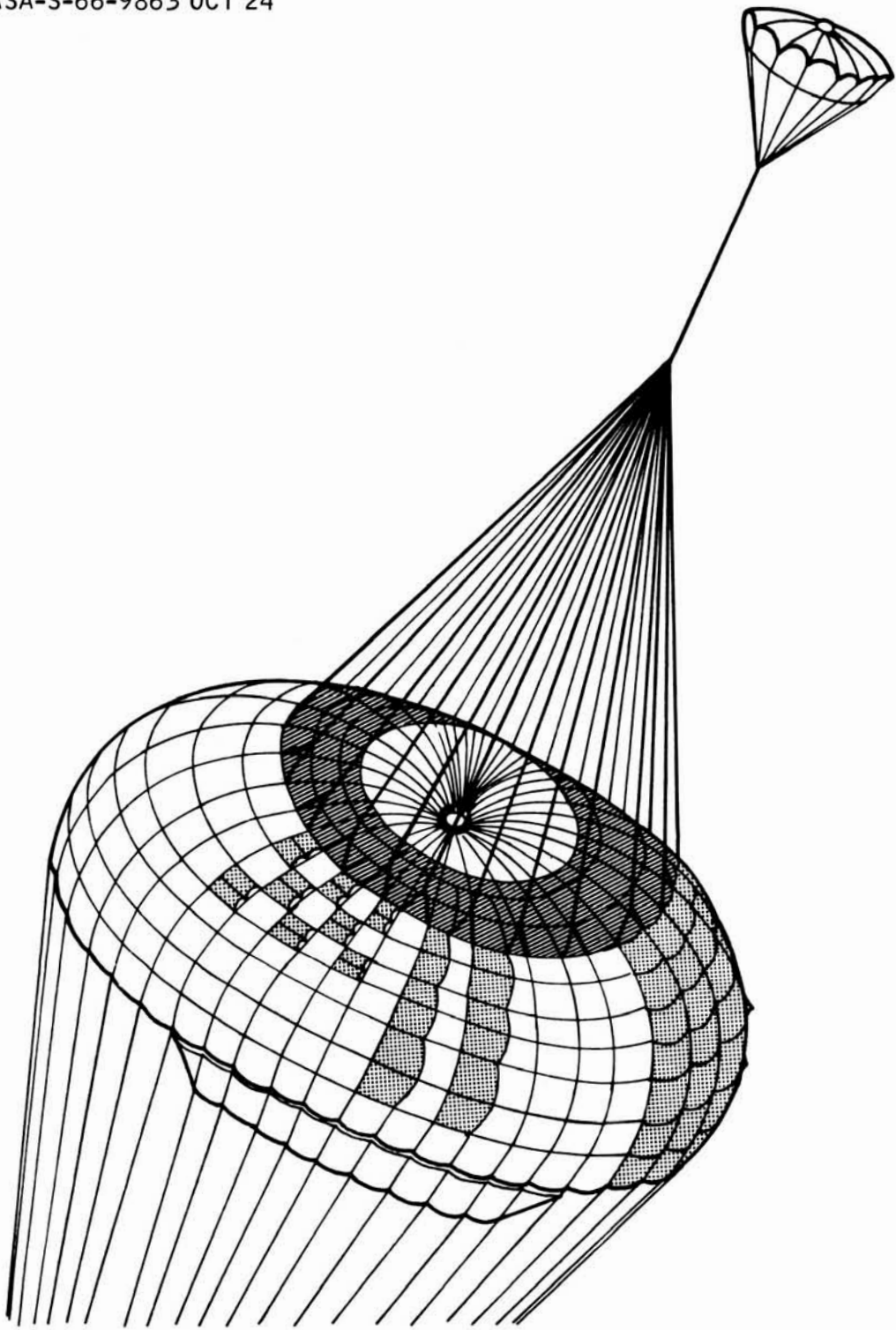


Figure III-17.- Thirty-six-line pilot parachute and bridle arrangement.

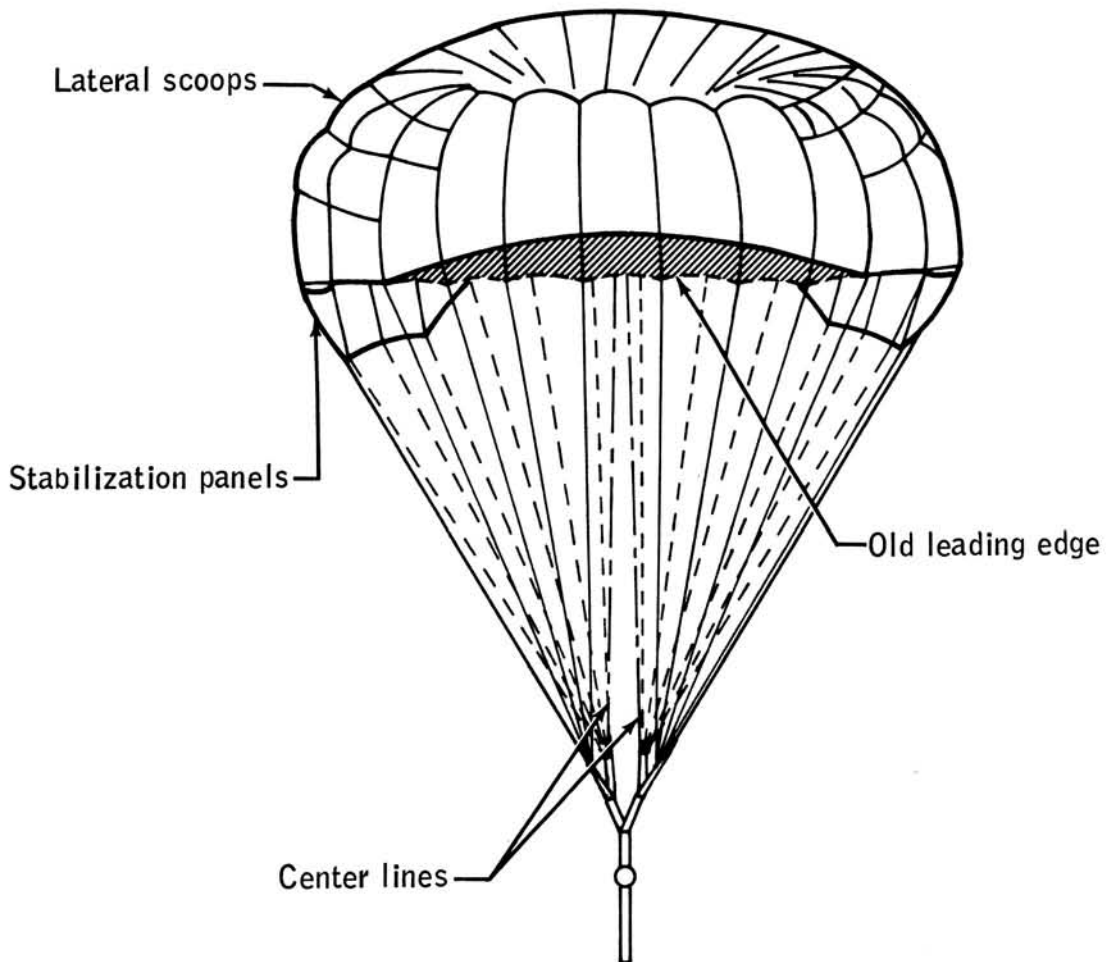
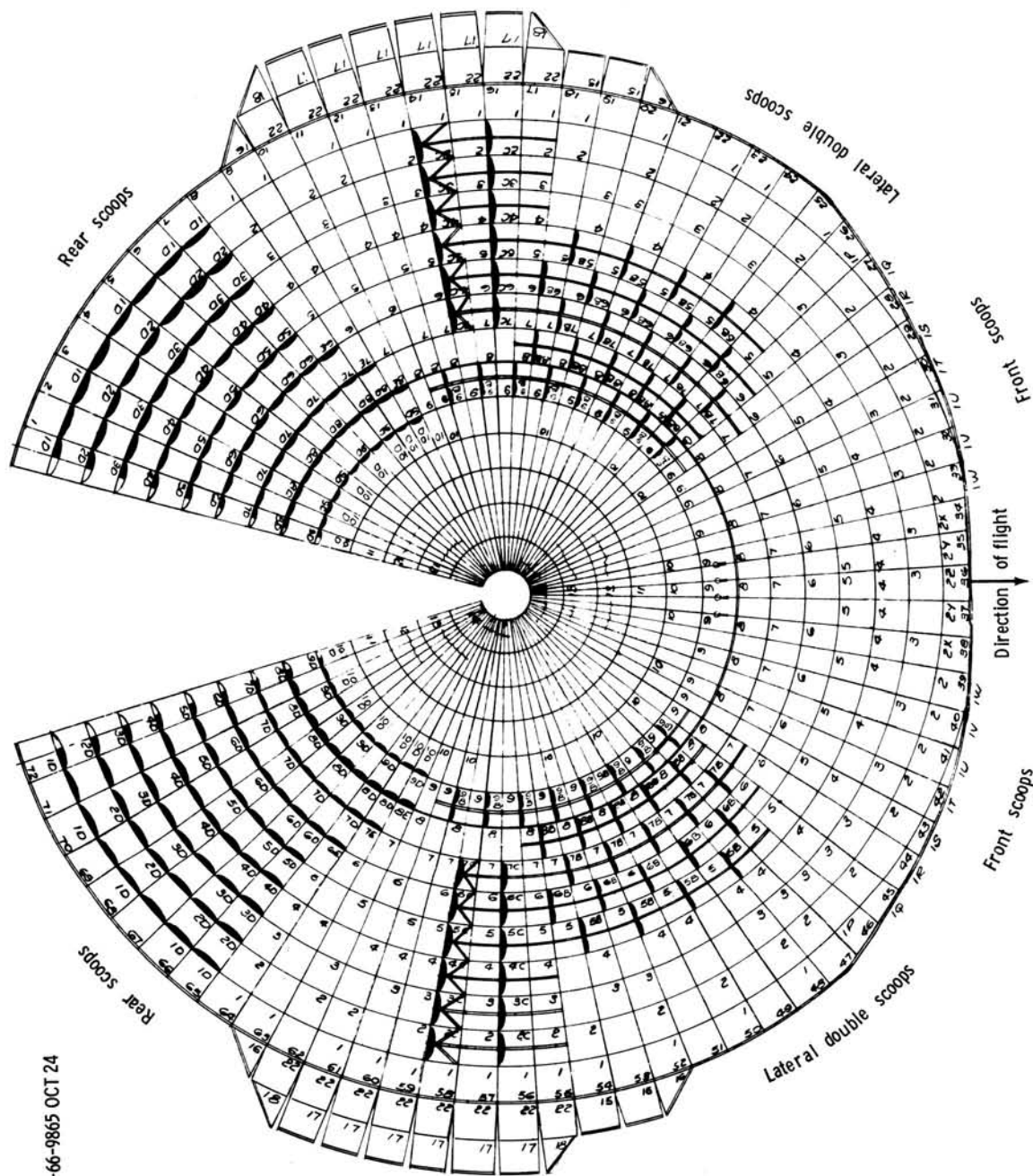
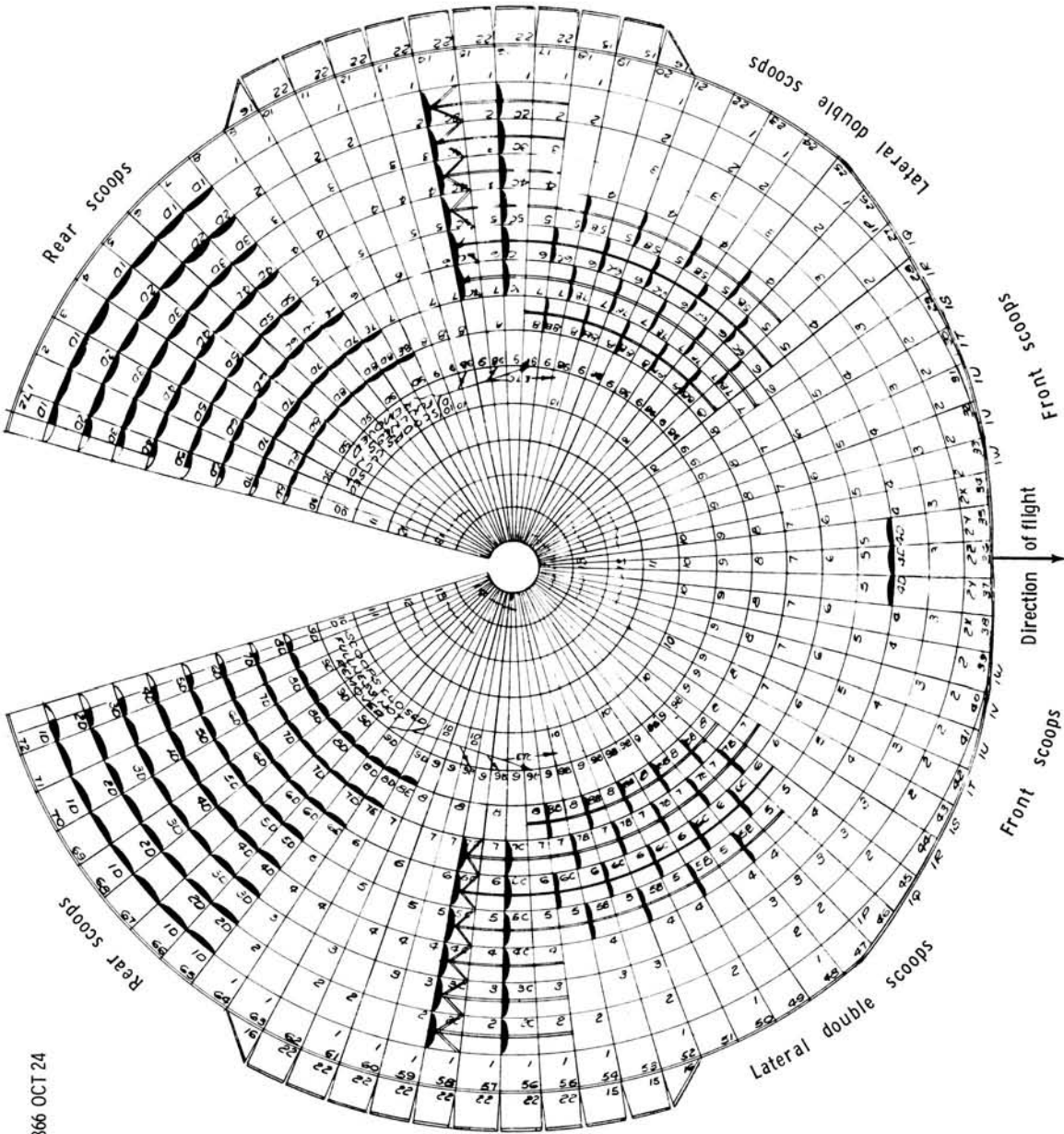


Figure III-18.- Twenty-four-foot d_0 Para-Sail, solid front elliptical cutout (front view).



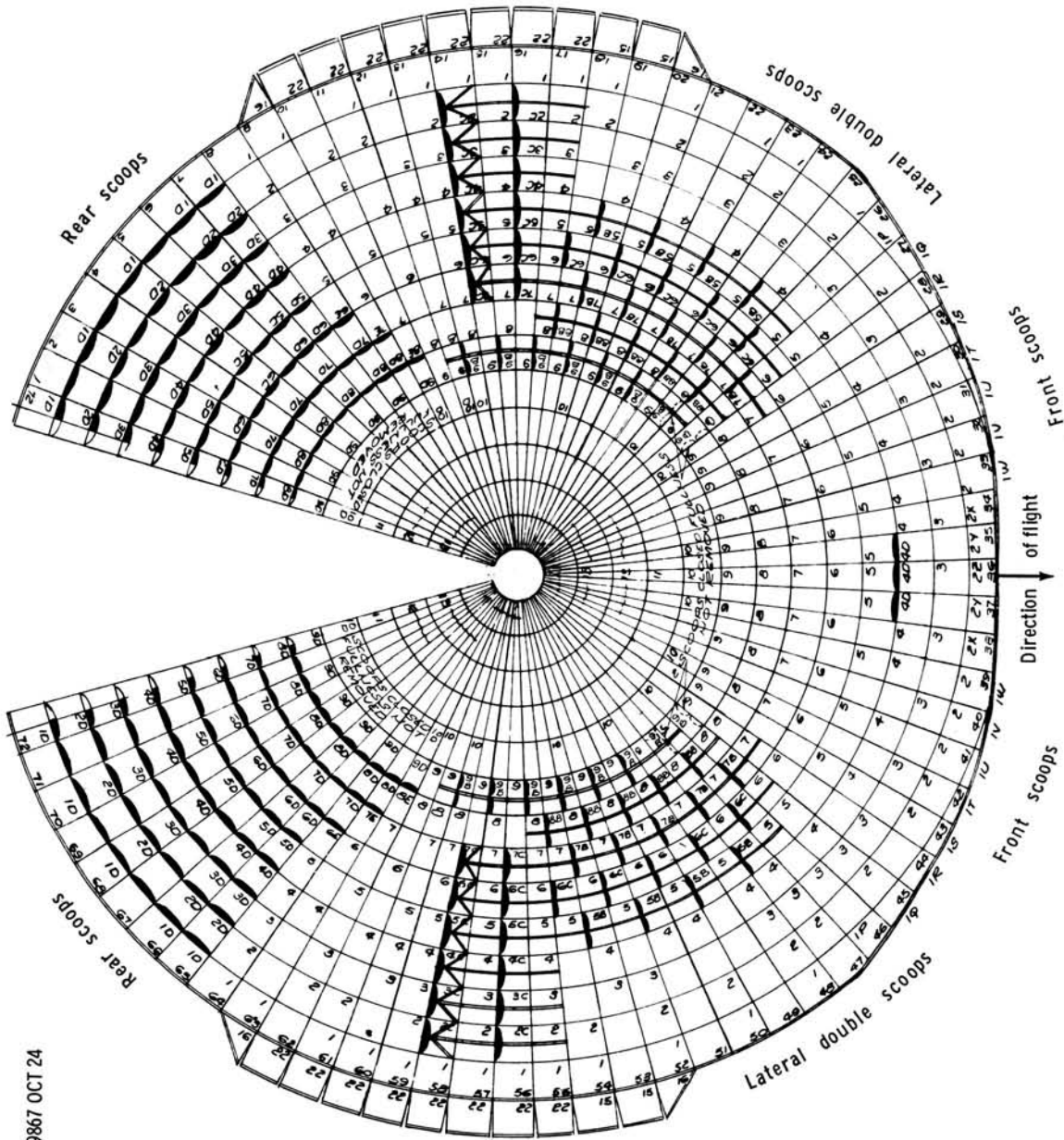
(a) Configuration for Houston tests 6 and 7.

Figure III-19.- Eighty-foot Para-Sail, solid front, elliptical cutout.



(b) Configuration for Houston test 8.

Figure III-19.- Continued.



(c) Configuration for Houston tests 9, 10, and 11; and El Centro tests 1, 2, 3, and 4.
Figure 19.- Concluded.

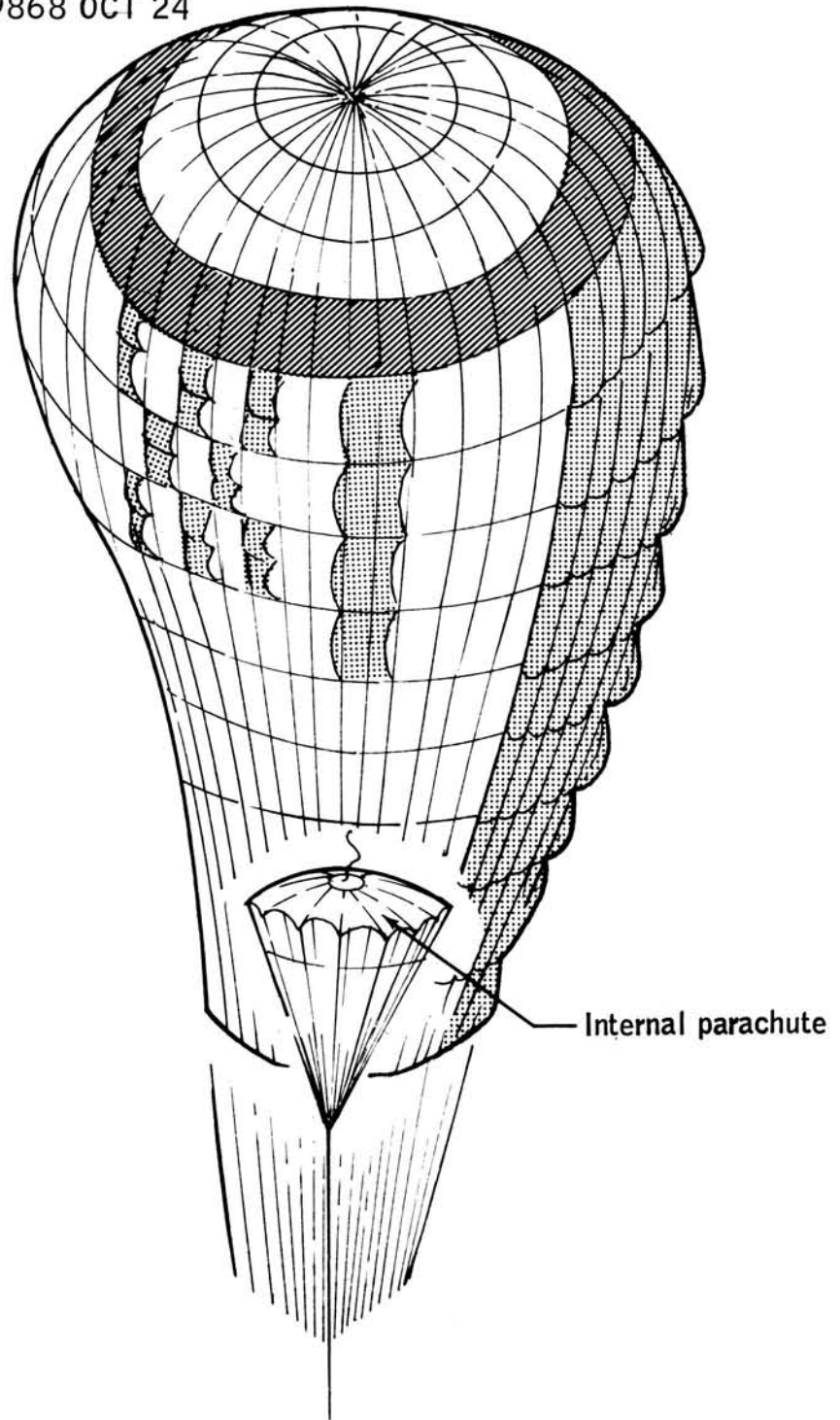


Figure III-20.- Internal parachute arrangement.

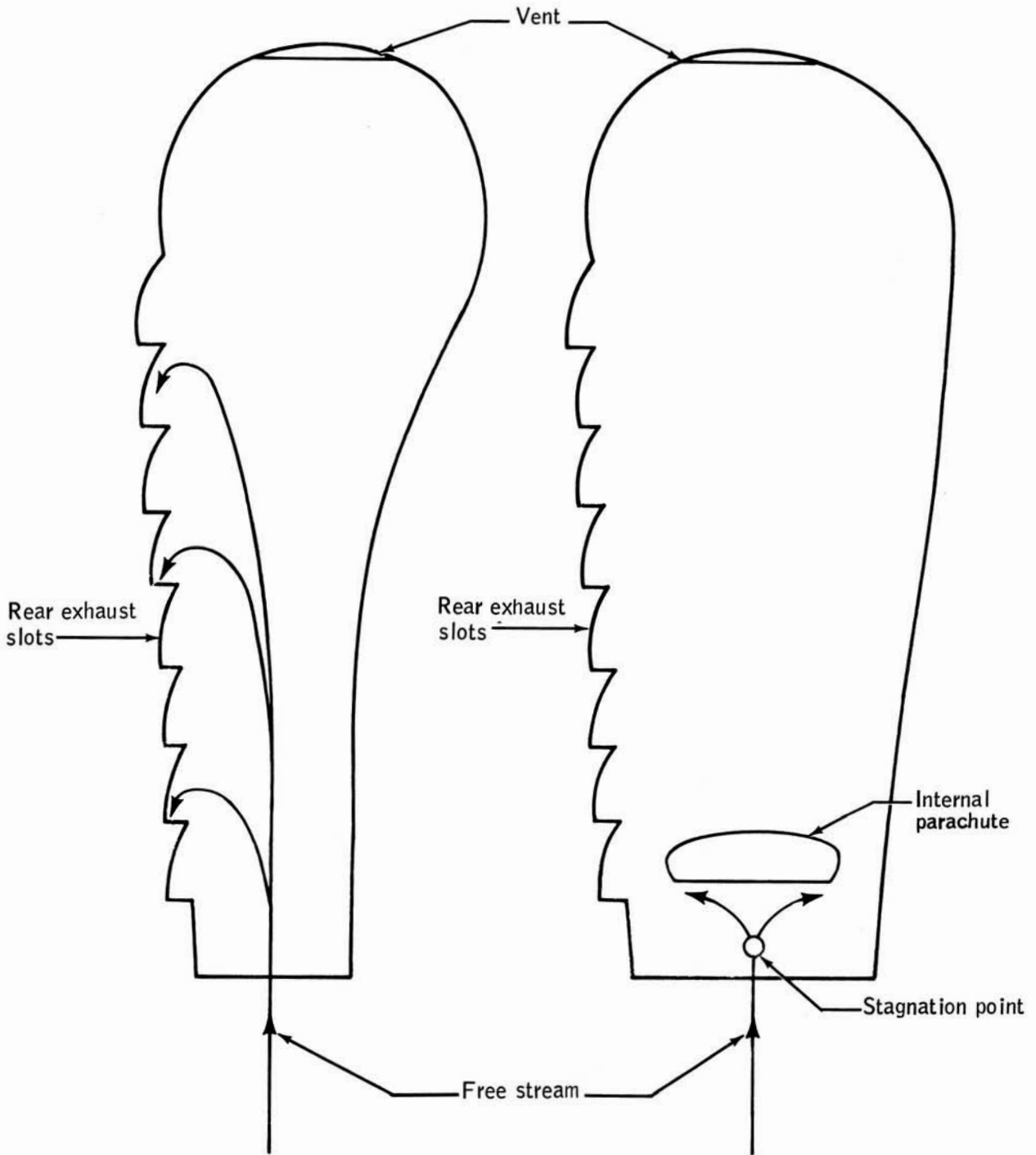
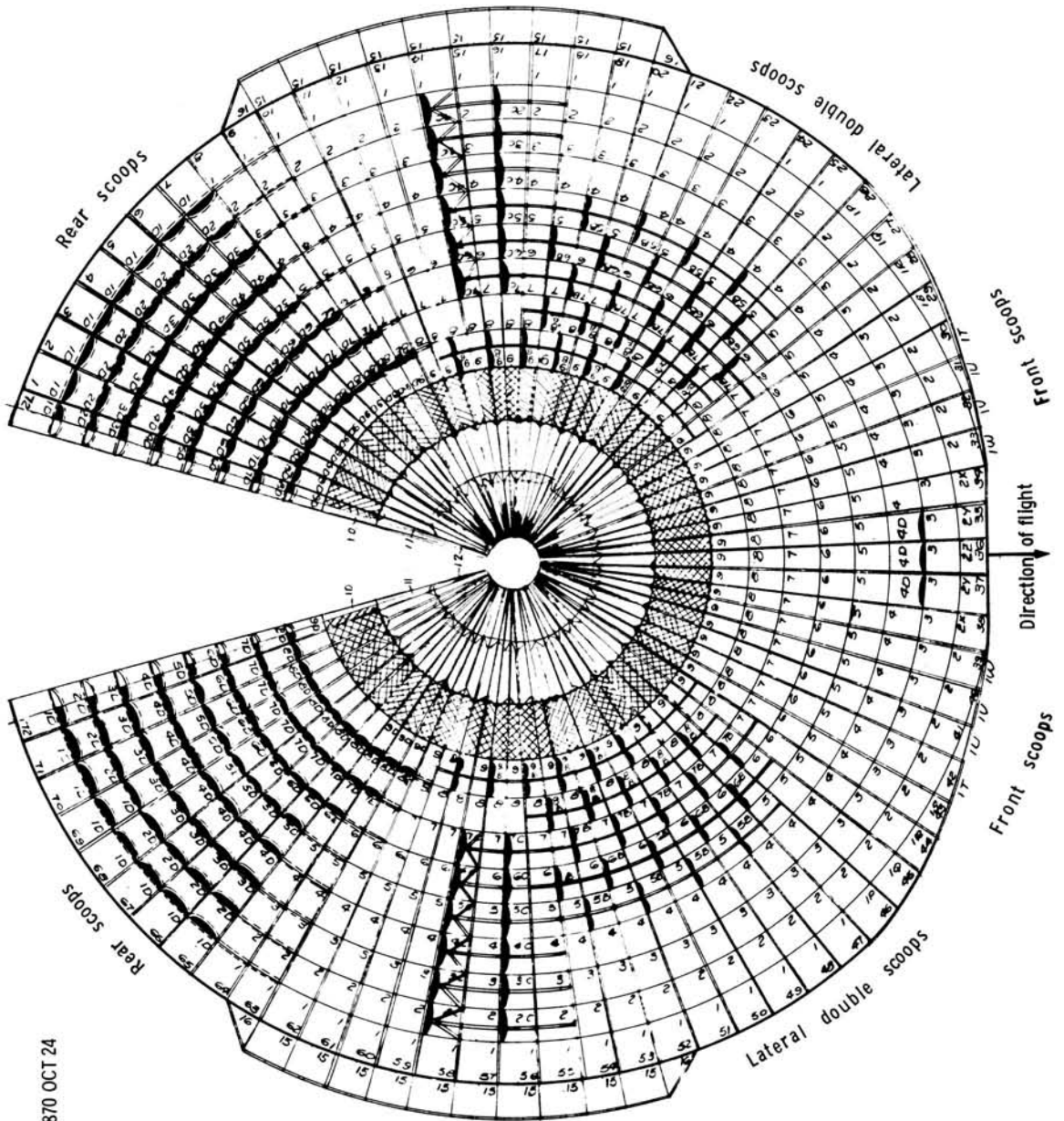
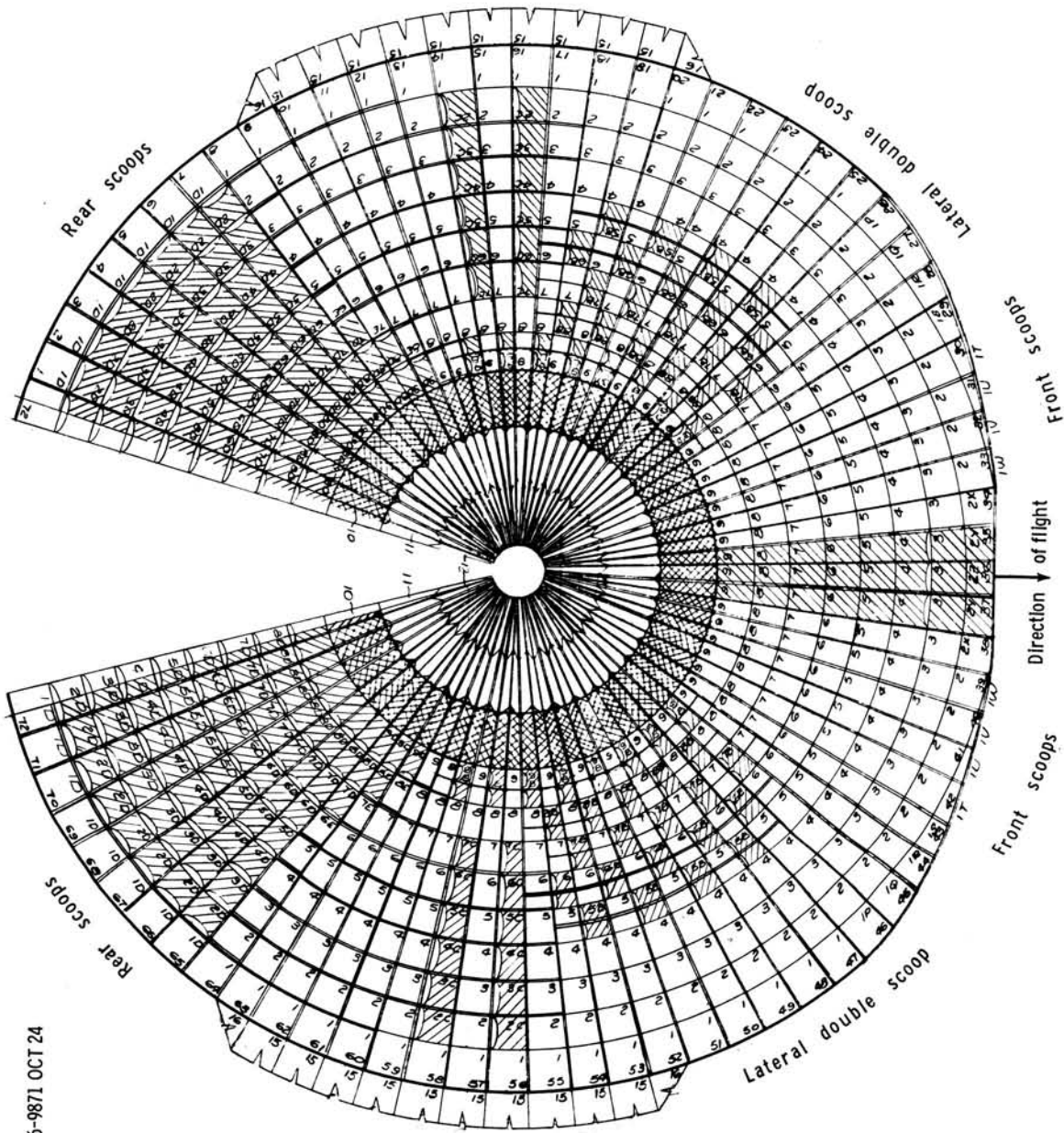


Figure III-21.- Reefed inflation, airstream lines.



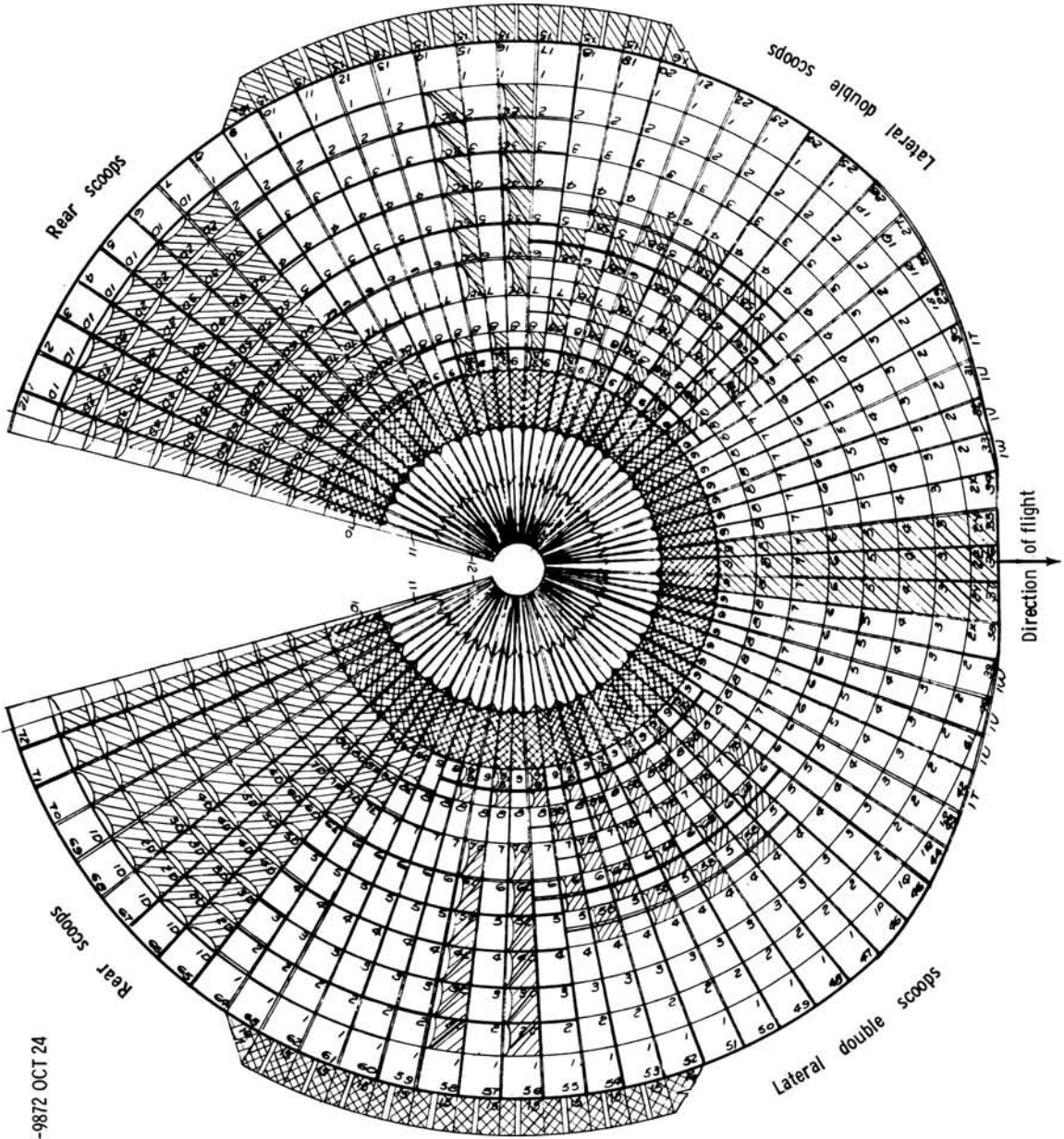
(a) Configuration for El Centro test 5.

Figure III-22.- Eighty-foot Para-Sail, no centerline.



(b) Configuration for El Centro tests 6 to 15 inclusive.

Figure III-22.- Continued.



(c) Final 80-ft configuration.
 Figure III-22.- Concluded.

NASA-S-66-9872 OCT 24

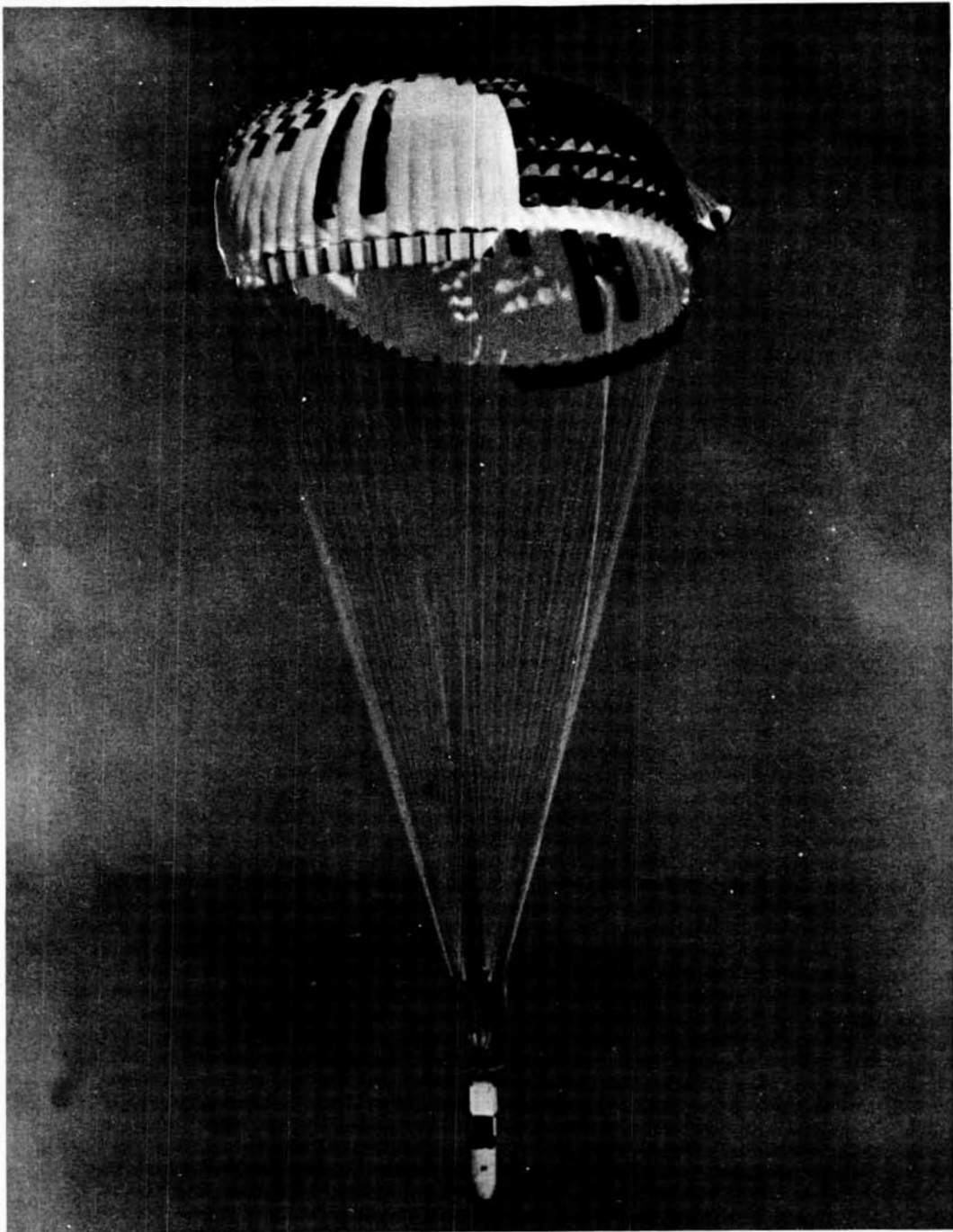


Figure III-23.- Eighty-foot Para-Sail, no centerline.

Altitude = 10 600 ft
Reefing = 12.35 percent for 6 sec
Payload weight = 4750 lb

○ Reefed opening shock
□ Full opening shock

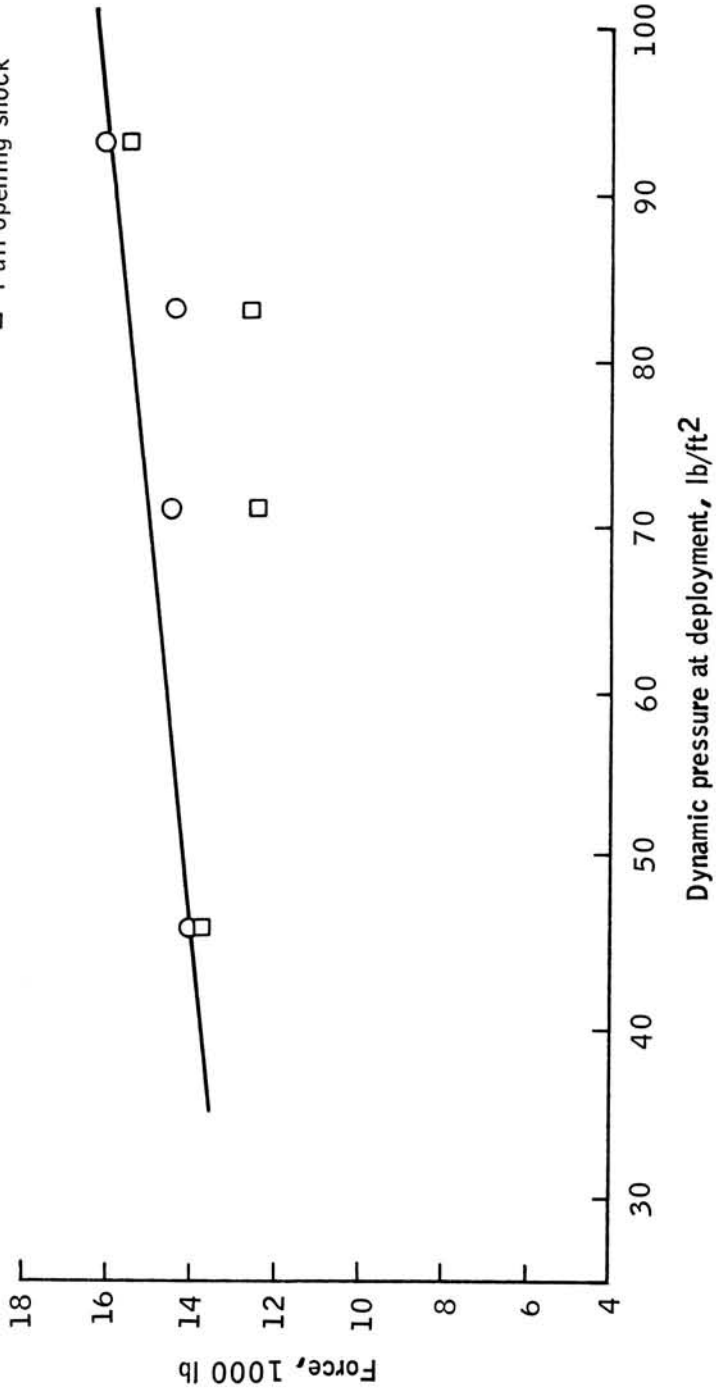


Figure III-24.- Expected opening loads.

Reefing = 12.35 percent for 6 sec
 Payload weight = 4750 lb
 Altitude 10 600 ft

—○— Expected time from line stretch
 to reefed opening shock
 - -□- - Expected time from disreef
 to full opening shock

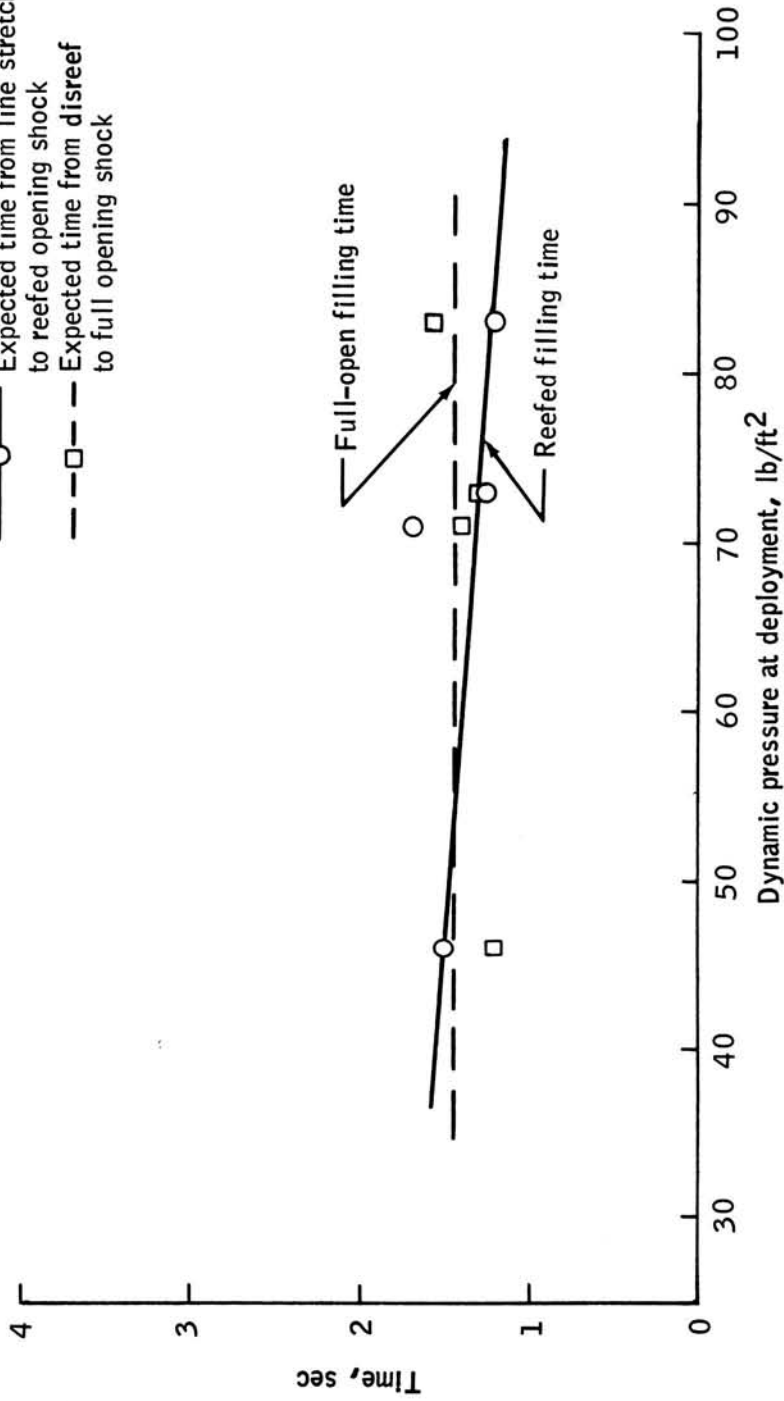


Figure III-25.- Expected opening times.

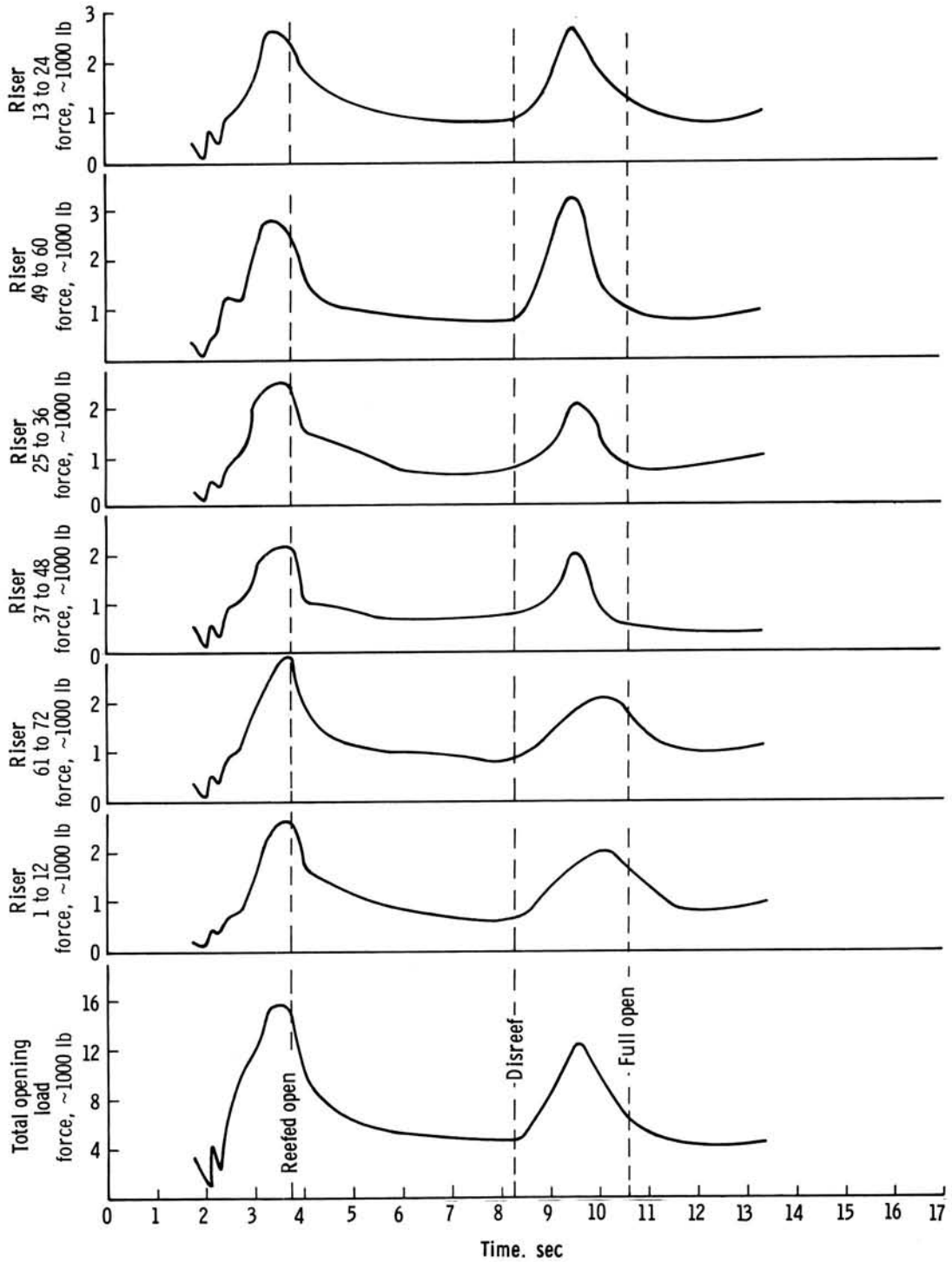


Figure III-26.- Individual riser loads, test 14.

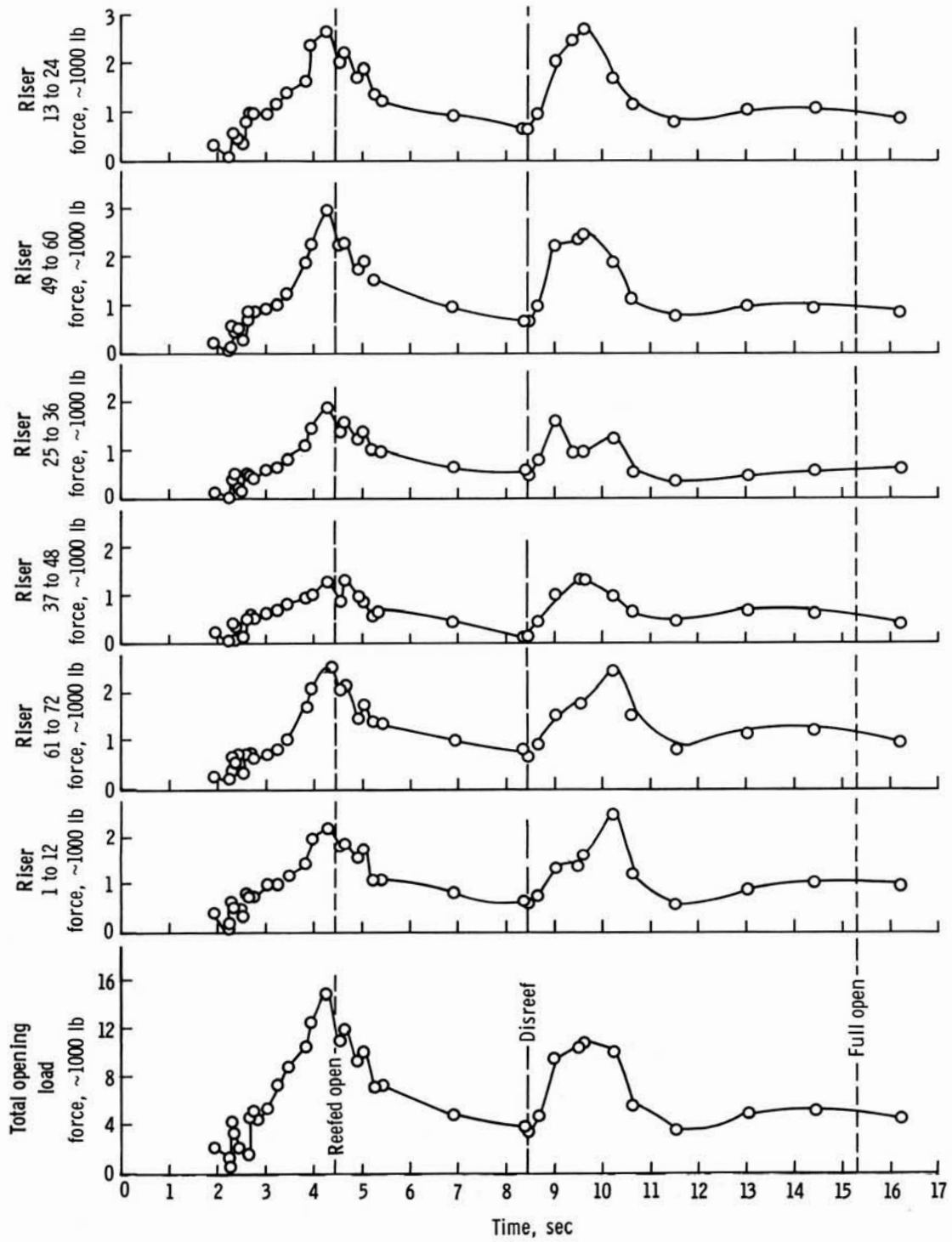


Figure III-27.- Individual riser loads, test 16.

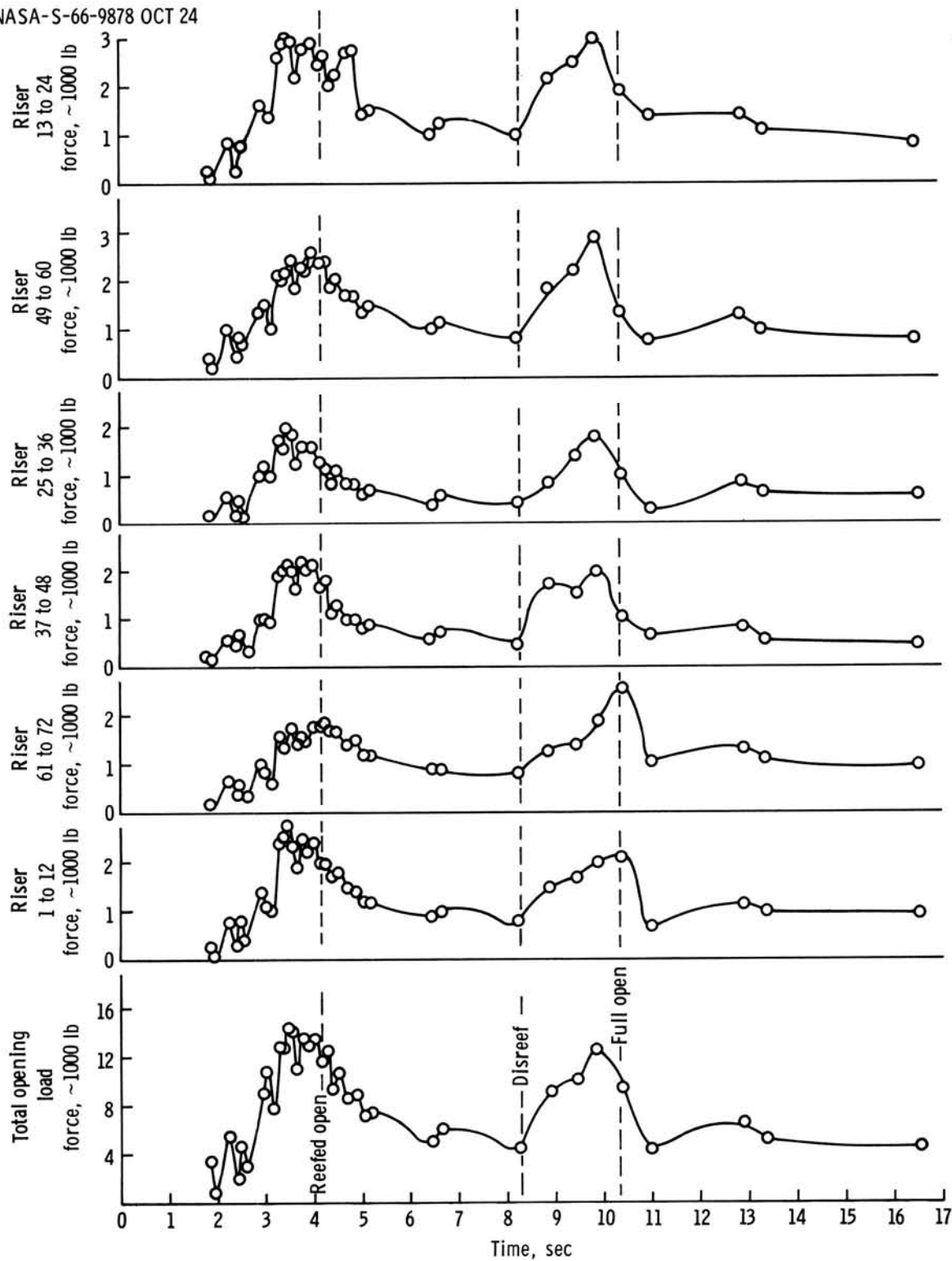


Figure III-28.- Individual riser loads, test 19.

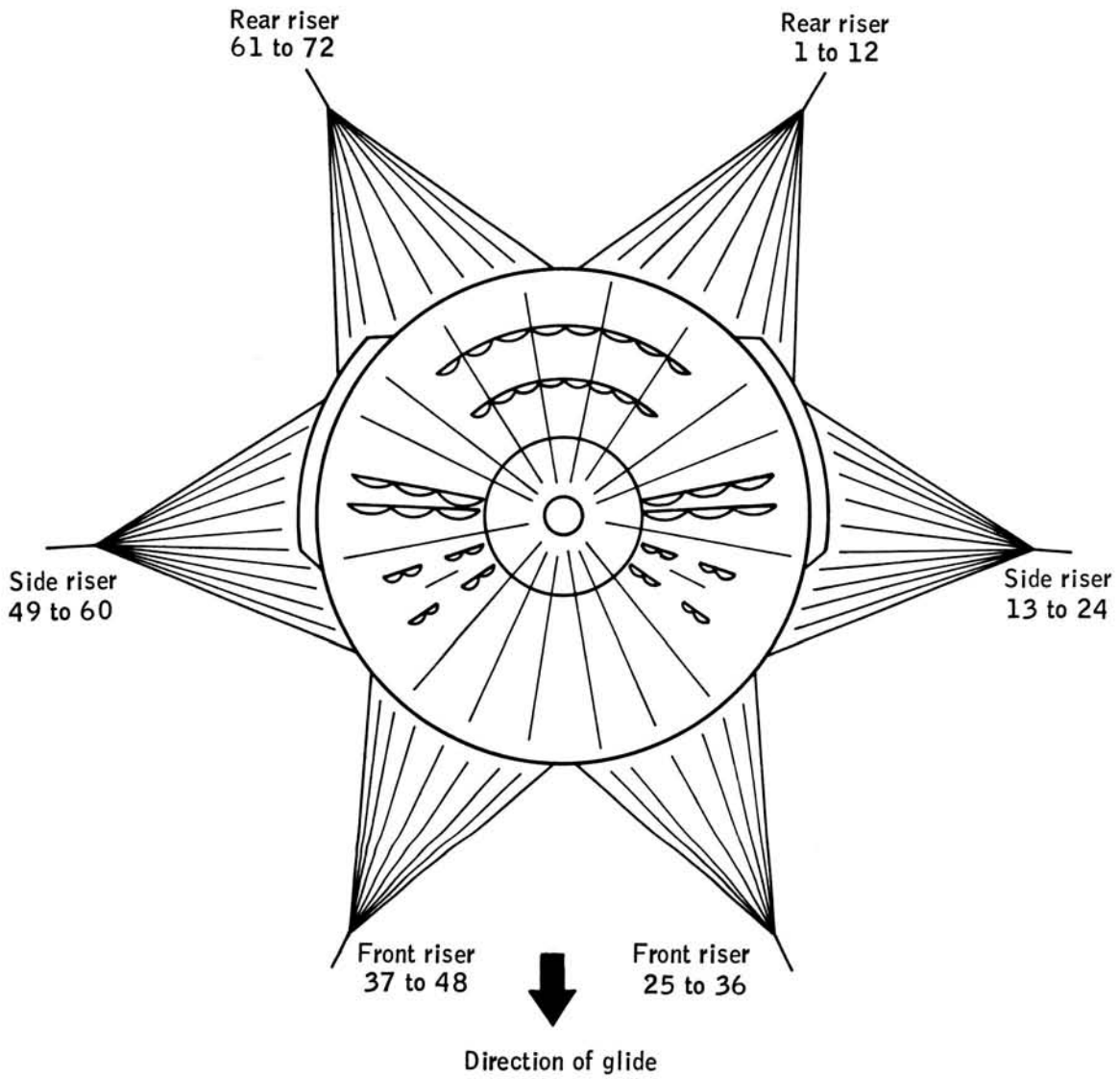


Figure III-29.- Riser schematic.

NASA-S-66-9880 OCT 24

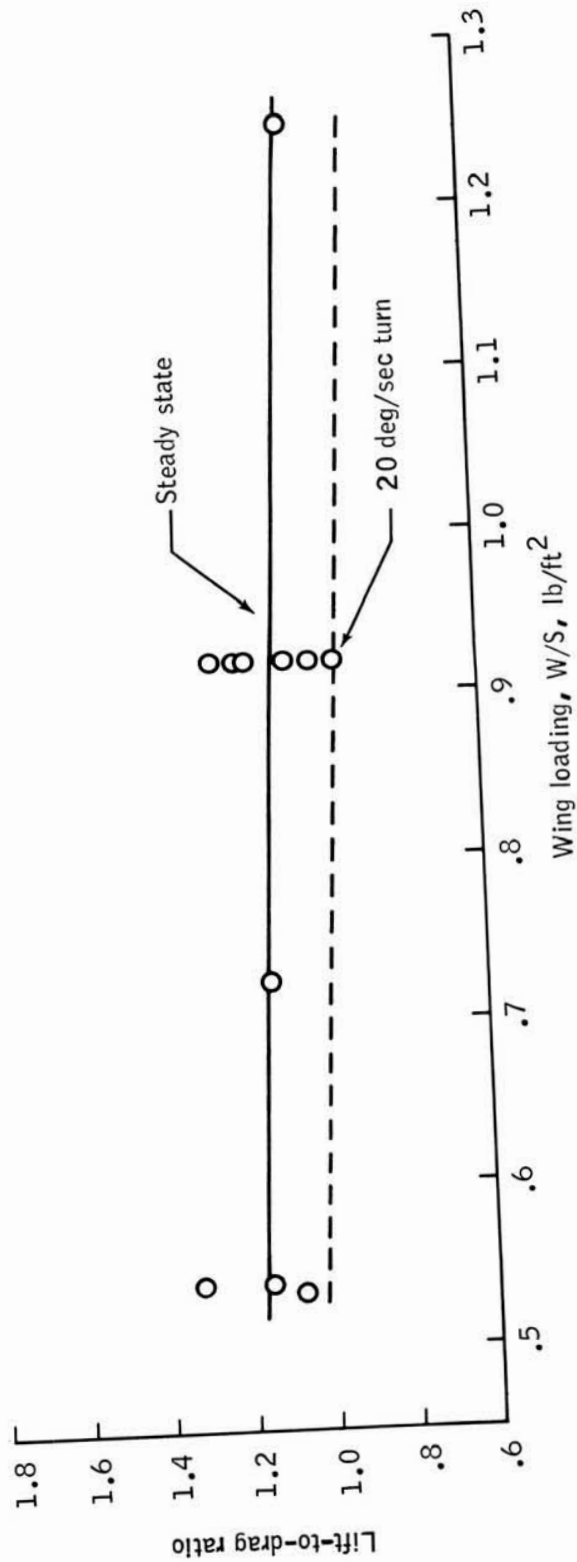


Figure III-30.- Glide ratio versus wing loading.

Altitude, 3000 ft msl

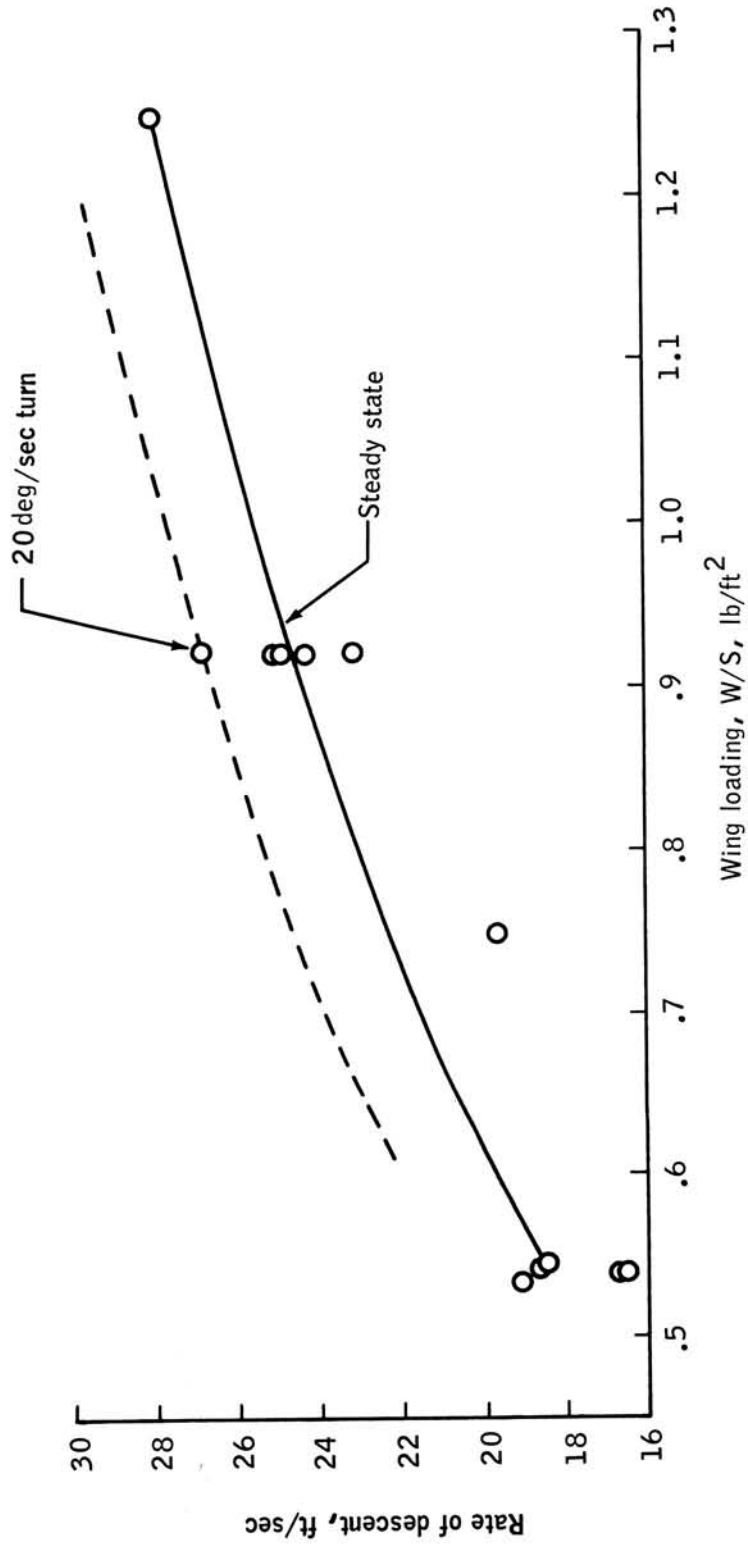


Figure III-31.- Rate of descent versus wing loading.

NASA-S-66-9882 OCT 24

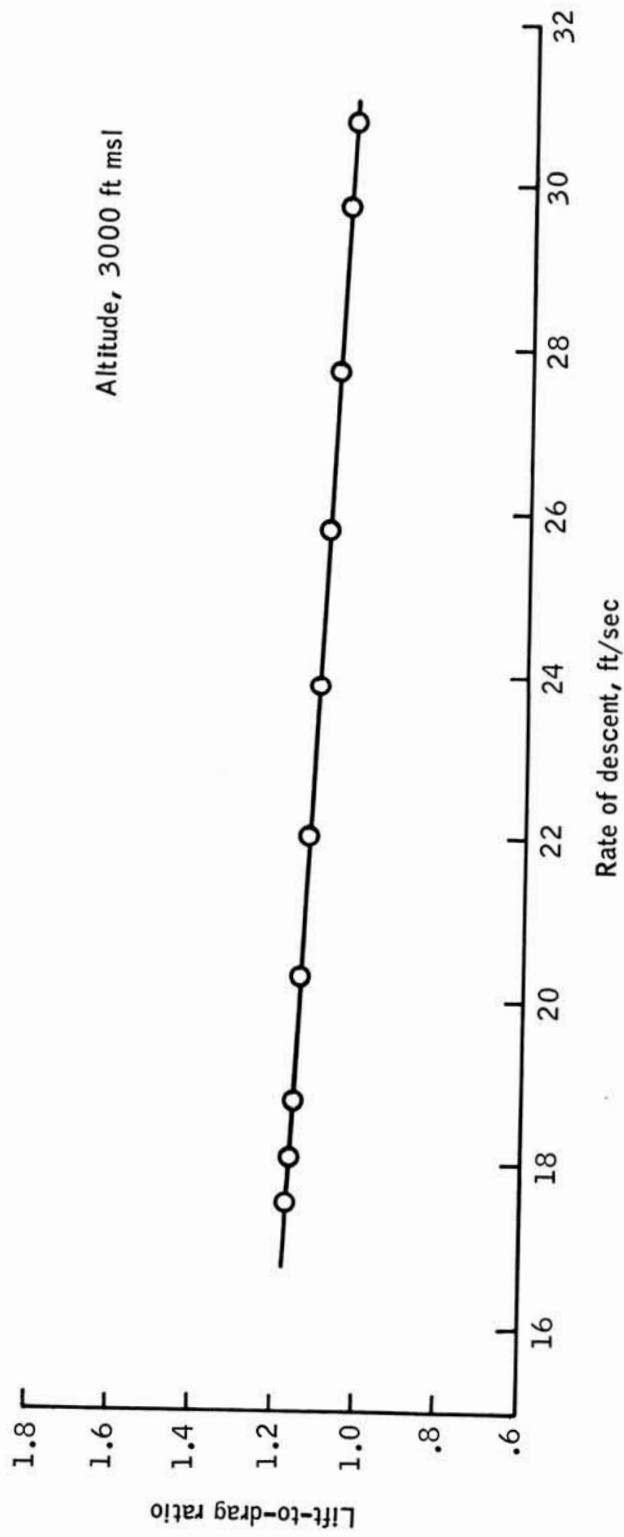


Figure III-32.- Lift-to-drag ratio versus rate of descent.

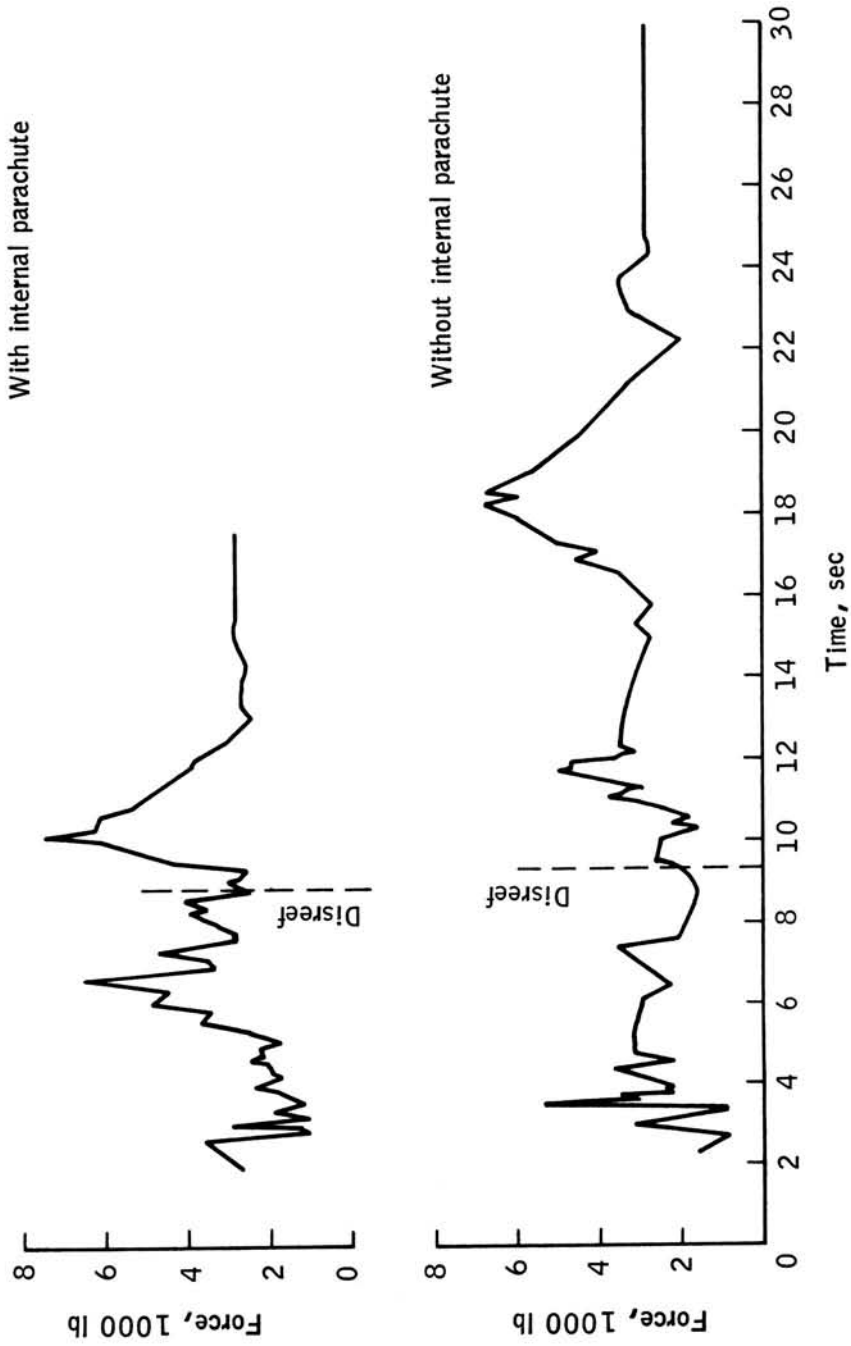


Figure III-33.- Opening dynamics with and without the internal parachute.

NASA-S-66-9884 OCT 24

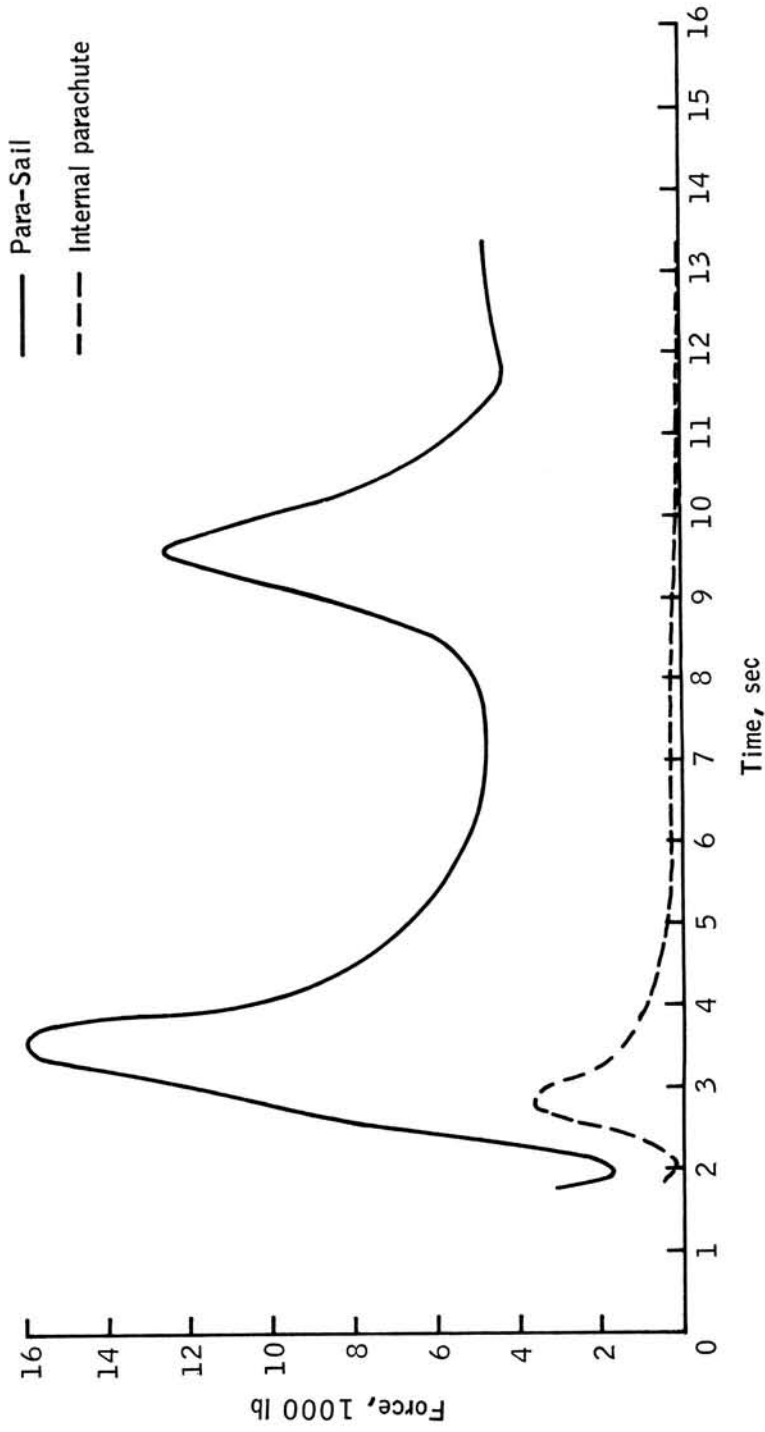


Figure III-34.- Force-time history, internal parachute and Para-Sail, test 14.

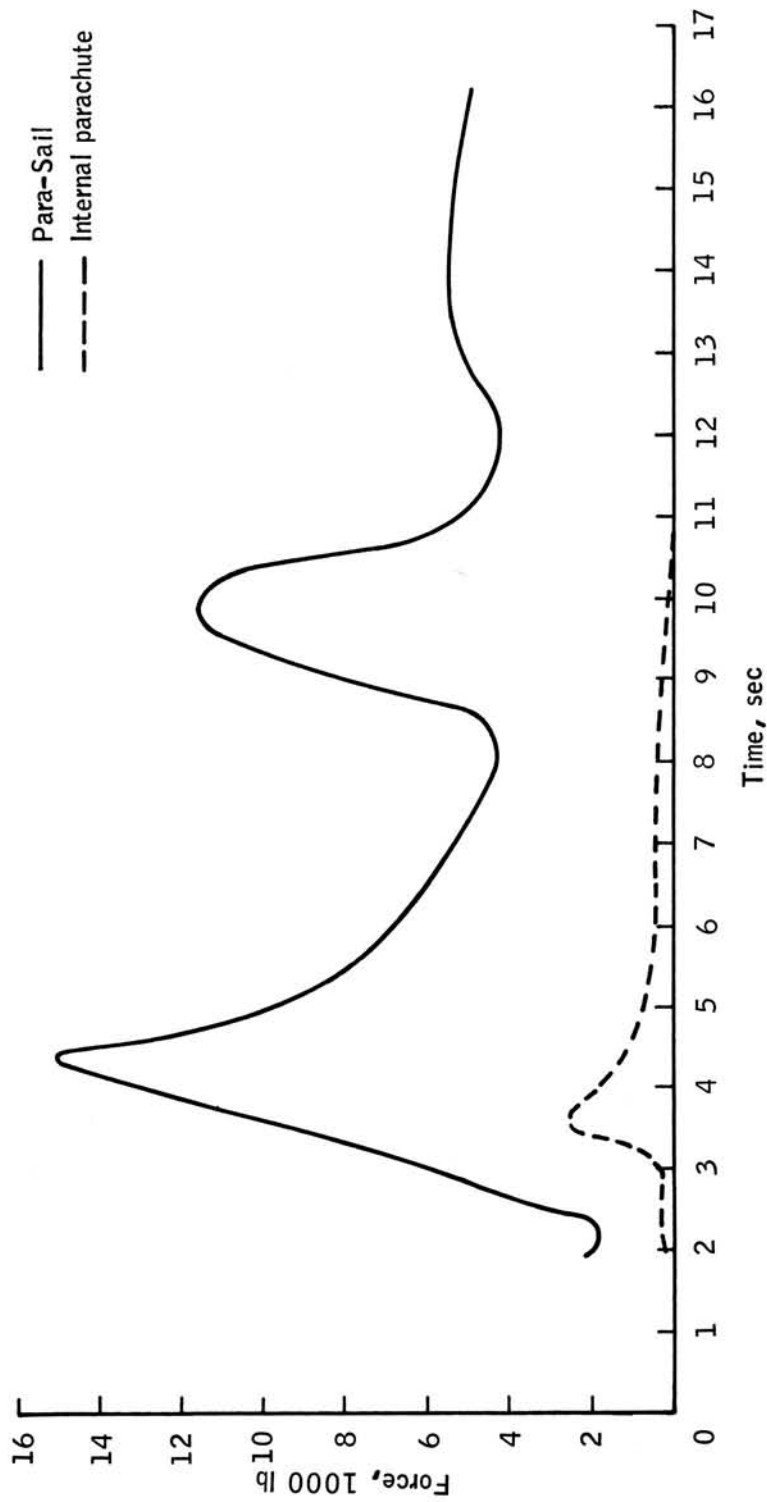


Figure III-35.- Force-time history, internal parachute and Para-Sail, test 16.

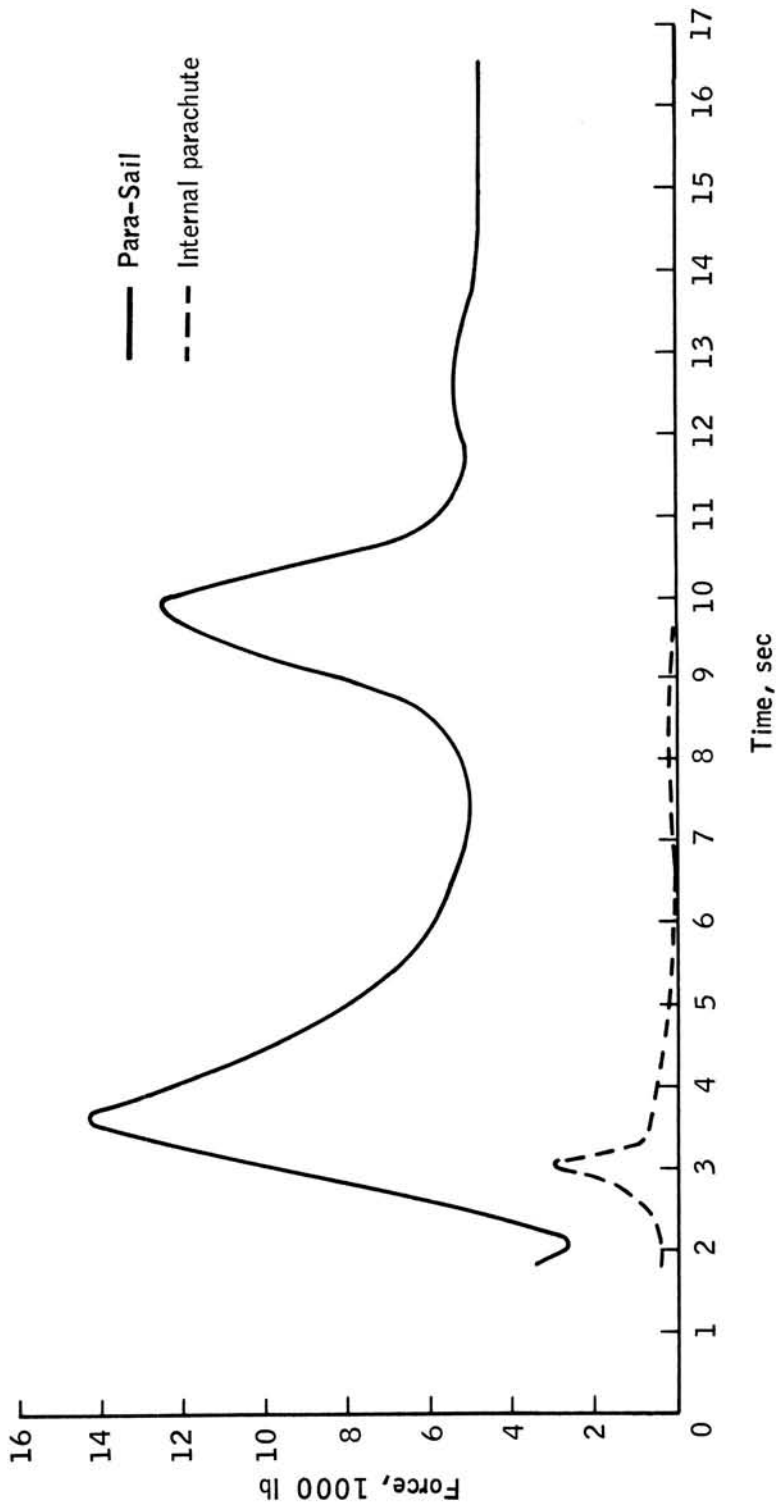


Figure III-36.- Force-time history, internal parachute and Para-Sail, test 19.

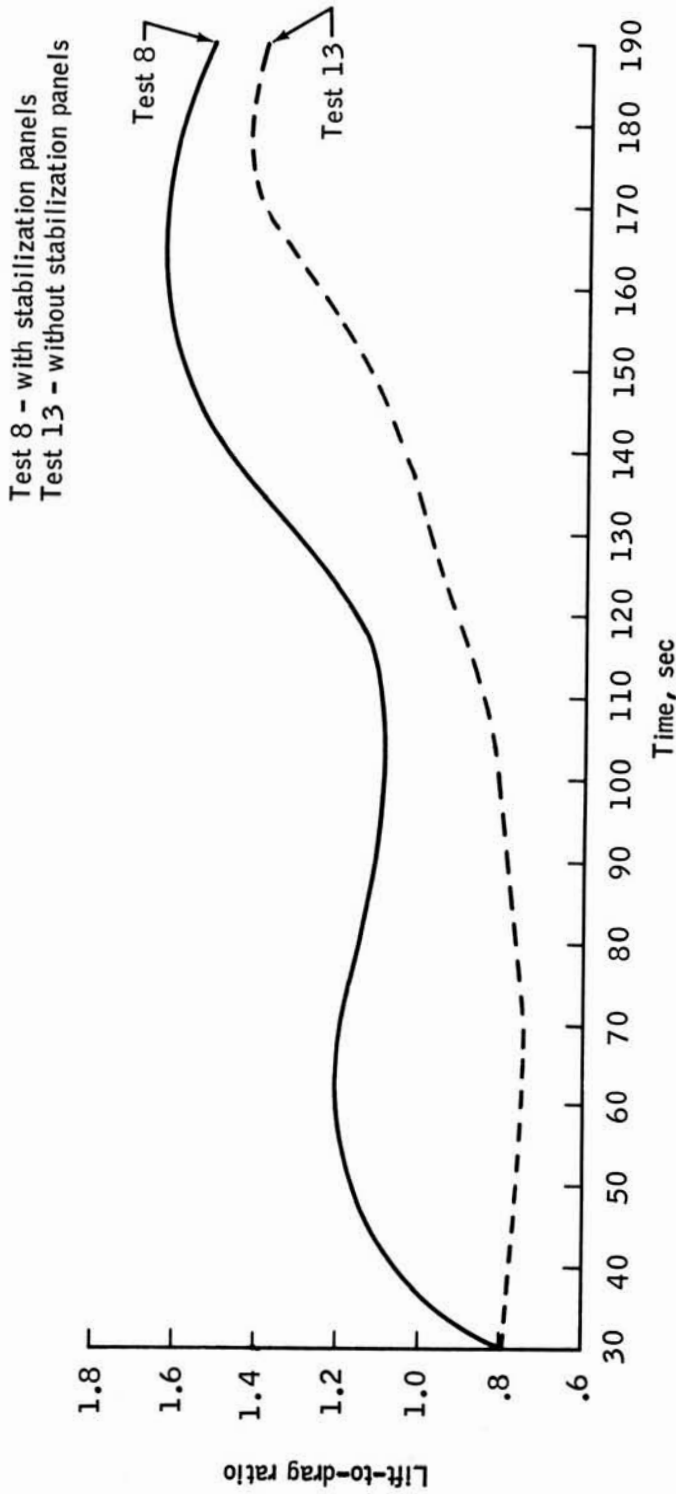


Figure III-37.- Lift-to-drag ratio with and without stabilization panels.

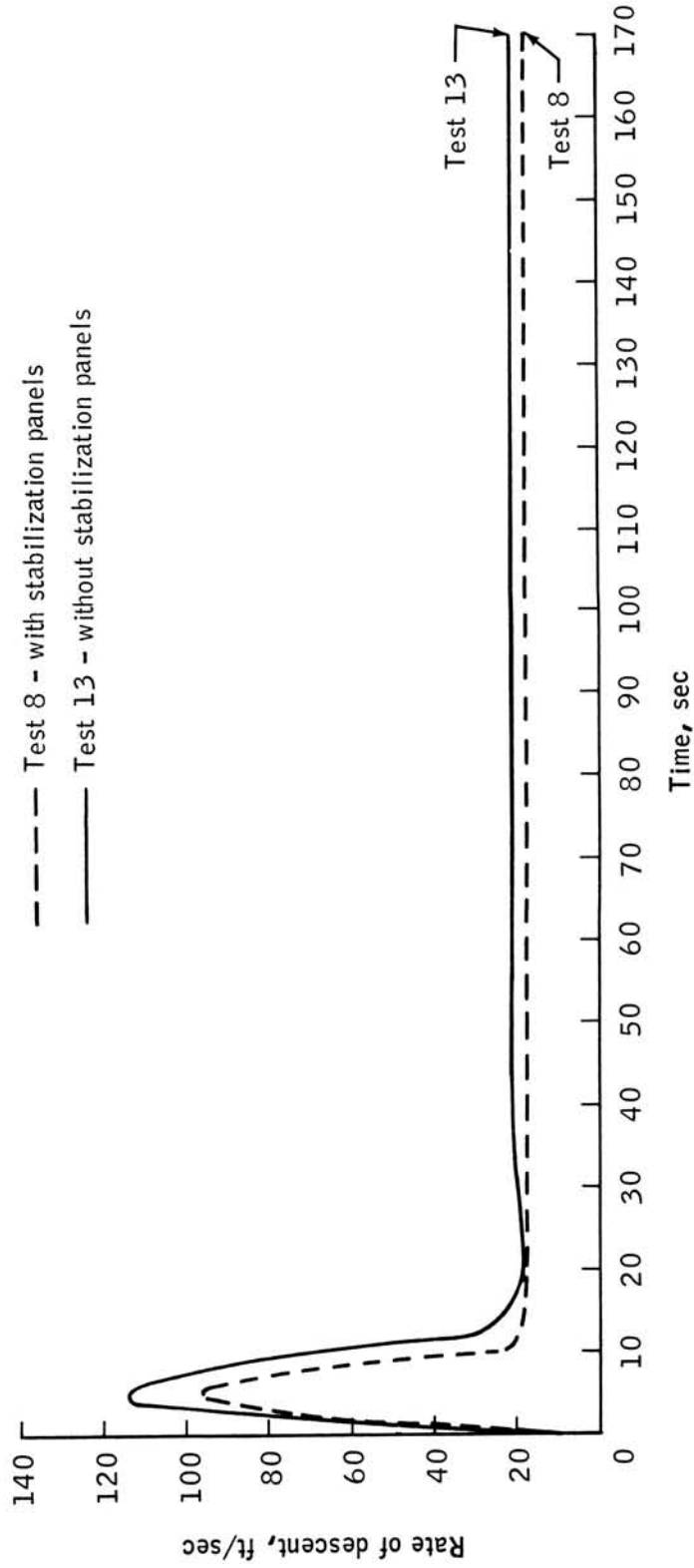


Figure III-38.- Rate of descent with and without stabilization panels.

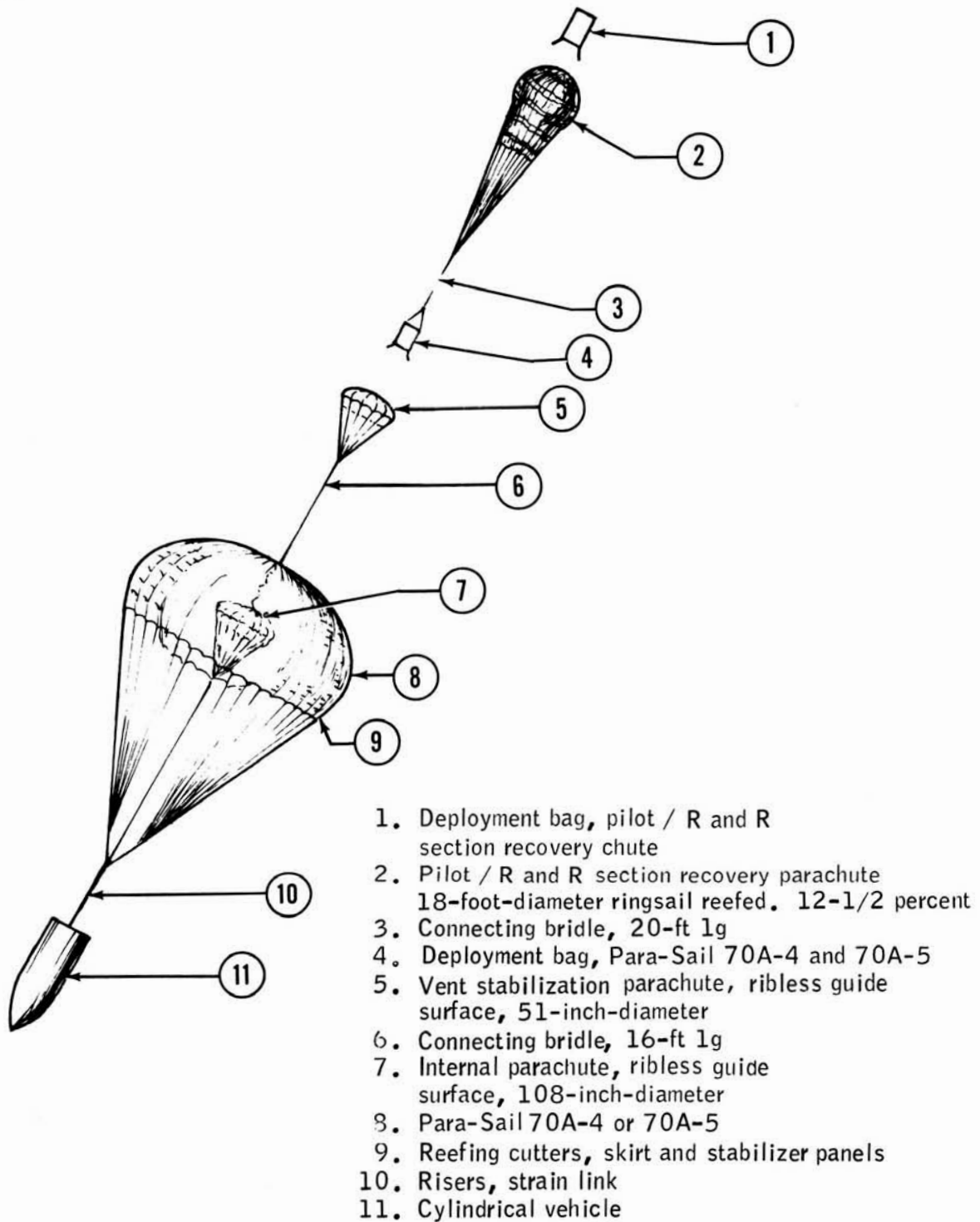


Figure III-39.- Schematic of parachute test items.

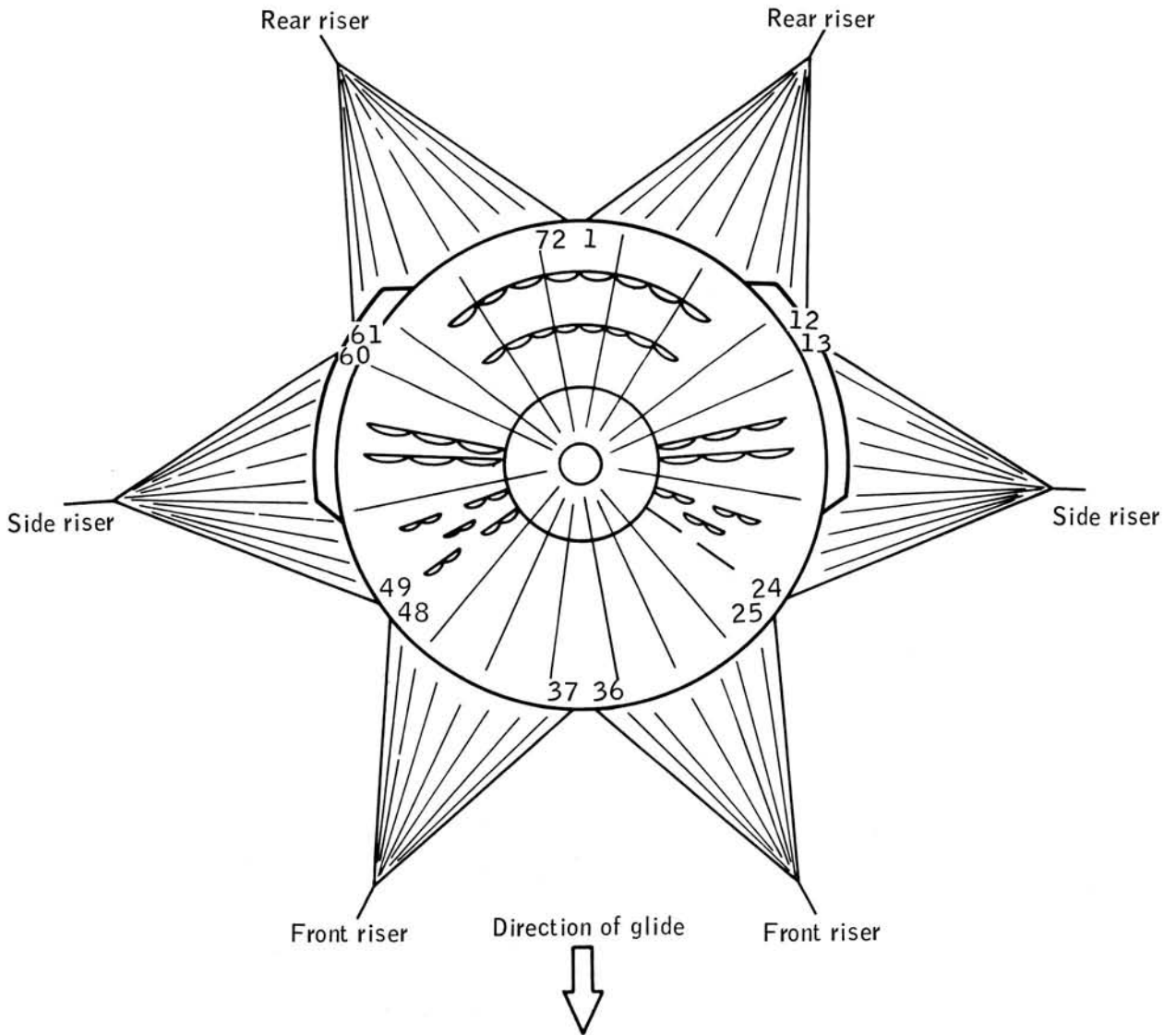


Figure III-40.- Schematic cording diagram for Para-Sails 70A-4 and 70A-5.

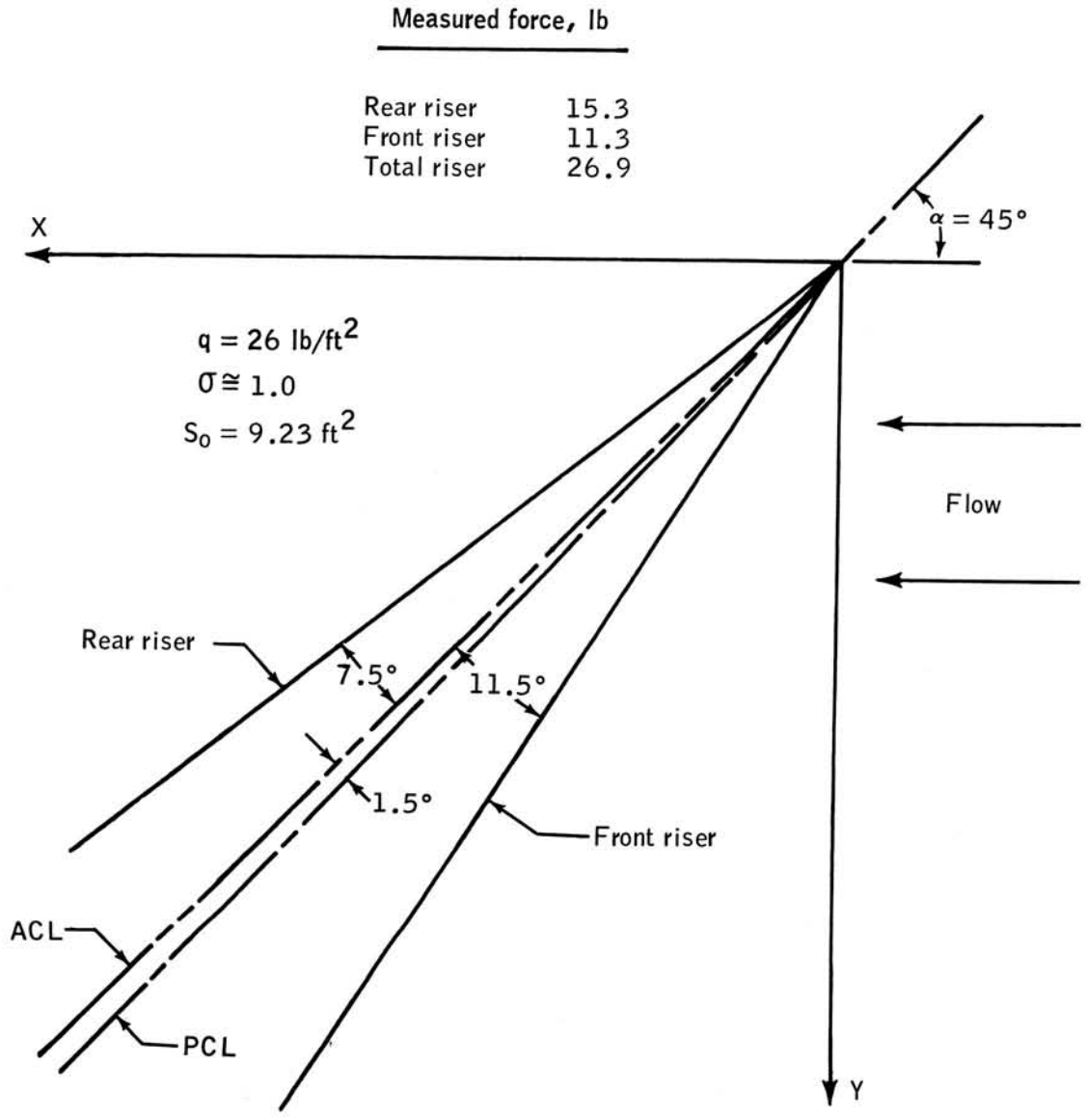


Figure III-41.- Location of aerodynamic centerline for a 69.8-ft Para-Sail (based upon wind-tunnel studies).

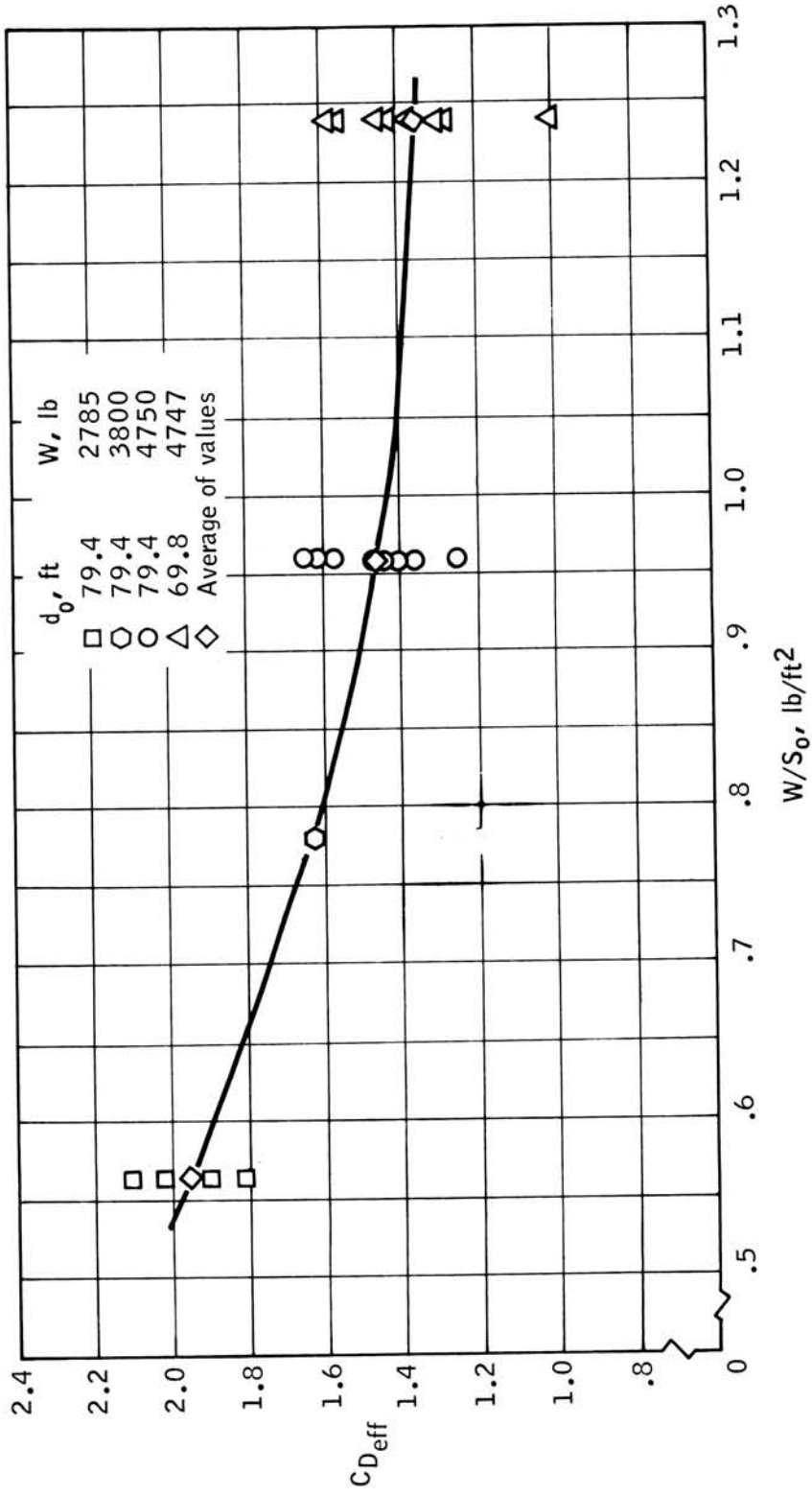


Figure III-42.- Average effective drag coefficient versus canopy loading for various Para-Sail configurations (based upon nominal area).

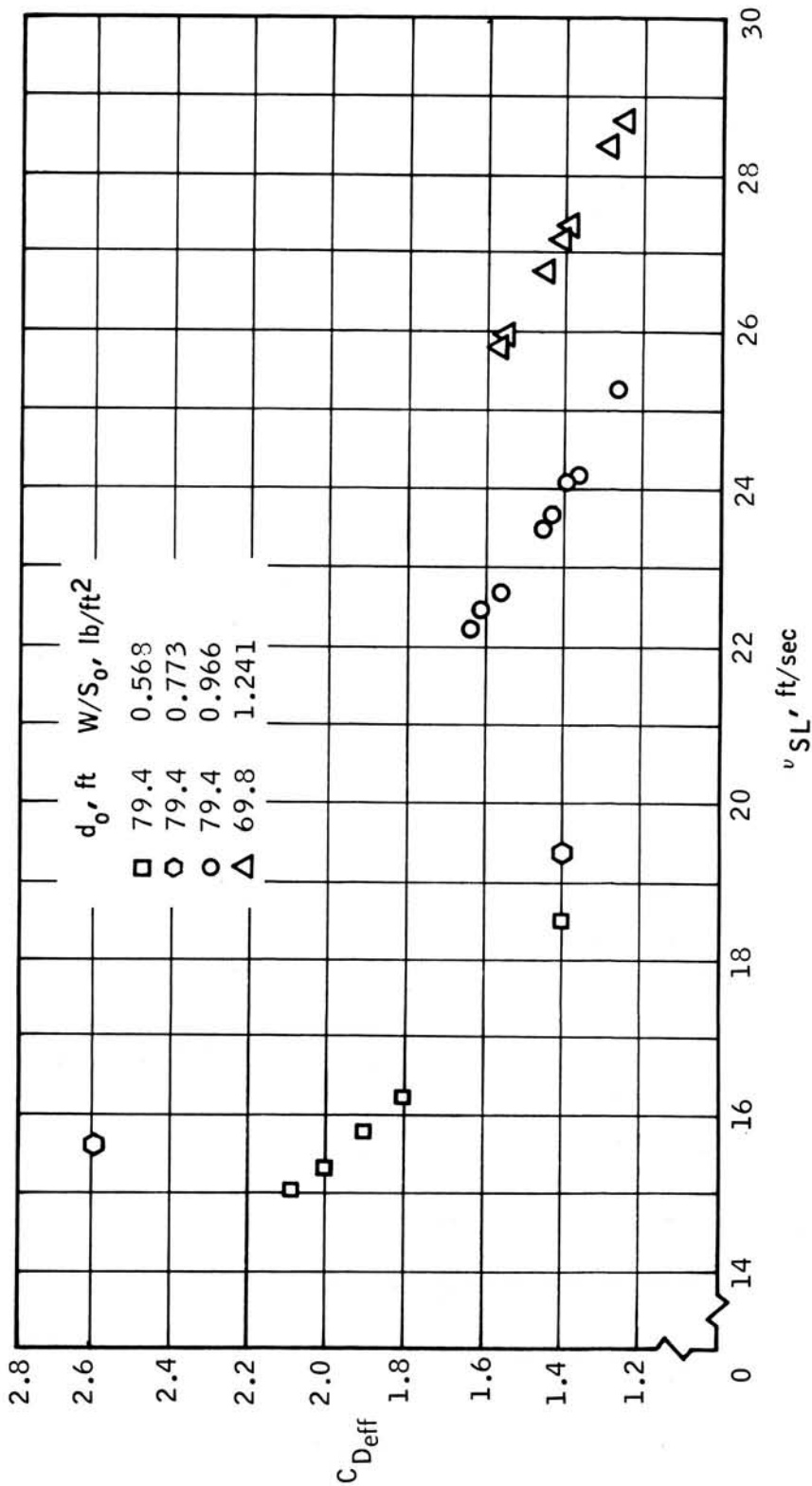


Figure III-43.- Average effective drag coefficient versus rate of descent at sea level for various Para-Sail configurations (based upon nominal area).

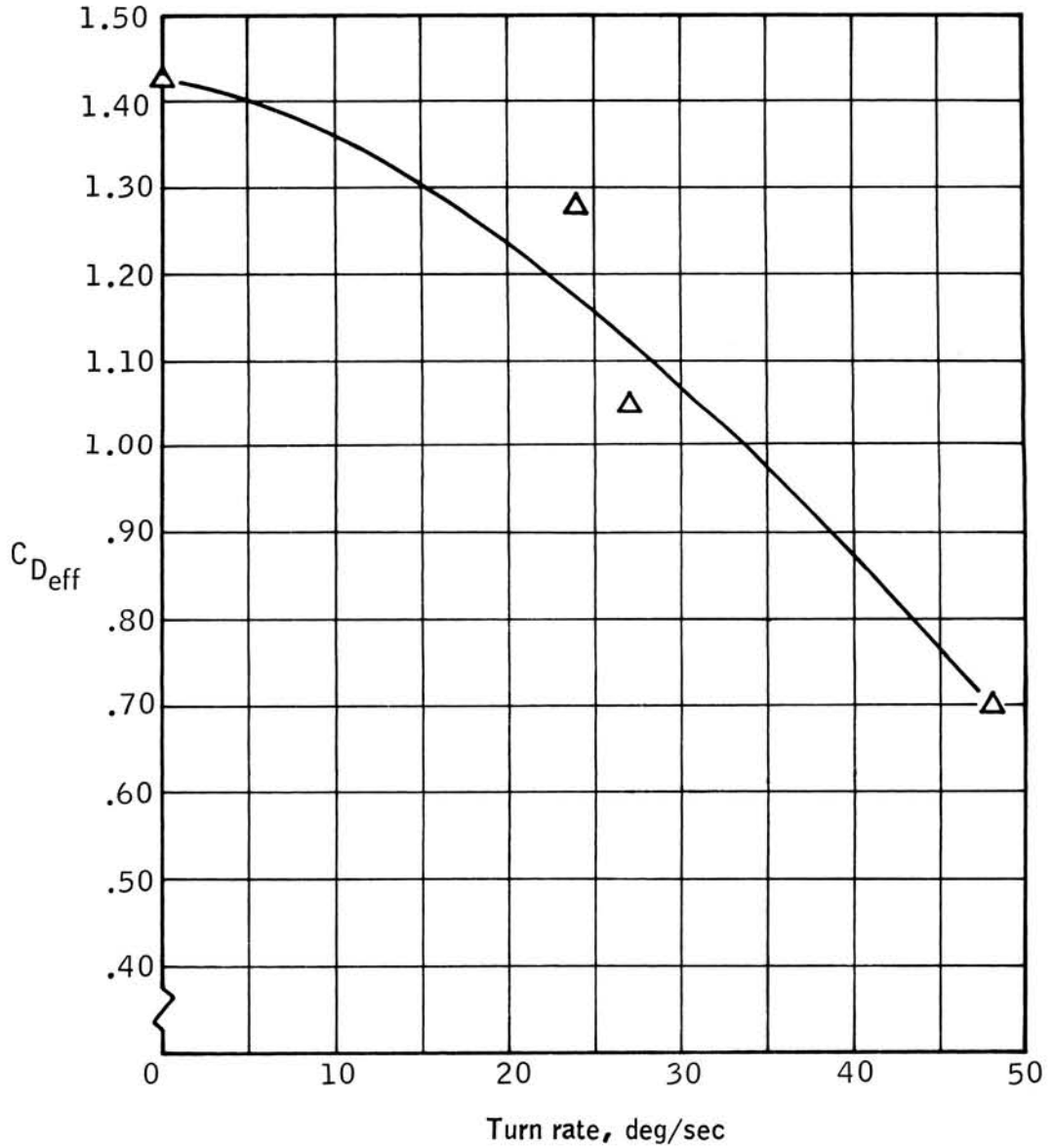


Figure III-44.- Average effective drag coefficient versus turn rate for 70-ft d_0 Para-Sail ($W/S_0 = 1.24 \text{ lb/ft}^2$; $C_{D_{eff}}$ based upon nominal area).

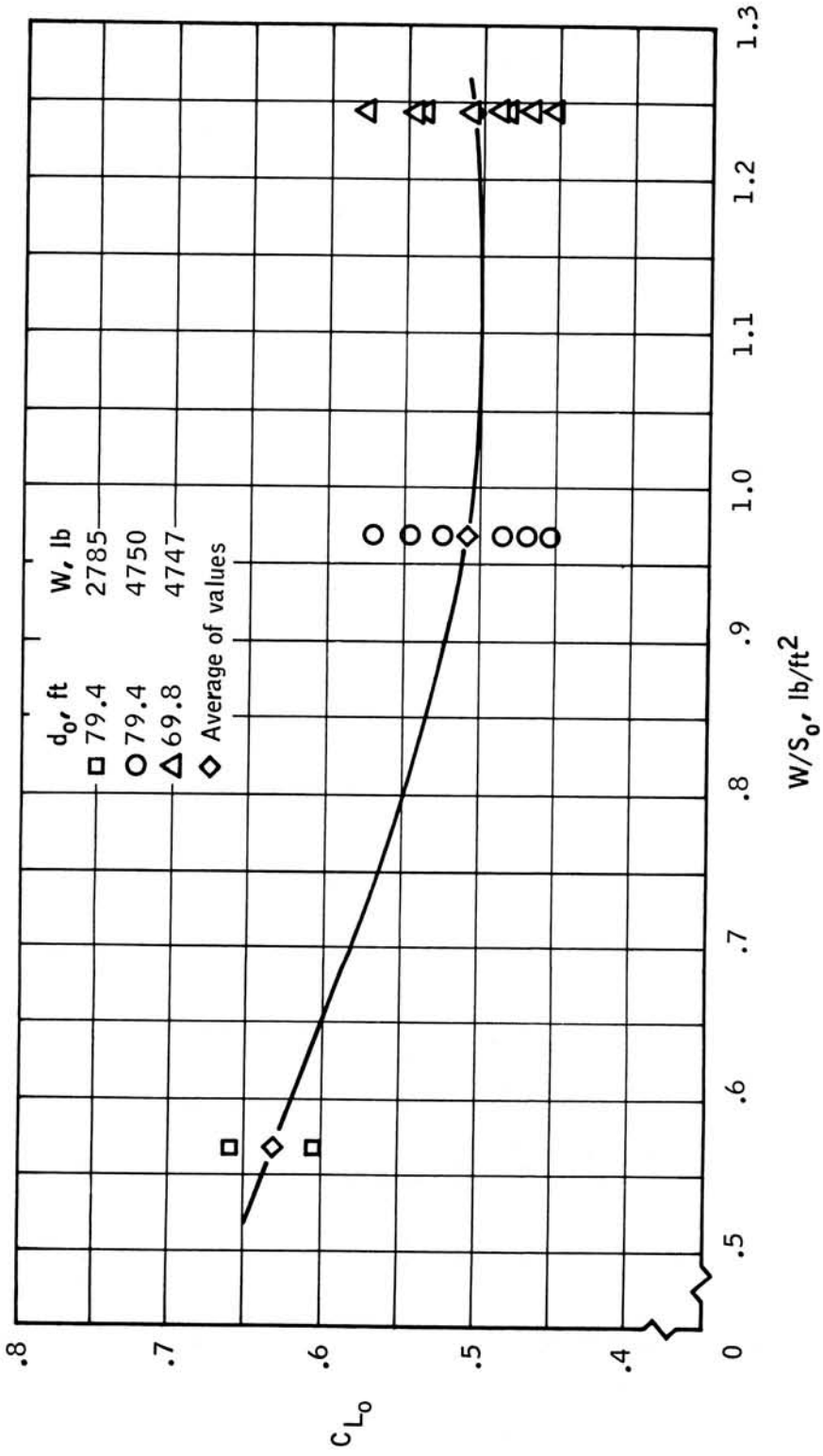


Figure III-45.- Average lift coefficient versus canopy loading for various Para-Sail configurations (based upon nominal area).

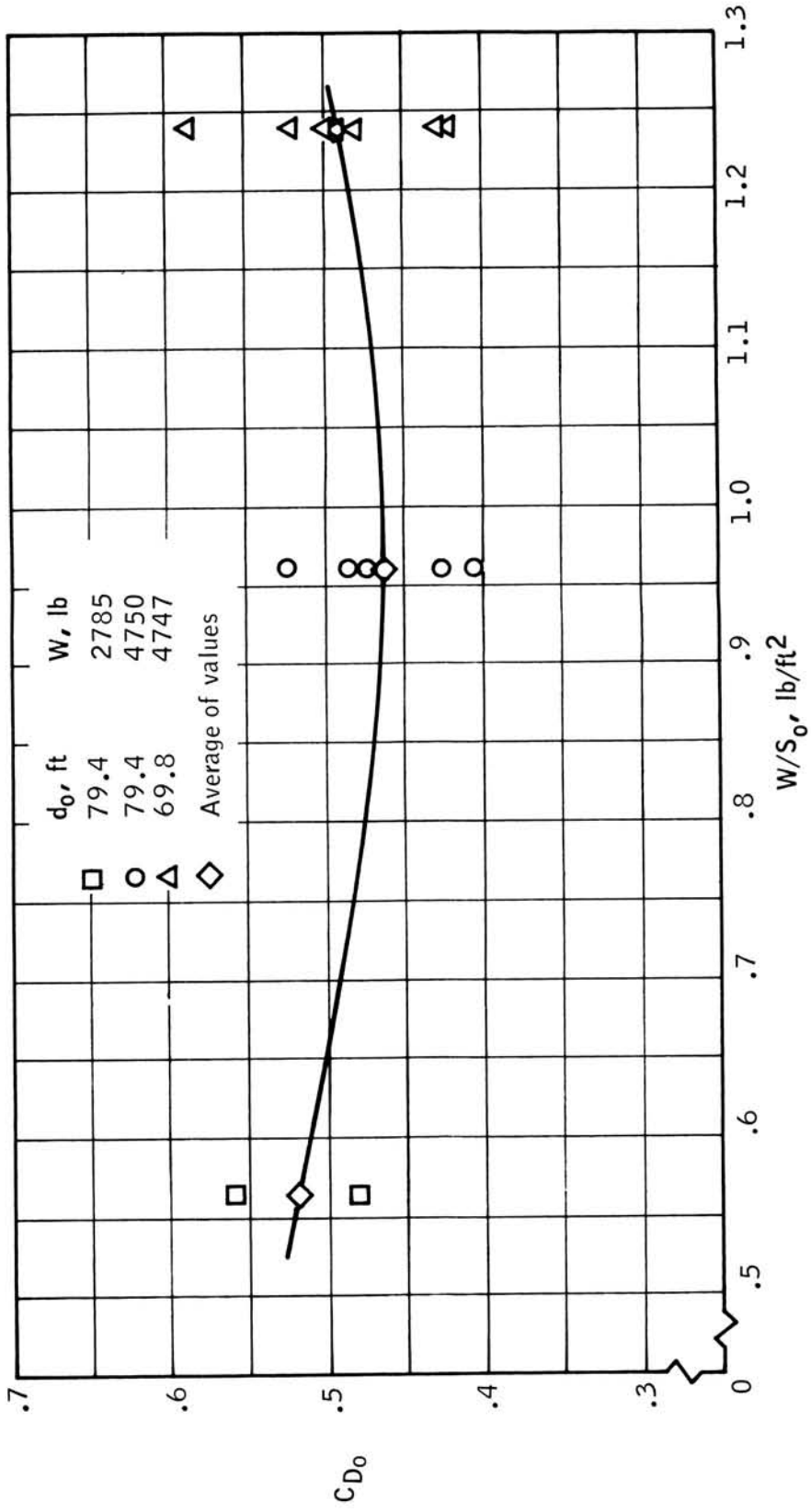


Figure III-46.- Average drag coefficient versus canopy loading for various Para-Sail configurations (based upon nominal area).

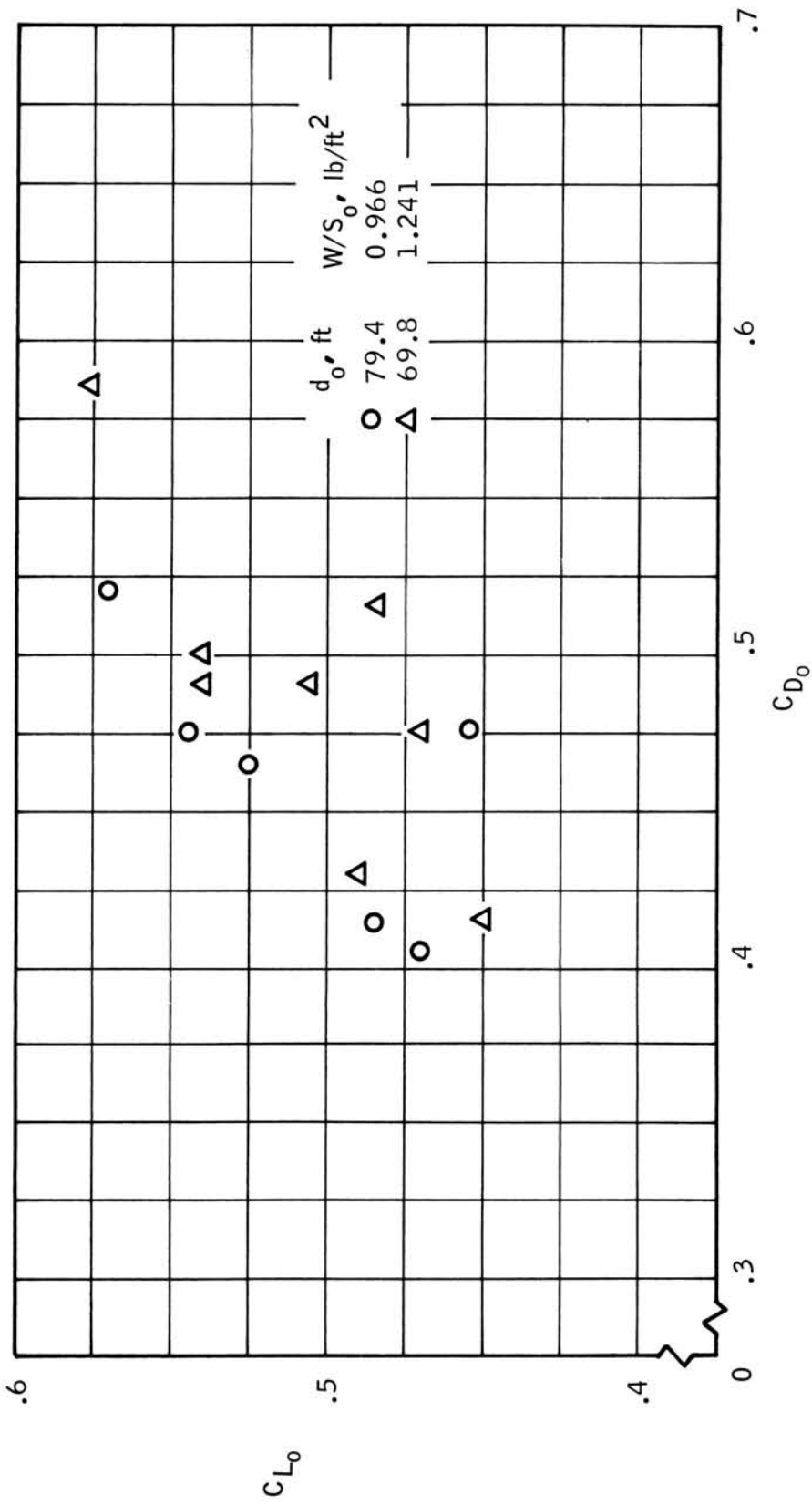


Figure III-47.- Lift coefficient versus drag coefficient for various Para-Sail configurations (based upon nominal area).

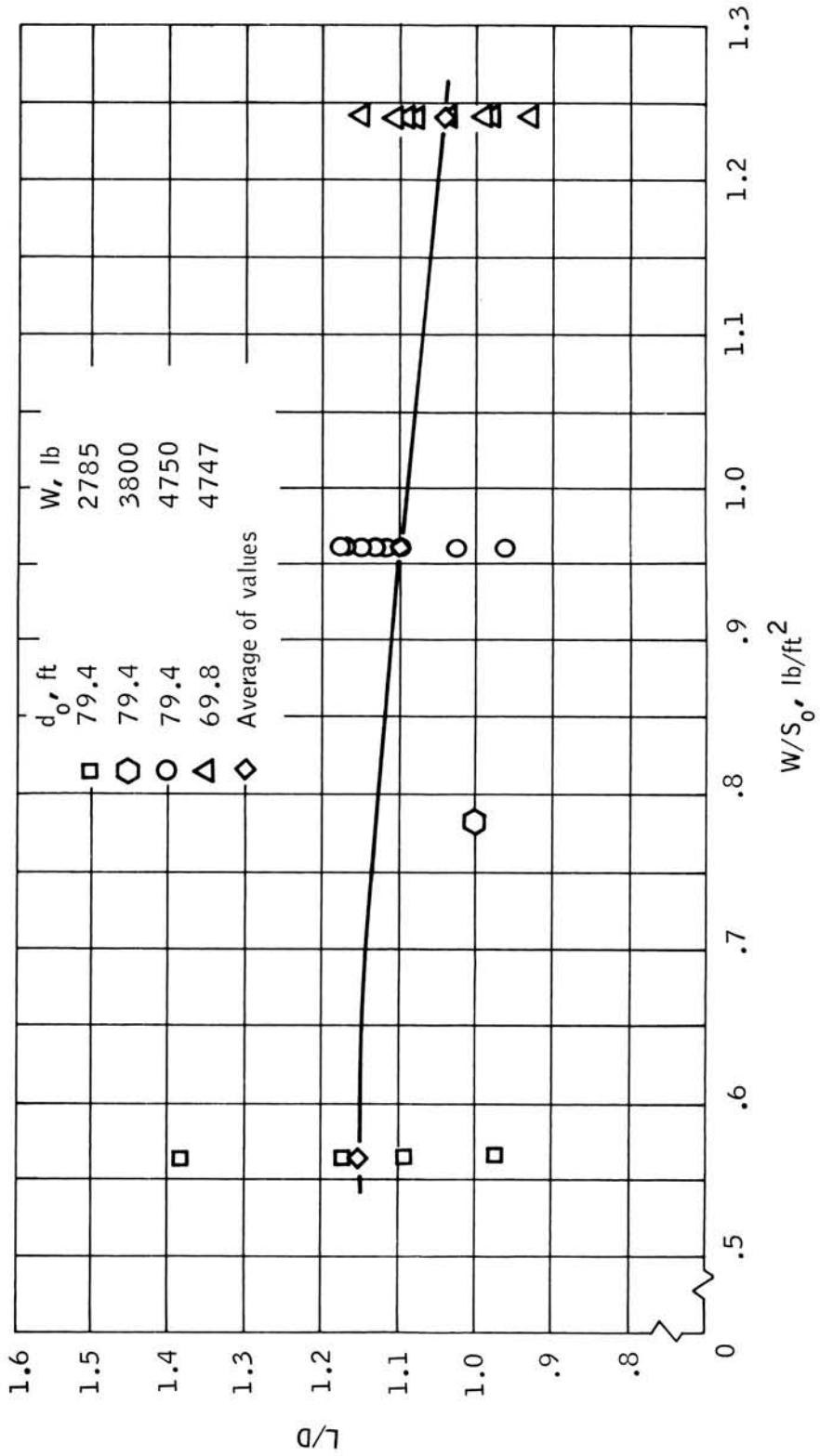


Figure III-48.- Average lift-to-drag ratio versus canopy loading for various Para-Sail configurations (based upon nominal area.)

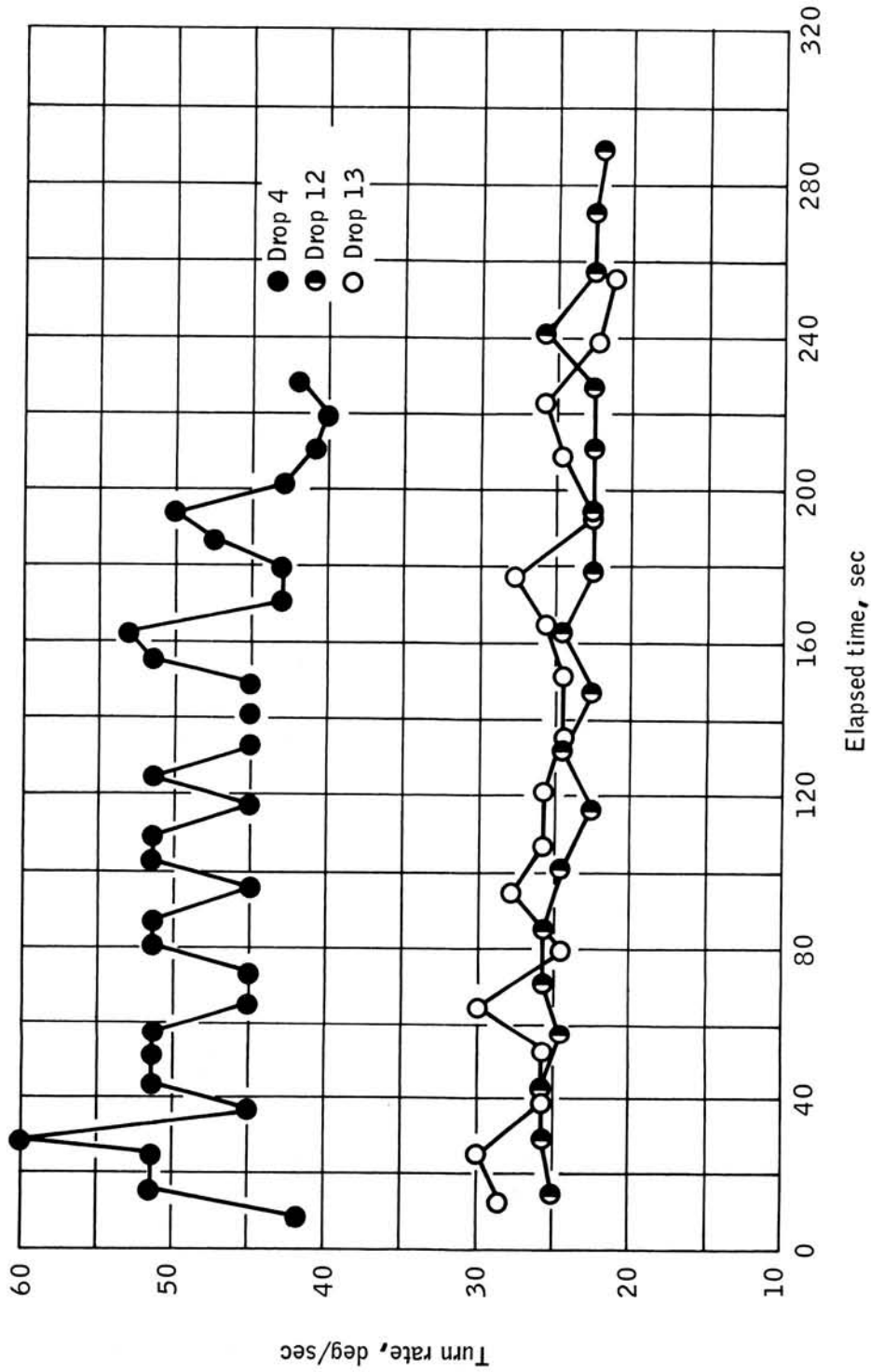


Figure III-49.- Turn rate versus elapsed time for a 69.8-ft d₀ Para-Sail.

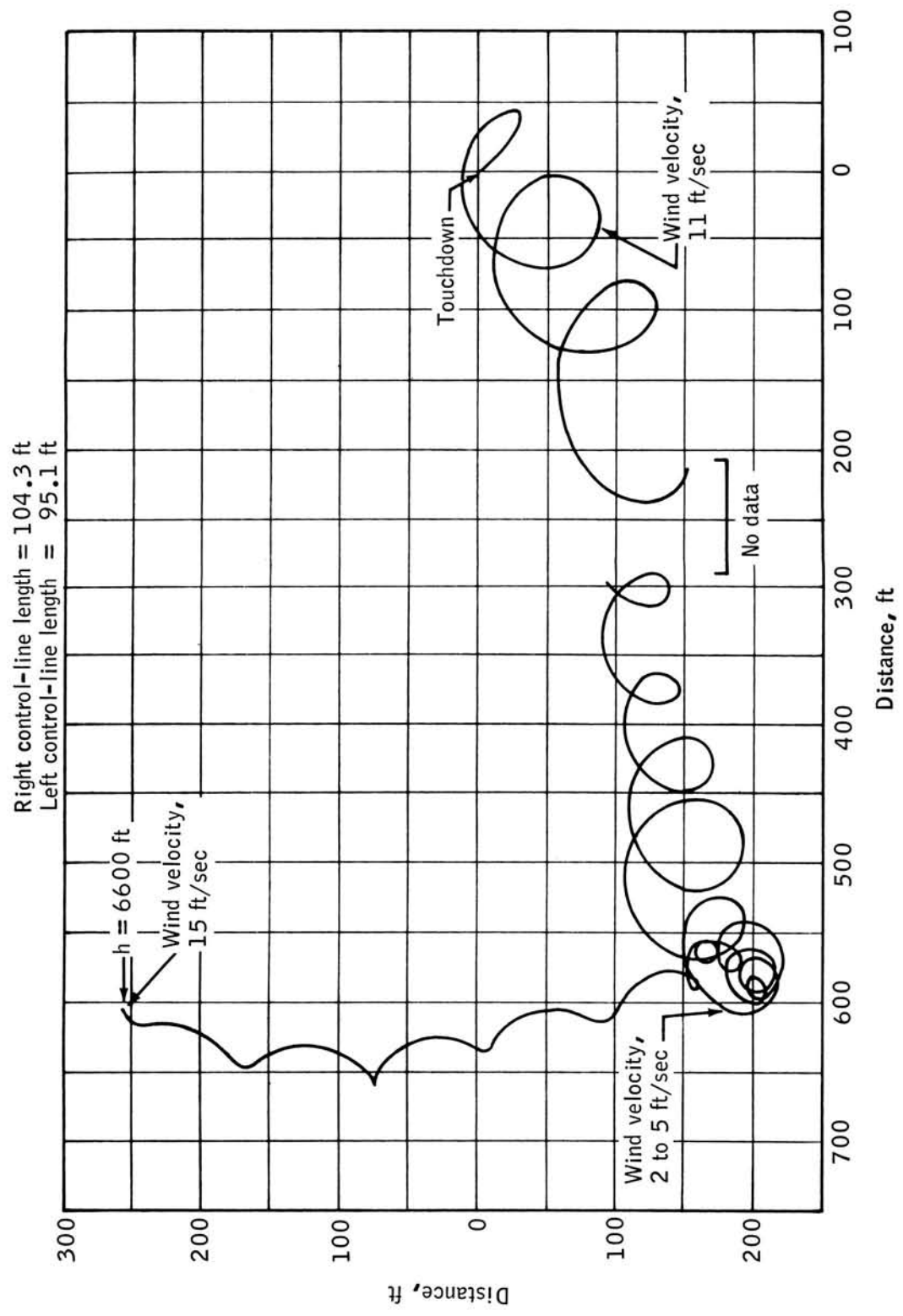


Figure III-50.- Ground Track for drop 4 (turn test).

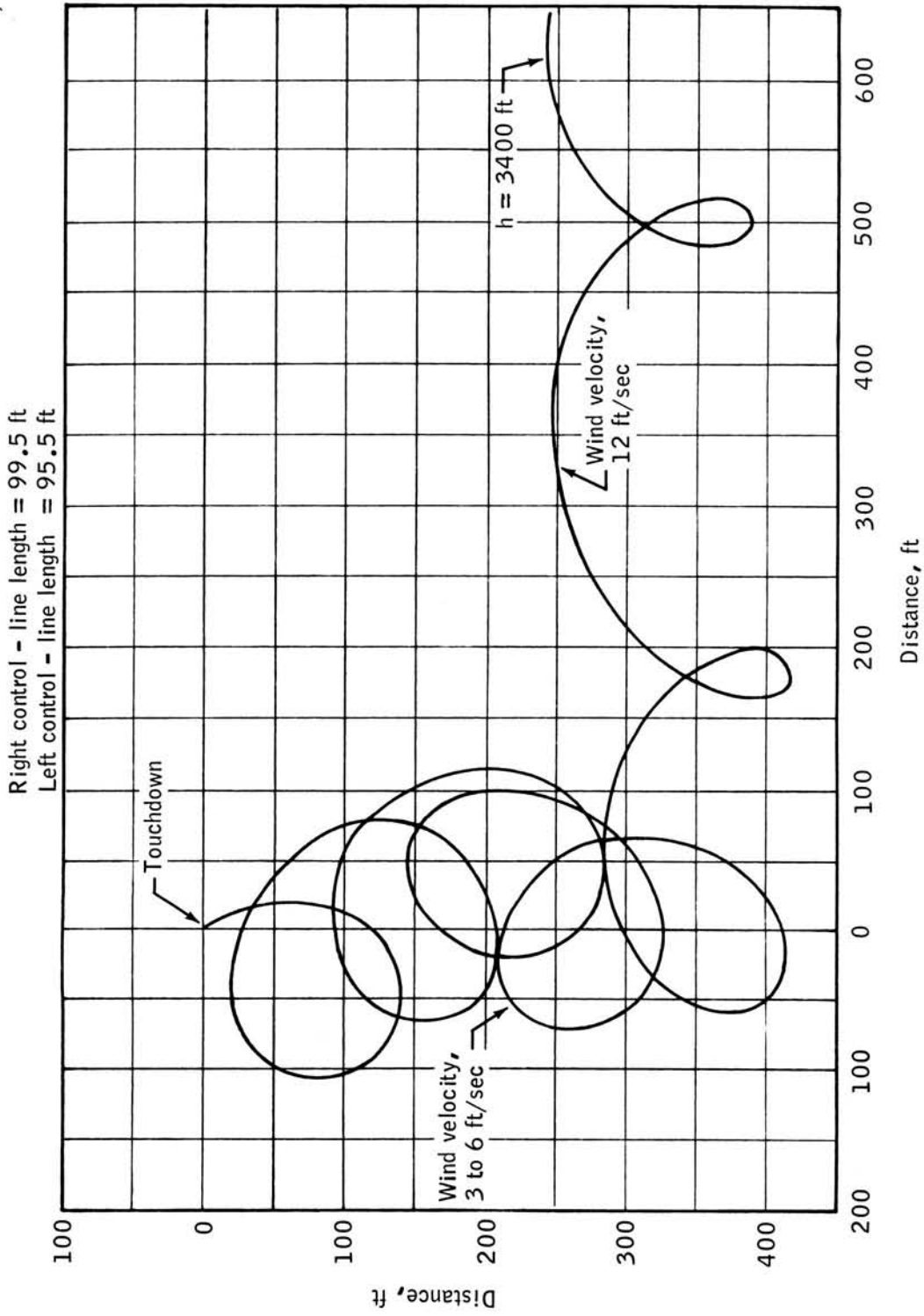


Figure III-51.- Ground track for drop 12 (turn test).

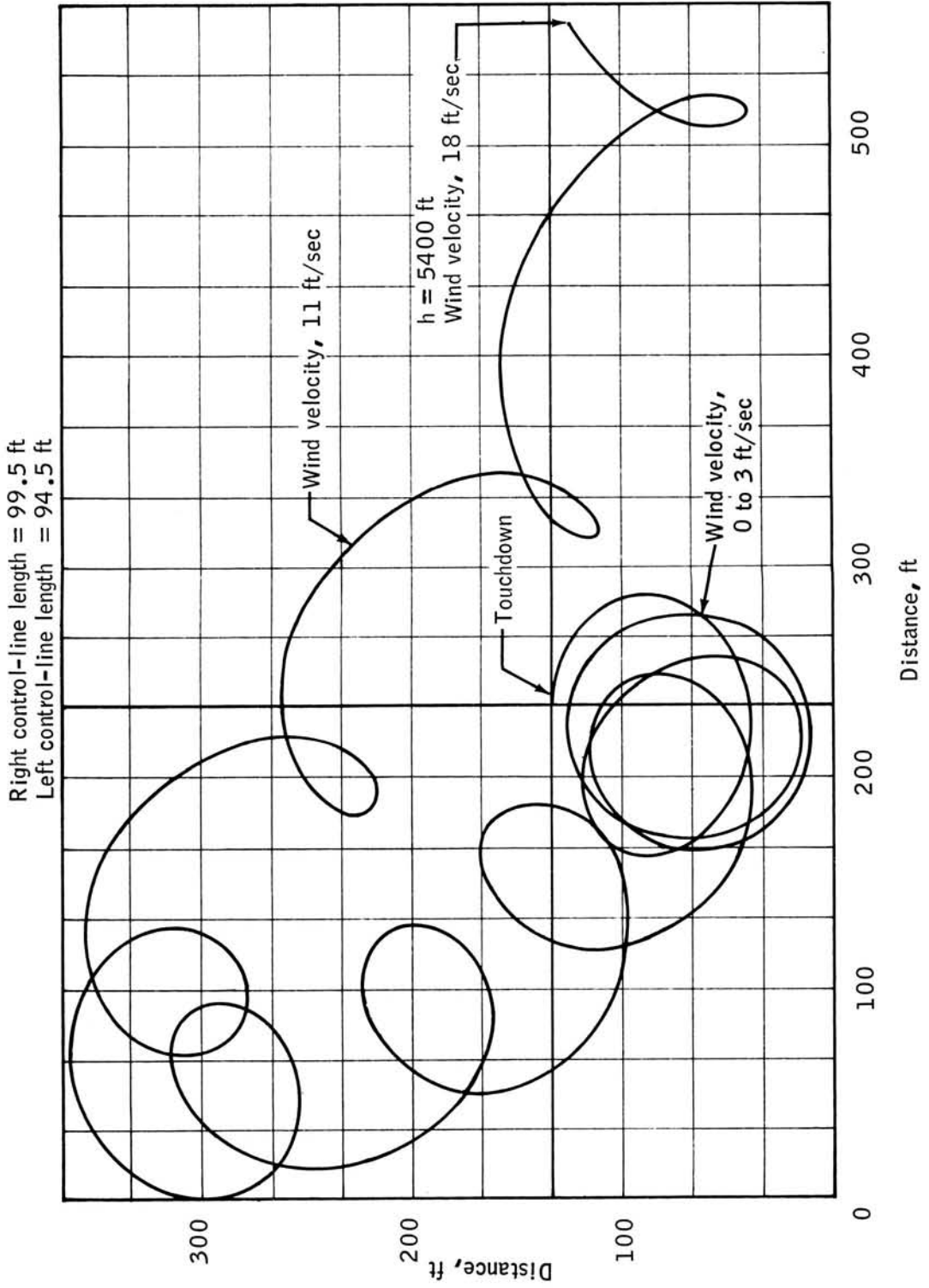


Figure III-52.- Ground track for drop 13 (turn test).

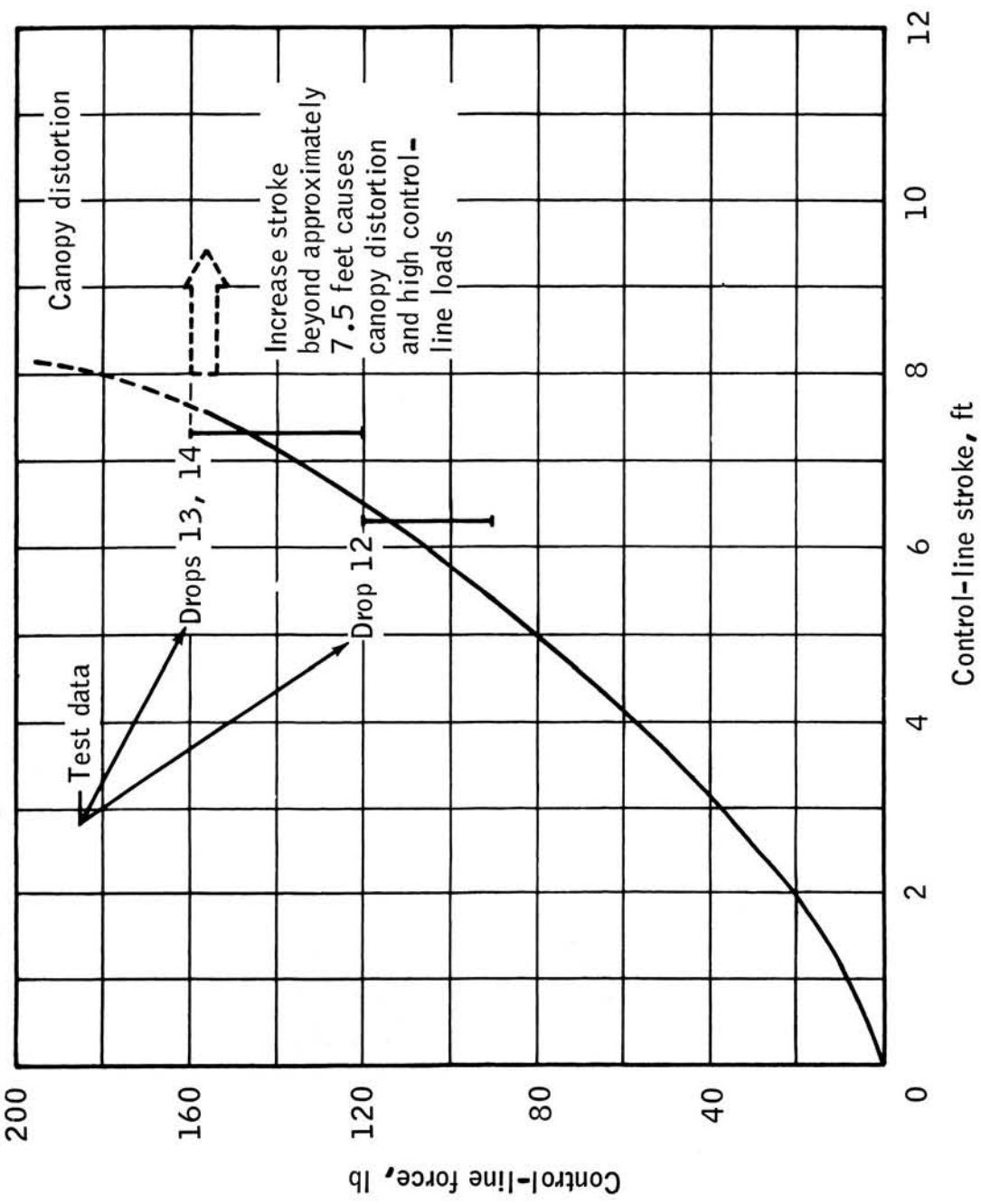


Figure III-53.- Control-line force versus control-line stroke for a 69.8-ft d_0 Para-Sail.

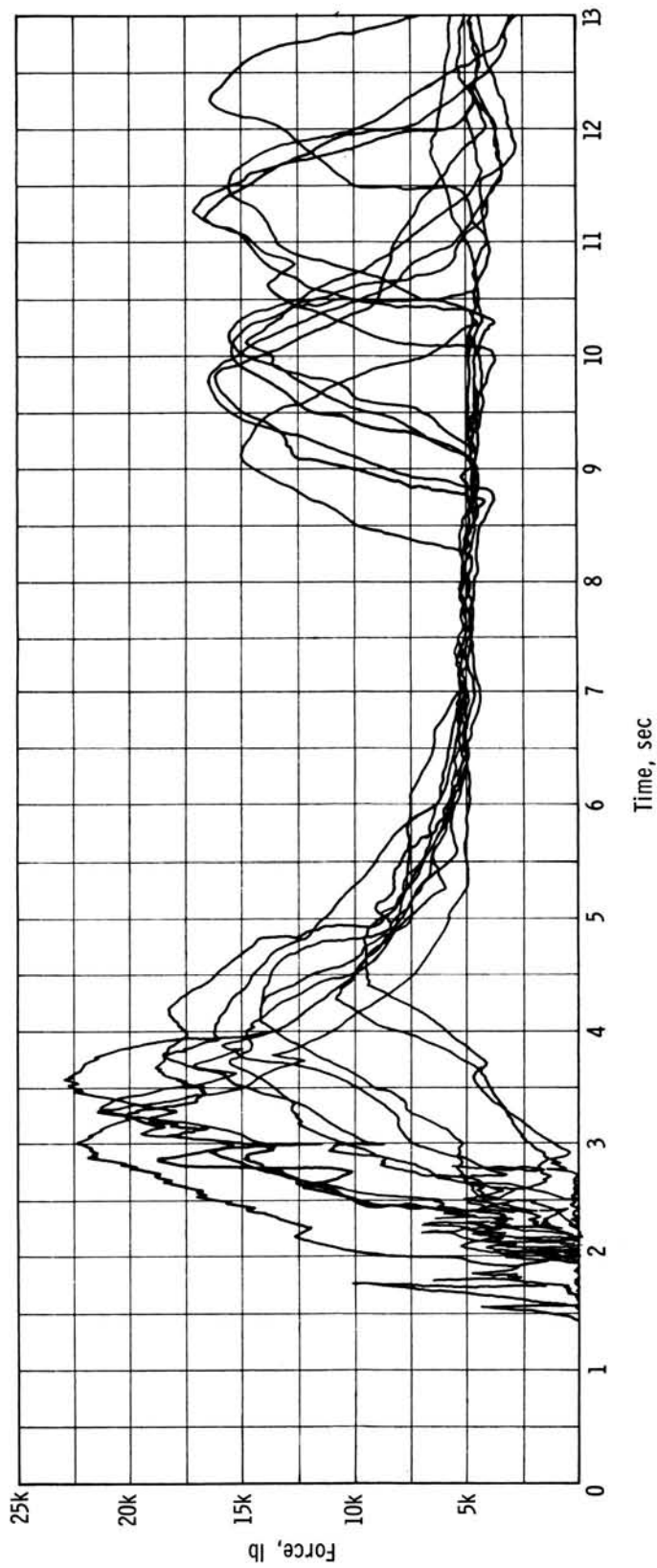


Figure III-54.- Force versus time traces for drops 2 to 5 (configuration 70A-4), and drops 6 to 11 (configuration 70A-5).

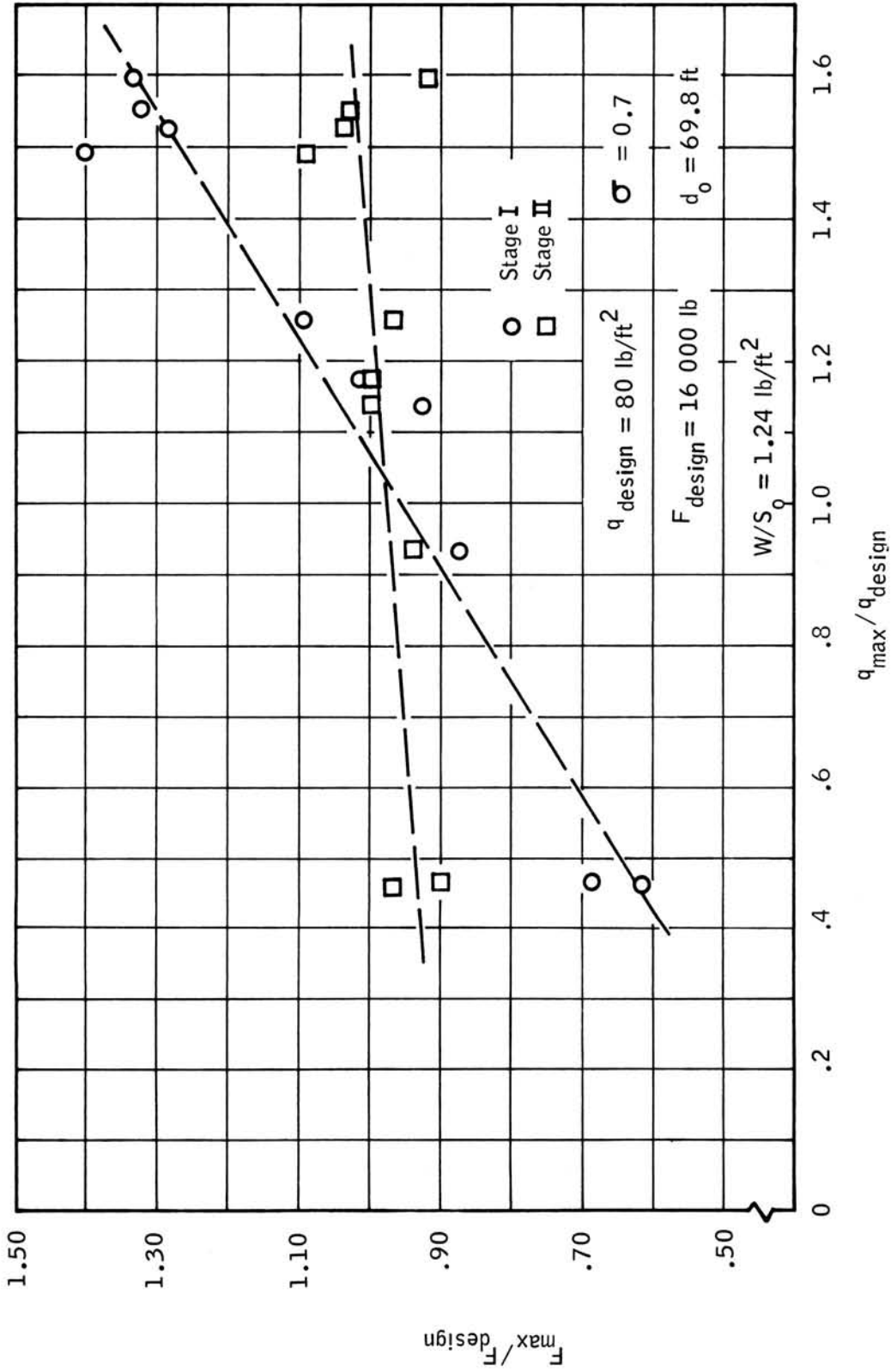


Figure III-55.- Maximum force ratio versus maximum dynamic-pressure ratio for a 70-ft Para-Sail.

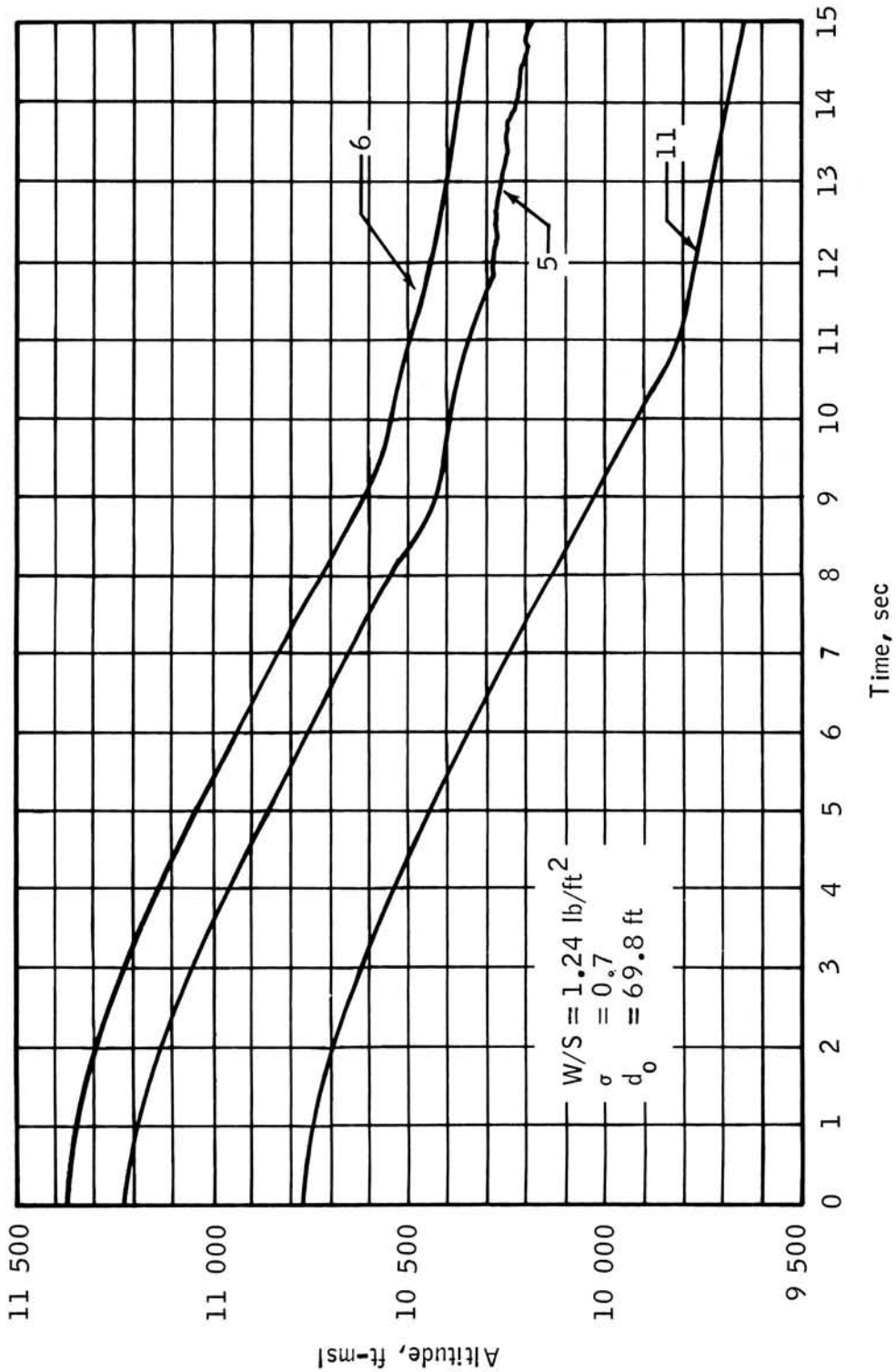


Figure III-56.- Altitude versus time curves for drops 5, 6, and 11.

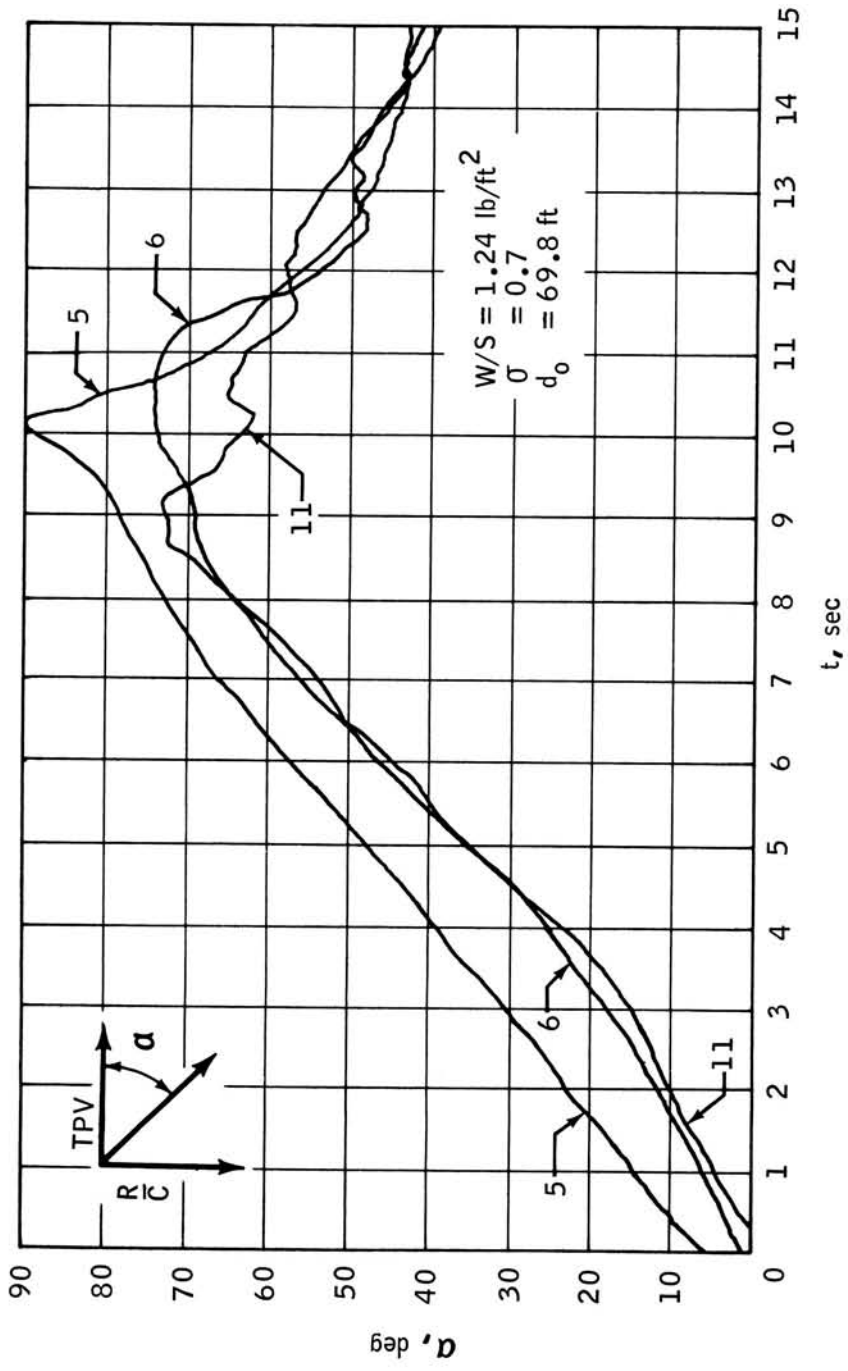


Figure III-57.- Trajectory angle versus time for drops 5, 6, and 11.

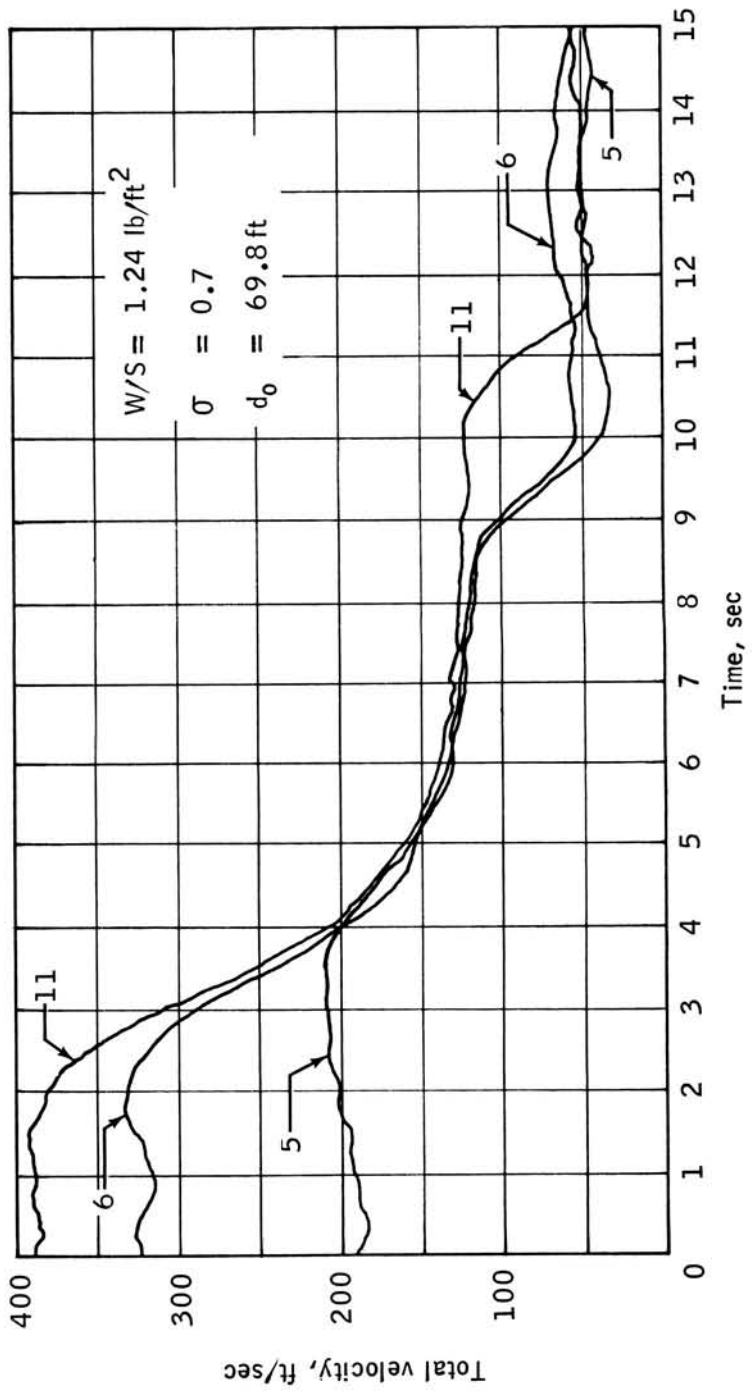


Figure III-58.- Total velocity versus time for drops 5, 6, and 11.

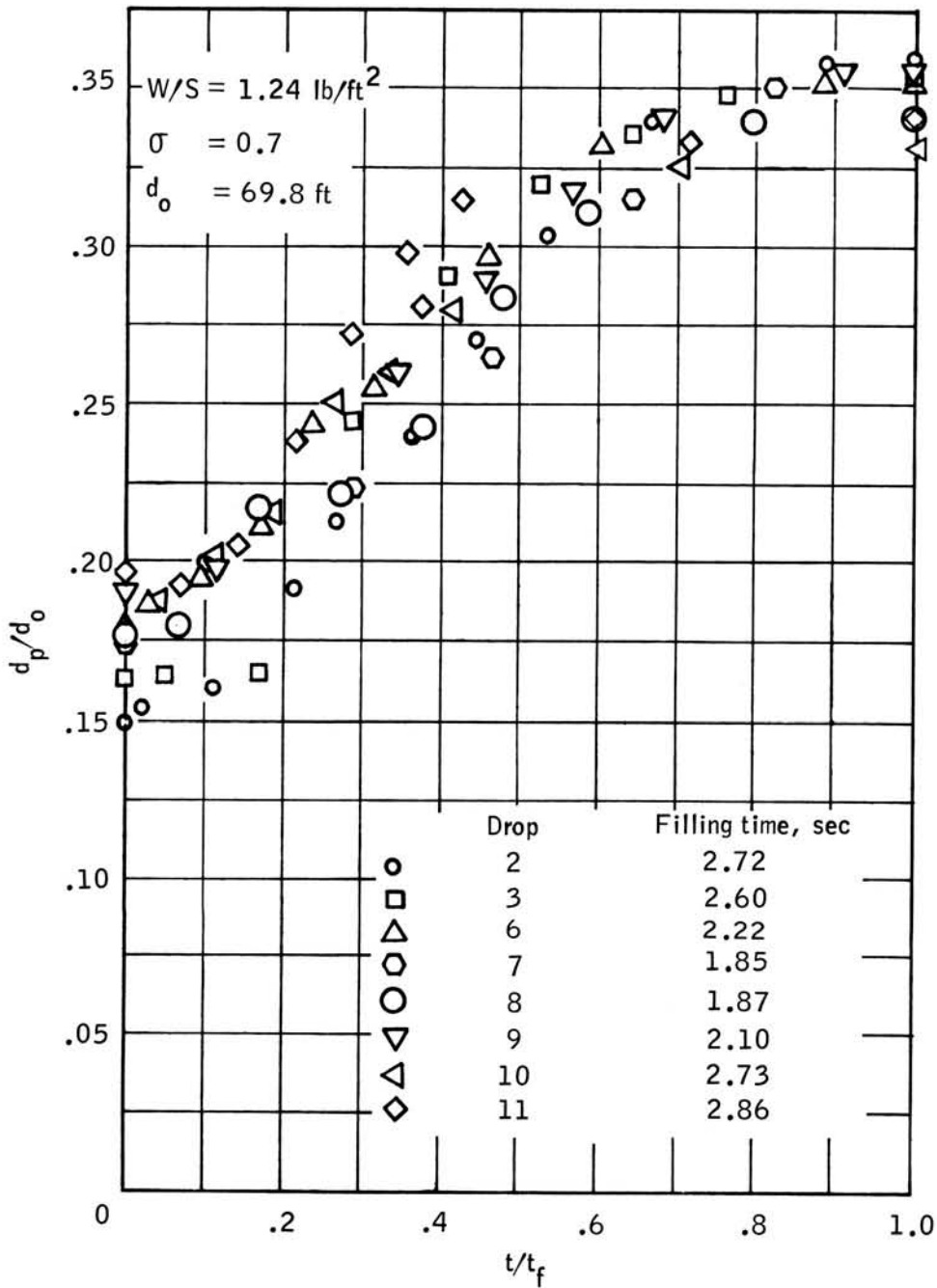


Figure III-59.- Projected diameter ratio versus time ratio, stage I.

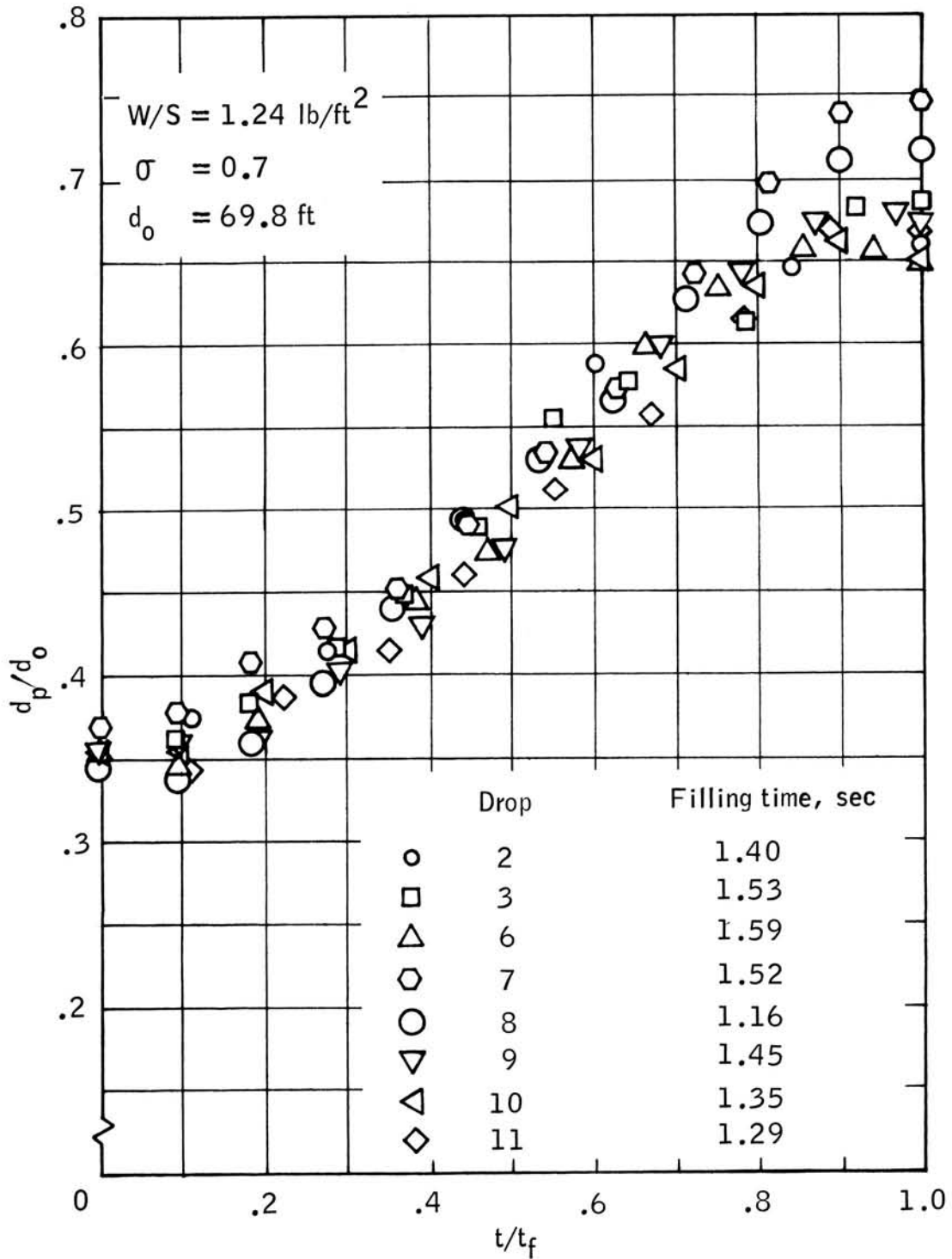


Figure III-60.- Projected diameter ratio versus time ratio, stage II.

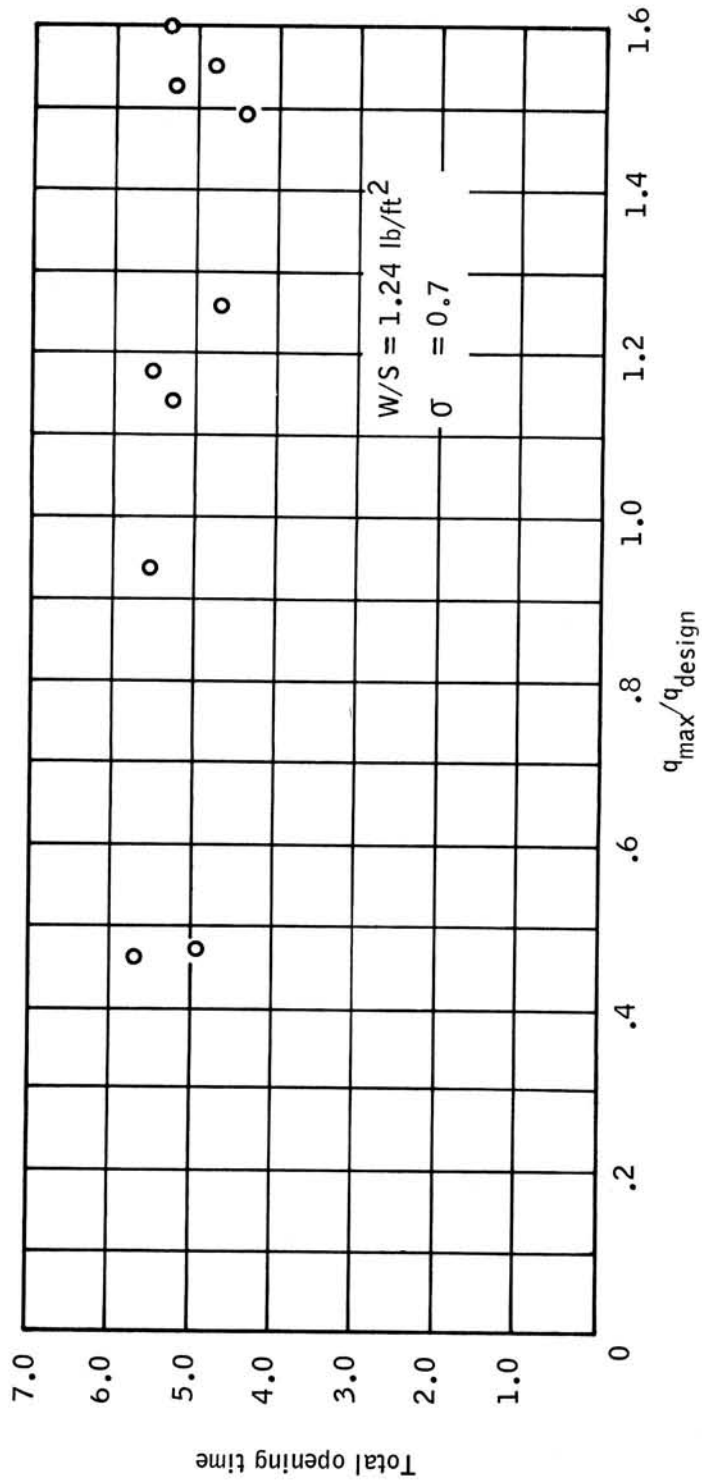


Figure III-61.- Total opening time versus maximum dynamic-pressure ratio for a 70-ft d_0 Para-Sail ($q_{\text{design}} = 80 \text{ lb/ft}^2$).

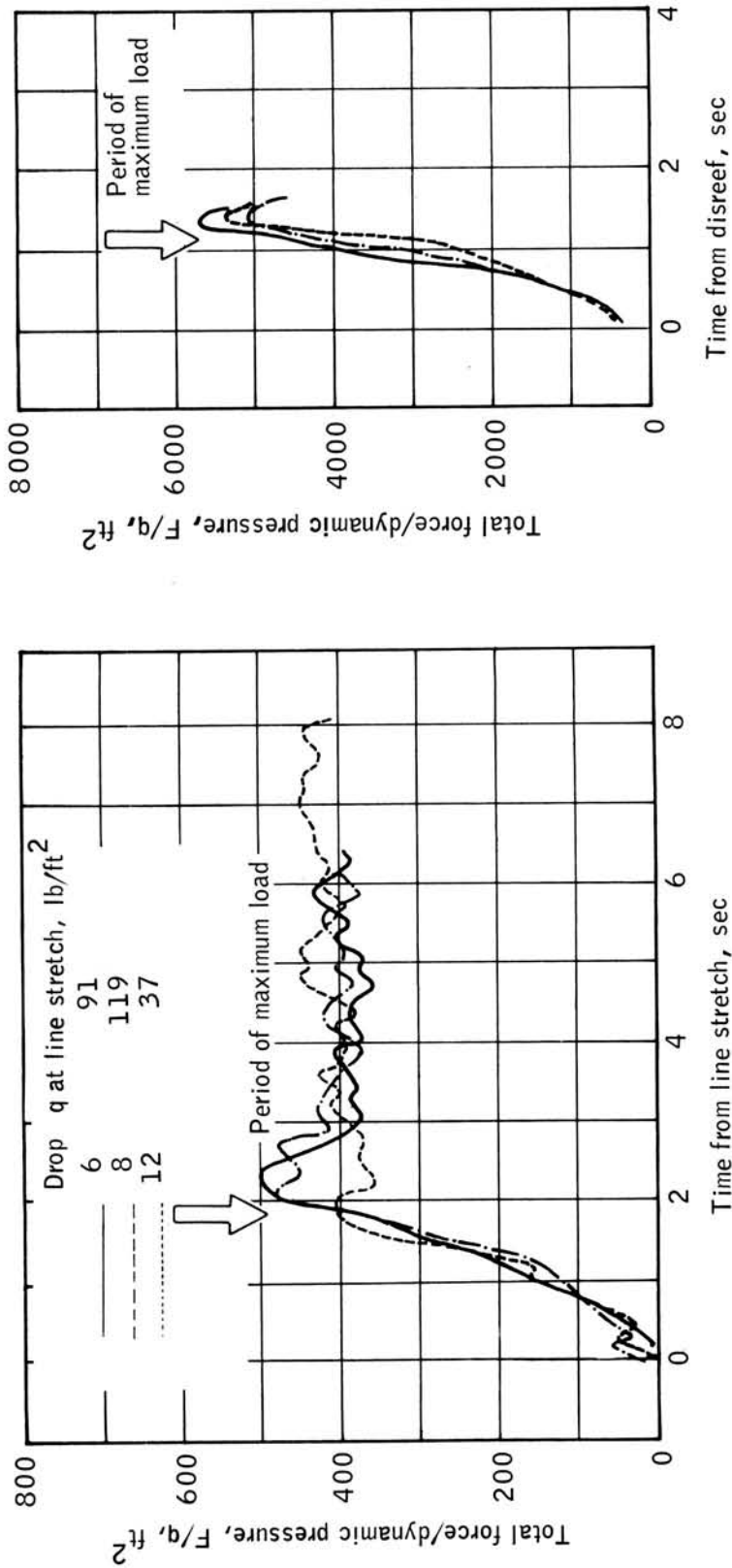


Figure III-62.- Total force-to-dynamic pressure ratio versus time.

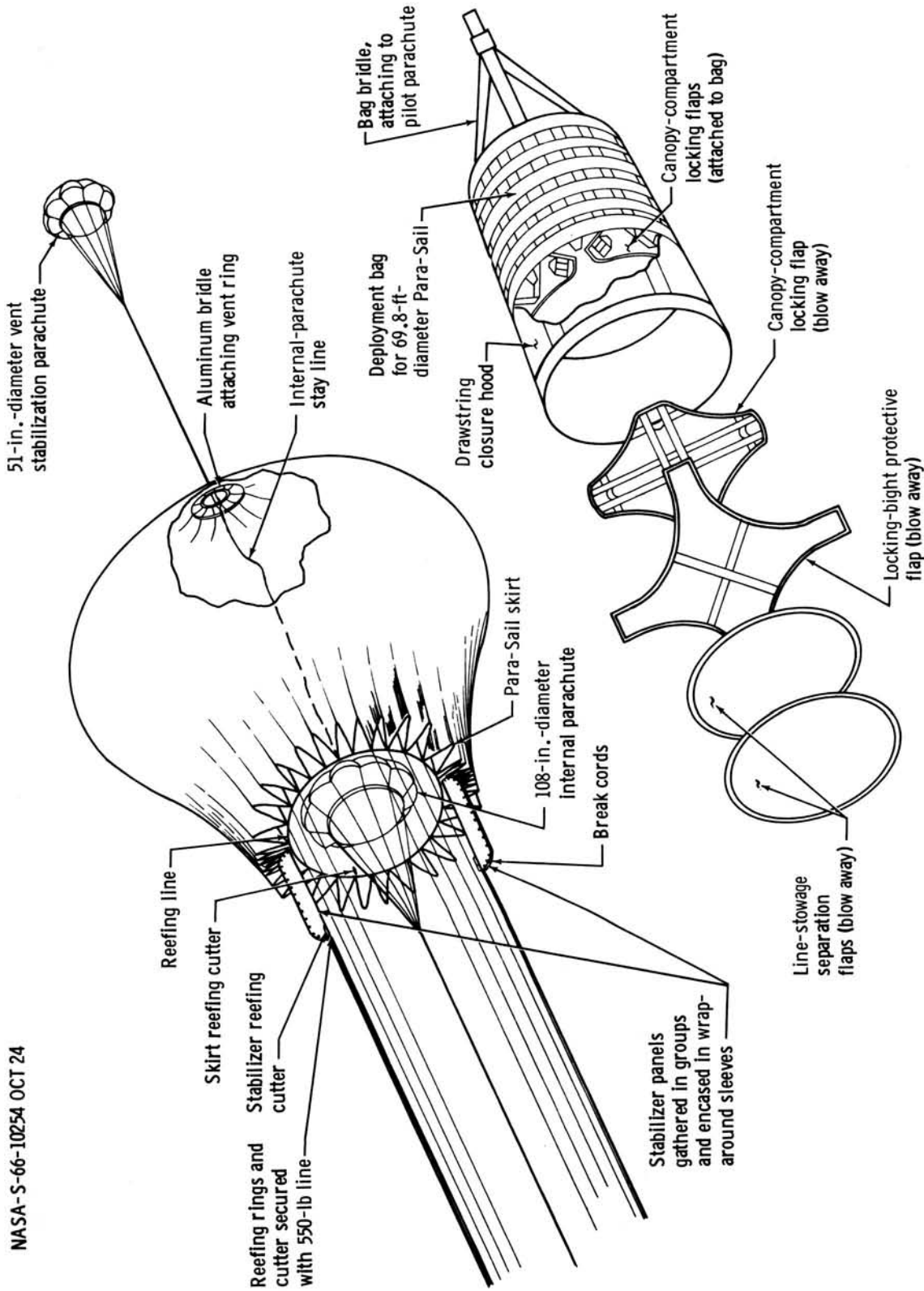


Figure III-63.- Pictorial view of Para-Sail deployment aids.

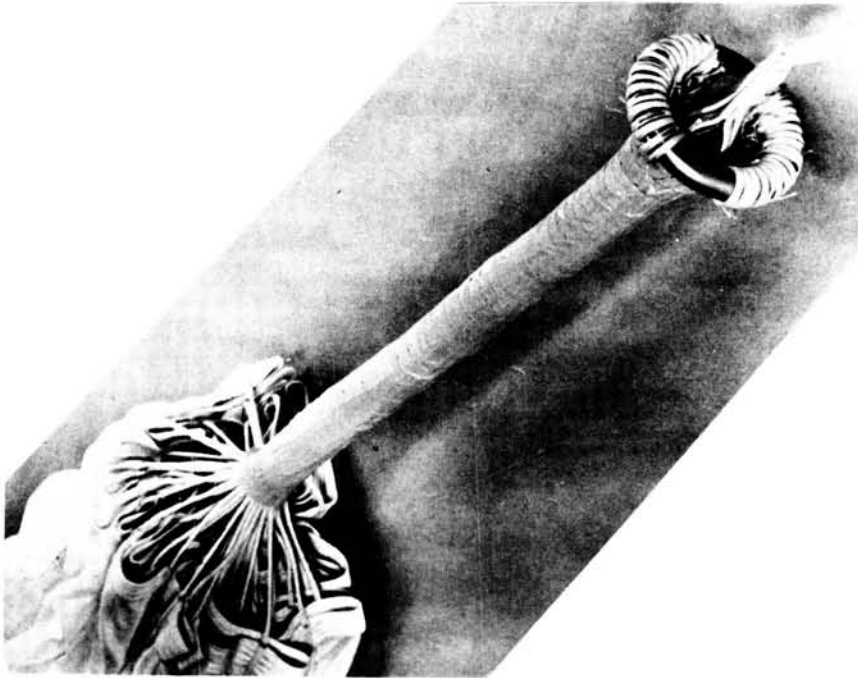


Figure III-64.- Aluminum bridle-attaching vent ring.

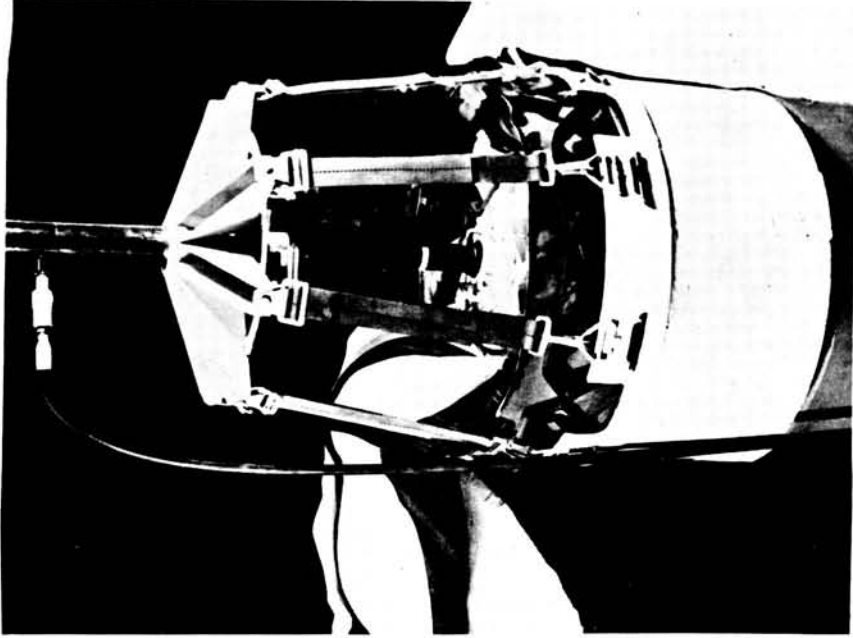


Figure III-65.- Para-Sail pressure packing equipment.

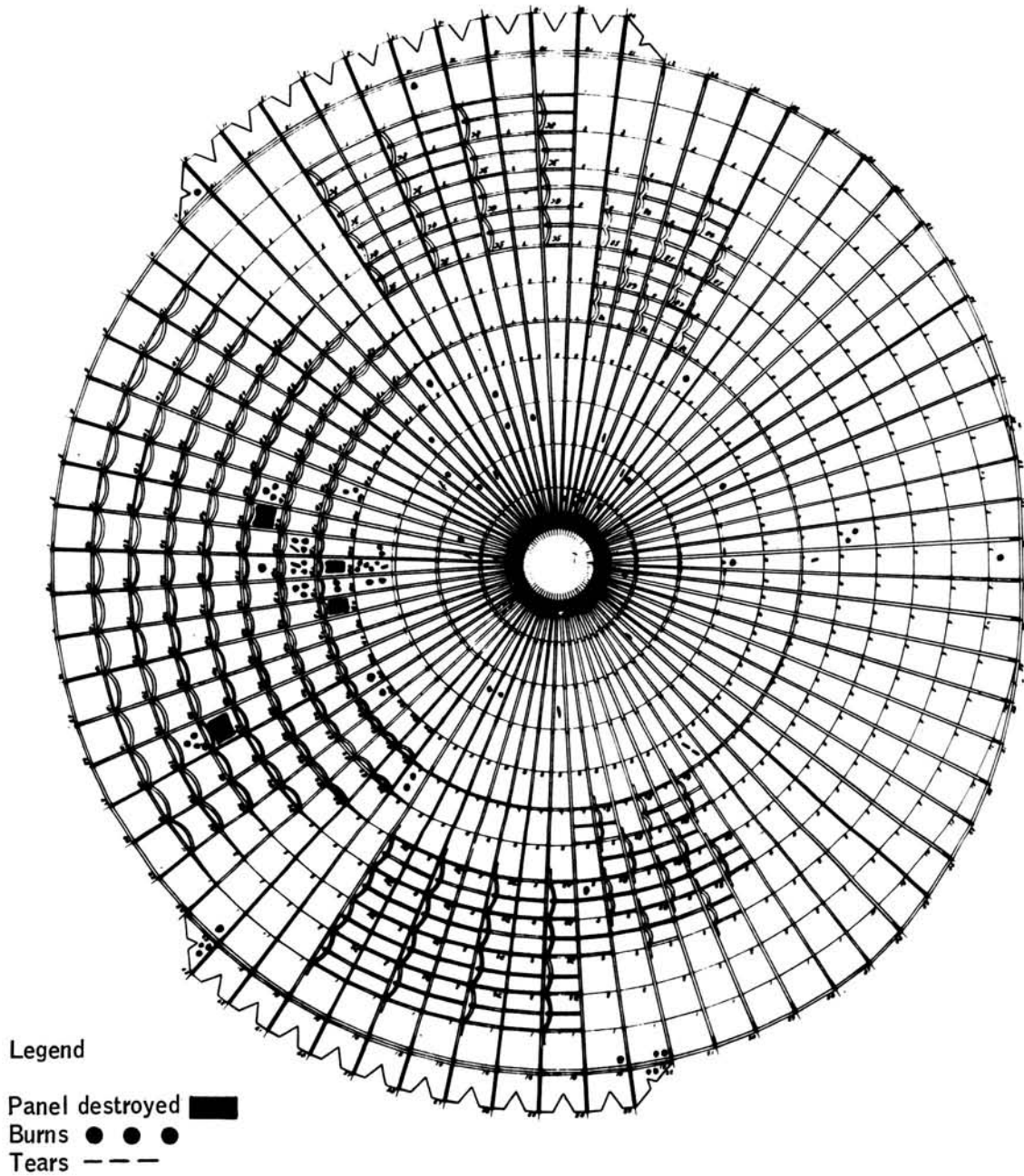


Figure III-66.- Composite damage chart, drop tests 2 to 15, configurations 70A-4 and 70A-5.

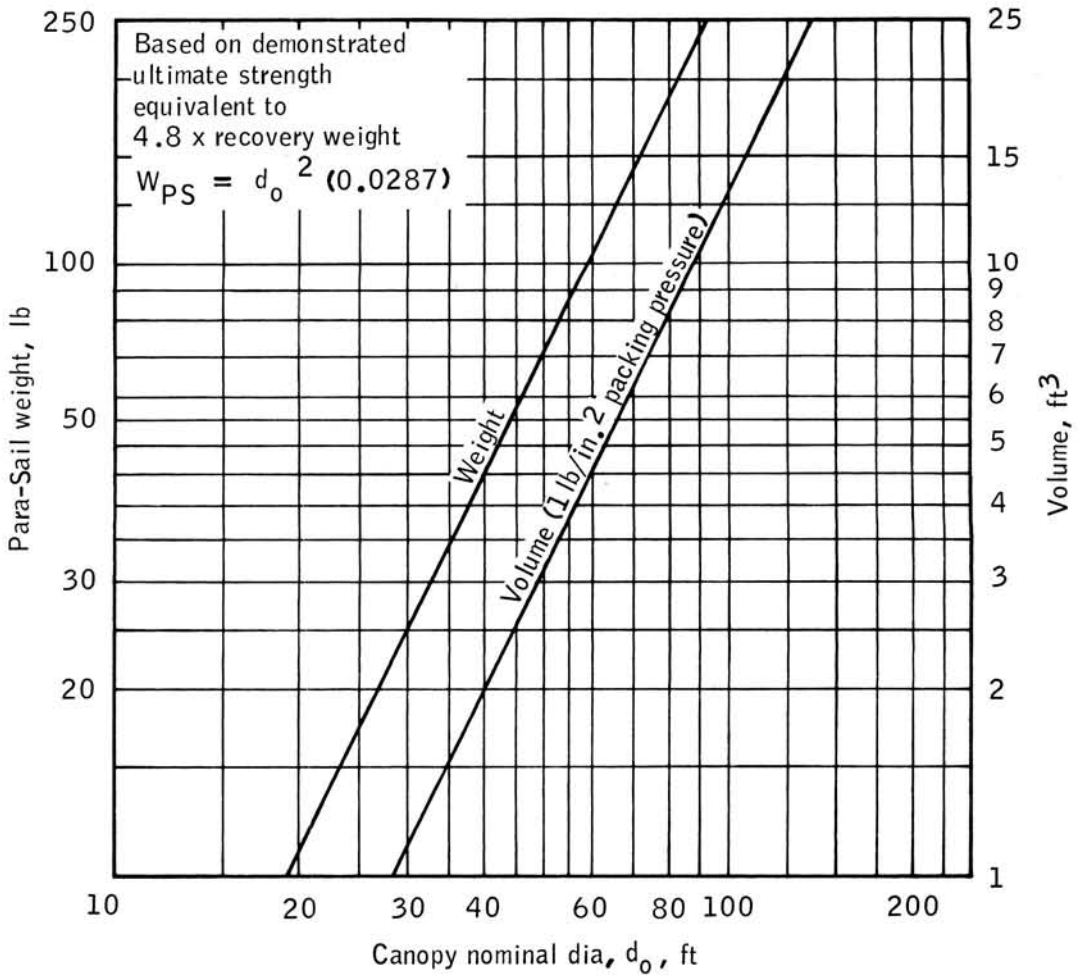


Figure III-67.- Calculated weight and volume for Para-Sail recovery parachutes.

NASA-S-66-10258 OCT 24

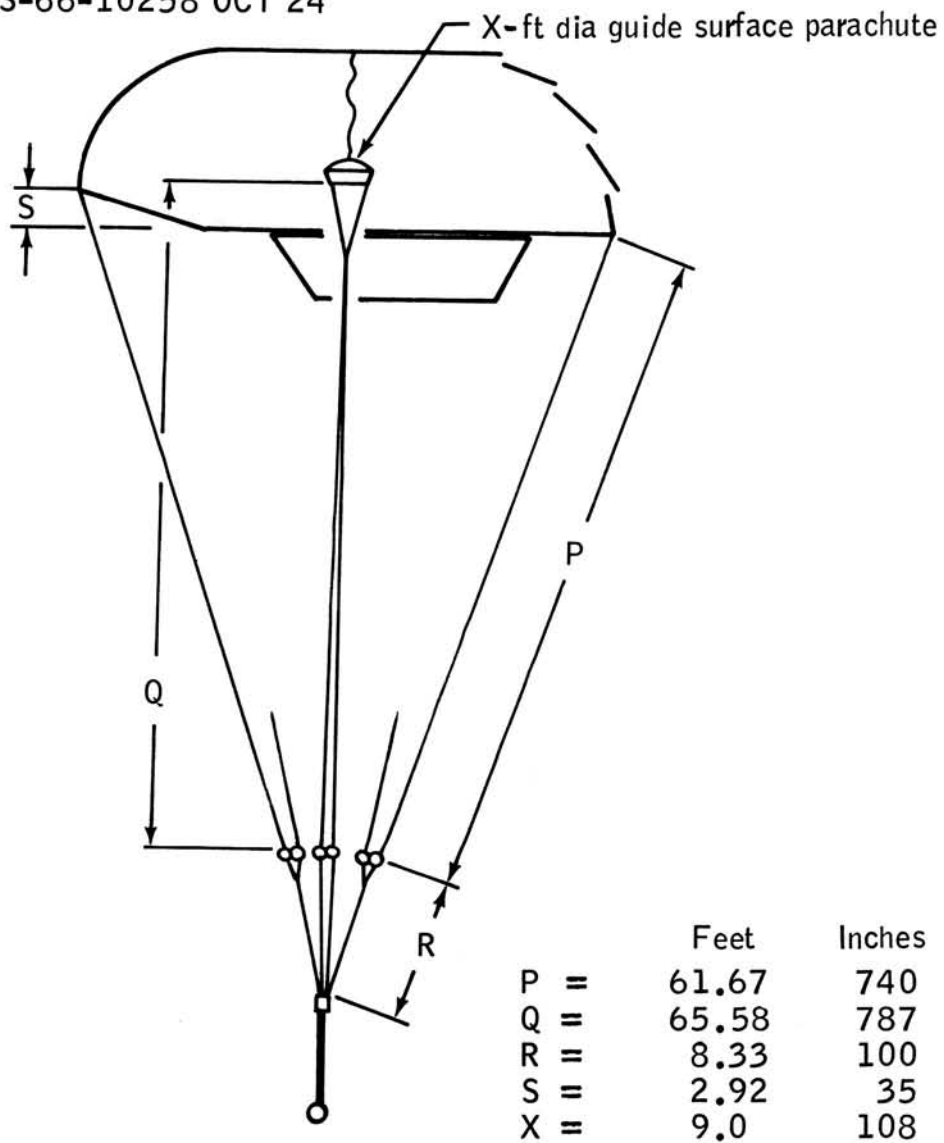


Figure III-68.- General geometry of a 69.8-ft d_0 Para-Sail (deflated condition). Configurations 70A-4 and 70A-5 (72 gores).

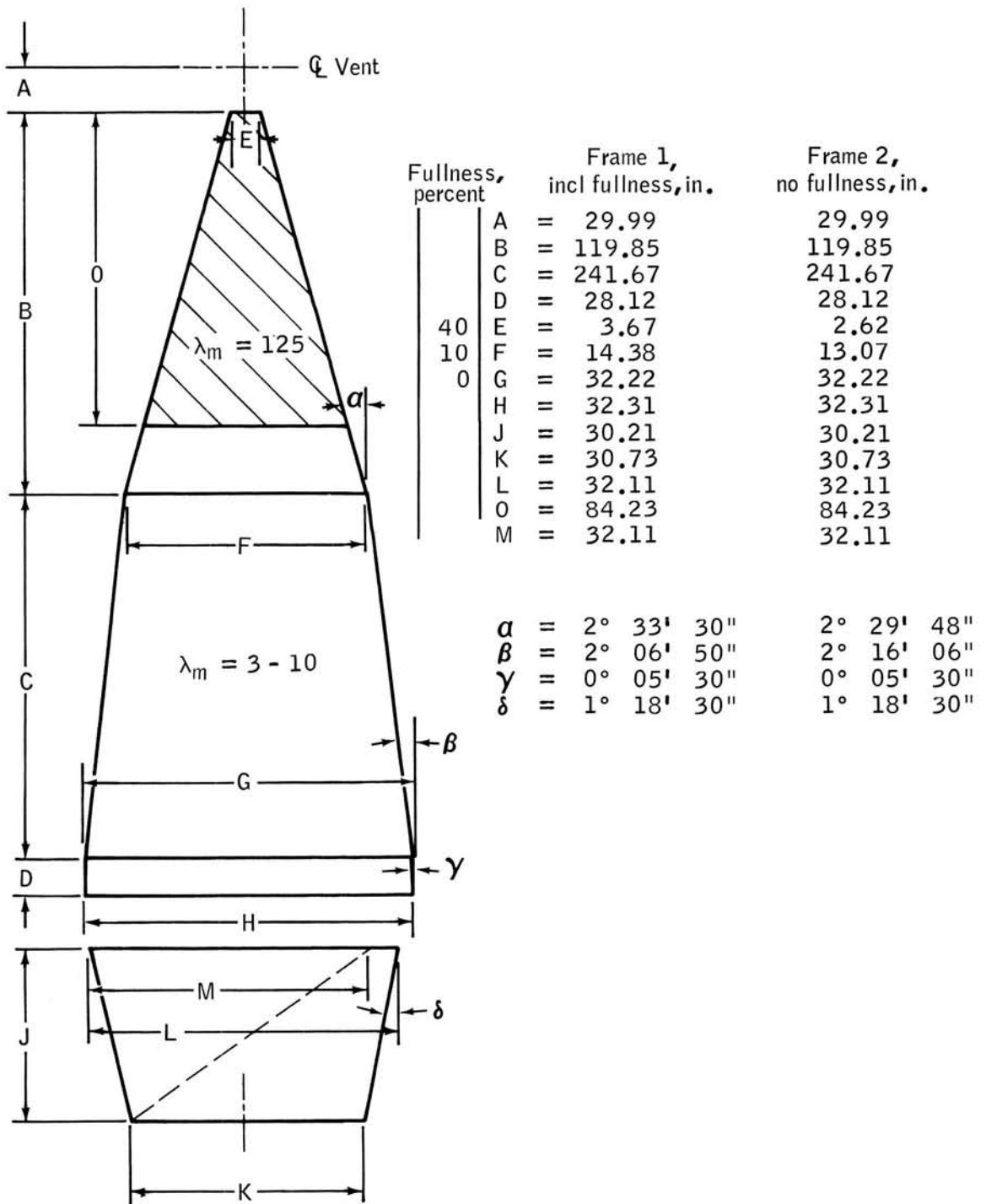
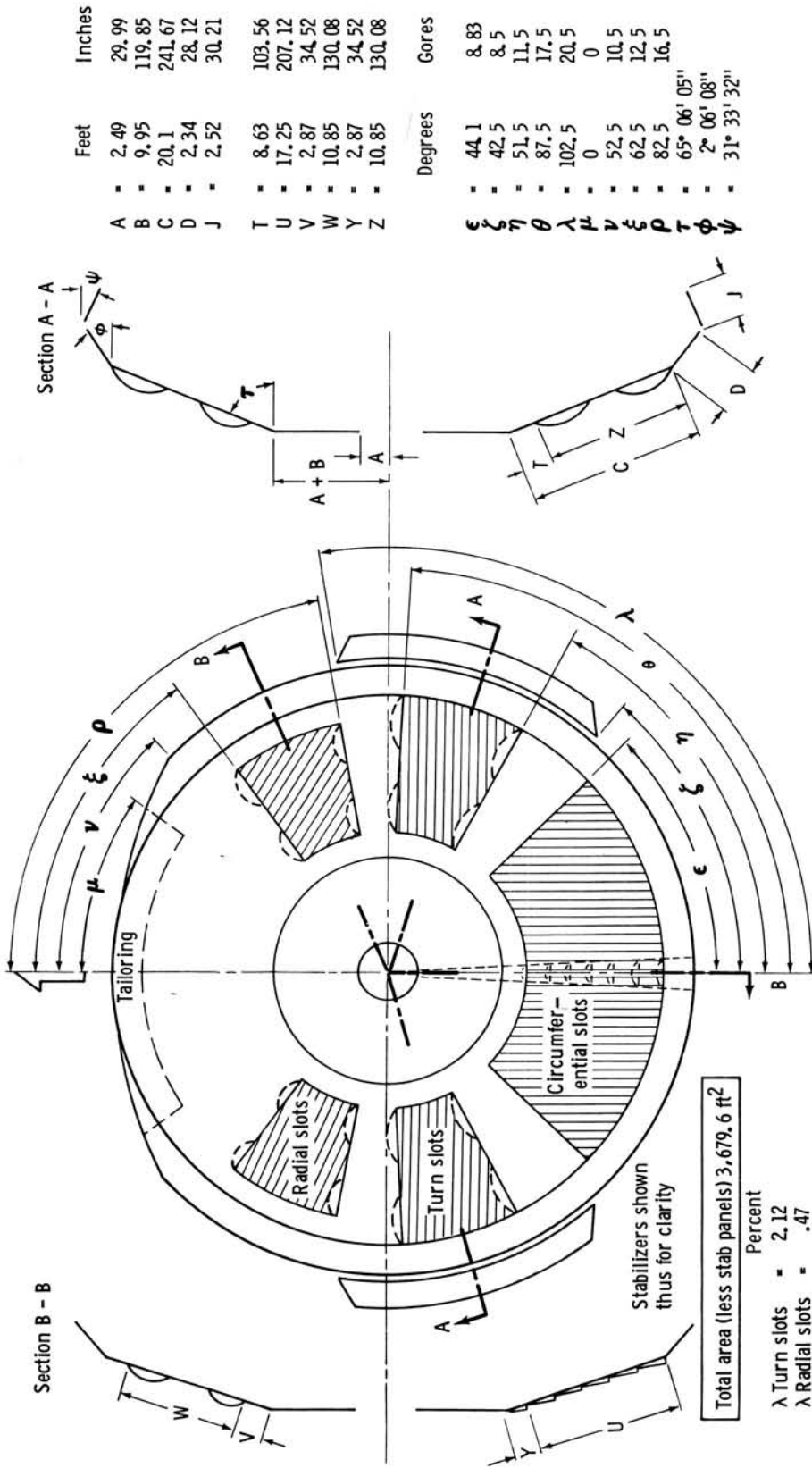


Figure III-69.- Typical gore pattern of a 69.8-ft d_0 Para-Sail. Configurations 70A-4 and 70A-5 (72 gores).



	Feet	Inches
A	2.49	29.99
B	9.95	119.85
C	20.1	241.67
D	2.34	28.12
J	2.52	30.21
T	8.63	103.56
U	17.25	207.12
V	2.87	34.52
W	10.85	130.08
Y	2.87	34.52
Z	10.85	130.08

	Degrees	Gores
ϵ	44.1	8.83
ζ	42.5	8.5
η	51.5	11.5
θ	87.5	17.5
λ	102.5	20.5
μ	0	0
ν	52.5	10.5
ξ	62.5	12.5
ρ	82.5	16.5
τ	65° 06' 05"	
ϕ	2° 06' 08"	
ψ	31° 33' 32"	

Total area (less stab panels) 3,679.6 ft²

	Percent
λ Turn slots	2.12
λ Radial slots	.47
λ Circumf slots	5.34
λ Vent	.53
λ Geom total	8.46
λ Mech total	.57
λ Total	9.03

Figure III-70.- Para-Sail, 69.8-ft d₀ engineer plan view, based upon gore without fullness. Configurations 70A-4 and 70A-5 (72 gores).

PRECEDING PAGE BLANK NOT FILMED.

SECTION IV - ROCKET-MOTOR DEVELOPMENT

By Lonnie W. Jenkins, Chester A. Vaughan,
and James W. Akkerman

USE OF PARAMETRIC EQUATIONS TO OPTIMIZE A LANDING

ROCKET AND SUBSEQUENT MODEL TESTING

By Lonnie W. Jenkins, Chester A. Vaughan,
and James W. Akkerman
Manned Spacecraft Center

SUMMARY

Parametric equations of motion for a retrorocket used in conjunction with a parachute for landing a spacecraft are derived. Their use in optimizing solid-propellant rockets for a Gemini-weight vehicle are discussed. A two-level thrust-time relationship is found necessary because of variations in vehicle velocity and rocket and altitude-sensor performance. The development and use of a pressurized gas-propulsion system for subscale testing is described.

INTRODUCTION

The use of parachutes for recovering a manned spacecraft after reentry was shown to be very reliable in Project Mercury. Due to the magnitude of the impact loads, all Mercury spacecraft landings were made in water. The achievement of land landings has become an objective of subsequent manned space programs. This goal requires an impact-attenuation system to reduce both the magnitude and the onset rate of deceleration or g-loading. In order to keep the weight of such a system as light as possible, it is necessary to consider a system which has maximum energy-absorption capability for a given weight. A good example is a solid-propellant rocket motor. In addition, it is simple, compact, and can be stored for extended periods of time without performance degradation. The solid-propellant rocket motor, in conjunction with an altitude-sensing device, can be ignited at a preset distance above the ground, thus decreasing the descent rate of the vehicle from the relatively high terminal velocity of the parachute to an allowable velocity at impact.

This section derives parametric equations of motion and describes their use in optimizing a solid-propellant landing rocket for use in conjunction with

the Para-Sail parachute. These components comprise the basis for a backup program for the Gemini spacecraft land landings being directed by the Landing Technology Branch, Structures and Mechanics Division, of the Manned Spacecraft Center (MSC), and supported in the analysis and development of the landing rockets by the Auxiliary Propulsion and Pyrotechnic Branch of the Propulsion and Power Division.

SYMBOLS

d	time delay, msec
d_D	time delay from sequencer triggering to signal to open dome vent valve, msec
d_N	time delay from sequencer triggering to signal to open the nozzle solenoid valve, msec
F	rocket thrust, lb
g	acceleration due to gravity, 32.2 ft/sec^2
H	thrust-to-weight ratio, boost phase
L	thrust-to-weight ratio, sustain phase
l	length, ft
m	mass (W/g), slugs
P_1	high value of dome pressure, psig
P_2	high value of nozzle manifold pressure, psig
P_3	low value of nozzle manifold pressure, psig
P_4	low value of dome pressure, psig
T	temperature, °F
t	time, sec

t_D	total time from sequencer triggering to signal to close the dome vent valve, msec
t_f	free fall duration to 90 percent of high pressure, msec
t_H	boost-phase duration, msec
t_N	total time from sequencer triggering to signal to close the nozzle solenoid valve, msec
t_T	total nozzle manifold-pressure duration, msec
V	velocity, ft/sec
W	weight, lb
x	distance traveled, ft
β	drag force proportionality constant
Δt_A	time from beginning of free fall to sequence triggering, msec
Δt_1	interval that dome vent valve is open $(t_D - d_D)$, msec
Δt_5	time from opening of nozzle solenoid valve to 90 percent of maximum nozzle manifold pressure, msec
Δt_6	time from closing of nozzle solenoid valve to beginning of decay of sustain-phase nozzle manifold pressure, msec
Δt_{11}	time from opening of dome vent valve to beginning of decay of boost-phase nozzle manifold pressure, msec
λ	constant
ν	reduced velocity ratio, $\frac{V}{V_0}$
π_k	temperature sensitivity of burning rate, ρ_F^{-1}

τ reduced time, $\frac{tg}{V_0}$

χ reduced distance traveled, $\frac{xg}{V_0^2}$

Subscripts:

A conditions pertaining to case A

B conditions pertaining to case B

del delay

f final

H horizontal

i initial

im impact

nom nominal

V vertical

0 initial value

1 value at end of boost phase

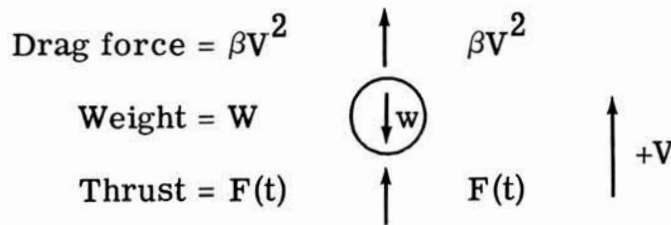
2 value at end of sustain phase

DERIVATION OF MOTION RELATIONSHIPS

In analyzing the motion of a spacecraft acted upon by the combined forces of gravity, parachute drag, and retrorockets, certain simplifying assumptions may be made.

1. The drag coefficient of the parachute is constant.
2. The drag force is proportional to the vertical velocity squared.
3. The vehicle is considered a rigid, point mass.
4. All forces are colinear.
5. There is no stretch in the parachute suspension lines.
6. There is no cross coupling between the horizontal and vertical forces.
7. The change of mass due to propellant loss is negligible.

The equations of motion may now be derived as



Summing the forces and using Newton's second law

$$\Sigma F = m \frac{dV}{dt} \tag{1}$$

$$F(t) + \beta V^2 - W = \frac{W}{g} \frac{dV}{dt} \tag{2}$$

Rearranging

$$\frac{dV}{dt} = \frac{F(t)}{W} g + \beta \frac{gV^2}{W} - g \tag{3}$$

Prior to rocket ignition, the vehicle has reached a steady-state velocity V_0 where the weight of the vehicle is equal to the drag force. The drag coefficient, therefore, can be determined by

$$\beta V_0^2 = W \quad (4)$$

or

$$\beta = \frac{W}{V_0^2} \quad (5)$$

Equation (3) now becomes

$$dV = \left(\frac{F(t)}{W} + \frac{V^2}{V_0^2} - 1 \right) g dt \quad (6)$$

The solution to this differential equation is dependent upon the variation of thrust with time and can be solved in closed form only when the thrust is constant. For a constant thrust-to-weight ratio H greater than one, the differential equation can be solved by separating the variables and direct integration.

Integration of equation (6) yields

$$V_1 = V_0 \sqrt{(H-1)} \tan \left(\frac{g}{V_0} \sqrt{(H-1)} t_1 + \tan^{-1} \left[\frac{1}{\sqrt{(H-1)}} \right] \right) \quad (7)$$

or rearranging

$$\nu_1 = \sqrt{(H-1)} \tan \left(\tau_1 \sqrt{(H-1)} + \tan^{-1} \left[\frac{1}{\sqrt{(H-1)}} \right] \right) \quad (8)$$

where

$$\nu = \frac{V}{V_0} \quad (9)$$

and

$$\tau = \frac{tg}{V_0} \quad (10)$$

with the subscript 1 or 2, as applicable, for V and t .

Integration of equation (7) yields

$$x_1 = \frac{V_0^2}{g} \left(\ln \left\{ \frac{\sqrt{(H-1)}}{\sqrt{(H-1)} \cos \left[\frac{gt_1}{V_0} \sqrt{(H-1)} \right] - \sin \left[\frac{gt_1}{V_0} \sqrt{(H-1)} \right]} \right\} \right) + x_0 \quad (11)$$

or rearranging

$$x_1 = \ln \left(\frac{\sqrt{(H-1)}}{\sqrt{(H-1)} \cos \left[\tau_1 \sqrt{(H-1)} \right] - \sin \left[\tau_1 \sqrt{(H-1)} \right]} \right) \quad (12)$$

where

$$\chi_1 = \frac{(x_1 - x_0) g}{V_o^2} \quad (13)$$

Figure IV-1 shows a family of curves generated from equations (8) and (12). Reduced velocity ν_1 is shown as a function of reduced distance traveled χ_1 , with the thrust-to-weight ratio H treated as a parameter. In addition, lines of constant reduced time τ_1 are shown. Any two terms may be used to determine corresponding values of the other two terms. For example, the resulting reduced velocity and the distance may be obtained for a given combination of reduced time and thrust-to-weight ratio.

The preceding results apply for the boost phase $H > 1$. It is further necessary to consider a sustain phase where the thrust-to-weight ratio L is less than one and constant. The initial conditions for this sustain phase are the end conditions for the boost phase.

Integration of equation (6) yields

$$V_2 = V_o \sqrt{(1-L)} \frac{\left(1 + \lambda \exp \left[\frac{2g \sqrt{(1-L)} t_2}{V_o} \right] \right)}{\left(1 - \lambda \exp \left[\frac{2g \sqrt{(1-L)} t_2}{V_o} \right] \right)} \quad (14)$$

where

$$\lambda = \frac{V_1 - V_o \sqrt{(1-L)}}{V_1 + V_o \sqrt{(1-L)}} \quad (15)$$

This may be rearranged to

$$\nu_2 = \sqrt{(1-L)} \left(\frac{1 + \lambda \exp \left[2\tau_2 \sqrt{(1-L)} \right]}{1 - \lambda \exp \left[2\tau_2 \sqrt{(1-L)} \right]} \right) \quad (16)$$

Integration of equation (14) yields

$$x_2 = V_o \sqrt{(1-L)} t_2 - \frac{V_o^2}{g} \ln \left(\frac{1 - \lambda \exp \left[\frac{2g \sqrt{(1-L)} t_2}{V_o} \right]}{1 - \lambda} \right) + x_1 \quad (17)$$

or, rearranging

$$\chi_2 = \tau_2 \sqrt{(1-L)} - \ln \left(\frac{1 - \lambda \exp \left[2\tau_2 \sqrt{(1-L)} \right]}{1 - \lambda} \right) \quad (18)$$

where

$$\chi_2 = \frac{(x_2 - x_1)}{V_o^2} g \quad (19)$$

Figures IV-2 to IV-12 each show a family of curves generated from equations (16) and (18) for values of reduced velocity at the end of boost phase ν_1 , ranging from 0 to 0.50. Reduced velocity ν_2 is shown as a function of reduced distance traveled in the sustain phase χ_2 , with the sustain thrust-to-weight ratio L treated as a parameter. In addition, lines of constant reduced time τ_2 are shown.

With the information presented in figures IV-1 to IV-12 and the assumptions mentioned, the rocket-performance envelope can be determined for any system.

APPLICATION

In determining performance requirements of solid-propellant rockets for the development program of the Para-Sail landing rocket system mentioned previously, it is necessary to consider variations, as well as the nominal values, of the parameters of the system. The magnitude and ranges of these, which were specified for the development program, were as follows:

1. Rate of descent, $V_o = 30 \pm 3$ ft/sec.
2. Impact velocity, $V_{im} \leq 10$ ft/sec.
3. Operating environment
 - a. Nominal temperature, 70° F.
 - b. Temperature limits, 40 to 140° F.
 - c. Altitude, sea level.
4. Altitude-sensor actuation-signal variation, ± 5 percent of the nominal distance.
5. Rocket ignition-time variation, ± 10 milliseconds.
6. Rocket-performance variation, ± 5 percent of the thrust at a given temperature.
7. Vehicle weight, 4550 pounds.

The nominal rate of descent listed is the terminal value of the proposed parachute. The maximum impact velocity given is approximately the design limitation of the present Gemini spacecraft landing gear. The expected temperature environment for the proposed location of the rocket motors in the Gemini spacecraft vehicle determined the operating temperature-limit range. From various studies of altitude sensors, it is felt that, for actuation heights of 5 to 40 feet above the ground, a sensor can be chosen that will

be accurate within ± 5 percent. By the use of present technology for solid-propellant rockets, the deviation in rocket ignition time of ± 10 milliseconds and the ± 5 percent variation in thrust level can be met without imposing undue hardships on the rocket manufacturer.

The variation of rocket performance with temperature is expressed by a temperature-sensitivity coefficient (π_k) which is dependent upon the particular propellant considered. For purposes of this analysis, the value of π_k is assumed to be 0.11 percent variation per degree of Fahrenheit change in temperature. The calculation of thrust and burning time with temperature variations is based upon the well established assumption that total impulse is constant. Thus

$$F_f = F_i \exp \left[\pi_k (T_f - T_i) / 100 \right] \quad (20)$$

$$t_f = t_i \exp \left[\pi_k (T_i - T_f) / 100 \right] \quad (21)$$

$$F_B = 1.05 F_{\text{nom}} \quad (22)$$

$$F_A = 0.95 F_{\text{nom}} \quad (23)$$

In determining the changes in vehicle motion caused by performance variation, this section considers their effect in worse-coupled conditions. These are:

1. The combination of the highest predicted initial velocity coupled with the lowest predicted thrust (case A).
2. The combination of the lowest predicted initial velocity coupled with the highest predicted thrust (case B).

In order to keep this system as simple as possible, altitude is the only parameter utilized to determine the proper time for igniting the rocket. Upon examining cases A and B, it is evident that case A results in a greater distance traveled during rocket firing than does case B. It is undesirable to impact with a net positive acceleration since this would result in a rebound with a second impact of unknown velocity and attitude. The altitude set for

igniting the rocket must, therefore, be at least as great as the distance traveled in case A. This means that in case B the rocket will burn out before impact, and the vehicle will free fall the remaining distance. Depending upon the magnitude of the free fall distance, the impact velocity may be excessive. For this event, a second, lower thrust level (sustain phase as opposed to the first or boost phase) with a thrust-to-weight ratio less than one is required to achieve the desired reduced velocity.

Case A

The minimum thrust occurs at $+40^{\circ}$ F, and the highest predicted initial velocity is 33 ft/sec with a maximum allowable impact velocity of 10 ft/sec. An upper limit of ν_{1A} can be established

$$\nu_{1A} = \frac{10}{33} = 0.30$$

There must be some allowance for altitude-sensor actuation and ignition-delay-time variances; however, this value will serve as a first approximation. After selecting a value of $H_A = 2.4$, τ_{1A} and χ_{1A} can be obtained from figure IV-1 with $\nu_{1A} = 0.30$ and $H_A = 2.4$. This results in $\tau_{1A} = 0.38$ and $\chi_{1A} = 0.238$; or $t_{1A} = 0.39$ second and $x_{1A} = 8.05$ feet. The use of figure IV-1 is better illustrated in figure IV-13.

Case B

The minimum predicted initial velocity is 27 ft/sec, and the maximum thrust will occur at 140° F. When equations (20) to (23) are used

$$H_B = \left(\frac{1.05}{0.95} \right) (2.4) \exp \left[0.0011 (140 - 40) \right] = 2.96$$

$$t_{1B} = 0.39 \exp \left[0.0011 (40 - 140) \right] = 0.35$$

The corresponding value of τ_{1B} is 0.42. From figure IV-1, $\nu_{1B} = 0.06$ and $\chi_{1B} = 0.204$, or $V_{1B} = 1.62$ ft/sec and $x_{1B} = 4.64$ feet.

For case B, the vehicle has to travel 3.41 feet after the end of boost thrust. If the vehicle were allowed to free fall for this distance, with an initial free fall velocity of 1.62 ft/sec, the velocity at impact would be 14.9 ft/sec. This value is greater than the maximum allowable impact velocity; therefore, a sustain-thrust phase is required.

SUSTAIN PHASE

The most efficient sustain phase thrust-to-weight ratio (L) allows an impact velocity of 10 ft/sec when the total distance traveled for both the boost and sustain phase in case B is equal to the distance traveled for the boost phase in case A.

The vehicle has to travel through a distance of 3.41 feet ($\chi_{2B} = 0.150$) during the sustain phase for case B. Values of L_B and τ_{2B} can be obtained by interpolation between figures IV-3 and IV-4 using $\nu_{1B} = 0.06$, $\chi_{2B} = 0.150$, and $\nu_{2B} = 0.37$. The results obtained are $L_B = 0.48$ and $\tau_{2B} = 0.68$. The use of figure IV-3 is better illustrated in figure IV-14.

It is now necessary to include the effects of altitude-sensor and ignition-delay-time variations. The ignition-delay variation may be converted to a distance variation by multiplying it by the maximum initial velocity

$$x_{del} = (0.010) (33) = 0.33 \text{ feet}$$

Thus the nominal altitude-sensor setting would be

$$x_{nom} = 8.05 + 0.33 + 0.05 x_{nom}$$

or

$$x_{\text{nom}} = 8.82 \text{ feet}$$

This value means that the vehicle must travel 0.77 foot, in case A, during the sustain phase ($x_{2A} = 0.023$). The corresponding reduced velocity ν_{2A} is obtained from figure IV-8 with $\nu_{1A} = 0.30$ and $L_A = 0.39$, giving a value of $\nu_{2A} = 0.34$ or $V_{2A} = 11.1 \text{ ft/sec}$. A lower value of impact velocity is required.

Either the burning time and/or the value of H must be decreased. The limit to these changes is the combination which would make the value ν_{1B} equal to zero. From figure IV-1, keeping $H_B = 2.96$, a value of $\tau_{1B} = 0.44$ will result in $\nu_{1B} = 0$. A first approximation for a new value of τ_{1B} is $(\tau_{1B} = \tau_{1B} + 0.44) \cdot 0.5 = (0.42 + 0.44) \cdot 0.5 = 0.43$, which is equivalent to $t_{1B} = 0.36$ second or $t_{1A} = 0.40$ second. A second pass through the calculation scheme gives the following values: $H_A = 2.4$, $x_{\text{nom}} = 8.96$ feet, $\tau_{1A} = 0.39$, $L_A = 0.46$, and $V_{2A} = 10.6 \text{ ft/sec}$.

The two values for τ_{1B} thus far used, and the resulting values of V_{2A} , are shown in figure IV-15. This suggests that a value of V_{2A} , less than 10.0 ft/sec, will not be attained with the set of values chosen and the restraints imposed. Indeed, using the limiting value of $\tau_{1B} = 0.44$, a value of $V_{2A} = 10.3 \text{ ft/sec}$ ensues. This analysis has been based upon a constant thrust with time in both the boost and the sustain phases. It also assumes that the transition between the boost and the sustain phases is instantaneous. Obviously, from an internal ballistics standpoint, the thrust will probably not be constant with time. Also, the transition from boost phase to sustain phase will require a finite amount of time. The result of these factors will, in general, be in a direction which increases the deceleration of the capsule.

Although the ramp function described is a good representation of the required performance, the actual thrust-time relationship should be used in equation (5) when it becomes available.

In summary, the nominal (70°) performance parameters of the landing rockets are as follows: $t_1 = 0.40$ second, $t_2 = 0.89$ second, $H = 2.61$, $L = 0.50$, and $x_{\text{nom}} = 9.0$ feet.

In the prototype vehicle selected for the Para-Sail landing-rocket program, the rockets are revolved 8° about the roll axis in opposing directions. This reduces the vertical component of thrust by the cosine of 8° . These factors may be combined to give the following required performance for each of the landing rockets for the Para-Sail landing-rocket system:

	Boost	Sustain
Thrust, lb_f	6000	1150
Burning time, sec	0.40	0.89

Thiokol Chemical Corporation (Elkton) was selected to manufacture solid-propellant rockets having these thrust-time requirements (appendix A). Appendix B describes a cold-gas propulsion system which was built for use in a subscale model.

CONCLUDING REMARKS

The thrust-time variation of a solid-propellant rocket used to provide impact attenuation for a vehicle descending to earth by means of a parachute may be designed to provide for many performance variations. These include variations in propellant burning rate and temperature, rate of descent, altitude-sensor actuation signal, and ignition delay time. For those systems where the variations are large, a second, lower thrust level must be provided.

The method is applicable for all parachute-landing rocket systems where the net force of the rocket (or rockets) acts vertically through the center of gravity. This includes a proposed military usage for palletized cargo.

APPENDIX A - DEVELOPMENT OF THE MODEL-100

LANDING ROCKET

As the concept of landing a Gemini spacecraft on land with a Para-Sail parachute and retrorockets (landing rockets) evolved, various locations for the rockets were considered. By the use of the concept of minimum change, the decision was made to utilize the main landing-gear bay. This fixed the rocket-motor envelope and angle between the thrust vectors of the two rocket motors. Furthermore, this location dictated the use of a scarfed nozzle; that is, the nozzle exit plane is oblique to the nozzle centerline. The required performance of the landing rockets was determined as detailed in section IV. Since the exact location of the center of gravity and the required cant angle were uncertain, the request for proposal (RFP No. 63-540P for the Model-100 Landing Rocket) indicated that only a design study of the canted nozzle was to be conducted. The first groups of delivered motors were to use a nozzle whose centerline was colinear with the motor centerline.

McDonnell Aircraft Corporation later suggested that the center equipment bay be used instead of the main landing-gear bay. This went beyond the original concept of minimum change, but allowed retention of the landing gear and the existing touchdown attitude. It also meant significant changes in the design of the rocket motor, although not in the method of approach. Changing the angle between the thrust vectors of the two motors from 51° to 13° meant a significant decrease in the thrust requirement. A larger motor-case diameter was permitted in the new location. This allowed more propellant; hence, a longer sustainer burn time. The longer burn time more easily accommodated the expected performance variations. The motor could also be more easily aligned in the new location. Perhaps as important was the fact that the nozzle exit plane could be perpendicular to the nozzle centerline.

A meeting was held on May 22 and 23, 1963, at the NASA Manned Spacecraft Center to clarify some questions in regard to the integration of landing rockets on a Gemini spacecraft. The following conclusions were reached:

1. The motor centerline and nozzle exit plane shall both be perpendicular to the nozzle centerline.
2. The envelope of the rocket shall be as defined in figure IV-16. In addition, the angle between the nozzle centerlines will be 13.0° .
3. Thrust will be transmitted to the vehicle through the aft attachment fitting and the collar of the igniter boss as shown in figure IV-16. In addition, a strap used to secure the rocket to the floor beams will be considered.

4. The igniter, without the squibs, shall have the same Interstate Commerce Commission classification as the rocket motor; or, it shall be designed such that the igniter can be shipped separately and installed in the rocket motor prior to installation of the rocket motor in the vehicle. In either case, the igniter shall be so designed that the squibs can be inserted after the rocket motor has been installed in the vehicle.

5. The maximum deviation of the thrust vector from the center of gravity (including center-of-gravity excursions) shall be less than 0.5 inch. The center of gravity can be measured to ± 0.25 inch.

6. Until additional information is available from drop tests, the vertical drag shall be considered proportional to the vertical velocity squared and independent of the horizontal velocity.

7. The maximum capsule reentry weight shall be considered 5050 pounds with 330 pounds and 170 pounds for the rendezvous and recovery canister section and the Para-Sail, respectively. The rocket motor shall be designed for the maximum vehicle touchdown weight, 4550 pounds. Provision shall be made for altering the thrust level by minimum alterations to the grain (such as by reducing the length of the grain).

8. The design philosophy shall be to consider worse-coupled conditions.

9. The rocket motor shall be designed to operate between the limits of -20° F and 180° F.

10. The expected operational temperature range shall be considered $+40$ to $+160^{\circ}$ F.

11. The Horex 3575 squib shall be used as the initiator. This item is being qualified for the Gemini spacecraft retrorocket.

12. The maximum average ignition time-delay shall be 60-milliseconds with a 10-millisecond dispersion allowed about the average.

13. The altitude-sensor error shall be considered to be ± 5 percent of the altitude but not less than 6 inches.

14. The vertical descent velocity shall be considered to be 30 ± 3 ft/sec. The current philosophy is to design for this velocity, changing the parachute diameter if necessary.

The design and development of the model-100 landing rocket (TE-421) was initiated by Thiokol Chemical Corporation on July 3, 1963, under

contract NAS 9-1772. Prior to this time, NASA and McDonnell Aircraft Corporation personnel arrived at envelope and interface requirements which were later finalized with Thiokol Chemical Corporation in July 1963. In particular, the interface with the space capsule and envelope was discussed. This envelope is shown in figure IV-17. The requirements are tabulated below.

	Original requirements	Modified requirements	Limits
Average thrust boost, lb	5950	5950	5650 to 6350
Average thrust sustain, lb . . .	1220	1220	1160 to 1280
Burning time, boost, sec40	.40	±.015
Burning time sustain, sec . . .	1.10	1.10	±.050
Ignition delay, sec06	.06	±.010
Length, in.	24.71	21.35	
Diameter, in.	5.5	5.5	
Nozzle cant angle, deg	90	90	
Nozzle exit diameter, in. . . .	3.26	3.396	
Nozzle length from centerline, in.	5.0	5.0	

The design of the propellant grain and inert components coupled with the initial available data on the high-pressure ballistic performance of the propellant, TP-H-1050, revealed that there would be erosive burning in the motor, resulting in high initial pressures. This required a strengthening of the pressure vessel. Since the envelope was restricted, the case and closure material had to be strengthened by changing to a high-strength material (Ladish D6AC steel versus 4130 steel as originally planned). As this change would have caused a considerable delay in the program, NASA decided to furnish heavyweight units for the immediate test program and to allow Thiokol to continue procurement of flightweight units for possible future evaluation.

There is only one essential difference between the two units. In the heavyweight unit, the metal parts, with the exception of the nozzle expansion cone, were made stronger by doubling the wall thickness of the exterior of the case and the aft closure.

BASIC MOTOR ASSEMBLIES

The motor consists of three basic assemblies: the loaded case, the insulated nozzle assembly, and the igniter.

The Loaded Case Assembly

The case is made of a steel tube which is threaded at one end to accept the nozzle assembly. A cap is welded to the other end. This head cap has a boss for the igniter. Sixteen pounds (nominal) of TP-H-1050 propellant are bonded to the case by liner TL-H-304. A 10-point-star grain configuration provides the required two levels of thrust. A cylinder 3 inches long and 1.5 inches in diameter is cut in the head end of the propellant to allow space for the igniter. The aft end of the propellant grain is finished flush with the case.

The Nozzle Assembly

The nozzle assembly, which screws on the motor case, consists of three parts: a hemispherical body, a nozzle expansion cone which is welded into the body at a 90° angle to the motor longitudinal centerline, and a nozzle throat insert which extends into the motor. A boss projects from the nozzle body along the longitudinal centerline. This 1.25-inch-diameter cylindrical boss is used as a motor attachment fitting. A small hole is tapped through the body within this boss so that motor pressure can be monitored. The nozzle body and exit cone are steel, and HLM 85 carbon is used as the throat insert.

The nozzle body is insulated with premolded polyisoprene rubber which has a thickness tapering from 0.284 inch at the pressure takeoff to 0.120 inch at the threads. The steel nozzle extension which extends down into the motor is protected by a cylinder of phenolic asbestos (RPD-150) that has been machined to fit the evolved part. A Thiokol adhesive (TA-D-310) is used as fillet insulation between the RPD-150 and the polyisoprene rubber.

The Igniter Assembly

The igniter assembly is mounted in the head of the motor by eight screws. The pressure seal is an O-ring. An aluminum mount 1.75 inches in diameter projects 1.95 inches from the rear of the igniter, providing a cylindrical surface which is used as the other attachment joint for the motor.

There are three bosses drilled into the end of the mount in a triangular arrangement. Two of the bosses are used for the initiators; the other provides access to motor Pyrogen pressure. Three grains of 2A boron pellets are used for the booster charge. A spacer establishes the required stand-off to the Pyrogen grain. The five-point-star Pyrogen grain is 2.75 inches long and 1 inch in diameter. This assembly (grain, spacer, and boron basket) is housed in a paper phenolic cartridge, which is bonded to the Pyrogen case. The case screws into the mount, making the igniter assembly self-contained. A ring of polyisoprene-type insulation protects that portion of the mount which protrudes into the motor case, while a sleeve of paper phenolic acts as an external insulator to protect the case from the hot motor gases.

The design objectives were to use existing technology as much as possible. The propellant, which was developed and qualified for the Dyna-Soar acceleration motor; and the initiator (Holex 3575), which was qualified for the Gemini spacecraft retrorockets were used. Some additional testing of the propellant was required in order to obtain ballistic parameters in the 1500 to 3000 psia range.

An igniter body and mount assembly were hydro-tested to destruction, failing at 4600 psig. The heavyweight case and nozzle were hydro-tested to 6000 psig with no failure or leakage; however, the bolts holding the igniter mount to the case were distorted. Two lightweight cases have been hydro-tested to destruction; one to 5310 psig and one to 4675 psig. The latter assembly had a case with walls 0.007-inch thinner than the minimum 0.050-inch requirement. Each of these is above the 4400 psia calculated burst pressure.

Two live igniter assemblies were static tested in the open air. Performance agreed with predicted levels and the components were in excellent condition. The development program was concluded with 12 motor firings. There were three statistical shots at 60° F and three at 125° F. The remaining six motors were subjected to sequential conditioning before they were tested.

All six motors were temperature cycled between 125° and -20°. Two motors were packaged together in a shipping container and dropped 4 feet on reinforced concrete in both lateral and longitudinal axes. These tests

occurred at 125° F. Two motors were shock tested to 5g both laterally and longitudinally; one motor at -20° F and one at 125° F.

The remaining two motors were subjected to a vibration test at 60° F consisting of a sweep of ±9g from 6 to 20 cps for 1 minute, and a ±0.05g to ±0.25g cycle from 6 to 20 cps for 4 hours in the longitudinal and lateral planes. There was no indication of resonant frequency during these vibration tests. All units were visually and radiographically inspected after the completion of each test and no discrepancies were found. Both motors subjected to drop tests were fired at -20° F. One of the motors subjected to vibration was fired at 125° F, and the other at -20° F; similarly for the two motors subject to shock testing.

Impulse and average thrust values were within specifications, but, because of erosive burning, the maximum pressure was exceeded. The peak pressure would not have been acceptable at 180° F in lightweight hardware. A typical thrust-time trace is shown in figure IV-18. There was also a minor potential problem with the nozzle insulation. Thiokol Chemical Corporation proposed a one-piece, molded-in-place, hard insulation of the RPD-150 type, which had been used successfully in other canted nozzle programs.

The initial development program was intended only to demonstrate an ability to withstand the expected NASA developmental environment; however, all Gemini spacecraft requirements were given as design requirements. A follow-on contract, NAS 9-3844, was issued to Thiokol to correct the problems noted and to verify the full-design requirements of temperature and vibration with lightweight hardware. The aft port of the propellant grain was enlarged in a successful attempt to reduce the erosive burning problem. This program was completed with all objectives achieved. One unresolved problem exists. Spalling of the graphite insert resulted in a burn through in the nozzle exit cone of two motors, one heavyweight and one lightweight case. These incidents are currently being investigated by Thiokol.

A contract for qualification of these rockets, NAS 9-4829, was issued June 29, 1965. The Project Apollo standard initiator was substituted for the Gemini spacecraft retrorocket initiator, and the environmental requirements were updated such that they would be compatible with Project Apollo environmental requirements for a comparable system.

APPENDIX B

PROPULSION-MODEL DESCRIPTION AND TESTING

Experimental verification of the previously described results was required to demonstrate the adequacy of the analytical method. A 1/3-scaled model of the Gemini spacecraft was chosen since it provided a vehicle of convenient size with which to work. Furthermore, this vehicle was chosen by the Mechanical and Landing Systems Branch (MLSB) of Structures and Mechanics Division (S & MD) for subscale tests of the Gemini spacecraft landing gear. The results of both the propulsion and landing gear tests would be applicable to the Para-Sail landing rocket study.

In order to include the effects of variations of the many parameters affecting system and vehicle performance, a flexible propulsion system was required. Also, the system had to be controllable within close tolerances and safe to operate. A pressurized gas system appeared most likely to meet these requirements; furthermore, it could meet the allowable vehicle weight and volume requirements. The system requirements generated in the main body of this report, scaled down to a 195-pound 1/3-scale vehicle, are:

Thrust, lb _f	Boost	Sustain
Maximum	580	110
Nominal	510	100
Minimum	470	90
Burning time, sec		
Maximum	0.22	0.49
Nominal	.23	.51
Minimum	.24	.53

The schematic shown in figure IV-19 describes the propulsion system selected. The magnitude of the pressure to the nozzle manifold is controlled by the pressure in the dome of the regulator valve. The second, lower pressure level (hence, thrust) is achieved by bleeding off some of the dome pressurant.

An electronic control unit was developed by the Guidance and Control Division to control the system's sequence of events. The sequencer used one R-C network channel for opening and closing the regulator-dome solenoid valve and one for the nozzle solenoid valve. A start signal was fed into the sequencer by the closing of a microswitch when the model physically separated from the drop tower. This signal initiated both R-C networks; however, both the time to energize and the time to de-energize each circuit were individually controlled by variable potentiometers. These times correspond to the opening and closing signals to each solenoid valve.

In order to effectively use the system, the various operating parameters had to be characterized. Figure IV-20 shows the thrust stand used to obtain the relationship between the manifold pressure and the resultant thrust. (The propulsion system described was for an earlier configuration, not the system shown in figure IV-20.) After the tanks were pressurized to approximately 2500 lb/in.², the regulator was locked open. The nozzle solenoid valve was then opened, allowing the tanks to blow down. After replicate runs, the relationship between the resultant thrust and the nozzle manifold pressure (fig. IV-21) was obtained. The dip in the curve was probably due to flow separation in the nozzle at low manifold pressures.

Before the subsequent steps of characterization, the propulsion system was installed within the framework of the model (fig. IV-22). These tests were performed with the vehicle tied down and the nozzles exhausting upward. Arbitrary values of dome solenoid valve and nozzle solenoid valve delay times d_D and d_N , respectively, and nozzle solenoid valve total time t_N were set on the sequencer. A series of tests was made of the propulsion system with various combinations of dome pressure and dome delay times. The dome pressure was varied in steps from 2000 psig down to 200 psig. The values of d_D ranged from 620 to 644 milliseconds. Figure IV-23 shows the typical relationship found between nozzle manifold and dome pressure, nozzle and dome solenoid valve current values, and time.

Values of nozzle manifold and dome pressure were determined for points 1, 2, 3, and 4 of figure IV-23. A summary of these time and pressure relationships is listed in table IV-I. The nozzle manifold pressures at points 2 and 3 were plotted as a function of the dome pressures at points 1 and 4, respectively. This determined the relationship of manifold pressure to the dome pressure (fig. IV-24).

The final correlation was obtained by plotting the ratio of dome pressures obtained at points 1 and 4 versus the difference between the sequencer settings t_D and d_D (fig. IV-25) or Δt_1 .

Since the 1/3-scaled model had negligible drag to help decelerate it, some drag compensation had to be made. The particular approach used was to match the velocity of the model at the end of the boost phase to the calculated velocity at the end of the boost phase if a parachute had been used. This velocity for the full-scale vehicle was calculated to be 4.8 ft/sec. The equation for initial velocity for a vehicle acted on by the opposing forces of gravity and constant rocket thrust (no drag) is:

$$V_o = V_1 - (H-1) gt_1 \quad (B-1)$$

A value of $V_o = 25.5$ ft/sec follows from the results described above for the full-scale vehicle, hence 14.7 ft/sec for the 1/3-scaled model.

The scheme for calculating the settings for the sequencer is summarized as follows:

1. Determine high and low manifold pressures from high and low thrust requirements using figure IV-21.
2. Determine high and low dome pressures from high and low manifold-pressure requirements using figure IV-24.
3. Determine the dome-pressure vent valve open time Δt_1 from the ratio of high to low dome pressures using figure IV-25.
4. Calculate the free-fall time required to give the necessary initial velocity from the relationship $t_f = \frac{V_o}{g}$.
5. Calculate the sequencer settings from the following relationships:

$$d_N = t_f - \Delta t_A - \Delta t_5$$

$$t_N = t_f + t_T - \Delta t_6$$

$$d_D = t_f + t_H - \Delta t_{11}$$

$$t_N = d_D + \Delta t_1$$

The vehicle was placed on the drop rig (fig IV-26), the sequencer settings were made, the tanks were pressurized to approximately 3000 psig, and the dome of the regulator was pressurized to the higher value. Figures IV-27 and IV-28 show typical results obtained by the system.

TABLE IV-1. - TIME AND PRESSURE RELATIONSHIPS OBTAINED
DURING SYSTEM CHARACTERIZATION

Run	P ₁	P ₄	P ₁ /P ₄	P ₂	P ₃	Δt_5	Δt_6	Δt_{11}	d _D	d _N	t _D	t _N	Δt_1
506	2000	349	5.74	1410	201	119	92	43	641	326	692	1242	50
509	1895	409	4.63	1360	170	119	93	42	644	328	694	1244	50
515	1370	268	5.10	946	170	119	94	43	641	326	691	1242	50
518	1580	268	5.90	1060	161	120	93	41	641	326	697	1242	56
521	1149	289	3.97	802	172	121	93	43	636	326	679	1243	43
527	1009	329	3.26	700	192	127	94	42	631	326	668	1245	37
530	809	273	2.97	517	163	126	94	42	633	326	670	1245	37
533	615	195	3.16	383	115	140	92	46	633	326	669	1244	36
541	1520	468	3.25	1071	144	117	97	49	631	327	667	1357	36
546	1763	477	3.67	1260	135	124	95	40	631	327	671	1250	40
551	1580	437	3.70	1338	292	119	93	42	629	326	669	1311	40
563	1792	467	3.65	1210	321	122	93	42	620	326	660	1320	40

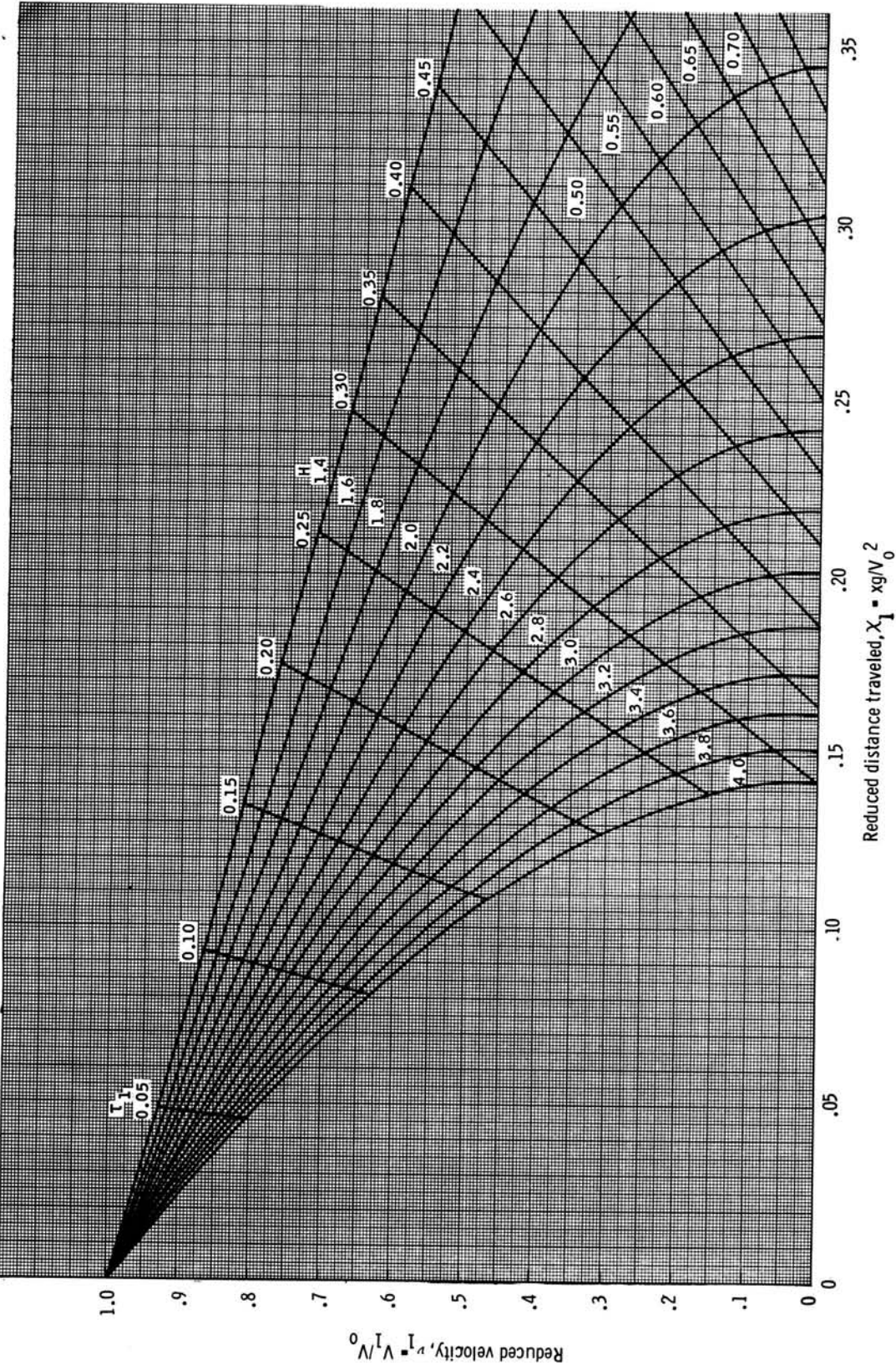


Figure IV-1.- Dimensionless performance, boost phase.

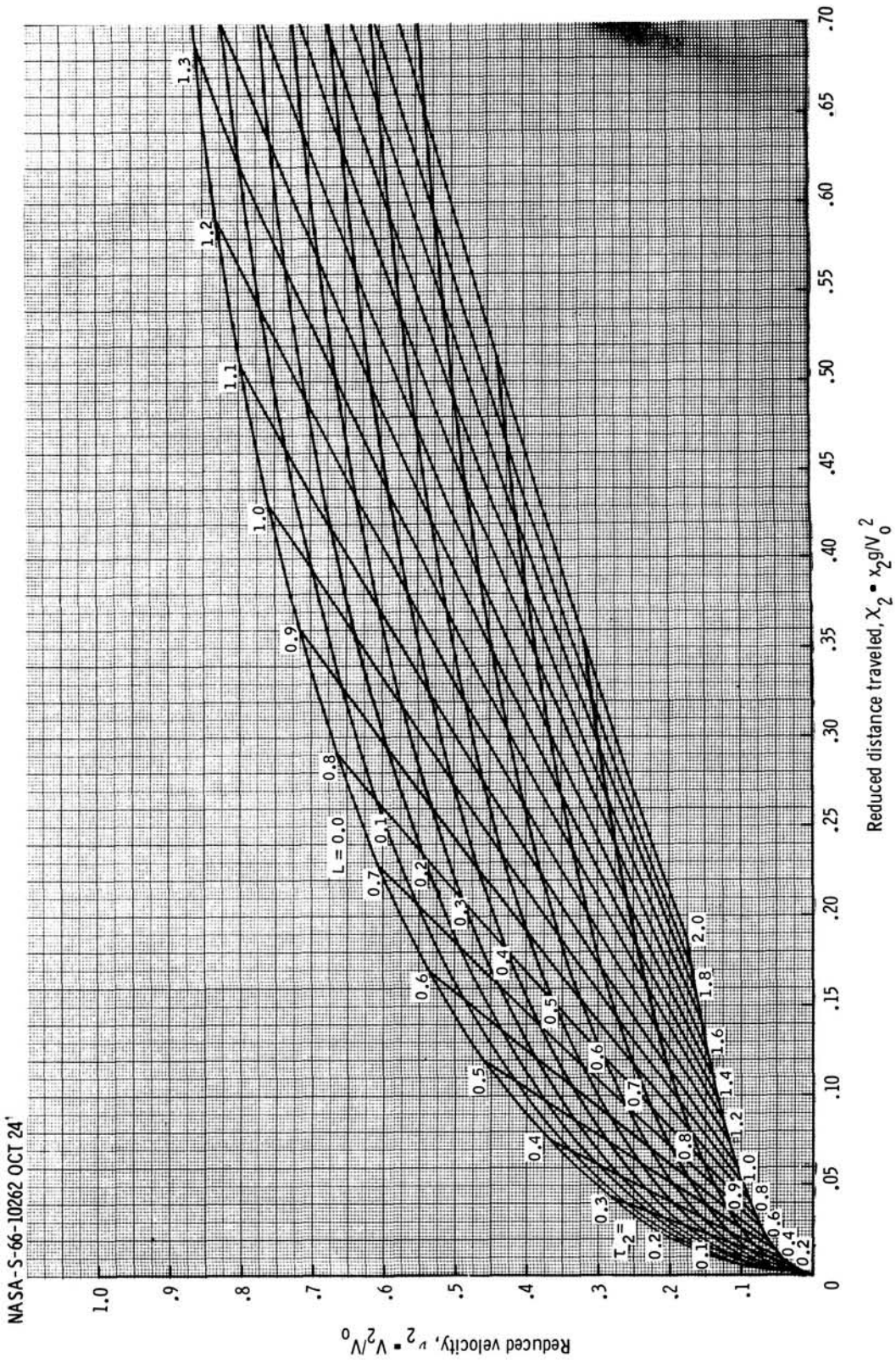


Figure IV-2.- Dimensionless performance, sustain phase, $\nu_1 = 0.00$.

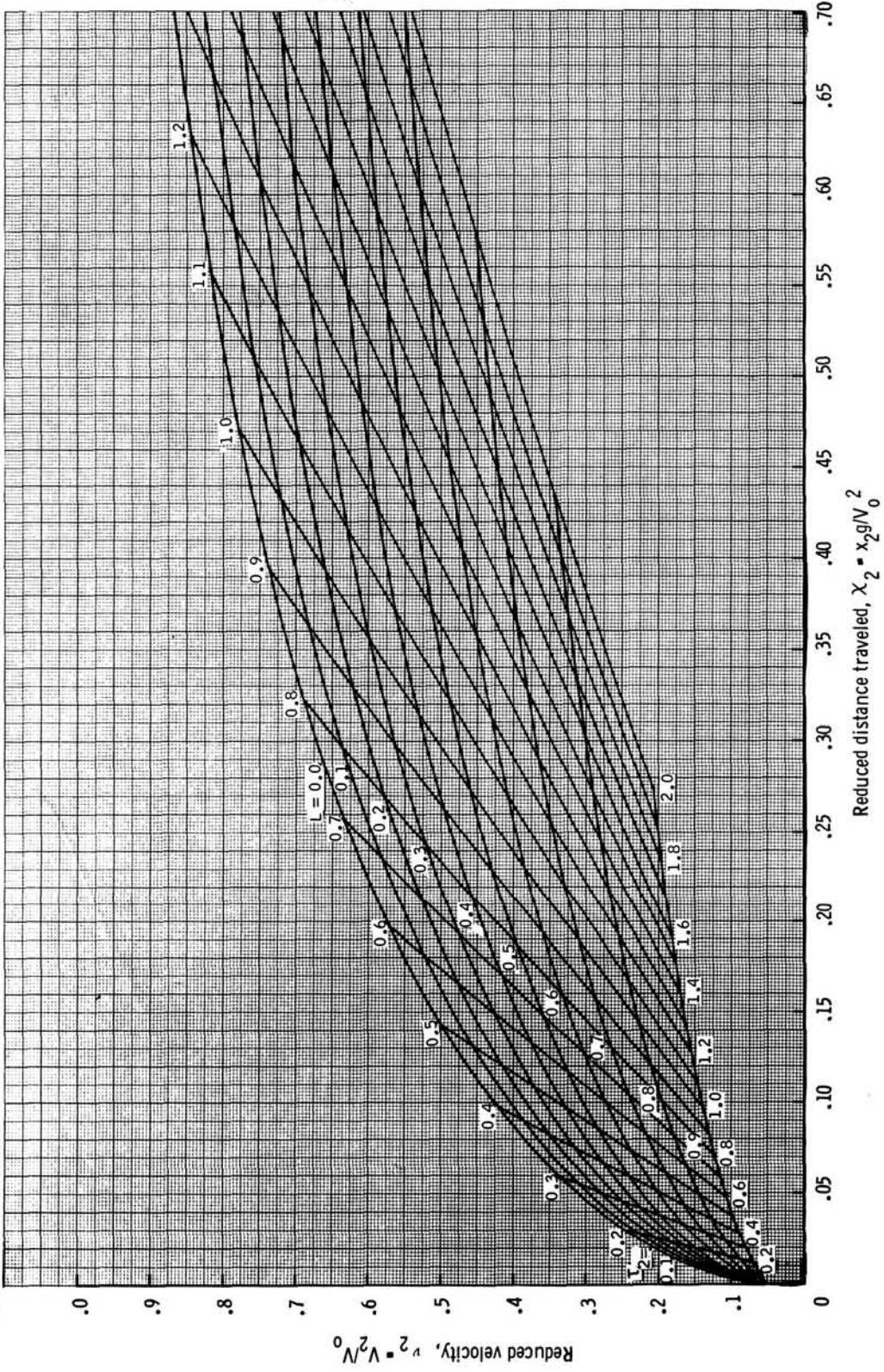


Figure IV-3.- Dimensionless performance, sustain phase, $\nu_1 = 0.05$.

NASA-S-66-10264 OCT 24

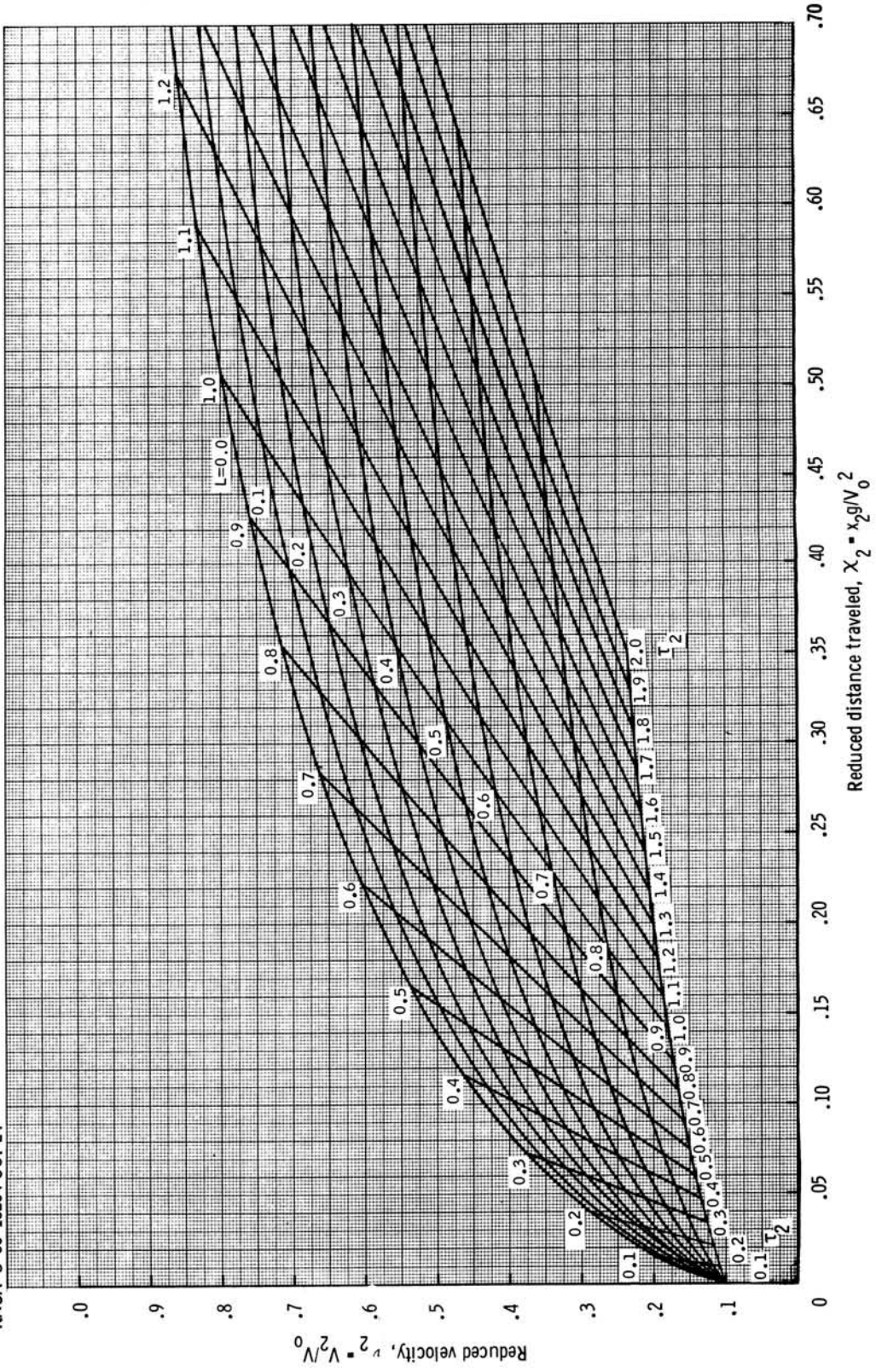


Figure IV-4.- Dimensionless performance, sustain phase, $\nu_1 = 0.10$.

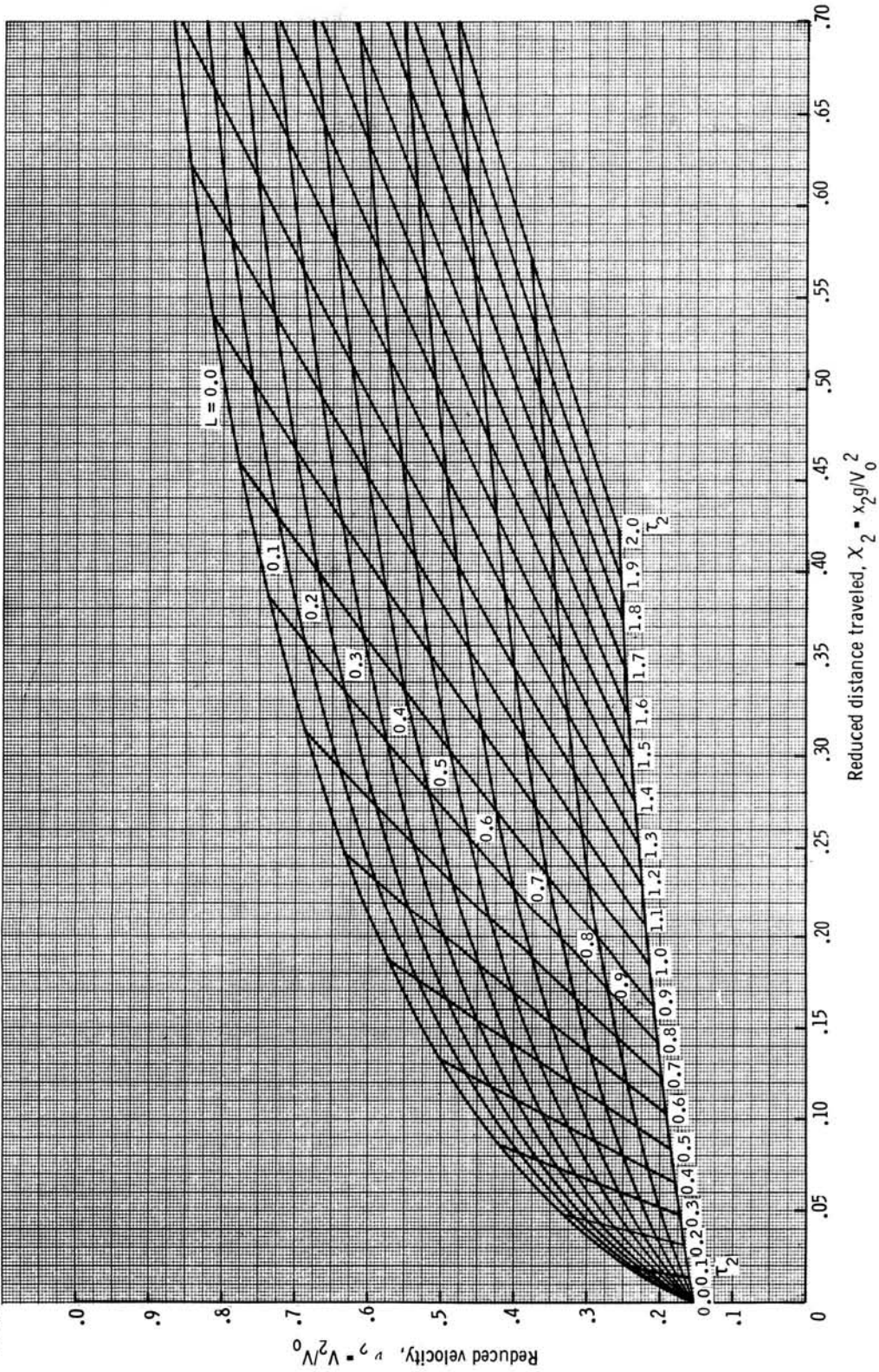


Figure IV-5.- Dimensionless performance, sustain phase, $\nu_1 = 0.15$.

NASA-S-66-10266 OCT 24

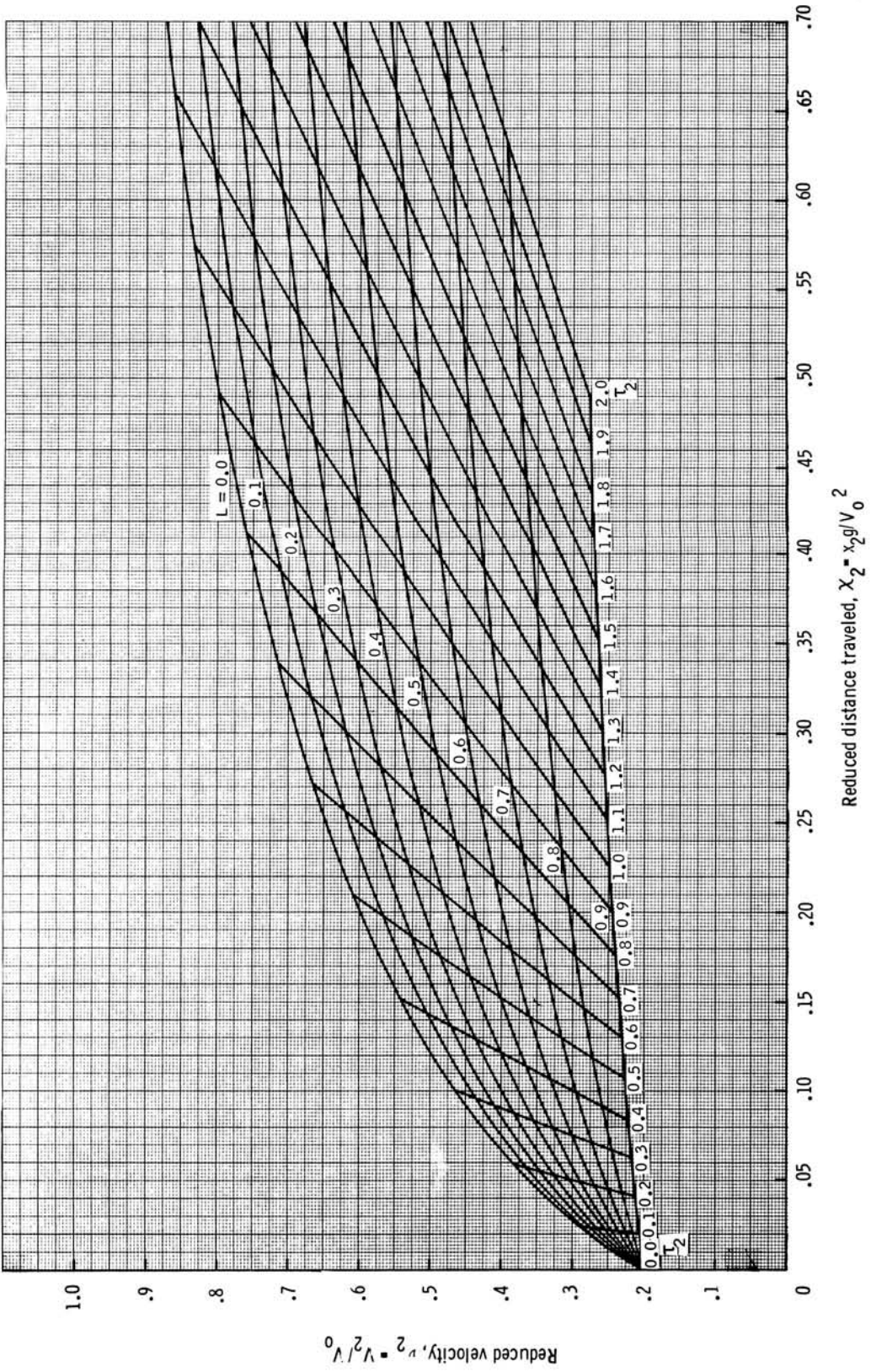


Figure IV-6.- Dimensionless performance, sustain phase, $v_1 = 0.20$.

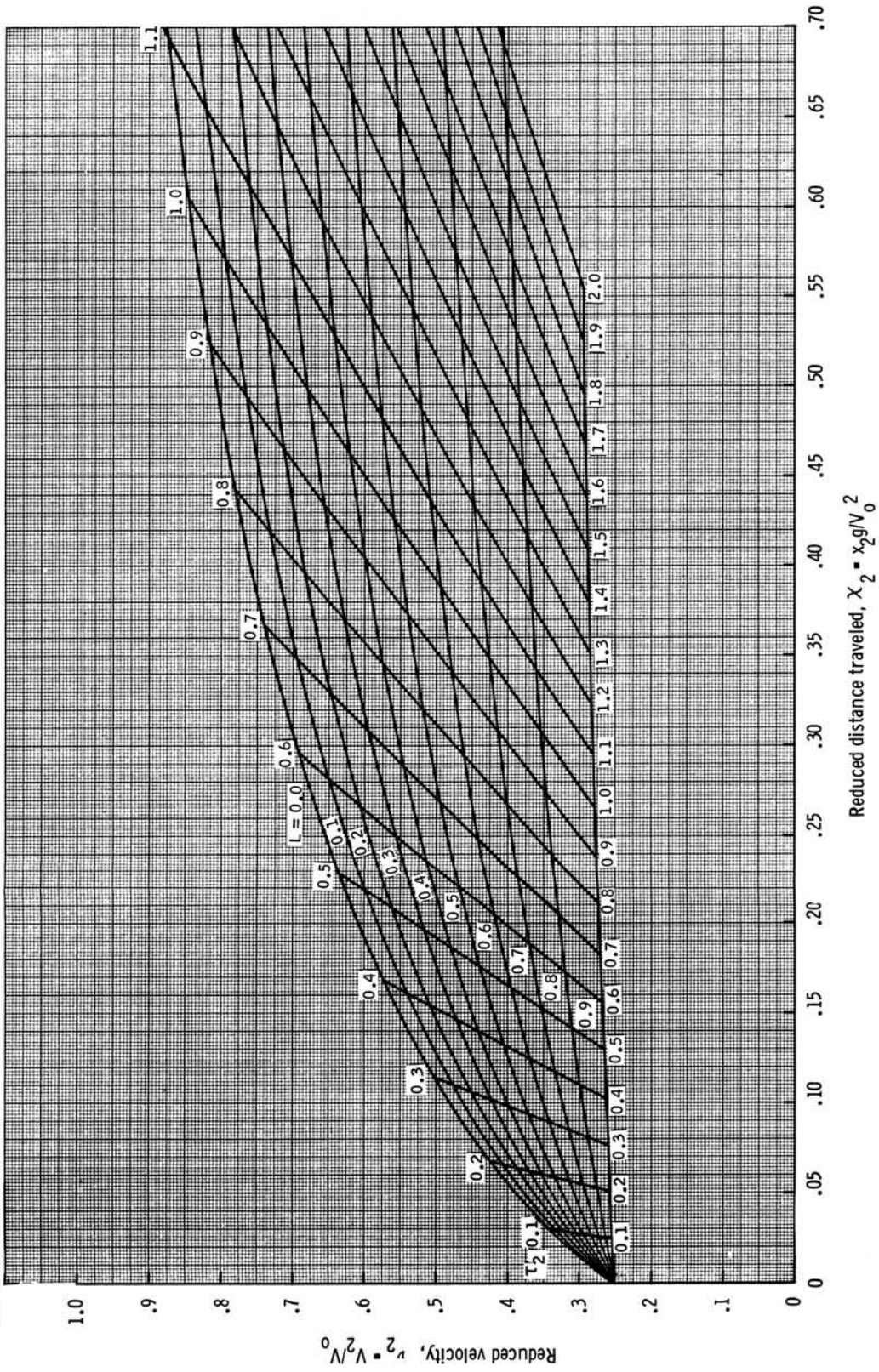


Figure IV-7.- Dimensionless performance, sustain phase, $\nu_1 = 0.25$.

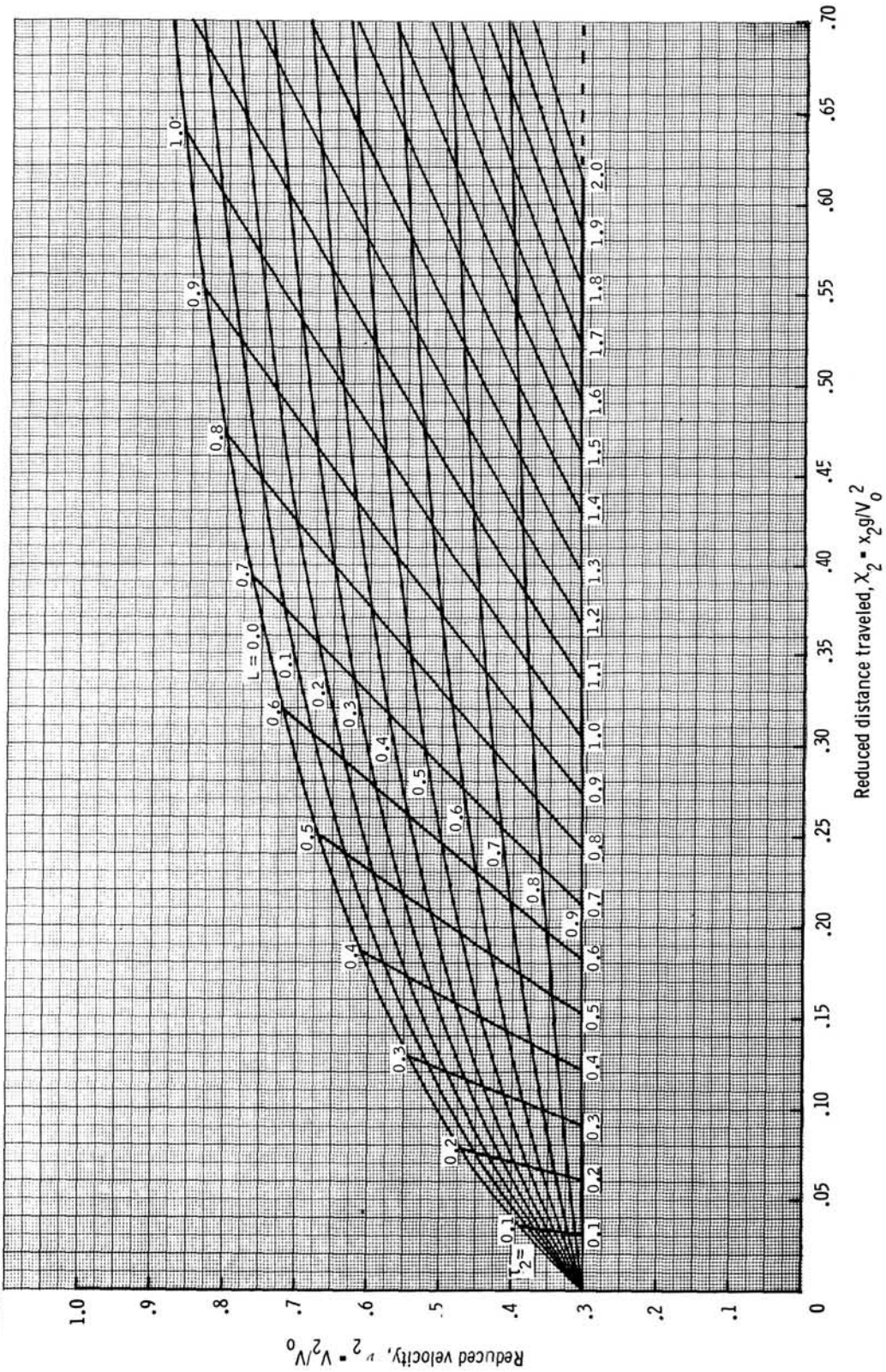


Figure IV-8.- Dimensionless performance, sustain phase, $v_1 = 0.30$.

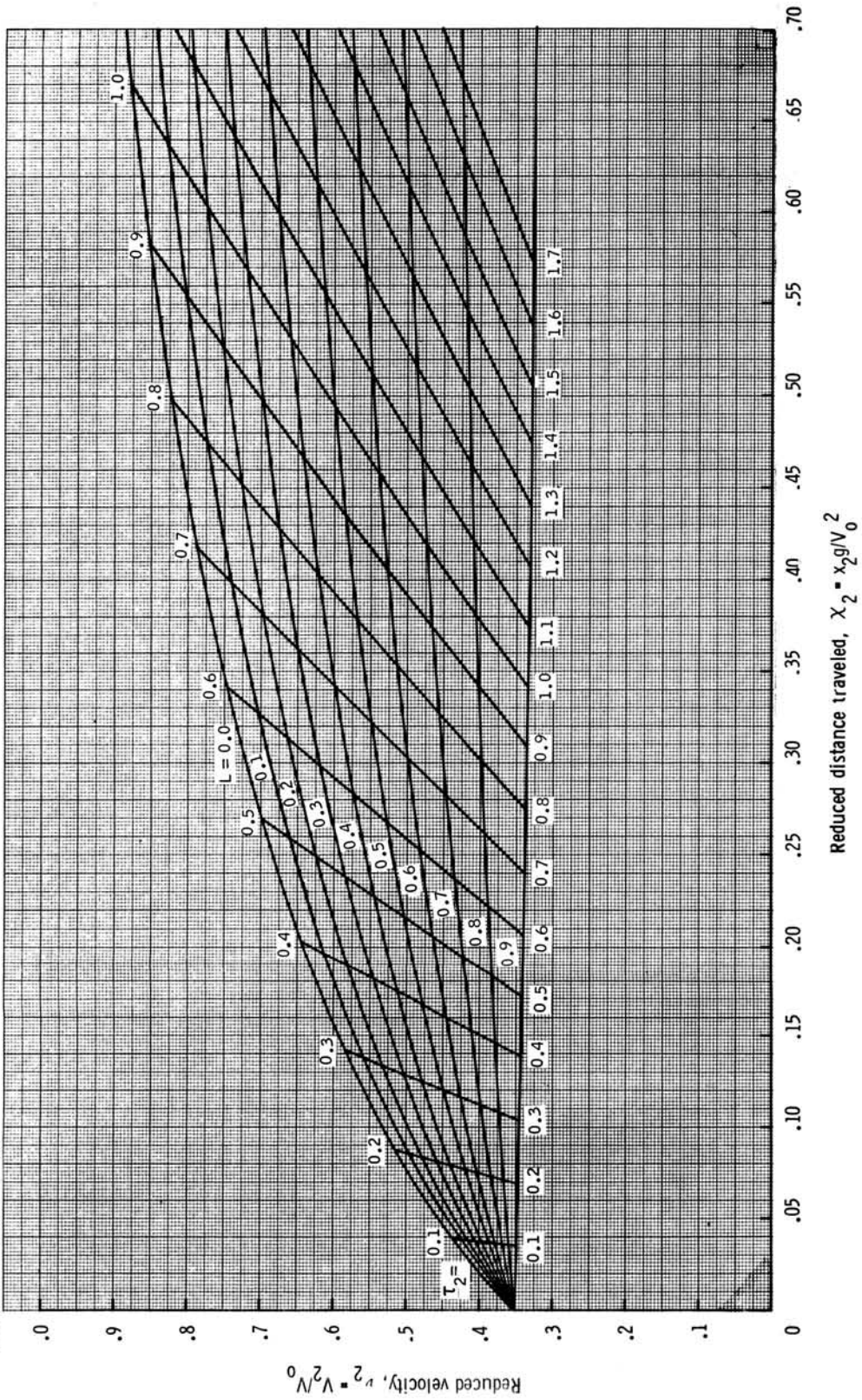


Figure IV-9.- Dimensionless performance, sustain phase, $\nu_1 = 0.35$.

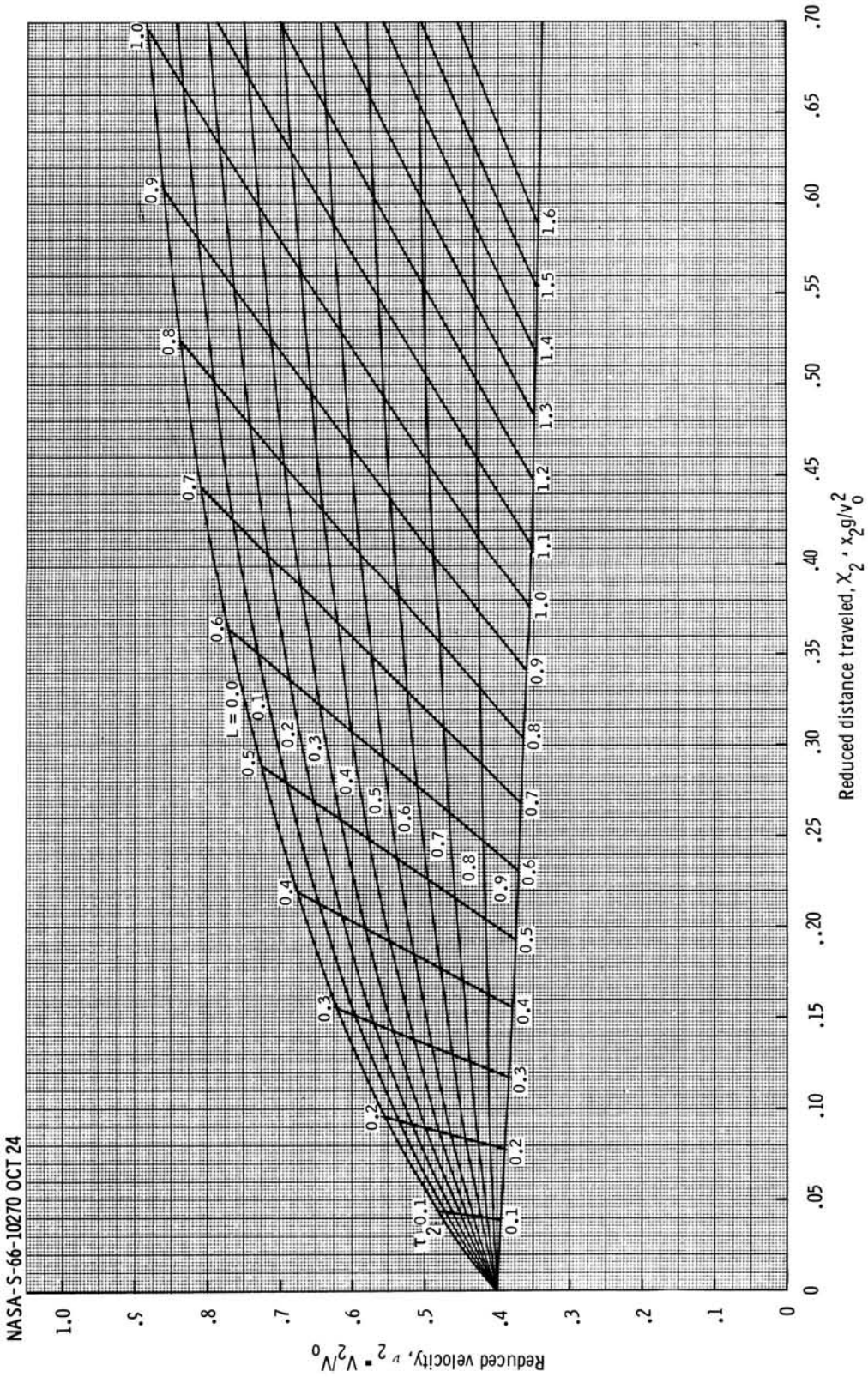


Figure IV-10.- Dimensionless performance, sustain phase, $\nu_1 = 0.40$.

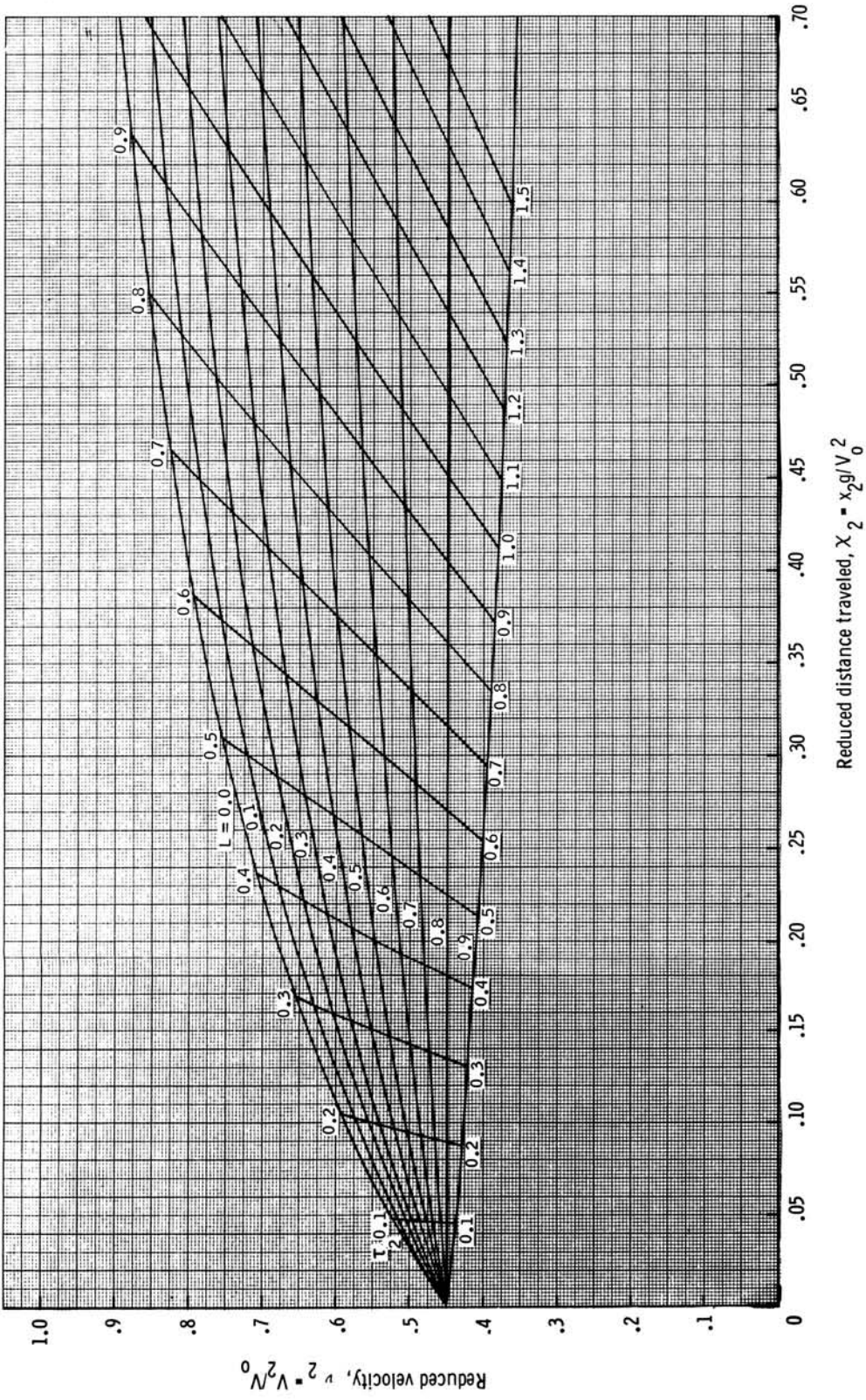


Figure IV-11.- Dimensionless performance, sustain phase, $v_1 = 0.45$.

NASA-S-66-10272 OCT 24

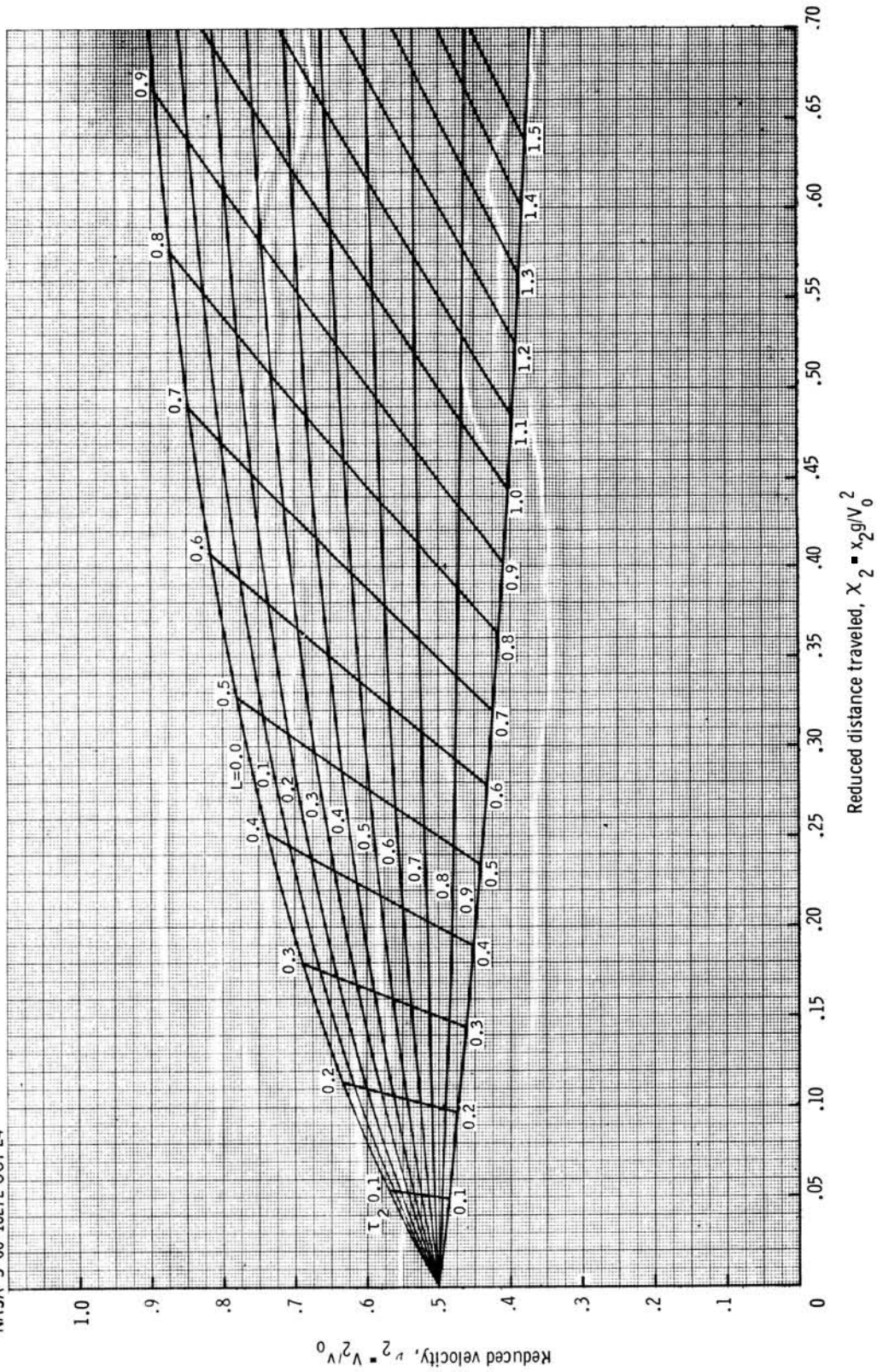


Figure IV-12.- Dimensionless performance, sustain phase, $\nu_1 = 0.50$.

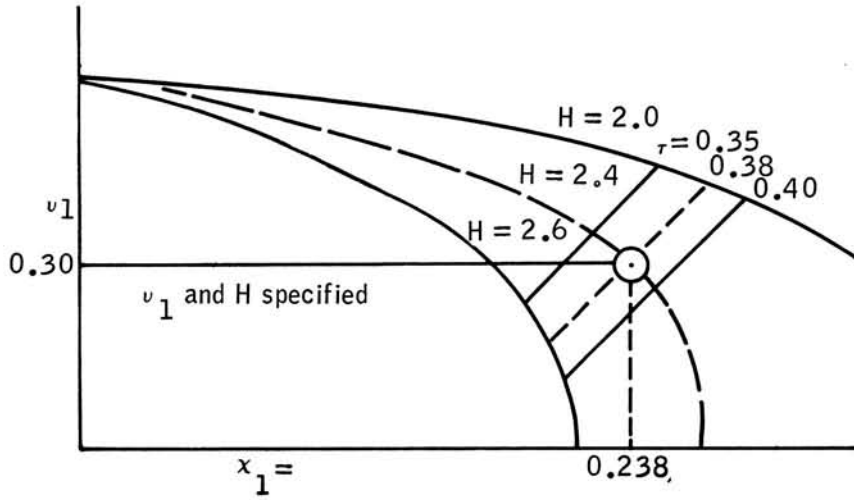


Figure IV-13.- Use of boost-phase parametric charts.

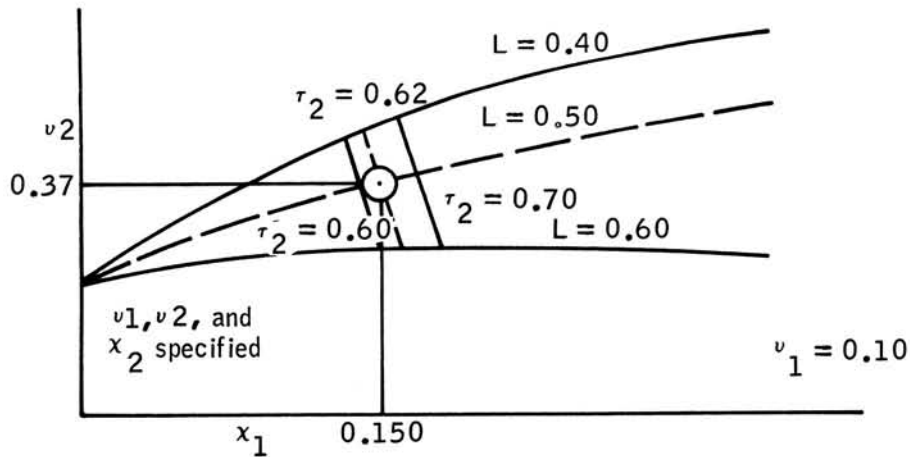


Figure IV-14.- Use of sustain-phase parametric charts.

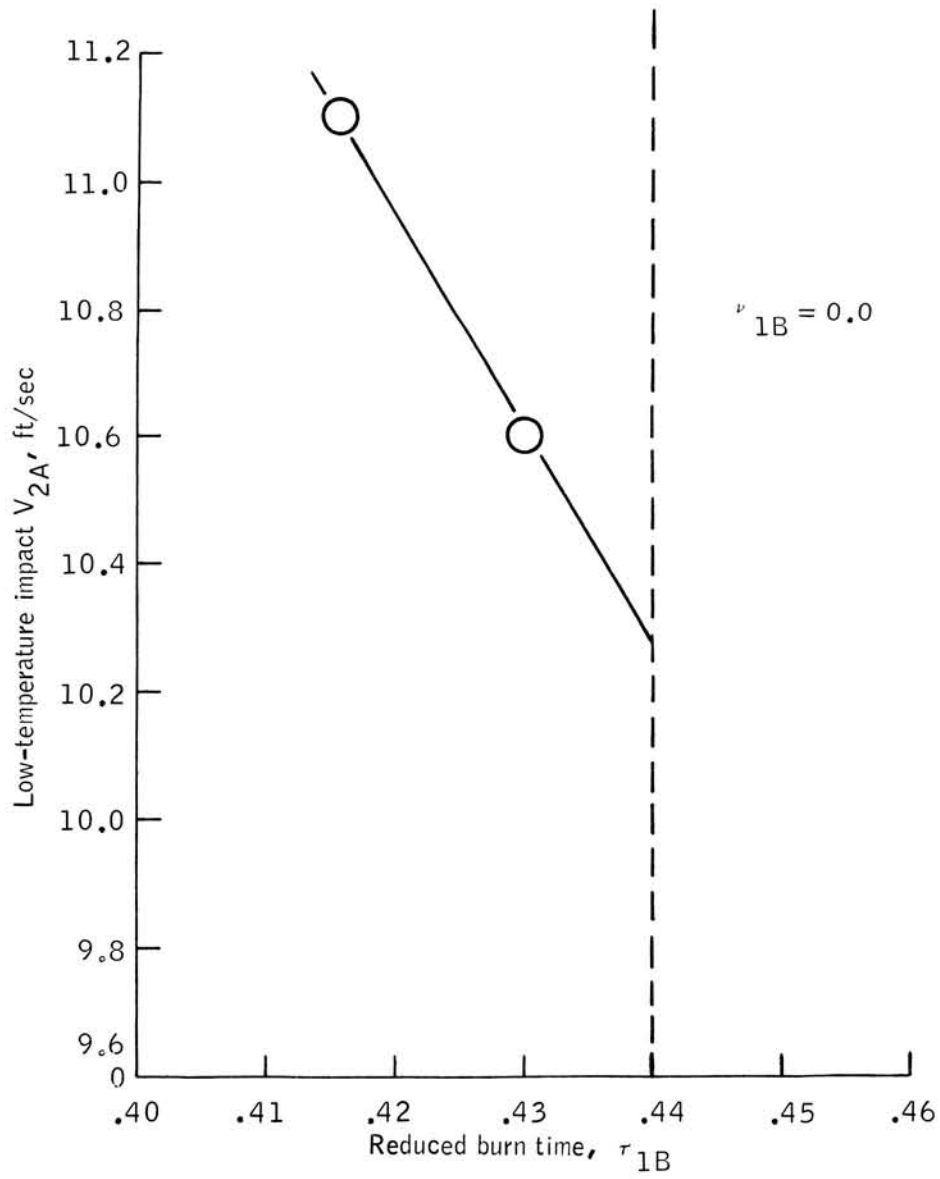


Figure IV-15.- Illustration of iteration scheme.

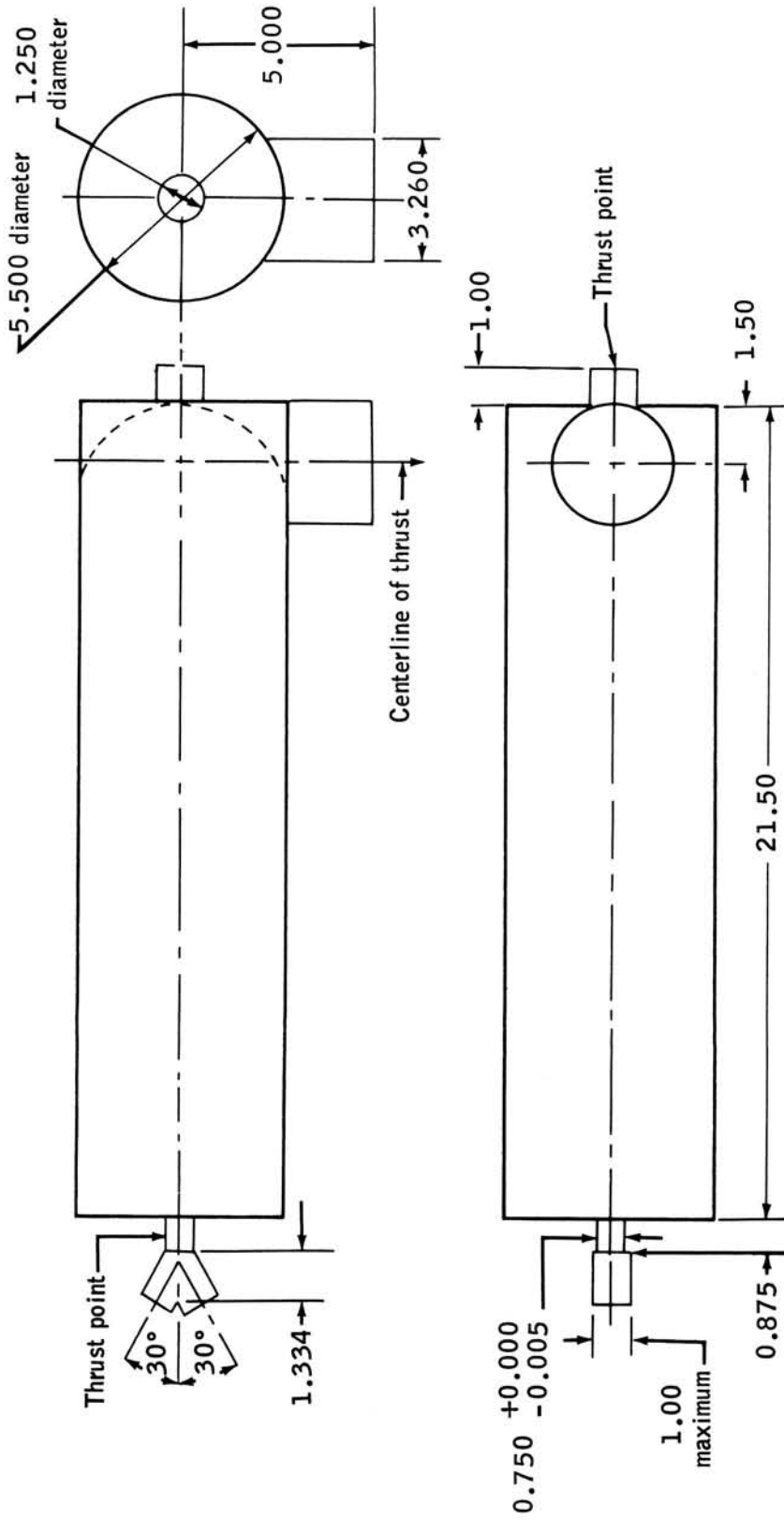


Figure IV-16.- Envelope requirements.

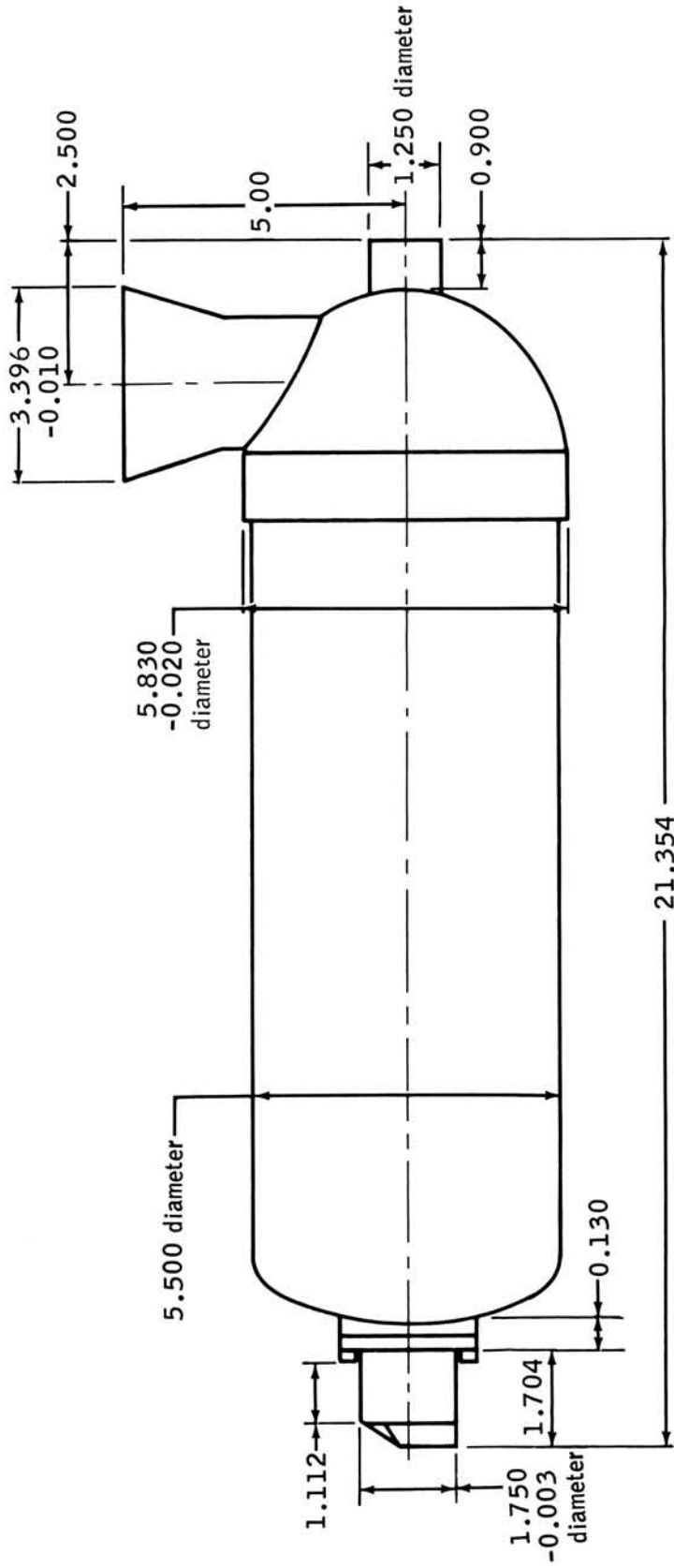


Figure IV-17.- Envelope of M-100 landing rocket (flight weight).

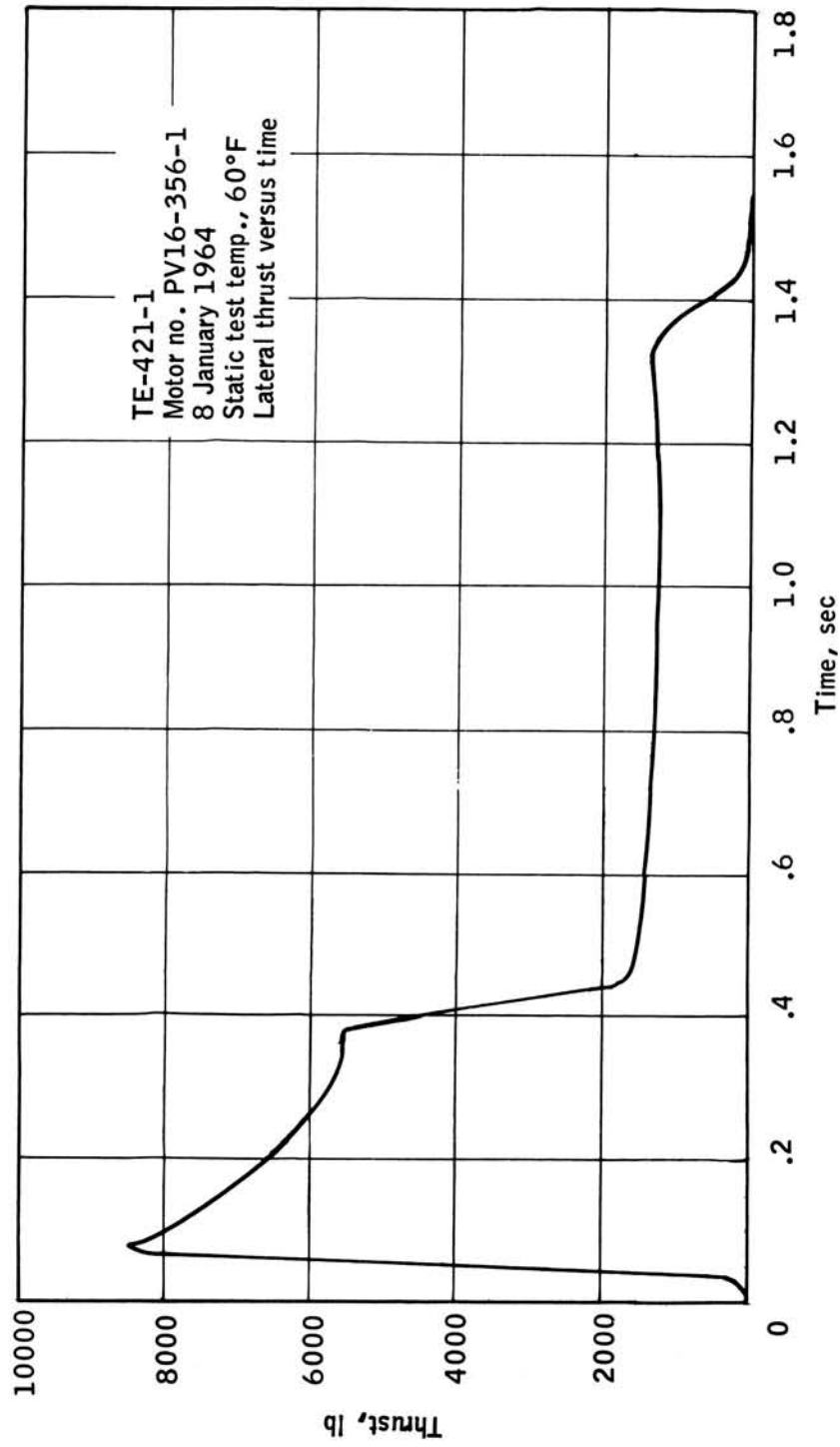


Figure IV-18.- Typical thrust-time trace.

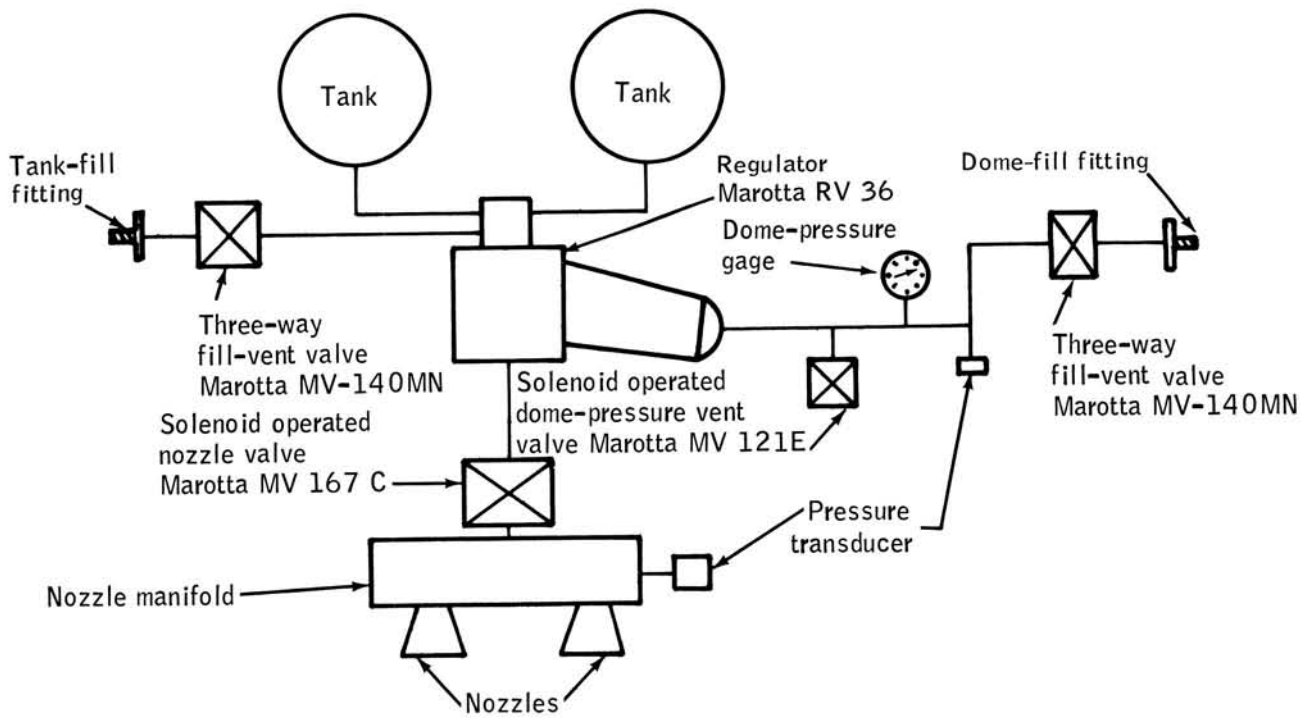


Figure IV-19.- Schematic of propulsion system (one-third-scale Gemini spacecraft).

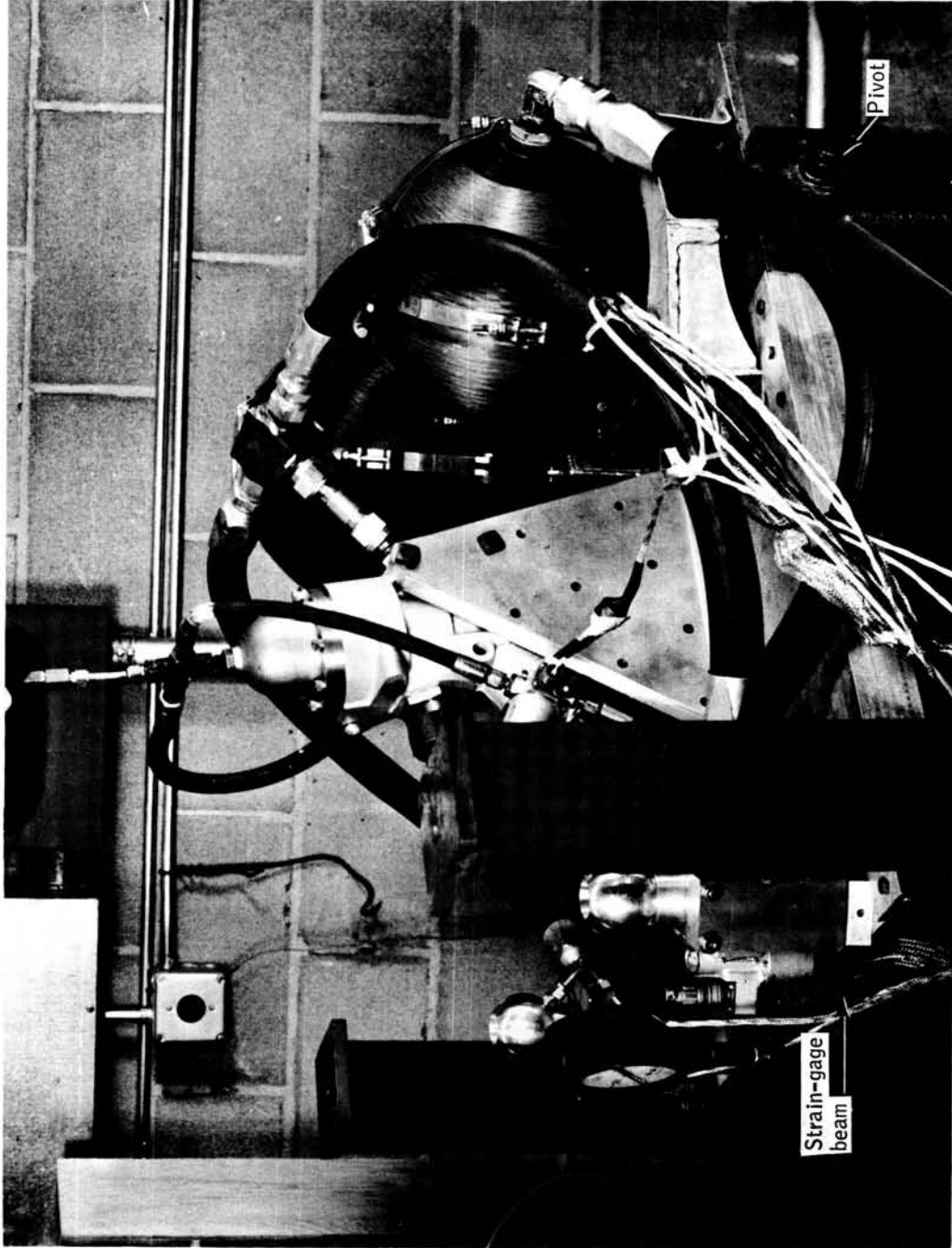


Figure IV-20.- Thrust stand used to calibrate cold-gas propulsion system.

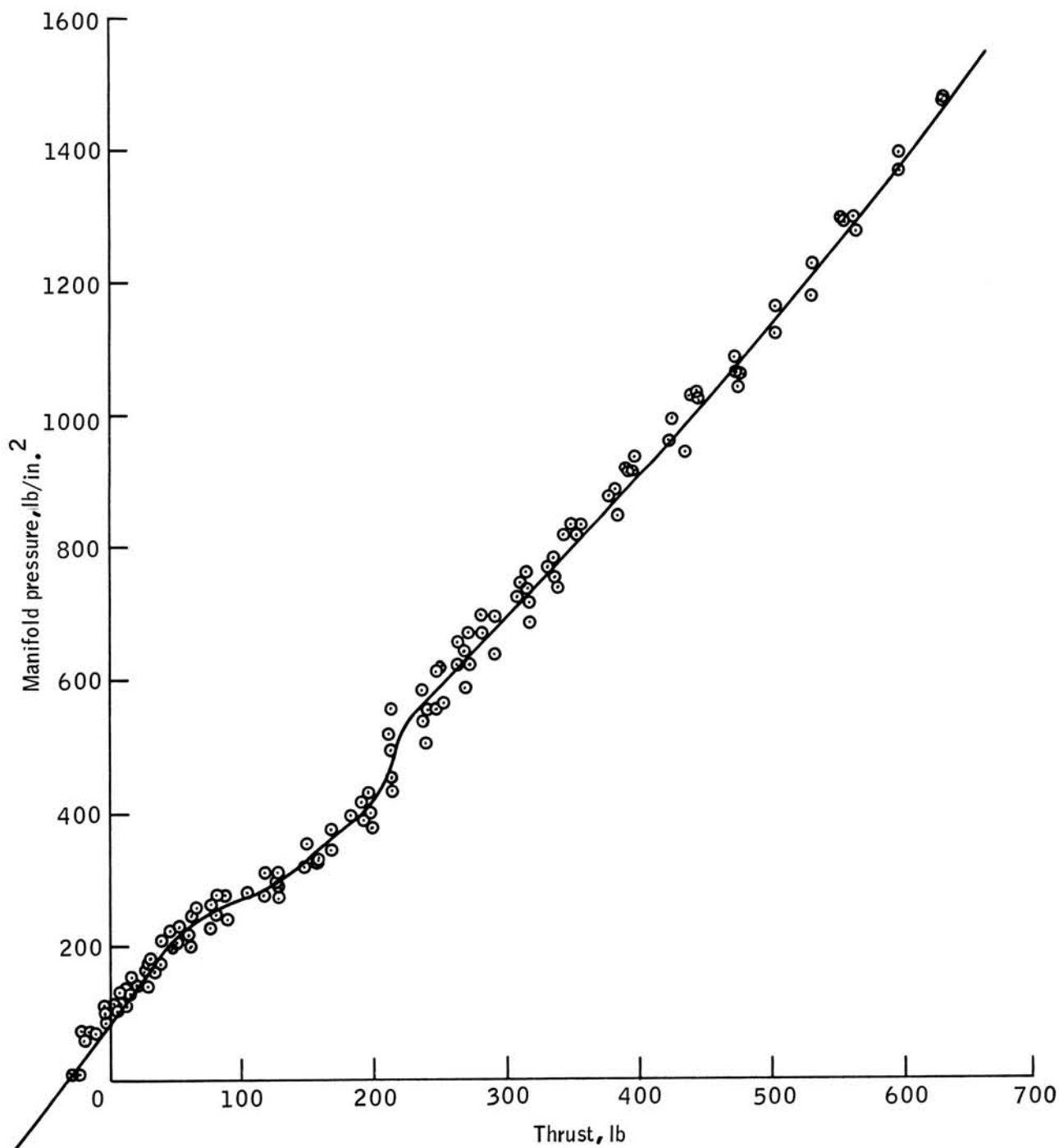


Figure IV-21.- Cold-gas system thrust-chamber pressure, calibrated curve.

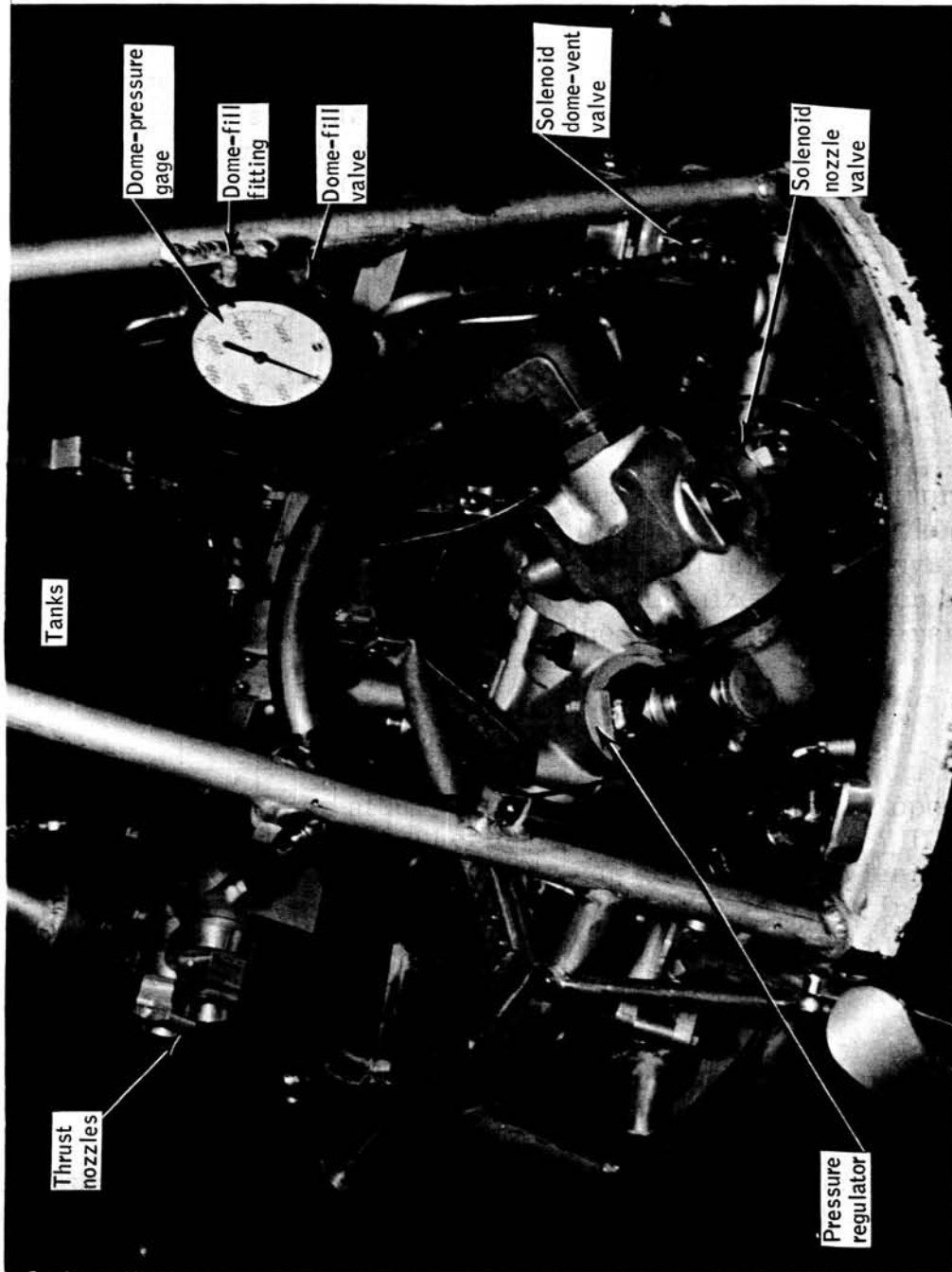


Figure IV-22.- Overall view of model propulsion system.

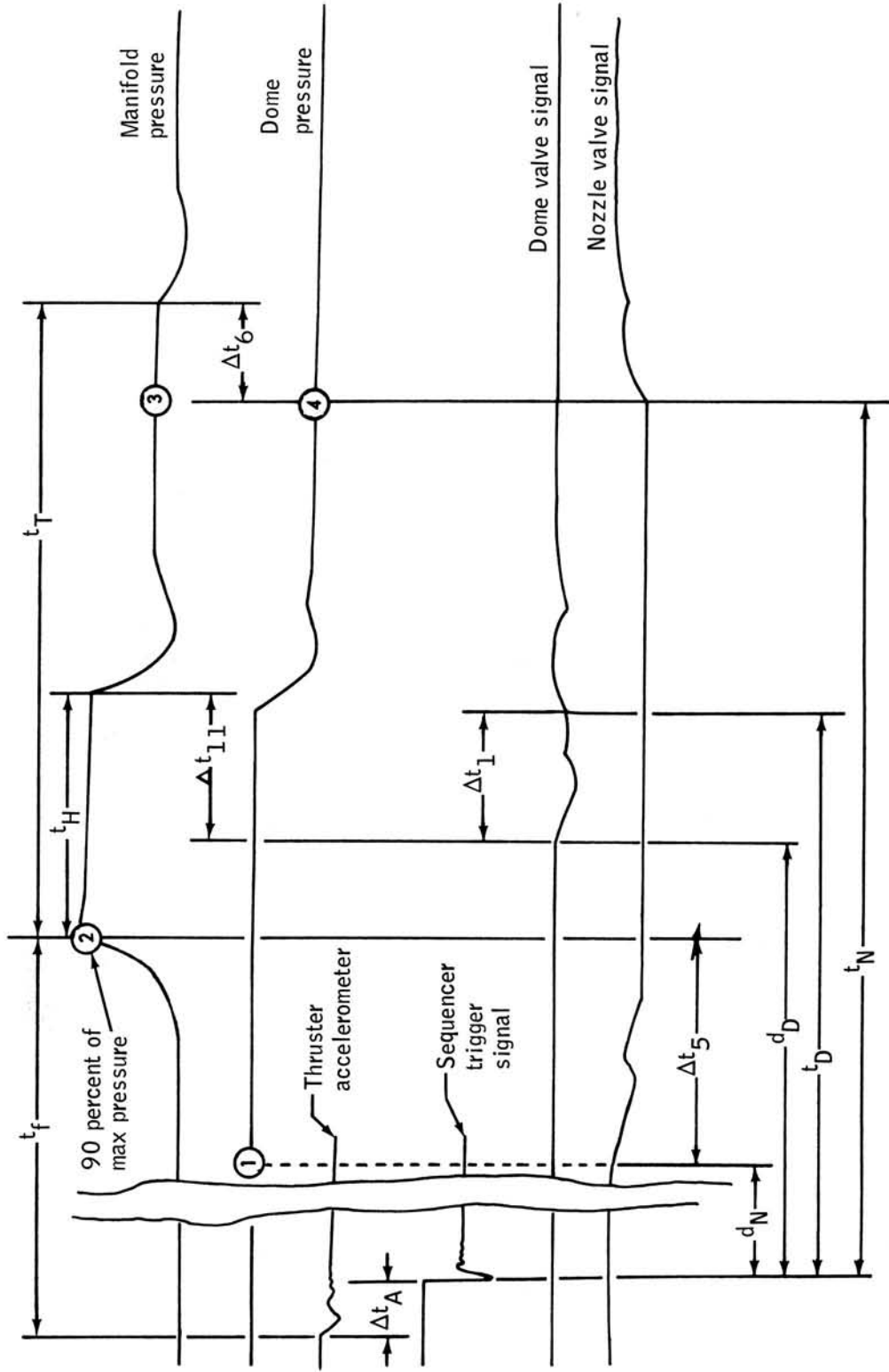


Figure IV-23.- Actuation time relationships for cold-gas propulsion system.

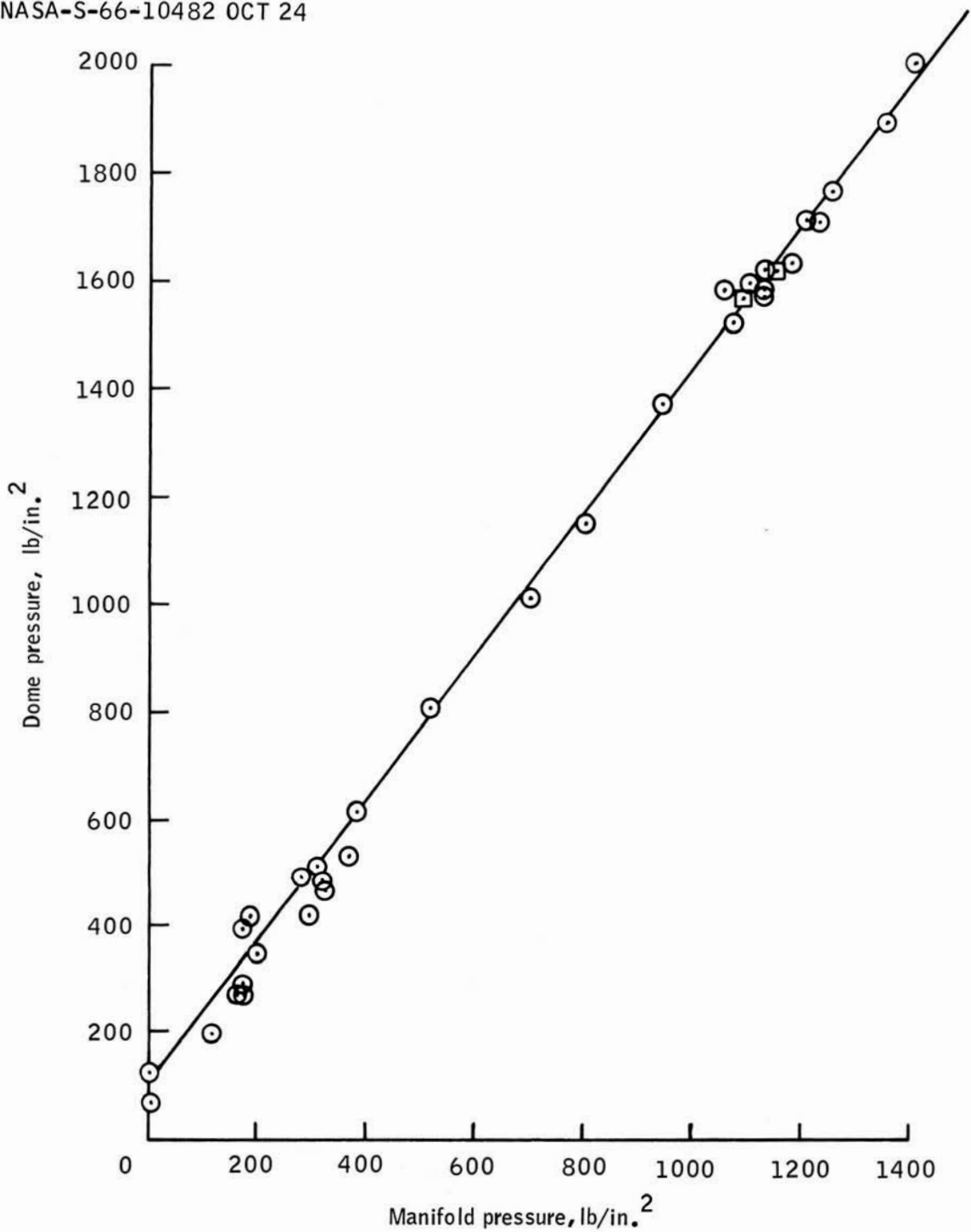


Figure IV-24.- Dome pressure-manifold pressure, calibration curve.

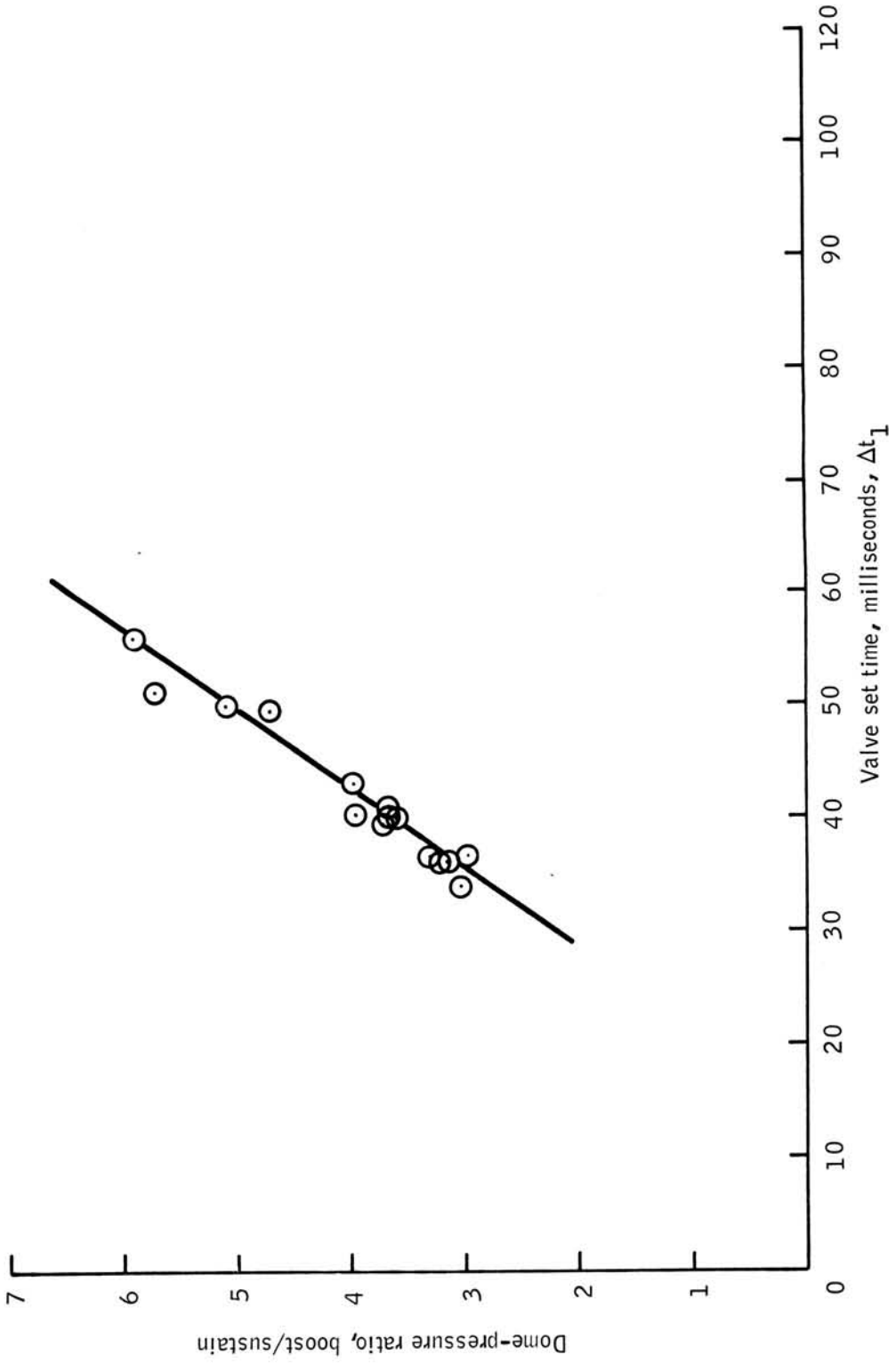


Figure IV-25.- Dome-pressure ratio as a function of valve open time.

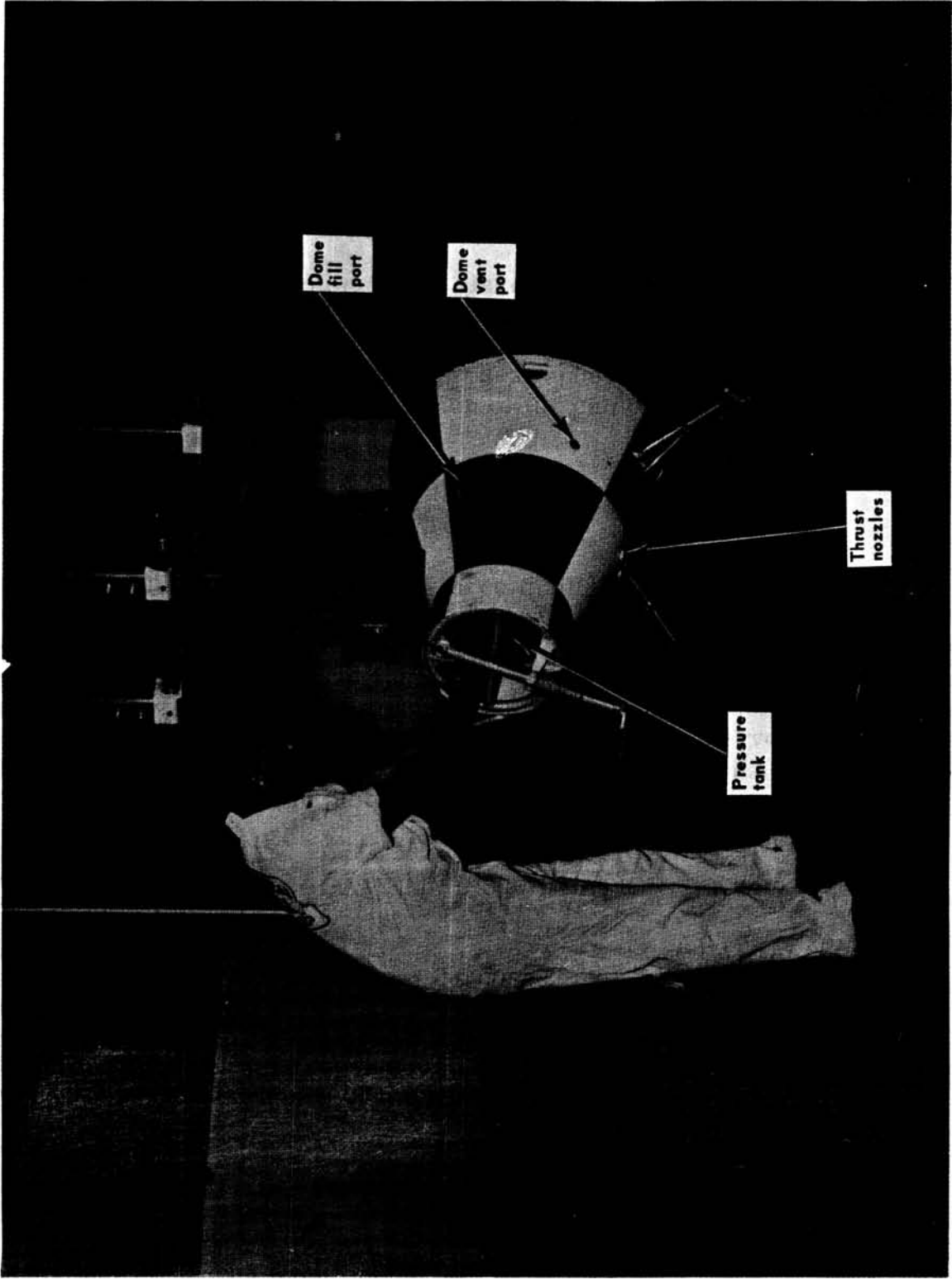


Figure IV-26.- Overall model test set up.

NASA-S-66-10485 OCT 24

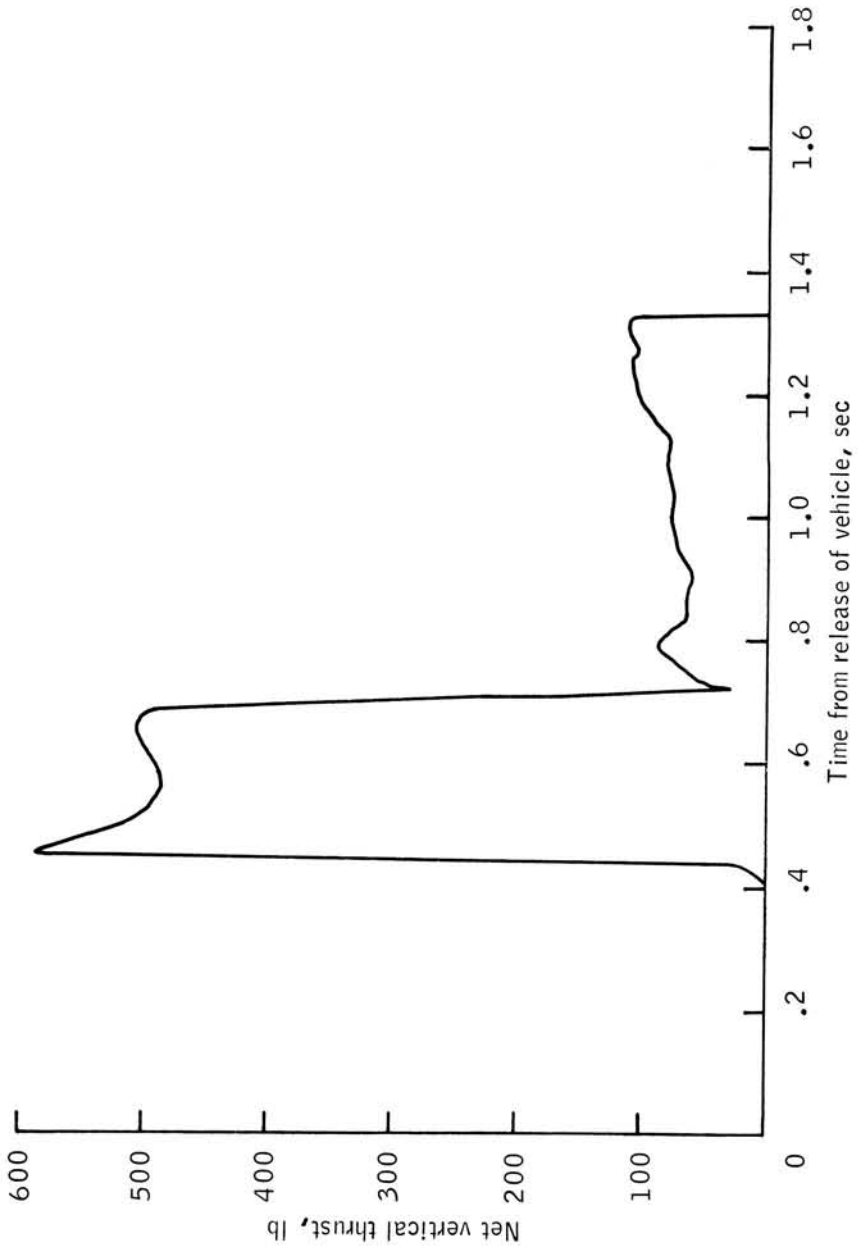


Figure IV-27.- Typical cold-gas thrust-time variation (drop 25).

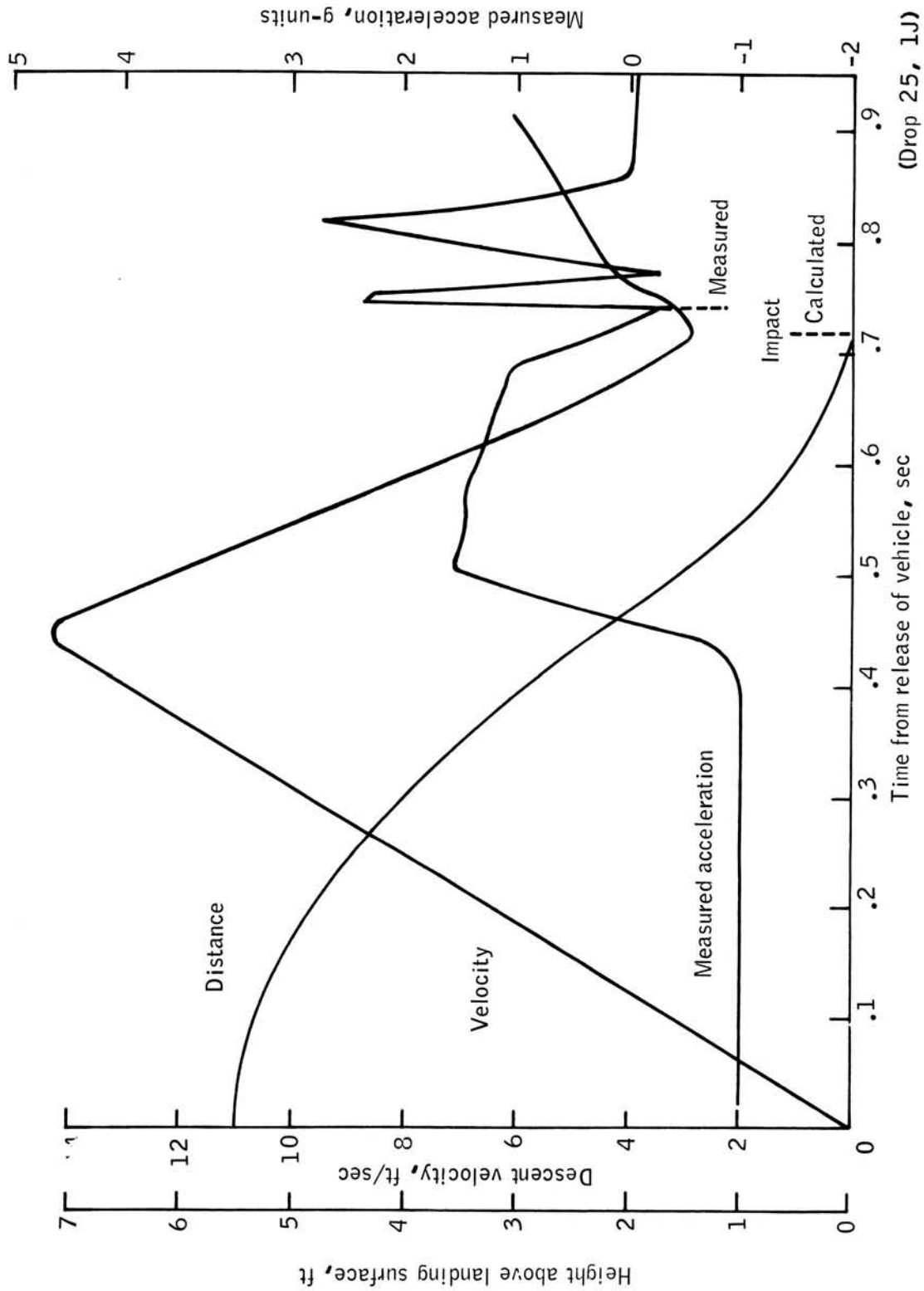


Figure IV-28.- Typical vertical acceleration, velocity, distance, and time relationships.

PRECEDING PAGE BLANK NOT FILMED.

SECTION V - ALTITUDE-SENSOR DEVELOPMENT

By Carlisle C. Campbell, Jr.

PRECEDING PAGE BLANK NOT FILMED.

ALTITUDE-SENSOR DEVELOPMENT

By Carlisle C. Campbell, Jr.
Manned Spacecraft Center

REQUIREMENT

An altitude sensor is necessary to achieve landing rocket ignition at the precise distance above the landing surface in order to achieve the desired final deceleration of the spacecraft. The device must be capable of withstanding all environmental conditions associated with space flight and perform reliably during parachute descent.

SCOPE

A thorough study was made of all conceivable altitude or distance sensing devices to permit selection of the one most practical for development within the given time span and within the funds available. The results of the study indicated that a homodyne system (continuous wave signals), as a primary system, along with a mechanical probe as a backup system, would prove to be a reasonable approach. The review of this study by the Manned Spacecraft Center and McDonnell Aircraft Corporation revealed that the present state-of-the-art of short range radar devices did not meet MSC requirements for a reliable short distance measurement device. For the Gemini spacecraft land landing system, it was decided to utilize two mechanical probes, either of which could initiate rocket firing.

Manned Spacecraft Center Development

Since the procurement of a mechanical-probe device would require several months, it was decided to develop a device at MSC to use as an interim altitude sensor until the contracted device became available. Because of its apparent simplicity and development reliability, a pendulum-type device was developed for use on crane drop tests and parachute drop tests. This system consisted of a microswitch sensing system located in the pendulum weight, and the electrical conductor served as the suspension line. The conductor was paid out from a type of spinning reel during deployment.

Mechanical Probe

A contract was let with deHavilland Aircraft of Canada, Ltd., to develop a mechanical-probe altitude-sensing system. The device was to be self-contained, automatically extendible, and mechanically and electrically redundant. The device developed utilized a storable, tubular, extendible boom having a force-sensitive tip which closed microswitches upon impact with either land or water. Two units were used on each test to provide mechanical redundancy, since it was expected that the reliability of the electrical system was satisfactory.

SYSTEM DESCRIPTIONS

Pendulum Type Device

Functional and physical description. - The pendulum device (fig. V-1) is suspended approximately 10 feet beneath the landing gear of the spacecraft on a six-conductor, shielded, electrical cable during parachute descent. The device is normally deployed a few seconds after the spacecraft has assumed a stable landing attitude while suspended beneath the main parachute. Prior to deployment, the cable is wrapped around a conical spool (fig. V-2). The sensor head (fig. V-3) nests against the open end of this cone; then a metal release strap is attached across the bottom of the sensor head to hold it in the stowed position. This metal strap has a fall-off hinge on one end and a pyrotechnically released bolt on the other end which, when fired, allows the hinge to fall free of the spacecraft. The sensor head falls out of the spacecraft due to the pull of gravity. The conductor cable pays off the reel in a spinning fashion, and the bloom thus formed softens full payout line loads.

The sensor head is constructed of a lightweight contact ball and a heavyweight housing (fig. V-4). The housing contains six microswitches, any one of which will fire one of the redundant rocket-ignition circuits. The device will function at impact angles from any direction. Tests were conducted which resulted in successful firings after inverted and sideward impacts.

Test results. - The development impact tests which were conducted on water were:

Number of tests	Velocity, ft/sec	Direction	Results	Date
4	15	Vertical	All successful	5/9/64
1	37	Vertical	All successful	5/9/64
3	15	Horizontal	All successful	5/9/64
1	30.2	Horizontal	All successful	5/9/64
9	37	Vertical	All successful	5/19/64
10	30	Horizontal	All successful	5/19/64
3	30.5	Vertical	All successful	9/14/64
4	21.2	Horizontal	All successful	9/14/64

The deployment tests consisted of twelve hand-released tests and two pyrotechnically released tests. The twelve hand-released tests were conducted on May 20, 1964, and all were successful. The intermittent firing signals were stopped after 7 seconds. The two pyrotechnically released tests were conducted successfully on July 14, 1964.

Preflight tests were conducted on all sensor heads which would be used on parachute or crane drop tests. All sensor heads were individually set for optimum operation and were dropped repeatedly a short distance to a soft surface to insure that the sensitivity was acceptable.

The data for the parachute and crane drop tests are:

Type	Length beneath to gear	Results	Date
Parachute (flashbulbs)	8.72 ft	Successful	5/14/64
Parachute (flashbulbs)	8.72 ft	Successful	5/26/64
Crane (rockets)	8.72 ft	Successful	7/31/64
Parachute (rockets)	8.75 ft	Successful	10/16/64
Crane (rockets)	8 ft 8-5/8 in.	Successful	3/12/65
Parachute (rockets)	9.02 ft	Successful	7/30/65

Problem areas and improvements. - Since all parachute and crane drop tests using the interim sensor were successful, it is apparent that there were no major problem areas. This device proved to be reliable because its operation was simple; it was easy to checkout; and its weight aided in deployment.

The sensing error due to oscillation beneath the spacecraft is negligible because the Para-Sail produces a relatively stable descent system. During a controlled flight, the spacecraft swings to the outside of a turn, and the altitude sensor likewise swings to the outside of the turn. Although each has its pendulum effect, this damps out quickly during a constant turn rate. The sensor also trails a negligible distance behind its attach point on the spacecraft due to air loads on the suspension cable and the sensor head.

Several minor improvements have been made on the system since it was originally fabricated. The six microswitches were relocated every 60° rather than having two located every 120° . The suspension cable was changed

from a lightweight cable to a six-conductor shielded cable 11/32 of an inch in diameter. To prevent inadvertent closing of the microswitches during a parachute descent, six 3/16-inch \times 1/2-inch \times 1/2-inch foam pads were inserted between the clapper and the main housing, thus requiring more force for actuation. The bolt which attached the clapper to the main housing was machined to have a ball-and-socket pivot action. The cable was attached to the spacecraft with two electrical clamps rather than one U-bolt which might pinch the conductor.

Present status. - As a test device, this system is relatively easy to install, and length adjustments are easily made. It is conceivable that a device of this type might be developed into a spacecraft-qualifiable system, but many refinements must be made. These include weight reduction and more positive initiation of payout. Since two devices of this type cannot be used in close proximity on the same spacecraft, every effort must be exerted to improve mechanical reliability of the system.

DeHavilland Type Altitude-Sensing Device

Functional and physical description. - The deHavilland altitude-sensing device developed under contract NAS 9-2810 was selected as the best of several mechanical types, including pendulum and other extendible boom designs. A deployment test of this device is shown in figure V-5.

A storable, tubular, extendible member (STEM) device is utilized as the boom element for the altitude sensor. The tube is nested in a container (fig. V-6) in the configuration of a steel tape, and it is restrained radially and axially under its own spring tension. The innermost coils are arranged to start their extension axially after the lid is pyrotechnically released, thus producing a jack-in-the-box effect. The sensor head (fig. V-7) is attached to the innermost coil, and a three-conductor shielded wire makes the electrical connection between the sensor head microswitches and the retrorocket firing circuit. This wire is stored in a spinning reel within the head, and it is paid out during extension. After the boom has fully extended, it progresses from a spiral seam, thin-wall tube to an axial seam tube; but, its seam actually consists of a 180° overlap of the wall to produce the necessary stiffness. At impact, the contact section of the sensor head pushes against the microswitches, producing the momentary signal necessary to lock in the firing circuit. The boom elements then bend or break under the weight of the spacecraft and, due to their thin-walled construction, do not upset the attitude of the spacecraft during impact.

The dimensions are as follows:

Overall length (set prior to installation), ft	5 to 20
Boom diameter (formed), nominal, in.	1
Sensor-head diameter, in.	2-3/8
Sensor-head stroke, in.	1/8
Sensor-head maximum force for actuation, lb	4
Boom-element thickness (per lamination), in.	0.005

The boom-element arrangement consists of four laminated sections at the root, three at the halfway section, two at the 3/4 section, and one at the head. The dimensions are as follows:

Coiled-element width before extension, in.	4
Boom-element material, stainless steel, no.,	304
Packaged, ready-to-use weight, lb	5 to 7
Packaged, ready-to-use dimensions	
Diameter, in.	5
Length, in.	7-1/2

Prior to the deployment of the two altitude sensors, the rocket-firing circuit is locked out; therefore, any actuation of the sensor microswitches during deployment is inconsequential. To release the boom from the canisters, a small bolt holding the lids in place is cut with a pyrotechnic bolt cutter. The lids fall free, and the booms fully extend in approximately 0.8 second. The sensor circuit is electrically inspected. Then the sensor is armed through a timer which was initiated after lid release.

The sensor head functions due to impact on either land or water. The impact angle can be vertical or from any direction up to 90° away from vertical. Impact velocities may range from 15 to 50 ft/sec. Microswitch-transfer time may require a maximum of 8 milliseconds, but this is satisfactory since the retrorockets will accommodate an altitude-sensor ignition height variation of ±5 percent.

Test results. - The sensors were tested under various deployment conditions.

At deHavilland: Approximately 100 development deployments, 6 qualification deployments, 2 demonstration deployments for MSC (which resulted in 1 extension malfunction on a 20-ft sensor), and impact tests on sand and water produced satisfactory firing signals.

MSC - Static deployments:

Two sensor units were tested on November 5, 1964. The results were successful.

Two sensor units were tested on January 5, 1965. Both units malfunctioned.

Two sensor units were tested on January 22, 1965. The results were successful.

MSC - Impact tests:

One sensor head was impacted on water at 25 ft/sec on November 5, 1964. It produced a good signal.

One sensor head was impacted on concrete at 51 ft/sec on December 8, 1964. A good signal resulted.

MSC - Para-Sail flight tests:

Two units were used on December 11, 1964. They deployed properly, but the left-hand unit trailed due to air loads. Satisfactory rocket-ignition signals were received from both units upon impact on water.

Two units were used on April 21, 1965. Both units deployed properly and apparently produced satisfactory rocket-firing signals upon impact with land. The right-hand unit trailed and bent backward during turns (fig. V-8).

Two units were used on June 3, 1965. The right-hand unit did not deploy. The left-hand unit deployed and trailed, but it automatically disarmed to prevent rocket ignition at altitude. The rockets did ignite 3-1/2 seconds after ground impact through a circuit which connected to the undeployed right-hand sensor.

Problem areas and improvements. - It is apparent from the results of the test conducted on June 3, 1965, that there are several potential malfunction modes in the deHavilland sensor. Therefore, it was decided to thoroughly redesign the components causing malfunctions and conduct 50 deployments under simulated wind-load conditions to confirm the reliability of the new system.

Status. - The deHavilland redevelopment program was successfully completed in October 1965 with a total of 50 reliability firings.

CONCLUSIONS

The deHavilland redevelopment program proved that their sensor system was reliable, and this type of system would be more practical for spacecraft employment since two devices could be used to provide mechanical redundancy. The original pendulum-type sensor has proved to be reliable although it offers no mechanical redundancy since the use of two pendulums, which might collide, could result in disaster. In addition, it would be wise to pass judgment on the pendulum device as a space-flight system only after it has been optimized for weight and volume to determine if these changes affect its performance.

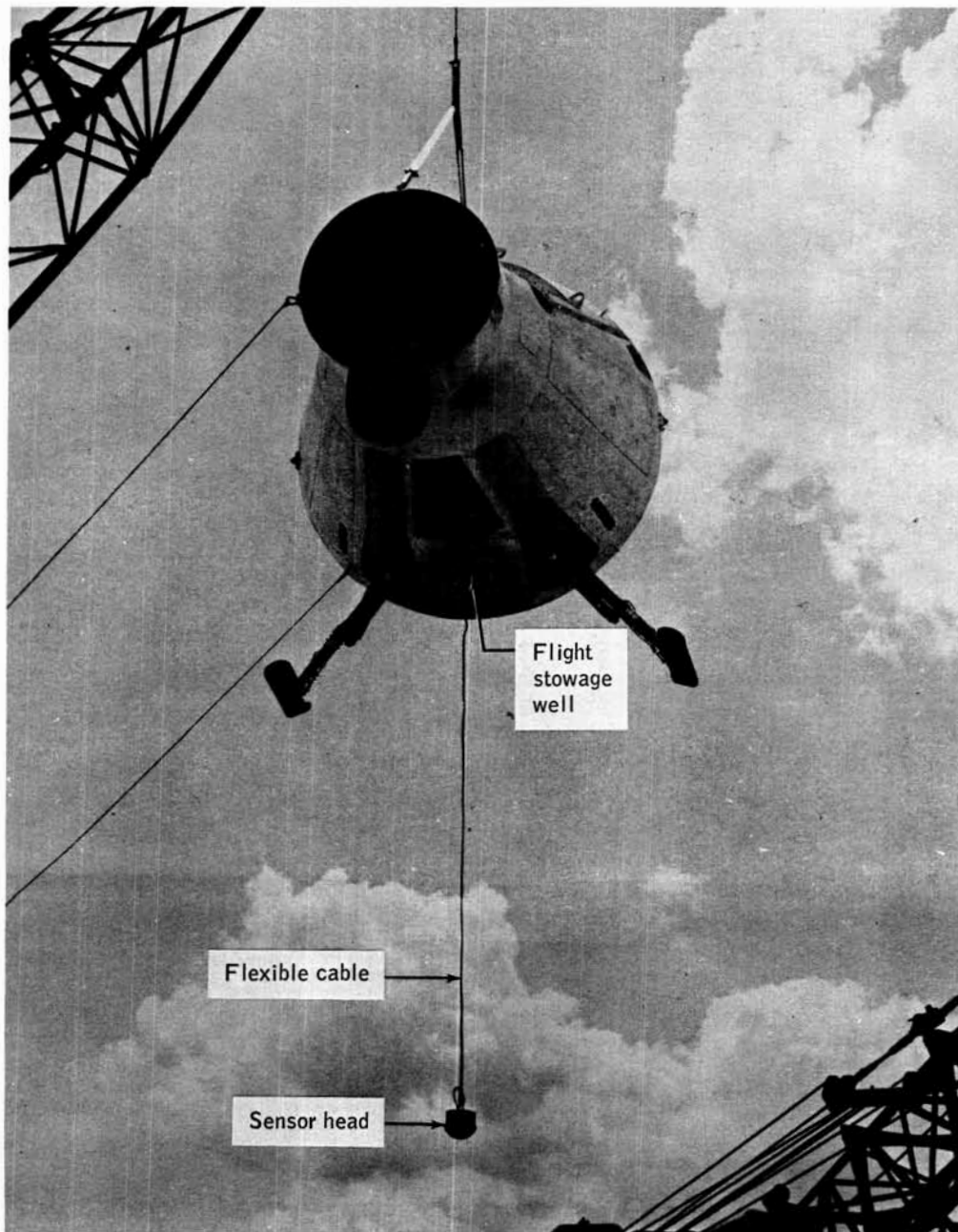


Figure V-1.- Full-scale landing-dynamics test using pendulum altitude sensor.

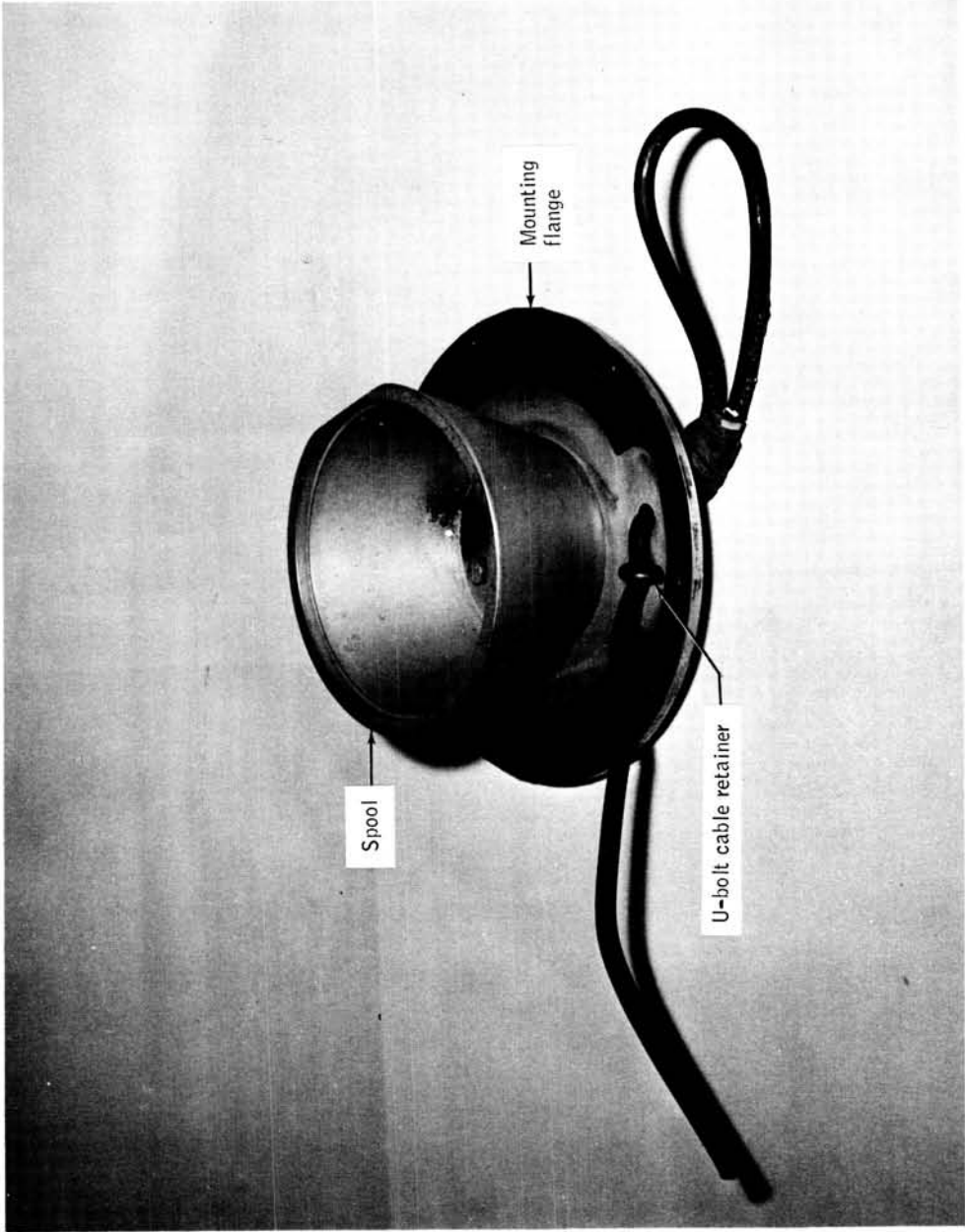


Figure V-2.- Cable storage spool for pendulum altitude sensor.

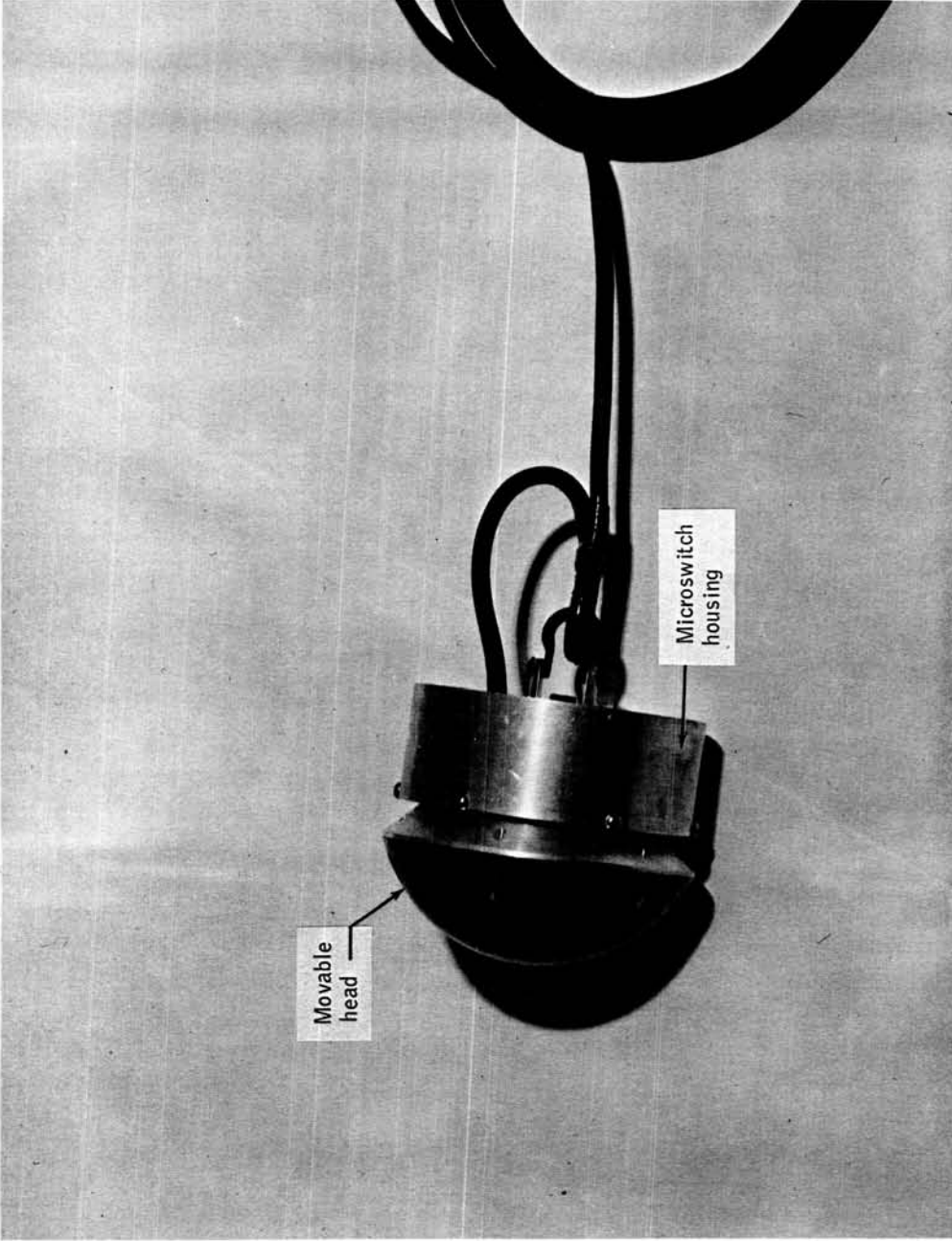


Figure V-3.- Pendulum sensor head.



Figure V-4.- Disassembled pendulum sensor head.

NASA-S-66-10282 OCT 24

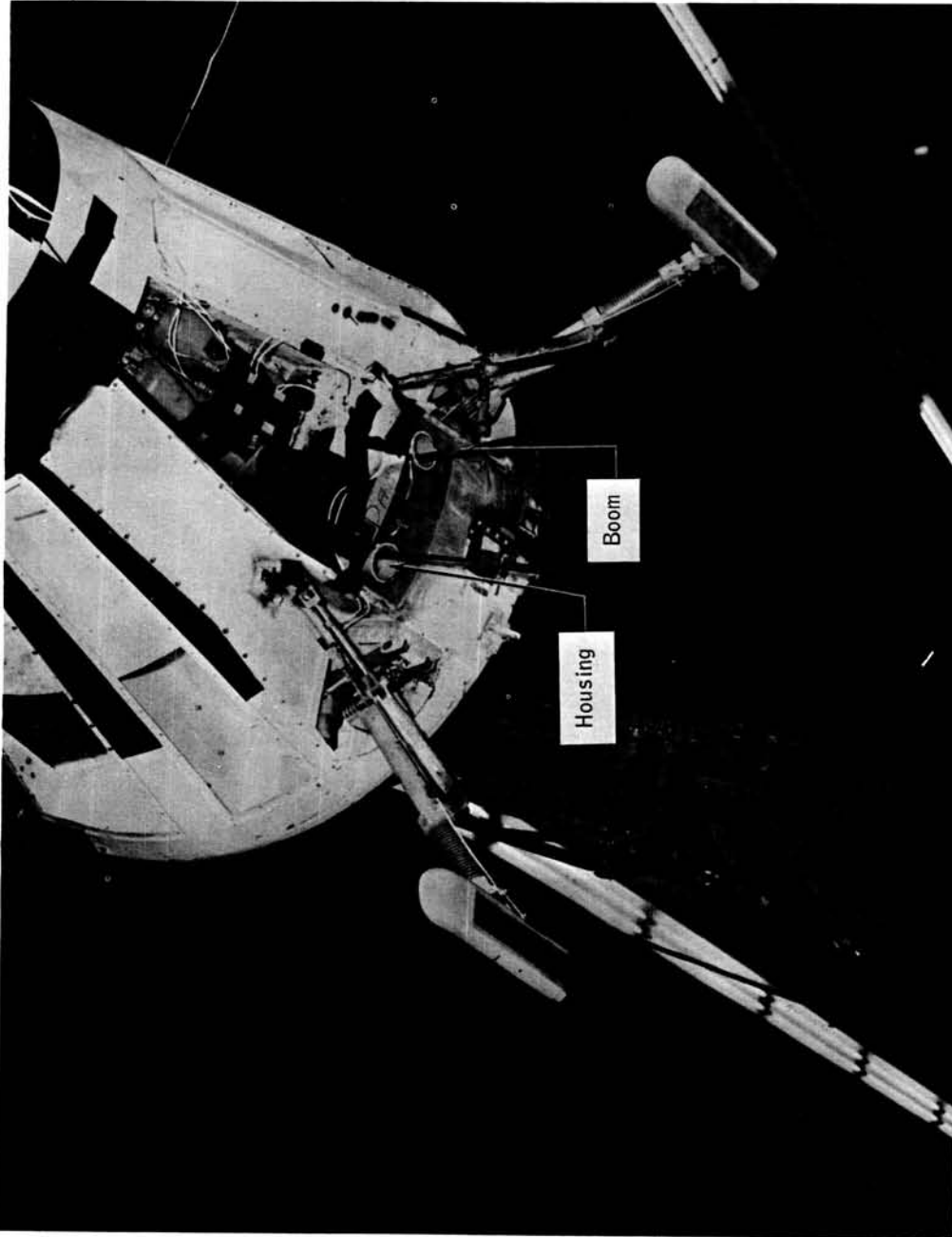


Figure V-5.- Deployment test of the deHavilland altitude sensor.

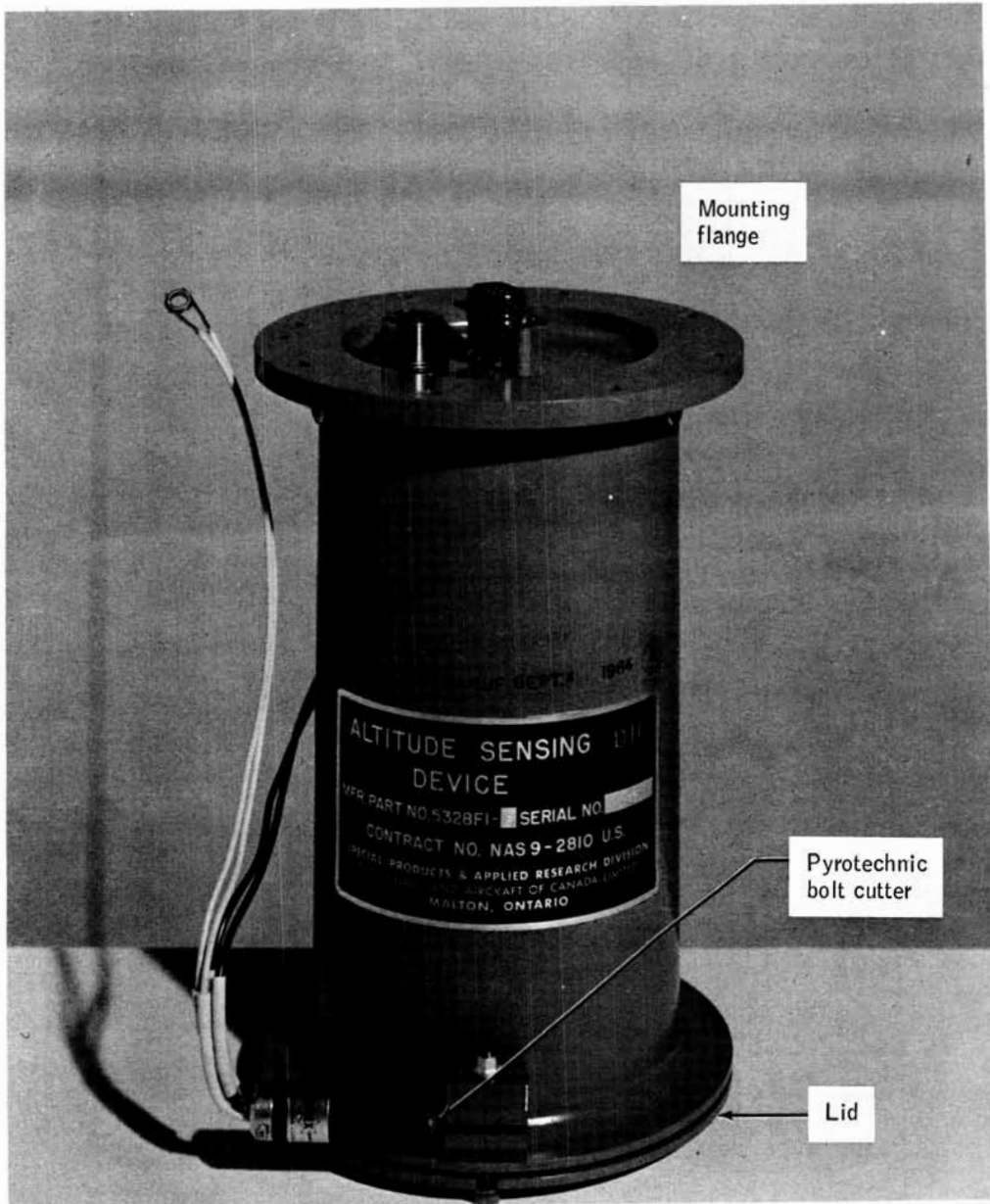


Figure V-6.- Container for the deHavilland altitude sensor.

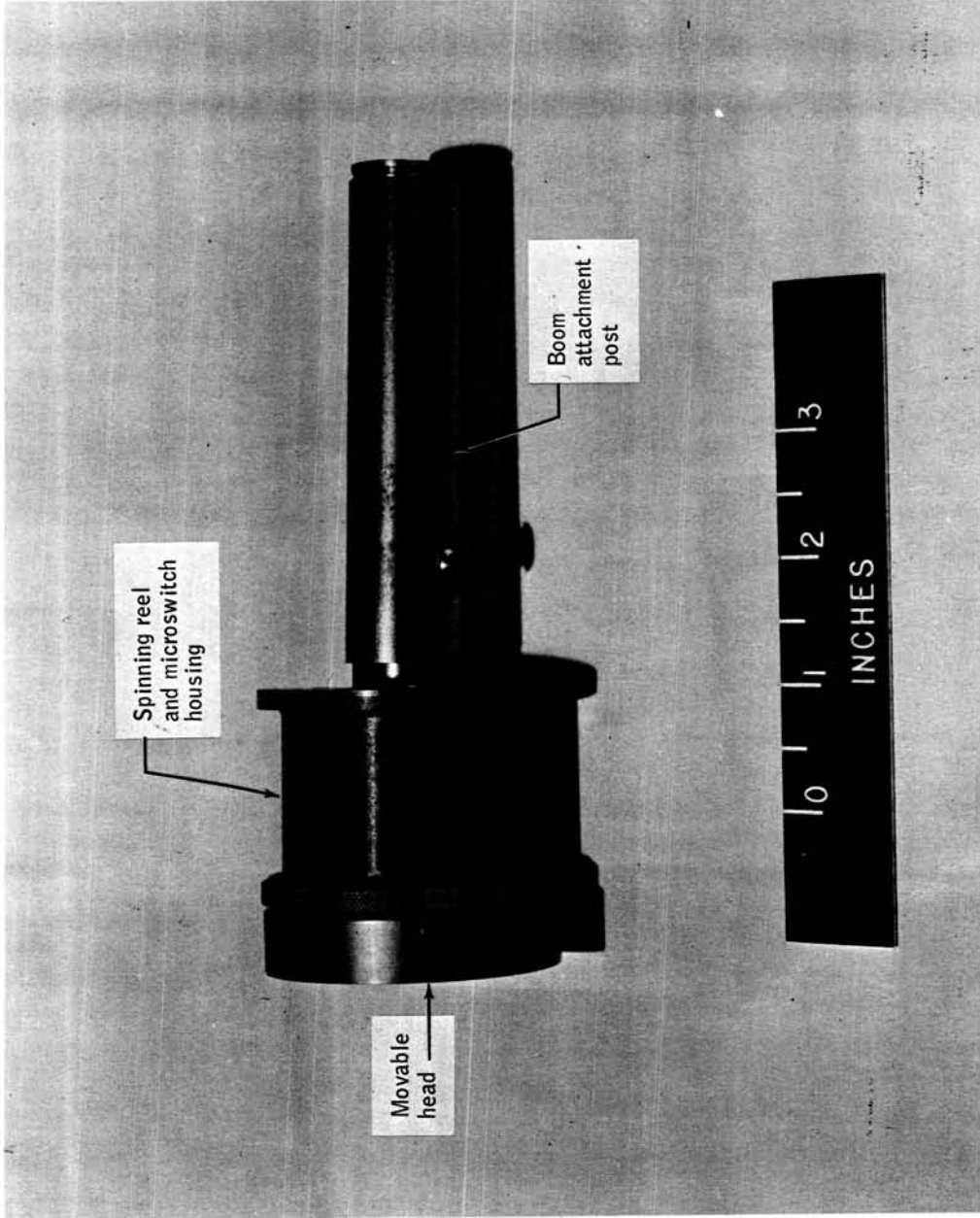


Figure V-7. - DeHavilland altitude sensor head.

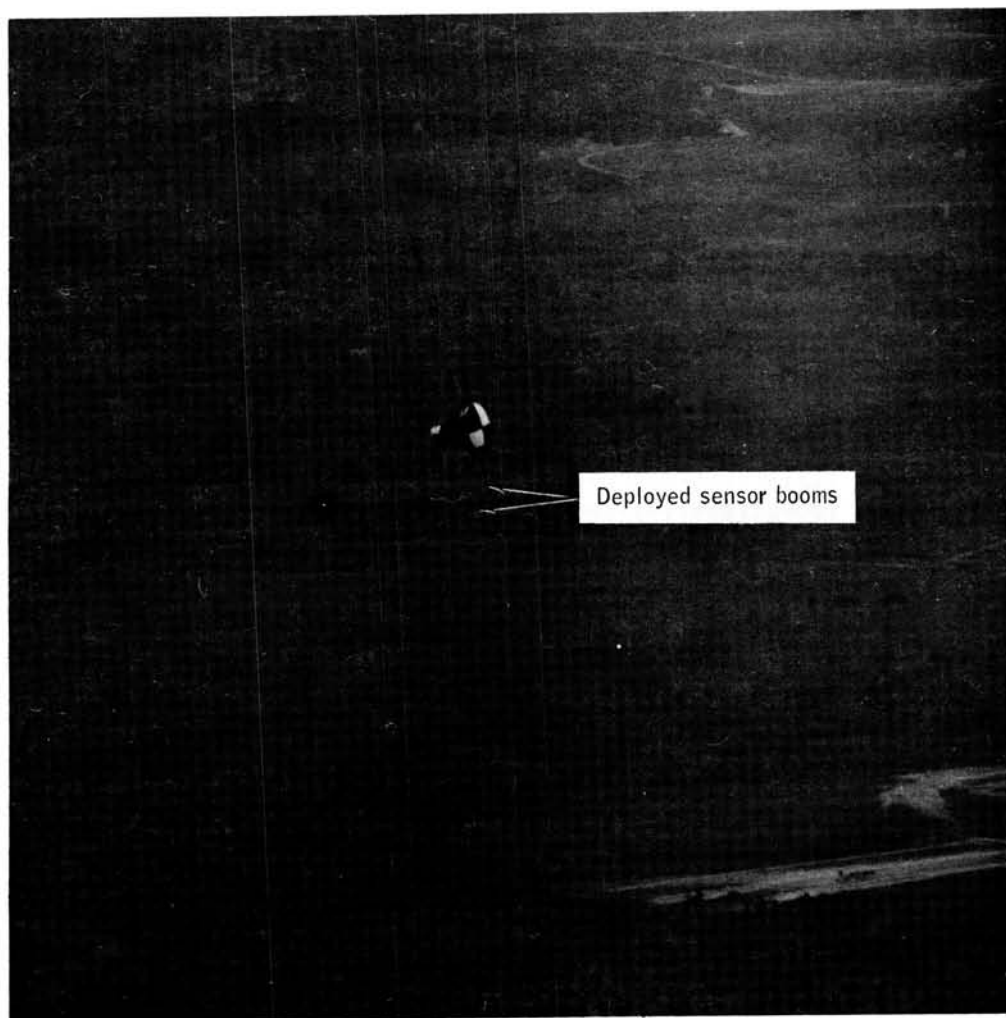
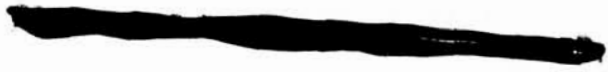


Figure V-8.- DeHavilland sensor deployment for spacecraft in flight.



SECTION VI - TURN-CONTROL MOTOR DEVELOPMENT

By Carlisle C. Campbell, Jr.

TURN-CONTROL MOTOR DEVELOPMENT

By Carlisle C. Campbell, Jr.
Manned Spacecraft Center

REQUIREMENT

The initial requirement for the turn-control system was to develop a motorized system suitable for parachute testing. The system should actuate the Para-Sail turn-control lines at the loads, strokes, and velocities necessary to produce effective turn maneuvers.

SCOPE

Aircraft Armaments Contract

A contract (NAS 9-1718, July 1963) was let with Aircraft Armaments, Incorporated, to develop two control-actuator systems for the Para-Sail. It was initially intended to control the Para-Sail glide angle by actuating a pitch system. This approach has since been discontinued and only the turn- or yaw-control system was flight tested. The performance envelope of this turn system along with the test results will be presented.

Manned Spacecraft Center Development

In order to achieve increased load and stroke capabilities, it was decided to modify one set of turn-control motors which would allow a heavier load to be moved at a slower rate, but for a greater distance. This development was not completed in time for use as flight-test hardware, but its performance capability is more nearly that which would be required for a space-flight item.

Future Development

In the event that the Para-Sail retrorocket system is to be utilized as a space-flight landing system, the design of the turn motors should be optimized,

and new motors would have to be tested against all space-flight conditions. The primary considerations for such a design would involve weight and volume restrictions; power requirements; force-stroke and velocity limitations; cable handling technique; and trim control. Presently, MSC is not conducting further development of this type of design.

SYSTEM DESCRIPTION

Functional and Physical Description

The turn-motor assembly (fig. VI-1) consists of a direct-current motor section, a gear drive, a cable-stowage reel, a limit-switching system, and a solenoid-actuated braking device. The limit switches are provided to remove power and apply the brake at either end of full or partial stroke. A potentiometer geared to the motor is provided to indicate cable positions. A strain-gage device was initially mounted on the motor to indicate cable loads during flight.

The motors may be commanded to reel in, payout, or brake at any position in order to affect proportional control movements. The cable takeup system is fail-safe; in that, upon loss of power, the solenoid-powered brake releases, allowing the turn cable to payout. This prevents locking the parachute in a continuous turn mode.

During parachute deployment and attitude change, the turn cables may receive shock loads which are considerably higher than normal flight-control loads. The cable and brake were designed to withstand loads several times higher than the loads measured on any flight test. Nevertheless, the 1/16-inch cable broke on several occasions either due to excessive bending around short radius surfaces or due to shock loads around sharp edges during parachute deployment.

The motors operate on 28-volt direct current (V dc) and have a permanent magnet stator. The rotating armature is of conventional construction with two carbon brushes for commutation. The motor is driven during reel-in direction only. The parachute load is allowed to turn the motor in reverse to provide reel out. The gear box contains a spur gear drive with an 11 to 1 reduction ratio. A worm-gear takeoff operates the cams which actuate the limit switches. Attached to the cam drive shaft is another set of spur gears which operates the position potentiometer. Three and one-half feet of 3/32-inch cable is wound on the grooved takeup drum. A brass retainer strap

and a feed-in roller prevent the cable from jumping grooves on the drum in the event the free end of the turn cable becomes loose prior to deployment of the parachute.

The mechanical brake acts as a lock and allows little or no slipping or clutch action. This device is a closely wound, coiled spring made of wire with a square cross section. One end is anchored and wound around a fixed drum which faces and touches a rotating drum attached to the takeup reel. The other end of the brake spring is attached to the solenoid mechanism which, when stroked, tightens the spring around the two drums. Friction between the wire and the moving drum during a stop signal causes this drum to lock against the spring in a payout direction only. Since the other end of the spring is fixed, this immediately locks the entire system or prevents rotation in one direction only. When the solenoid is released, the brake spring increases its diameter and releases from the moving drum, allowing the takeup drum to rotate and thus payout the turn line. A typical operational sequence is described.

If the control switch is in the stop position, power is applied to the brake solenoid, which locks the cable drum and prevents rotation. With the control switch in the wind position, power is removed from the brake solenoid and is applied through the wind-limit switch to the motor starting relay, which will close and apply power to the turn motor. The motor will turn and wind in the cable until the other wind-limit switch is mechanically actuated, which removes power from the motor starting relay and applies the brake.

With the control-system switch in the unwind position, brake power is removed, and the motor is turned in reverse under action of the parachute load. In this mode, the motor armature is short circuited, thus providing dynamic braking to limit cable speed during payout. The motor will continue to payout until the unwind limit switch is actuated, which applies power to the motor starting relay through the time-delay relay. The time-delay relay will remain closed for approximately the time required for the motor to bring the load to rest. At this instant, the motor speed is zero, or nearly so, and the time-delay relay closes, which removes power from the motor starting relay and applies brake power.

The performance limits and physical data are listed.

1. Weight: 10 lb/motor; two are required with a total weight of 20 lb.
2. Volume: $3\text{-}3/4 \times 6 \times 11$ in. /motor with a total volume of 0.287 ft^3 .

3. Voltage requirements: 18 to 32 V dc; brake solenoid must operate on 28 to 32 V dc.

4. Amperage range:

Running, 10 to 30 amperes.

Lock-rotor current, 80 amperes.

5. Fuse-time delay: slow blow after approximately 10 sec at lock-rotor conditions.

6. Battery:

Weight, 16.5 lb.

Capacity, 165 watt-hours.

Plates, nickel-cadmium.

Dimensions, $1.69 \times 4.64 \times 4.45$ in. /battery.

One battery will supply the necessary power for 32 turns, but two are used to increase the reliability and power available.

7. Motor output:

Available stroke, 42 inches.

Reel-in rate, approximately 4 ft/sec at 60 lb average cable load.

Payout rate, approximately 1 ft/sec at 60 lb average cable load.

Stall load, approximately 125 pounds. (See fig. VI-2.)

Test Results

Factory acceptance tests. - Each motor was required to reel in an average load of 100 pounds for a distance of 2 feet within 1-1/2 seconds for 16 consecutive cycles.

MSC development tests. - Numerous tests were conducted at MSC during familiarization and modification of the motors. Each motor has been cycled under load more than 250 times.

Between-flight qualification tests. - Prior to each parachute test, each motor was cycled under load 25 times. After these tests, the motor was disassembled and inspected, and the cable was replaced.

Preflight checkout tests. - After installation in the test spacecraft (fig. VI-3), each motor was cycled six times to confirm that it performed properly and to allow proper adjustment of the cable length.

Para-Sail flight-test results. - See table VI-I for the Para-Sail flight-test results.

Problem Areas and Improvements

Although the major problems have involved the use of steel cable, several other components were modified or changed to produce better turn-motor performance. To effect more positive braking action, a larger brake solenoid was installed. This made solenoid linkage adjustments less critical and allowed braking performance across a wider range of loads. The capacitors, which affect the length of time that power is applied to the turn motors to stop them after payout, were also changed to produce more desirable braking action.

The guides, which assist in feeding the cable onto the takeup drum, were changed from brass drag devices to steel cylindrical rollers. This change reduced system friction and increased cable life.

To gain more stroke which produced higher turn rates, the worm-gear drive which operates the limit-switch cams was changed. This resulted in an effective stroke of 42 inches rather than 23 inches. Originally, the cable-takeup drums held 48 inches of cable, but not all of the cable was used since doing so might result in a motor malfunction caused by traveling past the cam-limit switch setting.

Knowledge of actual parachute turn loads versus stroke was essential in predicting the best turn-line length-stroke combination. During the first few Para-Sail tests, an external load link was used to measure turn-line loads. It was subsequently decided to install a statically positioned load-measurement device inside the spacecraft. Although this device produced useful data, it contributed substantially to turn cable fatigue; therefore, it was eliminated on the last two tests. It should also be noted that the load-sensing system could not detect loads which exceeded 150 pounds even though the 1/16-inch cable was rated at 500 pounds. Therefore, all load data were not obtained.

The 1/16-inch-diameter cable originally supplied with the turn motors was 7/7-strand carbon steel and met Military Specification requirements. After several parachute tests which produced broken or frayed cables, it was decided to change to 1/16-inch-diameter, 302 stainless steel, 7/19-strand cable. Although this cable did not meet Military Specification requirements, it was proved to be more durable for this turn-motor system which required that the cable pass around several short radius rollers. Additional tests indicated that even this very flexible cable was subject to failure; therefore, the turn-motor takeup drum was modified to accommodate 3/32-inch

stainless-steel 7/19 cable which has a tensile strength rating twice that of 1/16-inch cable. In addition, the cable tension-measurement device was removed, and large radius Teflon guide surfaces were added to the outside of the spacecraft to insure that the cable would no longer be required to make any short radius bends. These changes proved to be highly successful. After the last two tests, examination of the cables revealed no apparent wear or excessive bending fatigue. Figure VI-4 illustrates the turn-motor assembly.

Final Configuration and Conclusions

The turn motor in its present configuration is basically the same as the original equipment, with the exception of the changes described. The major changes which produced the most significant results were the changes necessary to accommodate heavier stainless-steel cable. This motor can continue to be used as a test-system component since the motor has proved to be durable and is now reliable. Future systems may include the addition of a trim-control feature which does not require changes on the motor itself, but only the addition of an incidental number of electronic devices.

TABLE VI-I. - PARA-SAIL FLIGHT-TEST RESULTS

Date	Stroke, in.	Cable size, in.	Load range	Remarks	Motor results
2/2/64	--	--	--	No control system installed.	--
4/8/64	23	1/16	--	Main parachute failure.	--
4/28/64	23	1/16	9 to 109 lb	Satisfactory left-hand and right-hand turns.	Successful
5/14/64	23	1/16	Poor data	Broken main parachute riser. Produced slow turns.	Successful
5/26/64	42	1/16	Poor data	Right-hand turn cable broken during deployment. Poor left-hand turn rate.	Poor
10/16/64	42	1/16	Greater than 175 lb	Turn motor overloaded by preshortened turn lines, causing slow fuses to blow.	None
12/11/64	42	1/16	Poor data	Both turn lines broken during vehicle attitude change.	None
1/15/65	42	^a 1/16	40 to 135 lb	Improved cable stowage technique. Used stainless-steel 7/19 cable.	Successful
2/25/65	42	^a 1/16	16 to 113 lb	Same as above.	Successful
4/21/65	42	^a 1/16	Poor data	Cable frayed during flight. Right-hand cable broke prior to impact.	Fair
6/3/65	36	^a 3/32	No instrumentation	Para-Sail damaged during deployment. Poor canopy control. Turn system was satisfactory after flight.	Successful
7/30/65	36	^a 3/32	No instrumentation	Satisfactory turn control. Cable and motors were satisfactory after flight.	Successful

^aStainless-steel cable.

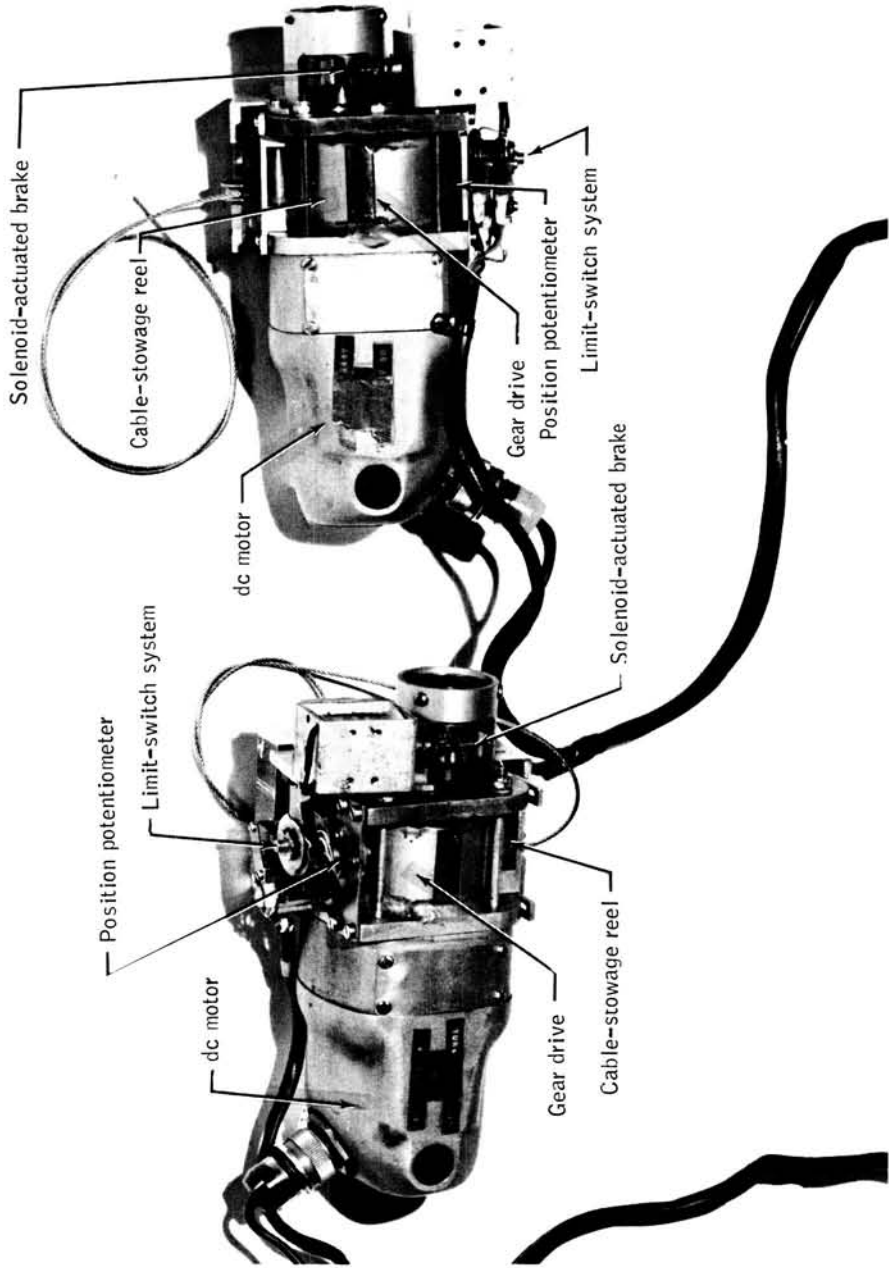


Figure VI-1.- Turn-control motors, assembled.

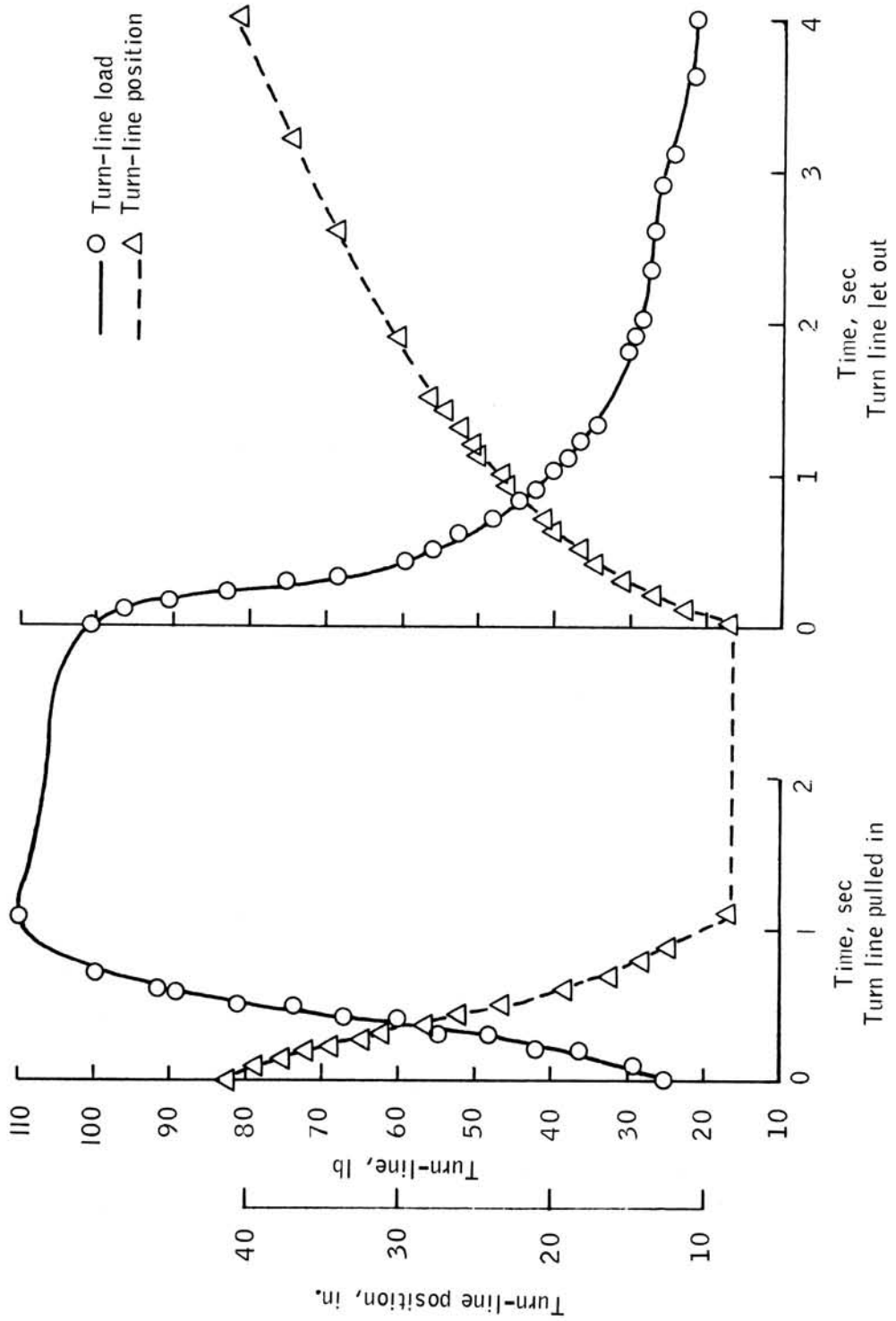


Figure VI-2.- Turn-line, load-stroke characteristics.

NASA-S-66-10288 OCT 24

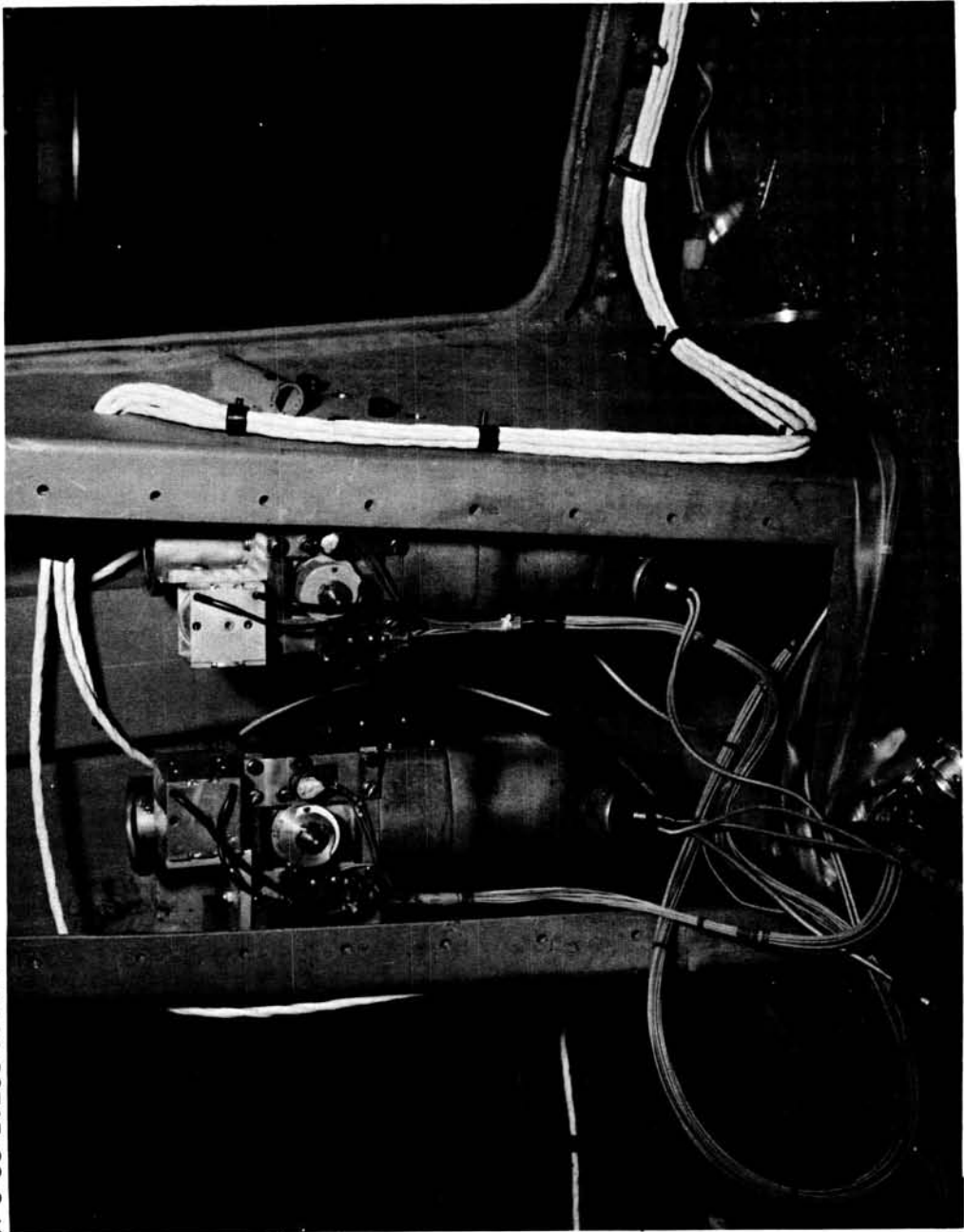


Figure VI-3.- Installation, left and right turn motors.

NASA-S-66-10289 OCT 24

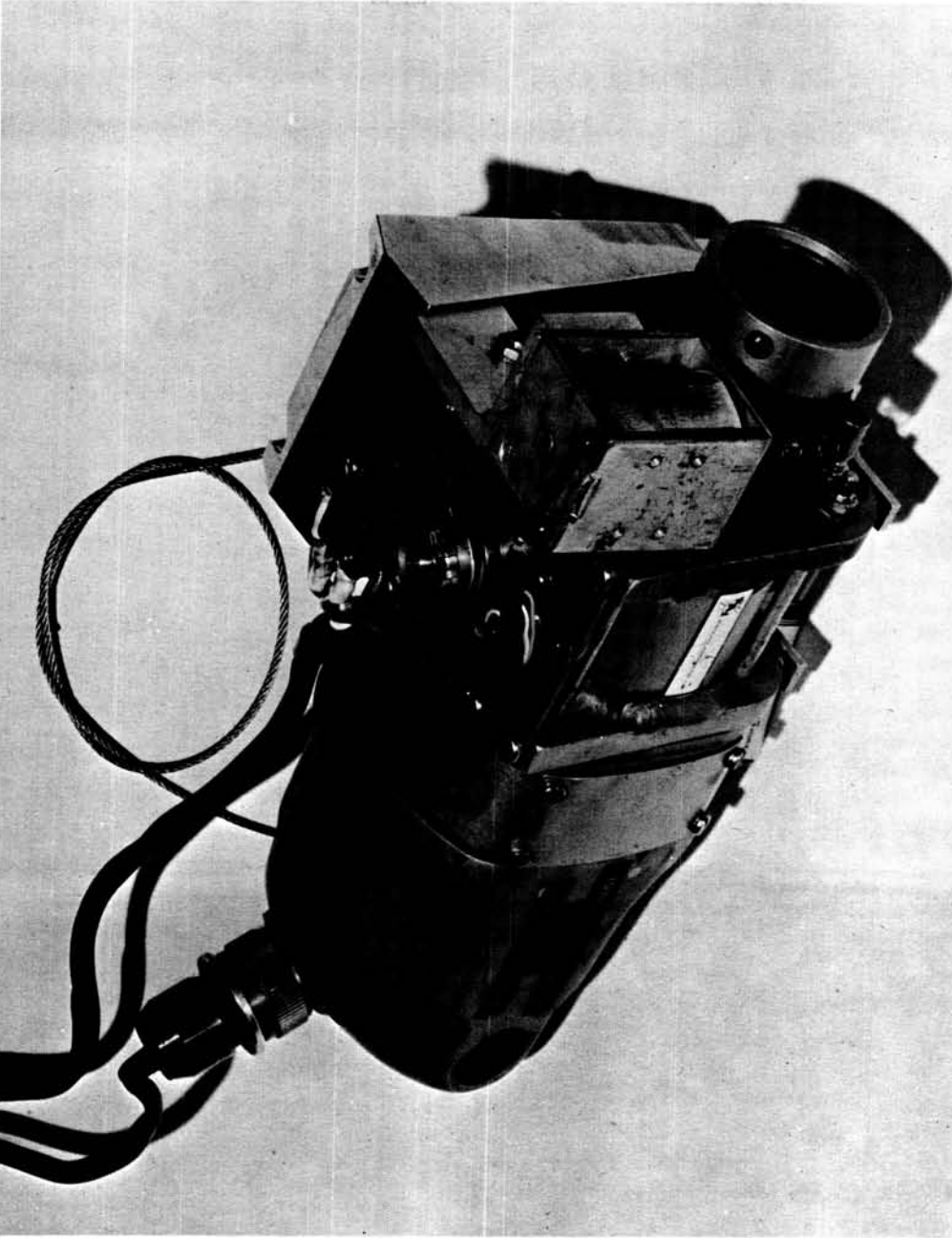


Figure VI-4.- Turn-motor assembly.

PRECEDING PAGE BLANK NOT FILMED.

SECTION VII - INVESTIGATION OF THE VISUAL-REFERENCE
REQUIREMENTS FOR PILOT CONTROL OF GLIDING PARACHUTES
FOR LAND LANDING OF SPACECRAFT

By James E. Burkett

INVESTIGATION OF THE VISUAL-REFERENCE REQUIREMENTS
FOR PILOT CONTROL OF GLIDING PARACHUTES
FOR LAND LANDING OF SPACECRAFT

By James E. Burkett
Manned Spacecraft Center

SUMMARY

A test program has been completed which investigated the problems associated with pilot control of a gliding, controllable parachute for land landing a spacecraft. The program was directed toward the Para-Sail parachute with the following characteristics: an L/D of 1; descent rate of 30 ft/sec; and turn rates to 20 deg/sec. Wind-drift determination, visual selection of a landing area, and obstacle avoidance were the major problems investigated during the program. The methods of testing included helicopter simulation of the Para-Sail parameters and scale-model air drops of an actual Para-Sail. The scale-model testing included motion-picture camera investigation for preliminary pilot-visual requirements determination, and later a television system for pilot-control investigations. A variety of test subjects was used to obtain different opinions on the system tested and the landing techniques used. It was found that with a system which gave the controller a view of a large percentage of the landing zone attainable and a simple reticle, landings could be successfully accomplished with visual control up to altitudes of 10 000 feet, providing the selected landing zone had a sufficient number of clear landing areas, and that wind and visibility conditions were within acceptable limits.

INTRODUCTION

General

The Manned Spacecraft Center, in keeping with the overall responsibility for manned space-flight operations, including landing and recovery, has given attention to the spacecraft systems and operational aspects of providing the

capability of a land landing at the termination of a space-flight mission. Such a capability at this point in spacecraft system development is desirable, but requires advances in the state-of-the-art of landing-system design and operation. Over the past 2 to 3 years, investigations have been made of several methods of providing spacecraft with a descent system which will allow pilot-visual control and maneuverability during the landing phase. These investigations have included such systems as paragliders, gliding parachutes, rotor systems, winged bodies, and so forth. Of these, the gliding parachute family of descent systems has shown great promise when considered for use in the semiballistic spacecraft shapes currently utilized for the NASA manned space-flight programs. Specifically, the controllable Para-Sail parachute has received the most attention, and has been developed and tested as a landing system in combination with a Gemini-sized spacecraft to the point where the operational aspects of landing such a system could be investigated profitably. This report gives the results of an operational test program to determine the visual-reference requirements for pilot control of gliding parachutes.

Mode of Operation

The gliding parachute family of descent systems has a relatively low L/D capability. This range of L/D for different types of systems is approximately 0.7 to 2.0 with an L/D of 1.0 to 1.2 more readily available with the Para-Sail. Thus, the maneuvering range of a spacecraft with such a system is limited, and this results in an operational constraint. If the L/D were large enough to overcome any errors in the reentry trajectory of the spacecraft, then a point landing could be made at a preselected site (airfield) contingent on local weather and winds. An L/D of the order of 3.0 to 4.0 would be required to provide this capability. (Other problems associated with high L/D, such as high horizontal landing velocity, are not considered here.) Low L/D (0.7 to 2.0), such as the Para-Sail system provides, has resulted in the zone landing concept. This concept is defined as: The capability of a spacecraft and its system to reenter to a point in the atmosphere from which a land landing can be made at any of a number of places within a selected but unprepared zone by avoiding existing obstacles. Thus, a zone is preselected which has a high percentage of clear and relatively flat terrain. The spacecraft pilot, under visual control with ground guidance as required, selects the best attainable landing area, determines the winds, and flies to that area to make an into-wind landing with the lowest possible horizontal velocity.

Test-Program Objectives

The Landing and Recovery Division initiated a program to study the operational aspects of using a controllable parachute for land landings. This program includes an investigation of those areas associated with pilot control and is currently being directed toward the Para-Sail parachute.

The program objectives were to determine: (1) The pilot display required to fully utilize the capability of the Para-Sail system; (2) The capability of the system to maneuver into areas of various sizes; (3) The altitude at which visual control can be obtained; and (4) The effect of wind drift on Para-Sail landing operations.

TEST-PROGRAM DESCRIPTION

A three-phase test program was initiated to determine the requirements for a visual-reference system to fully utilize the capabilities of a gliding parachute system for landing a spacecraft.

Phase I

The first phase was a preliminary investigation into the view of the ground required and a determination of the adequacy of the resolution attained with that view. This phase consisted of taking motion pictures from non-gliding parachute drops, helicopter descents, and scale-model Para-Sail drops.

Phase II

The second phase was a preliminary investigation into the size of landing area attainable and the amount of clear area required within the capability of the Para-Sail, plus further investigation into the field of view and resolution required. A controller was introduced at this point and helicopters were used for Para-Sail simulation.

Phase III

The third phase extended the investigations of phases I and II to an actual Para-Sail case. A scale-model spacecraft with a Para-Sail parachute and a television camera to simulate pilot view was used for phase III tests.

DESCRIPTION OF TEST VEHICLES AND SYSTEMS

Phase I

Nongliding parachute drops. - A metal container was fabricated which contained a parachute and a motion-picture camera aimed straight down. The container was weighted such that the descent rate was approximately 30 ft/sec.

Helicopter descents. - Four motion-picture cameras were mounted to a rack which was attached to the cargo floor of a UH-1 helicopter and extended outside the cargo door. The cameras were mounted so that their view was straight down from the helicopter (fig. VII-1).

Para-Sail drops. - During Para-Sail development tests, three motion-picture cameras were mounted in a 1/3-scaled Gemini space vehicle. The cameras were mounted such that one was aimed forward, one was aimed straight down, and one was at an angle forward of straight down. The latter camera could be adjusted to different angles prior to drop. The vehicle was suspended in the three-point Gemini spacecraft configuration from a 24-foot Para-Sail parachute.

Phase II

For phase II, three types of helicopters were used, the H-13, H-19, and H-34. A 6-foot fiber-optics bundle was used to give a view of the ground utilizing a lens at one end of the bundle to establish the field of view and a lens at the other end as an eyepiece. Figure VII-2 is a photograph of the fiber-optics bundle attached to the H-13 helicopter. A disc of Mylar with scribed lines was placed between the fiber-optics bundle and the eyepiece for use as a reticle. Different reticles (examples of which are shown in fig. VII-3) were evaluated during the test program. During a portion of the test program, the look angle of the field-of-view lens could be changed during flight from straight down to 60° forward of straight down. A motion-picture camera, with the same size lens and at the same look angle as the bundle, was used to record the descents. In addition to the fiber-optics bundle, other tests were

made with a closed-circuit television placed in the cargo compartment of an H-19, and descents were made with the test subject viewing the television monitor. An overlay was placed on the television monitor to serve as a reticle. Different lenses were also used on the television camera. A vane attached to a protractor card was used to give the helicopter pilot a reference to simulate the proper glide angle for the Para-Sail. The card was free-swinging and balanced to remain horizontal regardless of helicopter attitude.

Phase III

The same 1/3-scaled Gemini spacecraft vehicle and Para-Sail as in phase I tests was used for phase III testing. The only change was that a television camera replaced the three motion-picture cameras. The television camera was mounted so that the look angle could be changed from straight down to 45° forward of straight down. For all but two of the drops, the television camera was aimed 30° forward of straight down, and a 5.7-mm lens was used which had a field of view of 84° fore and aft and 65° side to side. The landing system consisted of a Para-Sail which could be controlled via radio link from a remote ground controller. The control system was nonproportional and was only capable of either full control-line travel or neutral, which resulted in control positions of full right turn, full left turn, or straight ahead with turn rates of 20 deg/sec. No control trimming capability was provided. The landing gear contained honeycomb to absorb impact loads, but was not intended to simulate the landing dynamics of the Gemini spacecraft. The drop vehicle was weighted to 400 pounds which resulted in a descent rate of approximately 20 ft/sec. It should be noted that this descent rate does not correspond to the operationally desired descent rate which has been determined as not lower than 30 ft/sec for the Para-Sail system. This desired descent rate resulted from a trade off between the requirements to attenuate as much of the spacecraft forward horizontal velocity as possible during an into-wind landing, and to provide an operationally reasonable wind limitation such that the spacecraft will not land with a backward velocity. Either a high forward velocity or a relatively low backward velocity would probably result in spacecraft tumbling or unacceptable landing-gear design criteria for landing on unprepared terrain.

A Para-Sail with an L/D of 1.0 will travel on a 45° glide slope in a no-wind condition (horizontal and vertical velocities equal). Thus, the horizontal velocity equals the maximum surface-wind velocity which can be attenuated without landing backward. Hence, the maximum surface-wind velocity is an operational constraint of which 30 ft/sec (17.8 knots) is considered acceptable. It was necessary to accept the 20 ft/sec descent rate for these tests due to the fact that the increased weight required to cause the 24-foot Para-Sail to descend at 30 ft/sec would have the following detrimental effects: (1) ground

handling would have been more difficult; (2) impact shock attenuation would have required a greater amount of shock material than was deemed practical; (3) the design strength of the available parachute would have been exceeded; (4) canopy shape on the particular size Para-Sail used for these tests was found to change if a higher descent rate was used, resulting in an unacceptably lower L/D capability.

The Para-Sail was suspended in the three-point Gemini spacecraft configuration with a split front riser and the apex of the Para-Sail pulled down. The vehicle was attached to the H-19 and UH-1 helicopters on specially constructed mounts which utilized a modified bomb rack for releasing the vehicle. The Para-Sail was deployed by a static line from the helicopter attached to the Para-Sail bag. A television receiver was placed in a van on the ground to give the controller a view of the landing area with a reticle (fig. VII-3, reticle 1). The point where the lines converge represents the point directly beneath the spacecraft. The short dashed lines represent 15° increments forward of straight down with the third one being over the no-wind landing point. The no-wind landing point is the point the spacecraft would land if there were no wind and the spacecraft were allowed to fly in a straight line. Figure VII-4 shows the vehicle in flight, while figure VII-5 is a photograph of the vehicle attached to the UH-1 helicopter. Figure VII-6 is a photograph of the interior of the control van showing the television monitor, the Para-Sail control box, and the video tape recorder.

TEST PROCEDURES

Phase I

Nongliding parachutes. - The containers with the motion-picture cameras and the nongliding parachutes were dropped from a UH-1 helicopter at altitudes to 10 000 feet over the Fort Hood Military Reservation.

Helicopter descents. - During the nongliding parachute drops, a helicopter attempted to follow the descending parachutes. Of the four cameras attached to the helicopter, two contained color film and two contained black and white film for comparison of the same terrain. Two different lenses were used on each set of cameras for resolution comparison.

Para-Sail drops. - The motion pictures from the onboard cameras were taken during Para-Sail development tests, which were not specifically for the visual-reference system tests. The vehicle was dropped from an H-19 helicopter at altitudes to 4000 feet over Ellington Air Force Base. The Para-Sail

was remotely controlled from a point on the ground with the controller watching the parachute. The angle of the adjustable camera was set prior to each flight.

Phase II

This phase introduced man into the system and several test subjects were used as controllers. The tests were conducted over uninhabited areas near Ellington Air Force Base and consisted of helicopter descents simulating the Para-Sail parameters. The helicopter would climb to the desired altitude, 5000 feet for the H-13 and H-19 and 10 000 feet for the H-34, and establish a 2000 ft/min descent with a 45° glide angle. The test subject would then use the view through the optical system to determine wind drift and select a landing area. Instructing the helicopter pilot to make the necessary turns, the test subject would maneuver the helicopter to the selected landing area. The helicopter pilot made flat rudder turns at rates of approximately 20 deg/sec and terminated the descents at approximately 500 feet above the ground. The descents were made into zones with various percentages of clear areas in order to determine the wind effect and the ability to maneuver into small landing areas.

Phase III

Phase III was performed in two parts. Part I consisted of low-altitude air drops at Ellington Air Force Base, and part II consisted of high-altitude air drops at the Fort Hood Military Reservation.

Part I. - Preliminary drops were made from altitudes to 4000 feet at Ellington Air Force Base for familiarization with and practice in wind-drift determination plus preliminary evaluation of the system. Due to the limited area of the drop zone around Ellington Air Force Base, the vehicle was released upwind of the intended target such that a nongliding parachute would reach the target. The controller was instructed to determine wind drift and its effect on the ground track and to land the vehicle at a specific point for these tests. The controller was in the NASA tower watching the television monitor, while a second controller was in the drop zone with the ground-control transmitter. The controller would radio commands to the person in the drop zone who would then control the vehicle. This second controller was used for safety so that in the event the television failed, the second controller could take over and land the vehicle near the target.

Part II. - At Fort Hood Military Reservation, the task of the controller was different in that the controller was instructed to select the landing point

after the vehicle was released from the helicopter. For these tests, the television and the controller were in a van in the drop zone where the vehicle was controlled directly. In the event of television malfunction, the controller could maneuver the vehicle by visual observation from outside the van. Three types of tests were performed at Fort Hood Military Reservation, all from 10 000 feet. The first test for each controller was to fly to a preselected area with the wind unknown. The second test was to select an area after release and fly to it. The third test was to simulate breaking out of an overcast. The latter test used two controllers: one controlled the vehicle to 2000 feet above the ground; the second controller took over at 2000 feet, selected a landing area, determined wind drift, and landed in the area.

Throughout the last two phases of the program, different test subjects were used as controllers to obtain a variety of opinions on the systems.

RESULTS AND DISCUSSION

Phase I

The phase I motion pictures provided a preliminary evaluation of the required field of view and its orientation. The pictures further gave an indication of the resolution that could be expected from a downward looking system with the various lenses used. From these tests, it was found that the best field of view would be one that encompassed the entire area attainable using the Para-Sail, and that some angle forward of straight down gave the most desirable line of sight. Considering the glide capability of the Para-Sail and a nominal wind, a 30° angle was selected for further testing. The 5.7-mm lens proved the most desirable for the required field of view. This lens is approximately equal to 85° from fore to aft and 65° from side to side. Although this was not quite the desired field of view, it was considered adequate for testing. Lenses available with larger fields of view caused an excessive amount of distortion at the periphery of the lens. During this phase, it was also determined that a helicopter could be used to simulate the Para-Sail descents.

Phase II

The lenses were again varied to verify the findings in phase I. Although the smaller angle lenses (less than 5.7 mm) presented somewhat better resolution, it was found that the area restriction was too severe. Even with the capability of changing the angle of the lens in flight, it was not possible to accomplish the landing task satisfactorily. Locating a suitable landing area

could be accomplished with a movable lens; however, the problem of determining wind drift was found to be extremely difficult and consumed an excessive amount of time. The field of view required is one which encompasses at least the area directly beneath the spacecraft and the no-wind landing point.

Reticle requirements were studied during this phase, and several patterns were investigated. Of the reticles tested, it was found that a simple, uncluttered presentation was best for wind-drift determination. The reticle should define the point directly beneath the spacecraft and the no-wind landing point for use as a reference for landing progress. Crosshairs were used to determine relative motion; and radials emanating from the straight-down point aided in determining direction of drift.

Descents were made into zones with various amounts of clear landing areas. These tests provided information as to the size of area required and the amount of clear area needed within the zone of capability. Approaches were made into areas that contained less than 50 percent clear area within the initial field of view at 10 000 feet. At 10 000 feet (using the optical system previously tested), large clearings, groups of trees, and roads and streams could be distinguished. However, during descent, fences powerlines, and similar, less easily defined local obstacles could not be seen until it was too late to avoid them. The inability to see these obstacles was due to at least a 50 percent light loss in the fiber optics. It is believed that a system specifically designed to provide a pilot with a view of the ground for spacecraft landing would eliminate this problem and provide the resolution necessary for distinguishing these objects. It was found that wind drift could be determined and a landing area selected within the limitations of the helicopter. Visual control could be accomplished from 10 000 feet, although wind drift was difficult to determine at altitudes above approximately 6000 feet.

It should be noted that exact simulation of the Para-Sail parameters could not be made with the helicopters flown under manual control. During the descents, the descent rate would vary within ± 500 ft/min of the desired descent rate, and the glide angle varied as much as $\pm 15^\circ$ of that desired. Pilot technique and experience was an important factor in the simulation. Also, the fact that the descents were terminated from 300 to 1000 feet above the ground made exact landing spots difficult to determine. However, the results of the testing gave an insight into the problems involved: a preliminary observation of the view and reticle required, and the size of the area that could be attained; and the techniques for using the system.

During the course of the helicopter simulation, a closed circuit television system was used to investigate the resolution obtained and to determine its suitability for further testing on an actual Para-Sail. A television monitor was placed in the cargo compartment of an H-19, and descents made from

6000 feet show that the television presentation actually provided better resolution than the fiber optics except that it did not show color. Flights at 10 000 feet in a C-119 showed that the resolution to 10 000 feet was adequate for further testing.

Phase III

Part I. - The drops during part I, as stated previously, were primarily for familiarization with the system as well as practice in wind-drift determination. Part I consisted of 18 drops using four different controllers. When these tests were performed, skies were clear, surface winds varied from 10 knots (17 ft/sec) to 20 knots (34 ft/sec), and gusts and winds at drop altitude were as high as 40 knots (68 ft/sec). These high winds exceeded the no-wind forward glide capability of the Para-Sail in that 20 ft/sec was the greatest forward speed attainable. The ability of the controller to perform the task of landing at a specific point was largely a function of the magnitude of the wind. As experience increased and familiarity with the peculiarities of the Para-Sail increased, the controller was able to land within approximately 200 yards of the desired target. At the higher winds and while flying into the wind, the view of the ground was not adequate to show the landing point. A technique to solve this problem was to make 90° turns cross wind to locate the landing point and then turn back into the wind just prior to touchdown. Typical ground tracks are shown in figures VII-7 to VII-10.

Part II. - Thirty drops of the 1/3-scale Para-Sail were made at Fort Hood Military Reservation during part II, again with four different controllers. The weather during these tests varied from clear skies with light and variable winds to broken clouds and surface winds to 15 knots. A problem resulting from weather conditions was fogging of the television lens at lower altitudes. This was alleviated by coating the lens with glycerin to prevent condensation from forming. Results of the test program showed that the optics used in the television system gave the astronaut an adequate presentation of the ground to control the Para-Sail to a suitable landing area. The resolution of the system was such that at an altitude of 10 000 feet, roads, streams, groups of trees, buildings, and large clear areas could be defined. Wind drift is difficult to determine at 10 000 feet of altitude due to low relative motion across the ground. At altitudes below 6000 feet, wind drift can be readily determined, and landing areas can be selected. Below 500 feet, it is again difficult to determine wind drift in an open area due to the lack of land reference points. Also, some local obstacles are difficult to see on the television monitor due to lack of contrast and loss of light. Examples of these obstacles are power lines, flat boulders in neutral-shade soil, and fences. As stated before, most of these obstacles probably could be seen with a television system having color and better contrast. This was indicated by the

motion pictures of earlier 1/3-scaled tests where color film was used in the recording camera.

In several drops, the controllers were instructed to purposely fly into areas that were predominantly undesirable due to trees and other obstructions. It was found during these tests that satisfactory landings could be made in zones with only 40 percent of the total area acceptable as a landing area. Advanced recovery planning for mission use had shown that landing zones could be selected which provided acceptable landing areas well in excess of the 40 percent attained at Fort Hood Military Reservation. Also, landings were made in areas as small as 150 yards square. Figure VII-11 is a map of the Fort Hood area showing the landing sites and a circle representing the area attainable from 10 000 feet under a no-wind condition. It should be noted that the terrain is not typical of that expected in a landing area that may be selected for an actual land landing mission, but represents a variety of terrains and conditions.

In general, the controllers, after several drops, were able to determine wind drift, select a landing area, and control the vehicle to that area. Except for instances where wind drift near the ground was difficult to determine due to lack of a reference point, they were able to land into the wind. Typical ground tracks of the Fort Hood Military Reservation tests are shown in figures VII-12 to VII-15.

In the course of the tests, several factors were brought out that indicated areas that require improvement prior to further testing. As stated before, wind drift was difficult to determine near the ground when no land reference points were available. It is recommended that, in areas where ground guidance and advice is available, the approach to the landing area should be selected such that turns are not required below 500 feet except to miss local obstacles. For landings without ground guidance, a compass or heading indicator should be included in the spacecraft so that the vehicle could be turned into the wind prior to touchdown. The wind direction could be considered as constant from the last wind obtained from the ground observation reference points, or obtained from a ground meteorology station. An altimeter should be included to give the pilot an indication of the height above the ground and the maneuvering time remaining.

Another factor involved in wind-drift determination is Para-Sail trim. Throughout the test series, various degrees of turn were built into the Para-Sail due to misrigging. Since a straight course could not be maintained, wind-drift determination was extremely difficult. The control system was such that when the system was activated, full turn was attained and when released the control lines returned to a neutral position. A proportional control system or

one with a trim capability would allow the controller to trim the system to straight flight.

These tests did not exactly duplicate the design parameters of the Para-Sail due to weight limitations of the vehicle and the parachute tested. The desired descent rate was 30 ft/sec, whereas the actual descent rate attained was approximately 20 ft/sec. This reduced descent rate lowered the capability of the system to negate the wind component; however, it increased the descent time and thereby gave the controller more time to determine wind drift and select a landing area. The system was hampered by a degradation in presentation due to the inherent resolution problem of using a noncolor television system. Resolution and obstacle detection could be greatly improved with the use of a clear optical system rather than a television camera. However, it was demonstrated that, even with the shortcomings mentioned and the lack of altitude and heading references, the landing task could be accomplished successfully. Any improvement to the system would add to the overall capability of the Para-Sail, simplify the pilot task requirements, and thus improve the accuracy of the landings.

The Para-Sail has the capability of variable L/D, although this capability was not used during this test program. Very little testing has been done to evaluate the effects of variable L/D except that of closing both turn vents simultaneously and thereby reducing the L/D. The advantage of having a variable L/D would be the capability to reduce forward motion just prior to landing and thus reduce the chances of tumbling. Further testing of visual-reference systems and operational landing problems should include a variable L/D capability so that the potential of the Para-Sail concept can be fully investigated.

CONCLUSIONS AND RECOMMENDATIONS

It was demonstrated that with the visual reference system tested, wind drift could be determined, a suitable landing area could be selected, and a gliding parachute could be controlled to the selected area. Also, visual control could be established at altitudes to 10 000 feet, and wind drift could be determined readily at altitudes below 6000 feet.

It is recommended that a system to be used for visual reference in conjunction with a controllable gliding parachute should include the following capabilities.

1. A field of view that would encompass as much of the attainable landing area as practical. (Min $\pm 30^\circ$ to the side, 10° beyond the no-wind point, and 30° behind the straight down point.)

2. Resolution sufficient to define major obstacles at altitudes to 10 000 feet and local obstacles at lower altitudes in time to avoid them.

3. A simple reticle showing the no-wind landing point and the point directly beneath the vehicle plus a crosshair arrangement for wind determination, similar to reticle 1 in figure VII-3.

4. An altimeter and compass, or heading indicator.

A need for further testing is indicated which, in addition to including an altimeter and heading indicator, should include:

1. Proportional control and/or trim capability for the parachute.

2. Study of the effects of variable L/D.

NASA-S-66-10290 OCT 24

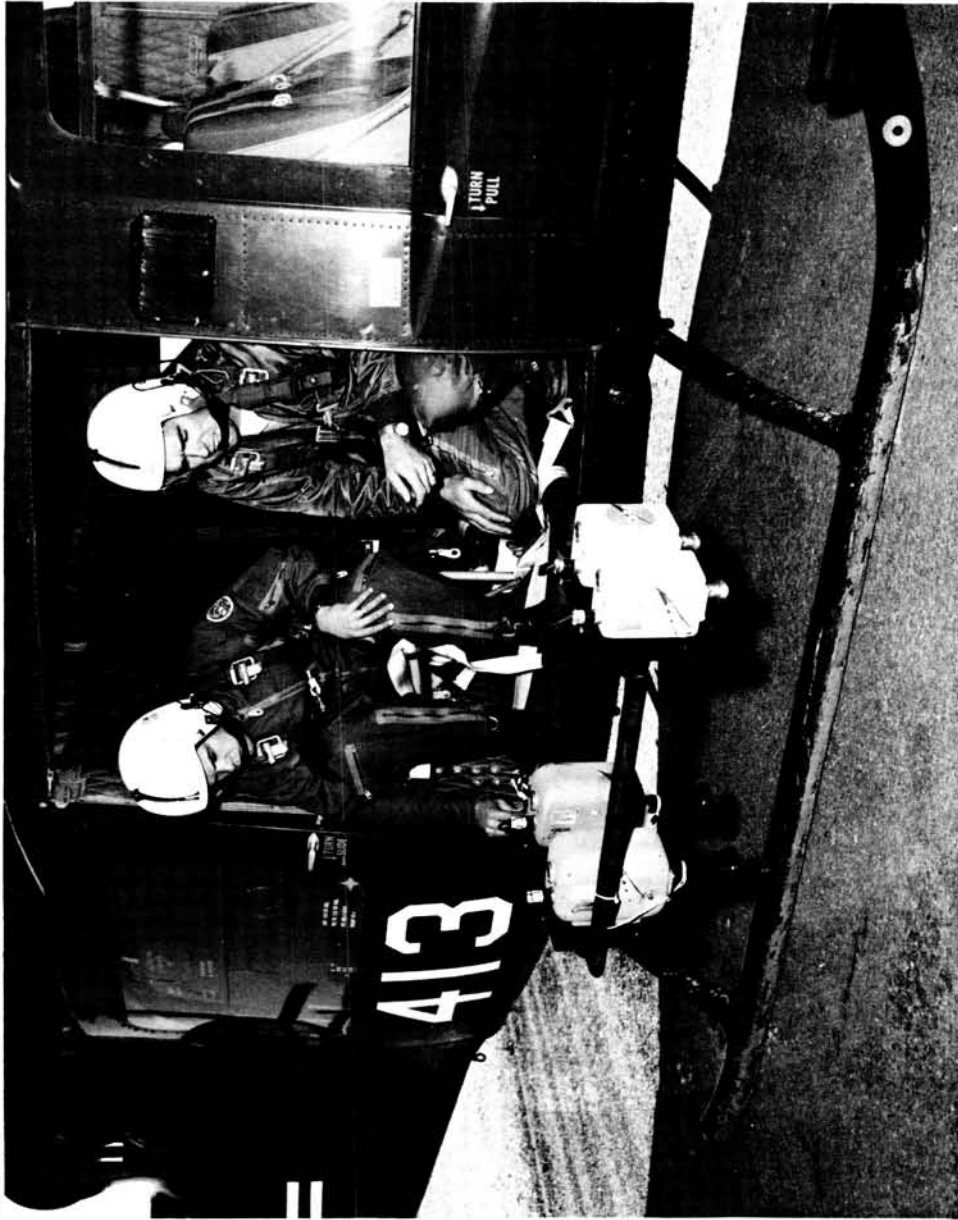


Figure VII-1.- UH-1 helicopter showing camera attachments.

NASA-S-66-10291 OCT 24

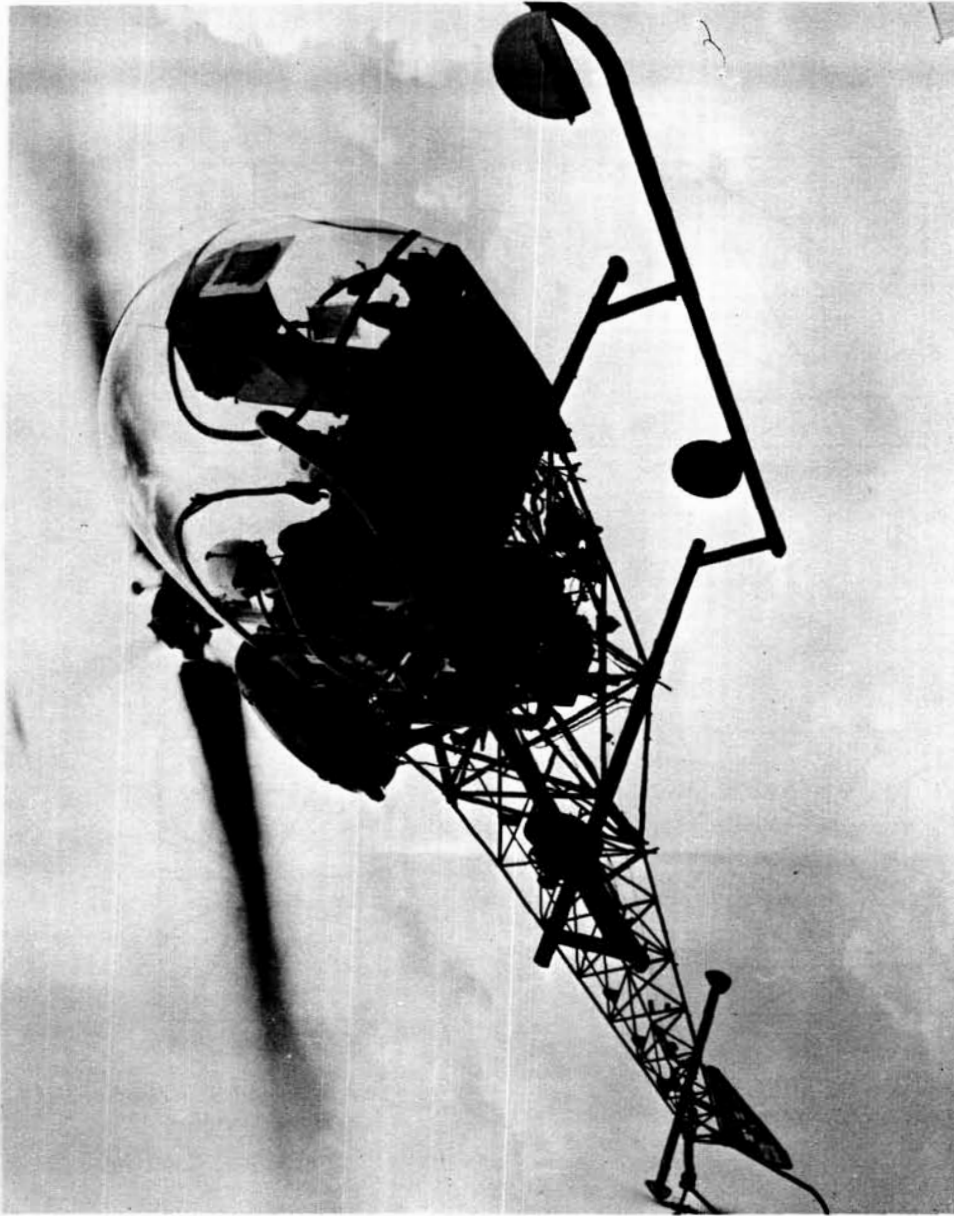


Figure VII-2.- H-13 helicopter with fiber-optics bundle and glide-angle indicator.

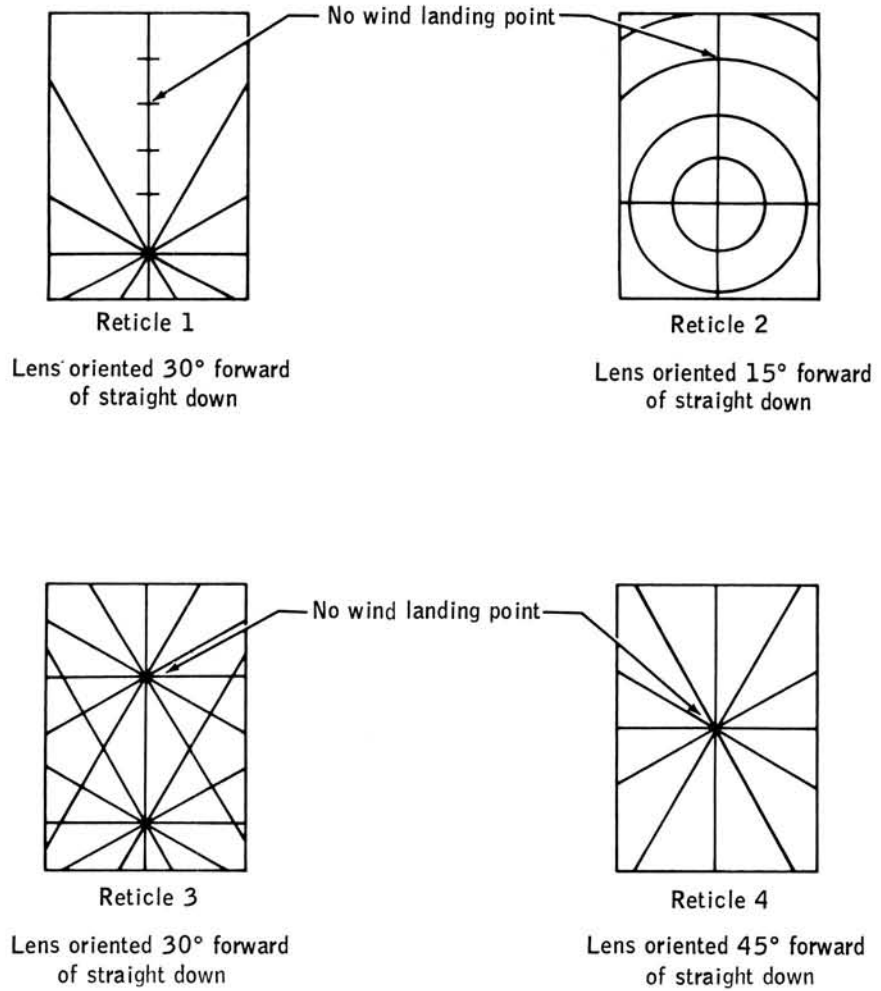


Figure VII-3.- Examples of reticles investigated.

NASA-S-66-10293 OCT 24

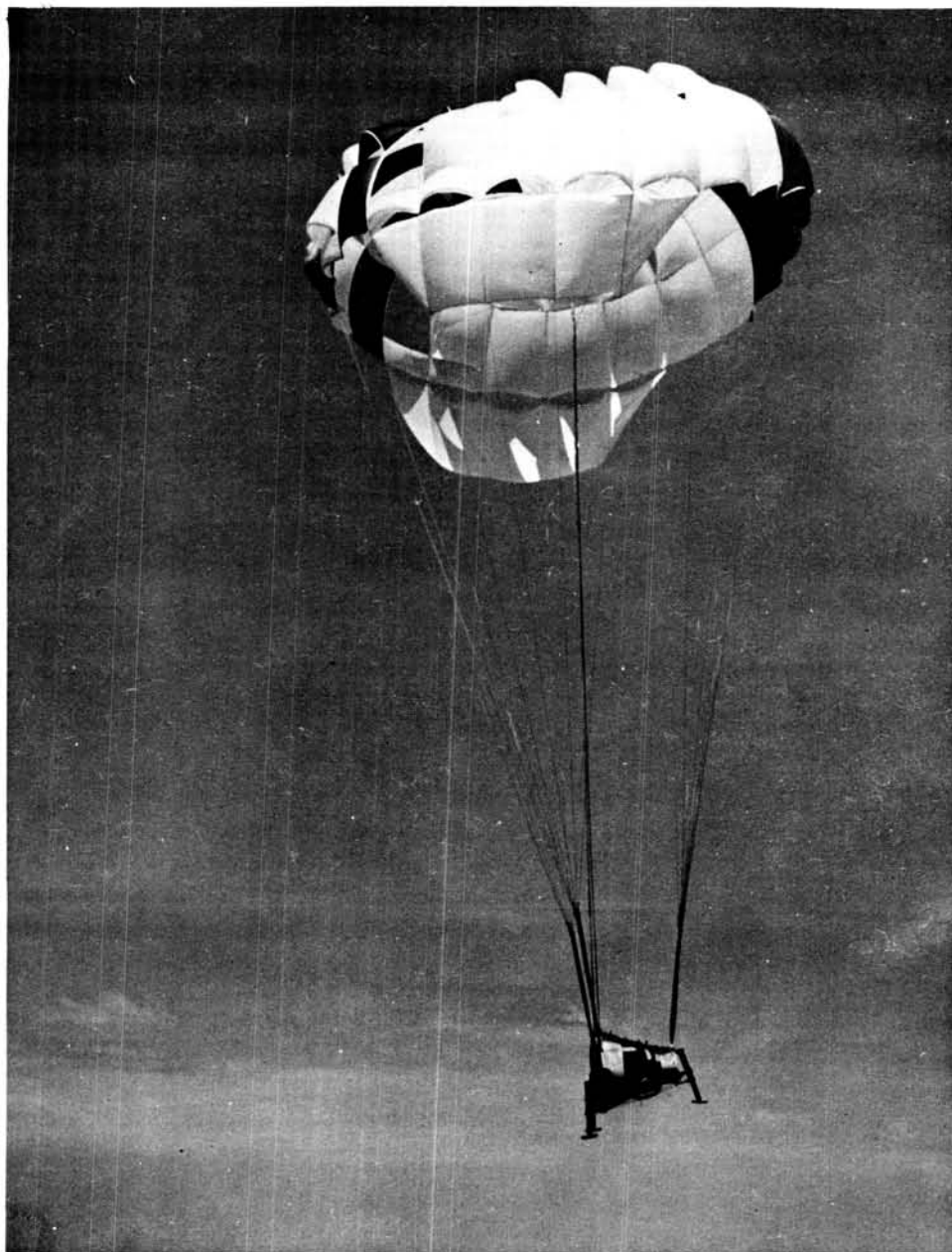


Figure VII-4.- One-third-scale Gemini spacecraft Para-Sail vehicle with television camera.

NASA-S-66-10294 OCT 24



Figure VII-5.- One-third-scale Gemini spacecraft vehicle attached to a UH-1 helicopter.

NASA-S-66-10295 OCT 24

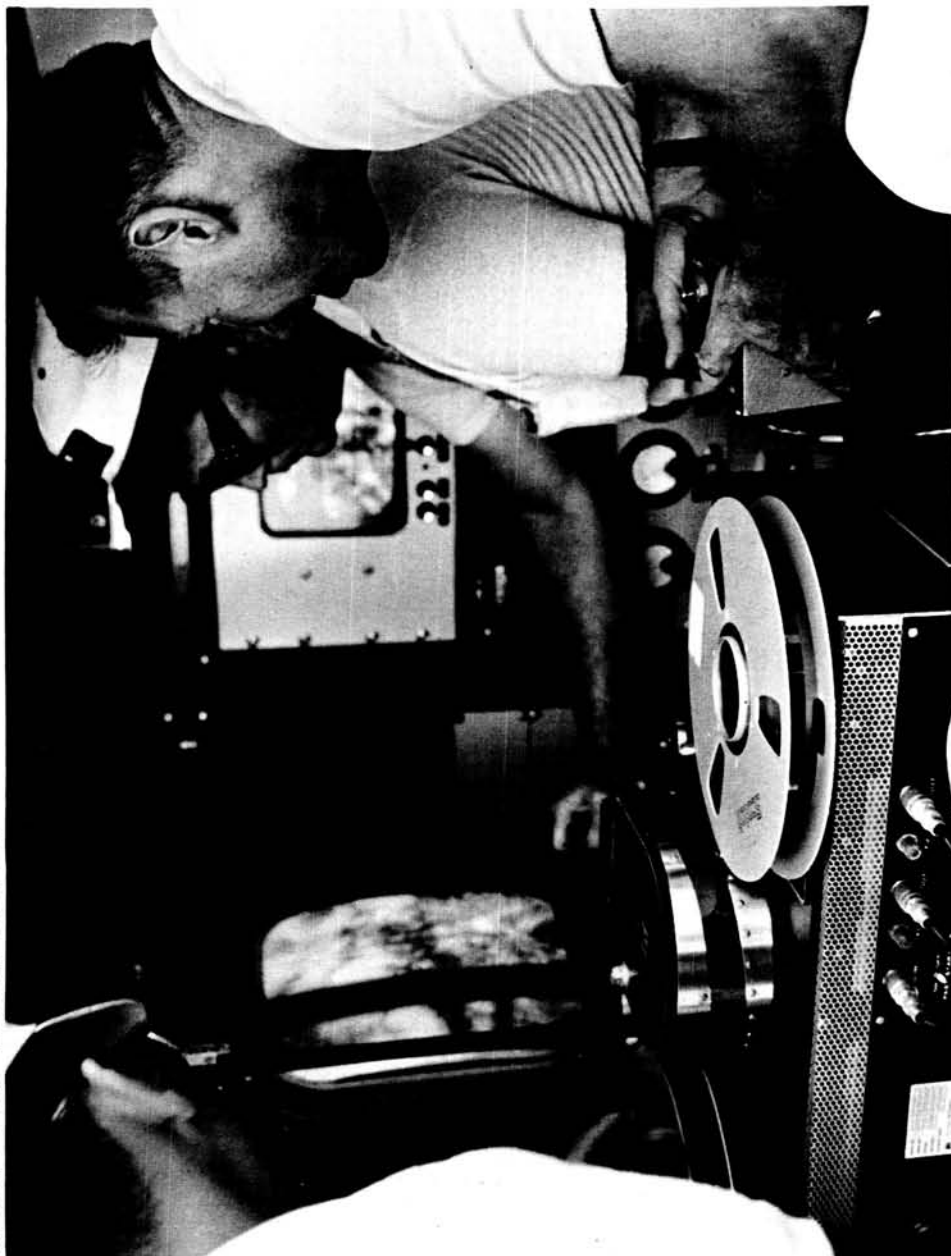
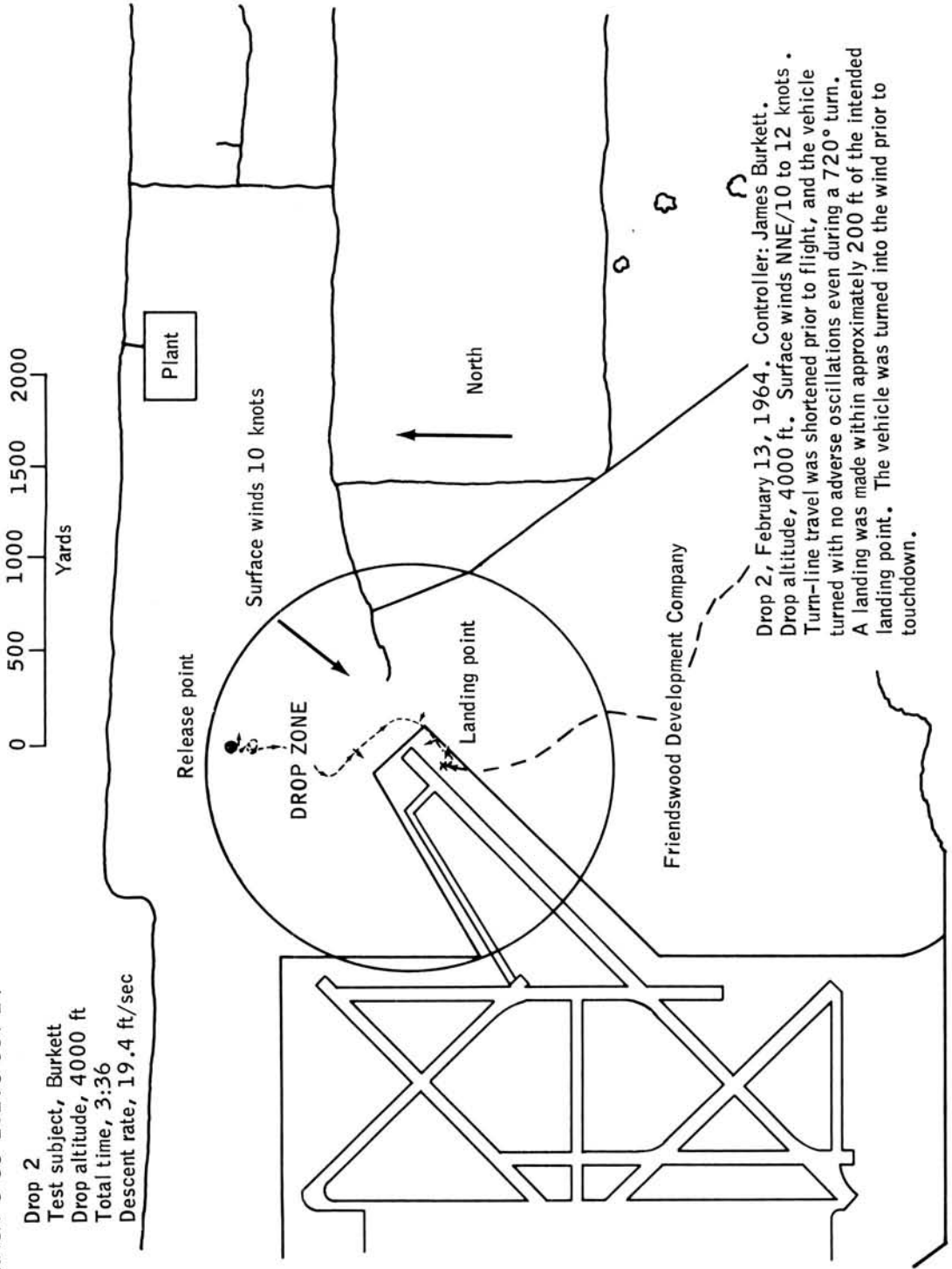


Figure VII-6.-Internal view of Para-Sail control van showing television monitor, control box, and video-tape recorder.

NASA-S-66-10296 OCT 24

Drop 2
 Test subject, Burkett
 Drop altitude, 4000 ft
 Total time, 3:36
 Descent rate, 19.4 ft/sec



Drop 2, February 13, 1964. Controller: James Burkett.
 Drop altitude, 4000 ft. Surface winds NNE/10 to 12 knots.
 Turn-line travel was shortened prior to flight, and the vehicle
 turned with no adverse oscillations even during a 720° turn.
 A landing was made within approximately 200 ft of the intended
 landing point. The vehicle was turned into the wind prior to
 touchdown.

Figure VII-7.- Typical ground track (Ellington Air Force Base, Texas).

NASA-S-66-10297 OCT 24

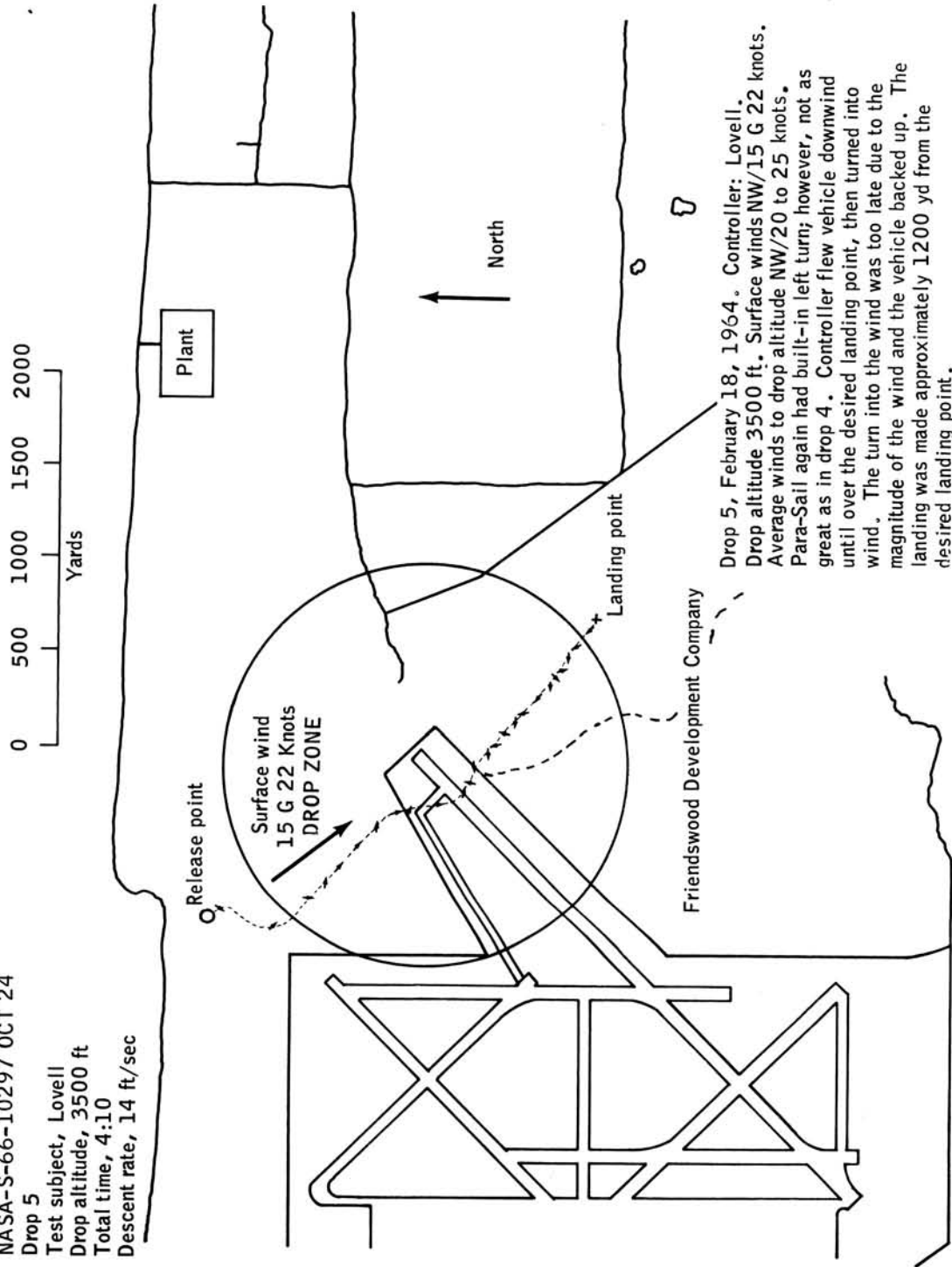
Drop 5

Test subject, Lovell

Drop altitude, 3500 ft

Total time, 4:10

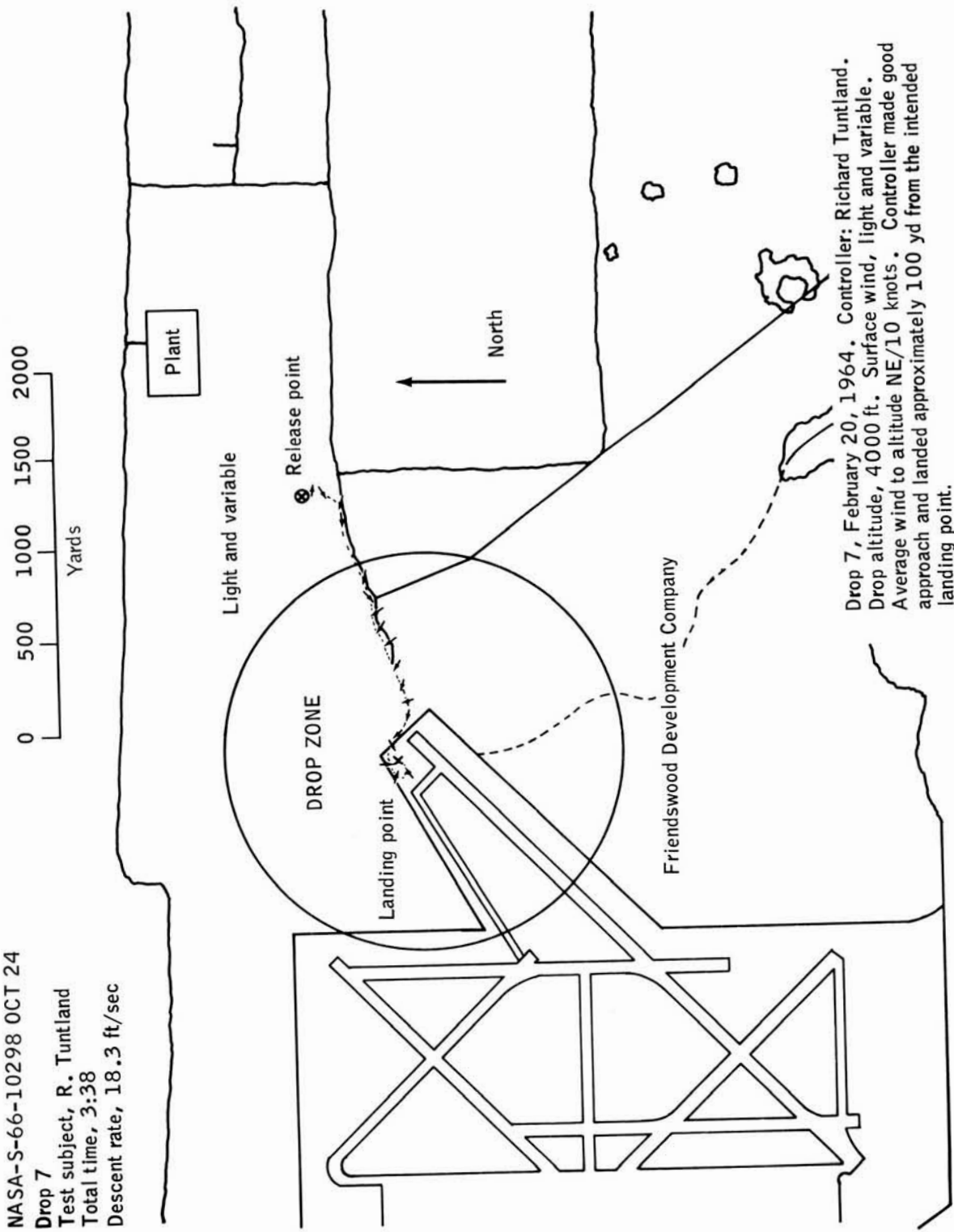
Descent rate, 14 ft/sec



Drop 5, February 18, 1964. Contoller: Lovell.
Drop altitude 3500 ft. Surface winds NW/15 G 22 knots.
Average winds to drop altitude NW/20 to 25 knots.
Para-Sail again had built-in left turn; however, not as great as in drop 4. Contoller flew vehicle downwind until over the desired landing point, then turned into wind. The turn into the wind was too late due to the magnitude of the wind and the vehicle backed up. The landing was made approximately 1200 yd from the desired landing point.

Figure VII-8.- Typical ground track (Ellington Air Force Base, Texas).

NASA-S-66-10298 OCT 24
 Drop 7
 Test subject, R. Tuntland
 Total time, 3:38
 Descent rate, 18.3 ft/sec



Drop 7, February 20, 1964. Controller: Richard Tuntland.
 Drop altitude, 4000 ft. Surface wind, light and variable.
 Average wind to altitude NE/10 knots. Controller made good approach and landed approximately 100 yd from the intended landing point.

Figure VII-9.- Typical ground track (Ellington Air Force Base, Texas).

NASA-S-66-10299 OCT 24
 Drop 8
 Test subject, Lovell
 Drop altitude, 4000 ft
 Time, 3:49
 Descent rate, 17.5 ft/sec

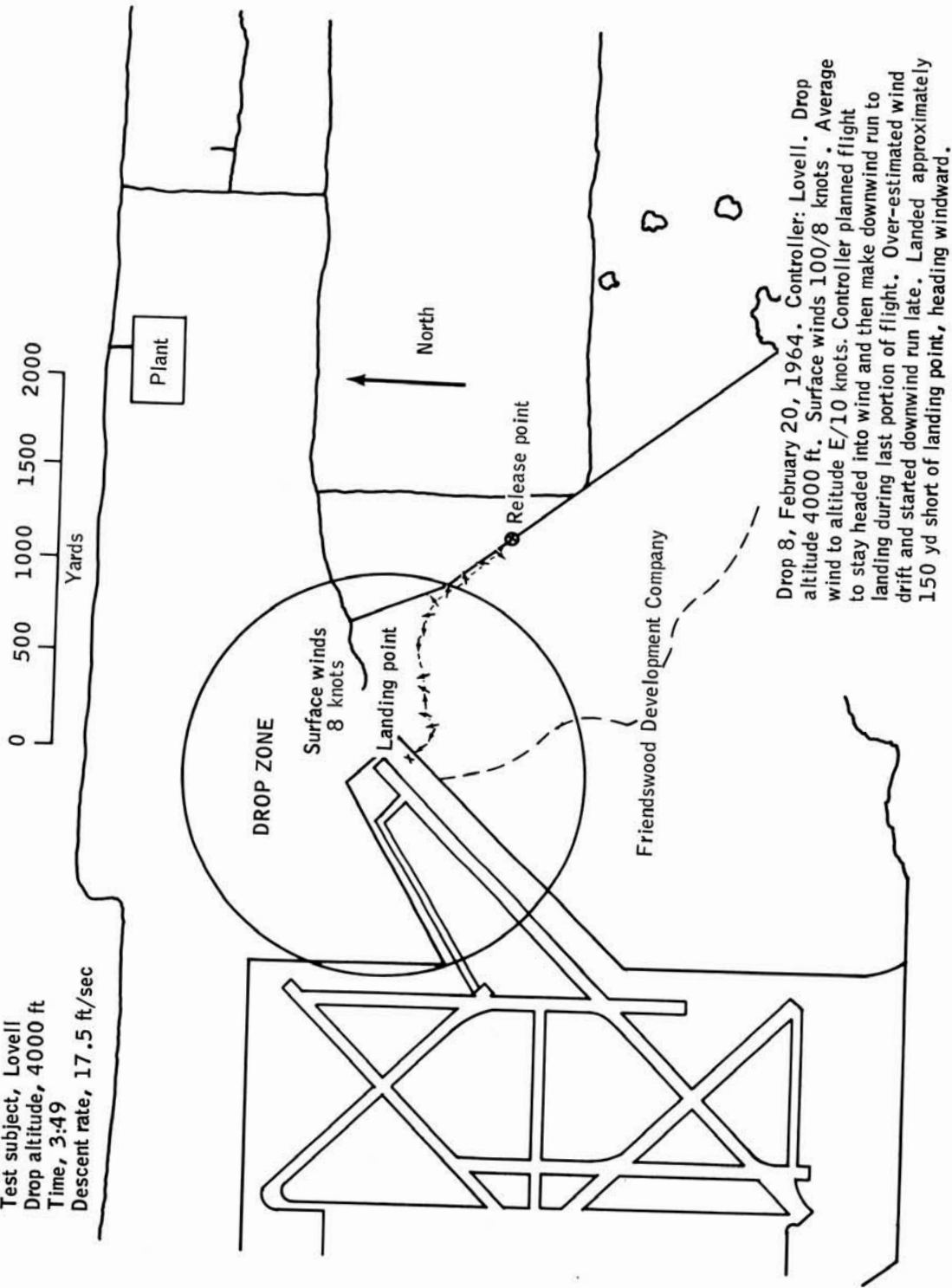
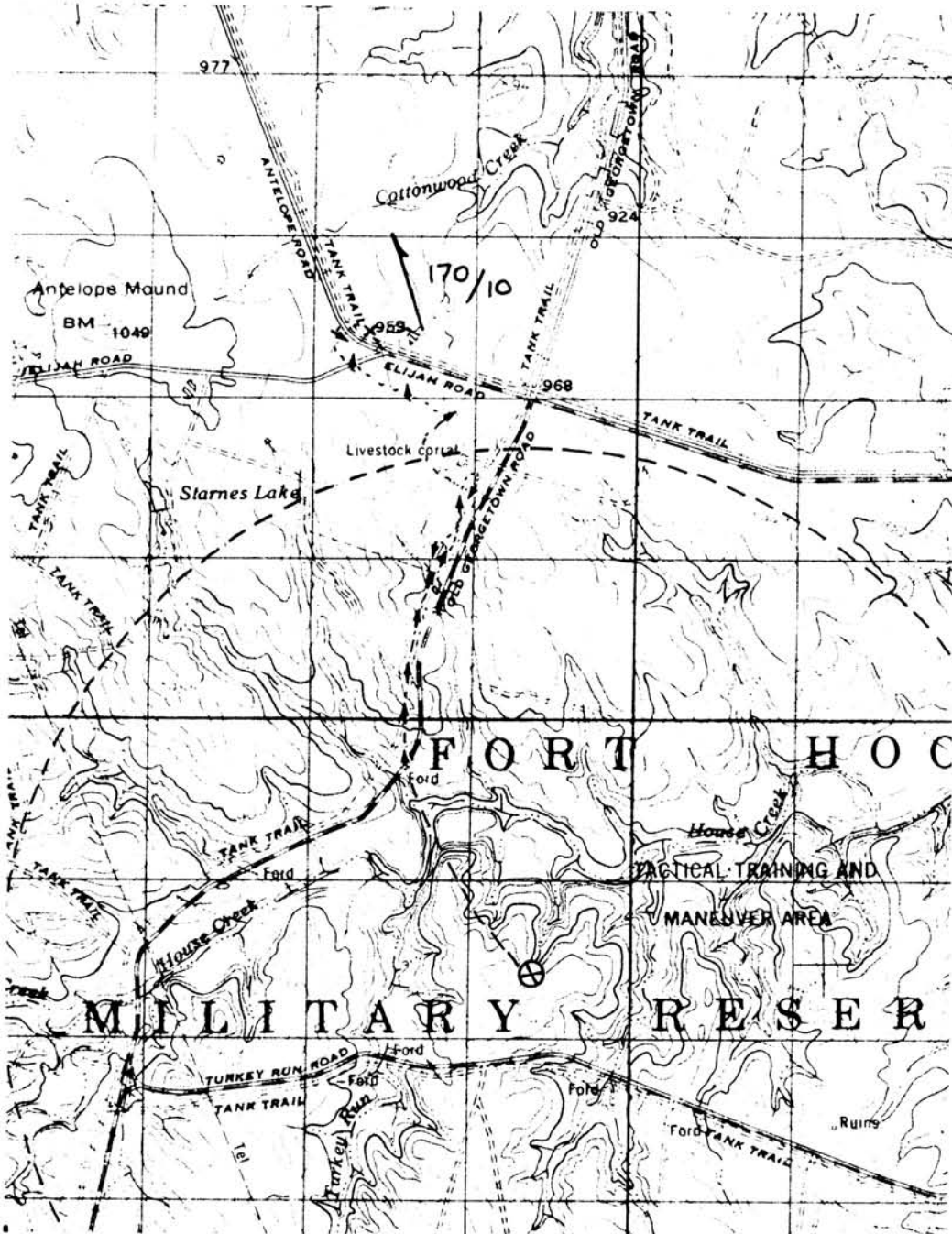
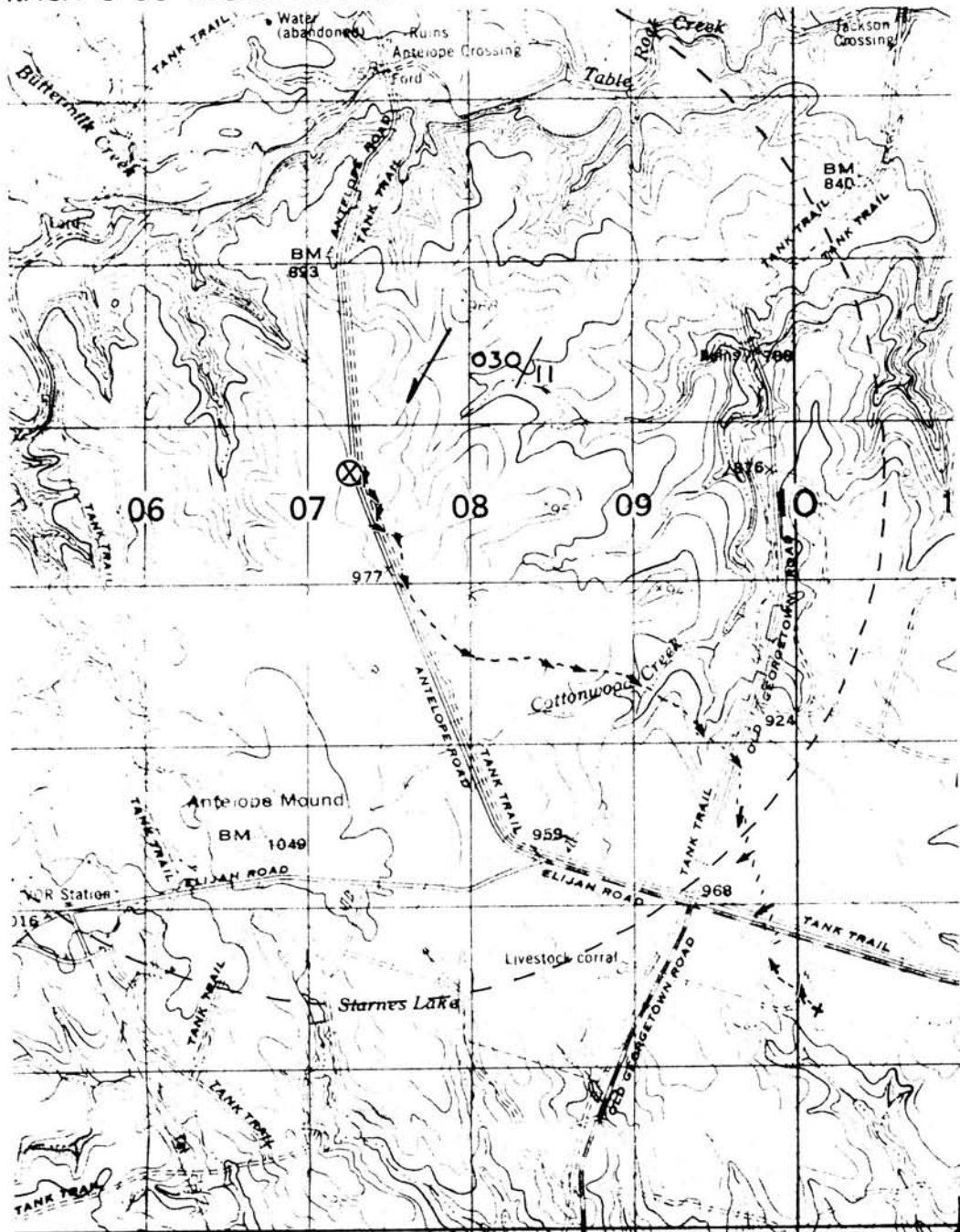


Figure VII-10.- Typical ground track (Ellington Air Force Base, Texas).



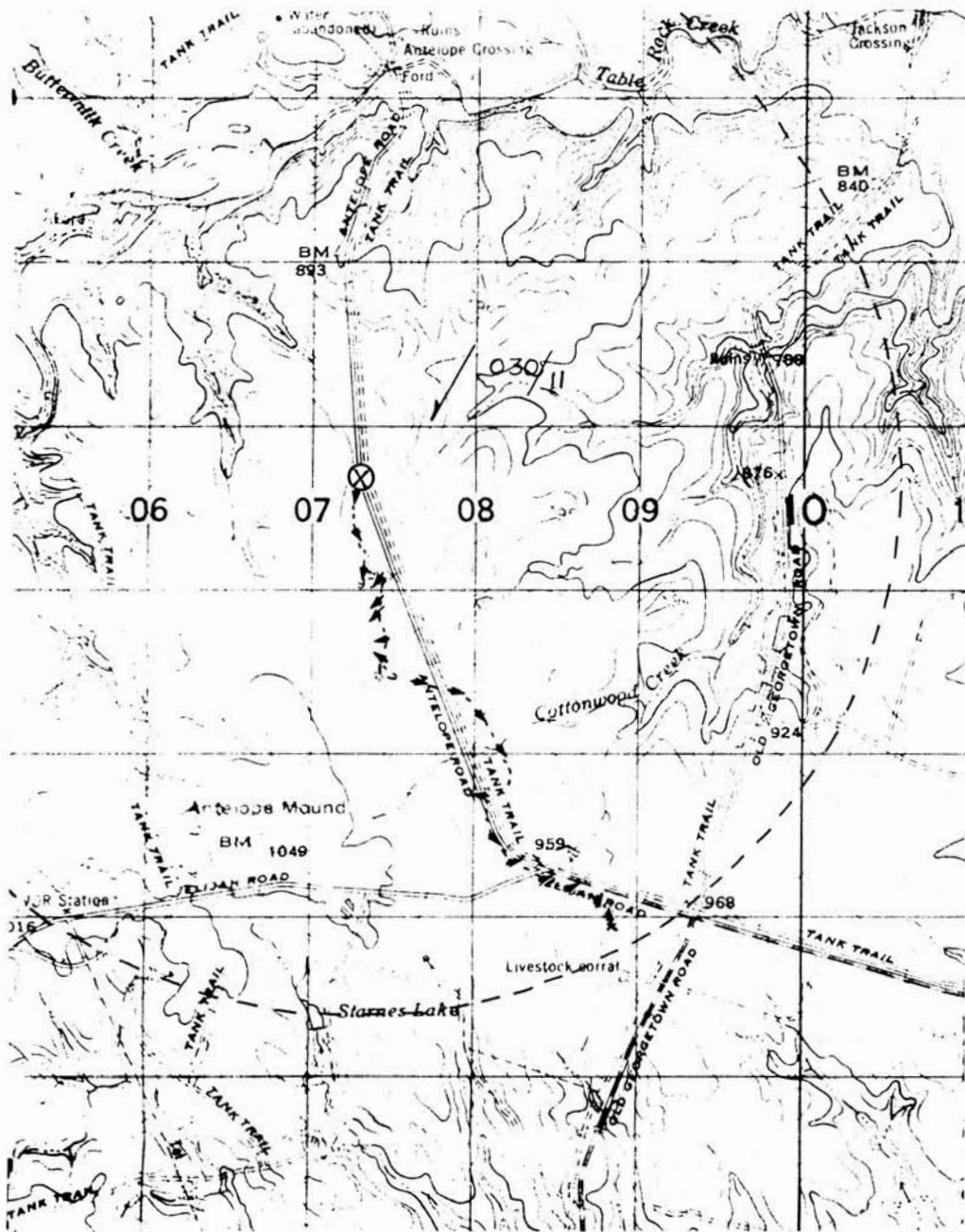
- | | |
|--------------------------|--|
| 1. ⊗ Release point. | 4. Dashed line shows ground track. |
| 2. x Impact point. | 5. Circle represents area attainable from 10 000 ft altitude, no wind. |
| 3. → Direction of flight | |

Figure VII-12.- Typical ground track (Fort Hood Military Reservation, Texas).



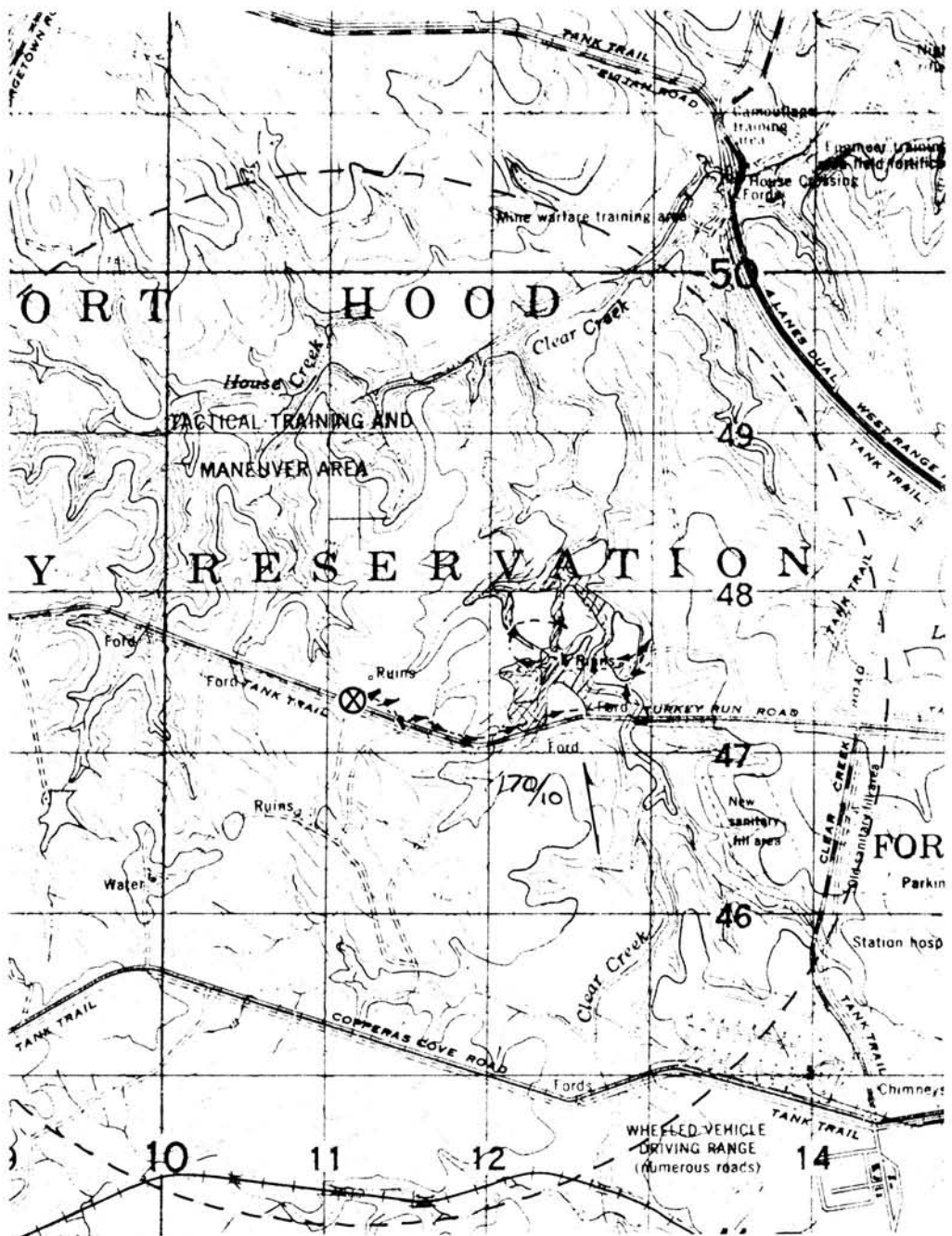
- | | |
|---|---|
| <p>1. ⊗ Release point.</p> <p>2. x Impact point.</p> <p>3. → Direction of flight.</p> | <p>4. Dashed line shows ground track.</p> <p>5. Circle represents area attainable from 10 000 ft altitude, no wind.</p> |
|---|---|

Figure VII-13.- Typical ground track (Fort Hood Military Reservation, Texas).



- | | |
|---------------------------|--|
| 1. ⊗ Release point. | 4. Dashed line shows ground track. |
| 2. x Impact point. | 5. Circle represents area attainable from 10 000 ft altitude, no wind. |
| 3. — Direction of flight. | |

Figure VII-14.- Typical ground track (Fort Hood Military Reservation, Texas).



- | | |
|---------------------------|--|
| 1. ⊗ Release point. | 4. Dashed line shows ground track. |
| 2. x Impact point. | 5. Circle represents area attainable from 10 000 ft altitude, no wind. |
| 3. → Direction of flight. | |

Figure VII-15.- Typical ground track (Fort Hood Military Reservation, Texas).

SECTION VIII - GEMINI FLIGHT-TEST VEHICLE
FOR PARA-SAIL/LANDING-ROCKET DEVELOPMENT PROGRAM

By Thomas M. Grubbs, Sr.

PRECEDING PAGE BLANK NOT FILMED.

GEMINI FLIGHT-TEST VEHICLE FOR PARA-SAIL/LANDING- ROCKET DEVELOPMENT PROGRAM

By Thomas M. Grubbs, Sr.
Manned Spacecraft Center

INTRODUCTION

Forty-one test hardware items were designed, manufactured, and developed to meet the specific needs of the full-scale test program. This section provides a brief description of the physical and operating characteristics of the more important of these items. Verification tests were conducted where required and are discussed in Section IX.

TEST VEHICLE

A flight-test vehicle to simulate the Gemini spacecraft reentry vehicle was required in support of the Gemini oriented Para-Sail landing-rocket program. The vehicle used in the program was a boilerplate model fabricated in Houston, Texas, from mild cold-rolled steel, which was originally designed for Gemini spacecraft flotation studies. The boilerplate was converted to its present configuration in the NASA MSC shops.

Structural modifications included those installations which required cutting and welding to the basic vehicle; and nonstructural modifications included brackets required for installation of flight equipment (cameras, instrumentation, landing gear, and so forth). In building up the boilerplate for the test series, it was required that certain flight components (altitude sensor, separation switch, and so forth) be designed and built at MSC.

The structural modifications, the nonstructural modifications, and the flight components designed and/or fabricated in Houston are briefly described and illustrated in this report. The exterior dimensions and nomenclature used for the boilerplate are shown in figure VIII-1. Basic structural modifications are shown in the remaining illustrations.

EXTERIOR MODIFICATIONS OF THE GEMINI SPACECRAFT BOILERPLATE

The following modifications are presented together because they are permanently attached to the exterior of the boilerplate (figs. VIII-2 and VIII-3). The purpose of each modification is included in the brief description:

1. Two arming-bar wells and one umbilical well, each 5 inches in diameter, were recessed so that the arming bars and umbilical plug would not extend past the outer mold line of the vehicle. The wells were permanently welded in the pressure vessel.
2. An arming-bar box was installed to supplement the arming-bar wells. This installation was a recessed box with positions for 12 Deutsch connectors for arming the various pyrotechnic circuits. The box was accessible when the vehicle was in the drop cradle. A cover was fitted to the contour of the skin and was held in place with four one-quarter-turn fasteners which allowed rapid and easy access to the panel. The box was a welded installation. The plate which held the 12 Deutsch connectors was removable.
3. Riser rip-out channels permitted the parachute risers to be stowed flush with the outer mold line (OML). The risers were held in place with 80-pound breakcord on 6-inch centers. The rip-out channels formed an inverted T along the OML at top Y. At configuration change these risers were extracted and the vehicle pitched over to the flying configuration. The rip-out channels were a permanent welded installation.
4. Side attach-point wells were installed for recessing the parachute side-attach load cells and release hardware. These wells were located about 2 inches forward of the heat shield and about 10 inches above the left and right X-axes. The recess was large enough to enable the load cell and disconnect to be stowed inside the projected mold line of the boilerplate.
5. A top Y recessed attach-point well was welded in the rip-out channel at station Z 115.43. This well provided for a flush installation of the disconnect and for storage of the load cell. The attachment brackets for the load cell were precisely aligned to insure proper operation of the load cell.
6. Hatch windows were installed to duplicate the size, shape, and location of the flight spacecraft. The window was made of clear plastic and was bolted in place. Gaskets were provided to make the installation airtight. Both crew hatches were equipped with the windows.

7. Clear plastic windows were provided for the three cameras that were located inside the pressure vessel. The windows were bolted to a permanently welded flange. Rubber gaskets were provided to prevent leakage.

RENDEZVOUS AND RECOVERY CANISTER

Purpose

A primary function of the R and R canister was to store the main Para-Sail parachute. A drogue-stabilization parachute was attached to the top of the R and R canister. After the boilerplate had fallen clear of the drop aircraft and had been stabilized by the drogue parachute, the R and R canister was mechanically released from the boilerplate. The drag of the drogue parachute caused separation. As separation occurred, the main parachute was pulled from its storage cavity in the R and R canister. The drogue parachute lowered the R and R canister so that it could be recovered, refurbished, and reused.

Description

The R and R canister was an all aluminum structure. The skin was 1/16-inch aluminum sheeting riveted to the frame structure. The storage cavity for the Para-Sail parachute was welded inside the structure. The cavity was a cylindrical canister which measured 24 inches inside diameter by 22.69 inches in length (fig. VIII-4).

The R and R canister was locked to the vehicle with two pivoted over-center links (fig. VIII-5) which extended past the parting line and engaged the release mechanism in the Gemini spacecraft boilerplate (fig. VIII-6). These links were adjusted to secure a tight fit between the R and R canister and the Gemini spacecraft boilerplate.

The drogue parachute loads were transferred from the top of the R and R canister to the overcenter links by means of two aluminum channels.

All unused space in the R and R canister was filled with foam which caused the canister to float when dropped in water.

RENDEZVOUS AND RECOVERY RELEASE MECHANISM

Purpose

The R and R canister was securely locked to the Gemini spacecraft boilerplate at the time it was released from the drop aircraft. After the boilerplate had cleared the aircraft, a drogue parachute was deployed to stabilize the fall. It was the function of the R and R release mechanism to initiate separation of the R and R canister from the boilerplate. The R and R release mechanism had to be able to withstand the opening shock load of the drogue parachute.

Description

The release mechanism was mounted in the forward end of the Gemini spacecraft boilerplate within the first 5 inches adjacent to the parting line between the R and R canister and the boilerplate (fig. VIII-6). The release mechanism was actuated by two pyrotechnic squibs fired simultaneously. Either squib was capable of initiating separation. The mechanism consisted of two pivoted dogs mounted diametrically opposite each other. One end of each of the dogs latched on to the overcenter links which extended down from the R and R canister. The other ends of the dogs were connected to each other through a linkage across the diameter of the boilerplate. The linkage was a three-piece member which was held together with two shear pins. One end of each shear pin was open while the other end was enclosed with the pyrotechnic gas generator. Upon the signal to release, the gas generator was ignited; the pins were forced free; and the linkage was separated. The dogs were then free to pivot and release the R and R canister links, and the drogue parachute pulled the R and R section from the boilerplate.

RESERVE PARACHUTE INSTALLATION

Purpose

A standard ringsail parachute was used as a backup for the Para-Sail parachute. This parachute was located in the forward cylindrical section of the Gemini spacecraft boilerplate. A radio signal from the ground separated the main parachute and activated the parachute extraction gun which initiated the deployment of the reserve parachute system.

Description

The parachute was stored in a wedge-shaped aluminum canister. The canister was rigidly attached to the inside of the cylindrical section of the Gemini spacecraft boilerplate between stations Z 160 and Z 192 (fig. VIII-7). Once the canister was in place, an aluminum fairing was placed between the parachute canister and the nose landing gear. This fairing prevented the emergency parachute from snagging on the nose landing gear (NLG) when it was deployed. The NLG was fitted with a bracket which held the extraction parachute gun. The emergency parachute did not release automatically on impact as did the main parachute.

MAIN LANDING-GEAR INSTALLATION

Purpose

The production Gemini spacecraft landing gear was used on the boilerplate in the Para-Sail landing-rocket program. The basic boilerplate had to be reworked to provide the necessary hard points and bracketry to adapt the production landing gear.

Description

The main landing gear (MLG) was installed with three mating brackets (fig. VIII-8). These brackets were very similar to the brackets designed by McDonnell Aircraft Corporation for the Gemini spacecraft. The brackets, weldments of high-strength steel, were machined to McDonnell Aircraft Corporation tolerances. The brackets were attached with high-strength bolts and press-fitted dowel pins.

The structural modification to the boilerplate consisted of mild steel plates welded to the inside of the landing-gear bay and to the inside of the pressure vessel. These plates sustained the landing loads and limited the structural deflection. Warping and distortion during construction and during rework for MLG hard points made it necessary to hand fit all brackets.

NOSE LANDING GEAR

Purpose

The Gemini spacecraft production nose landing gear (NLG) was used in the Para-Sail landing-rocket program. Due to the location of the main parachute attach point on the gear, the top Y-bracket took about 80 percent of the parachute opening load. Installation of the NLG required three brackets and structural modification to the capsule.

Description

The NLG attachment points were T-shaped with the single end at top Y and the ends of the T at lower Y, left and right X-coordinates. The three brackets used to install the NLG were similar to the McDonnell Aircraft Corporation brackets with some exceptions (fig. VIII-9). The bracket at lower Y right X served the dual purpose of NLG attach point and as a pivot point for the R and R canister release mechanism. The brackets were made of high-strength steel and were hand fitted to the capsule. Installation was made with a combination of high-strength bolts and dowel pins.

INSTRUMENTATION INSTALLATION

Purpose

The purpose of the instrumentation mounting surfaces was to provide attachment for equipment so that: (1) accelerometers and rate gyroscopes were as near the capsule center of gravity as possible, (2) all equipment was mounted securely, (3) individual components were easily removed, and (4) individual components were accessible for adjustment while operating with the rest of the equipment.

Construction

Onboard instrumentation was mounted in one of four ways. Accelerometers and rate gyroscopes were mounted on a 4-inch-wide flange beam that was welded inside the pressure vessel. The longitudinal axis of the beam coincided with the Z-axis of the Gemini spacecraft boilerplate. The sensing elements were grouped as close to the Z center of gravity as possible.

Much of the pyrotechnic sequencing system was mounted directly to the interior of the pressure vessel. Holes were drilled and tapped into the bulkheads. After the equipment was in place the holes and protruding bolts were covered with a potting compound in order to maintain an airtight pressure vessel.

The remaining equipment was mounted on four removable pallets (fig. VIII-10), which allowed the equipment to be mounted in a breadboard fashion.

DEHAVILLAND ALTITUDE-SENSOR INSTALLATION

Purpose

The purpose of the deHavilland altitude sensor was to fire the landing rockets at a preselected altitude and to decelerate the boilerplate so that it was within the velocity capability of the landing gear.

Description

The Landing Technology Branch of MSC purchased an extendible boom altitude sensor from deHavilland Aircraft of Canada. The deHavilland sensor was unlike the interim pendulum altitude sensor and could be man-rated. Redundancy in altitude sensing was accomplished by using two identical deHavilland assemblies mounted in separate containers.

The two deHavilland sensors were mounted at Station 121 (fig. VIII-11). The boom centerline of the sensors was pitched forward 13° off the Y-axis. The booms were mounted with a 15° included angle. The installation consisted of a trough-shaped box made from 5/32-inch steel plate on the sides and 1/4-inch steel plate on the back surface. The trough was recessed so the sensor containers were flush with the outer mold line.

ZERO ALTITUDE SENSOR

Purpose

The purpose of the zero altitude sensor was to indicate to the onboard control system that the capsule was in the water. Once this signal was

received, a command was sent to disconnect the parachute and to make the boilerplate watertight.

Operation

The zero altitude sensor consisted of three main parts: two brass electrodes and the body (fig. VIII-12(a)). The body was made of clear plastic. The brass electrodes were 3/4-inch diameter and were threaded. The threads mated with the threads in the body and were so oriented that the electrodes lay on the same axis. The threads allowed for adjustment of the gap between the ends of the electrodes. A 24-volt source was applied across the ends of the electrodes and in series with the pyrotechnic circuit that initiated parachute release. When the electrodes were immersed in salt water, sufficient current was established to fire the pyrotechnic circuit. This sensor was used for water drops only.

INTERIM ALTITUDE SENSOR

Purpose

The purpose of this interim altitude sensor was to signal the onboard control system that the Gemini spacecraft boilerplate was a prescribed distance above the landing surface; nominally this height was 7 to 10 feet. This sensor was not man-rated nor was any attempt made to man-rate it. This particular design was an interim step between no altitude sensor and one that would be eventually man-rated.

Operation

The basic sensor consisted of a convex cone mated with a concave cone (fig. VIII-12(b)). These cones were linked together with a shoulder bolt which allowed a small amount of relative motion in all directions. Snap-action miniature switches were mounted so that their plunger extended into the void between the mated cones. Upon impact with the landing surface, the cones were driven together, the switch plungers were displaced, and the required signal was generated. The miniature switches were grouped in two sets of three each. The actuation of any one switch in either group was sufficient to send the required signal.

The basic sensor assembly was suspended beneath the boilerplate by the electrical conductor which carried the signal. The length of the conductor determined the altitude at which the signal was generated.

The sensor was stored in a well which was flush with the outer mold line of the boilerplate. The sensor was not deployed until after the Gemini spacecraft boilerplate had gone through the attitude change, at which time a pyrotechnic device released the strap which held the sensing head in place. Free fall of the head was restricted by winding the electrical conductor on a spinning-rod-type drum that slowed the line payout.

Twenty seconds after deployment the sensor circuit was checked to determine if it was open. If the circuit was open, the sensor was then connected into the retrorocket firing circuit. If the circuit was closed, the altitude sensor was not connected to the retrorocket circuit.

SEPARATION SWITCH

Purpose

For reasons of safety, the onboard sequencing was not started during each drop until after the boilerplate had been released and was moving down the launch cradle. The signal to start the onboard sequence was initiated by a separation switch after the capsule had moved approximately 12 inches.

Description

The separation switch consisted of a steel housing welded to the capsule, a group of snap-action switches, a phenolic slide block, and an 18-inch nylon lanyard (fig. VIII-13(a)). The switches were spring loaded in the closed-circuit position. These switches were mounted to the housing with their actuators on the inside. The slide block was pushed into the housing depressing all the switches and thus opening the circuits. The lanyard was tied to the cradle and the phenolic slide block. As the boilerplate slid down the cradle, the normally slack lanyard tightened and removed the slide block. The switches snapped shut and the sequence was started. Four switches were used to isolate the various circuits. The switches were used in the following manner: (1) one switch was a spare, (2) two switches (for redundancy) were used to start the pyrotechnic system, and (3) one switch was used to start the onboard cameras.

RETRACTABLE ATTACH POINT

Purpose

Immediately prior to launch from the aircraft, the boilerplate was retained by a single attach point. Due to the configuration of the release mechanism, it was necessary that this attach point would extend well beyond the outer mold line of the boilerplate. Some means were required to retract this attach point immediately after the boilerplate was released to prevent its hitting the drop cradle during launch or snagging some portion of the parachute.

Description

A hook eye was attached to a rod which was inserted in a cylinder where a large spring acted against the end of the rod, spring loading it in the retracted position (fig. VIII-13(b)). When the hook eye was attached to the release mechanism on the cradle, the rod pulled out compressing the spring until an enlarged diameter of the rod bottomed out on the forward end of the cylinder. When the hook was released, the spring quickly retracted the hook to a position inside the mold line of the boilerplate.

RETROCKET ALINEMENT HARDWARE

Purpose

It was the purpose of the rocket alinement hardware to insure that the thrust vector of the retrorockets passed through the center of gravity of the boilerplate.

Description

The retrorockets were attached at both ends of the rocket casing. At the nozzle end a nipple on the casing fitted into a pivoted plate (fig. VIII-14, bottom). This plate allowed the igniter end of the rocket to pivot in and out of the surface of the boilerplate. The adjustment of screws on this plate also permitted the rocket body to be rotated about its own axis. Thus, the rocket had angular freedom in two planes. The lower swivel plate was attached to the boilerplate structure.

The rocket was restrained on the igniter end by a threaded eye bolt (fig. VIII-14, top). The eye slipped over the end of the igniter and the threaded portion mated with a positioning nut which was rigidly fastened to the boilerplate. By adjusting this nut and the screws on the plate, the rocket could be alined.

The determination of the line of action of the thrust vector was accomplished with the retrorocket alinement fixture (fig. VIII-15). This fixture consisted of a plug and a pointer. The plug was placed solidly in the retrorocket nozzle. When the plug was securely in position, the pointer duplicated the thrust vector of the rocket. A watertight panel was removed during rocket alinement to allow the pointer to extend into the pressure vessel.

BLAST DEFLECTOR

Purpose

The Gemini spacecraft boilerplate carried two solid-fuel retrorockets. The retrorockets were installed after the boilerplate had been checked out and placed in the drop aircraft. The danger of accidental ignition always existed; therefore, a rocket blast deflector was used to minimize the danger by canceling the thrust and venting the exhaust out the rear of the drop aircraft.

Operation

The blast deflector was attached to the boilerplate by three open hooks on one end and a shear pin on the other end (figs. VIII-16(a) and VIII-3). After configuration change to the flying attitude, a gas generator was ignited and the shear pin was dislodged allowing the blast deflector to swing free of the Gemini spacecraft boilerplate. A small diameter parachute was used to control the descent of the blast deflector. The blast deflector was recovered after the drop test and was reused on subsequent drops.

The blast deflector was constructed of 6-inch standard-weight steel pipe and extra strong elbows and tees (see fig. VIII-16(b)). The blast of the rocket was directed into the elbows and was carried downward parallel to the boilerplate skin where the exhaust was split by the tees and sent in opposite directions. The blast of the retrorockets was equally divided, and the resultant thrust was reduced to zero.

LOAD CELLS

Purpose

The onboard load cells measured opening parachute loads, steady-state single-point parachute loads, configuration-change transient loads, and load fluctuations during a controlled descent.

Descriptions

The load cells were built in two sizes. The large load cell was designed for loads to 20 000 pounds, and the small cells were designed for loads to 7000 pounds. Externally, both load cells were the same size. The difference was the diameter of the hole bored through the shank of the cell. The cells had a cylindrical shank with a pin connector on each end (fig. VIII-17). One pin attached to the capsule through the pyrotechnic-disconnect fitting while the other pin mated with the parachute webbing. The cylindrical shank was fitted with a small strain gage to record the load. There were four 7000-pound load cells and one 20 000-pound load cell on the boilerplate.

PARACHUTE DISCONNECT AND ATTITUDE-CHANGE MECHANISM

Purpose

The Gemini spacecraft boilerplate left the aircraft and fell heat shield first. The parachute opening loads were taken through a single attach point until the parachute had disreefed and had reached steady-state descent. The single attach point was then released and the Gemini spacecraft boilerplate pitched over approximately 100° to the flying attitude. In this configuration, the boilerplate was suspended from the parachute at six places; two points were for control lines. Upon impact with the desired landing surface, the main parachute had to be disconnected to prevent the boilerplate from being dragged by surface winds.

The purpose of the attitude-change mechanism was to release the single-point attachment and allow the boilerplate to pitch over. This function was also required to disconnect the main parachute in an emergency. The main parachute disconnects released the parachute at impact from the six attach points mentioned. In the event of main parachute failure prior to the pitch-over maneuver, a radio command to deploy the reserve system would

fire the main disconnect on the NLG and the other six attach points. After a time delay, the reserve system would then be deployed.

Description

The attitude-change mechanism was located above the large load cell that measured opening shock (fig. VIII-18). The mechanism consisted of a pivoted post that held the parachute webbing. The post was held in place with a high-strength shear pin. The signal for attitude change initiated a pyrotechnic squib which dislodged the shear pin. The post was free to rotate and released the parachute. A single squib initiated by dual bridge wires and dual firing circuits was used on this disconnect.

There were four main parachute disconnects (figs. VIII-18 and VIII-19). These were the four load carrying attach points in the flying position. (The two turn-control attach points are discussed under cablecutters.) The attach points incorporated a small diameter retaining pin in double shear. For release, the squib was fired by dual-firing circuits. The pressure generated dislodged the retaining pin and released the load-cell attachment link. The retaining pin impacted lead washers and remained within the disconnect mechanism. The load-cell instrumentation wires were connected to the Gemini spacecraft boilerplate with a quick-disconnect cannon-type plug which pulled free when the load cell was released.

TENSION-MEASUREMENT DEVICE

Purpose

In the development of the Para-Sail landing-rocket program, it was necessary that all operational parameters be investigated. One such parameter was the tension in the parachute turn-control lines. The tension-measurement device was designed to determine the control-cable tension (fig. VIII-20(a)).

Description

The tension-measurement device was mounted directly on the turn-control motor (fig. VIII-20(b)). It consisted of two small-diameter pulleys. The control cable left the motor drum and wrapped 5° on the smaller pulley and then went partially around the larger pulley and then up to the parachute. As viewed from an end section, the cable contacted three pulleys in a fixed

position so that the angle of incidence and departure to the middle pulley was fixed. The load on the middle pulley was proportional to the load in the cable. The middle roller was mated with a strain-gage link, and load could be measured directly and could be read while the cable was stationary or in motion.

The pulleys, mounted on small diameter rods, were free to translate along their axis of rotation. This was necessary since the cable translated as it wound and unwound on the motor drum. This tension-measurement device was used only with the original Aircraft Armaments, Incorporated, turn-control motor.

NEW TURN-CONTROL MOTORS

Purpose

The Para-Sail was a steerable parachute in which direction control was accomplished by the extension and retraction of two, 3/32-inch-diameter steel cables. When signaled from the ground, the turn-control motors reeled in and paid out these cables which controlled the positioning of the parachute control panels. There were two motors on the Gemini spacecraft boilerplate.

Description

The latest turn-control motors were an MSC modification of turn motors purchased from Aircraft Armaments, Incorporated (fig. VIII-20). The modified motors (fig. VIII-21) had a 250-pound capacity, a 6-foot cable travel, and a 1/2 ft/sec cable reel-in speed.

Mechanically, the system had three basic parts. The motor consisted of a 24-V dc permanent-magnet field motor, a planetary gear train, and a ball-bearing spline shaft.

The motor armature was keyed directly to a planetary gear train that reduced the speed 45:1. The gear-train output was coupled to a ball-bearing spline shaft. The cable drum was keyed to the ball housing and, due to the design of the ball spline, it was able to translate along the axis of the spline shaft. A brass guide, which reflected the cable grooves in the drum, mated with the drum. The drum and guide acted as a nut and bolt (fig. VIII-21). The position of the cable as it unwound from the drum was stable since the drum was traveling at the same speed as the position of the cable on the drum.

The turn-control motor was equipped with a normally unlocked brake, adjustable limit switches, a cantilevered tension-measurement device (not similar to the one previously described), and an electrical position read-out.

CABLE CUTTER

Purpose

The turn-control motors were placed inside the pressure vessel for protection. The turn-control cables had to pass through the pressure vessel to the parachute. It was the purpose of the cable cutters to cut the turn-control lines and to make a watertight seal upon impact with the desired landing surface. A secondary function of the cable cutters was to serve as pressure-vessel vents.

Description

The cable cutter consisted of three main parts: the piston, the body, and the end plate (fig. VIII-22). The body was drilled axially to accommodate the piston. The body also had a $1/4 \times 1.0$ -inch slot perpendicular to the piston for cable passage. To cut the cables, a pyrotechnic charge was ignited which fired the piston toward the cable in the slot. The cable was trapped against the far end of the slot and was sheared. The reservoir between the end of the slot and the end plate was filled with grease which the piston forced back along the sides of the piston thus producing an effective watertight seal.

CAMERA INSTALLATION

Purpose

Onboard cameras were required to supplement the data obtained from rate gyroscopes, strain gages, accelerometers, and so forth. Four onboard cameras covered all phases of the flight.

Operation

Three of the four onboard cameras were located inside the capsule pressure vessel. The fourth camera was located in the cylindrical section

and was encased in an aluminum waterproof box with a clear plastic window. The four cameras scanned the following directions (fig. VIII-23):

Camera 1. This camera was located in the cylindrical section and was focused to view the opening of the Para-Sail parachute.

Camera 2. This camera was located in the pressure vessel and was focused to view the parachute after the configuration change.

Camera 3. This camera was located inside the pressure vessel and was mounted so that its focal point was in the same position as the eyes of the astronaut. Consequently, the picture presented was that which the astronaut would see through his window.

Camera 4. This camera was located in the pressure vessel and was focused to view the ground during flight. It was used to record blast-deflector separation and the deployment of the altitude sensors.

RADIO ANTENNA INSTALLATION

Purpose

Radio signals between the Gemini spacecraft boilerplate and the control station were used to telemeter information recorded on board, to command the steerable parachute, and to deploy the emergency parachute, if necessary. The antennas were an important part of the radio system.

Description

Two types of antennas have been used on the Gemini spacecraft boilerplate; flat antennas, and spring-steel whip antennas. Two flat antennas were installed in the equipment-bay panels below the X-axis in the early stages of the drop program. These antennas have been replaced with whip antennas. In the later configuration, there were six whip antennas.

The whip antennas were made up of 1/2-inch-wide steel strips that had a slight curve on the cross section. The antenna and a bulkhead single-pin connector were soldered together. This assembly was mated in a small cup and covered with a potting component (fig. VIII-24). This was fitted in the capsule skin and bolted in place. For airtight installations, room temperature, vulcanizing white silicon rubber adhesive sealant (RTV 102) was used to seal the installation.

AIRBORNE LAUNCH CRADLE

Purpose

The Gemini spacecraft boilerplate used in the Para-Sail landing-rocket program was launched from an Air Force C-119 aircraft. The cradle was used to insure a safe and smooth exit from the aircraft.

Description

The airborne launch cradle was made of mild steel and was designed to hold the Gemini spacecraft boilerplate during all possible flight attitudes and loads. The cradle was also designed to restrain the boilerplate should one or both of the landing retrorockets accidentally fire. The cradle presented a minimum volume envelope since the C-119 aircraft was barely large enough to contain the boilerplate (fig. VIII-25).

In operation, the cradle was tied down to the aircraft. The boilerplate was restrained at three points while the dead weight of the boilerplate was carried at two points: the forward carriage and the aft rollers. Two of the restraint points were located on the side of the boilerplate while the third was located near the forward cylindrical section of the boilerplate. The two side points consisted of pins which allowed the boilerplate to back away when it was released. The forward single attach point had provisions for a helicopter cargo hook which was attached to the retractable attach point on the boilerplate (fig. VIII-13). When the launch signal was given, the cargo hook was released and the boilerplate was free to move down the slight incline built into the cradle. The boilerplate moved freely down the incline because of the aft rollers and the wheels on the forward carriage.

The capsule was carried with the blast deflector (fig. VIII-16) rotated up toward the right X-axis about 72°. This large off-center weight gave the boilerplate a tendency to roll when moving down the cradle. This roll was checked by an antiroll plate welded to the boilerplate. This plate fitted against the forward carriage and stopped all roll until after the boilerplate left the aircraft.

GEAR-STROKE SENSOR

The gear-stroke sensor (fig. VIII-26) was a microswitch mounted between the main landing-gear damper and the damper retaining plate so

that the switch was in the closed position before the gear stroked and was opened by the gear stroke.

NOSE LANDING-GEAR SKID PROTECTOR

Purpose

The purpose of the skid protector was to shield the NLG skid during R and R canister separation, and to keep the parachute shroud lines from snagging on the NLG.

Description

The skid protector was made from 1-1/4-inch mild steel tubing and 5/16-inch mild steel gussets and plates. The protector was formed to follow the outline of the NLG skid when the NLG was in the stowed position. The fit between the protector and the skid was as close as possible with the maximum daylight gap not exceeding 3/8 inch. On the left X side of the protector, the tubing was bent 90° away from the skid for 8.0 inches and then down to the boilerplate (fig. VIII-27). This was done to protect the torque link from the parachute riser. The skid protector was held to the boilerplate by eight 5/16-24-NF aircraft bolts. The skid protector was welded throughout.

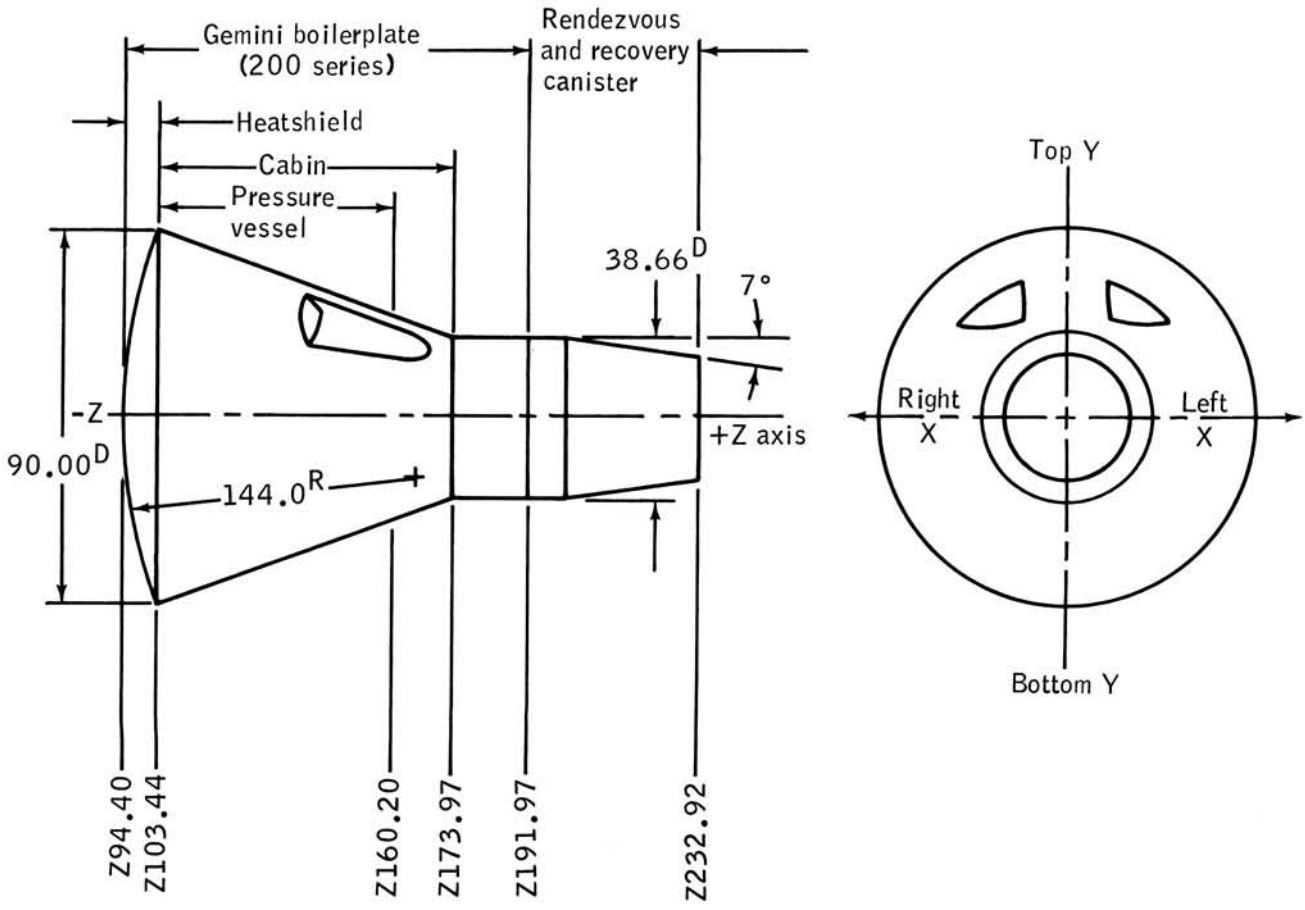


Figure VIII-1.- Gemini spacecraft boilerplate station and nomenclature diagram (200 series).

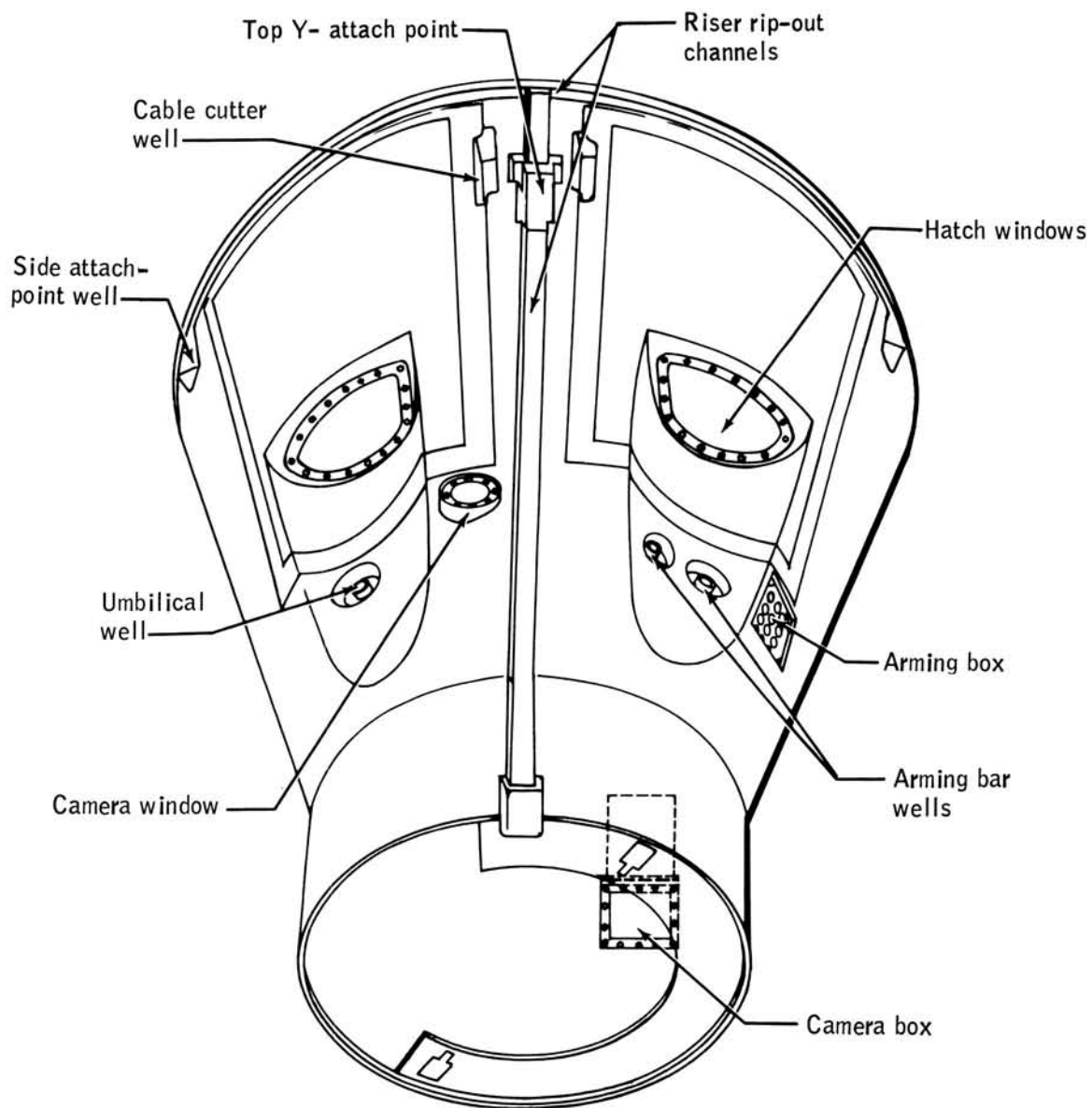


Figure VIII-2.- Top view of Gemini spacecraft boilerplate (200 series).

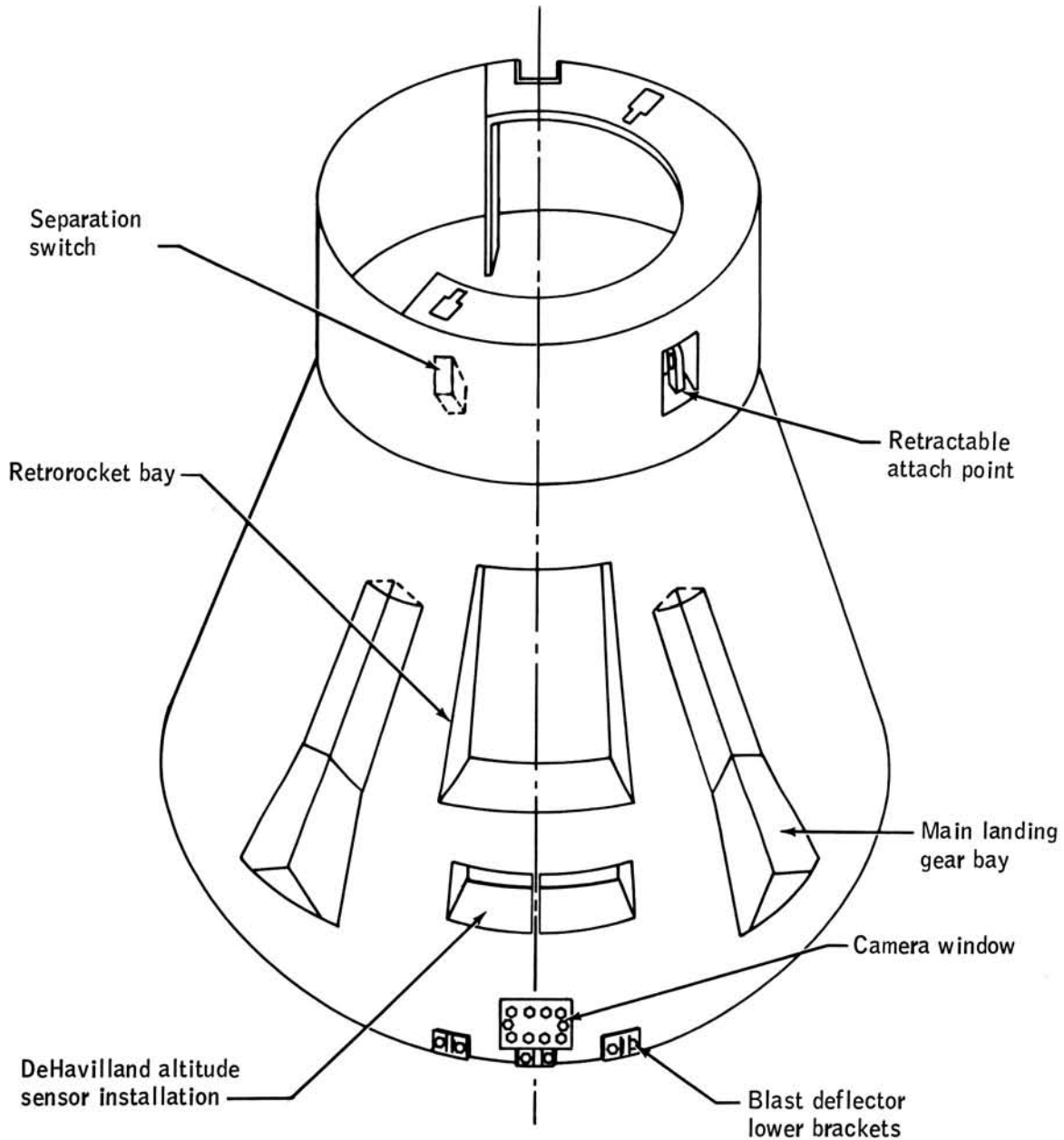


Figure VIII-3.- Bottom view of Gemini spacecraft boilerplate (200 series).

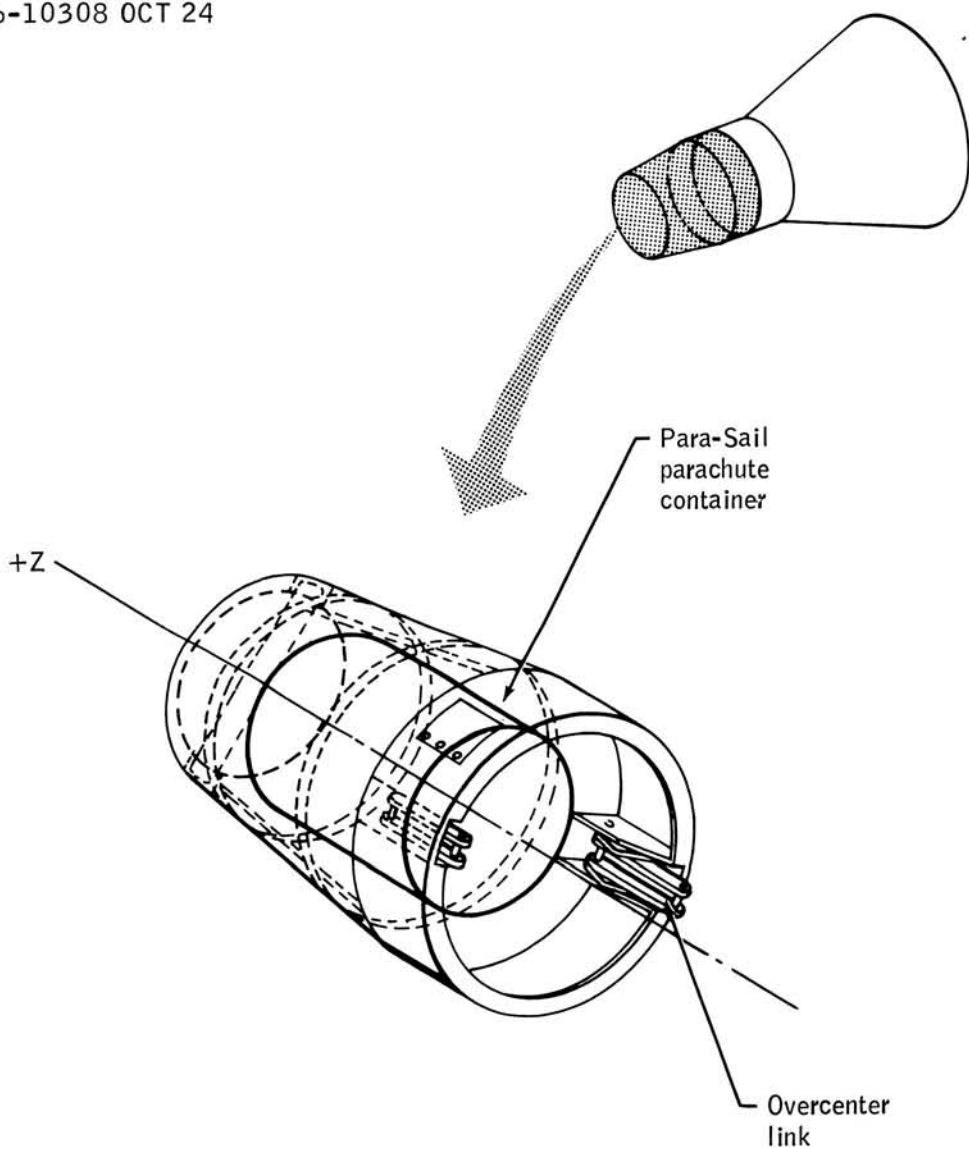


Figure VIII-4.- Rendezvous and recovery canister. (See fig. VIII-5 for detail.)

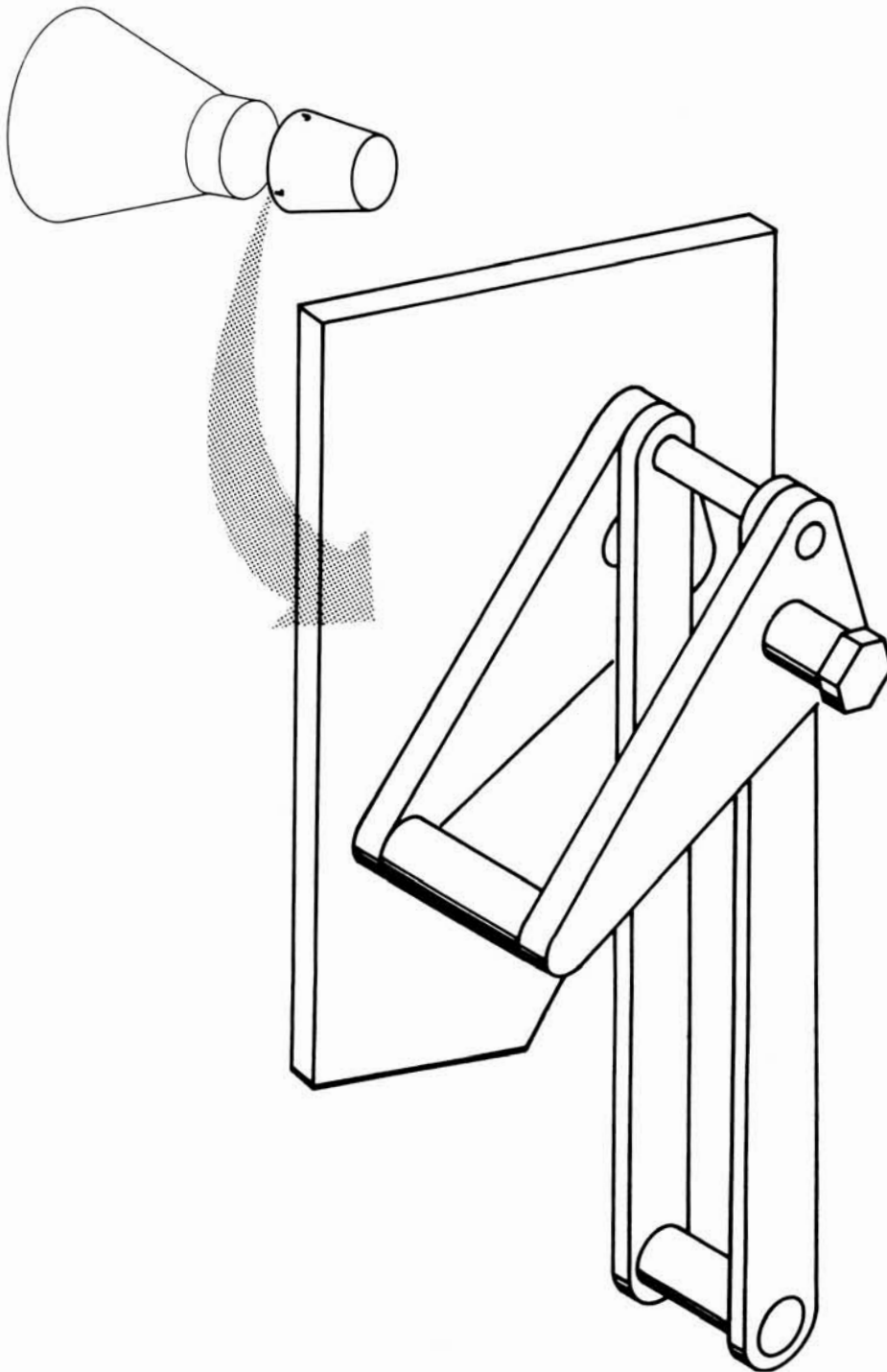


Figure VIII-5.- Overcenter link.

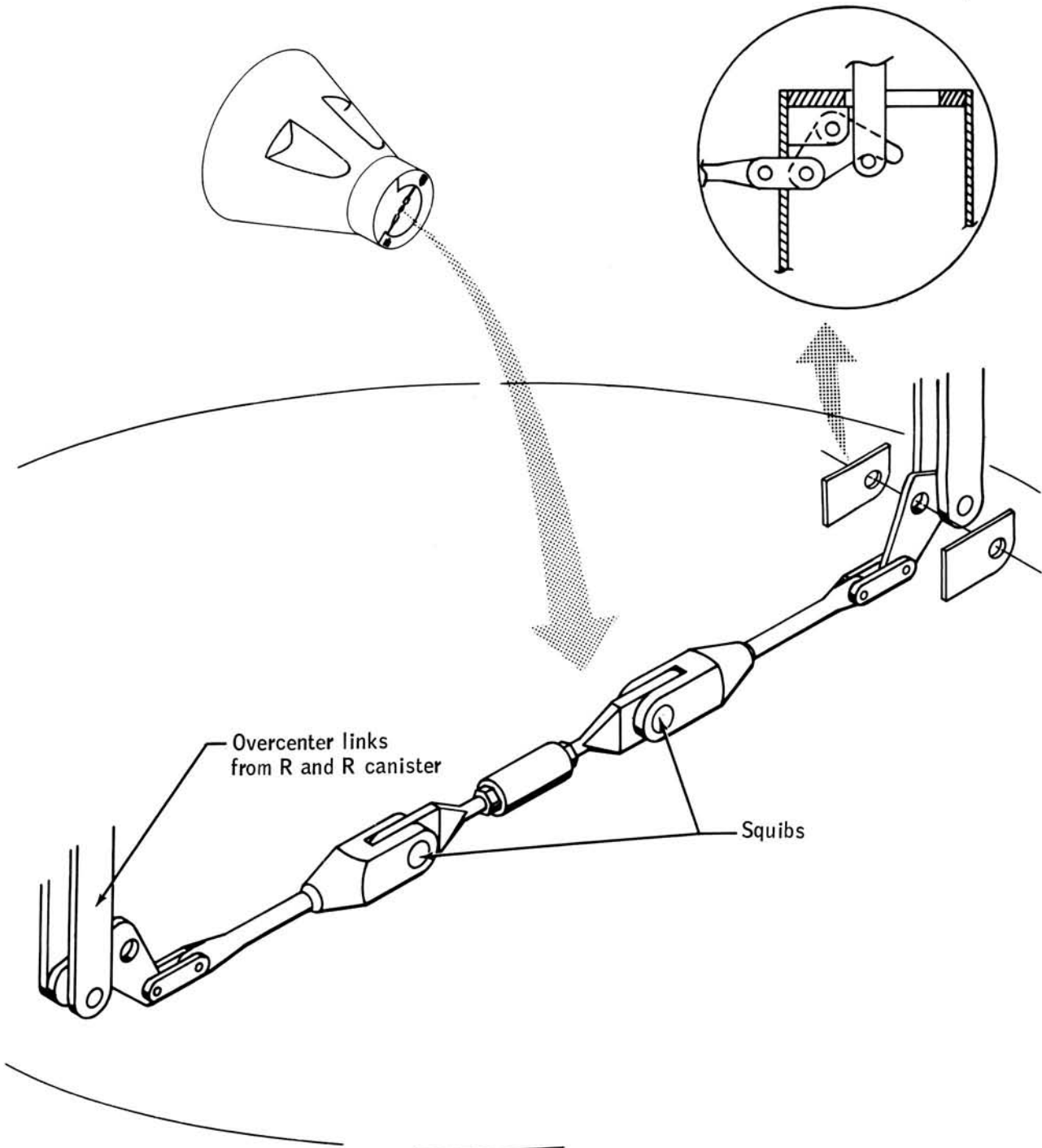


Figure VIII-6.- Rendezvous and recovery release mechanism.
(See fig. VIII-5 for detail.)

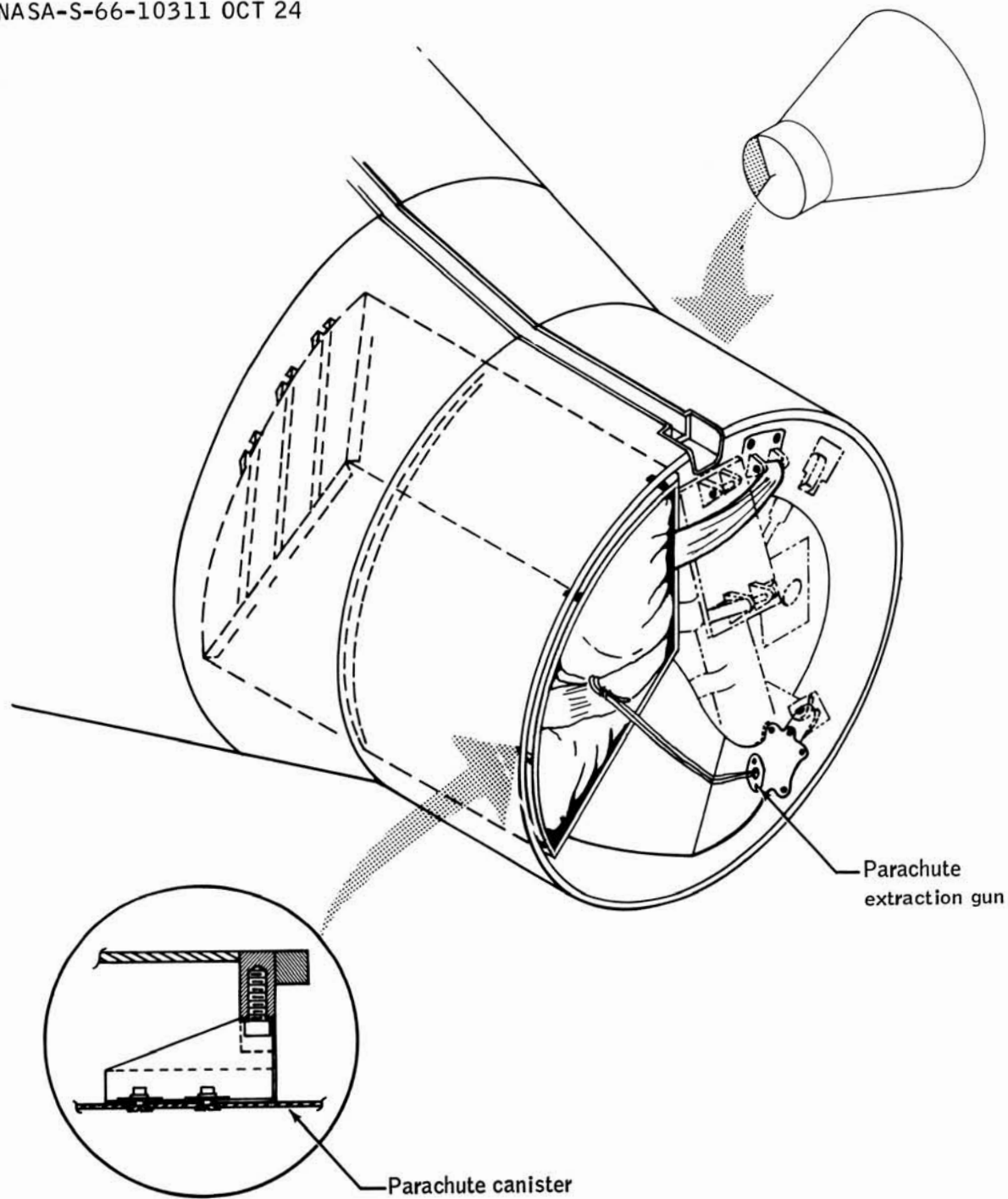


Figure VIII-7.- Reserve parachute installation.

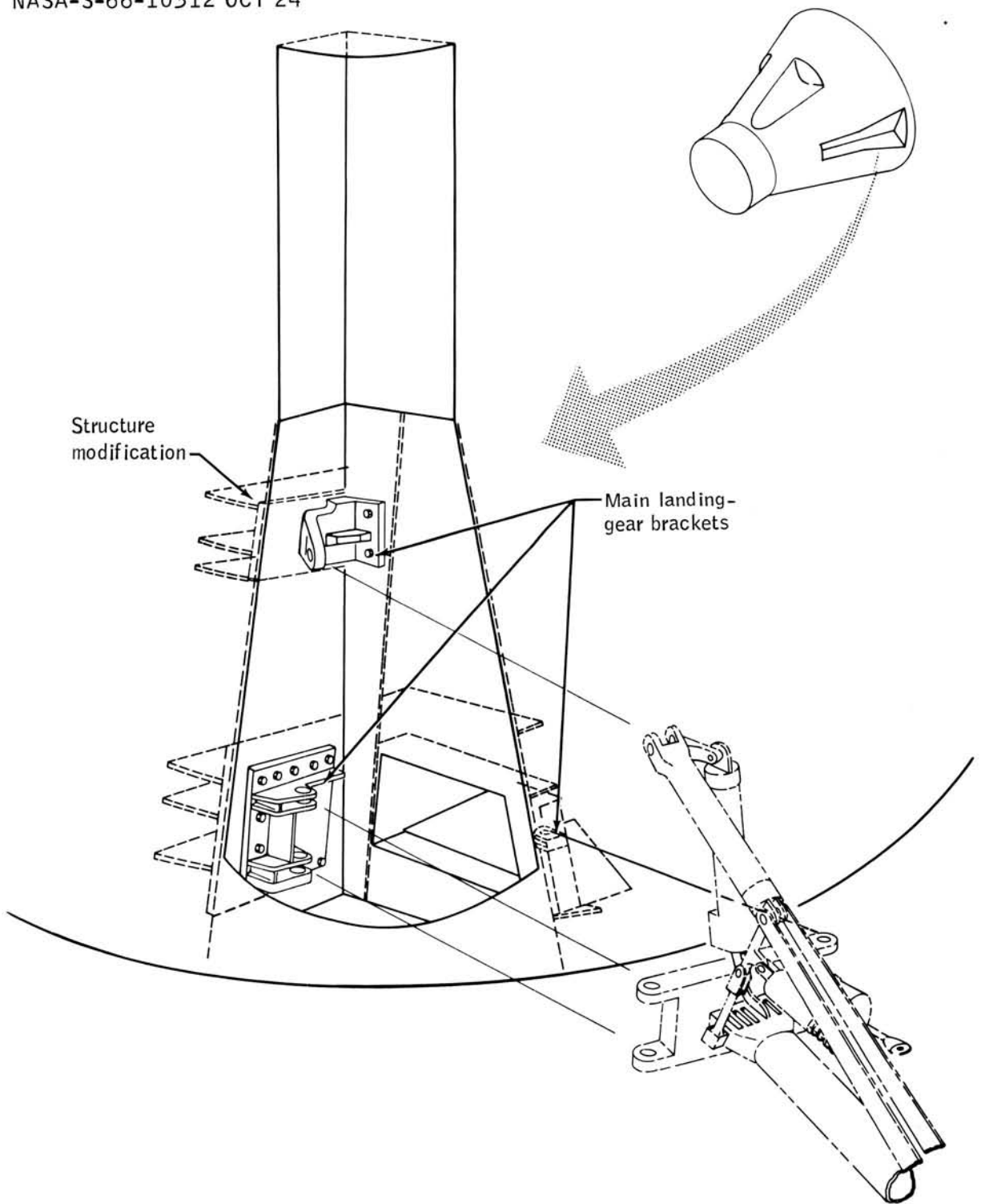


Figure VIII-8.- Main landing-gear installation.

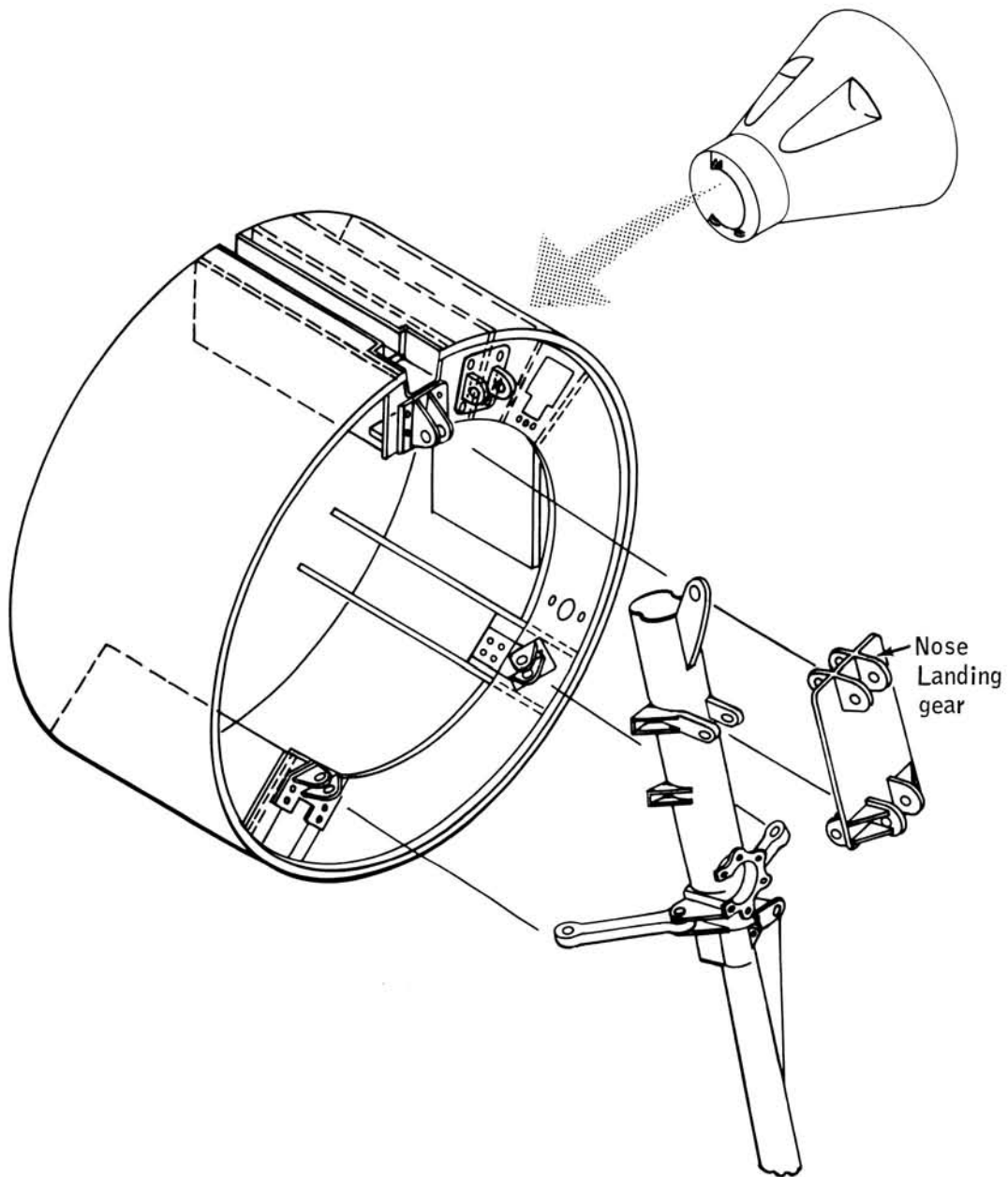


Figure VIII-9.- Nose landing-gear installation. (See fig. VIII-18 for detail.)

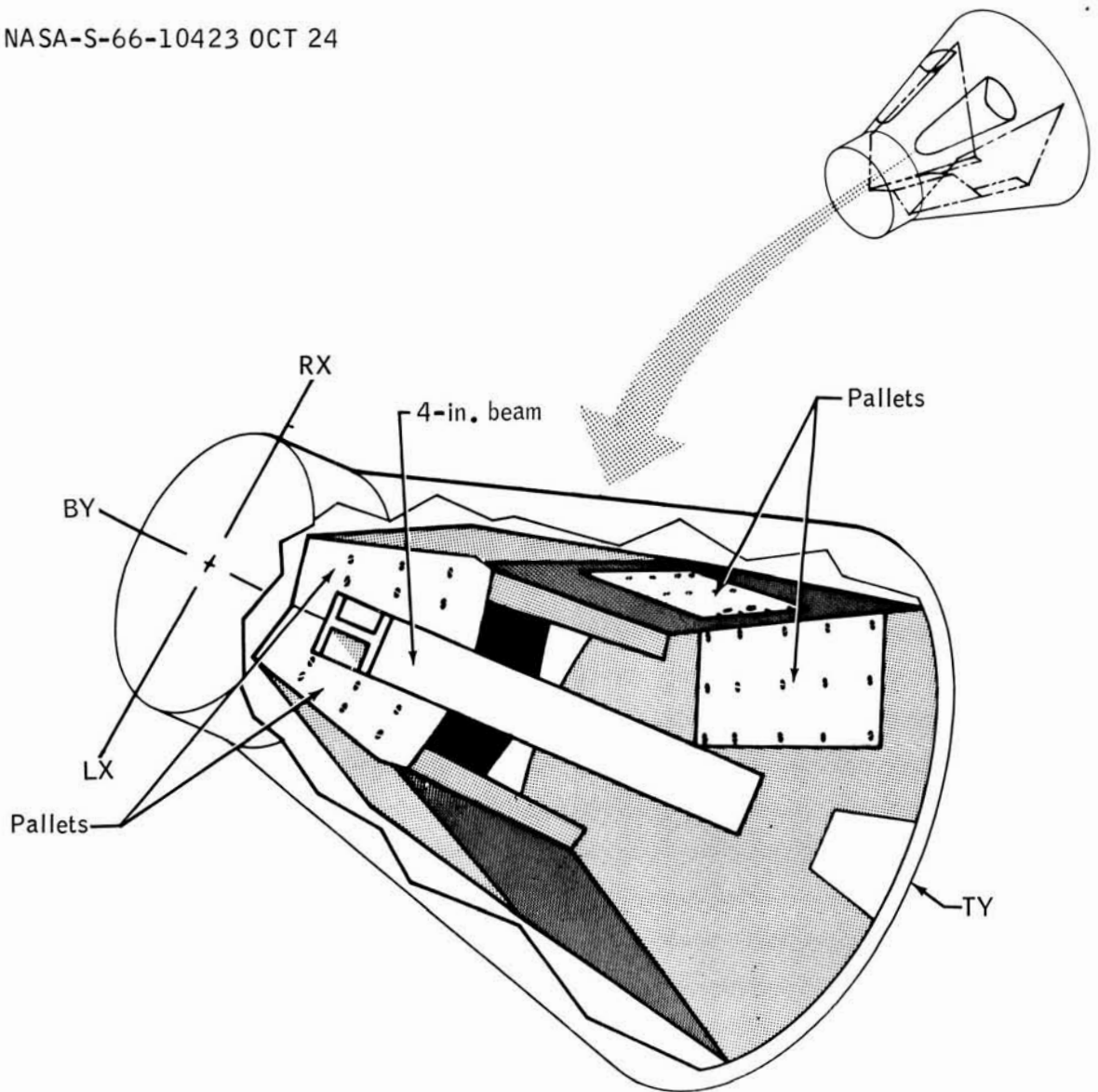


Figure VIII-10.- Instrumentation mounting surfaces.

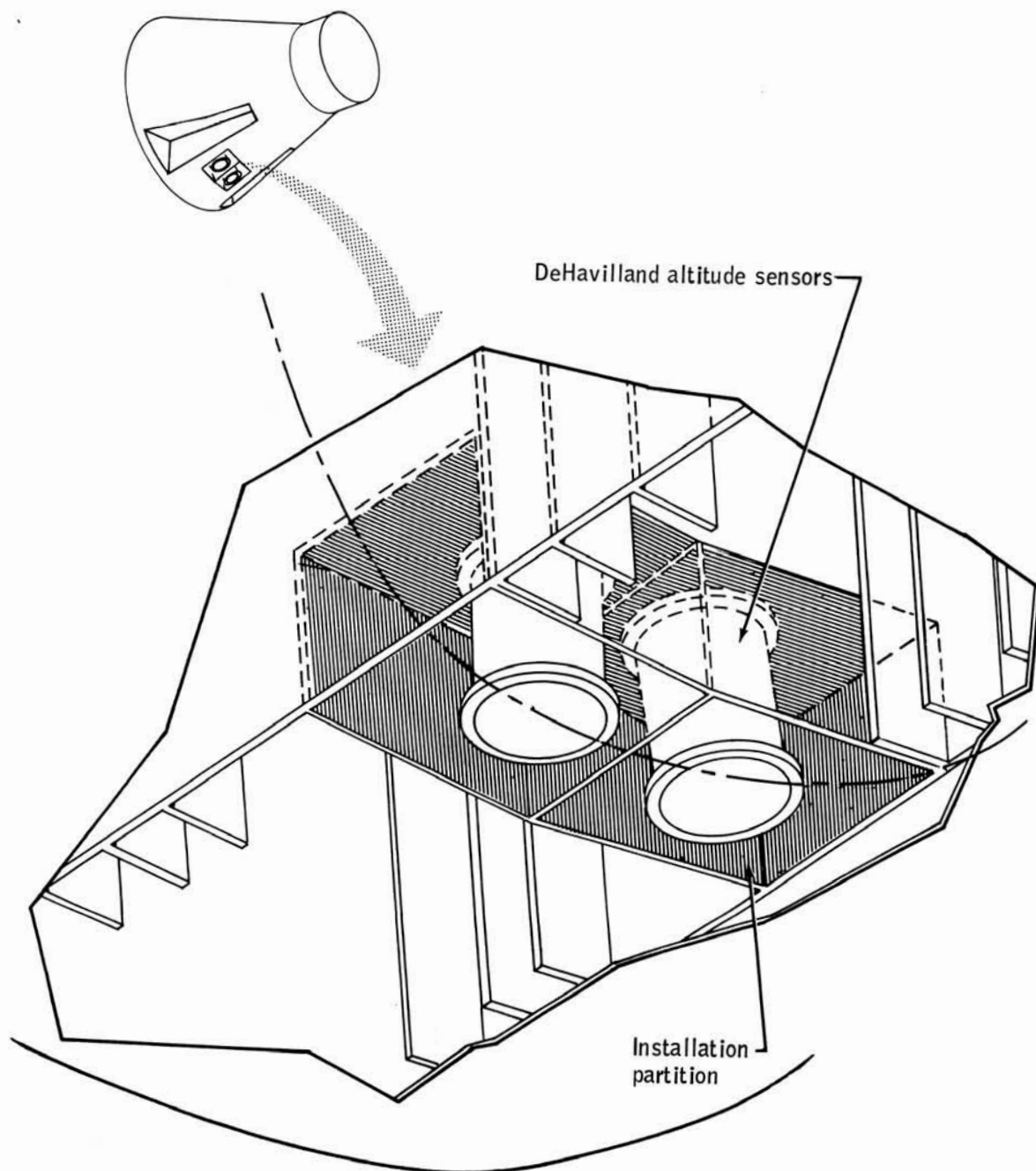
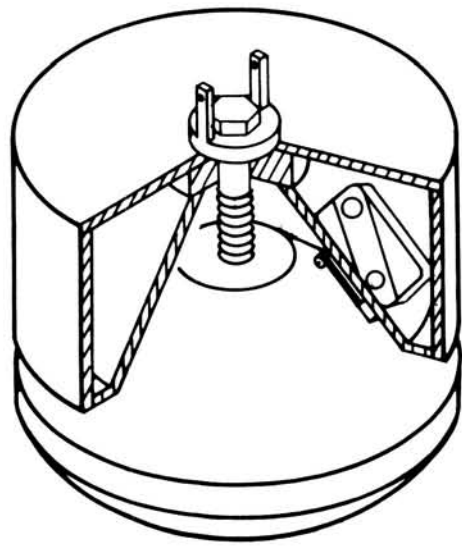
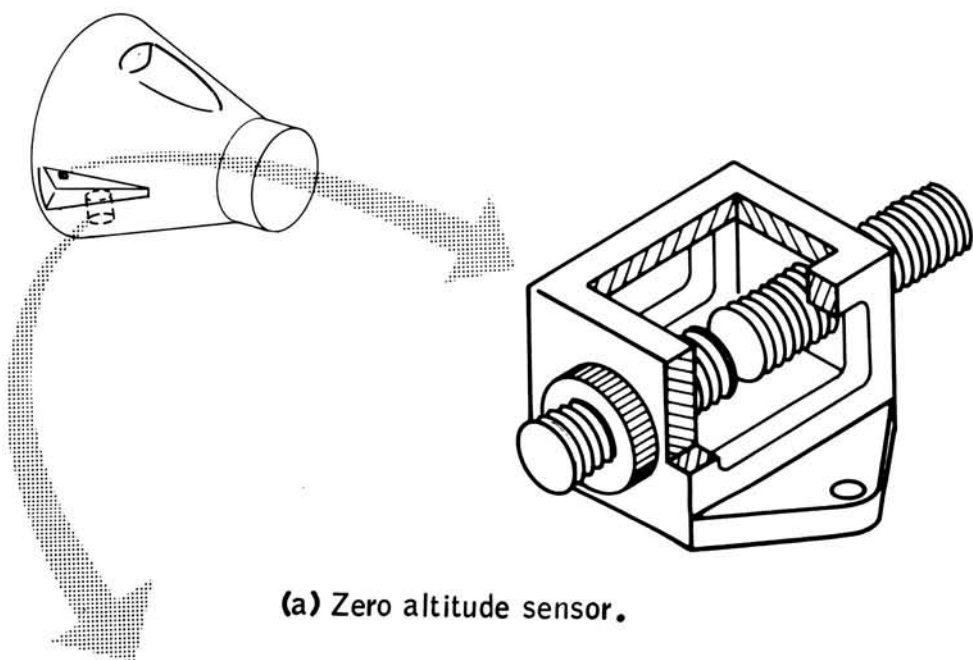
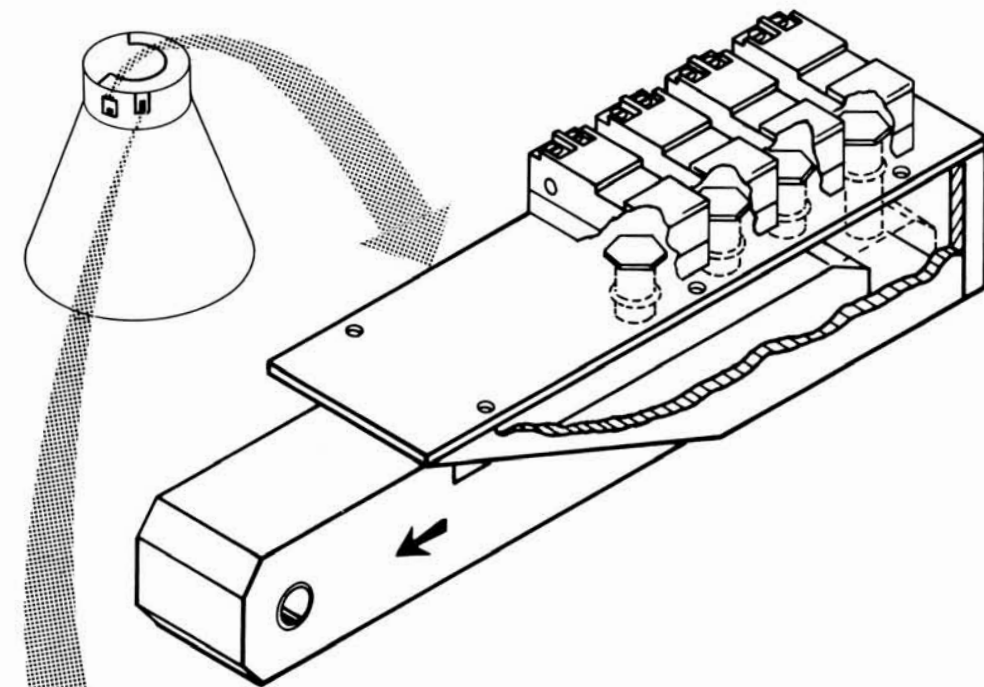


Figure VIII-11.- DeHavilland altitude-sensor installation.

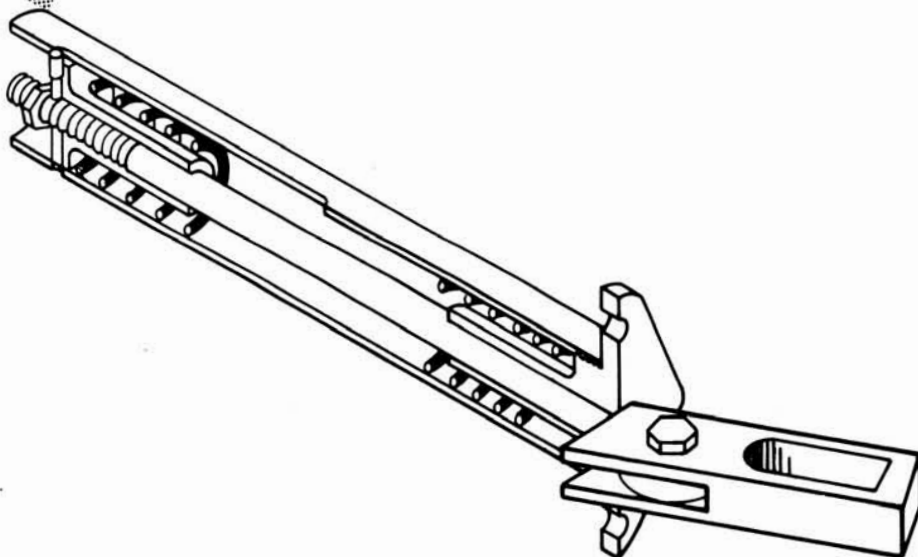


(b) Interim altitude sensor.

Figure VIII-12.- Altitude sensors.



(a) Separation switch



(b) Retractable attach point.

Figure VIII-13.- Gemini spacecraft boilerplate equipment.

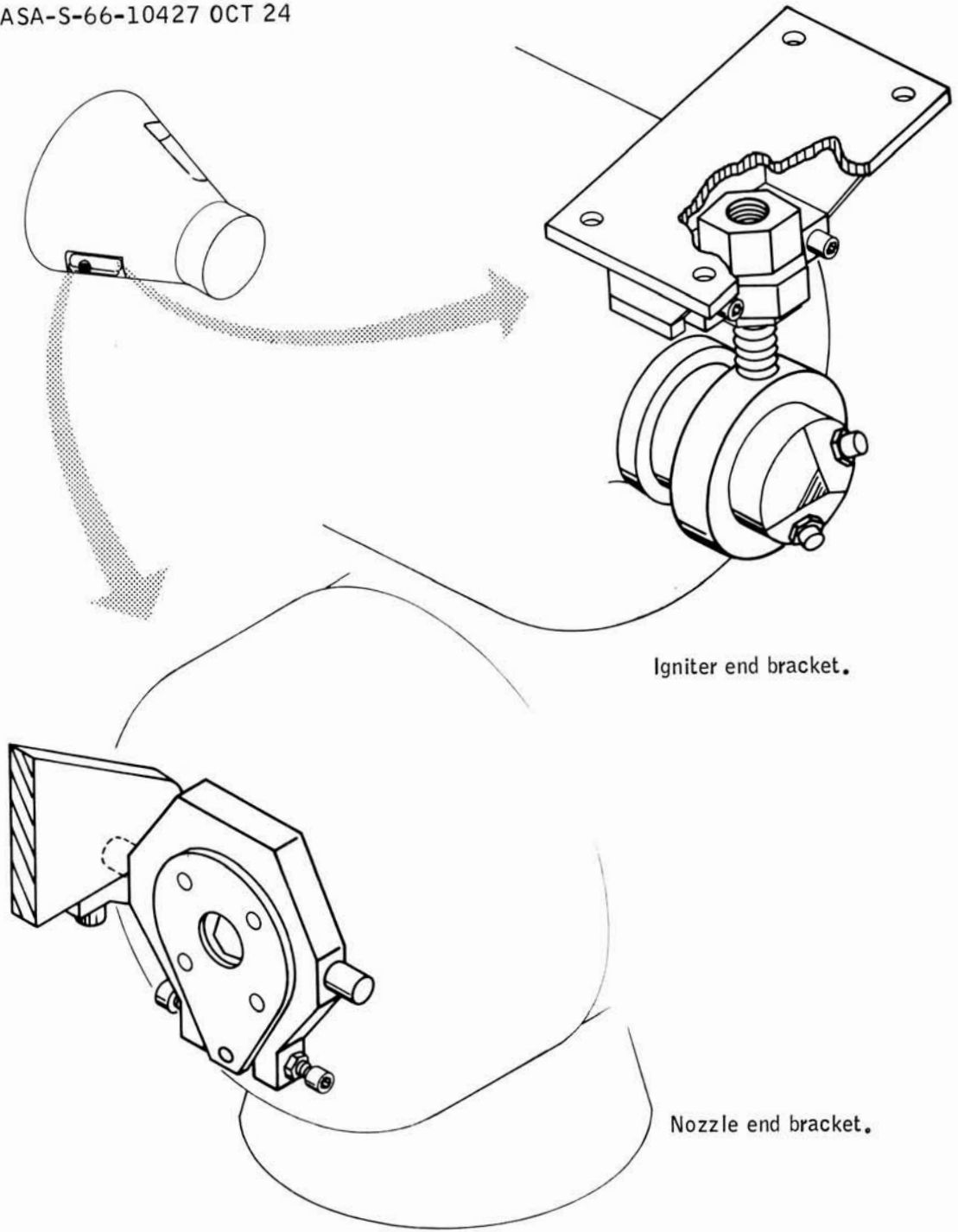


Figure VIII-14.- Retrorocket alinement hardware.

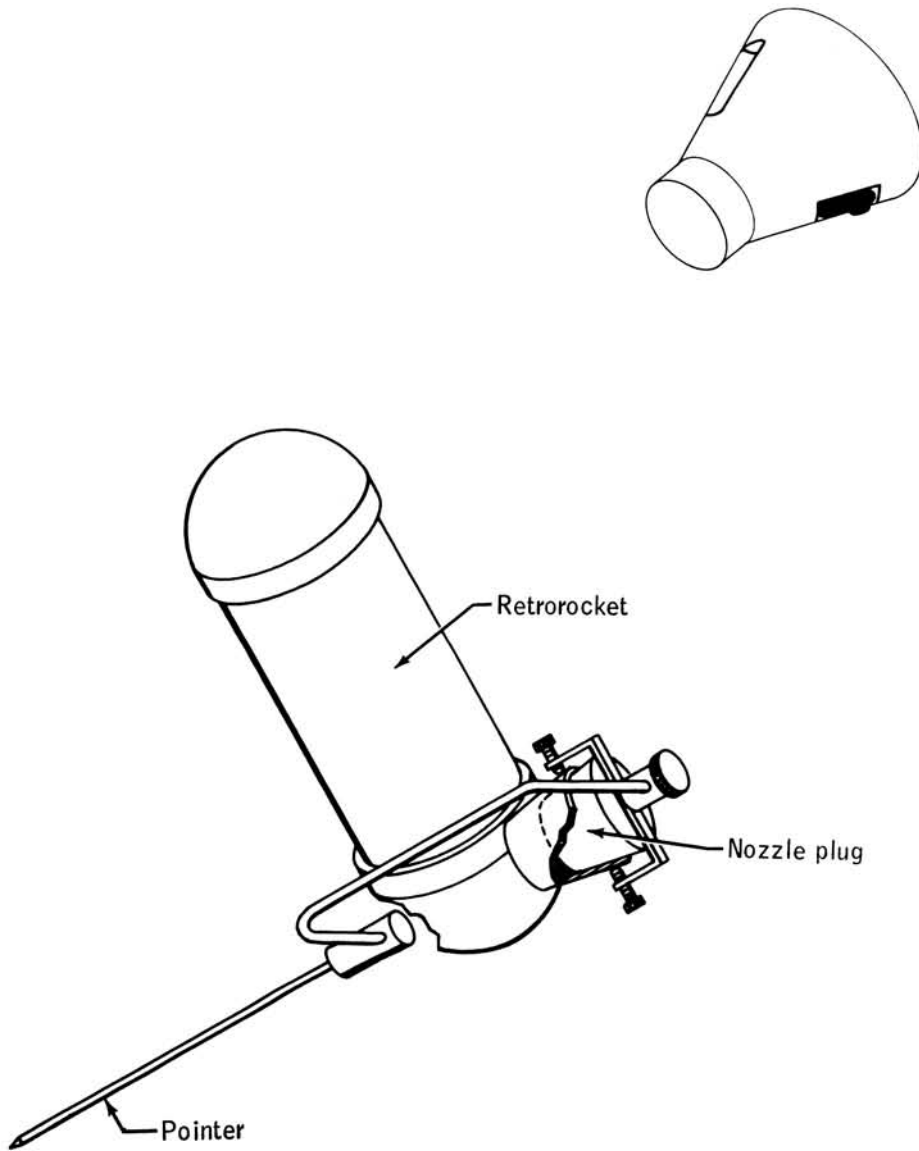


Figure VIII-15.- Retrorocket alinement fixture.

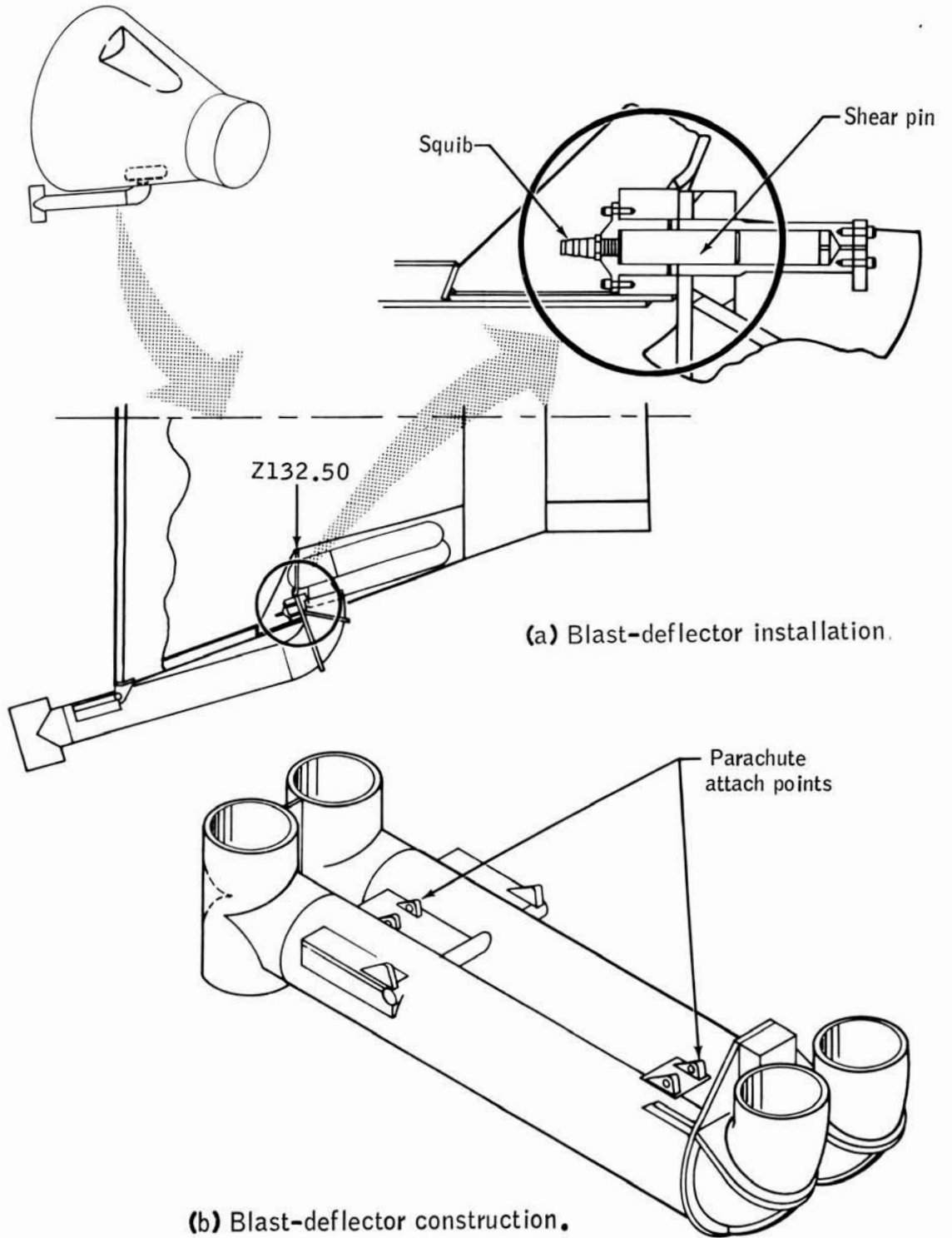


Figure VIII-16.- Blast deflector and installation.

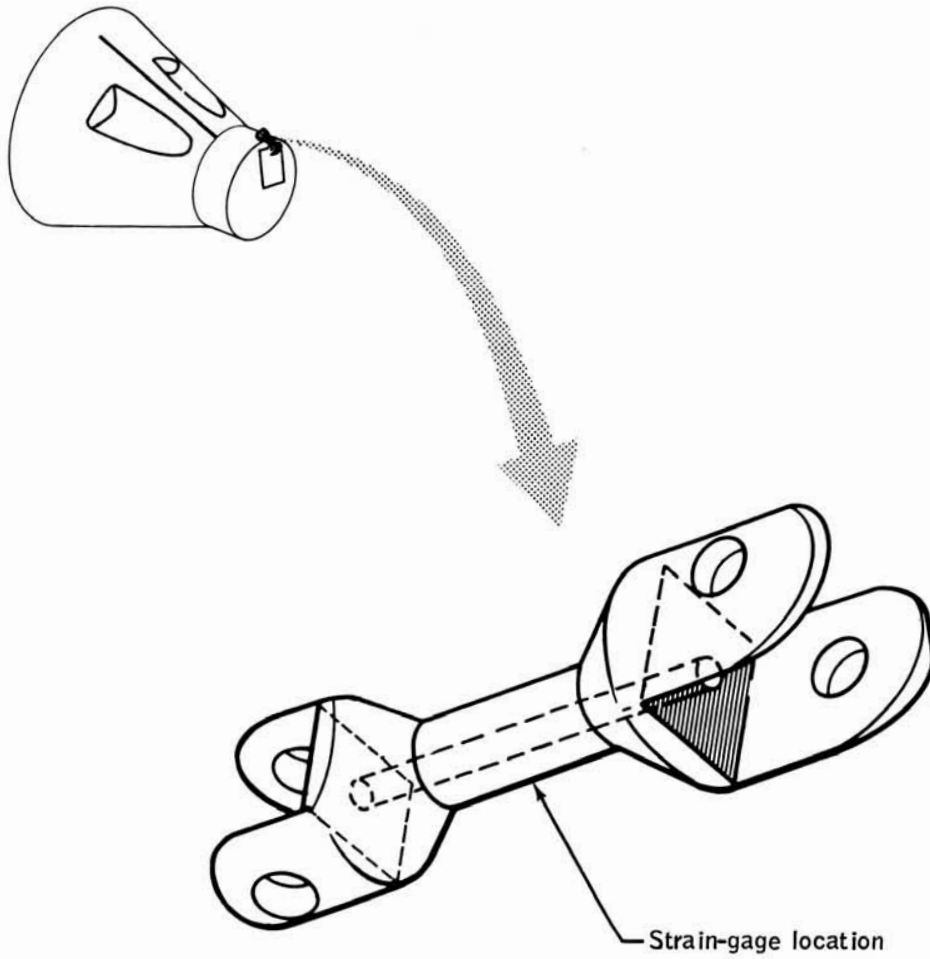


Figure VIII-17.- Load cell.

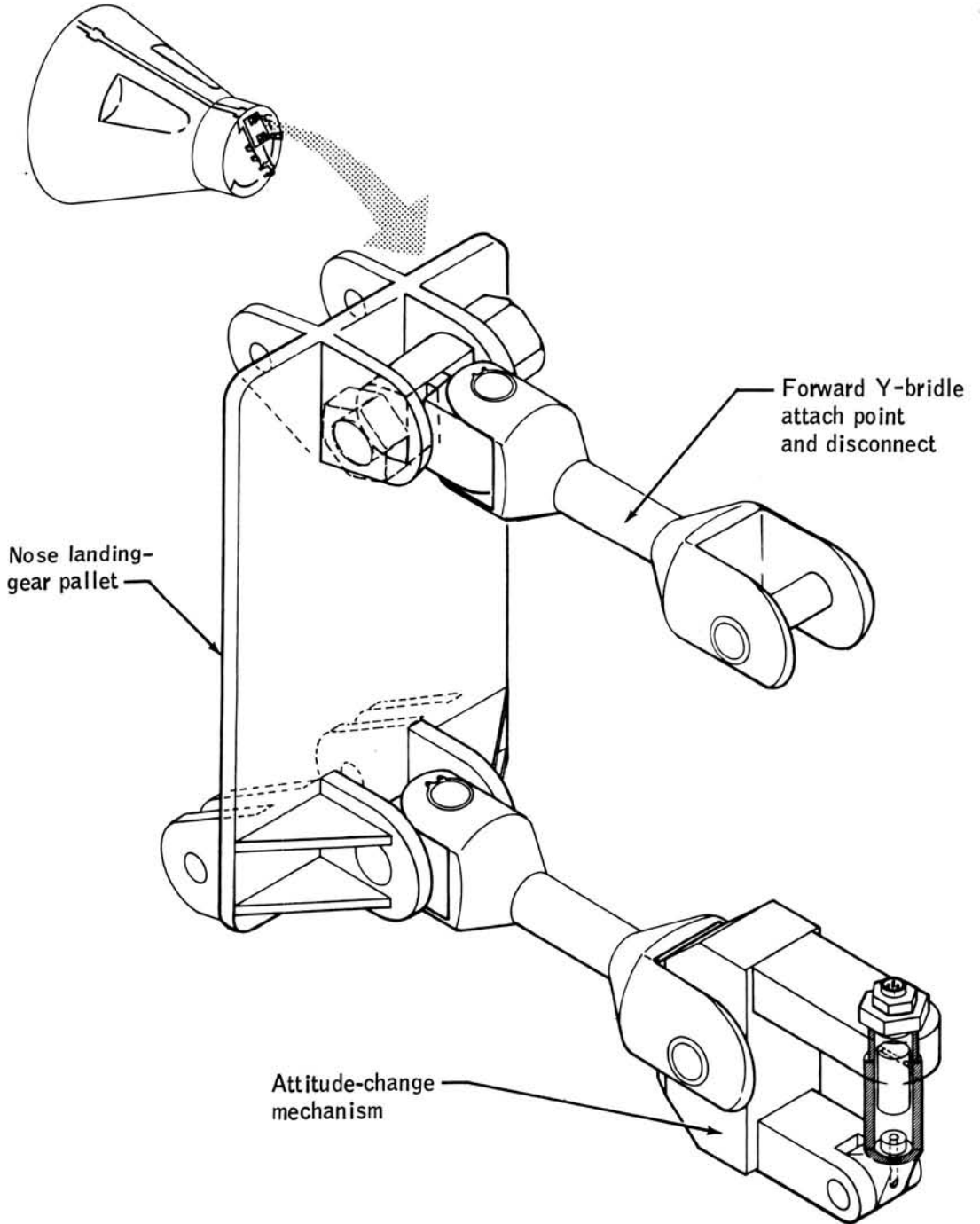


Figure VIII-18.- Parachute disconnect hardware.

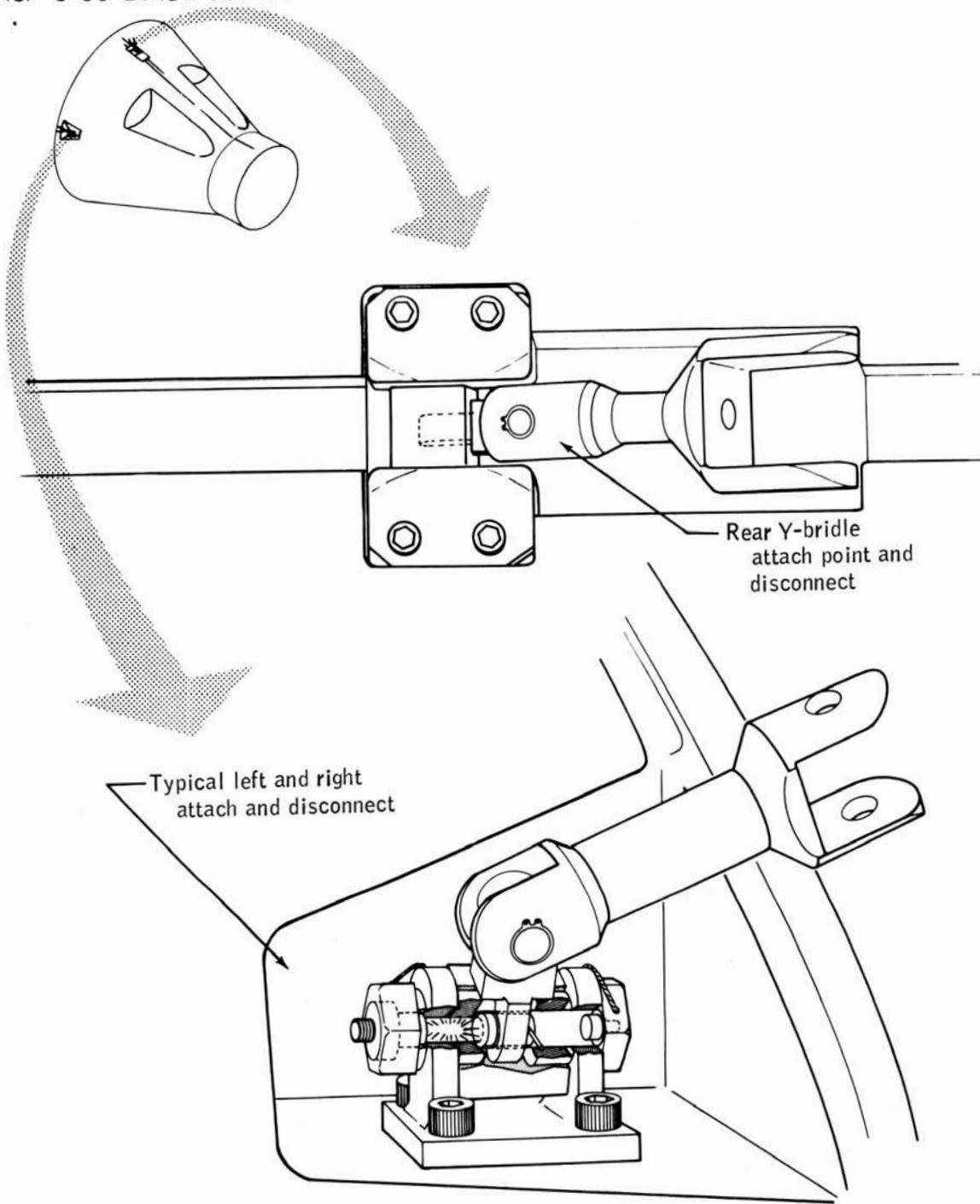


Figure VIII-19.- Parachute attach and disconnect hardware.

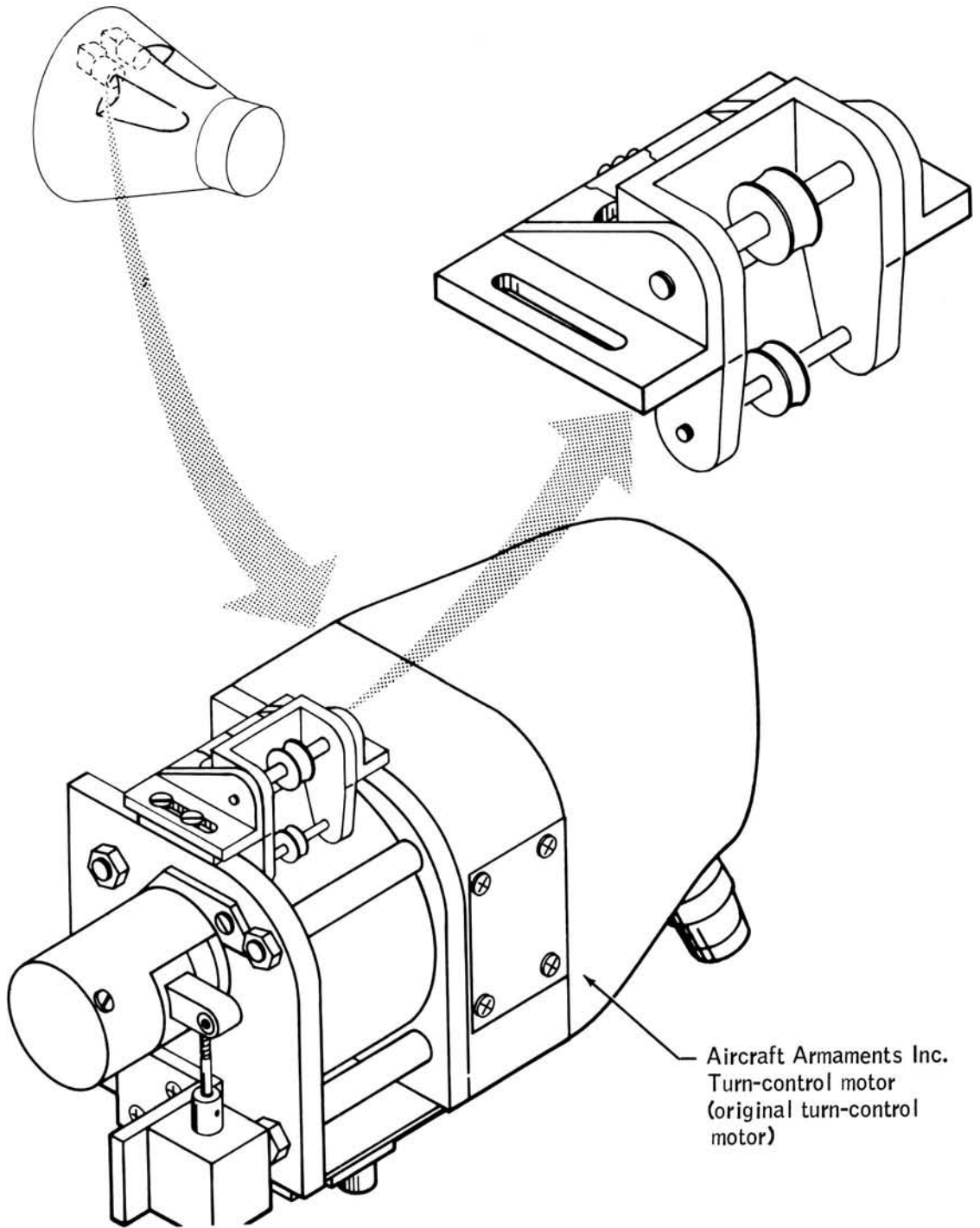


Figure VIII-20.- Tension-measurement device installation.

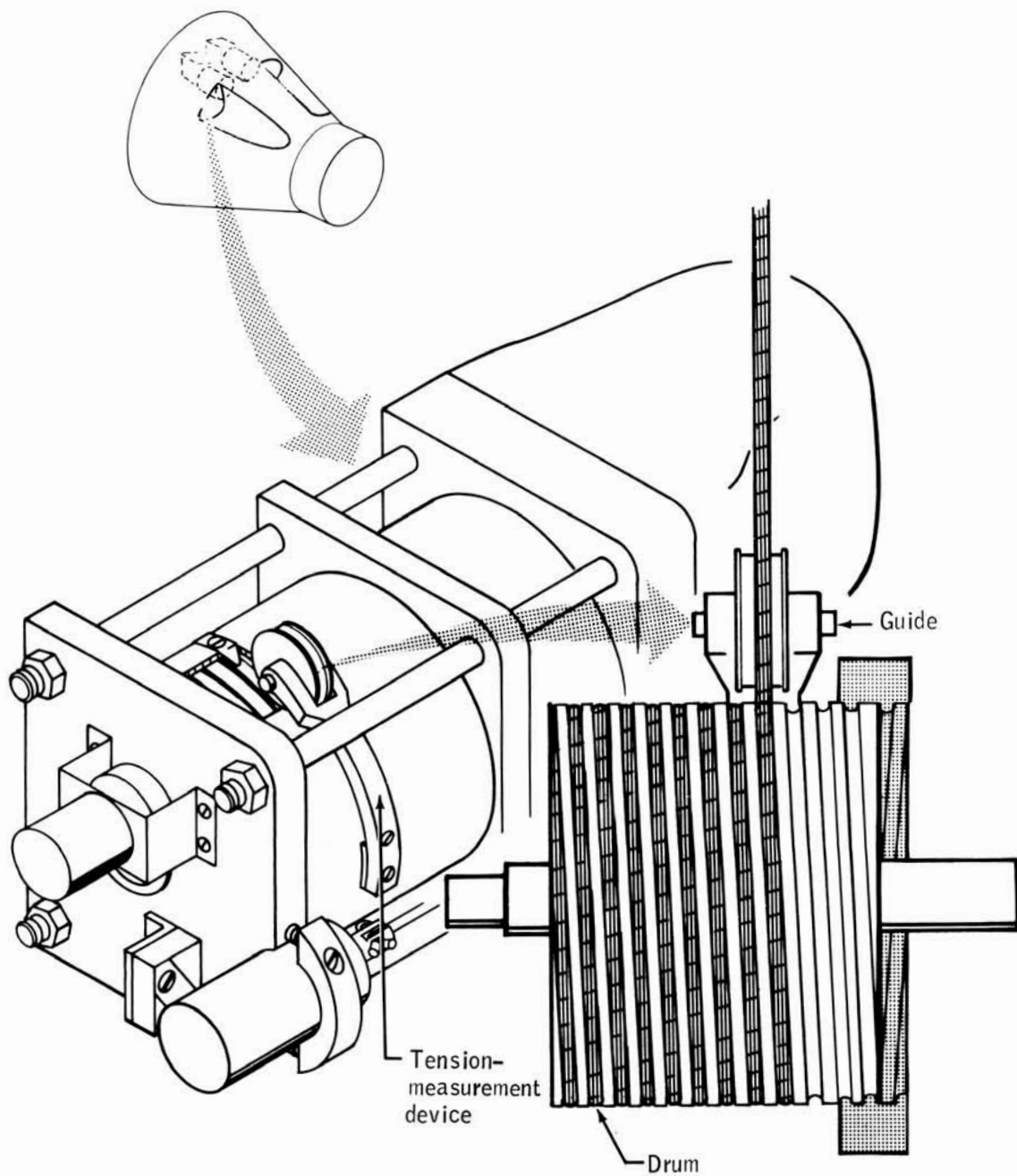


Figure VIII-21.- Modified turn-control motor.

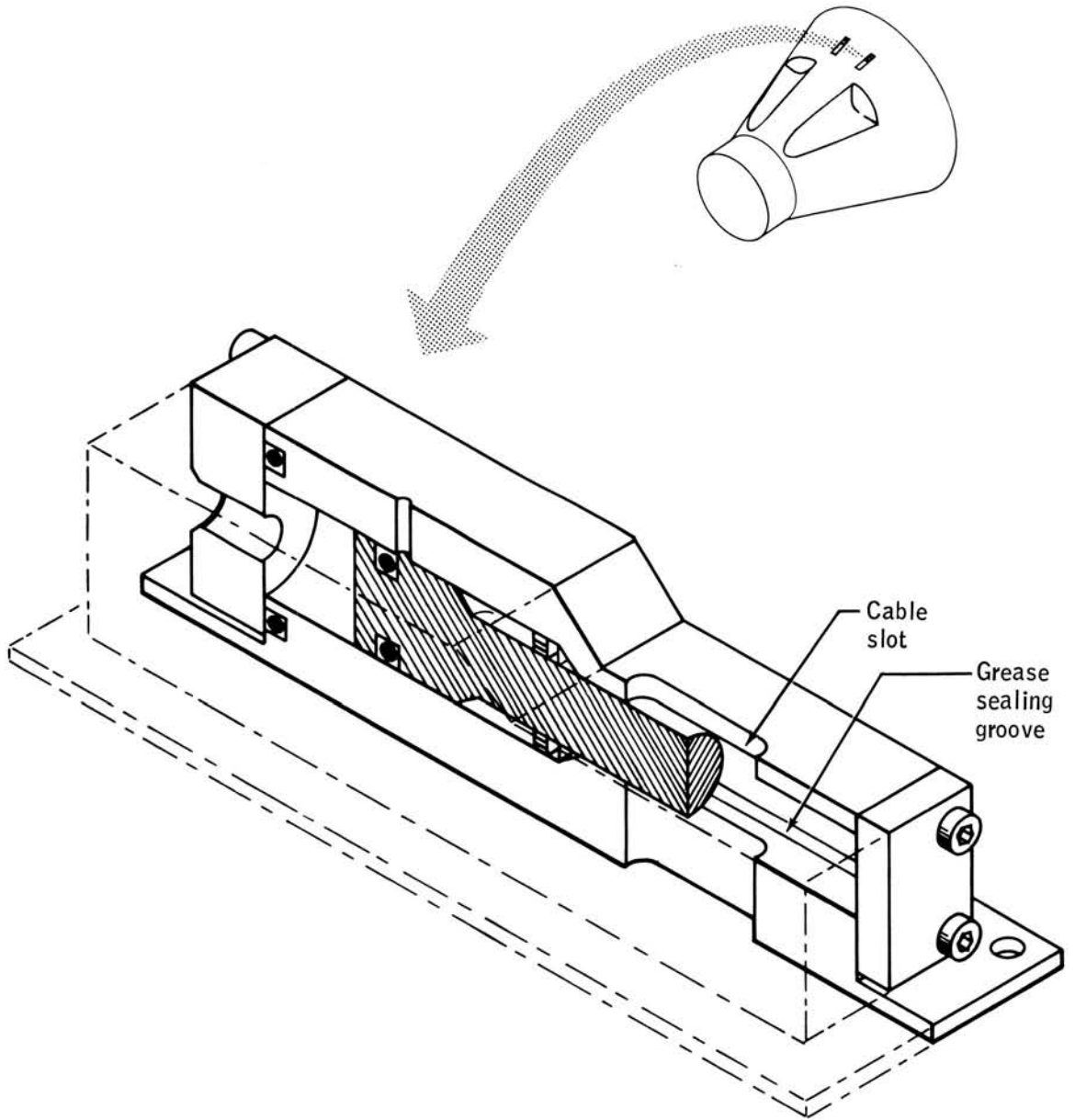


Figure VIII-22.- Cable cutter.

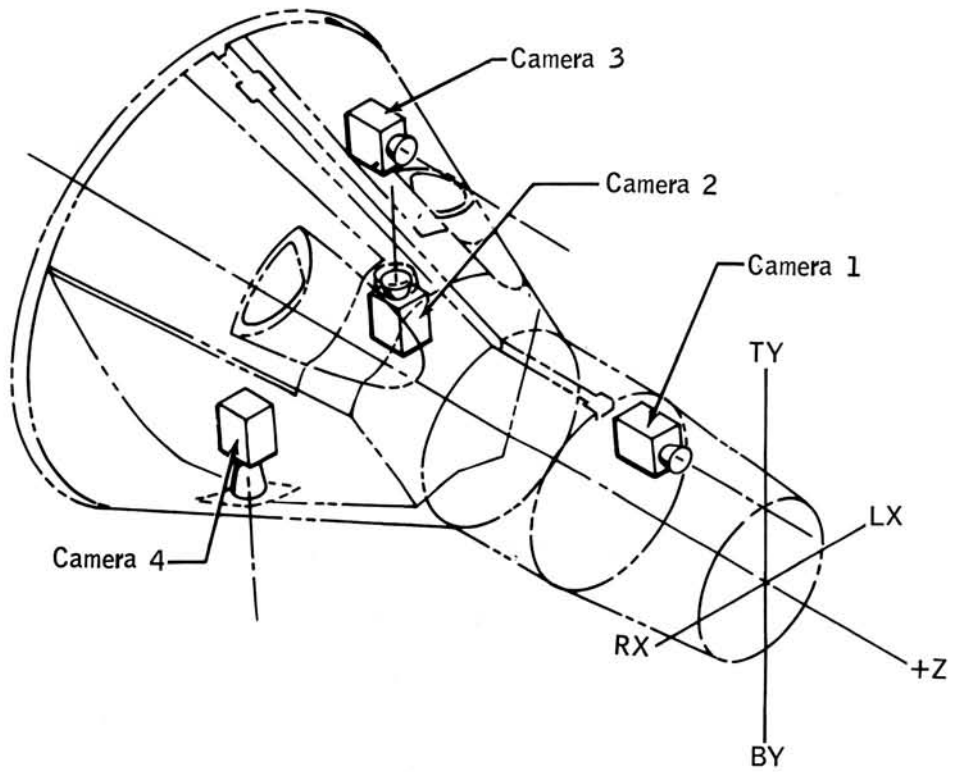
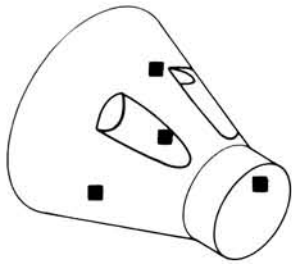


Figure VIII-23.- Camera locations.

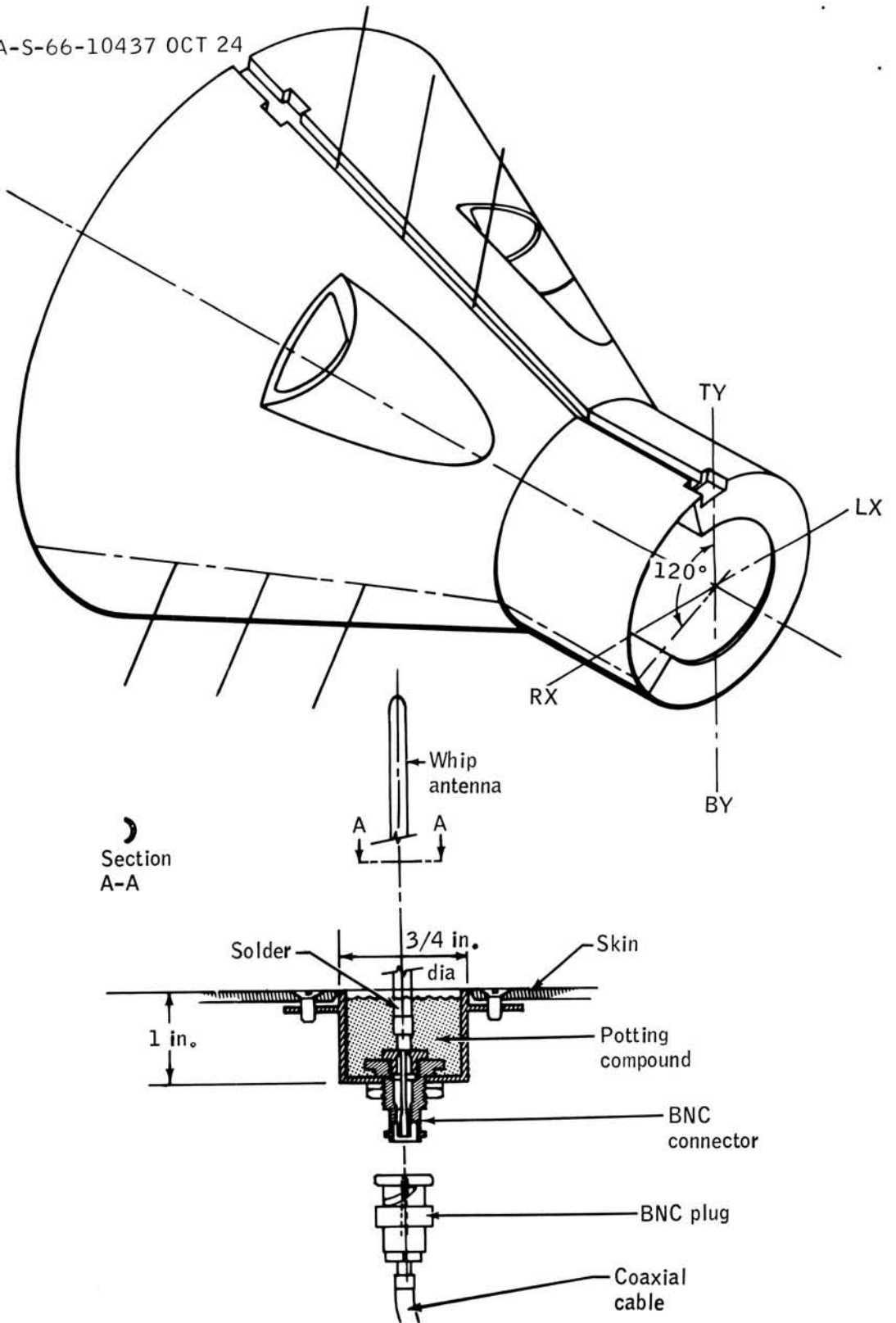


Figure VIII-24.- Whip antenna installation and location.

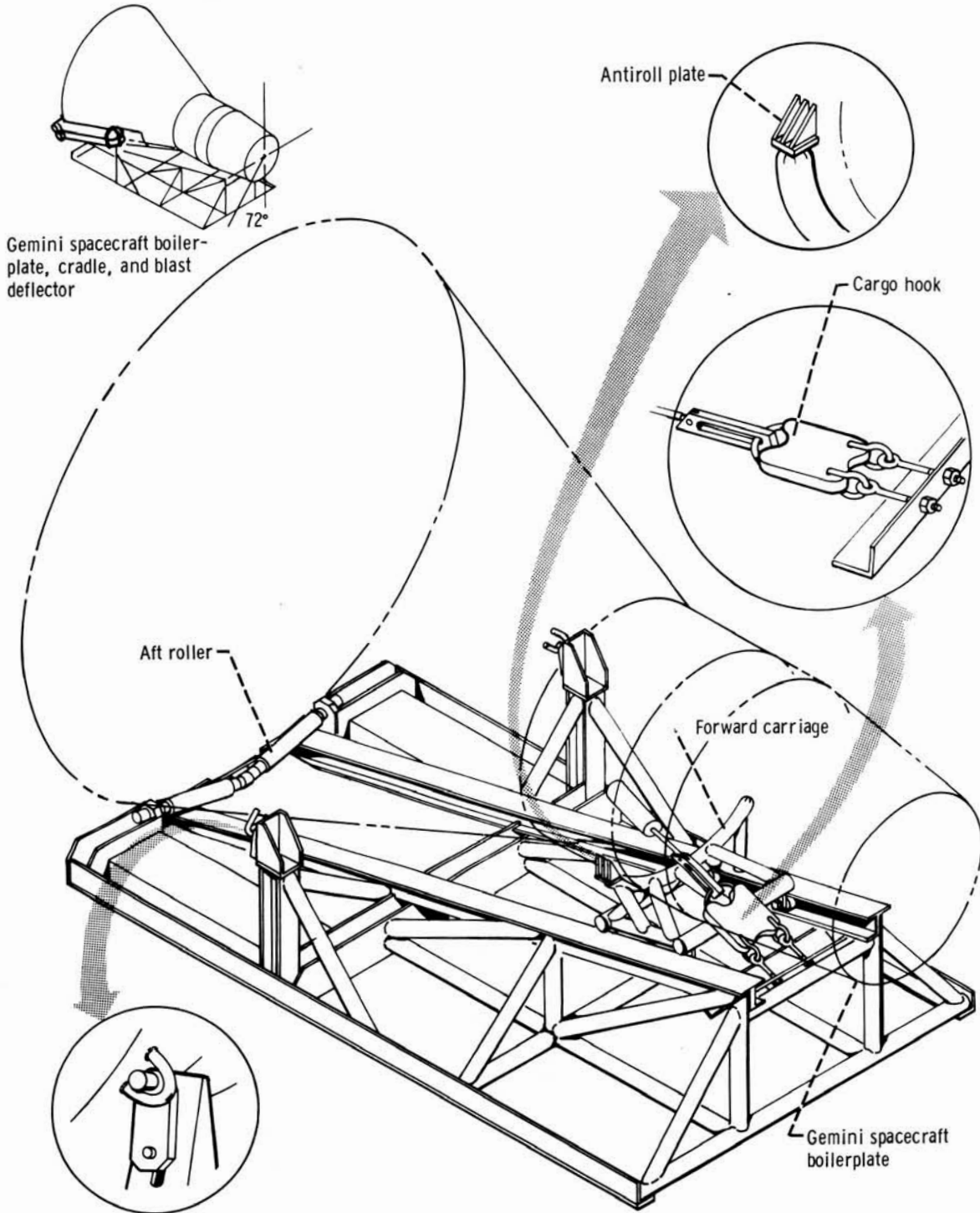


Figure VIII-25.- Airborne launch cradle.

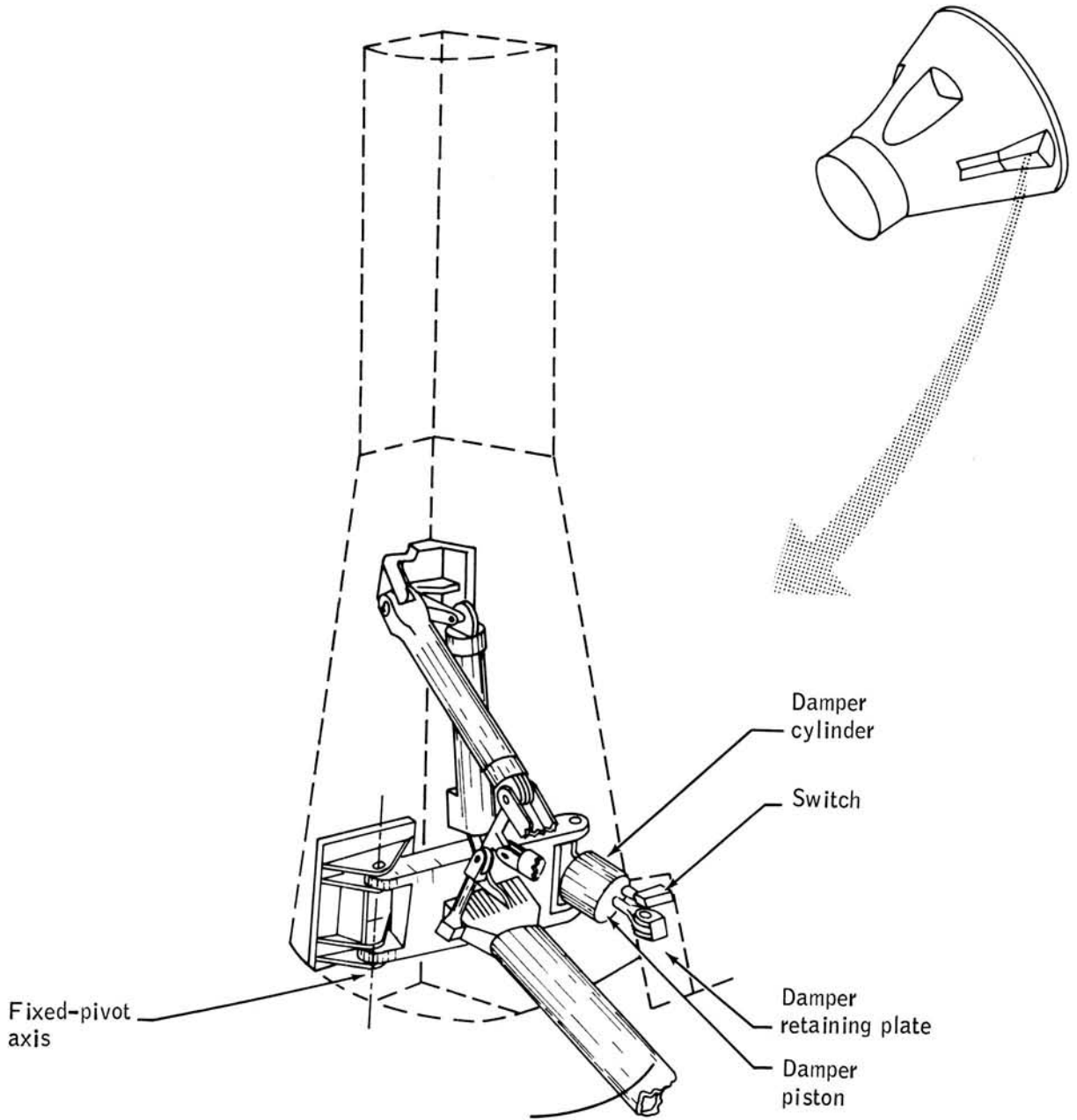


Figure VIII-26.- Gear-stroke sensor.

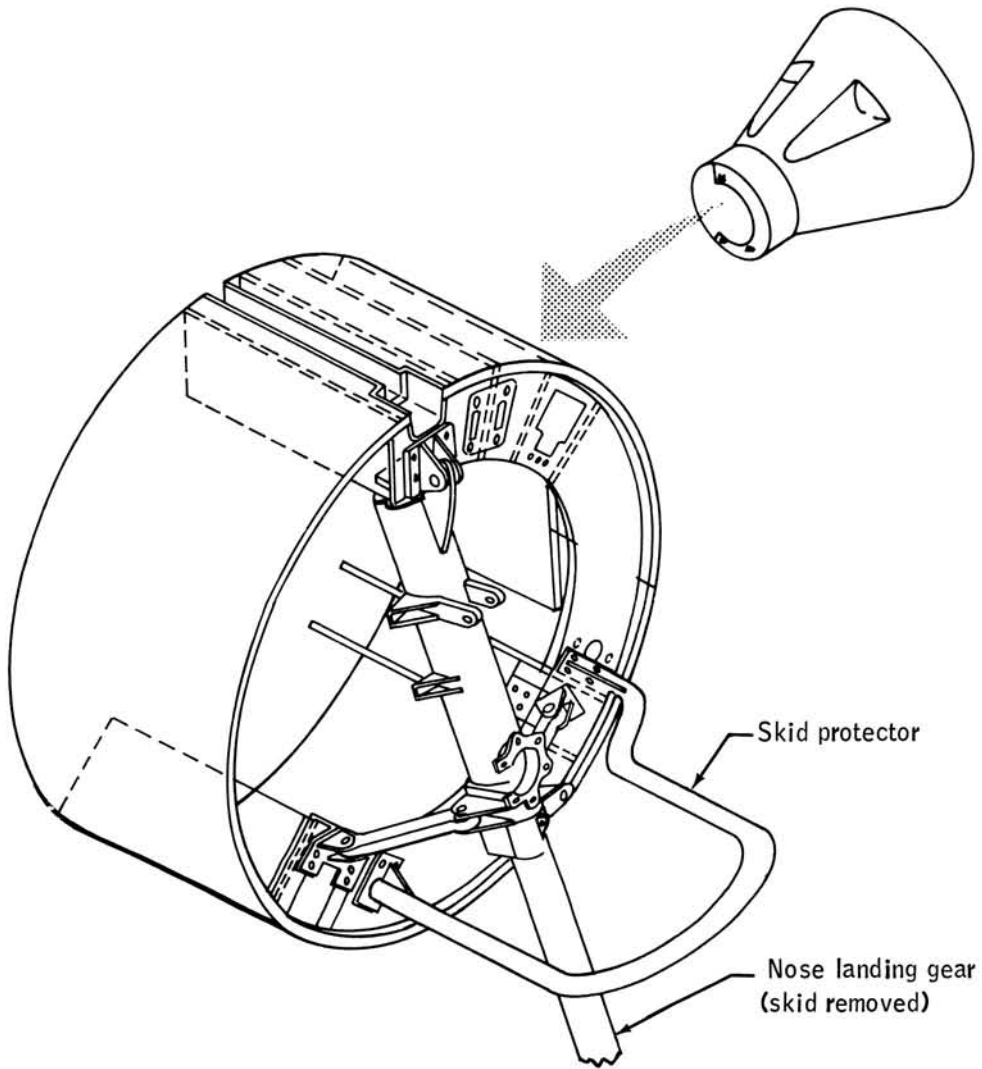


Figure VIII-27.- Skid-protector installation.

PRECEDING PAGE BLANK NOT FILMED.

SECTION IX - VERIFICATION OF THE LANDING GEAR
AND THE TEST HARDWARE

By Leland C. Norman

VERIFICATION OF THE LANDING GEAR AND THE TEST HARDWARE

By Leland C. Norman
Manned Spacecraft Center

SUMMARY

The landing gear originally designed for use with the Gemini spacecraft paraglider was incorporated into the land landing system without change. This section reports the series of tests conducted to verify performance of this landing gear as a system component. In addition, many other hardware and vehicle preparatory tests were conducted to verify individual performance and are contained herein.

INTRODUCTION

The landing gear utilized in the development program was designed and constructed for use with the paraglider, but was eliminated from the Gemini Program before its development was completed. Consequently, the design was fixed at program initiation and a basic development effort such as that necessary for other system components was not required. It was necessary to verify deployment and impact-attenuation characteristics.

In addition to the landing gear, many other hardware items and test implementation devices were employed that were designed and fabricated especially for this program. A mechanical description of these devices is contained in Section VIII. The procedure established and followed was to conduct tests of each device and insure acceptable performance prior to employment in the test program. The more important of these tests are discussed.

LANDING-GEAR VERIFICATION

Deployment Tests

The landing gear is a tricycle-arranged system composed of one air-oil telescopic nose gear and two cantilever main-gear struts which are capable of deflecting as springs. The nose gear is deployed, or extended, by actuating two pyrotechnic valves which open a line connecting two high-pressure nitrogen supply bottles to the strut. This pressurizes the strut and shears a tear link, extending and locking the nose gear in the down position. Each pressure bottle is capable of supplying 125 lb/in.^2 , and the nose gear is designed to extend with only one of two bottles supplying pressure. Figure IX-1 shows the nose-gear pressurization system.

The main gears are extended by pyrotechnic actuators which shear the locking links, pull the struts into position, and lock the overcenter links. Each main gear has two actuator cartridges capable of furnishing approximately 2900 lb/in.^2 , and the main gears are designed to extend and lock with only one of the two available actuator cartridges firing.

The maximum allowable tensile force in the main-gear actuator assembly is 1000 pounds. They also must be manually operable when a force of 50 pounds is applied. Figure IX-2 shows the main-gear actuators.

Pretest simulation. - Before the actual deployment tests, simulated tests were conducted by attaching a high-pressure nitrogen supply line containing a gage and a regulator valve into the pyrotechnic cartridge port of the main-gear actuators and immediately preceding the check valve on the nose gear. The gears were then extended by pressurization with nitrogen. The nose gear required an average value of 55 lb/in.^2 to actuate. The left and right main gears required an average of 1945 lb/in.^2 and 2167 lb/in.^2 , respectively, for extension. These pressure values are well within the design requirements discussed. Following the pressurization tests, a series of pyrotechnic deployments was conducted.

Test setup. - The test vehicle was suspended in the flying attitude from an overhead crane, with the gears in the stowed position. A pressure gage was installed to record nose-gear extension pressure. The main gears are designed to stroke with a pressure range of 400 to 500 lb/in.^2 in the hydraulic damper. This pressure should remain unchanged by deployment. To verify

the end points, the left main damper was pressurized to 500 lb/in.² and the right main damper was pressurized to 400 lb/in.² for these tests. The pyrotechnic actuators, pressure bottles, and so forth, were installed and remotely fired. Figure IX-3 shows the system during test.

Test 1. - All actuators installed and fired.

Results. All three gears extended smoothly. The nose-gear check valve allowed a slight feedback of hydraulic fluid into the pressure bottles. Deployment times were:

Nose gear, sec	0.125
Left main gear, sec58
Right main gear, sec587

Inspection of the main-gear actuators indicated no signs of damage. The nose gear held a pressure of 225 lb/in.², well within the design pressure range previously discussed. The pressure in the main-gear hydraulic dampers did not change.

Test 2. - The test setup was modified to include the installation of three axis-linear accelerometers, located at the vehicle center of gravity, to record resulting vehicle motion. Strain gages were also attached to the main-gear actuators to determine deployment loads. All actuators were again installed and fired.

Results. All three gears extended smoothly. Deployment times were:

Nose gear, sec	0.162
Left main gear, sec60
Right main gear, sec575

Inspection of the main-gear actuators showed no evidence of damage, and extension forces of 500 pounds in the left actuator and 400 pounds in the right actuator were recorded. These tensile loads approximate the midpoint

of the design load range. The peak accelerations recorded at the vehicle center of gravity were 0.25g in both the X and Y planes. The nose gear held a pressure of 230 lb/in.².

Test 3. - This test was conducted to verify the one-actuator deployment case. One actuator per gear was installed and fired.

Results. All three gears extended smoothly. Deployment times were:

Nose gear, sec	0.28
Left main gear, sec688
Right main gear, sec763

The nose-gear check valve again allowed a slight feedback of hydraulic fluid. No evidence of damage was found on the main-gear actuators, and deployment forces of 350 pounds were recorded in each actuator. The nose gear held a pressure of 130 lb/in.², and the main-gear hydraulic-damper pressure remained constant. Accelerations recorded at the vehicle center of gravity were negligible.

Conclusions. - All gear components, with the exception of the nose-gear check valve, operated satisfactorily; and gear deployment was acceptable in every case. One actuator was sufficient for deployment. Gear loads and pressures recorded were in the operable-design range. The nose-gear check valve was reworked prior to incorporation into system testing.

Impact Attenuation Tests

The main gear consists of two cantilevered struts which are capable of deflecting as springs once deployed and locked in the extended position. These gears are pivot mounted and connected to a hydraulic damper which strokes as the gear deflects. The damper action allows a 10-inch vehicle center-of-gravity stroke before the damper piston bottoms out. The hydraulic damper is designed to operate while pressurized with from 400 to 500 lb/in.² of nitrogen. If the vehicle rebounds, this nitrogen pressure forces the damper piston back to the original position so that full stroke is again available for attenuation. After the damper piston bottoms out, an additional 2 inches of

vehicle center-of-gravity stroke are available, due to deflection of the gears. The nose gear is composed of a hydraulic shock-absorber strut with 12 inches of vertical travel. All gears have flat shoes for slideout dissipation of horizontal velocity.

Figure IX-4 contains the gear extension and stroke dimensions. As shown in the figure, the gear-touchdown plane is at an angle of 18.3° to the spacecraft centerline. With the spacecraft suspended in the 13° nose-down attitude, this allows the main landing gear to touch down first, before the spacecraft rotates downward and the nose gear touches down. This method provides the greatest margin of impact stability.

The mathematical landing capabilities of these gears are:

Pitch, 10° nose up to 18.5° nose down

Yaw, $\pm 37^\circ$

Roll, $\pm 10^\circ$

Ground coefficient of friction, 0.2 to 0.5

Sink speed, 10.0 ft/sec limit; 12.9 ft/sec ultimate

Horizontal speed, not critical from the standpoint of accelerations at initial impact.

Attenuation characteristics of the landing-gear system were based upon the following maximum impact accelerations.

Nose landing gear:

Vertical, 3.5g down

Horizontal, 4.0g forward at the center of gravity of the spacecraft

Horizontal, 8.0g forward at the pilot's head

Main landing gear:

Vertical, 2.0g down

Horizontal, 1.0g forward at the center of gravity of the spacecraft

Horizontal, 1.3g aft at the pilot's head

Prior to incorporation of the landing gears into the system testing, a series of static and crane-drop tests was conducted to verify gear-attenuation characteristics and to obtain vehicle landing-dynamics data under closely controlled conditions.

Static tests. - The design pressure limit at which the nose-gear strut and the main-gear damper must exhibit structural integrity is 3000 lb/in.²

Each gear system used in the development program was structurally verified by hydrostatically pressurizing the nose strut and main dampers to this value. No failures were encountered.

In addition to pressure tests, static design loads were applied to each gear to verify structural integrity of the total gear assembly. This was accomplished by securing the inverted test vehicle to a heavy equipment tie-down pad and incrementally applying the range of design loads in the correct vertical, drag, and side directions. Figure IX-5 shows the test setup during the main-gear vertical-load test. No failures were encountered. These tests completed the static verification of the gear assemblies. Following these tests, a series of 13 crane-drop tests was conducted.

Test setup. - The gears were predeployed and the test vehicle was suspended in the flying attitude from an overhead crane, then released to free fall and land. The test vehicle was ballasted to the following conditions: the weight of the test vehicle was 4691 pounds; and the center-of-gravity location was X, 0.00, Y, +2.438, and Z, 132.25. Three axis-linear accelerometers and a pitch angular-rate indicator were located at the vehicle center of gravity to record vehicle motion. Nose-gear stroke was measured by dusting powder on the inner cylinder of the strut before the test and measuring the amount of powder scrubbed off after the test. The coefficient of friction of the landing surface was calculated at 0.41 by measuring the force required to slide the vehicle.

The landing gears were predeployed and pressurized with nitrogen. The nose gear was pressurized to 225 lb/in.², and the main-gear dampers were pressurized to 500 lb/in.² each. Wooden bumpers were attached to the bottom of the test vehicle to prevent the gears from bottoming out and suffering structural damage if the loads should exceed the capability of the gear. Three high-speed cameras recorded the tests. Figure IX-6 shows the test system just prior to release.

Test conduct. - Tests were conducted at each of three pitch attitudes (18.7°, -13°, -8°) for vertical impact velocities of 7.2, 8.4, 9.5, and 12 ft/sec for a total of 12 tests. This series was conducted on a sod surface. A 13th test was conducted on concrete at nominal impact conditions.

Test results. - Table IX-I presents the recorded results for each test. The two values presented are the two major acceleration peaks. The first occurs at initial main-gear contact, and the second occurs when the nose gear contacts, following pitch rotation. All accelerations were measured at the vehicle center of gravity. The absence of certain data points is due to the loss of instrumentation. All times given are in seconds and based on

zero at release. Since no roll conditions were tested, accelerations in the X-axis were negligible.

At all pitch attitudes and velocities tested, initial peak accelerations are in the vicinity of 4g in the Y plane and 1g to 2g in the Z plane. Angular accelerations recorded indicate peak values of from 7 to 16 radians/sec² in the positive direction. The secondary acceleration peaks, occurring when the nose gear impacts, show a range of from 3g to 6g in the Y plane and around 2g in the Z plane. Peak angular accelerations were from 5 to 10 radians/sec² in the negative direction. No gear damage was received during these tests.

Conclusions. - The landing-gear system has successfully demonstrated structural integrity throughout design loading and limiting burst pressures. It will successfully attenuate a vertical velocity envelope from 0 to 12 ft/sec throughout a pitch attitude range from -8° to -18.7° (nominal -13°, ±5°).

TEST VEHICLE AND SUPPORTING HARDWARE

These test series concern verification of specific devices designed and developed to achieve various Gemini spacecraft simulation functions.

Rendezvous and Recovery Canister Release Mechanism

Since deployment of both the main and reserve parachute systems was dependent upon successful separation of the R and R canister, a redundant separation system was designed and statically tested prior to drop tests. The R and R canister separation was accomplished by means of a squib-actuated release mechanism (section VIII). This mechanism consists of two pivoted dogs restrained by a common linkage. The dogs engage steel straps on the R and R canister and mate the two vehicle sections. Separation occurs when the linkage is broken. The linkage is a three-piece member held together with two shear pins. Pyrotechnic squibs are ignited on signal and eject the restraining pins, thus separating the linkage. Activation of either pyrotechnic squib is sufficient to separate the linkage. The drogue parachute attached to the R and R canister furnished the force to separate the two vehicle sections.

Test setup. - The R and R canister was mated to the test vehicle in the vertical position. The drogue parachute force was simulated by a system of weights rigged through two pulleys and attached to the R and R canister bridle such that the pulloff angle coincided with the drogue parachute riser.

Since the R and R canister movement was vertical, the weight of the R and R canister (246 pounds) was added to the listed weight for each test condition. These tests were conducted with the basic test vehicle primarily to verify the separation mechanism.

Test 1. Nominal conditions: (1) both squibs activated; (2) 500-pound separation force; and (3) force evenly distributed through the R and R canister V-bridle.

The results showed that the R and R canister separated cleanly, with no evidence of binding.

Test 2. Asymmetric overload conditions: (1) one squib activated; (2) 1200-pound separation force; and (3) force applied through one V-bridle leg, 35° pulloff angle.

The results indicated that the R and R canister separated cleanly, with no evidence of binding. It pitched approximately 25° after separation.

Test 3. Failed drogue conditions: (1) one squib activated; (2) 50-pound separation force; and (3) force applied through one V-bridle leg, 35° pulloff angle.

The results indicated a clean separation, with no evidence of binding.

Conclusions. - The separation mechanism provided positive separation of the R and R canister under the range of conditions in which it must operate during tests. When the nose landing gear and emergency parachute were added to the system, separation clearance tests were conducted to insure that binding would not occur at separation.

Attitude-Change Tests

The vehicle changes from the heat-shield down attitude to the horizontal flying attitude after the main parachute has fully inflated. Prior to attitude change, the rear risers, the V-bridle, and the turn lines are stowed in the ripout channel. During the test program, failures occurred wherein the turn lines broke at attitude change. Film coverage of the drop tests was inadequate to pinpoint the strip-out action of the risers. In order to determine the riser action and to verify the turn-line stowage, two static attitude-change tests were conducted. The forces resulting from attitude change while rigidly suspended were significantly higher than those resulting from attitude change while elastically suspended; however, the critical part of the action occurs during strip-off and prior to assumption of loads by the risers.

Test setup. - The vehicle was suspended in the heat-shield down attitude from two cranes, with the risers and turn lines stowed in the ripout channel as for flight. The attitude-change disconnect was then remotely fired. For the first test, the 19-inch elongation allowance was erroneously omitted. Four 16-mm cameras at 400 frames/sec and one at 3000 frames/sec recorded the tests. Figure IX-7 shows the risers and turn lines in the stowed position. Figure IX-8 shows the suspended vehicle prior to release.

Test 1. The risers stripped from the channel and cleared the turn-line area, and the turn lines deployed evenly. Strip-out began at the cylindrical section and progressed rapidly down the channel. As the vehicle reached the lowest position, both turn lines failed in tension due to the error in elongation.

Test 2. The risers stripped from the channel, as previously described, and cleared the turn-line area. Both turn lines deployed correctly. As the front risers reached peak load at the end of attitude change, the front riser extensions (test-implementation device) failed in tension due to loading approximately three times that experienced in flight, allowing the vehicle to take a 25° nose-down attitude. This did not affect the turn lines.

Conclusions. - The risers strip from the channel evenly and rapidly, beginning at the cylindrical end. The turn-line stowage method shown in figure IX-7 is acceptable.

Zero Altitude Sensors

Three types of zero altitude sensors were employed during the test program to disconnect the parachute at impact.

Inertia switch. - During tests without the rocket motors when the system impacted on water, a simple inertial impact switch was used. This device is a preset, g-sensitive series of mechanical contacts that mate when the preset g-loading is met or exceeded. The mating contacts complete an electrical circuit which, in turn, fires the parachute disconnects.

Prior to each test, the inertia switch was set at the desired acceleration level and checked by mounting it on a centrifuge in all three planes and measuring the g-loading at closure. This was repeated three times in each plane. In all tests, closure accelerations were repeatable within 5 percent.

Zero altitude sensor for salt water use (fig. VIII-12(a)). - When the rocket motors were incorporated into the test program, the impact switch was no longer feasible for use since the accelerations experienced during rocket fire were approximately the same as those resulting from water impact. The

zero altitude sensor for salt water use was developed to allow retention of the parachute during rocket fire and still facilitate separation at touchdown. This device is a pair of brass electrodes with an adjustable gap. A 24-volt source is applied across the ends of the electrodes. When the switch is immersed in salt water, sufficient current is established to complete the disconnect circuit.

To verify the functioning of this switch prior to incorporation into the test program, a 24-volt power source was placed across the electrodes, and the switch was immersed in a bucket of salt water obtained from Galveston Bay. An ammeter was placed in the circuit to measure the current. The electrode gap was varied from $9/32$ to $31/32$ inch.

During these tests, a minimum current of 4 amperes was measured at any setting up to $3/4$ inch. A match squib was installed in the circuit and fired at all settings. It was concluded that the salt water switch was acceptable for operation and that an electrode gap of $3/8$ inch should be used.

Gear-stroke sensor. - In the drop tests conducted over land, a sensor was developed which allowed retention of the parachute during rocket fire but jettisoned the parachute at touchdown. This device was a microswitch mounted between the main landing-gear damper and the damper retaining plate so that the switch was in the closed position until the gear stroked. As the gear deflected, the gear damper cylinder moved along the piston, releasing pressure on the microswitch and allowing it to open and trigger the disconnect circuit.

To verify this gear-release method, the microswitch was mounted in position while the gears were stowed. Flashbulbs and a power source were placed in series with the microswitch such that activation of the switch would fire the flashbulbs. The gears were then pyrotechnically deployed. This process was repeated three times. The switch did not activate during deployment. Following each deployment, one main gear was stroked by hand. The flashbulbs fired each time after approximately 2 inches of gear stroke.

It was concluded from these results that this device had adequately met the performance requirements, and it was incorporated into system testing.

Disconnect Hardware

The disconnect hardware is used to allow instantaneous jettisoning of the Para-Sail in the event of malfunction and at impact to prevent vehicle tumbling due to being dragged. Two basic types of disconnects are used. The attitude-change disconnect (fig. VIII-18) is located on the nose-gear pallet and

retains all the risers while the vehicle is in the heat-shield down attitude. This mechanism consists of a pivoted post held in place with a high-strength shear pin. A pyrotechnic squib dislodges the shear pin and allows the post to rotate, freeing the risers.

There are four riser disconnects (figs. VIII-18 and VIII-19) which support the spacecraft while in the flying attitude. These disconnects incorporate a high-strength retaining pin in double shear which is dislodged by a pyrotechnic actuator. In both disconnect types, lead buffers are used to dissipate the shear-pin energy and prevent rebound.

Test setup. - Static firings and pull tests were conducted on each disconnect to verify the following:

1. The structural integrity of the disconnect assembly at maximum load; 10 000 pounds on each riser disconnect, 20 000 pounds on the attitude-change disconnect.
2. The size of the pyrotechnic charge required to activate.
3. Disconnect operation at maximum load.
4. Disconnect operation at zero load (failed parachute case).
5. The amount of lead buffers required.

Test conditions. - The disconnect devices were mounted on a fixed block with a three-ply, 10 000-pound webbing attached to the riser end. A load link was attached to the webbing and to a crane hoist. Force was then applied until the desired load was reached. The pyrotechnic actuators were then remotely fired. All actuators were 3/8-inch, electrically-initiated pyrotechnic pressure cartridges (RSPC 58080).

Test results. - All disconnect devices demonstrated structural integrity at the rated maximum loads. The attitude-change disconnect and three of the four riser disconnects actuated satisfactorily under zero and maximum load conditions. The rear V-bridle disconnect (fig. IX-9) failed to separate at the maximum load condition. A small booster charge was added to supplement the actuator, and the disconnect was satisfactorily separated in two additional tests.

Conclusions. - The disconnect devices are satisfactory for use in the test program. Each device should be inspected for damage and pull-tested to maximum load before each system test.

Cable Cutters

The turn cable cutters are located on either side of the rear V-bridle attach point where the turn cables exit the spacecraft structure (fig. IX-9).

The cable cutters are used to sever the turn-line cables and perform with the riser releases to allow instantaneous jettisoning of the Para-Sail in the event of malfunction and, at impact, to prevent vehicle tumbling due to being dragged. Since the early drop tests were conducted over water, the cable cutters also had to effect a watertight seal after severing the turn cables to prevent water from leaking into the pressure vessel.

The turn cables are routed through slots in the cutters while in operation. When activated, a pyrotechnic gas generator fires a piston into the cable, shearing it on the far end of the slot. The reservoir between the end of the slot and the end plate of the housing is filled with grease. As the piston moves forward, it forces this grease back along the sides of the piston and forms the watertight seal. Lead buffers are used to dissipate the piston energy and prevent rebound.

Test conditions. - Four static firings of each device were conducted to determine and verify the following:

1. The structural integrity of the cutter assembly.
2. The size of the pyrotechnic charge.
3. The amount and type of sealant.
4. The amount of lead buffers.

Test setup. - The cable cutters were affixed in a vise with the cables inserted through the slots. Tests were conducted with zero load in the cable and with 100-pound tension. For one test, the turn-line load-link lead was also inserted through the slot.

The entire piston reservoir was filled with vacuum grease as a sealant. Leakage tests were conducted by mounting the cable cutter to the bottom of a bucket with a slot cut to allow free passage of the turn cable. After the cutter was fired, the bucket was filled with water and observed for leakage. A 3/8 inch, electrically-initiated pyrotechnic pressure cartridge (RSPC 58080) was used as the cutter actuator in each test.

Results. - The cutter cleanly severed the cable in each test. When the instrumentation lead was included in the cutter slot, it was also cleanly severed. No leakage was observed in tests of the sealant.

Conclusions. - The cable cutters demonstrated satisfactory performance.

Load Cells

Load cells were employed to measure and continuously monitor all parachute loads and were operated in conjunction with the disconnect devices. These cells have a cylindrical shank, with a pin connector at each end for attachment to the disconnect and the risers. Strain gages are mounted on the shank to record loads. Load carrying capability is varied by varying the diameter of the hole bored through the shank of the cell. A 20 000-pound cell is used with the attitude-change disconnect, and 10 000-pound cells are used on the individual risers. Prior to each test, each cell was inspected by X-ray for damage and pull-tested to insure structural integrity and calibration repeatability.

Test setup. - Loops of three-ply, 10 000-pound webbing were fixed in each end of the load cells. One end was fixed while the other was attached to a load recorder and then to a crane hoist. Force was gradually applied until the desired maximum load was reached.

Results. - While this was a continuing process as the development program proceeded, the load cells bore up remarkably well. A total of five cells was replaced during the twelve-test program as a result of the pretest verifications described here. One load cell failed during an actual system test due to an inadvertent bending load.

Rocket-Motor Mounting and Alinement Hardware

The alinement of the rocket-thrust line through the vehicle center of gravity is critical since misalignment would create a moment tending to upset the vehicle.

The rockets are mounted to a pivoted plate at the nozzle end (Vol. II, Sec. VIII, fig. VIII-14) and to a threaded eyebolt (fig. VIII-14) at the igniter end. Adjustment of these mounts allows both roll and pitch movement of the motors to facilitate alinement.

The determination of the thrust-line axis is accomplished by the alinement fixture (fig. VIII-15). The fixture plug fits in the motor nozzle, and the pointer duplicates the thrust axis.

Test setup. - Several static tests of alinement travel and accuracy were conducted, and the motor mounts were pull-tested to 1.5 times the expected peak loads.

1. Alinement fixture: One rocket motor was mounted on the vehicle and the alinement tool affixed. The thrust line was marked on a plate inside the vehicle. The fixture was removed, reinstalled, and the thrust vector re-marked five times.

2. Motor mounts: (1) Adjustment travel. The rocket motor was mounted in the vehicle and the alinement tool affixed. The mounts were then traversed the full range of pitch travel to determine if alinement could be achieved throughout the Gemini spacecraft center-of-gravity range. (2) Pull tests. The mounts were individually loaded by a hydraulic jack simulating rocket thrust.

Test results. - The test results are noted.

Alinement fixture: The alinement pointer scribed a circle of approximately 3/16-inch diameter. When alining the motors for systems testing, this variation was accounted for by rotating the pointer and fixing the vehicle center of gravity in the center of the circle thus inscribed.

Adjustment travel: The travel was sufficient to allow alinement at any point within the Gemini spacecraft center-of-gravity range.

Pull tests. - These tests demonstrated the structural integrity of the motor mounts. (Although the mounts showed no permanent deformation in these tests, a 5° vehicle pitch change occurred during the first system crane drop that was attributed to elastic deflection of these mounts. As a result, the mounts were thickened structurally, and the pull tests, just described, were repeated with satisfactory results.)

Conclusions. - The means of alinement are acceptable and the motor mounts perform satisfactorily. A discussion of alinement during the system-test program is contained in the analysis of the results in Volume I.

Flotation Tests

To allow passive attenuation of impact accelerations while the system was being developed, the first nine full-scale tests landed in the water. A flotation-test series was conducted to insure that the test vehicle was compatible with water landings. The objectives of these tests were to verify the integrity of the pressure shell and door seals and to determine the flotation attitude and the amount and location of flotation aids.

Test setup. - The test spacecraft was ballasted to 4800 pounds and the Gemini spacecraft center-of-gravity location, lowered into a water tank by means of a crane, and the flotation characteristics were noted. The vehicle was then rolled in the water to a point where the doors were submerged. This is shown in figure IX-10.

Results. - Without buoyant material located in the conical and cylindrical sections, the spacecraft floated heat shield up. Several leaks around the door were noted. Figure IX-11 presents the flotation attitude with the forward section flooded. Figure IX-12 presents the flotation attitude with 2/3 of the forward section sealed against flooding. The pressure vessel showed no evidence of leakage other than at the door seals.

Test series 2. - Styrofoam (14 ft³) was added to the conical section forward of the pressure vessel and to the upper access hatch sections, and the door seals were reinforced with RTV. The test vehicle was then placed in the water tank and rechecked for leakage and flotation attitude. These tests verified pressure-vessel and door-seal integrity and indicated a nominal Gemini spacecraft horizontal-flotation attitude. Figure IX-13 shows the test vehicle following an actual water landing.

TEST IMPLEMENTATION DEVICES

Launch-Cradle Tests

The drop cradle (figs. IX-14 and IX-15) was designed and employed to launch the test vehicle from a C-119 aircraft. Launch was accomplished by releasing a helicopter cargo hook attached to a retractable arm (fig. VIII-13) in the test vehicle. After release, the test vehicle slid down the cradle by means of rollers at the aft end of the cradle and a cylindrical section support that rolled down the incline with the vehicle.

Pitch-attitude tests. - This means of launching imparted a pitch moment to the test vehicle as it left the aircraft. Tests were conducted to determine the pitch travel to be expected before the drogue parachute opened and to insure that the possibility of drogue entanglement did not exist.

Test setup: The vehicle and cradle were placed on the rear of a flat-bed truck, simulating the drop aircraft, and released. High-speed film coverage was employed to determine pitch travel and rate.

Results: These tests indicated that the test vehicle would rotate 140° to 190° at drogue parachute opening. This range is compatible with effective drogue operation, with no possibility of drogue fouling due to pitch.

Roll moment tests. - When the blast deflector was added to the system, tests were conducted to determine if the rolling moment due to the blast deflector would cause the vehicle to roll as it slid down the incline. Roll travel could result in the blast deflector striking and/or hanging up on the cradle at release.

Test setup: The test vehicle and cradle were placed on the rear of a flat-bed truck, simulating the drop aircraft, and released. High-speed film coverage was employed to discern roll and possible fouling.

Results: The test vehicle rolled when released, causing the blast deflector to strike the cradle arm and impart a yaw moment to the spacecraft. It was concluded from analysis of the film that the vehicle could have hung on the cradle or struck the rear of the aircraft as it exited.

Following this test, a metal plate was welded to the cylindrical section of the test vehicle (fig. IX-15) such that it mated with the end of the carrier on the cradle and formed a rotation stop. In addition, the top of the left cradle post was cut off to provide additional clearance for the blast deflector.

When these modifications were made, two additional release tests were conducted in the manner previously described. Both of these tests resulted in a clean launch with no evidence of roll or binding. This launch method was successfully used throughout the test program.

Blast Deflector

Since activation of the landing rockets either inside the drop aircraft or during launch would jeopardize the aircraft and crew, a mechanical device was designed as a backup to the electrical lockouts to neutralize the rocket thrust

and to vent the exhaust gases. This design also included a release mechanism so that the blast deflector could be jettisoned once the test vehicle had cleared the aircraft. A static test was conducted to determine the effectiveness of the design.

Test of blast deflector I. - Deflector I (fig. IX-16) was constructed from welded aluminum plate, weighed 125 pounds, and was attached to the test vehicle by two points at the tee section and one point at the motor nozzle end. In operation, the motor gases exhaust from the rockets into a common manifold, are turned 90° , and travel through the deflector body to the tee section where they are split into two 180° exhaust streams, canceling any resultant thrust. While the test vehicle is in the launch aircraft, the tee section extends outside the aircraft. The inside of the blast deflector was lined with RTV to reduce erosion during rocket fire.

Test setup: The test vehicle was suspended between two cranes with the Z-axis horizontal and rolled 90° so that the rocket motors exhausted in a horizontal plane. In this manner, any thrust not canceled would cause the vehicle to swing. Four cables were attached to the vehicle to restrict motion (fig. IX-16).

Three linear accelerometers and one angular accelerometer were installed at the center of gravity of the vehicle to determine the net resultant thrust vector. Four high-speed 16-mm cameras and one 70-mm Hulcher sequence camera recorded the test.

Test procedure: The vehicle was ballasted to the correct weight and center-of-gravity location and suspended from the two cranes. After installation of the rocket motors and the blast deflector, the motors were remotely ignited.

Test results: Approximately 0.2 second after ignition, the forward deflector attach point failed structurally, and the deflector was blown 75 feet from the vehicle. Examination of the failure indicated that the overall design loads were too low. This under design was accentuated by a faulty weld on the forward attach point. The deflector body was bulged outward due to the high internal pressure. This swelling increased the load on the attach points by pushing the side of the deflector against the vehicle before failure.

Conclusions: The existing blast deflector and attach points were unsatisfactory and a redesign was necessary.

Blast deflector II. - The second deflector (fig. IX-17) resulted from the design information gained from the test of the initial configuration. Deflector II was constructed of 6-inch steel pipe, with reinforced elbow and tee

sections. Splitter vanes were placed at the tee section to separate the exhaust equally. The RTV reinforced with expanded metal was installed in the elbows and splitter sections to prevent erosion. The total weight was 350 pounds.

Test setup: The vehicle was suspended from the two cranes as previously described. A load cell was attached to the vehicle at the approximate center of gravity to verify the accelerometer data. A cable connected the load cell to a stationary point. Instrumentation and camera coverage were identical to the previous test.

Test results: Figure IX-18 shows the test in progress. The blast deflector maintained its structural integrity throughout rocket fire. The peak acceleration recorded by the linear accelerometers was 0.28, which corresponds to approximately 1000 pounds. The peak angular acceleration was 1.245 radians/sec, which equals a force of 624 pounds applied at the exit plane of the blast deflector. The load cell recorded a resultant force of 515 pounds. This net resultant force was caused by the exhaust gases tending to follow the outside curvature of the deflector, thereby being separated into two unequal streams, creating torque on the vehicle. The resulting forces and accelerations were well below the gust loads experienced by the drop aircraft and posed no threat to the aircraft or crew.

Conclusions. - Blast deflector II was satisfactory in that it provided adequate protection to the aircraft and crew should an accidental firing occur. It was recommended that the launch crew wear masks for protection against the toxic fumes that could remain inside the aircraft should the rockets fire.

Blast-deflector attach points and structural integrity. - The blast deflector is attached to the test vehicle by three open hooks at one end and a high-strength shear pin at the other (fig. VIII-16). Release is accomplished by dislodging the shear pin and allowing the blast deflector to rotate free of the open hooks. Prior to conducting the test of blast deflector II, a static test was conducted to verify the integrity of the attach points.

Test setup: The blast deflector was attached to the vehicle with the rocket alignment ports removed. A hydraulic jack was placed inside the vehicle, mounted on the center-of-gravity post so that the ram extended through the alignment port and pushed outward on the blast deflector. Load was then gradually applied until the peak high-thrust value was reached.

Results: This test initially demonstrated the structural integrity of the attach points. Final verification was made by the test firing previously discussed.

Blast-deflector jettison mechanism. - Once the test vehicle has cleared the launch airplane, the blast deflector has served its test purpose and can be jettisoned and recovered. The blast deflector is attached to the test vehicle by means of three open hooks on the vehicle that mate with fixed pins on the blast deflector at one end and a shear pin through a restraining collar at the other end. The blast deflector is jettisoned by igniting a gas generator that forces the shear pin free of the restraining collar, allowing the blast deflector to rotate free of the open hooks and fall away. A detailed description of this mechanism is contained in section VIII.

Lead buffers in the shear-pin restraining cylinder dissipate the generated energy and prevent the shear pin from rebounding. A 28-foot d_0 parachute, with the deployment bag permanently attached to the heat shield, is used for recovery. The blast deflector deploys this parachute from the fixed bag as it falls away from the test vehicle. A static blast-deflector jettison test was conducted prior to incorporation into the system test program.

Test method: The test vehicle with the blast deflector attached was suspended from a crane in the 13° nose-down flying attitude; then the pyrotechnic gas generator was remotely ignited. High-speed cameras were employed to determine jettison dynamics.

Results: The blast deflector separated cleanly at the motor nozzle end, rotated approximately 80° about the open hooks, and fell vertically. Jettison was almost immediate, with no evidence of binding or recontact.

Conclusions: The blast-deflector jettison mechanism was satisfactory.

CONCLUDING REMARKS

With the exception of the landing gear, the hardware test items were developed to implement the land landing system development effort and were generally unique in design and function. The hardware test series validated individual performance prior to incorporation into system testing. The most important verification came as a part of the successful full-scale test program.

TABLE IX-I. - GEAR IMPACT TEST RESULTS

Drop	Pitch alti- tude, deg	Vertical velocity, ft/sec	Main gear impact						Nose gear impact						Nose- gear stroke, in.	Com- ments (a)
			Y		Z		Angular		Y		Z		Angular			
			g	t	g	t	Rad/ sec ²	t	g	t	g	t	Rad/ sec ²	t		
1	-18.7	7.2	--	--	--	--	--	--	--	--	--	--	--	--	--	B
2	-18.7	8.4	1.9	0.272	--	--	7.1	0.300	--	--	5.1	0.33	--	--	--	
3	-18.7	9.5	3.9	.310	--	--	9.1	.321	--	0.414	2.2	0.40	5.6	.35	--	
4	-18.7	12	7.7	.384	2.6	0.370	12.1	.394	--	--	--	--	9.1	.44	--	A, B
5	-13	7.2	3.1	.240	1.5	.248	9.1	.250	3.9	.340	--	--	8.1	.34	10	A, B
6	-13	8.4	3.9	.275	--	--	11.1	.286	4.6	.40	--	--	8.1	.36	10.5	A, B
7	-13	9.5	4.3	.313	1.4	.330	11.6	.319	6.2	.432	-1.47	.460	9.1	.39	10.75	A, B
8	-8	7.2	3.1	.240	1.4	.280	9.1	.252	6.2	.400	-1.8	.480	6.1	.40	9.5	A, B
9	-8	8.4	3.5	.273	1.4	.298	10.6	.287	5.8	.405	-2.2	.400	8.1	.40	9.5	
10	-8	9.5	3.1	.315	1.4	.325	10.1	.321	5.4	.442	-2.6	.420	6.6	.418	10.0	
11	-8	12	2.7	.381	--	--	12.1	.393	3.1	.489	--	--	10.1	.500	10.5	A, B
12	-13	12	3.1	.369	1.1	.410	16.7	.390	3.1	.414	--	--	8.1	.45	--	
13	-13	7.2	--	--	--	--	--	--	--	--	--	--	--	--	10.0	C

^aA = Nose bumper hit surface; B = sod surface; C = concrete surface.

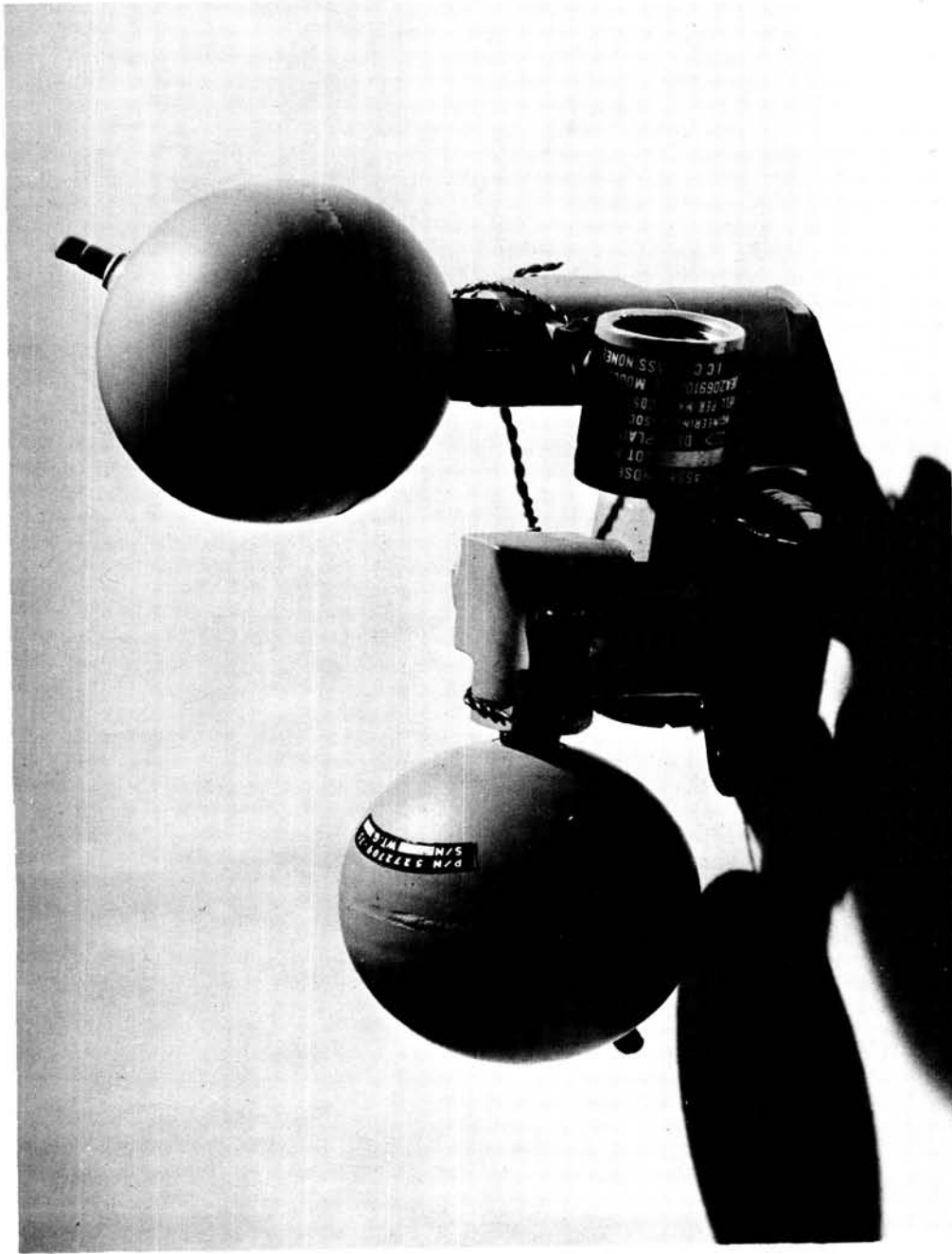


Figure IX-1.- Nose-gear pressurization system.

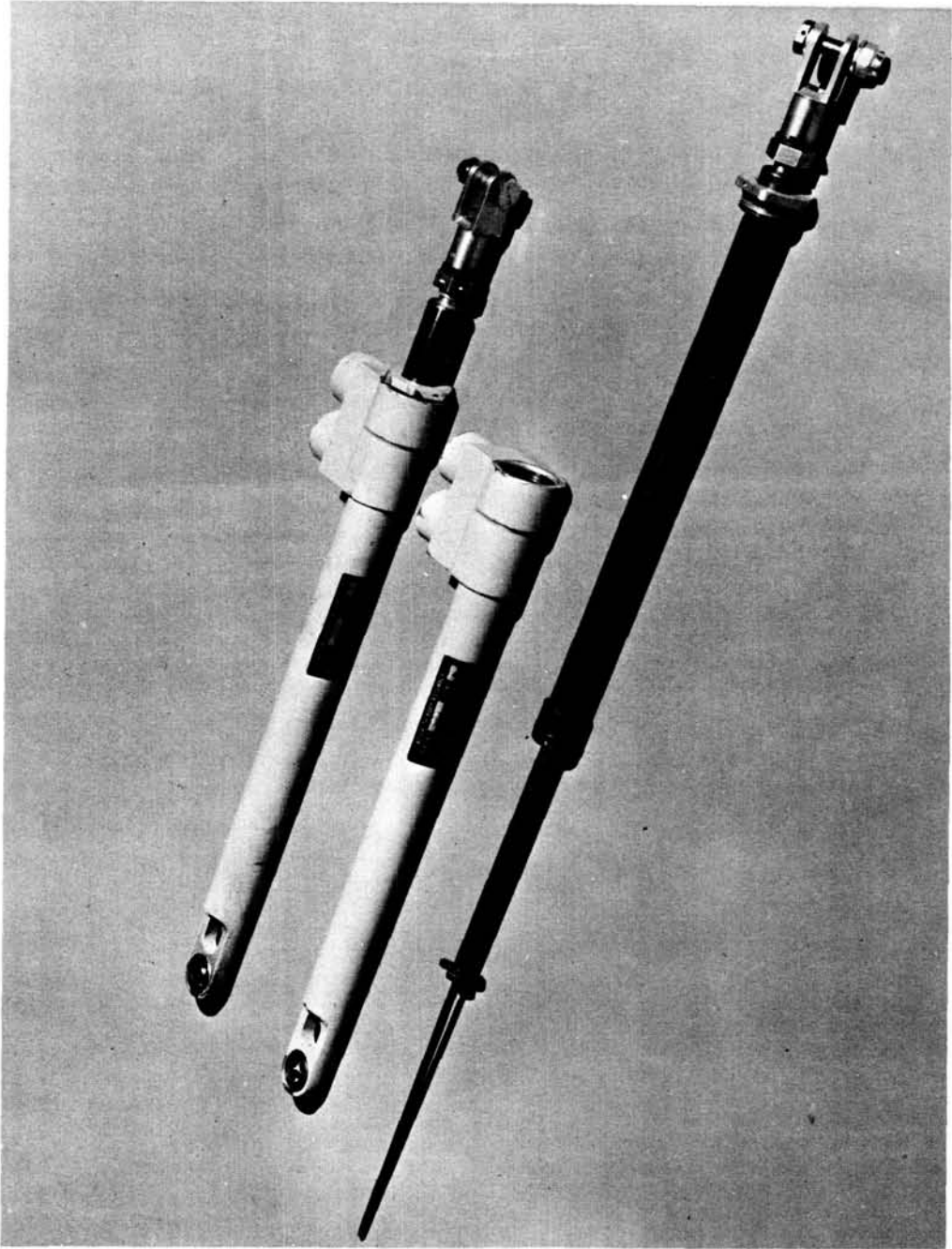


Figure IX-2.- Main-gear deployment actuators.



Figure IX-3.- Gear deployment test.

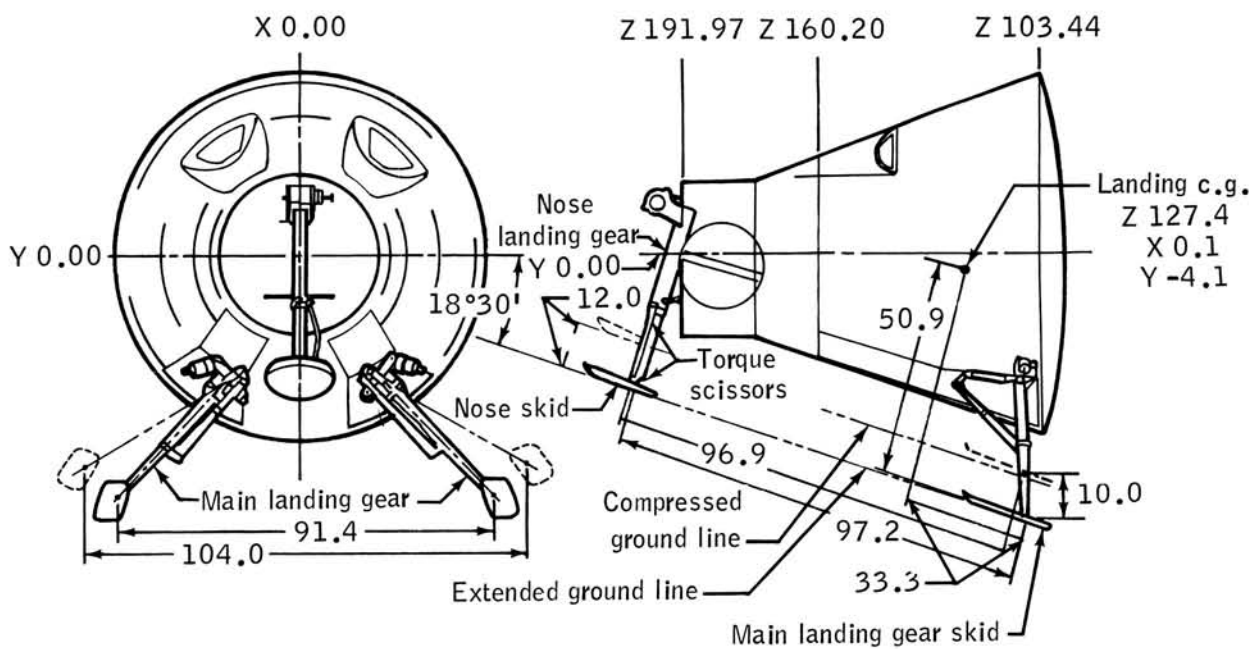


Figure IX-4.- Landing-gear extension and stroke dimensions.

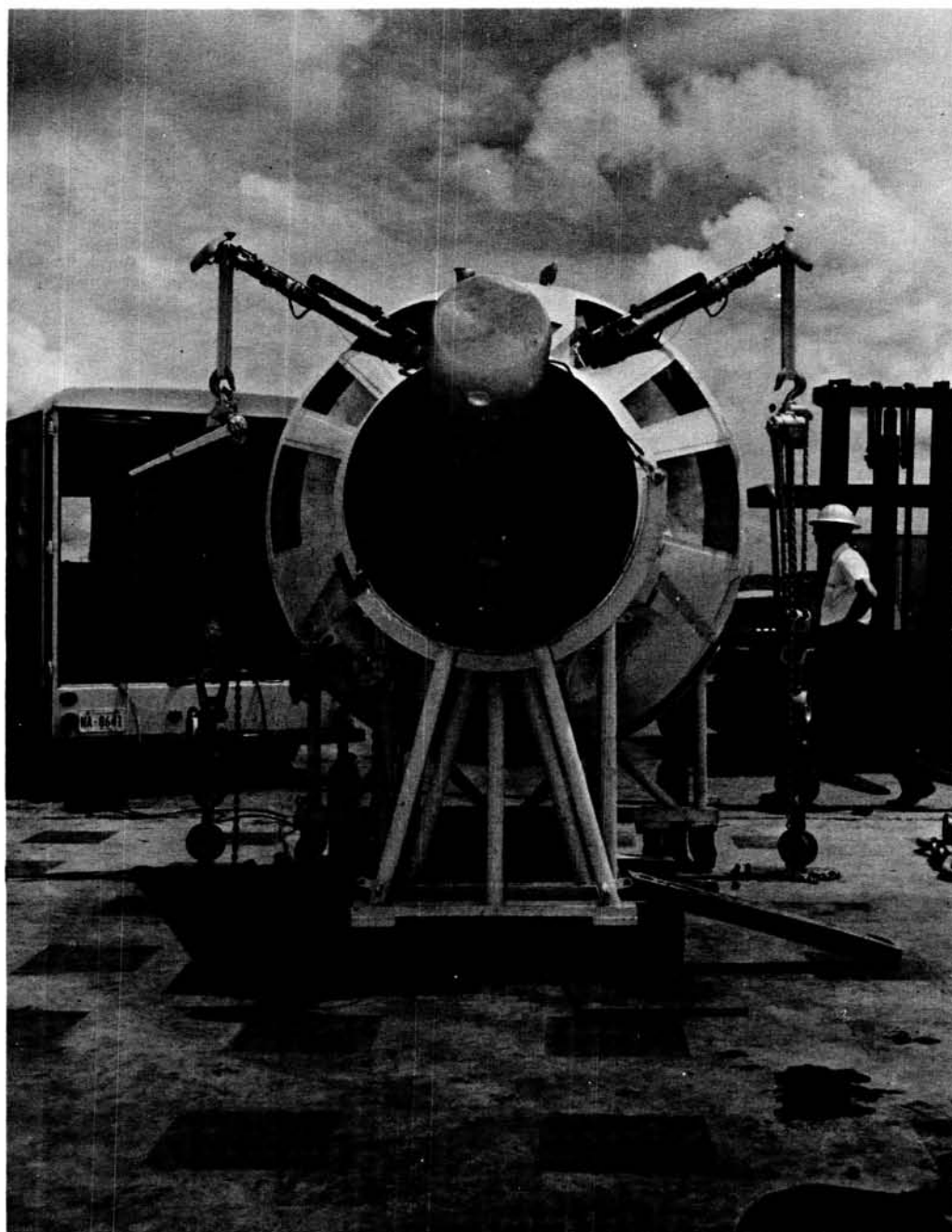


Figure IX-5.- Landing-gear static-load test.



Figure IX-6.- Landing-gear crane drop.



Figure IX-7.- Riser and turn-line stowage.



Figure IX-8.- Attitude change, test setup.

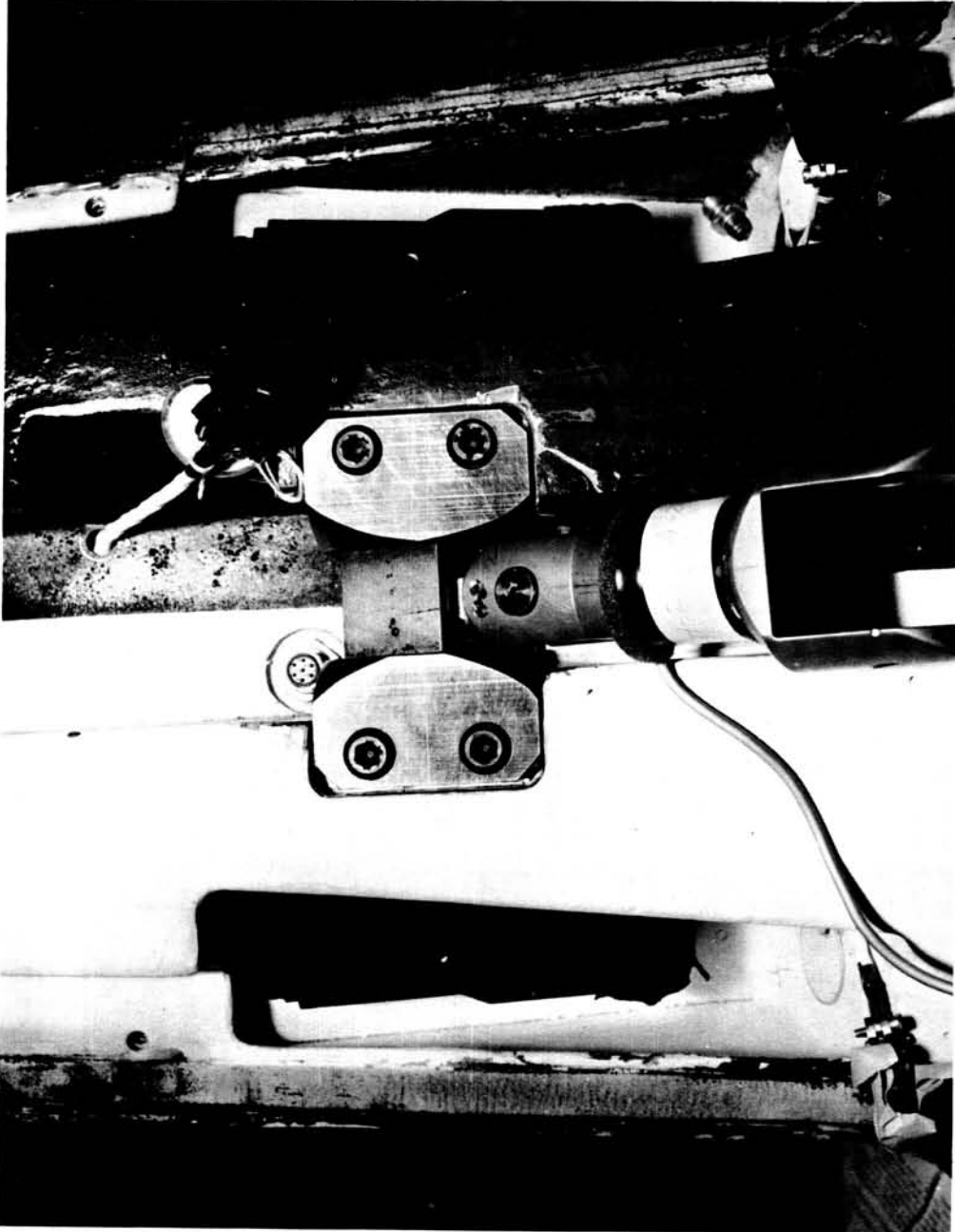


Figure IX-9.- Rear V-bridle disconnect and cable cutters.

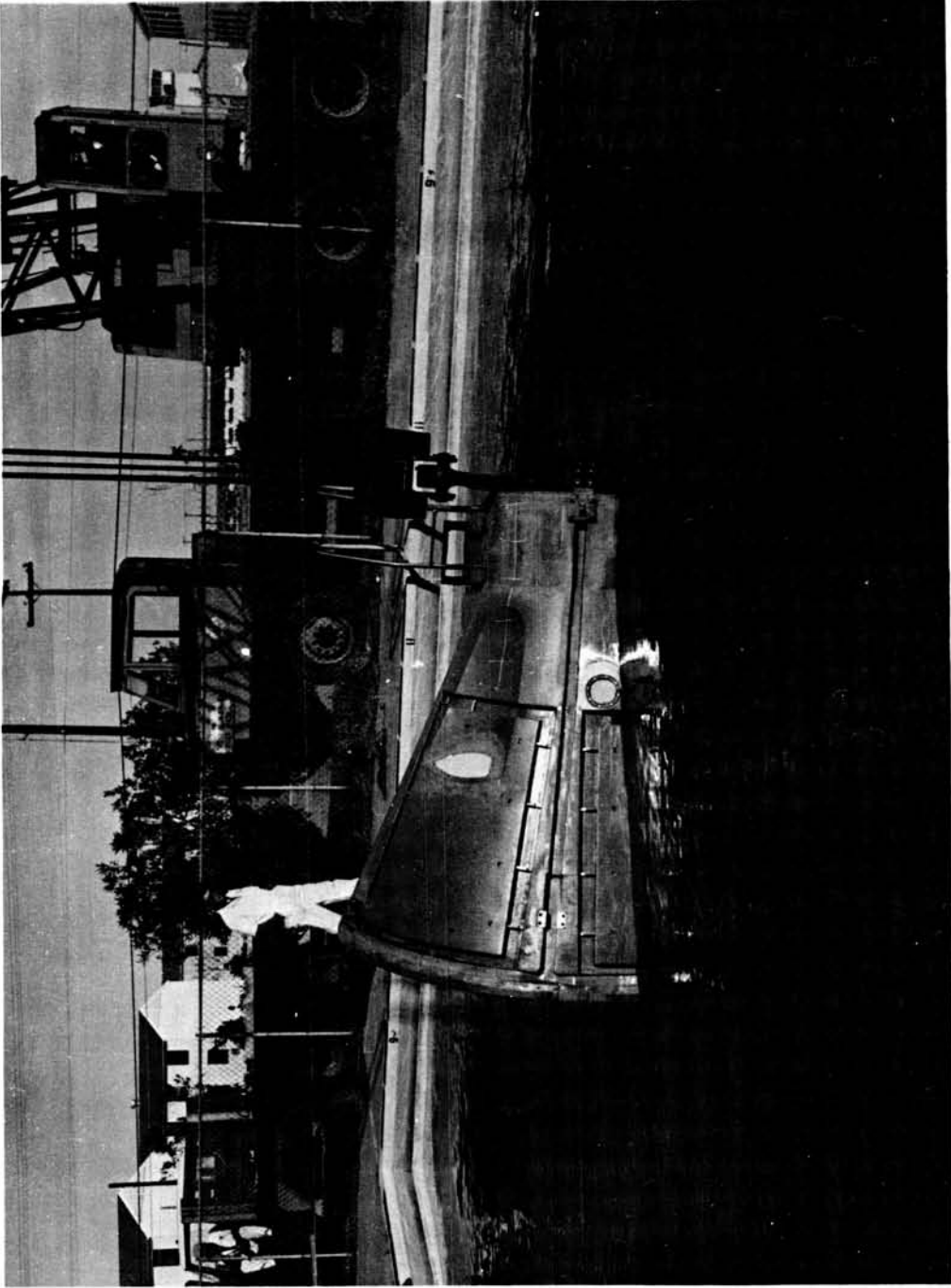


Figure IX-10.- Door-seal integrity test.

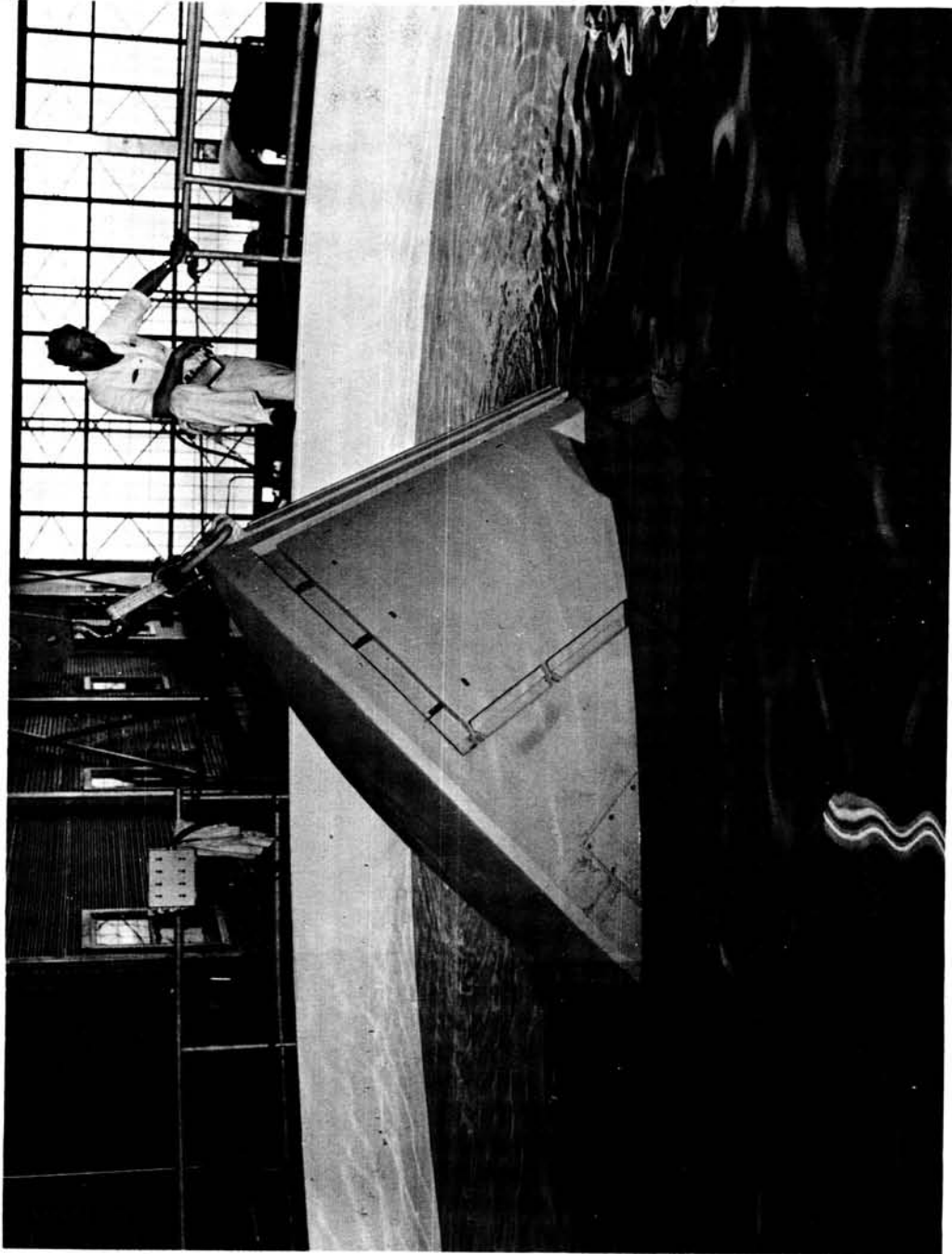


Figure IX-11.- Flotation attitude, forward section flooded.

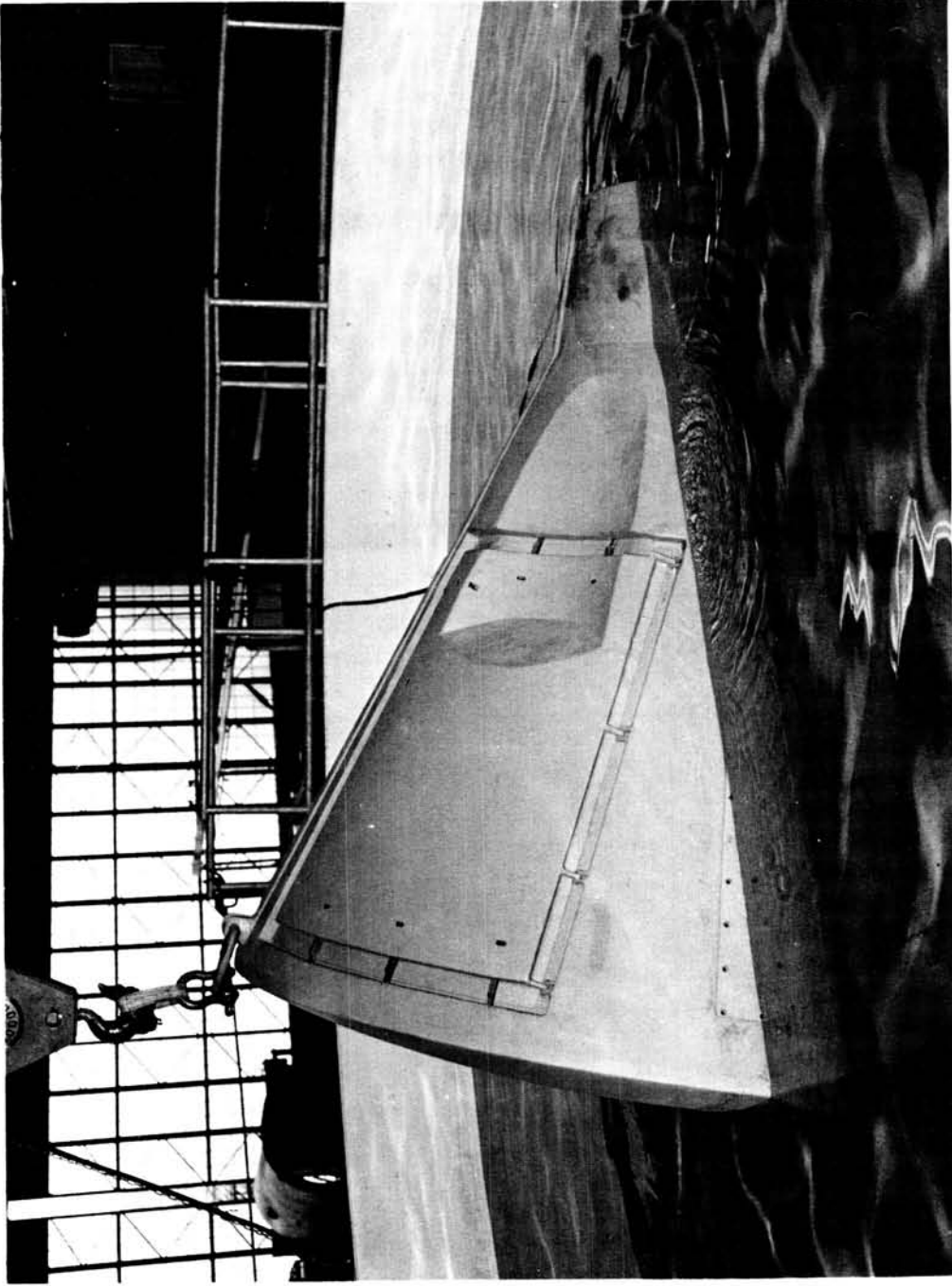


Figure IX-12.- Flotation attitude, two-thirds of forward section sealed.

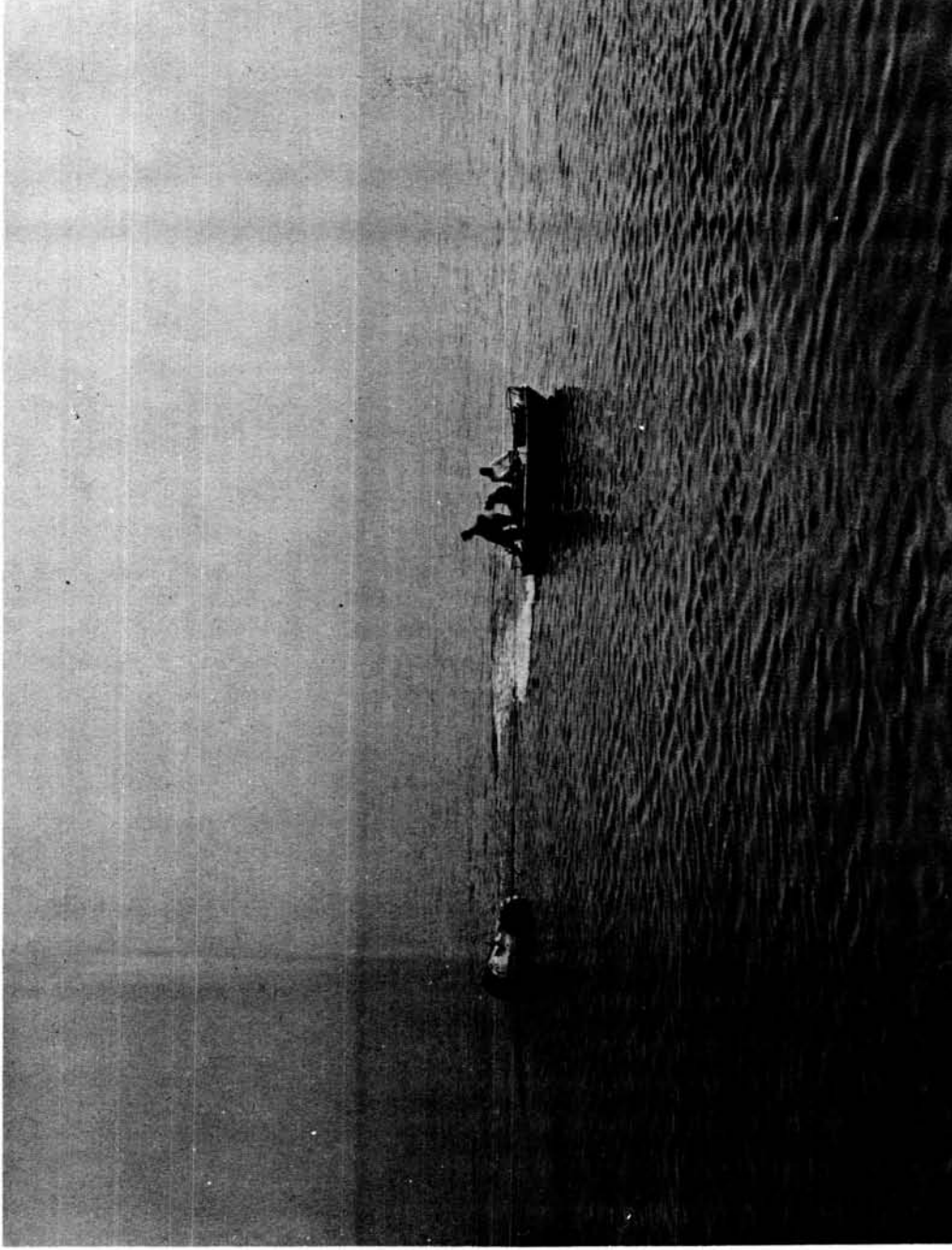


Figure IX-13.- Test vehicle after a water landing.

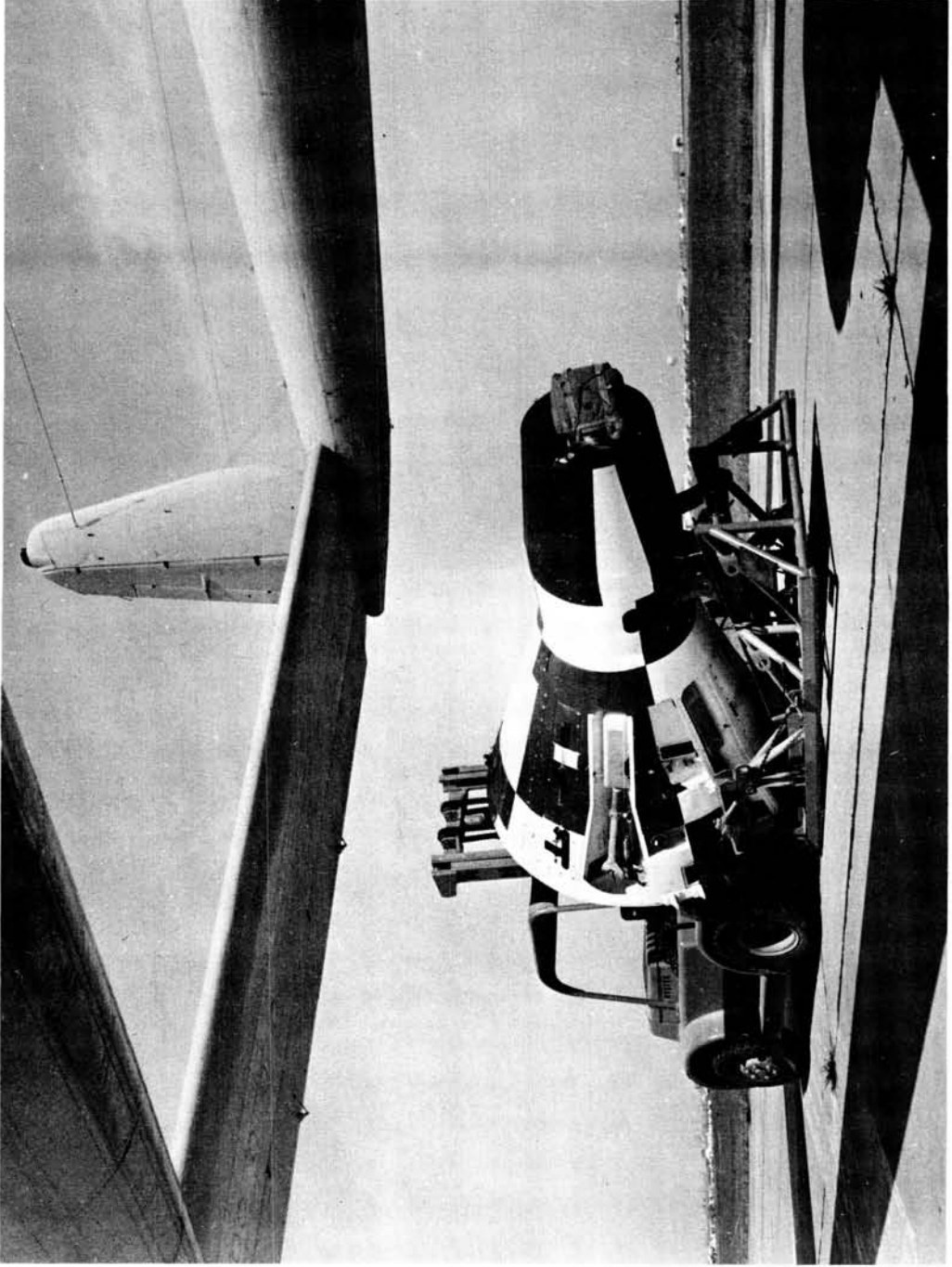


Figure IX-14.- Test vehicle and launch cradle.

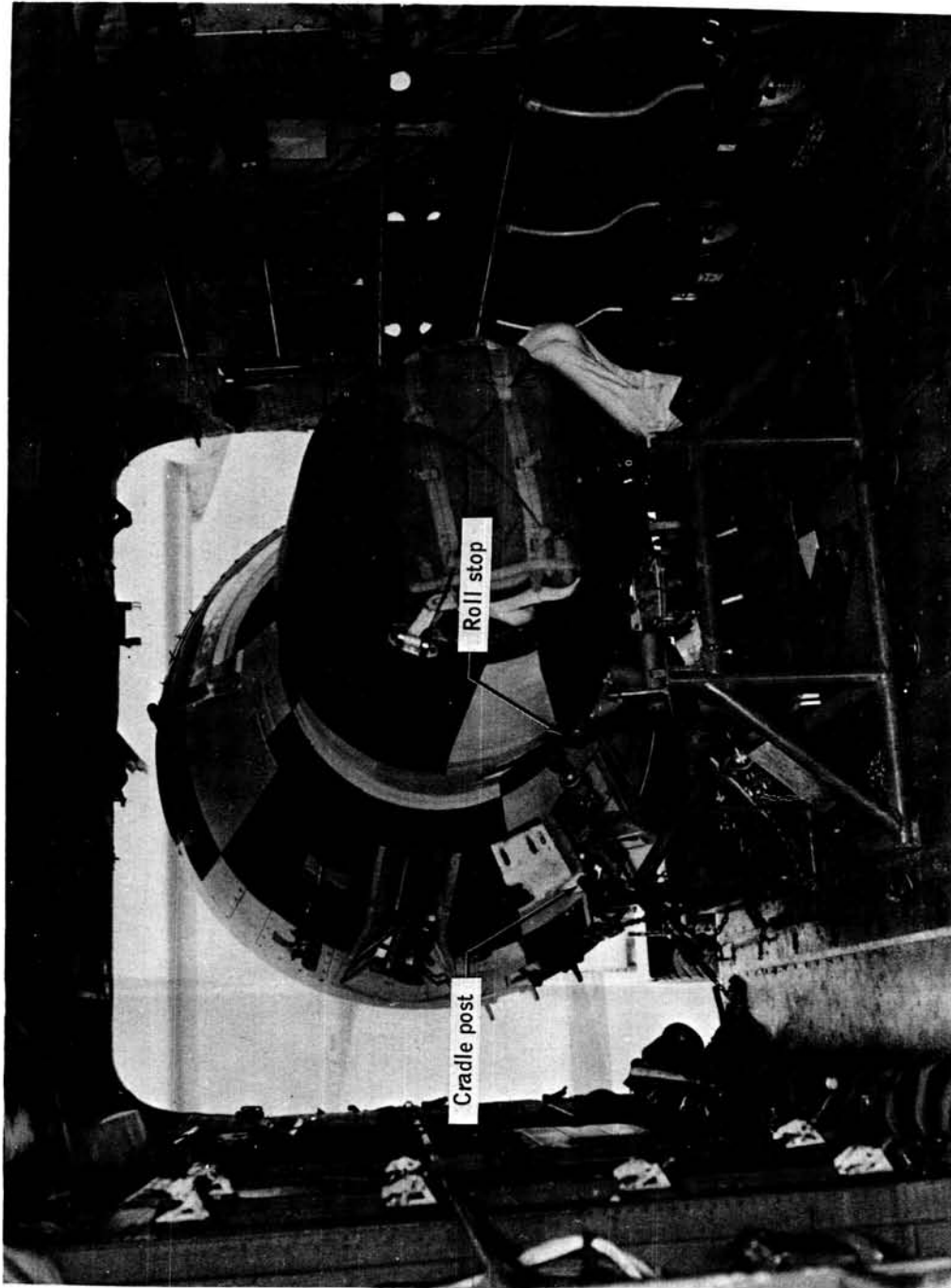


Figure IX-15.- Test vehicle and launch cradle, in aircraft.

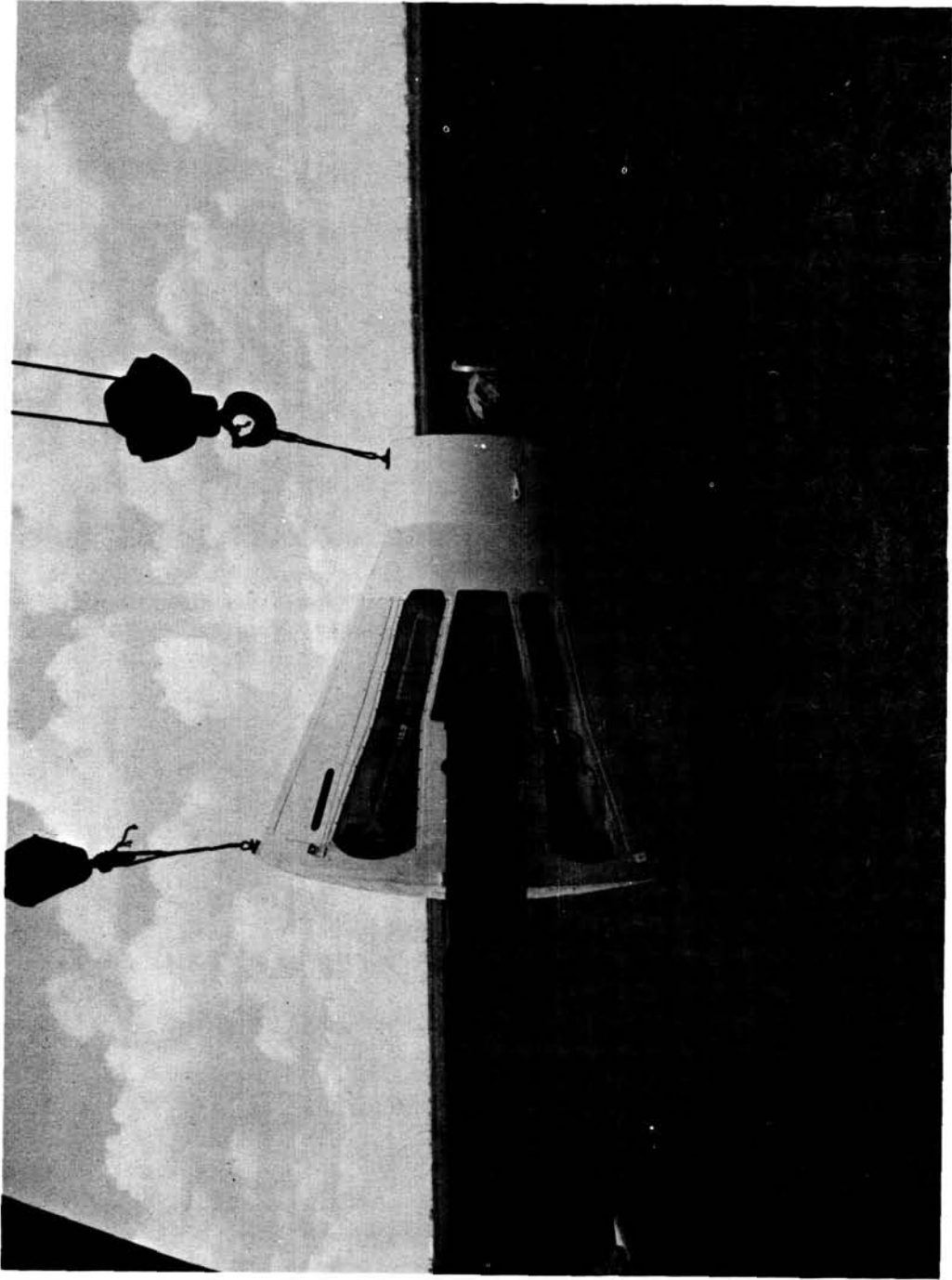


Figure IX-16.- Blast deflector I.

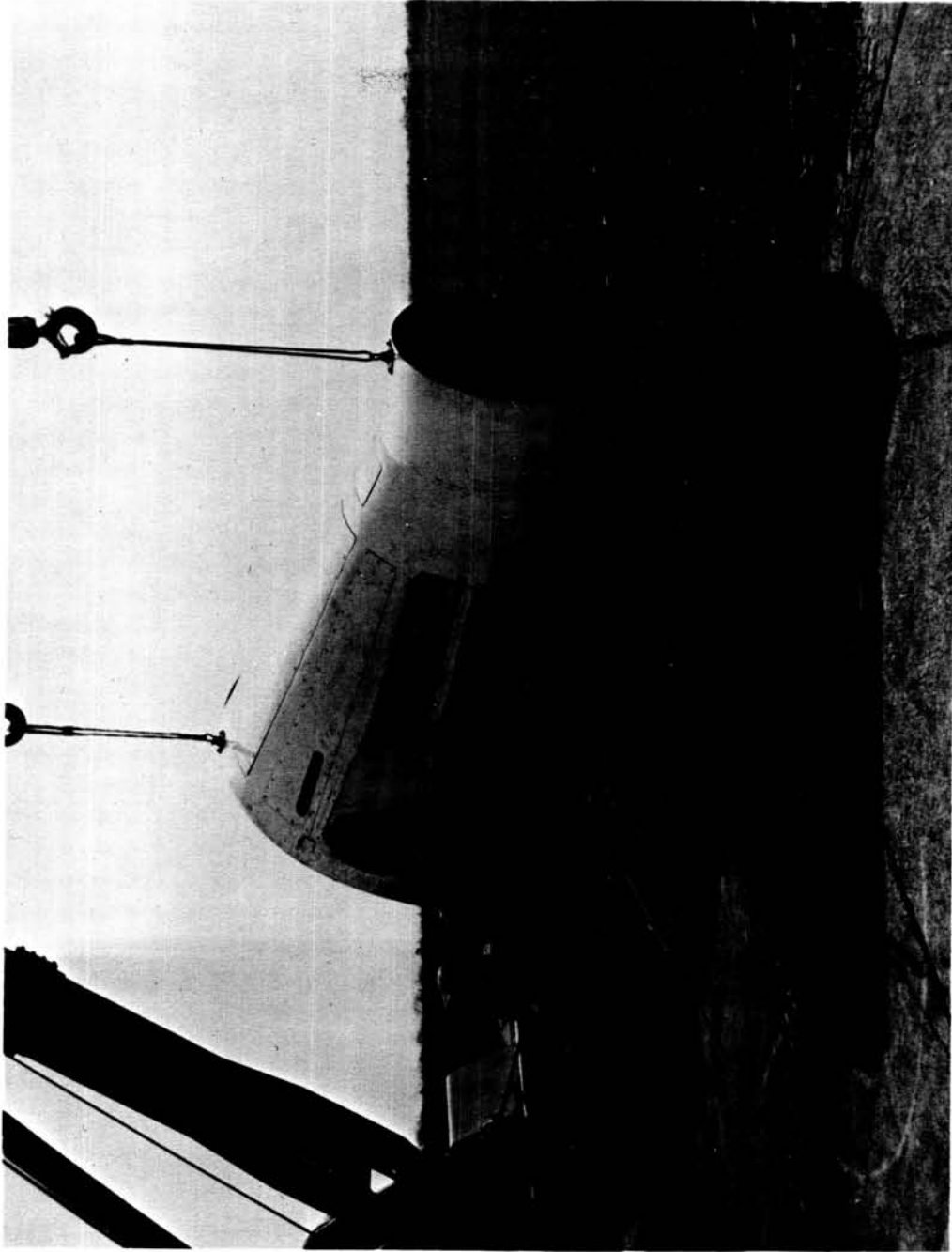


Figure IX-17.- Blast deflector II.

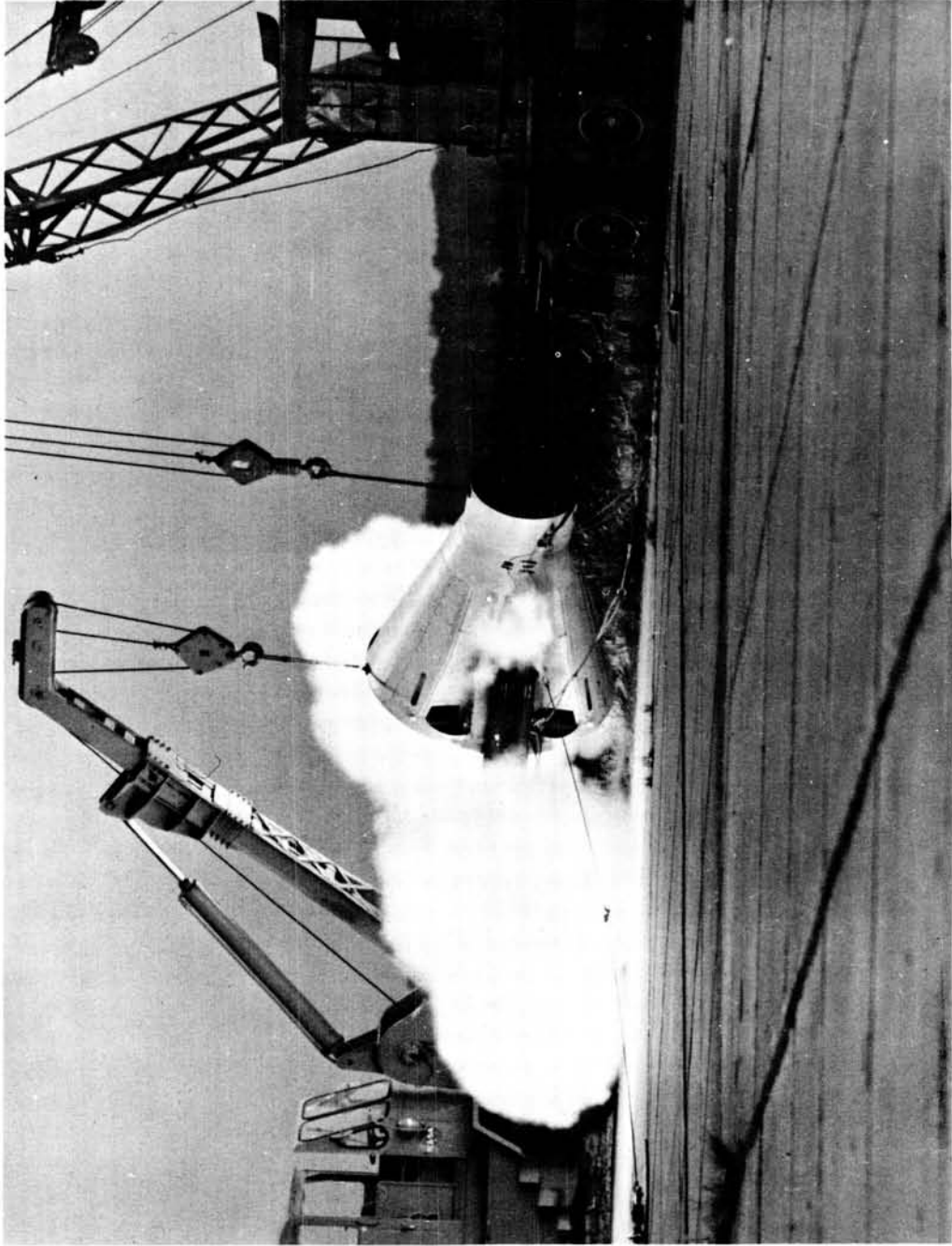


Figure IX-18.- Blast deflector II, test in progress.

SECTION X - OPERATIONAL PERFORMANCE STUDY

By Richard Tuntland

PRECEDING PAGE BLANK NOT FILMED.

OPERATIONAL PERFORMANCE STUDY

By Richard Tuntland
Manned Spacecraft Center

The Landing and Recovery Division (LRD) of MSC, early in the Para-Sail/landing-rocket program, began an extensive operational analysis to determine the operational limitations, to define the landing site requirements, to establish the level of support required to operate the system within its design constraints, and to define the pilot visual requirements. This analysis determined that the system has the inherent capability to attenuate winds up to 17.5 knots, to avoid local obstacles, to land on a relatively smooth unprepared surface, and can be aligned with the wind vector with a relatively simple visual system. However, the landing system does not have the maneuver capability to effect a point landing; therefore, the zone concept of operation was developed. The zone landing concept is defined as follows: the capability of a spacecraft and its system to reenter to a point in the atmosphere from which a land landing can be made at any of a number of places within a selected but unprepared zone by avoiding existing obstacles.

The size of the landing zone required was established as a circle with a 20-nautical-mile diameter based upon the 3-sigma dispersion of the spacecraft guidance and navigation system with single-station tracking. An area of this size, optimally positioned, also afforded potential landing sites for several orbits during a long duration mission. The landing zone criteria including slope, terrain, hydrology, cultural features, vegetation, statistical meteorology and area availability were then established into two categories; primary and emergency. The primary areas were in the continental United States and were within the Gemini Program envelope. The basic criterion for a primary area was that it would be 90 percent free of obstacles and have no more than a 5° slope. The emergency landing area sites were selected on a worldwide basis within the Gemini Program envelope and excluded the communist bloc countries. The criterion for these areas was that they would be at least 50 percent free of obstacles and have slopes no greater than 5°. This analysis established that there were sufficient landing zones within the continental United States to support the primary landing requirements and enough worldwide emergency landing sites available to support contingency land landings, if a land landing were selected as the emergency mode.

Once it was determined that the zone concept was the optimum mode of operation for the Para-Sail landing configuration, LRD formulated the

ground-support requirements. It was determined that a ground-based radar coupled with real-time display of the spacecraft center-of-maneuver capability, available landing sites, and integrated wind profile and voice communications with the spacecraft were desirable.

An analog computer-program simulation was accomplished to verify this concept; and a prototype terminal landing system was procured to further define the operational requirements, to verify the system capability and to provide the base for an operational system to complement the Para-Sail landing system when it is integrated into an operational spacecraft. Further studies are being accomplished to evaluate the use of guidance up-dating during reentry to limit landing-area dispersion.

The pilot visual requirements portion of the LRD portion of the program was accomplished to insure that the visual system incorporated in a manned spacecraft would be compatible with the established landing-zone criterion and the spacecraft control performance. An elaboration of the program is contained in Section VII of this report.

SECTION XI - INSTRUMENTATION AND ELECTRONIC SYSTEMS
IMPLEMENTATION FOR THE GEMINI SPACECRAFT PARA-SAIL
RETROCKET SYSTEM

By Marvin Perry

INSTRUMENTATION AND ELECTRONIC SYSTEMS IMPLEMENTATION
FOR THE GEMINI SPACECRAFT PARA-SAIL
RETROCKET SYSTEM

By Marvin Perry
Manned Spacecraft Center

INTRODUCTION

The Instrumentation and Electronic Systems Division (IESD) has provided the instrumentation for a program to evaluate the performance of the Para-Sail-type parachute and its application to a Gemini spacecraft earth landing. This was done in support of the Landing Technology Branch of the Structures and Mechanics Division (S & MD), who initiated and directed the program. Instrumentation was provided to measure the loads and aerodynamic parameters of these Para-Sail parachutes and the boilerplate Gemini spacecraft capsules. The impact loads, retrorocket system, and landing-gear performance were monitored.

Three distinct instrumentation systems were used on two Gemini boilerplate spacecrafts (BP-205, figs. XI-1 and XI-2; and BP-206, fig. XI-3). The first system (figs. XI-4 and XI-5) was designed to provide load data on the Para-Sail parachute. This system was used for airdrop 1 and consisted of seven measurements (table XI-I and fig. XI-6) with an onboard recording system. The second system (figs. XI-7 and XI-8) was used on airdrops 2 to 5. It consisted of 31 measurements (table XI-II), telemetry, and command systems (figs. XI-9 to XI-12). The third system (figs. XI-13 and XI-14) was designed and used on airdrops 6 to 12. It consisted of 43 measurements (table XI-III) which were added to handle the additional measurement requirements of the retrorocket subsystem (fig. XI-15).

These systems were designed, fabricated, and calibrated in a joint effort by all branches of the IESD. The following is a list of each branch and their responsibilities.

1. General instrumentation: Overall systems responsibility, instrumentation, power, and signal distribution.

2. Flight data systems: Onboard telemetry systems, telemetry ground station, and A-D conversions.
3. Standards and quality assurance: Calibration and inspection.
4. Electromagnetic systems: Telemetry transmitters, command system, and all antenna systems.

MEASUREMENT CHANGES, PROBLEMS, AND TECHNIQUES

Signal Conditioning

The signal conditioning used to amplify the low signal-level transducers for airdrops 2 to 5 was Statham carrier amplifiers (Model CA17-64). These amplifiers were found to be unacceptable for this type of test because the drift in the output circuit that was observed from the final instrument checkout to the airdrop was too great. Drifts were found to be as great as 8 percent of full scale. The time between the final instrument checkout and airdrop was about 30 hours. The Gulston dc amplifier (Model EM2000 D2) was incorporated on airdrops 6 to 12 and the drift problem was corrected.

Control-Line Load Measurements

The load links which were used for these measurements on airdrops 2 to 6 were found not to be compatible with this test article. This first configuration was a small strain-gage load link which was inserted into the control line between the turn-control motor and the parachute. These links were designed for 250 pounds. Because these links and their connecting cables had to be placed in the control line outside the boilerplate, problems were experienced during deployment. The connecting cables were tangled in the control lines during deployment because proper storage could not be made on the boilerplate. This problem was solved by designing and fabricating a load-measuring device which could be placed on the inside of the boilerplate (fig. XI-16). This device was placed between the turn-control motors and their exits inside the boilerplate, thereby eliminating the external sensor and cable.

Chamber Pressure Measurement P-42 and P-44

Preliminary tests were made on the retrorocket motor prior to flight tests. During these tests, the chamber pressure of the motors was monitored (fig. XI-17). The normal chamber pressure which was expected was approximately 3100 lb/in.² with a peak pressure of 3500 lb/in.². For the best resolution, a Consolidated Electronics Corporation (CEC) Model 4-326 unbonded strain-gage transducer was selected (0 to 3500 psig range). Following the first test, an analysis of the data revealed a large zero shift at the end of the data run. It was also noted that a rather large pressure transient existed at the rocket ignition. On the next static firing 0 to 10 000 lb/in.² transducers were used, and this transient was found to be 7100-lb/in.² and existed for about 4 milliseconds. This time was the upper limit of the frequency response of the transducers. The upper limit of the frequency response was required of the transducer in order to define the transient condition. Procurement was made on 0 to 5000-lb/in.² transducers which had a two-times-overload capability. These transducers functioned properly, for no other shifts were noted and data were considered reliable on all flights.

Attitude Gyroscope

An adequate pitch-angular-attitude measurement was never made because a reliable gyroscope could not be obtained which would withstand the environment of this test. Some data were taken with a Giannini Model 3416DV.06, but because its range was continually exceeded during attitude change, its reference was lost and the data were considered unsatisfactory thereafter.

Angle of Attack

Although an angle-of-attack measurement was not made, this measurement would have added considerably to the aerodynamic characteristics data which were gathered. Considerable effort was made to acquire an instrument to make this measurement, but an accurate one (10 to 40 ft/sec) could not be found that would be applicable to the environment of these tests or that could be physically located on the test boilerplates. A good low-velocity angle-of-attack measuring device was needed.

Batteries

Because of economy and the availability of equipment, four Eagle Picher Model MAR-8000 (5 ampere-hour) batteries were used to power all instrumentation electronic systems. These were nickel-cadmium batteries and could be readily recharged following each sequence test or airdrop. Problems were encountered during the first three drops because of a low resistance to ground that was noticed following the completion of each drop. This low resistance was due to leakage caused by broken cells within the battery. Ground tests were made and it was found that after the recharging of the battery, the vent caps were replaced tightly too soon, resulting in a residual pressure build-up within each cell. The batteries were then installed on the boilerplate and when the boilerplate was carried to the drop attitude of 11 000 feet, the outside pressure decreased; therefore, the differential pressure was greater than 40 lb/in.² and several of the seals of the cells burst. The vent valves on the batteries apparently failed. The water from the cells leaked out and a low-resistance short occurred; however, the short was never great enough to cause a power failure. This problem was eliminated by venting each cell at least 12 hours each time the battery was recharged. The vent caps were secured just prior to their installation in the spacecraft, which was about 6 to 8 hours before the drop. No further shorts were observed following this operation.

Ground Receiving Station

When this program was initiated in October 1963, a ground telemetry receiving station was required which could be readily moved from the ground checkout station to the drop site. The drop sites were Trinity Bay and Fort Hood, Texas. The IESD provided two telemetry receivers and six discriminators. A number of real-time data channels were required so that the test conductor would have the necessary information to intelligently control the Para-Sail. The control-line positions and loads were monitored real time. Additional real-time channels were needed, but equipment and funds were not available.

Launch release time. - All of the sequence times which were on the spacecraft were initiated from launch release. This time was accurately recorded, but had to be placed on a commutated channel because of the number of high-frequency measurements required which had to be placed on the straight telemetry channels. This is an important measurement that should have been recorded real time. This would have enabled the test conductor to receive an accurate time of launch release so that corrective

action could be taken if other events did not occur at predetermined times. These real-time requirements were handled by voice communication with the drop aircraft (C-119) and a ground communicator who started a timer.

Rocket arm (lockouts 1 and 2). - In addition to the launch-release time, two other important real-time measurements were needed. These were the events which indicated that each rocket motor was armed, and that the altitude sensor had been deployed. Knowledge of this event was important on the earth landing tests; because, if these motors were not armed, the landing gears would not be deployed. Damage to the landing gear would be incurred if the motors were not fired. This measurement was also placed on a commutated channel. Real-time readouts were made by displaying the pulse amplitude modulation (PAM) wave train on an oscilloscope and these events were visually monitored. This is a difficult task and a great deal of error can be introduced.

Antenna Systems

A signal was required from the boilerplate to the ground station for the primary and secondary commands and telemetry during the time when the spacecraft was in the drop aircraft, in all attitudes of flight, and after impact in the water. The command-systems antennas were designed in order to provide linear polarization on the spacecraft and circular polarization omnidirectional coverage on the ground. The initial telemetry antenna system was a slot type. This was found to be incompatible because following the spacecraft impact, the jar would de-tune the capacitive-tuned slot and result in a loss of signal. This type was replaced by 1/4-wave whip antenna. Three whip antennas were fed in phase, two of which were mounted diametrically opposite near the vehicle base, and one mounted between the hatches. This arrangement was used for the primary command and telemetry antennas. The secondary command-systems antenna consisted of two whip antennas which were fed in phase diametrically opposite and mounted on the base of the vehicle. No problems were encountered with this system.

On airdrops 5 to 12 the antennas mounted on the spacecraft had to be moved because of the location of the retrorocket motors. The antennas were then mounted so that they were diametrically opposite the hatches rather than the vehicle base. The television antennas were also mounted at this time.

CALIBRATIONS

All sensors were calibrated by the IESD calibration laboratory. These calibrations were made with certified standards and were calibrated prior to each test. The auxiliary test equipment (oscilloscopes, digital voltmeters, counters, and so forth) was also calibrated and certified by this laboratory.

DATA HANDLING

Following the calibration of each measurement, the calibration data were forwarded to the Computation and Analysis Division (C & AD), where the data were placed within the computer program for each test. Normally, the calibration data did not change except when new transducers or requirements were made. Each airdrop was recorded on magnetic tape. The data were received from two telemetry receivers. The data were sent through discriminators and then digitized by the IESD and given to the C & AD. At the C & AD, the data were tabulated and plotted as requested by the S & MD and IESD. The IESD also made an analog oscillograph record of each measurement. These were primarily made for quick-look data trends and failure analysis. (See data flow chart, fig. XI-18.)

TABLE XI-I. - MEASUREMENT REQUIREMENTS, AIR DROP 1

Measurement number	Measurement description	Range	Transducer		Frequency response, cps	Recording	
			Make	Model		Mode	Channel
^a A-27	Impact acceleration, Y-axis	± 15g	Statham	AJ15-15-350	135	Oscillograph	6
^b F-11	Combined riser load	0 to 20 klb	MSC		135	Oscillograph	1
F-12	Front riser load	0 to 5 klb	MSC		135	Oscillograph	2
F-13	Middle riser load	0 to 5 klb	MSC		135	Oscillograph	3
F-14	Right aft-riser load	0 to 5 klb	MSC		135	Oscillograph	4
F-15	Left aft-riser load	0 to 5 klb	MSC		135	Oscillograph	5
^c P-32	Rate of descent	0 to 15 psia	CEC	4-328-0002	135	Oscillograph	7

^aA = acceleration.

^bF = force.

^cP = pressure.

TABLE XI-II. - MEASUREMENT REQUIREMENTS, AIR DROPS 2 THROUGH 5

Measurement number	Measurement description	Range	Transducer		Frequency response	Recording	
			Make	Model		Mode	Channel
^a A-24	Linear acceleration, Y-axis	± 2g	Statham	AJ17-2-350	10 sps	PAM	27
A-25	Linear acceleration, X-axis	± 1/2g	Statham	A4-0.5-350	10 sps	PAM	28
A-26	Linear acceleration, Z-axis	± 1/2g	Statham	A4-0.5-350	10 sps	PAM	29
A-27	Impact acceleration, Y-axis	± 15g	Statham	AJ15-15-350	330 cps	VCO	14
A-28	Impact acceleration, X-axis	± 10g	Statham	A69 TC-10-350	110 cps	VCO	11
A-29	Impact acceleration, Z-axis	± 10g	Statham	A69 TC-10-350	160 cps	VCO	12
A-54	Angular acceleration, pitch axis	100 rad/sec ²	Statham	AA20-100-350	220 cps	VCO	13
^b D-22	Left control-line position	0 to 2 ft	Pot (spectrol)		14 cps	VCO	5
D-23	Right control-line position	0 to 2 ft	Pot (spectrol)		20 cps	VCO	6
^c E-59	Launch release				10 sps	PAM	31
E-60	R and R canister separation				10 sps	PAM	32
E-61	Attitude change				10 sps	PAM	57
E-65	Backup parachute activation				10 sps	PAM	59
E-66	Left-turn command (unwind)				10 sps	PAM	73
E-67	Right-turn command (unwind)				10 sps	PAM	76
E-69	Left-turn command (wind)				10 sps	PAM	74
E-70	Right-turn command (wind)				10 sps	PAM	75

^aA = acceleration.^bD = positions or strokes.^cE = events.

TABLE XI-II. - MEASUREMENT REQUIREMENTS, AIR DROPS 2 THROUGH 5 - Concluded

Measurement number	Measurement description	Range	Transducer		Frequency response	Recording	
			Make	Model		Mode	Channel
^d F-11	Combined riser load	0 to 20 klb	MSC		80 cps	VCO	10
F-12	Front riser load	0 to 5 klb	MSC		60 cps	PAM	3, 18, 33, 48, 63, 78
F-13	Middle riser load	0 to 5.0 klb	MSC		60 sps	PAM	4, 19, 34, 49, 64, 79
F-14	Left aft-riser load	0 to 5.0 klb	MSC		60 sps	PAM	5, 20, 35, 50, 65, 80
F-15	Right aft-riser load	0 to 5.0 klb	MSC		60 sps	PAM	6, 21, 36, 51, 66, 81
F-16	Left control-line load	0 to 100 lb	MSC		6 cps	VCO	2
F-17	Right control-line load	0 to 100 lb	MSC		8 cps	VCO	3
^e O-21	Pitch attitude	0 to 360 deg	Giannini	3416-DV.06	11 cps	VCO	4
O-68	Inner gimbal	0 to 360 deg	Giannini	3416-DV.06	10 sps	PAM	61
^f P-32	Rate of descent	0 to 15 psia	CEC	4-328-0002	10 sps	PAM	47
^g R-18	Yaw rate	± 180 deg/sec	Humphrey	RG01-1601-1	10 sps	PAM	13
R-20	Pitch rate	± 120 deg/sec	Humphrey	RG01-2601-1	10 sps	PAM	15
^h T-46	Ambient temperature	20 to 60° C	Trans-Sonic	T4082A-4	10 sps	PAM	16
ⁱ V-53	Power distribution	0 to 32 V dc	MSC		10 sps	PAM	30

^dF = force.

^gR = rates.

^eO = attitude.

^hT = temperature.

^fP = pressures.

ⁱV = voltage.

TABLE XI-III. - MEASUREMENT REQUIREMENTS, AIR DROPS 6 THROUGH 12

Measurement number	Measurement description	Range	Transducer		Frequency response	Recording	
			Make	Model		Mode	Channel
^a A-24	Linear acceleration, Y-axis	± 2g	Statham	AJ17-2-350	10 sps	PAM	27
A-25	Linear acceleration, X-axis	± 1g	CEC	4-205	10 sps	PAM	28
A-26	Linear acceleration, Z-axis	± 1g	CEC	4-205	10 sps	PAM	29
A-27	Impact acceleration, Y-axis	± 15g	CEC	4-202	330 cps	VCO	14
A-28	Impact acceleration, X-axis	± 10g	CEC	4-202	110 cps	VCO	11
A-29	Impact acceleration, Z-axis	± 10g	CEC	4-202	160 cps	VCO	12
A-31	Thrust acceleration, Y-axis	± 10g	CEC	4-202	450 cps	VCO	15
A-33	Footwell acceleration, Z-axis	± 10g	CEC	4-202	35 cps	VCO	7
A-34	Footwell acceleration, X-axis	± 10g	CEC	4-202	45 cps	VCO	8
A-35	Footwell acceleration, Y-axis	± 10g	CEC	4-202	59 cps	VCO	9
A-54	Angular acceleration, pitch axis	100 rad/sec ²	Statham	AA20-100-350	220 cps	VCO	13
^b D-22	Left control-line position	0 to 42 in.	Pot		14 cps	VCO	5
D-23	Right control-line position	0 to 42 in.	Pot		20 cps	VCO	6
^c E-47	Altitude-sensor arm				10 sps	PAM	43
E-48	Altitude-sensor lockout number 1				10 sps	PAM	44
E-59	Launch release				10 sps	PAM	31
E-60	R and R canister separation				10 sps	PAM	32
E-61	Attitude change				10 sps	PAM	57

^aA = acceleration.^cE = events.^bD = positions or strokes.

TABLE XI-III. - MEASUREMENT REQUIREMENTS, AIR DROPS 6 THROUGH 12 - Continued

Measurement number	Measurement description	Range	Transducer		Frequency response	Recording	
			Make	Model		Mode	Channel
E-62	Landing-gear deployment				10 sps	PAM	87
E-63	Blast-deflector release				10 sps	PAM	58
E-64	Rocket fire				10 sps	PAM	88
E-65	Backup parachute activation				10 sps	PAM	59
E-66	Left-turn command (unwind)				10 sps	PAM	73
E-67	Right-turn command (unwind)				10 sps	PAM	76
E-69	Left-turn command (wind)				10 sps	PAM	74
E-70	Right-turn command (wind)				10 sps	PAM	77
F-11	Combined riser load	0 to 20 klb	MSC		80 cps	VCO	10
^d F-12	Front riser load	0 to 5 klb	MSC		60 sps	PAM	3, 18, 33, 48, 63, 78
F-13	Middle riser load	0 to 5 klb	MSC		60 sps	PAM	4, 19, 34, 49, 64, 79
F-14	Left aft-riser load	0 to 5 klb	MSC		60 sps	PAM	5, 20, 35, 50, 65, 80
F-15	Right aft-riser load	0 to 5 klb	MSC		60 sps	PAM	6, 21, 36, 51, 66, 81
F-16	Left control-line load	0 to 125 lb	MSC		6 cps	VCO	2
F-17	Right control-line load	0 to 125 lb	MSC		8 cps	VCO	3
^e O-21	Pitch angular attitude	0 to 360 deg	Giannini	3416-DV.06	10 cps	VCO	4
O-68	Inner gimbal	0 to 360 deg	Giannini	3416-DV.06	10 sps	PAM	61

^dF = force.

^eO = attitude.

TABLE XI-III. - MEASUREMENT REQUIREMENTS, AIR DROPS 6 THROUGH 12 - Concluded

Measurement number	Measurement description	Range	Transducer		Frequency response	Recording	
			Make	Model		Mode	Channel
f P-32	Rate of descent	0 to 15 psia	CEC	4-328	10 sps	PAM	47
P-42	Rocket-chamber pressure, left	0 to 5000 psia	CEC	4-326 Special	790 cps	VCO	17
P-44	Rocket-chamber pressure, right	0 to 5000 psia	CEC	4-326 Special	600 cps	VCO	16
g R-18	Angular rate, yaw	± 30 deg/sec	Humphrey	RG02-2320-1	10 sps	PAM	13
R-19	Angular rate, roll	± 120 deg/sec	Humphrey	RG02-2320-1	10 sps	PAM	14
R-20	Angular rate, pitch	± 120 deg/sec	Humphrey	RG02-2320-1	10 sps	PAM	15
h T-46	Ambient temperature	20 to 60° C	Trans-Sonic	T4082A-4	10 sps	PAM	16
i V-53	Power distribution, voltage	0 to 32 V dc			10 sps	PAM	30

f P = pressures.

g R = rates.

h T = temperature.

i V = voltage.

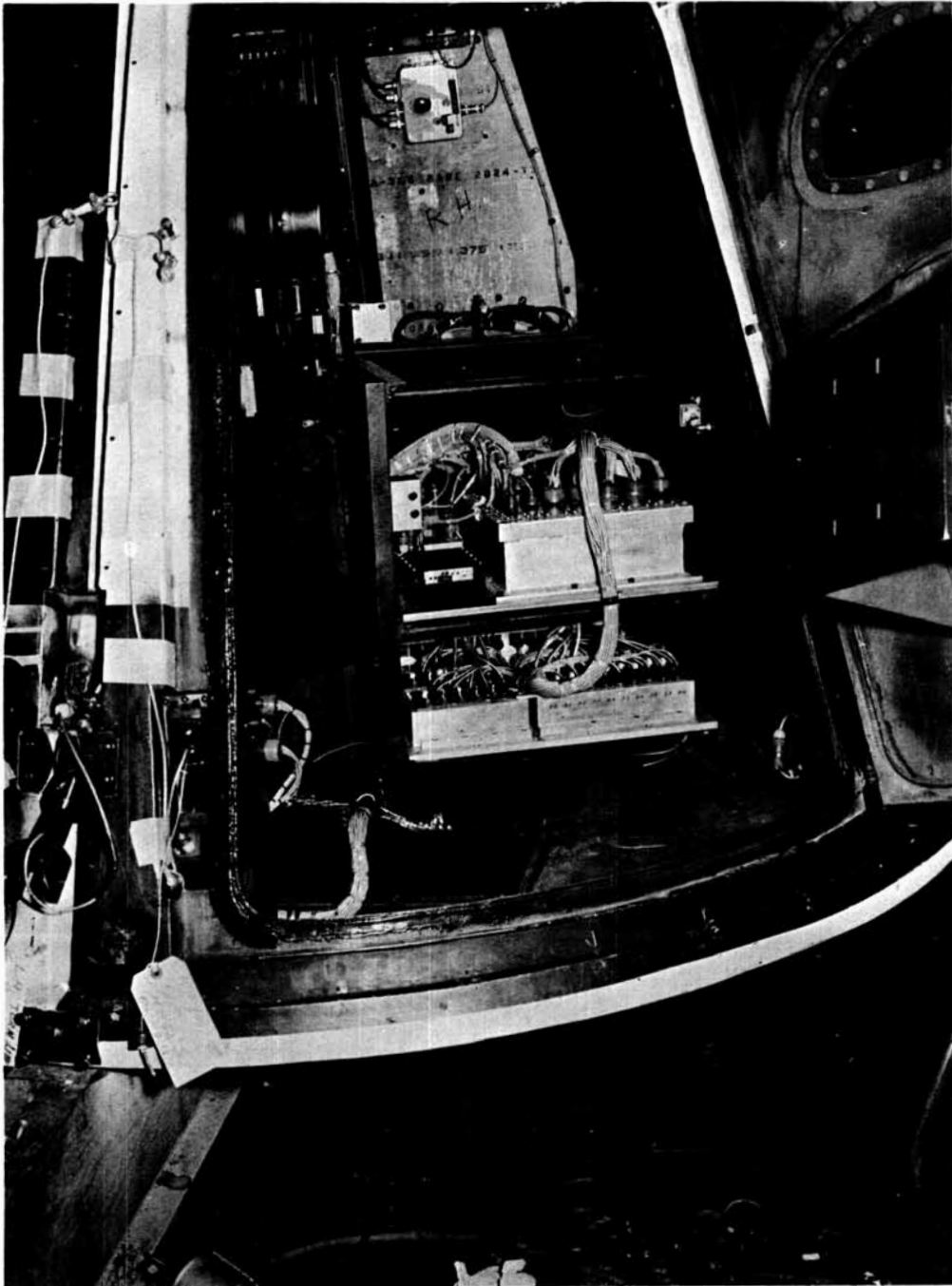


Figure XI-1.- Instrumentation pallet, BP-205.

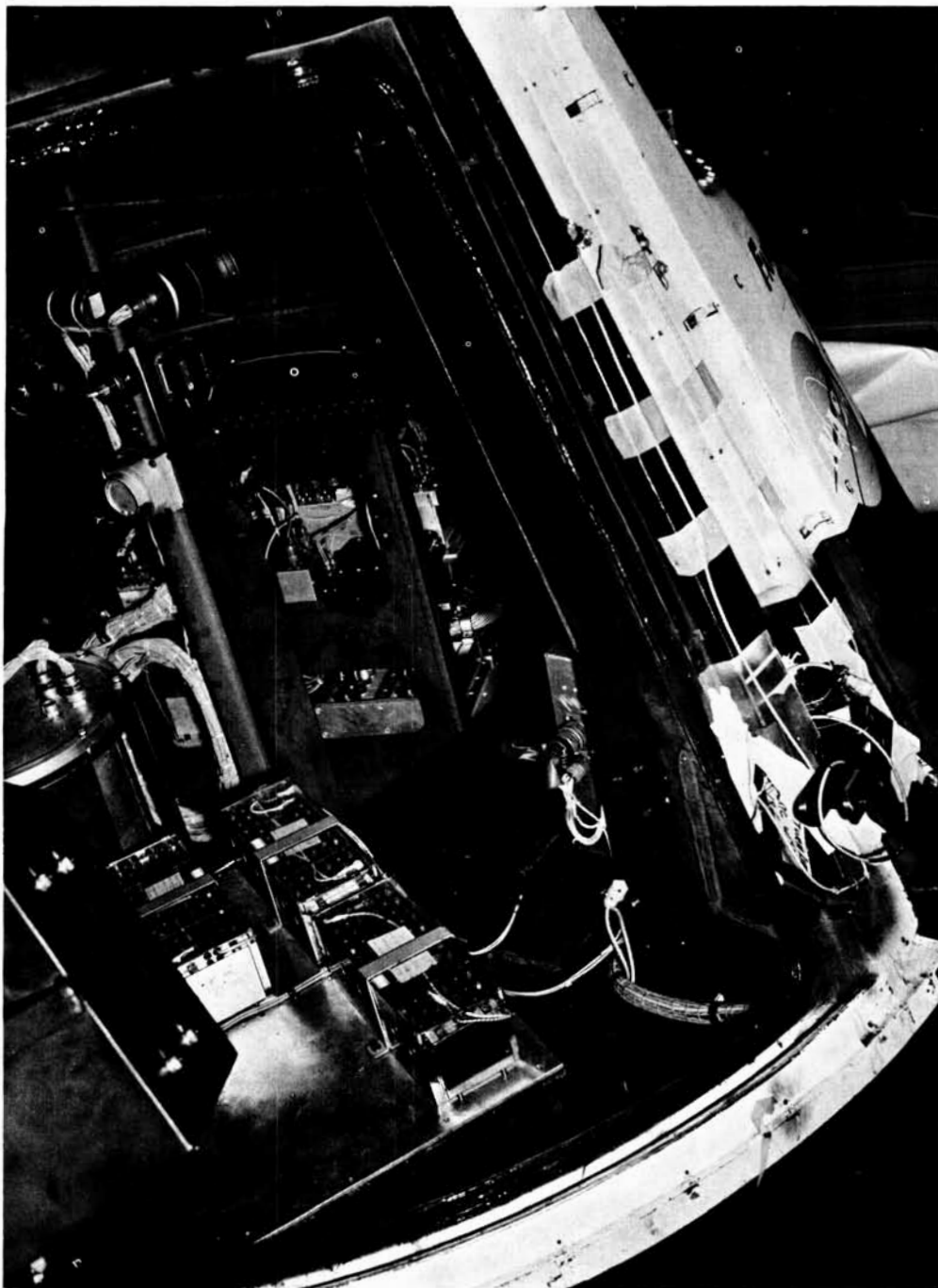


Figure XI-2.- Complete instrumentation system, BP-205.

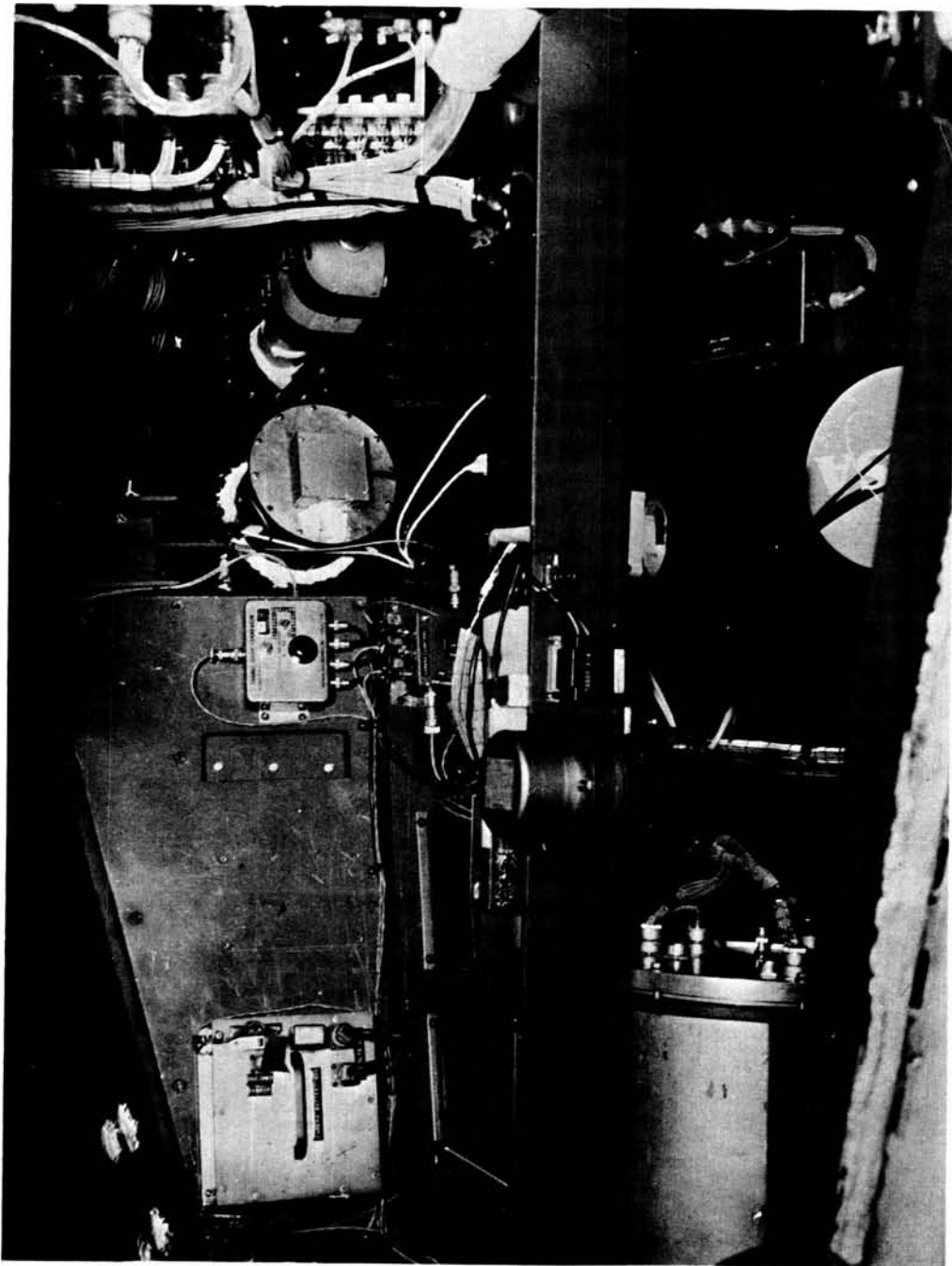


Figure XI-3.- Instrument systems, BP-206.

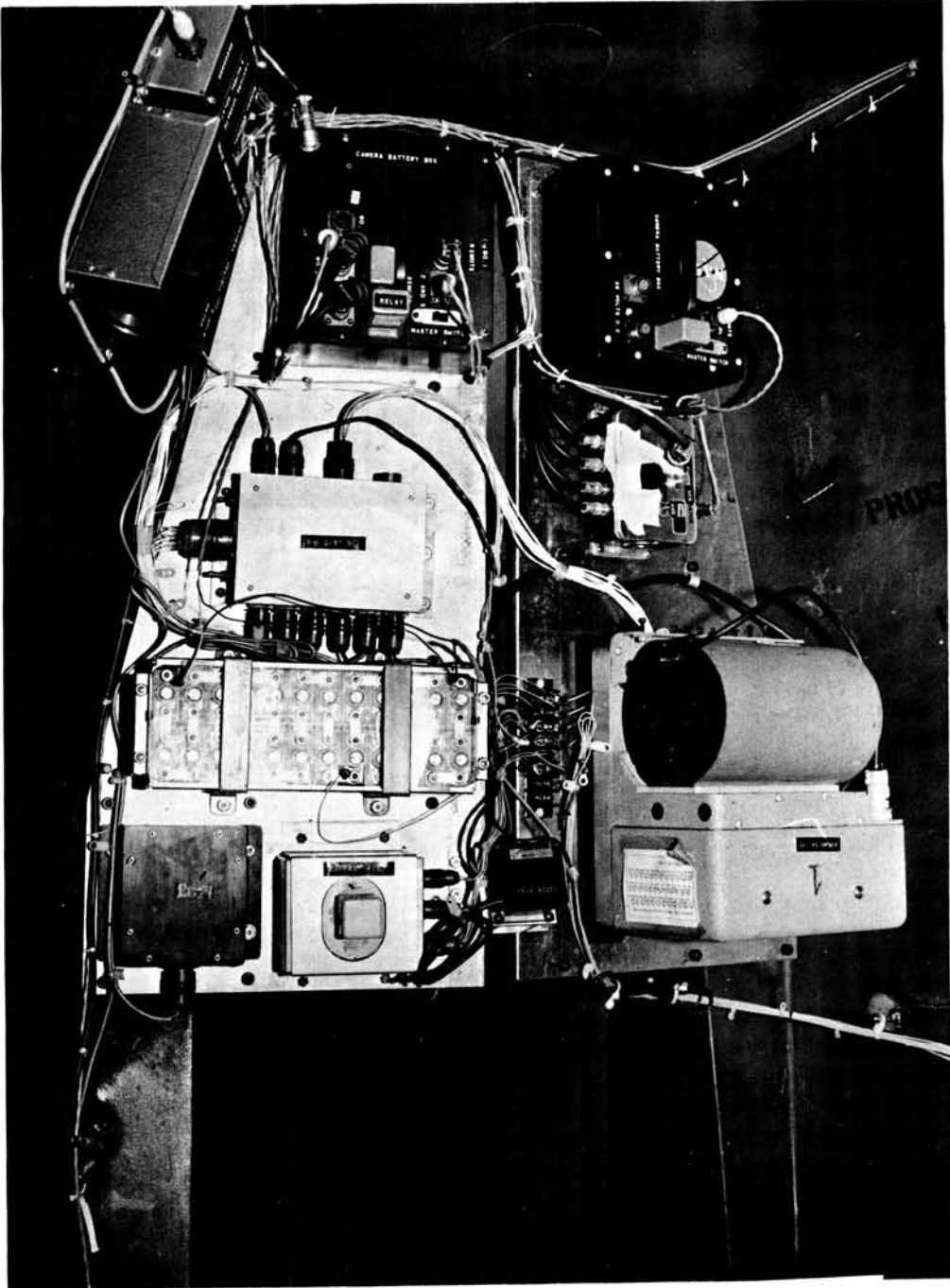


Figure XI-4.- Instrumentation for first deployment test.

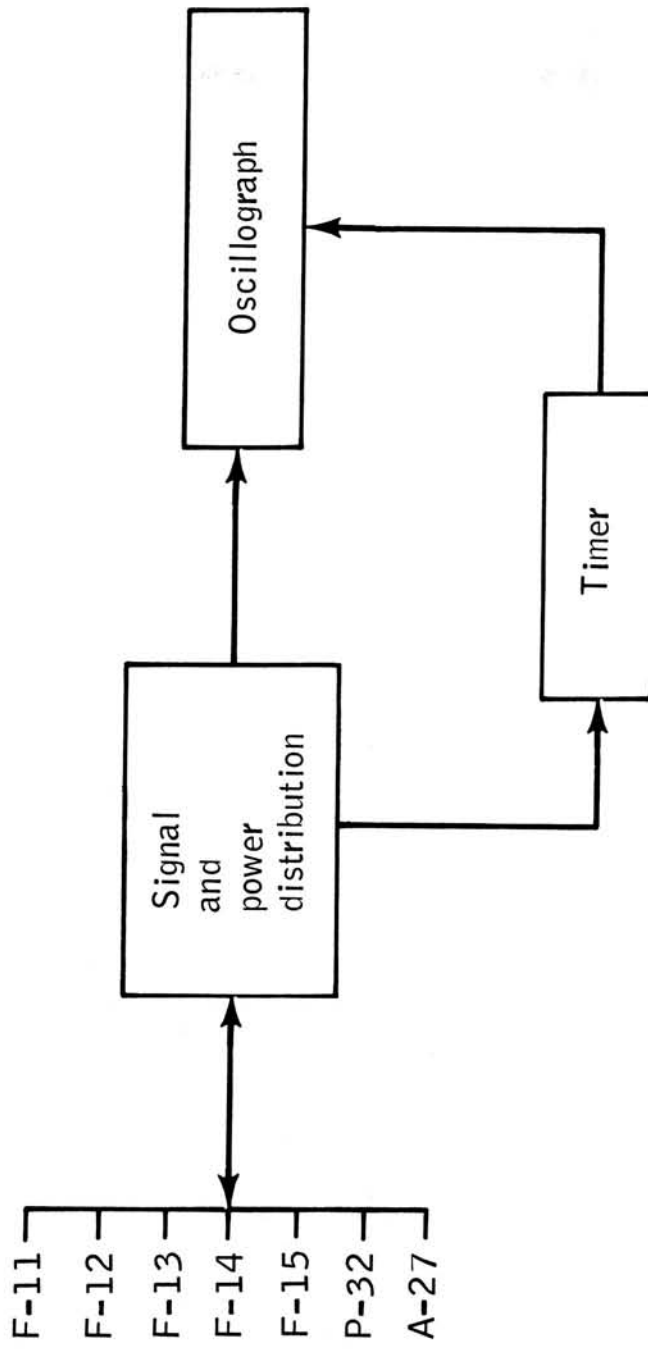
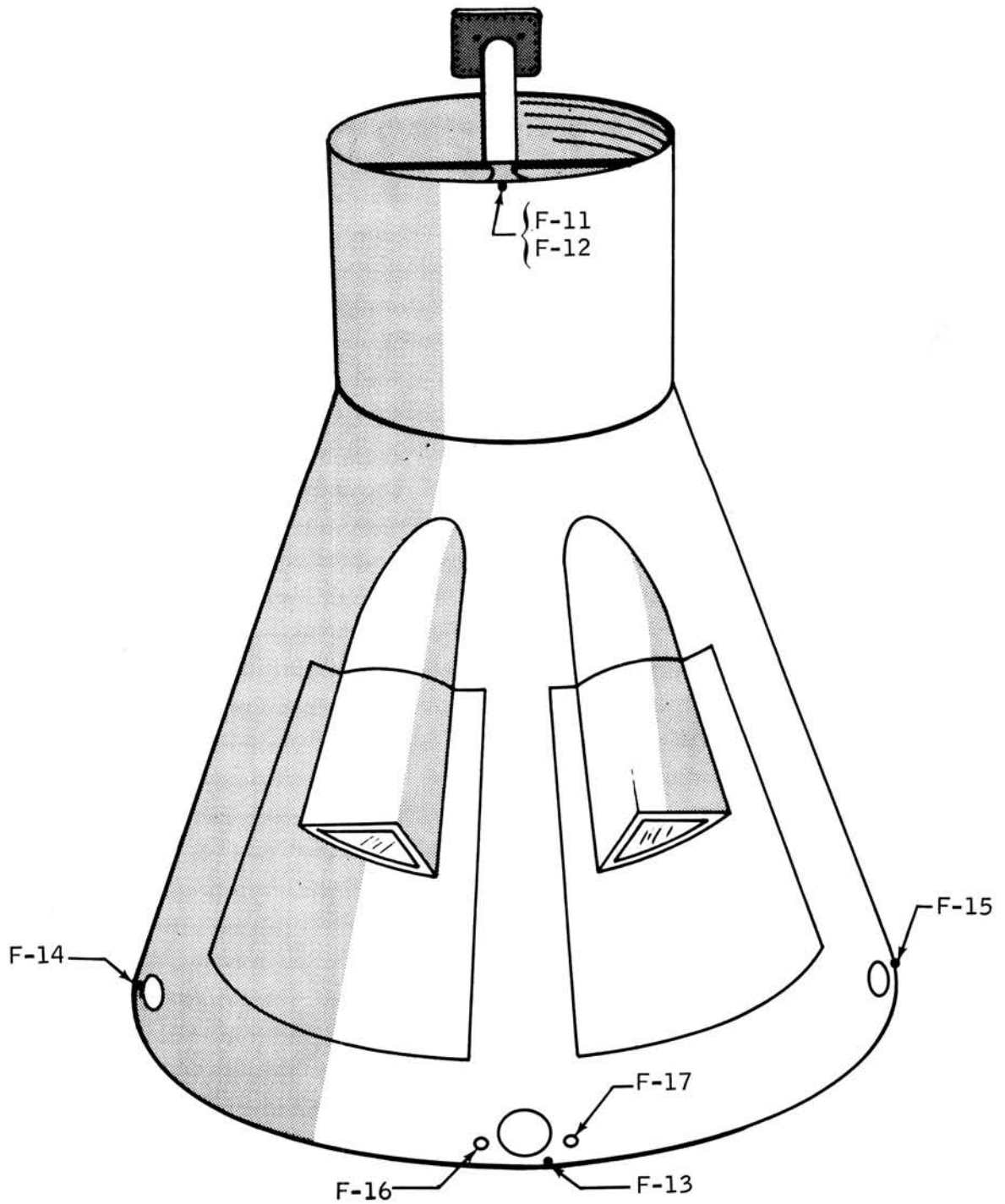


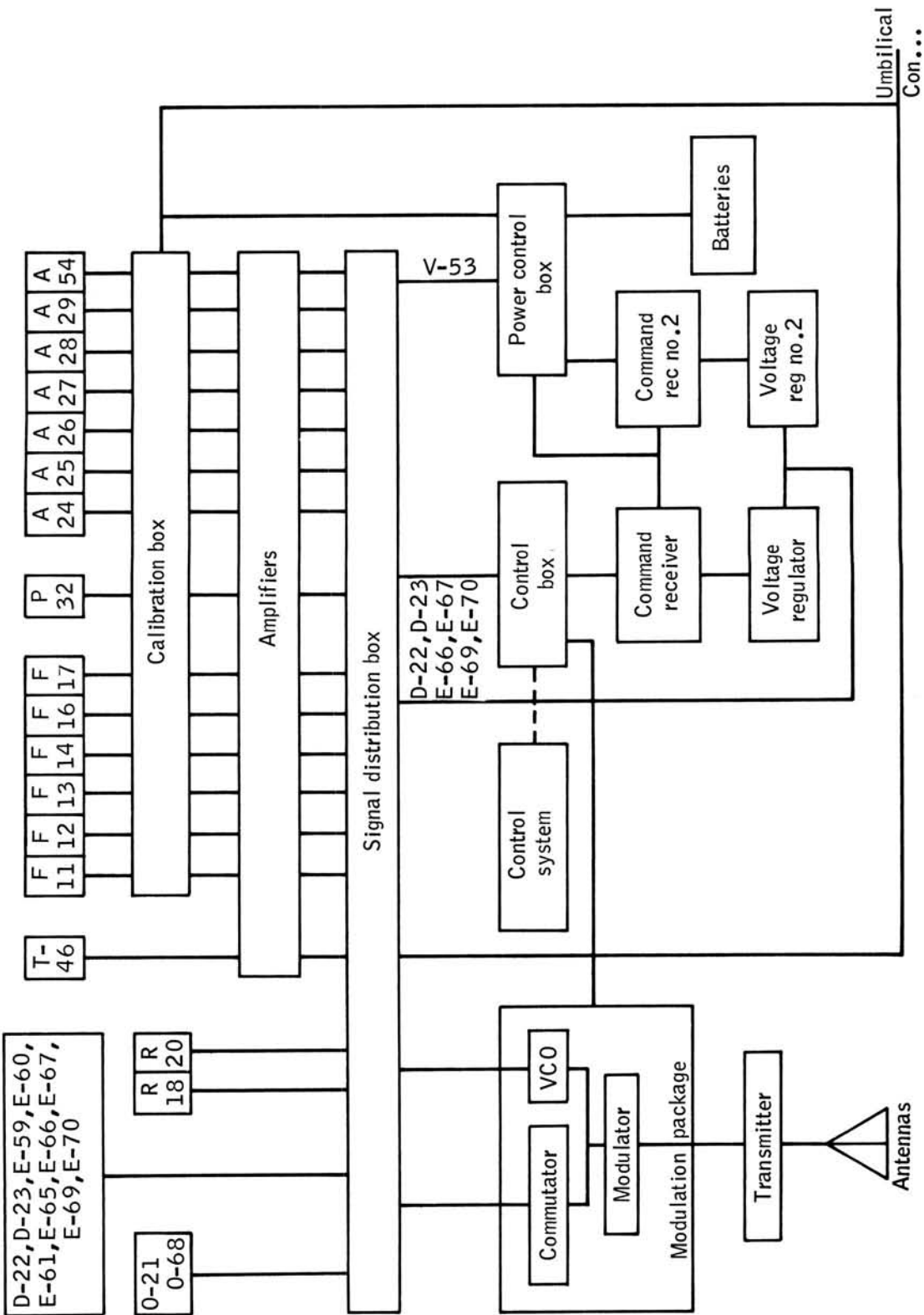
Figure XI-5.- Instrumentation and electronic systems for airdrop 1.
(F, force; P, pressures; and A, acceleration.)



XI-6.- Measurement locations, top view. (F, force.)



Figure XI-7.- Instrumentation breadboard, airdrops 2 to 5.



Umbilical
Con...

Figure XI-8.- Instrumentation and electronic systems for airdrops 2 to 5.
(A, acceleration; D, positions or strokes; E, events; F, force; O, attitude;
P, pressures; R, rates; T, temperature; and V, voltage.)



Figure XI-9.- Telemetry system.

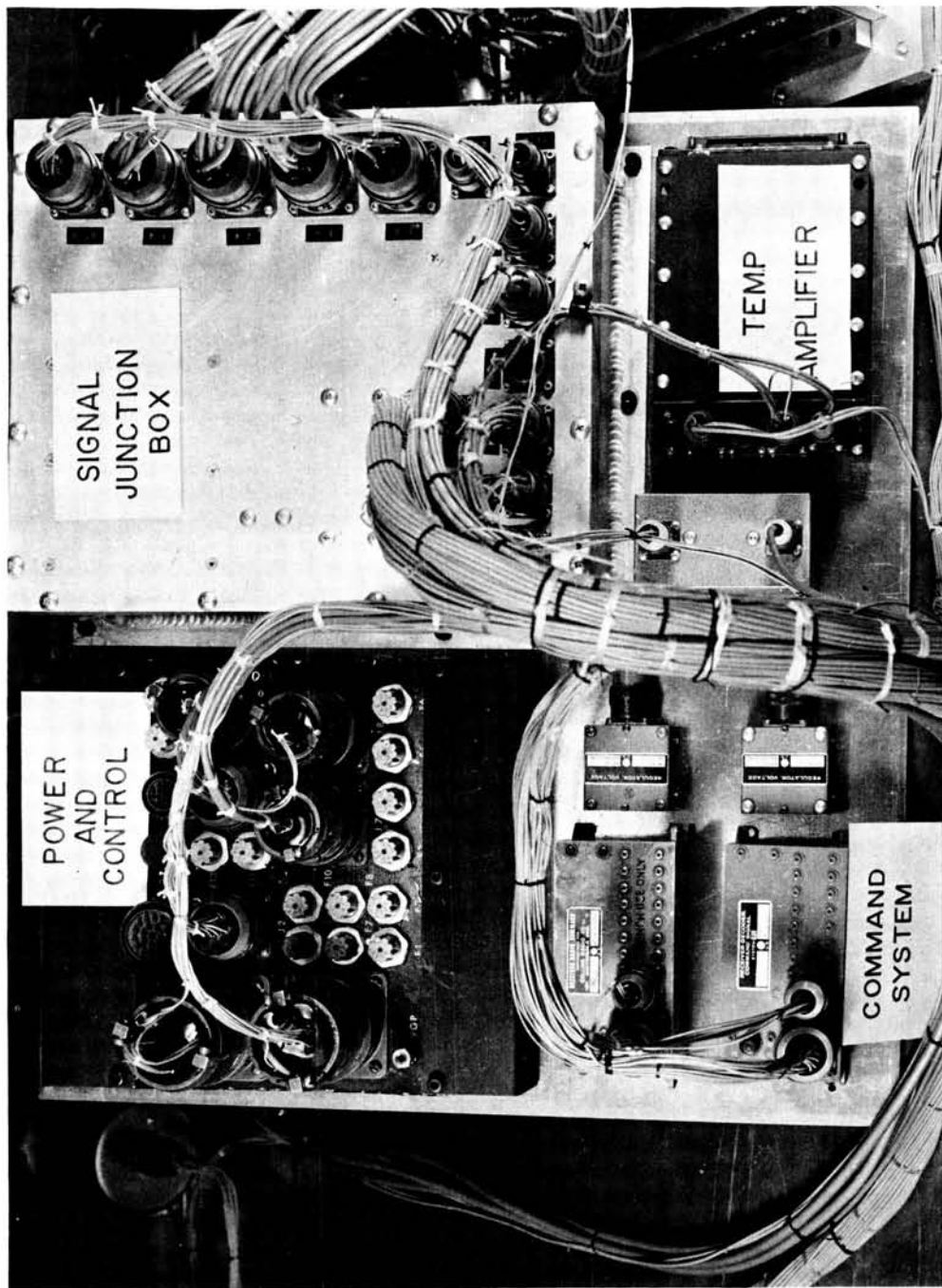


Figure XI-10.- Instrumentation and electronic systems.

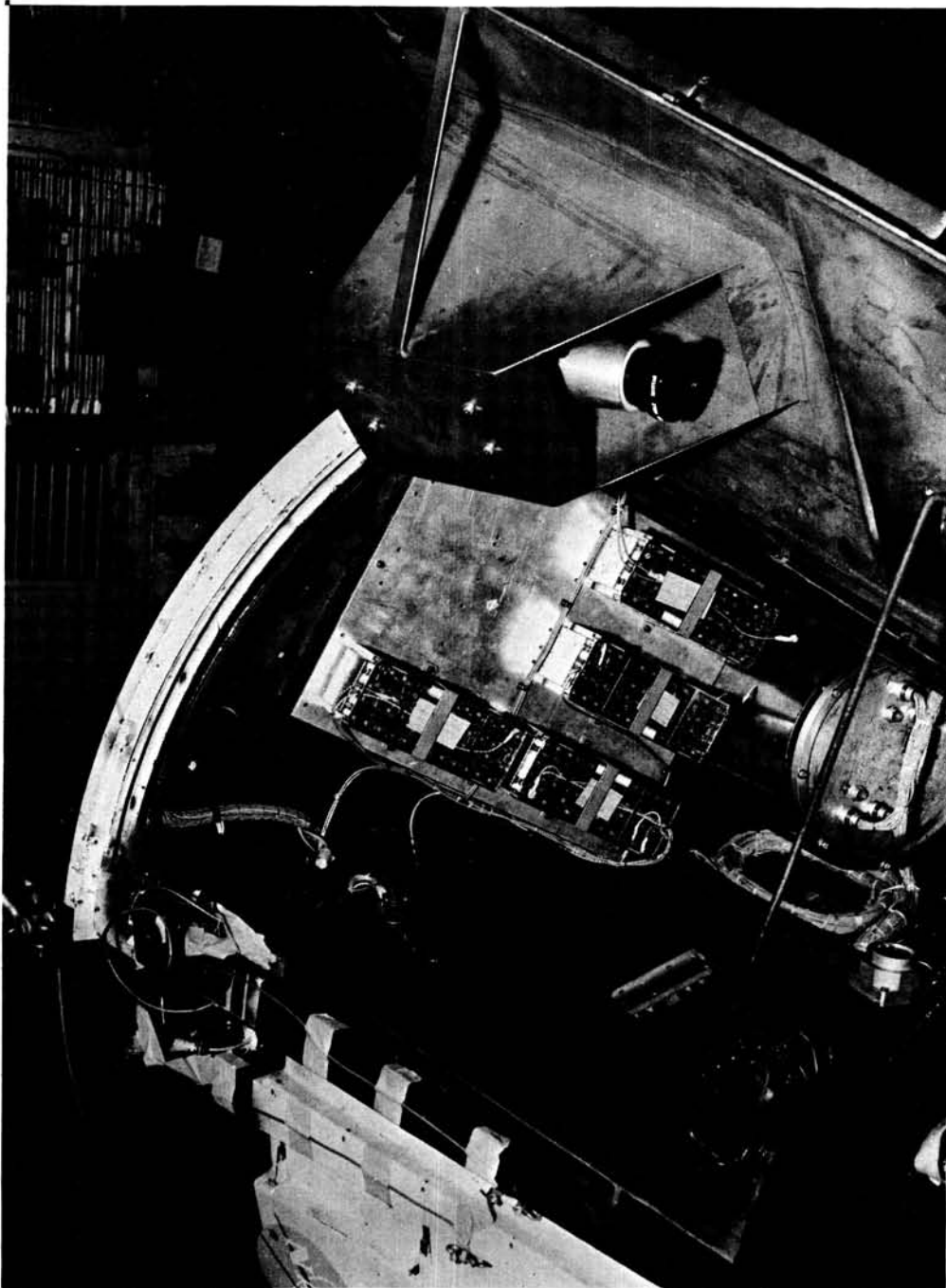


Figure XI-11.- Battery pallet.

NASA-S-66-10470 OCT 24

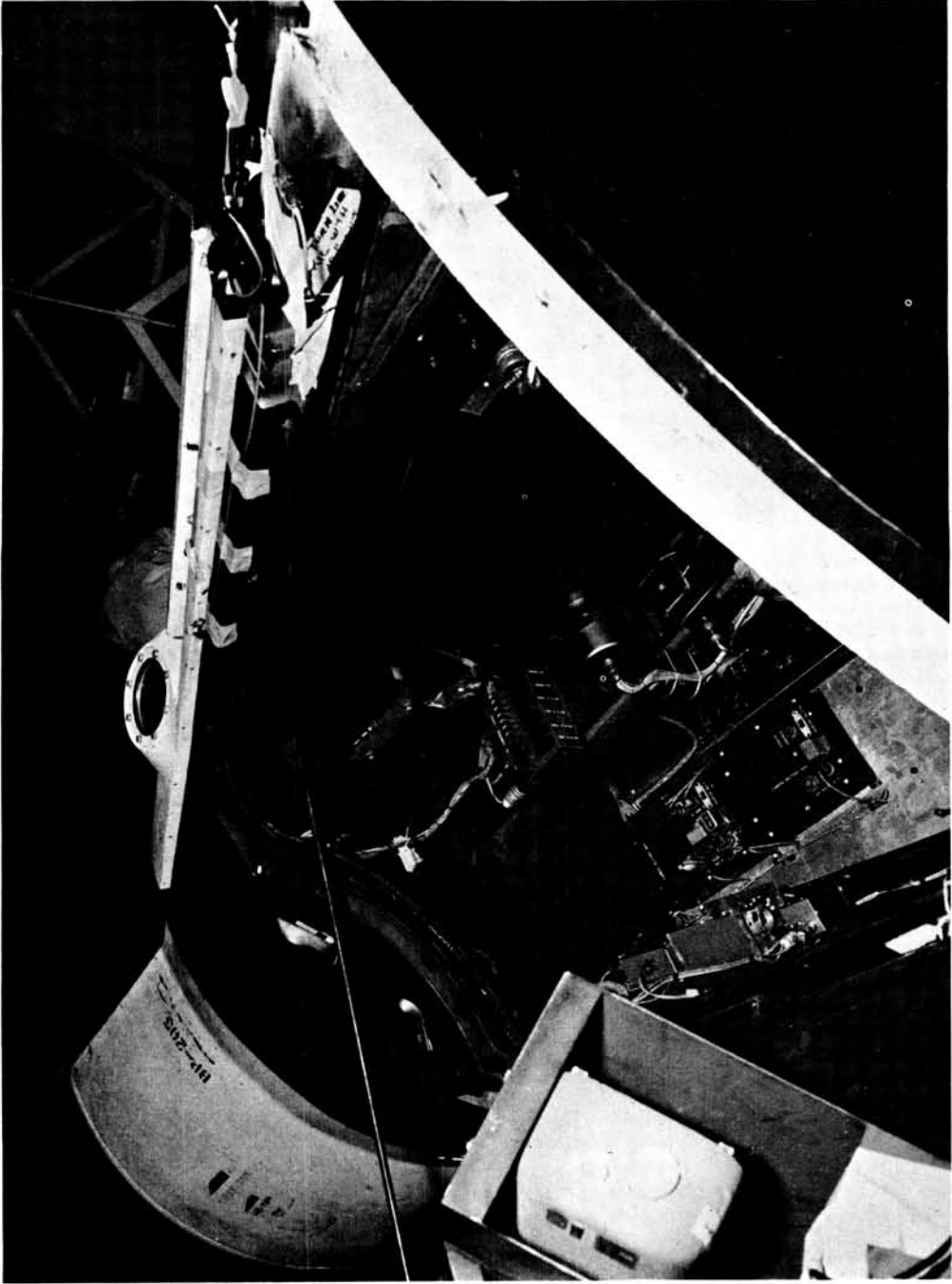


Figure XI-12.- Instruments at the center of gravity.

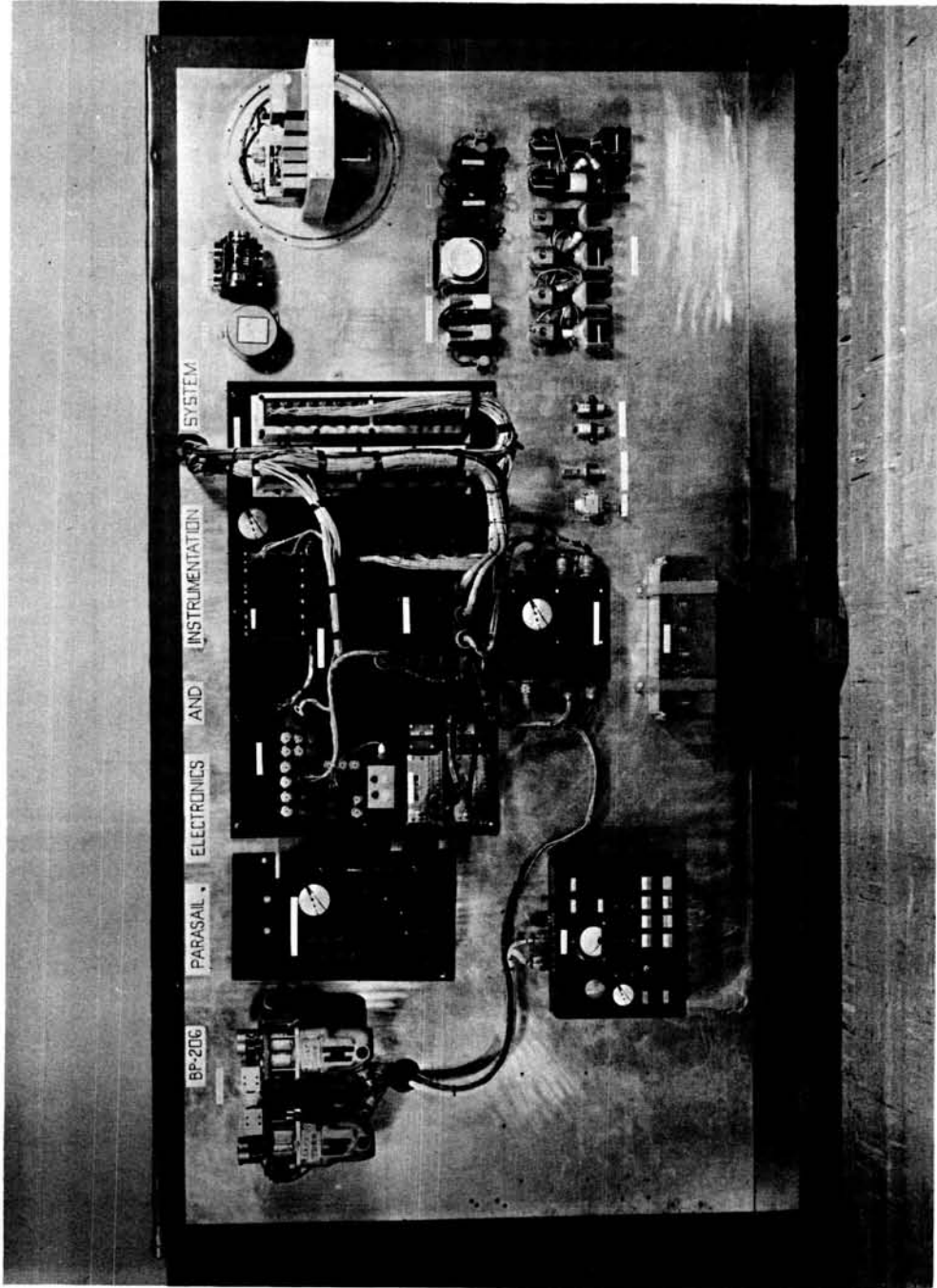


Figure XI-13.- Instrumentation breadboard, airdrops 6 to 12.

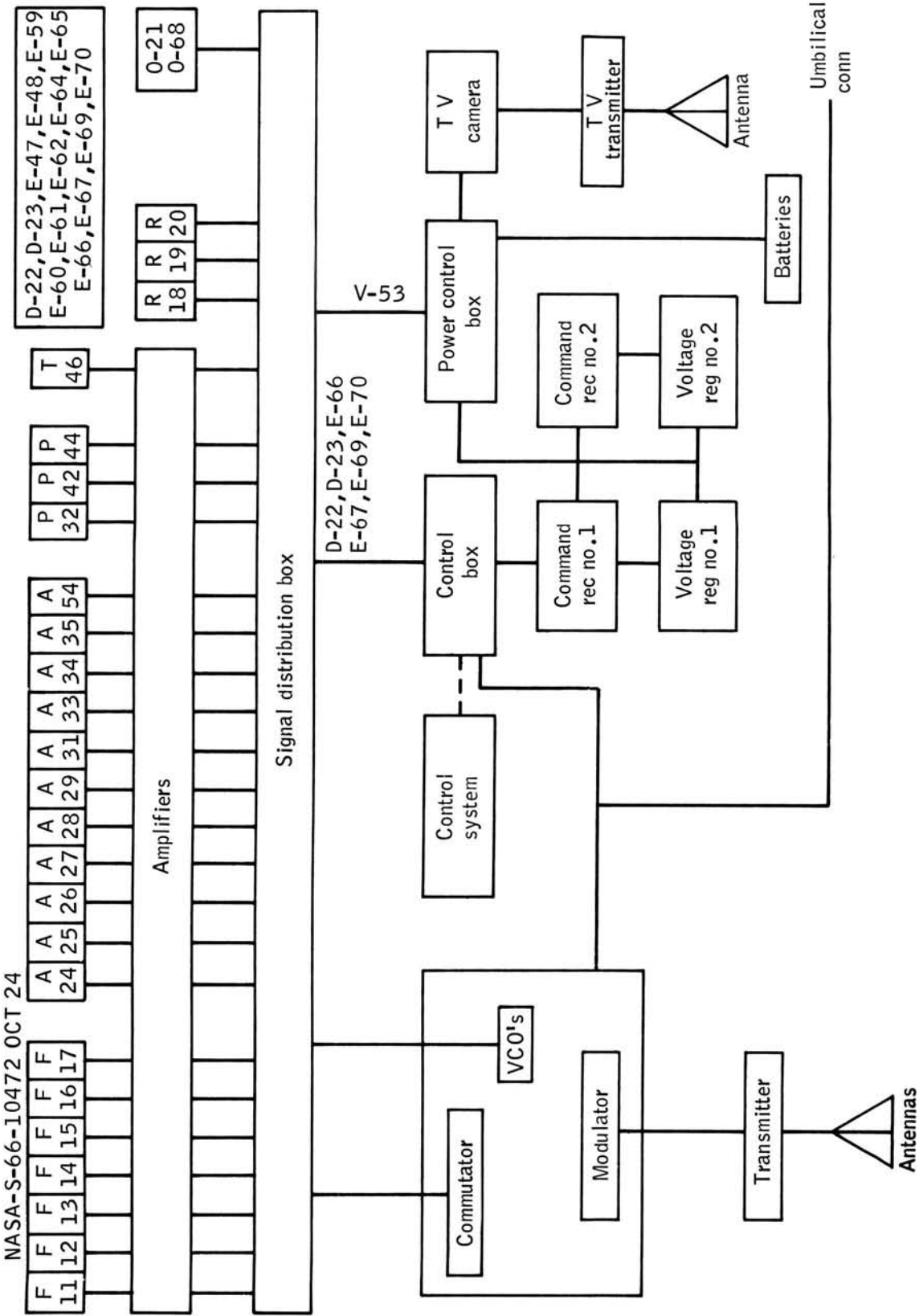


Figure XI-14.- Instrumentation and electronic systems for airdrops 6 to 12. (A, acceleration; D, positions or strokes; E, events; F, force; O, attitude; P, pressures; R, rates; T, temperature; and V, voltage.)

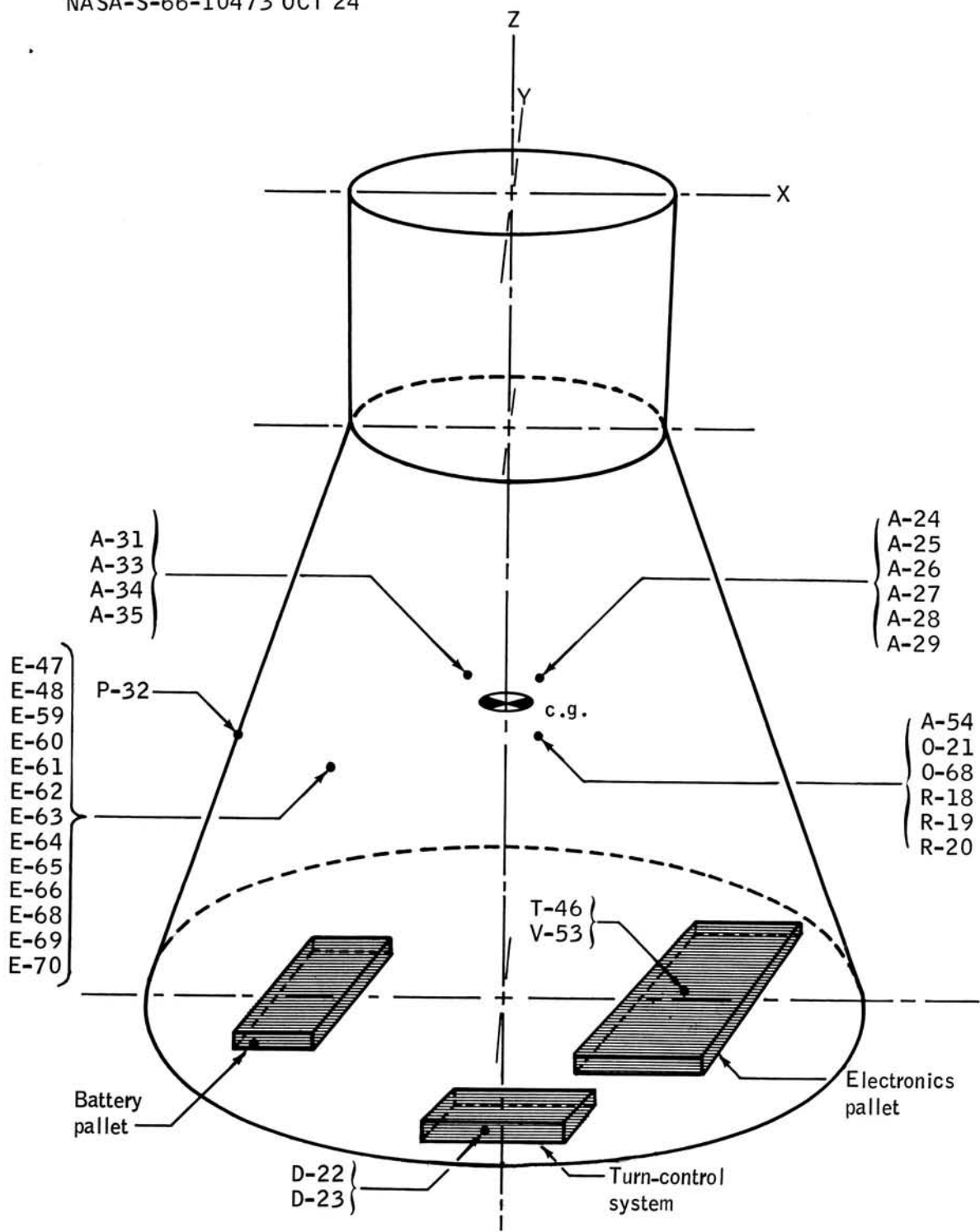


Figure XI-15.- Measurement locations, inside view. (A, acceleration; D, positions or strokes; E, events; O, attitude; P, pressures; R, rates; T, temperature; and V, voltage.)

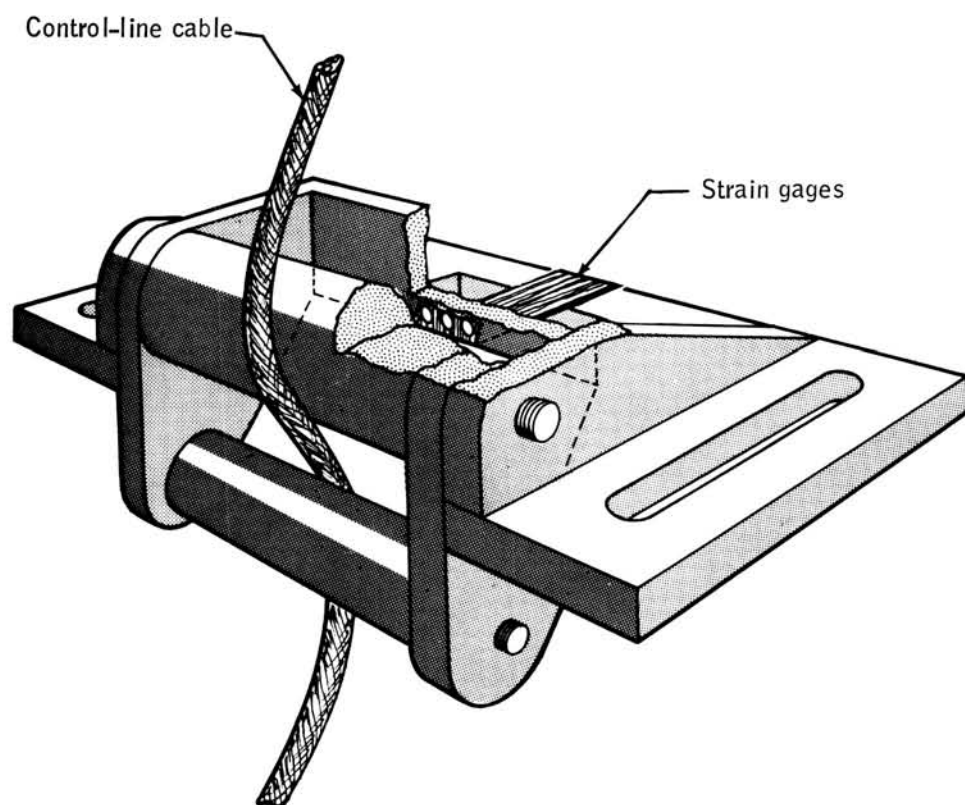


Figure XI-16.- Control-line transducer.

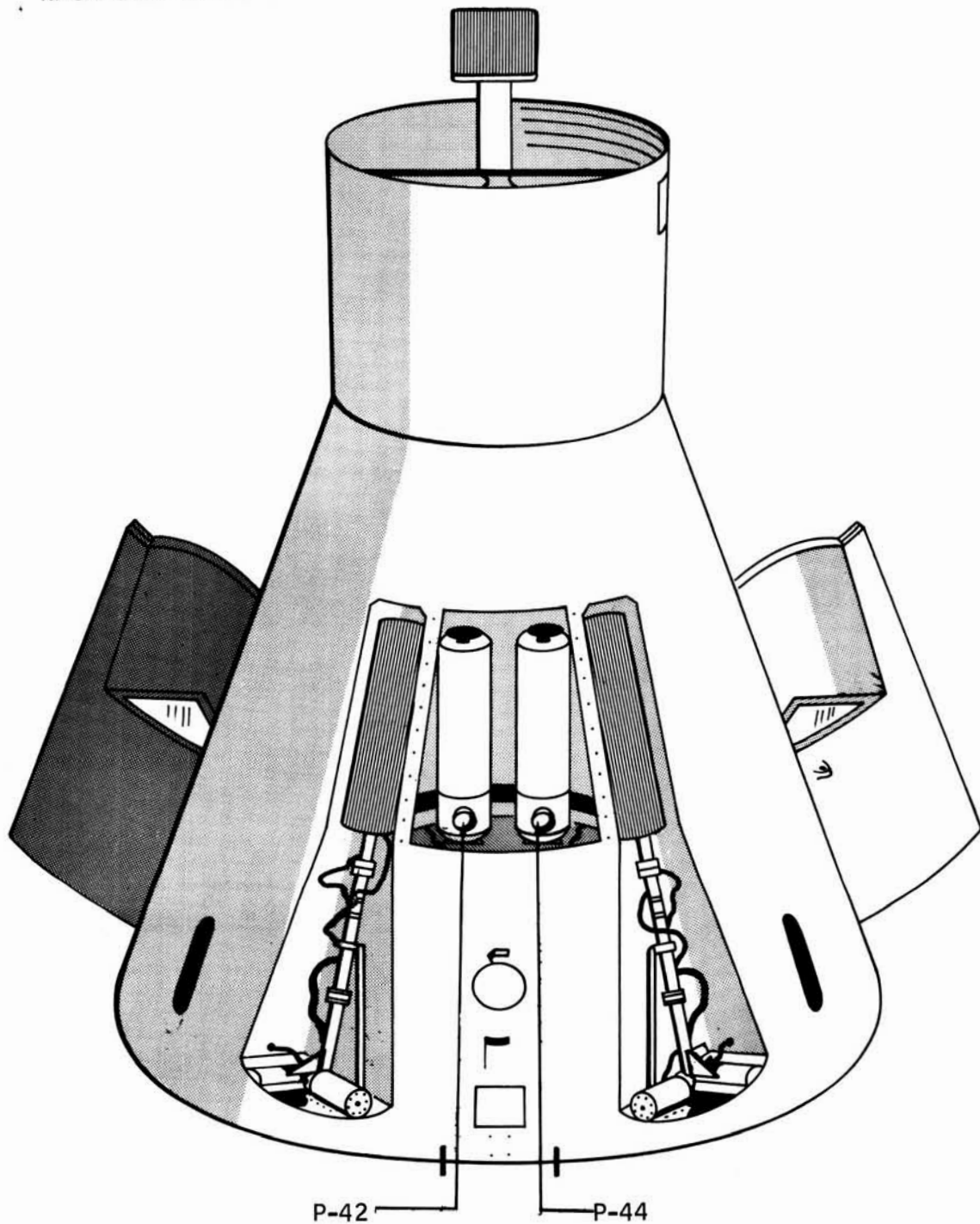


Figure XI-17.- Measurement locations, bottom view. (P, pressures.)

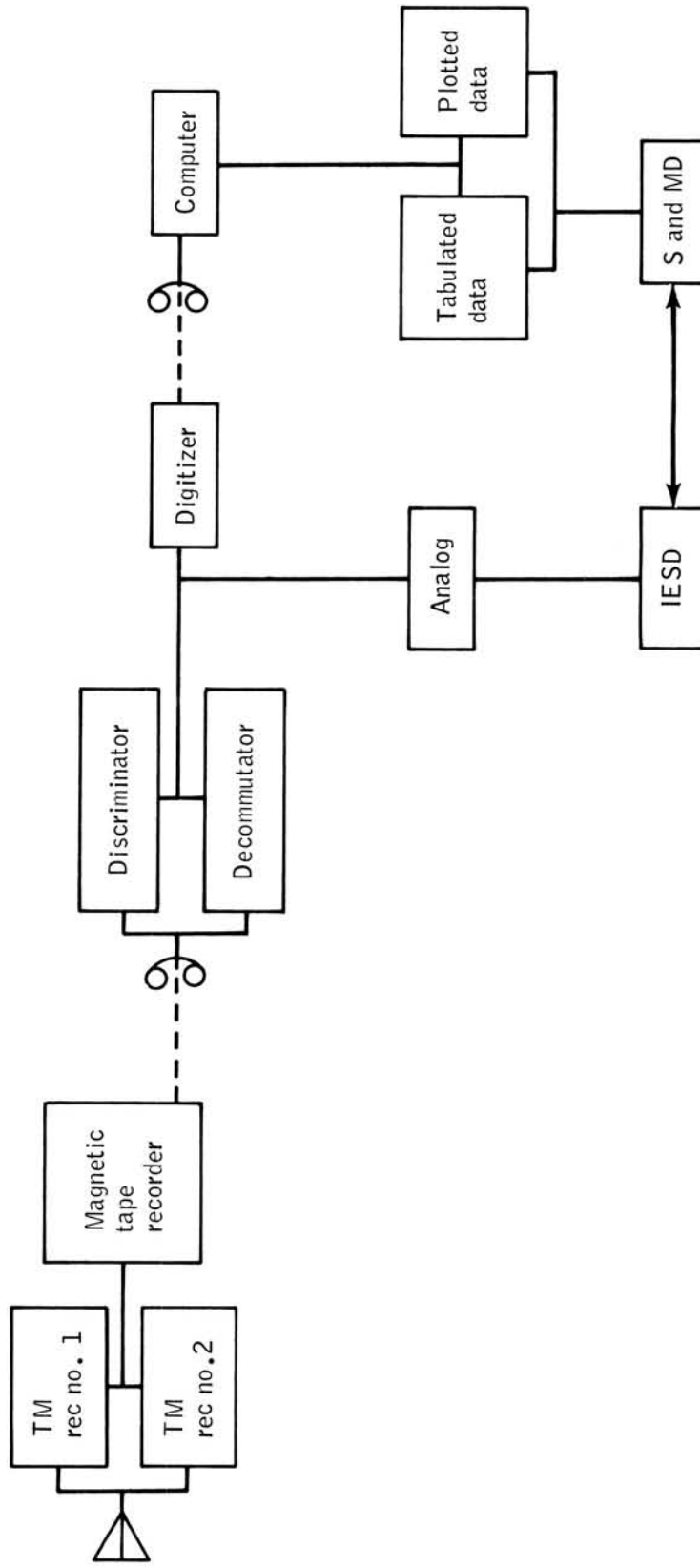


Figure XI-18.- Data flow chart.

SECTION XII - SEQUENCING AND IGNITION SYSTEMS FOR THE
GEMINI SPACECRAFT LAND LANDING PROGRAM

By Roger N. Messier

PRECEDING PAGE BLANK NOT FILMED.

SEQUENCING AND IGNITION SYSTEMS FOR THE GEMINI SPACECRAFT LAND LANDING PROGRAM

By Roger N. Messier
Manned Spacecraft Center

INTRODUCTION

The Gemini spacecraft land landing system provides a safe rate of descent to return the spacecraft to the surface of the earth, and furnishes the proper attitude for a soft impact in a predetermined landing area. During descent, the rendezvous and recovery section is released, the Para-Sail is deployed, the emergency landing system is armed, the main Para-Sail suspension is repositioned from a single point to a four-point system, the blast deflector is released, the landing gear is activated to a landing position, the altitude sensor is deployed, the parachute disconnect switch is armed, and the altitude sensor for rocket firing is armed. These events are dependent upon sequential systems comprised of indicators, relays, bridges, squib switches, sensors, pyrotechnics, rocket motors, and timing devices which provide automatic control during the critical landing period.

The sequencing system is the method employed to control automatically the events that are required to function in a specific order and at a precise time. It performs the events necessary to attain mission objectives by initiating pyrotechnic actuated functions such as those described.

DISCUSSION

The heart of the programming system is composed of squib switches. These switches are manufactured by the Atlas Chemical Industries, Inc., and are of the OM series, with varying time delays. The ignition and sequential systems are completely redundant, and neither system is ever electrically connected to the other. The circuitry is isolated from all other spacecraft circuits and utilizes a floating concept which employs twisted, shielded, paired wiring with Teflon sleeves; the pairs being encapsulated within a Teflon jacket. The shielding of this system is grounded at a single

point on the sequence board. The ignition circuitry for pyrotechnics and the rocket motors are wired through an arming-bar technique which greatly enhances the checkout and arming capabilities and permits the shorting of pyrotechnics after they have been installed.

A monitoring capability was designed into the system which greatly expedited the checkout procedures during pyrotechnic installation, pre-arming, checkout, and final arming. It also provided the capability of validating the ignition system and performing the final arming in the drop zone, thus increasing confidence and reliability and providing means of detecting any possible last minute malfunctions in the system.

A composite pyrotechnic checkout unit was designed to accommodate this monitoring capability. This unit is also adaptable to other ignition systems or sequencing systems that might be designed with a monitoring feature.

The emergency landing system is activated by a ground command. The activation of this system is dependent upon the reception of two coded frequencies which close two series relays in each receiver. The closure of these two series (relays) activates the emergency system on the sequential board and automatically locks out all normal events that have not sequentially functioned. The emergency programmer simultaneously fires all Para-Sail suspension release mechanisms and the configuration change, completely releasing the Para-Sail from the test vehicle. At 0.8 second later, the emergency parachute deployment gun is fired, extracting and deploying the emergency parachute.

The emergency sequential lockout prevents the release of the blast deflector, landing-gear deployment, altitude-sensor release, and the rocket-motor ignition. If all events have functioned prior to the initiation of the emergency systems, it will still lock out the rocket-motor ignition.

After a normal flight, the only pyrotechnic that has not been utilized is the emergency parachute gun. Therefore, the arming bars are located on the test vehicle so as to be easily accessible on the ground, enabling the removal of the arming connector and installation of shorting connectors prior to the de-arming of the parachute gun.

System Checkout Philosophy

The sequencing and ignition systems were designed with features which enable a complete system checkout. After complete installation of the systems and the associated hardware in the spacecraft, the following procedures were followed.

Meggar check. - A meggar check was performed on each individual wire to every other wire in both systems and each wire to ground and shield. The equipment used to verify the insulation resistance of each wire was designed and assembled by Hazardous Materials Branch, Technical Services Division personnel and consisted of a unique grouping of motorized switches and a meggar.

Circuitry lead resistance. - Circuit resistance was determined with an Alinco circuit tester and recorded in the resistance reading procedure. The circuit reading and the squib bridge resistance were used to calculate the final resistance by which each circuit was verified during checkout and arming procedure.

Sequencing board checkout procedure. - The sequence board checkout procedure verified each wire, squib-switch contact, and squib-switch bridge on the board and also the altitude sensor, lanyard switch, and parachute disconnect switches. This check was accomplished by verifying and recording continuity and resistance with an E-80 Blasting Galvanometer and a 101-5BF Alinco circuit tester. An ignition battery voltage check is also performed in this procedure.

Pyrotechnics and rocket-motor installation and checkout, and pre-arming checkout. - The first part of this procedure is self-explanatory, but it should be stated that a policy of verification of no voltage, no continuity, and no ground is rigidly followed prior to the installation and connection of any pyrotechnics. This procedure also established a complete system checkout and required the use of the pyrotechnic checkout unit.

Final internal/external capsule check sheet. - This procedure was performed to assure last minute readiness of all systems and components prior to door closure.

Flight checkout and arming. - Immediately after takeoff, the R and R canister release was checked out and armed in order to save the test system in the event of an aircraft emergency which required ditching of test equipment. Final arming and checkout were completed in the drop zone. All checkout and system verification in this procedure was performed with the pyrotechnic monitor checkout unit.

During buildup preparation, a simulated mission was performed on the vehicle. (The checkout procedures described were followed.) Instrumentation, television, command systems, and onboard camera systems were operated as in an actual mission. This included physical checkout of the normal and emergency sequencing systems. In lieu of actual pyrotechnics, match squibs were used to simulate the **squib** bridges and eliminate the

explosive danger of an actual pyrotechnic. The simulated mission was performed as the last phase of the vehicle buildup and test prior to actual flight buildup.

A checkout and qualification testing of components and hardware was performed on all pyrotechnically actuated or sequencing oriented devices prior to flying on actual missions. As an example, parachute disconnects, cable cutters, blast-deflector release, altitude-sensor deployment, configuration change, R and R canister release, and landing-gear deployment testing were performed under simulated flight conditions. Two rocket firings with the blast deflector installed were also accomplished to qualify structural design and its ability to negate the rocket thrust. As a result of this type of testing, no MSC designed and fabricated hardware or component failed during a flight test.

Sequencing System

The sequencing system block diagrams depict the basic sequencing systems that were used during the 12 test drops and the 2 crane drops. A brief explanation of each diagram is included to assist the reader in understanding the philosophy of the system. Table XII-I contains a listing of all of the pyrotechnic devices used.

Block diagram 1 for test 1. - This sequencing system (fig. XII-1) was employed in the first test, which was conducted primarily to verify capabilities of configuration change (ability to go from a single-point suspension to a four-point suspension) and to investigate steady-state characteristics. The sequence of events was as follows: At T - 0 seconds, the lanyard switch was closed and the sequencing was begun by firing an 8-second-delay squib switch and activation of a dimple motor which programed the Triad camera cutoff; at T + 8 seconds, the 8-second-delay squib switch closed, triggering a 20-second-delay squib switch and firing two R and R canister release cartridges, either of which was capable of performing R and R canister release; at T + 28 seconds, the 20-second-delay switch closed, activating the configuration change. This drop did not have a control system or an emergency system, but the sequencing used was fully redundant.

Block diagram 2 for tests 2, 3, 8, and 9. - This sequencing system (fig. XII-2) was designed to accommodate Para-Sail deployment evaluation and to assist in further engineering and development of the control system. In addition to the features described in figure XII-1, this system contained an impact switch, Para-Sail suspension releases, control-line cable cutters, and an emergency system. This system was used in tests 2 and 3 primarily

and again for tests 8 and 9, when improvement in control-line deployment became necessary prior to attempting an earth landing. During these last two tests, the turn system was developed to the required degree of reliability necessary for land landing.

Block diagram 3 for tests 4 and 5. - This chart (fig. XII-3) reflects the addition of an MSC developed altitude sensor and simulated rocket motors (flashbulbs). This system was used to evaluate and verify altitude-sensor techniques in attaining rocket-motor firing at the proper altitude (approximately 10 feet above the water) prior to impact. It was also used in the development of the altitude sensor. The R and R canister release time was reduced to 5 seconds. In summary, the system contained an emergency system, R and R canister release, configuration change, altitude-sensor release, altitude-sensor arming, simulated rocket-motor firing, and Para-Sail release at impact.

Block diagram 4 for tests 6 and 7. - This system (fig. XII-4) included the addition of the blast-deflector release, simulated landing-gear release, conversion from impact switch to salt-water switch, Para-Sail disconnect at landing, and a check circuit in the altitude sensor at deployment which validated the position of the sensor switches prior to arming of the sensor circuit. In case of improper switch position, the sensor was locked out, eliminating a possible premature rocket-motor ignition in midair. Each system had an independent check circuit and locked only its own system. For example, if system one was at fault, only system one was locked out; system two still retained the capability of rocket-motor ignition when the sensor contacted.

This sequencing system was completely automatic except for initiation of the emergency system, which was activated by ground command. The emergency system activation was the closing of two series relays in each receiver, and this furnished a path for the current to activate the emergency system on the sequence board. After ground activation, this emergency system was also fully automatic. It locked out all the events that had not functioned, starting with blast-deflector release up to and including rocket firing, and it also initiated the release of the Para-Sail suspension and the control-cable cutters, plus the configuration change. After a 0.5-second delay, the emergency parachute gun deployment was initiated.

Block diagram 5 for tests 10, 11, and 12. - This system (fig. XII-5) was designed to accommodate land landings and contained all the features of previously discussed systems. The changes included redesign to accommodate landing-gear deployment by ground command, addition of switches in the landing gear to accomplish Para-Sail release upon landing, and a system which allowed the removal of circuits from the system after it had

functioned, thus eliminating electrical shorts or other possible battery drains.

Block diagram for a crane drop. - This system (fig. XII-6) was designed to evaluate rocket-motor performance and altitude-sensor capabilities prior to installation in the actual drop vehicle. The test was accomplished by suspending the vehicle from a predetermined height and releasing it to free fall. Instrumentation was hardlined to the vehicle and recorded acceleration, rate of attitude change (if any), rocket-motor pressure, and g-impact.

This block diagram illustrates the advance sequence design of these drops. To illustrate, the rocket motors were installed; the initiators were installed; and the pre-arming check was performed prior to hoisting the vehicle. After hoisting, the system was checked and armed by hardline. This was the verification of proper altitude-sensor switch position and also system arming and consequent final arming of the ignition system. Release was initiated by firing explosive cutters. The altitude sensor was backed up by the lanyard switch, which was activated approximately 1 foot after the sensor contacted the ground.

Two crane drops were made. One was performed on a hard surface, and the other was performed on soil to evaluate soil erosion during actual landing.

Squib switch. - Squib switches were selected to be used in the sequencing system because of the high degree of reliability in past performances. The squib switch was an electrically initiated, explosive device with the capability for operating in a time increment of milliseconds or in varying delays up to 30 seconds. The squib switches used in this system were manufactured by Atlas Chemical Industries and were of the OM series. Each squib switch had two switch contacts that were normally closed and two contacts that were normally open. This configuration provided the means of initiation or elimination of events, as required in the design of the sequencing system.

Sequence of event monitoring. - The real time of various events was required for proper evaluation of systems and interpretation of the recorded data. This was done by monitoring a separate contact of the squib switch that initiated the function. This design provided the means of monitoring the actual time of the event with the ability to retain sequencing and ignition system isolation. The event time was transmitted by the onboard telemetry system to the ground station.

Sequencing and ignition batteries. - The battery packs for the sequencing and ignition systems were designed and built by Hazardous Materials Branch, Technical Services Division personnel. These packs were assembled from

cells produced by Nicad, Model MP702T, Type M-1718055. Each cell had a voltage of 1.25 V dc and was originally assembled by the vendor in packs with a voltage output of 12 V dc, 4 ampere-hour capacity. The assembly did not meet project standards; hence, the assembly had to be modified to perform as required. The modifications included replacing the metal straps between cells with wire; potting the packs in rubber-lined metal cases, which were fastened to the bottom of the sequence boards; and wiring the packs in series to attain a 24-V dc output. Additional packs were parallel to attain the desired amperes in accordance with the requirements of the system.

Sequencing programmer board. - Figure XII-7 illustrates the sequencing programmer board for systems one and two which were used on tests 10, 11, and 12. The battery packs were mounted on the reverse side of each sequence board.

Conclusions. - In all tests, the sequencing system performed as designed, without failure in attaining the test objective.

Manned Spacecraft Center
National Aeronautics and Space Administration
Houston, Texas, October 25, 1966
904-02-15-01-72

TABLE XII-I. - PYROTECHNIC NOMENCLATURE LIST

Nomenclature	Application	Vendor	Part number
Electrically initiated pressure cartridges	Para-Sail suspension disconnects; control cable cutter; R and R canister releases; MSC altitude-sensor release	Ordnance Assoc., Inc., Atlas Chemical Industries, Inc.	RSPC 58080 IGN 121
Reefing cutters, mechanically actuated	Parachute systems	Atlas Chemical Industries, Inc. Ordnance Assoc., Inc.	A-1SE152 - Series A-1SE153 - Series OA-D2 - Series OA-E3 - Series
Drogue gun (emergency parachute deployment gun)	Deploy the emergency parachute	Ordnance Assoc., Inc.	101070-33
Pressure cartridge	Drogue gun	Ordnance Assoc., Inc.	101070-33
Electrically initiated pressure cartridge	Drogue gun	Ordnance Assoc., Inc.	RSPC58082
Squib switches	Sequencing system	Atlas Chemical Industries, Inc.	OM - Series
Dimple motor	Raymond timer for camera system	Hercules Powder Co.	DM25N4
Electrically initiated pressure cartridge	With OA-A15 cutter for landing gear release strap	Ordnance Assoc., Inc.	OA-B10E
Electrically initiated pressure cartridge	Landing-gear deployment	Ordnance Engineering Assoc., Inc.	Nose gear, OEA2-69100-17 MAC52-72709-17 Main gear, OEA2069200-9 MAC52-72709-9

TABLE XII-I. - PYROTECHNIC NOMENCLATURE LIST - Concluded

Nomenclature	Application	Vendor	Part number
Electrically initiated pressure cartridge	Configuration change, blast-deflector release	Atlas Chemical Industries, Inc. Ordnance Assoc., Inc.	2GN6 C-210-12 without base charge. Add 5.5 grains unique pistol powder.
Electrically initiated pressure cartridge	Rocket motor ignition	Holex Corporation	P/N-E-15948-01
Electrical guillotine cutter	DeHavilland altitude-sensor release	Holex Corporation	Dual-bridge guillotine cutter
Rocket motors	Reduce impact load, soft landing	Thiokol Chemical Corporation	TE-421-1

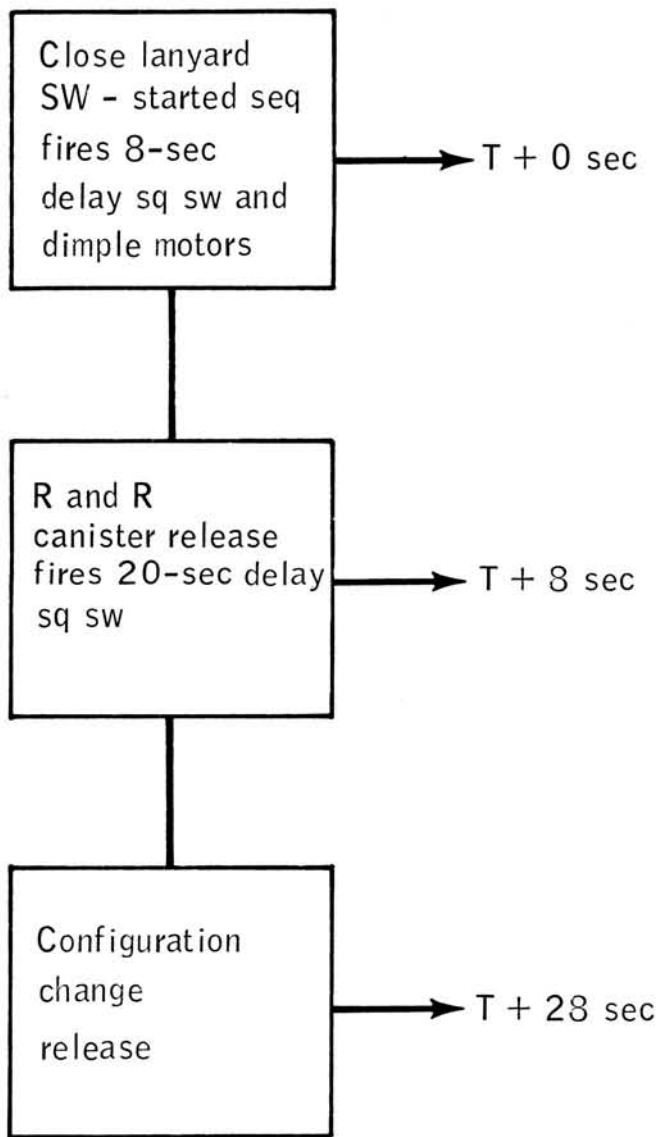


Figure XII-1.- Block diagram of event-sequencing system for drop 1 of the Gemini spacecraft land landing system.

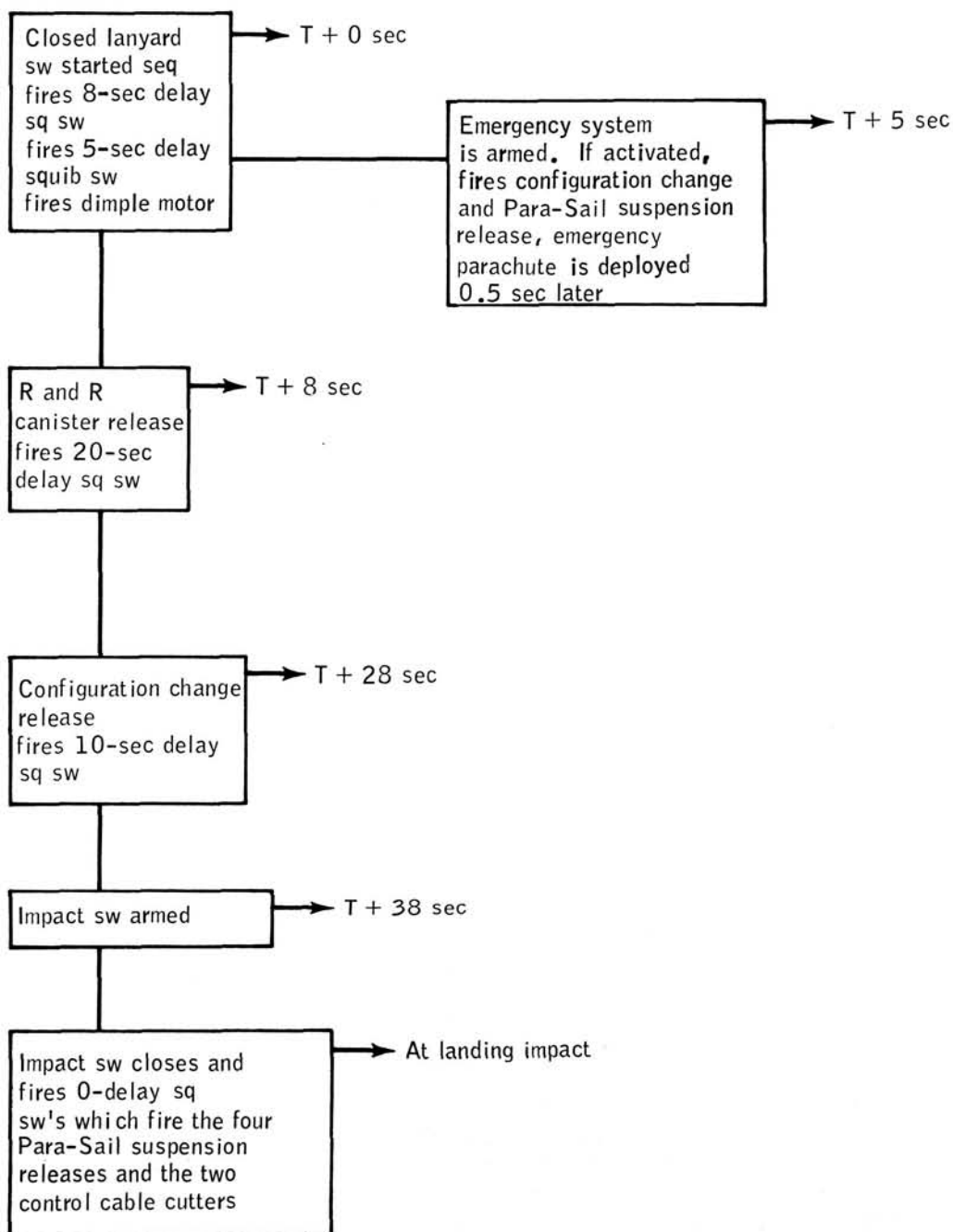


Figure XII-2.- Block diagram of event-sequencing system for drops 2, 3, 8, and 9 of the Gemini spacecraft land landing system.

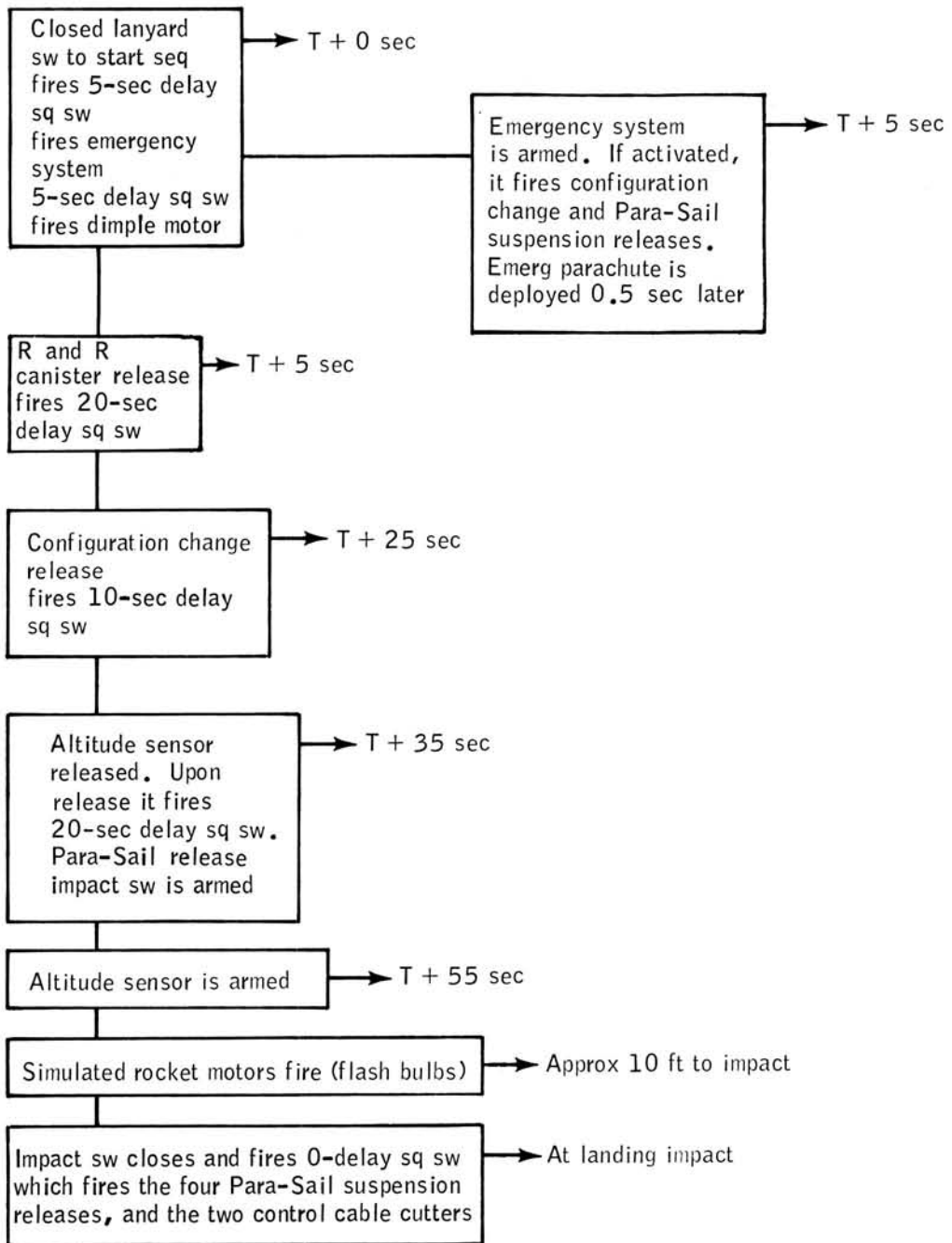


Figure XII-3.- Block diagram of event-sequencing system for drops 4 and 5 of the Gemini spacecraft land landing system.

NASA-S-66-10490 OCT 24

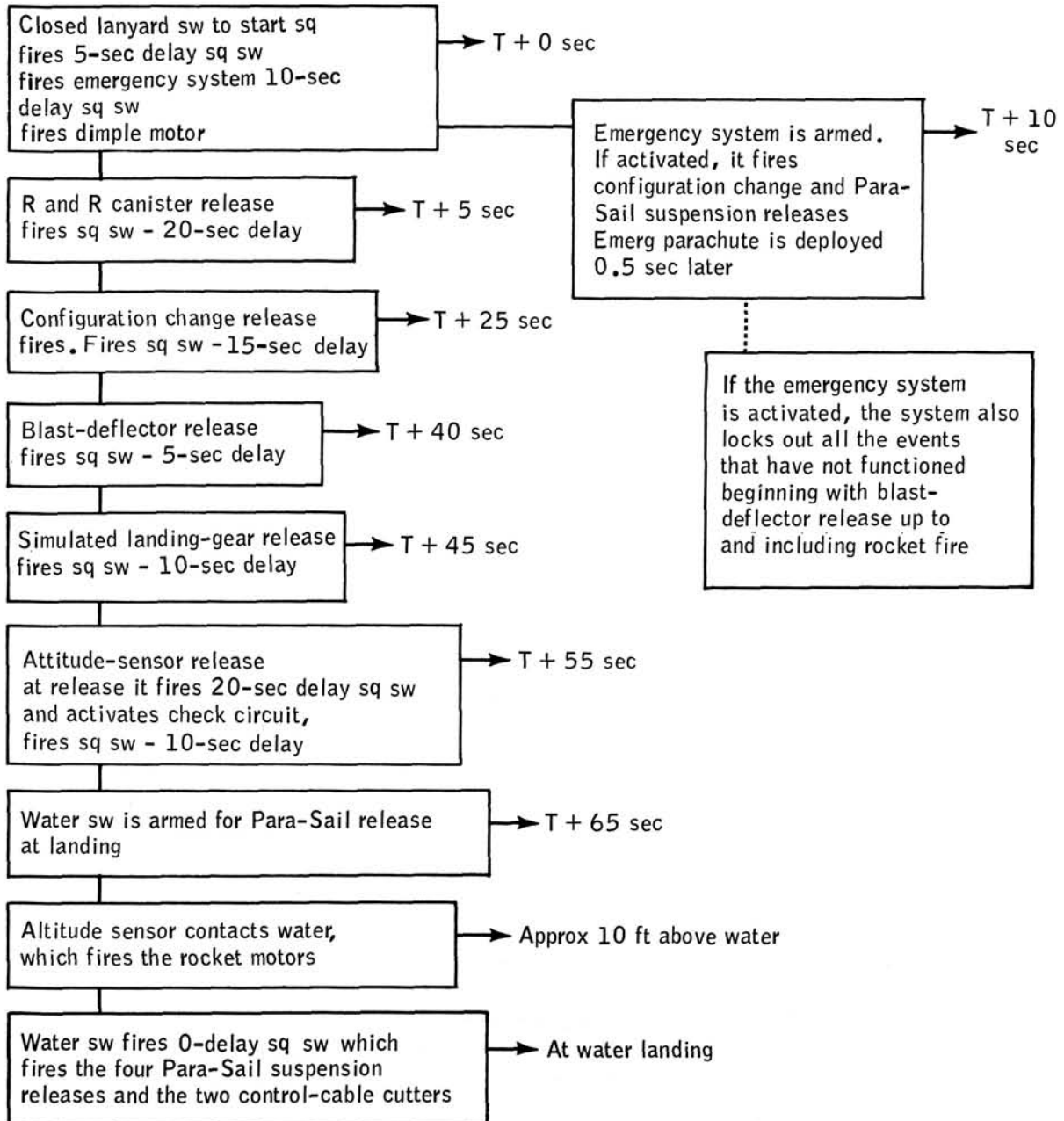


Figure XII-4.- Block diagram of event-sequencing system for drops 6 and 7 of the Gemini spacecraft land landing system.

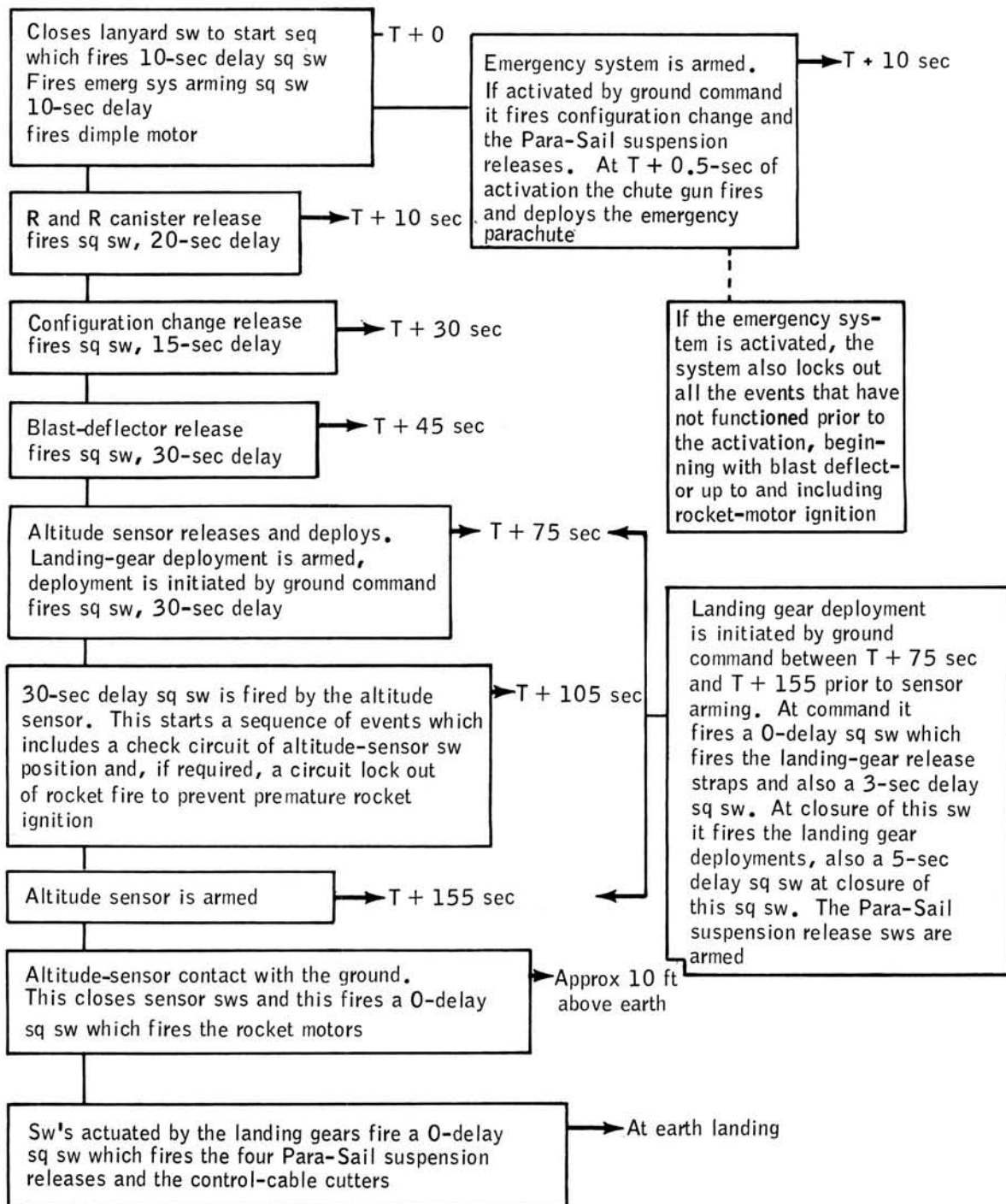


Figure XII-5.- Block diagram of event-sequencing system for drops 10, 11, and 12 of the Gemini spacecraft land landing system.

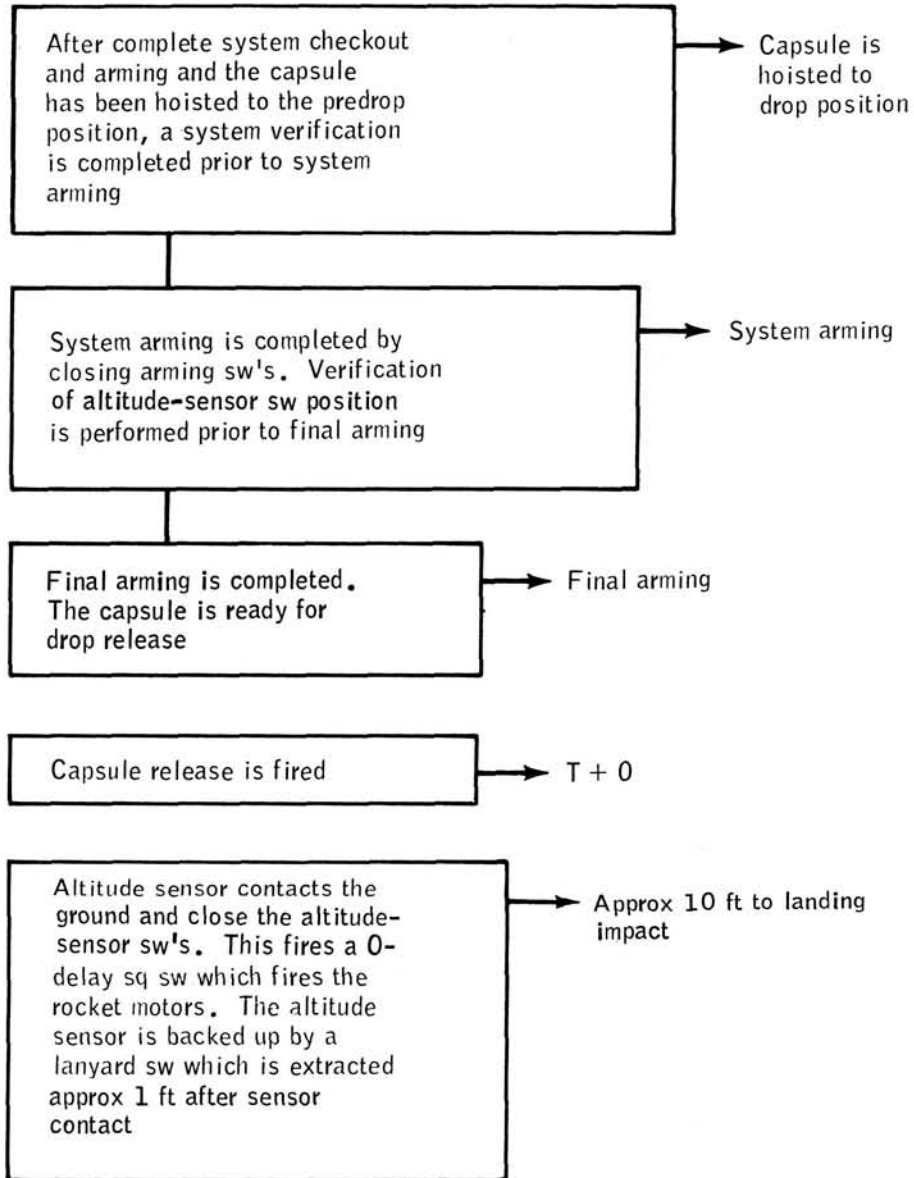


Figure XII-6.- Block diagram of event-sequencing system of crane-drop tests of impact-attenuation system.

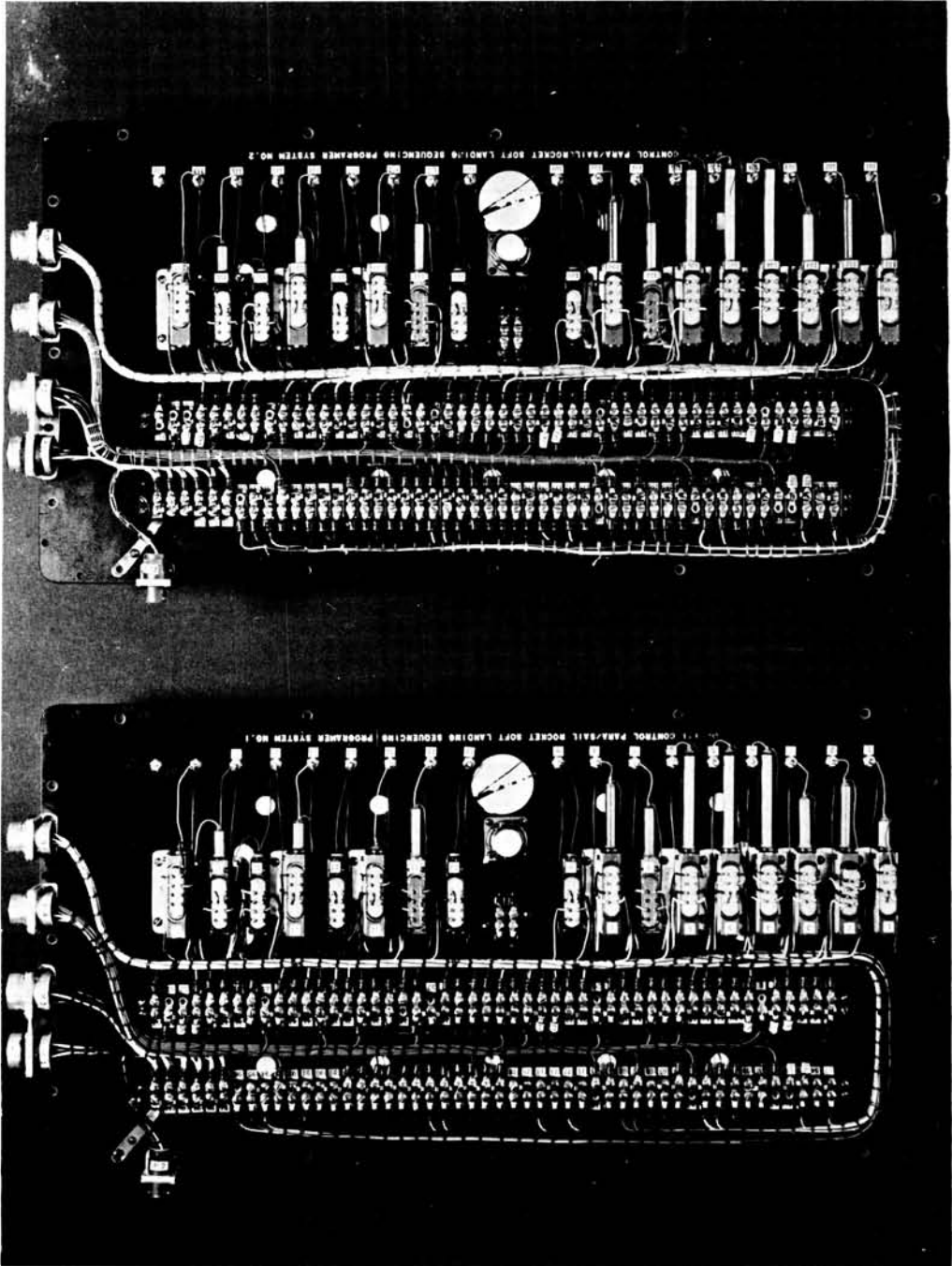


Figure XII-7.- Sequence board for drops 10, 11, and 12.

"The aeronautical and space activities of the United States shall be conducted so as to contribute . . . to the expansion of human knowledge of phenomena in the atmosphere and space. The Administration shall provide for the widest practicable and appropriate dissemination of information concerning its activities and the results thereof."

—NATIONAL AERONAUTICS AND SPACE ACT OF 1958

NASA SCIENTIFIC AND TECHNICAL PUBLICATIONS

TECHNICAL REPORTS: Scientific and technical information considered important, complete, and a lasting contribution to existing knowledge.

TECHNICAL NOTES: Information less broad in scope but nevertheless of importance as a contribution to existing knowledge.

TECHNICAL MEMORANDUMS: Information receiving limited distribution because of preliminary data, security classification, or other reasons.

CONTRACTOR REPORTS: Scientific and technical information generated under a NASA contract or grant and considered an important contribution to existing knowledge.

TECHNICAL TRANSLATIONS: Information published in a foreign language considered to merit NASA distribution in English.

SPECIAL PUBLICATIONS: Information derived from or of value to NASA activities. Publications include conference proceedings, monographs, data compilations, handbooks, sourcebooks, and special bibliographies.

TECHNOLOGY UTILIZATION PUBLICATIONS: Information on technology used by NASA that may be of particular interest in commercial and other non-aerospace applications. Publications include **Tech Briefs**, **Technology Utilization Reports and Notes**, and **Technology Surveys**.

Details on the availability of these publications may be obtained from:

SCIENTIFIC AND TECHNICAL INFORMATION DIVISION
NATIONAL AERONAUTICS AND SPACE ADMINISTRATION
Washington, D.C. 20546